Azoheteroarene photoswitches: Structure-property relationship towards photoswitching using visible light, in the water medium, and solid state

Ankit Kumar Gaur

A thesis submitted for the partial fulfillment of

the degree of Doctor of Philosophy

Department of Chemical Sciences

Indian Institute of Science Education and Research (IISER) Mohali

Sector 81, Knowledge City, S. A. S. Nagar, Manauli PO, Mohali, 140306 Punjab, India.

June 2023

Declaration

The work presented in this thesis has been carried out by me under the guidance of Dr. Sugumar Venkataramani at the Indian Institute of Science Education and Research Mohali. This work has not been submitted in part or full for a degree, a diploma, or a fellowship to any other university or institute. Whenever contributions of others are involved, every effort is made to indicate this clearly, with due acknowledgment of collaborative research and discussions. This thesis is a bona fide record of my original work; all sources listed within have been detailed in the bibliography.

Ankit Kumar Gaur

In my capacity as the supervisor of the candidate's thesis work, I certify that the above statements by the candidate are true to the best of my knowledge.

Dr. Sugumar Venkataramani

DEDICATED TO

MY PARENTS, MY WIFE, AND MY HERO, SHIVAY

Acknowledgements

First and foremost, I would like to express my heartfelt gratitude to my thesis supervisor Dr. Sugumar Venkataramani for his exceptional guidance, unwavering support, and invaluable contributions throughout my doctoral journey. His expertise and passion for science have been a constant source of inspiration for me. I am immensely thankful for the countless hours devoted to our discussions, meticulously reviewing my drafts, and providing invaluable feedback that shaped the direction of my research. His constructive criticism and thought-provoking suggestions challenged me to think critically and refine my ideas. His vast knowledge and keen insights have pushed the boundaries of my research and greatly enriched the quality of my work. Beyond his professional contributions, I want to acknowledge him for his exceptional personal qualities, patience, kindness, and approachability created a nurturing environment that allowed me to thrive academically and emotionally. His dedication to my success, coupled with his genuine interest in my well-being, made this journey all the more rewarding.

Finally, I would like to express my profound gratitude to him for believing in me and giving me the opportunity to pursue my Ph.D. Being his student has been an honor and privileged. I am forever grateful for his guidance, mentorship, and unwavering support.

A special thanks to Manju Ma'am for inviting us for dinner and lunch and giving us a home-like environment.

I would especially like to thank my Doctoral Committee Members, Prof. S. Arulananda Babu and Prof. Santanu Kumar Pal, for their valuable discussions and suggestions and for evaluating my research improvement yearly and for spending their valuable time. My genuine thanks to Prof. J Gowrishankar, present director of IISER Mohali and former director Prof. N. Sathyamurthy, Prof. Debi P. Sarkar, Prof. Arvind, and Prof. Siva Umapathy for providing the facilities and infrastructure to carry out my research work smoothly. I am sincerely thankful to the Head of the chemistry department Prof. Sanjay Singh, and former heads of the chemistry departments: Prof. S. Arulananda Babu and Prof. K. S. Viswanathan, for making the various departmental facilities available for use. I gratefully thank all the faculty members of the Department of Chemical Sciences for allowing me to use the departmental facilities. I sincerely thank Prof. Sanjay Singh and Dr. Sandeep Kumar Thakur for their help in solving the crystal structures. I sincerely thank Prof. Gopalan Rajaraman for his support, guidance, and sharing of knowledge for photoswitchable metal complexes work.

Furthermore, I am deeply grateful to everyone who has contributed to my research journey and supported me throughout the completion of this thesis. The success of this work would not have been possible without the unwavering dedication and collaboration of my labmates, whose contributions have enriched my experience in countless ways. I want to extend my gratitude to all my present and past lab members (Dr. Mayank, Dr. Chitranjan, Dr. Surbhi, Dr. Anjali, Dr. Pravesh, Dr. Sudha, Dr. Archana, Anjali, Sapna, Himanshu, Debapriya, Subham, Rajani, Piyush, Navneet, Gayathri, Raman, Sonam, Dheeraj, Ashish, Amal, Vaithesh, Irin, Sabhana, Anees, and Roshan). Especially, I would like to thank Debo for helping me a lot starting with healthy discussion for a project, collecting data, writing manuscripts, and manuscript revision. She was the only person who took care of my research work when I was at my home with my father during his last time. She is a true example of a dedicated researcher.

I would like to thank Btech (Himanshu) for supporting me a lot many times. He supported me financially whenever I needed it. He also supported me when I was frustrated or depressed. I would like to thank a special cool personality, Pravesh. He inspired us with his punctuality in the lab.

To all my labmates, thank you for your companionship, encouragement, and the countless memories we have shared. Your contributions have enriched my Ph.D. experience beyond measure, and I am truly grateful for each and every one of you.

I would like to thank a special person, “My younger brother DNN (Dhanyaj Naryanan Nampoothiry).” I used to memorize his words when he discussed “You know bhaiya”. Very hard to find such a nice and supportive person in life.

Sometimes we don’t have any blood relation, but we are more than a blood relation. For me, Gaurav bhai, Akash, and Deepanshu, Pankaj are more than any blood relations. These are pillars of my life. Specially thanks to Anuj and Prasoon also. Special thanks to my M.Sc. mate Rahul, Gaurav, and Darlington, Sitikant. Without these guys, my M.Sc. was not have been possible.

Very special thanks to my Ph.D. mates Yogesh, Captain, Pavit, Gurdeep, Feroz, Bara, Sandeep, Prashant, Prateek, Sai and others Ph.D. mates. All are very kind-hearted and helpful people. Thanks to Feroz and Gurdeep for helping me during my toughest time. Special thanks to Mayank (physics) and Jaskaran (physics), Gaurav Sharma too. Special thanks to all neighbor labs.

During my Ph.D., the lab is like our family, lab environment is the most impactful thing in life. Thanks to all my colleagues and juniors for the wonderful environment. Thanks to Arun Chauhan for entertaining. He is most entraining guy.

I am very thankful to all my teachers (All my school teachers, my college ones). I want to thank my M.Sc. supervisor Dr. Usharani Subuddhi, who encouraged me to pursue Ph.D.

I want to thank all my relatives. I want to especially thank all my Mausi-Mausa ji, my maternal uncles and aunties, and their children for caring for my mother. These are the people always stand with us in any situation. I want to thank my mother-in-law and father-in-law and their family for caring for my wife and our baby during this period. Thanks to my wife and my hero Shivay for coming into my life.

I can’t express my sincere thank just in words to my parents and my sister and her family; without them, I couldn’t imagine this journey. My amma ji is a great lady. Though she is illiterate, she is the only one who knows the value of education in life. She faced many challenges without education. Today I am writing this thing just because of her.

Abbreviations

ACN	Acetonitrile
AcOH	Acetic acid
Aq	Aqueous
brs	Broad singlet
$CHCl_3$	Chloroform
clcd	Calculated
cm	Centimetre
δ	Chemical shift
$CDCl_3$	Chloroform-D
J	Coupling constant
DCE	Dichloroethane
DCM	Dichloromethane
Et_2O	Diethyl ether
°C	Degree celsius
DMSO	Dimethyl sulfoxide
DBU	1,8-Diazabicyclo[5.4.0]undec-7-ene
d	Doublet
dd	Doublet of doublet
ddd	Doublet of doublet of doublet
dt	Doublet of triplets
EWG	Electron withdrawing
ESI	Electrospray ionization
EtOH	Ethanol
EtOAc	Ethylacetate
equiv	Equivalents
FT-IR	Fourier transform infrared spectroscopy
Hz	Hertz
HRMS	High-resolution Mass Spectrum
h	Hour(s)
IR	Infrared
LED	Light-emitting diode
m/z	Mass/Charge

MHz	Megahertz
m.p.	Melting point
MeOH	Methanol
ml	Milliliter(s)
mM	Mili Molar
mmol	Millimole(s)
min	Minute(s)
MOST	Molecular solar thermal energy
µL	Microliter (s)
M.S.	Molecular sieves
m	Multiplet
DMF	*N*,*N*'-Dimethyl formamide
q	Quartet
rt	Room temperature
sept	Septet
s	Singlet
NaH	Sodium hydride
tert	Tertiary
THF	Tetrahydrofuran
TMS	Tetramethylsilane
t	Triplet
td	Triplet of doublets
tt	Triplet of triplet
UV	Ultraviolet
Vis	Visible

List of Schemes and Figures

List of tables

Abstract

Azobenzenes are one of the prominent classes of molecular photoswitches that exhibit widespread applications, from smart materials (photo-controlled actuators, adhesives, energy storage materials, non-linear optics, etc.) to biology (bioimaging, drug delivery, photopharmacology, etc.). They are known for photoisomerization between a thermodynamically stable *E*-isomer and a metastable *Z*-isomer. The forward (*E*-*Z*) isomerization is mainly driven by UV light, whereas reverse (*Z*-*E*) isomerization can be induced by visible light or heat. However, UV light is harmful and potentially causes damage to the surface of the material. The utility of azobenzenes in real-life applications demands excellent bidirectional performance, long *Z*-isomer stability, photoswitching with visible light, photoswitching in aqueous media, and photoswitching in the bulk state, some of which are challenging. Recent explorations on replacing one of the six-membered azobenzene rings with a five-membered heterocyclic ring led to outstanding photoswitching behavior and exceptional thermal stability of *Z*-isomer. Motivated by the recent progress in this direction, we considered designing bidirectional visible light photoswitchable azo compounds with a long stable *Z*-isomer, photoswitching in water, and the bulk state as the major objectives of the thesis.

Towards designing bidirectional visible light-driven azo photoswitches, we introduced cyclic aliphatic amine at the *ortho* position of azoheteroarenes. Furthermore, we synthesized 22 derivatives with different azoheteroarenes (azopyrazole, azoisoxazole, and azopyrrole), varying the size of the cyclic aliphatic amines using a simple synthetic strategy with excellent yields. To understand the effect of substitution on the photoswitching properties and *Z*-isomer stability, we performed UV-Vis and ^{1}H-NMR spectroscopic studies. Substitution at 3,5-position of azoheteroarenes (azopyrazole and azoisoxazole) with phenyl shows further red-shifted absorption compared to methyl substitution. To stabilize the *Z*-isomer, fluorine substitution is introduced at the *ortho* position of azoheteroarenes and cyclic amines. All the molecules exhibit bidirectional photoswitching under visible light with tuneable half-lives between minutes to hours/days. More importantly, moderate to good conversions were observed with forward (*E*-*Z*) isomerization with violet to green light and reverse (*Z*-*E*) isomerization with blue to red light. Through this, a structure-activity relationship has been established.

The next aim was to construct azo compounds capable of bidirectional photoswitching in water with tunable or high *Z*-isomer stability. In the first approach, we quarternized the

pyridine nitrogen of pyridylazoheterarenes to make the ionic photoswitches. We synthesized eight derivatives of heteroaryl azopyridinium ionic photoswitches (HAPIPs) with varying azoheteroarens (azopyrazole and azoisoxazole), substitution at azoheteroarene ring (Me vs Ph), counter anions. All the molecules showed moderate to good bidirectional photoswitching in water. Apart from that, the derivatives exhibit thermal stability of *Z*-isomer from seconds to days. Further, to achieve quantitative photoswitching with the exceptional thermal stability of *Z*-isomer, we have designed 36 arylazopyrazolium ionic photoswitches (AAPIPs) derivatives by quaternization of substituted arylazopyrazoles. All the derivatives showed quantitative forward photoisomerization, while reverse photoisomerization was moderate to excellent in water and organic solvents such as DMSO, CH_3CN, MeOH, chloroform, and toluene. The parent derivative shows 157 days half-life in the water and 55 days in DMSO at room temperature.

In the last part of the work, to achieve photoswitching in the bulk state in multiple azo(hetero)arenes synthesized in a tripodal C_3-symmetric mode. The azopyrazole-based C_3 derivatives show excellent photoswitching in solution, solid state with photochromic behavior confirmed by UV-Vis, ^{1}H-NMR, and PXRD techniques. The solid-state photoswitching was exploited towards fully light-driven image writing and erasing applications. Upon bringing flexible connection, the phenomena can be observed as photochromism in the forward and thermochromism in the reverse direction.

Chapter 1. General Introduction

1.1 Photochromism

Photochromism is one of the oldest phenomena which express toggling of a chemical species between two isomeric states by light.[1] Historically, photochromic materials were used during the era of Alexander the Great (356–323 BC), but scientifically, in 1867, Fritsche stated about the fading of an orange solution of Tetracene in daylight and color recovery in the dark (**Scheme 1.1**).[2] Similarly, ter Meer discovered potassium salt of dinitroethane, which showed a color change in the solid state from yellow in the dark to red in the daylight.[3] Another early example comes from Phipson, who observed that fence posts turn black during the day while in the night it was white. This came from a zinc pigment probably lithopone.[4] The interest in photochromism was in the aftermath continuous, although limited, until between 1940 and 1960 increased mechanistic and synthetic studies especially in the working groups of Hirshberg and Fishermen in Israel. In the early 1950s, Hirshberg first time presented the term "Photochomism" of dianthrone by ultraviolet irradiation at low temperatures.[1] This name is valid even today. However, the phenomenon is not limited to colored compounds, but encompasses systems ranging from short-wave UV to long-wave IR absorbtion, very fast ones as well as very slow thermal processes.

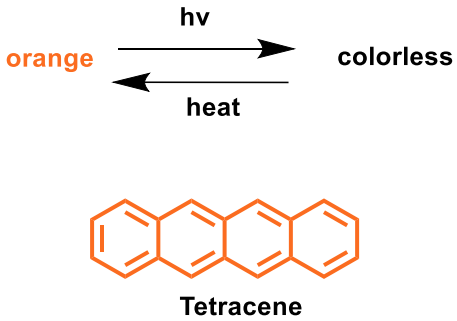

Scheme 1.1. Photochromism in tetracene.

In the case of photochromic molecules, light can induce various physical changes such as melting point, dipole moment, size, shape, etc., as well as chemical processes such as, isomerization, tautomerization, bond cleavage, cyclization, coordination changes, redox reactions, electron-hole pair generation, spin crossover, etc.[5] Through the photochemical processes, the more stable state or the isomeric form of the photochromic molecule can be converted into a less stable state or isomer. The reversal or attainment of the original status of

the photochromic molecules can be achieved either thermally or photochemically (by irradiating the sample with a different wavelength of light).

In recent times, several organic photochromic compounds such as azobenzenes, stilbenes, spiropyranes, fulgides, diarylethenes, chromenes, donor-acceptor Stenhouse aducts (DASAs), etc. have been explored. Most of these compounds show excellent photochromic behaviour and reversibility. Based on the mechanism associated with the molecular transformation, these photochromic compounds may belong to one of the following three major classes:

(i) *E-Z-E* isomerization (C=C bond or N=N bond): Azobenzene, stilbenes, indigo, hemiindigoid, hydrazone.

(ii) Electrocyclic reaction: Spiropyran, diarylethenes, fulgides, dihydropyrene, norbornadiene, DASAs

(iii) Photoinduced cyclization and tautomerization: Chromene, dihydoazulene

Depending on the energy barrier between the two-isomeric species involved, there can be two possible types of photochromic molecules.[5]

(i) T-type (Thermally reversible type): If the barrier is low, the metastable can spontaneously be converted back to the more stable isomer. Such systems are called T-type referring to the thermally induced reaction. e.g., stilbenes, spiropyranes, chromenes and azobenzenes.

(ii) P-type (photochemically reversible type): If the barrier is high, only light can be able to induce the isomerization between them. The resulting bistable system is called as P-type, which represents photo-induced photochromism. e.g., stilbenes, diarylethenes and fulgides.

In the case of photochromic molecules, light can induce various chemical processes such as, isomerisation, tautomerisation, bond cleavage, cyclization, coordination changes, redox reactions, electron-hole pair generation, spin crossover, etc.

1.2 Important classes of organic photochromic molecules

1.2.1 Spiropyrans

From the beginning of 20th century, spiropyrans are one of the important and oldest class of organic photochromes till present time due to their unique structural isomerisation in response to a variety of orthogonal stimuli, e.g., light, temperature, metal ions, redox potential,

and mechanical stress. The spiropyran molecules contain two types of orthogonally bound heterocyclic groups, an indoline and a chromene moiety through a spiro junction at carbon atom. Electronic spectra of such systems exhibit typically a band at wavelength 272–296 nm, which is attributed to the π–π* electronic transition in the indoline part, and band between 323–351 nm corresponds to the chromene moiety. The native spiropyran (closed ring isomer) can be isomerized into structurally distinct ring open isomer (known as merocyanine) by the cleavage of the C_{spiro}–O bond. The ring-opening phenomenon presented either as a heterolytic C–O bond or as a 6π electrocyclic ring opening, leading to the zwitterionic or the quinoidal resonance forms, respectively (**Scheme 1.2.1**).[6]

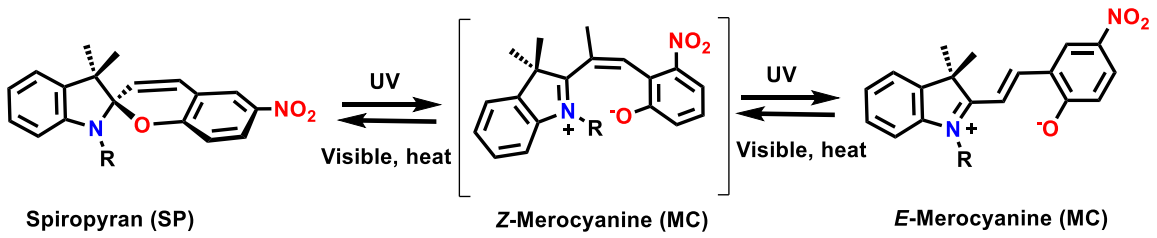

Scheme 1.2.1. Photoswitching behaviour of spiropyran.

1.2.2 Fulgides

Fulgides are eminent thermally stable photochromic (P-type) switch, which have at least one aromatic ring on the exo-methylene carbon atom. Fulgides show 6π-electrocyclization to form a 1,3,5-hexatriene structure.[7] The photochromism of fulgide occurs between one of the colorless open form and the coloured cyclized species, which can be interconverted by light-driven electrocyclic ring closing and ring opening mechanism. Typically, these molecules possess a heteroaromatic ring in their structure. It exhibits three thermally stable isomers *E*-, *Z*- and C-forms (**Scheme 1.2.2**).

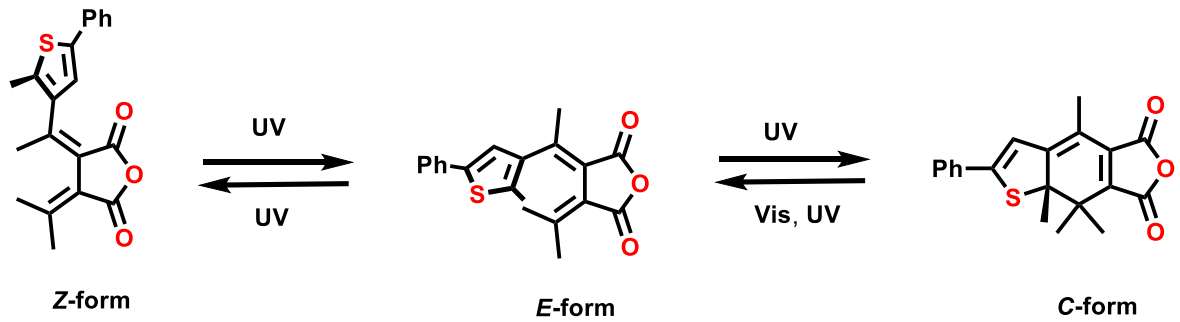

Scheme 1.2.2 Photoswitching behaviour of fulgide.

Among the three, *E*- and *Z*-isomers exist in the ring opened form, which can undergo photoisomerization between them. Indeed, the *E*-*Z* isomerization channel competes with the ring-closing reaction of the *Z*-isomer leading to the C-form. During the isomerization, polarity changes occurred to a small extent. Once the C-isomer is formed, this reaction is thermally irreversible. However, C-isomer can photochemically revert back to the *Z*-isomer in an electrocyclic ring-opening reaction. The substituents present around the triene influence the conformations of *E*- and/or *Z*-isomers of the fulgides in the ground state. These substituents also effect the quantum yields in photoisomerization reaction.

1.2.3 Stilbenes

Stilbenes are widely studied class of photochromic switch, which can isomerize between two states, *E*-isomer and *Z*-isomer. In stilbene, *E*-*Z* isomerization leads through C=C bond isomerization. The *Z*-isomer (*cis*) of stilbene can further undergo 6π electrocyclisation, resulting in a cyclized product, dihydrophenanthrene.[8] Further, in the presence of an oxidant dihydrophenanthrene can undergo, irreversible aerial photooxidation (dehydrogenation) yielding phenanthrene. This irreversible nature of stilbene makes it limited for various applications (**Scheme 1.2.3**).

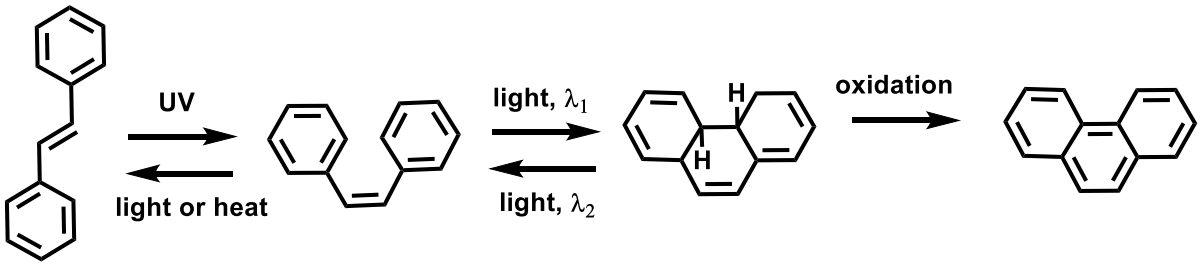

Scheme 1.2.3. Photoswitching behaviour of stilbene.

1.2.4 Diarylethenes

Diarylethenes with heterocyclic aryl groups are a recently developed popular class of P-type photochromic switch. Diarylethene photoswitch can exhibit reversible photocyclization between their unconjugated open-ring isomer (o) and conjugated closed-ring isomer (c) under irradiation using appropriate wavelength (**Scheme 1.2.4**).[9] Dithienylethene molecules in the open form may exist as two conformational isomers, anti-parallel and parallel conformations, The conformers exchange even at room temperatures.

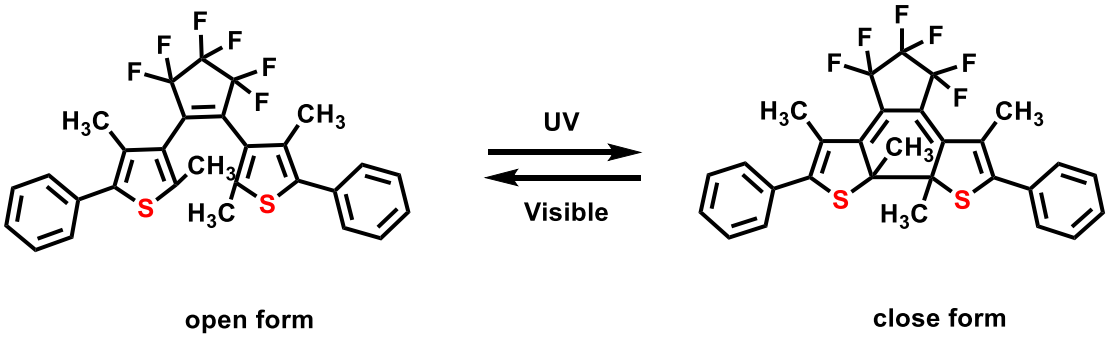

Scheme 1.2.4. Photoswitching behaviour of diarylethene.

The photocyclization reaction can occur only from the anti-parallel conformer upon irradiation with UV light, indicating that the anti-parallel conformation is photoactive, while the parallel conformation is photochemically inactive. Therefore, the quantum yield for the cyclization reaction is dependent on the ratio of these conformations.

1.2.5 Chromenes

Chromenes are photochromic compounds with a benzpyram moiety that can reversibly open its ring (**Scheme 1.2.5**). Becker and co-workers have studied the photochromic behaviour of chromenes.[10] These chromenes show excellent resistance to photodegradation, which is similar to that of spirooxazines.

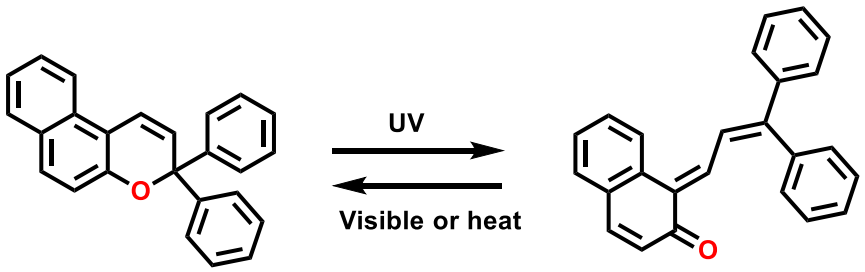

Scheme 1.2.5. Photoswitching behaviour of chromene.

1.2.6 Donor–acceptor Stenhouse adducts (DASAs)

DASAs are new class of visible light driven photoswitches, which consist a donor, acceptor, and triene-enol groups.

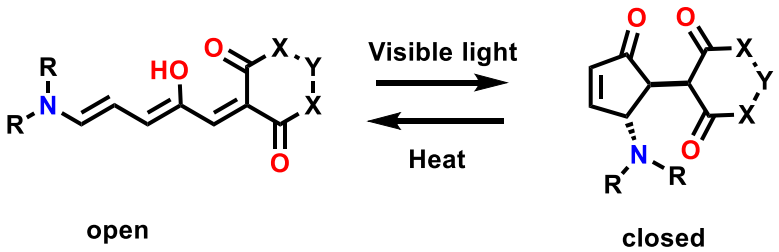

Scheme 1.2.6. Photoswitching behaviour of DASAs.

Upon irradiation, DASAs are isomerized from a strongly absorbed colored form into a colorless (**Scheme 1.2.6**). These switches show interesting negative photochromism and solvatochromism (negative photochromism-isomerization from strongly absorbs colored form to a colorless form, solvatochromism- changing the absorption pattern of a species upon changing the solvents).[11]

Among all photoswitches, azobenzene is one of the widely used photoswitches for numerous applications due to ease of synthesis, functionalization prospects and fatigue resistant photoswitching.

1.3 Azobenzenes

1.3.1 Introduction of azobenzene

Since the discovery (Noble 1856), azobenzenes are undoubtedly mostly used photoswitch due to their easy synthesis, tuneable physical properties, and several insightful photophysical properties.[12] In the beginning of 19th century, azobenzenes were mainly used as dye molecules in texile industries and popularly known as azo dyes. Later, azobenzene derivatives such as prontosil were identified as antibiotics due to the resemblance of their metabolites mimicking *para* aminobenzoic acid, a bacterial metabolite that interfere with the metabolic channel of the microorganism.[13] Apart from that, they played significant role as the pH indicators due to colour changes at different pH.

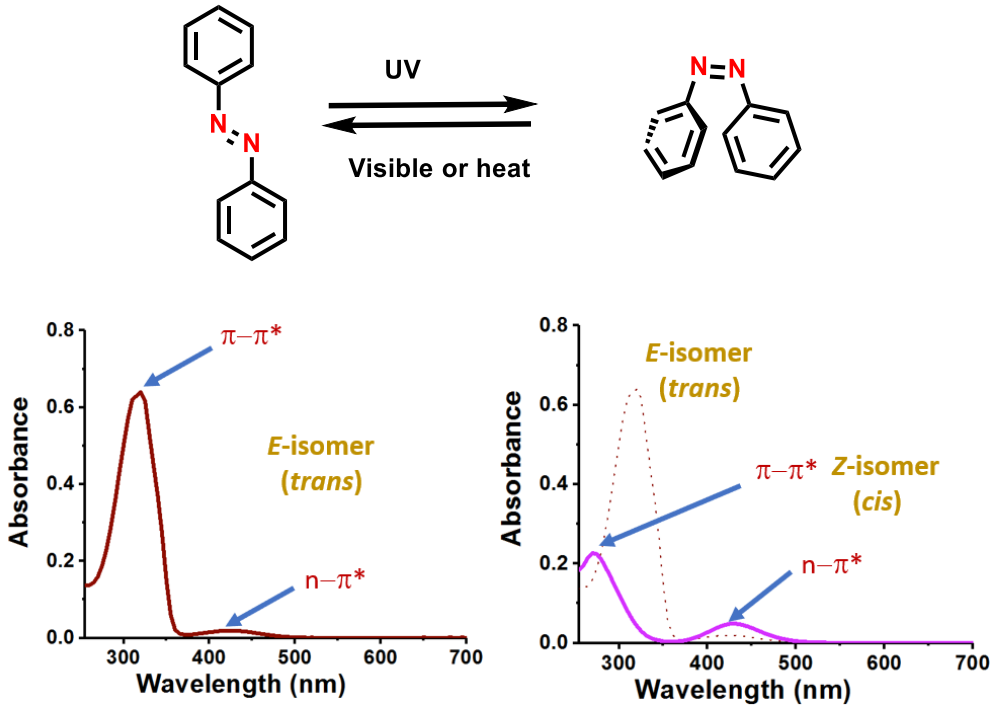

Scheme 1.3.1. Photoswitching behaviour of azobenzene.

Photoisomerization ability of azobenzene has been explored with the discovery of *cis* isomer (*Z*-isomer) in 1937 by Hartley.[14] Furthermore, this delightful journey of photoisomerization of azobenzene has been explored by Fischer, Frenkel, and Wolovsky with introduction of wavelength dependent phtotoisomerization of *trans* (*E*) to *cis* (*Z*) or *cis* to *trans*.[15] Both isomers have different physical properties such as dipole moment, molecular length, melting point, planarity and π-conjugation etc.[16,17] Generally, azobenzenes exhibit two electronic transitions, which are identified in absorption spectra as π–π* and n–π* bands (**Scheme 1.3.1**). The *E*-isomer of azobenzene has planar structure and exhibits a strong π–π* absorption, which is symmetry allowed, and a weak symmetry forbidden n–π* band. Upon *E*-*Z* photoisomerization, the *Z*-isomer exhibits a blue shifted and weak π–π* band, whereas the n–π* band gains enhancement due to vanishing of planarity and symmetry of *Z*-isomer (**Scheme 1.3.1**).

1.3.2 Azoheteroarenes

Although heterocycle-based azoheteroarenes are known for several decades mainly investigated as dyes or drug candidates, recently they devolved into an emerging class of photoswitches. The photoisomerization journey of azoheteroarenes starts from photoisomerization behaviour of 2, 2'-azopyridine studied by Le Favre in 1951.[18] Later, Campbell et al. have explored the symmetrical and unsymmetrical geometrical isomers of azopyridines.[19] Indeed, azopyridines are one of the broadly studied analogues among the various azoheteroarenes. In spite of extensive studies on azopyridine photoswitching, studies on photoisomerization aspects of other heterocyclic analogues were scarce for several decades. The heterocyclic analogues of the azoarenes acquired an important status in recent times. Attempts have been made towards achieving the important goals in improving the photoswitching behaviour, and bringing tunability as well as stability to the azoheteroarenes.[20-26] Prior to this situation, major attention was given to the detailed investigations on the kinetics and mechanistic aspects of azo coupling reactions in the formation of several azoheteroarenes,[27-33] whereas, their photoswitching behavior has been seldom reported. The role of azoheteroarenes with photoswitching applications attained a new era after the reports on photoswitchable contrast agents reported by Herges group.[34] By using nickel porphyrin and the azopyridine, they were able to modulate the magnetic properties by light.[35-37] As an extension, they have also developed a synthetic strategy to access phenylazoimidazole.[20,38] This report kick started the chemistry of azoheteroarene-based photoswitches. Following the footsteps of this work, Fuchter and co-workers further improved

the *Z*-isomer stability by replacing the imidazole with *N*-methylpyrazole unit.[23] In yet another extensive work, they utilized different five-membered heterocyclic based azoheteroarenes and demonstrated that the *N*-methylation is crucial, whereas the *ortho* substitution decreases the stability of *Z*-isomer in azopyrazoles.[23] Quite recently, König and co-workers have developed azoindoles that can be tunable between nanoseconds to days.[22] Apart from the steric and electronic effects through substituents, the hydrogen bonding is equally important in controlling the stability of the *Z*-isomer in arylazopyrazoles.[24] Following the recent trend in visible light-induced molecular photoswitching, Kolarski et al. have synthesized azoheteroarenes based on the purine scaffold for photopharmacological applications.[39] All these results support the possibility of using azoheteroarene as better photoswitches in futuristic applications. Particulalrly, the introduction of five-membered heterocyclic systems such as azothiophene,[40] azoisoxazole,[41] etc. tremendously influenced the *Z*-isomer stability, photoswitching efficiency, and several interesting properties. Now the stage is reached for several novel applications and improvement in the existing systems.

1.4 Classification(s) and types of azoheteroarenes

1.4.1 General Classification

Numerous heterocyclic-based azoarenes available in the literature. Azoheteroarenes classified into the following four different types based on the number and nature of heterocycles (**Scheme 1.4.1**):

A. Class–I (Monoheteroaromatic ring containing azoheteroarenes)

B. Class–II (Bisheteroaromatic rings containing azoheteroarenes)

C. Class–III (Fused heteroaromatic ring(s) containing azoheteroarenes)

D. Class–IV (Partially or fully saturated heterocyclic ring containing/miscellaneous azoheteroarenes)

1.4.1A Class–I Azoheteroarenes

This is the most frequently reported class of azoheteroarenes. Overall, this class of azoheteroarenes contains one heterocyclic ring, which is directly attached to the azo group (**Figure 1.4.1A**). Simple or substituted phenyl group used to be the attachment at the other side of the azo group. This class of azoheteroarenes can be further divided into sub-classes based on the ring size of the heterocycle, and the number of heteroatoms. Monoazoheteroarenes can be divided into two sub-types, based on the ring size, i.e., 5-membered heterocyclic rings and 6-membered heterocyclic rings.

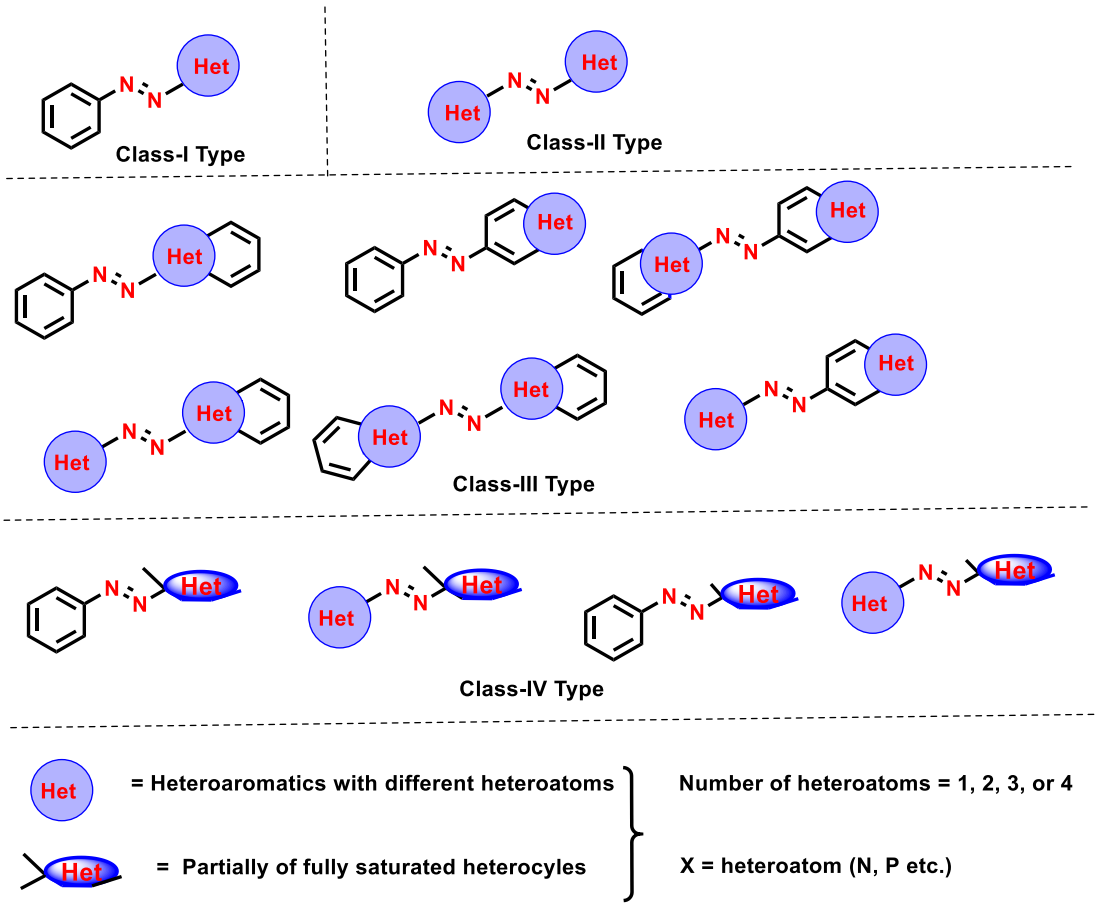

Scheme 1.4.1. General classification of azoheteroarenes.

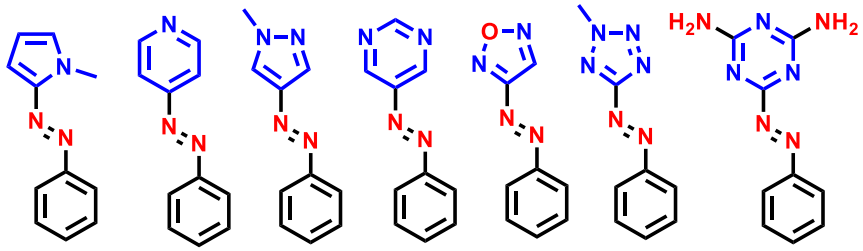

Figure 1.4.1A. Class-I type azoheteroarenes: Examples of five-membered and six-membered monoheterocyclic azoheteroarenes.

Further, these can be classified on the basis of the number of heteroatoms on heterocyclic ring as mono-, di-, tri- and tetra-heteroatom containing rings.

1.4.1B Class–II Azoheteroarenes

The second important class of azoheteroarenes is the one having two heteroaromatics in either side of the azo group (**Figure 1.4.1B**). Indeed, both the heterocycles are directly attached to the azo group. Furthermore, these systems can be either symmetrically or unsymmetrically connected with respect to the azo group. Likewise, in the previous class,

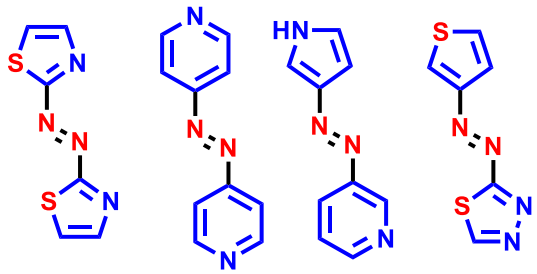

Figure 1.4.1B. Class-II type azoheteroarenes: Examples of symmetrical, unsymmetrical with five-/six-membered and mixed type bis-heterocyclic azoheteroarenes.

these can also be sub-divided based on the size of the ring (5 or 6 members) and the number of heteroatoms.

1.4.1C Class–III Azoheteroarenes

In this class, one or two fused heterocycles will be directly attached to the azo group (**Figure 1.4.1C**). These can once again be symmetrical or unsymmetrical with respect to the azo group. Besides that, the fused heterocyclic unit can be connected either at the heterocyclic part or through the benzene (non-heterocyclic) part. Furthermore, they can be classified as systems with five-membered or six-membered fused heterocyclic rings.

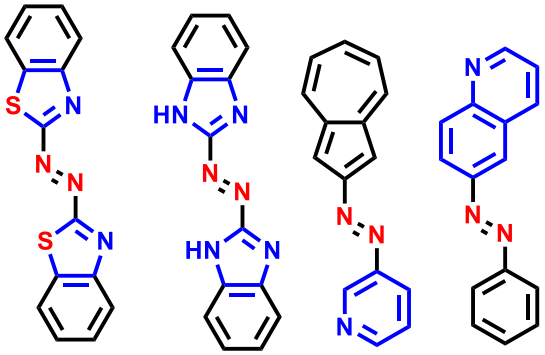

Figure 1.4.1C. Class-III type azoheteroarenes: Examples of symmetrical, unsymmetrical with five-/six-membered and mixed type fused heterocyclic based azoheteroarenes.

1.4.1D Class–IV Azoheteroarenes

In this class, heterocycles with fully or partially saturated rings are connected to the azo group (**Figure 1.4.1D**). More examples are available in which the azo group is connected to the ring nitrogen atom forming a triazene link. Several miscellaneous types of azoheteroarenes, which cannot be classified under other three categories will also be accommodated in this class. But these type azoheteroarene photoswitches also showed photoisomerization with half-lives in minutes to hours.[42]

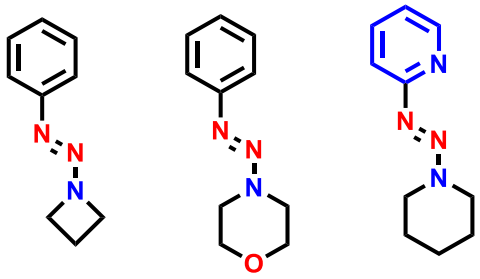

Figure 1.4.1D. Class-IV type azoheteroarenes: Examples of fully or partially saturated heterocyclic based and miscellaneous azoheteroarenes.

1.5 Visible light azo(hetero)arene photoswitches

Typically, azo(hetero)arenes absorbs strongly in the UV region. Hence, most of azo(hetero)arene derivatives exhibit photoisomerization under the irradiation of UV light.[15] High-energy UV light is very harmful for biological window due to the possible tissue damage, high scattering and low tissue penetration. Since the emergence of fields such as photopharmacology, energy storage, etc. demand visible and NIR irradiation, design and synthesis of azo photoswitches capable of isomerizing under such irradiation conditions are increasing. In this regard, various azo photoswitces have been developed for visible light photoswitchable azo(hetero)arenes.

1.5.1A *Ortho*-tetra substituted azobenzenes

Ortho-tetra substituted azobenzenes are important class of visible light photoswitch. In 2011, Woolley and co-workers designed tetra substituted azobenzene with four -OCH_3 groups on the *ortho* positions of the azo unit.[43] Interestingly, their n–π* band in *cis* isomeric state showed a blue shift with respect to their respective *trans* isomer in visible region. This is because of *ortho* methoxy groups destablize the n-orbital of *E*-isomer. The difference between the bands of *cis* and *trans* isomers allowed the photoswitching by green light (530-560 nm) to achieve forward (*E*-*Z*) isomerization; whereas blue light was used to revert (*Z*-*E*) it. Similar to tetra methoxy substituted derivative, *ortho*-tetra thiomethyl substituted azobenzenes also showed bidirectional photoswitching ability under visible light.[44] Later in 2012, Hecht and co-workers devolved *o*-tetra fluoro substituted azobenzene, which showed a similar blue-shift of n–π* in *cis*-isomer compared to the *trans*-isomer.[45] The blue-shift of n–π* in *cis*-isomer is due to all four electron-withdrawing (σ withdrawing) fluorine atoms on *ortho* positions of azo unit could reduce the n-orbital energy of *cis*-isomer.[45]

Similar to fluorine other halogens (chlorine and bromine) also showed bidirectional photoswitching under visible light.[46] In the case of tetra -OCH_3 substituted azobenzene case, the separation between *trans* and *cis* isomers arises from repulsion between n oribital of azobenzene and lone pair of oxygen atoms. On other hand tetra fluoro substituted azobenzene, separation arises due to stabilization of n orbital with electron withdrawing fluorine atom. Recently, Langton and co- workers also demonstrated photoswitching of heavy atoms (Se, Te) substituted azobenzenes with near IR light. However, these systems showed very fast thermal relaxation (**Figure 1.5.1A**).[47]

1.5.1B Bridged azobenzenes

Bridged azobenzenes are special class of azobenzenes, in which the native form is thermally stable *cis* isomer. The photoswitching behaviour of the bridged azobenzene was firstly reported by Herges and co-workers in 2009.[48] In bridged azobenzene, *E*-*Z* photoisomerization happens with green light however *Z*-*E* photoisomerization happens with violet light. Bridged azobenzenes show high quantum and excellent photoisomerization. Later the same group replaced CH_2 unit with other heteroatoms (S, N, and O) in bridged azobenzene. These derivatives show photoisomerization with red to near IR light (**Figure 1.51B**).[44]

1.5.1C BF_2 connected azobenzenes

In 2012, Aprahamian and co-workers developed azophotoswitches by connecting a BF_2 group with the azo nitrogen.[49] Such systems exhibit bidirectional photoswitching in under visible regions. Later by introducing electron donating groups at the *para* position, photoswitching can also be induced with near IR light. However, these derivatives are very sensitive to oxygen and water (**Figure 1.5.1C**).

1.5.1D *Ortho*-aminoazobenzenes

Introducing cyclic aliphatic amines at the *ortho* or *para* position of azobenzene leads to the photoswitching under visible light. Woolley introduced a series of aliphatic cyclic amines connected to azobenzene derivatives (Figure 1.5.1D).[50] As the number of electron-donating groups increase, it led to the shift in absorption band towards the red region. Later, Priimagi and co-workers used a similar approach to introducing visible light photoswitching. Also, to enhance the thermal stability of the *Z*-isomer, they introduced a fluorine atom at the ortho position along with cyclic amines (Figure 1.5.1D).[50] Introducing the electron donating and electron withdrawing at opposite sides at *para* positions also make them to absorb in the visible region.

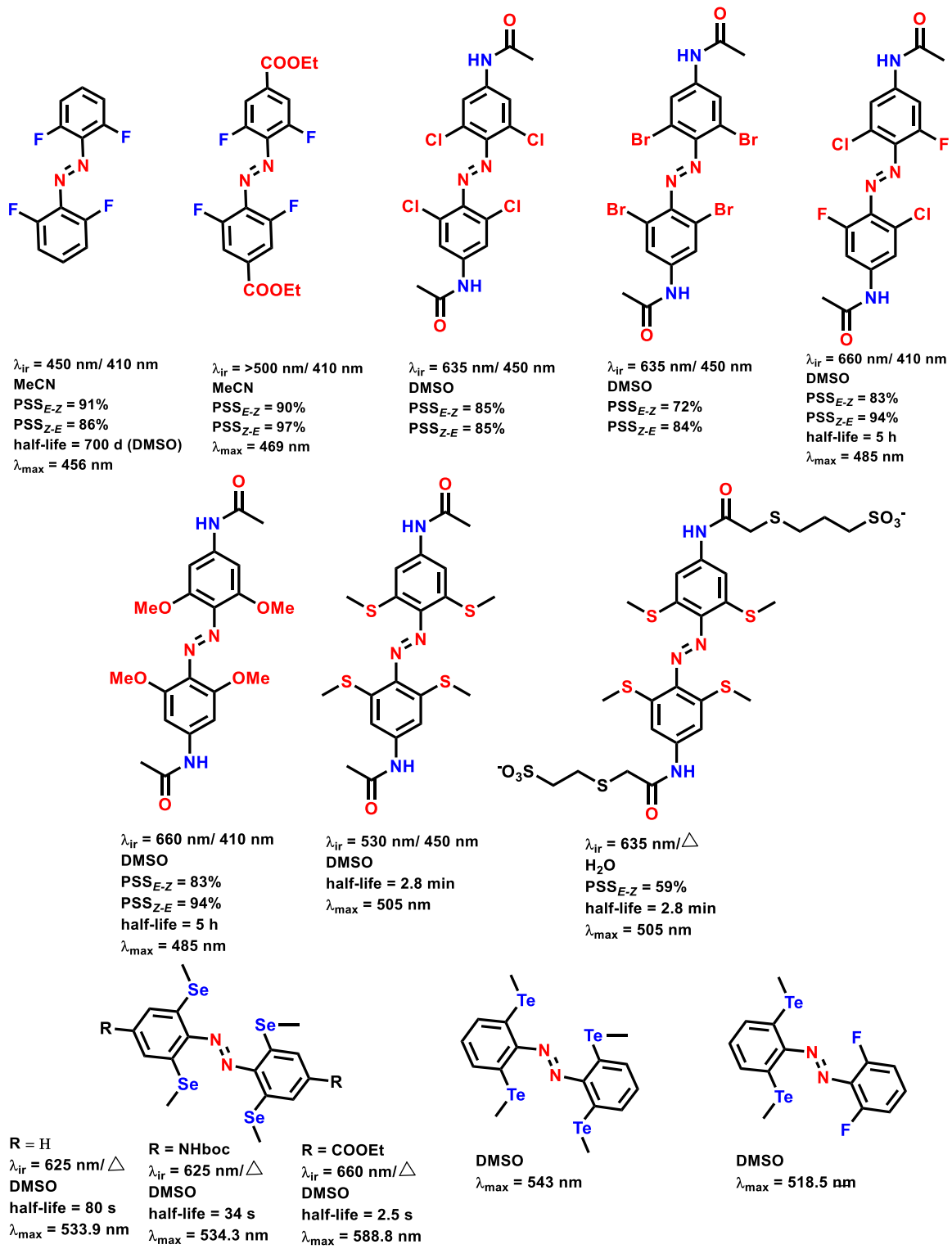

Figure 1.5.1A. Examples of *ortho* tetra substituted azobenzenes.

However, such types of azobenzenes, commonly called as push-pull type photoswitches, exhibit fast thermal relaxation of *Z*-isomers.[51]

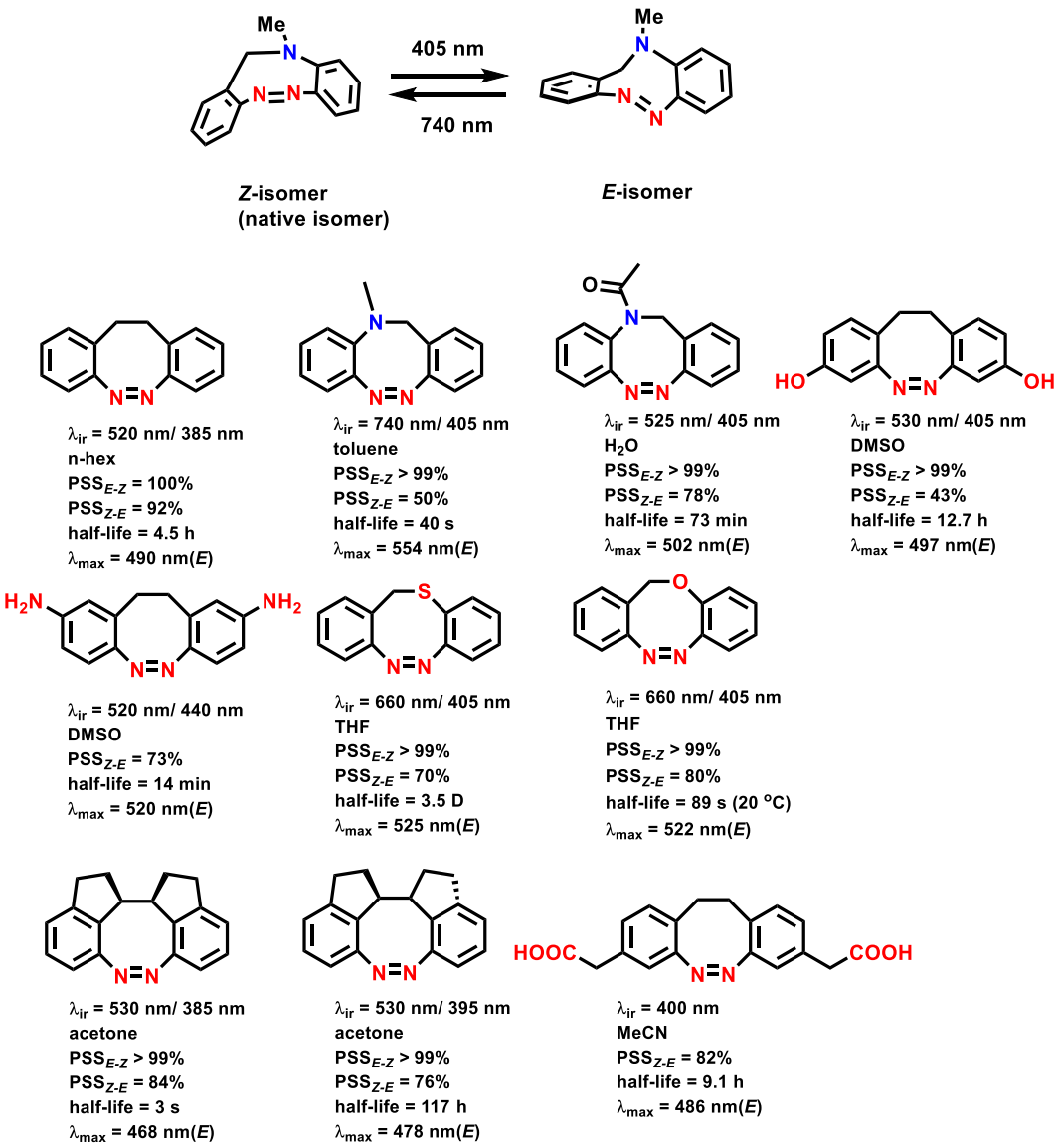

Figure 1.5.1B. Examples of bridged azobenzenes.

1.5.1E Protonated azobenzenes

Nitrogen atom of azogroups can take proton under acidic conditions. Such protonation induces red shift in the absorption spectrum of azobenzene. Particularly, *ortho* methoxy group can form H-bonding with the protonated azo group, as a result, the *Z*-isomer can be stabilized.[52] Similarly, heterocyclic ring at azo group can also make the H-bonding (**Figure 1.5.1E**).[53]

1.5.1F Push Pull azo(hetero)arenes Introducing of electron donating and withdrawing group on the opposite ring of the azobenzene. Generally, push-pull type photoswitches exhibit red shifted absorption band with very fast reverse thermal isomerization (**Figure 1.5.1F**).[54]

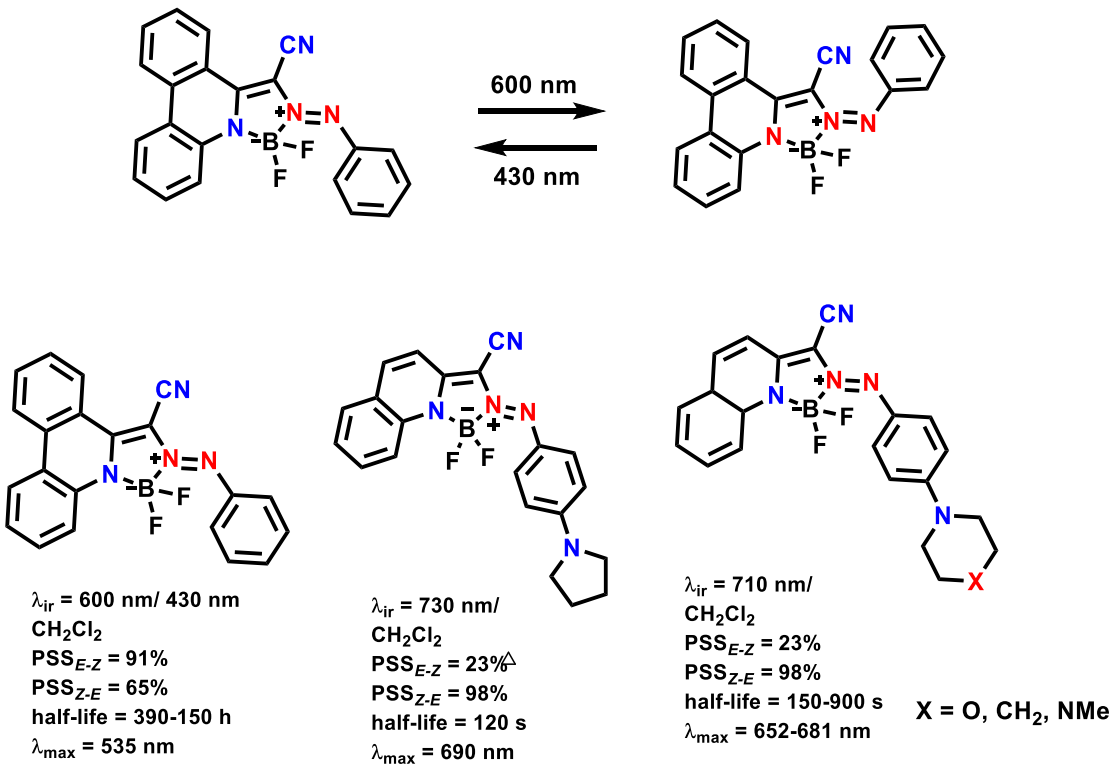

Figure 1.5.1C. Examples of BF_2 connected azobenzenes.

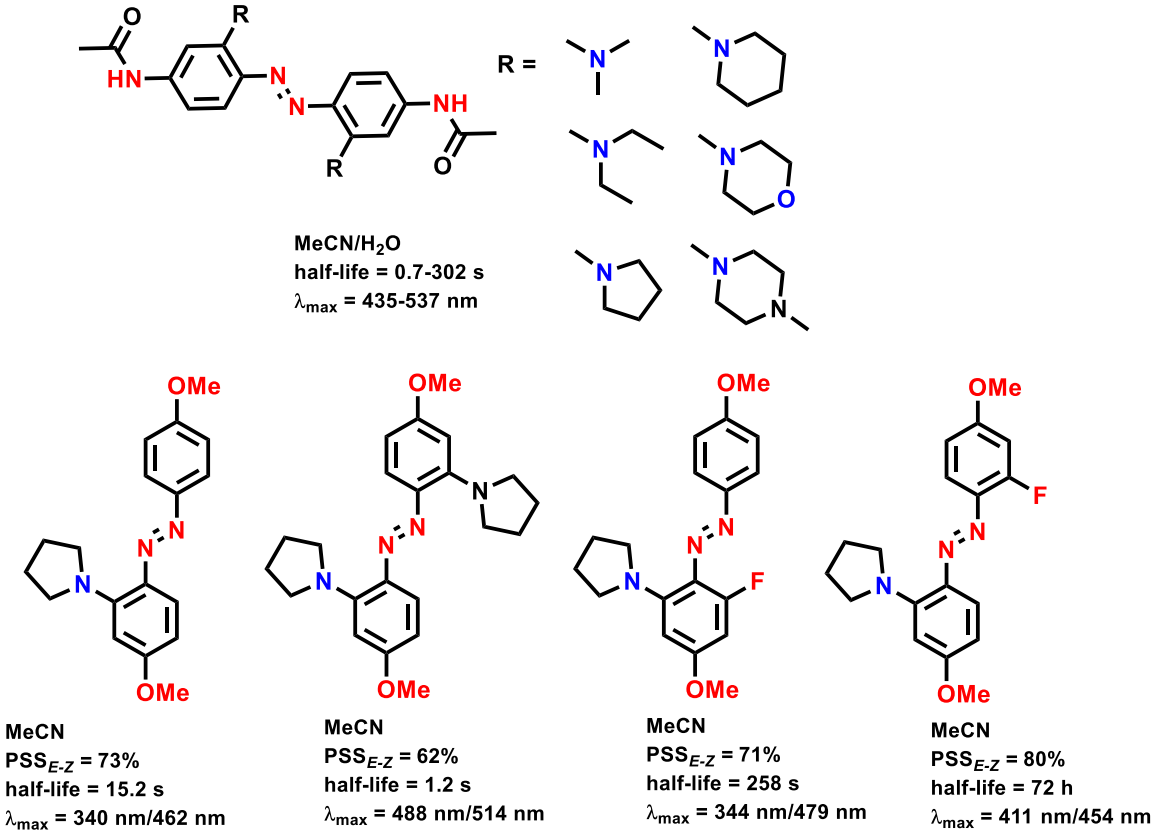

Figure 1.5.1D. Examples of *ortho*-amino azobenzenes.

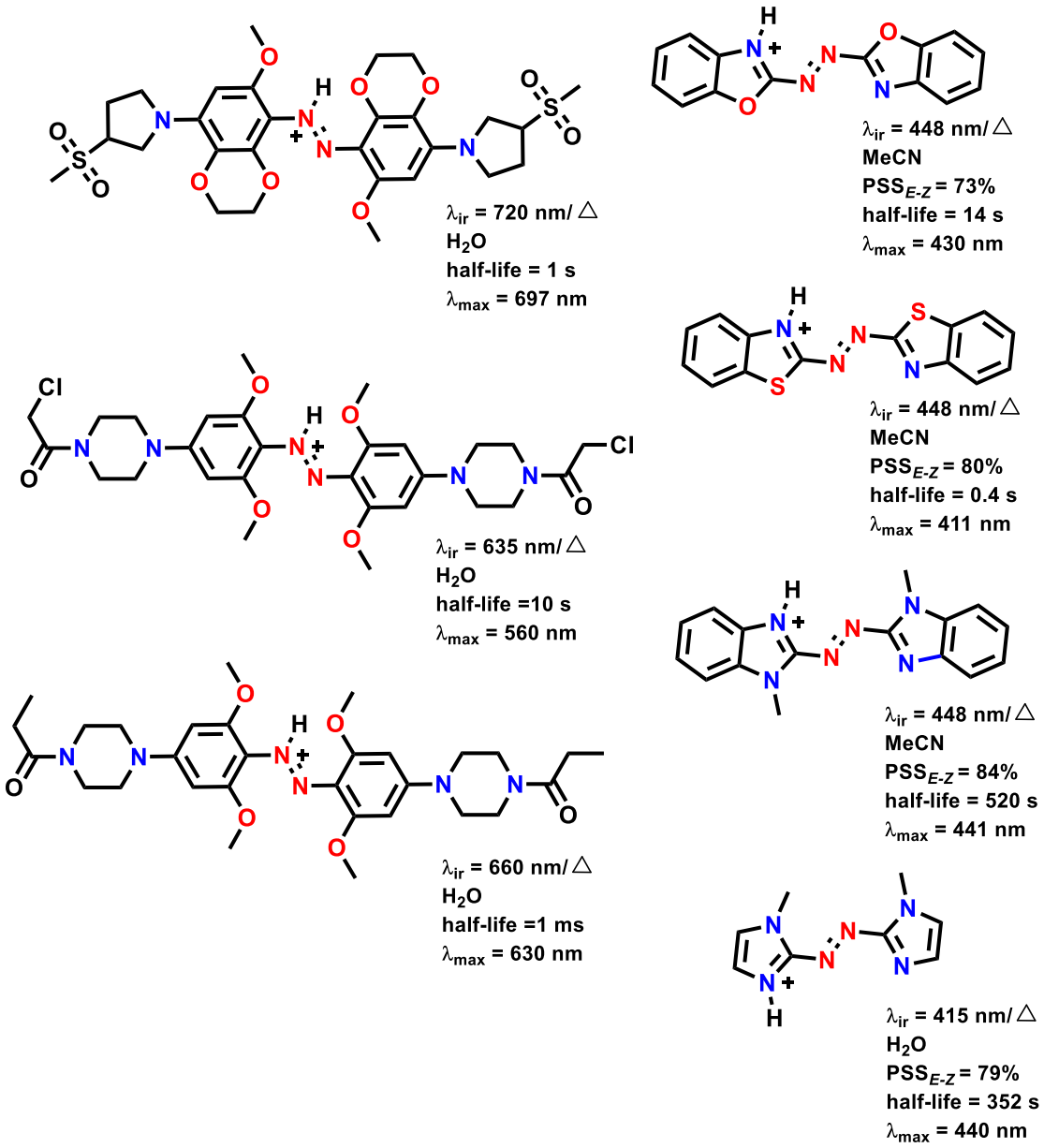

Figure 1.5.1E. Examples of protonated azobenzenes.

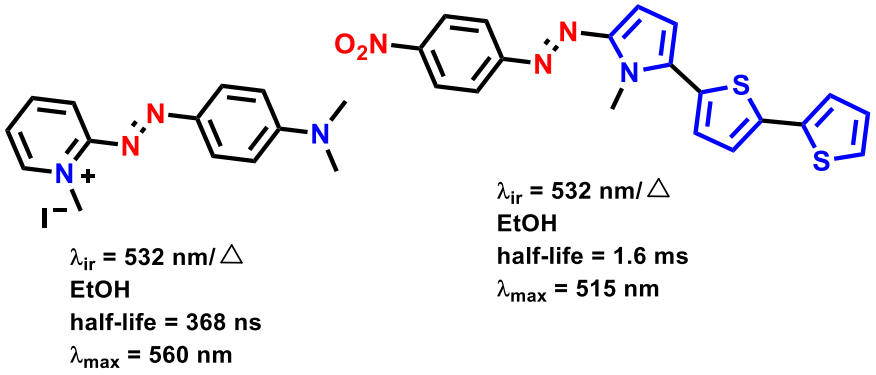

Figure 1.5.1F. Examples of push pull azo(hetero)arenes.

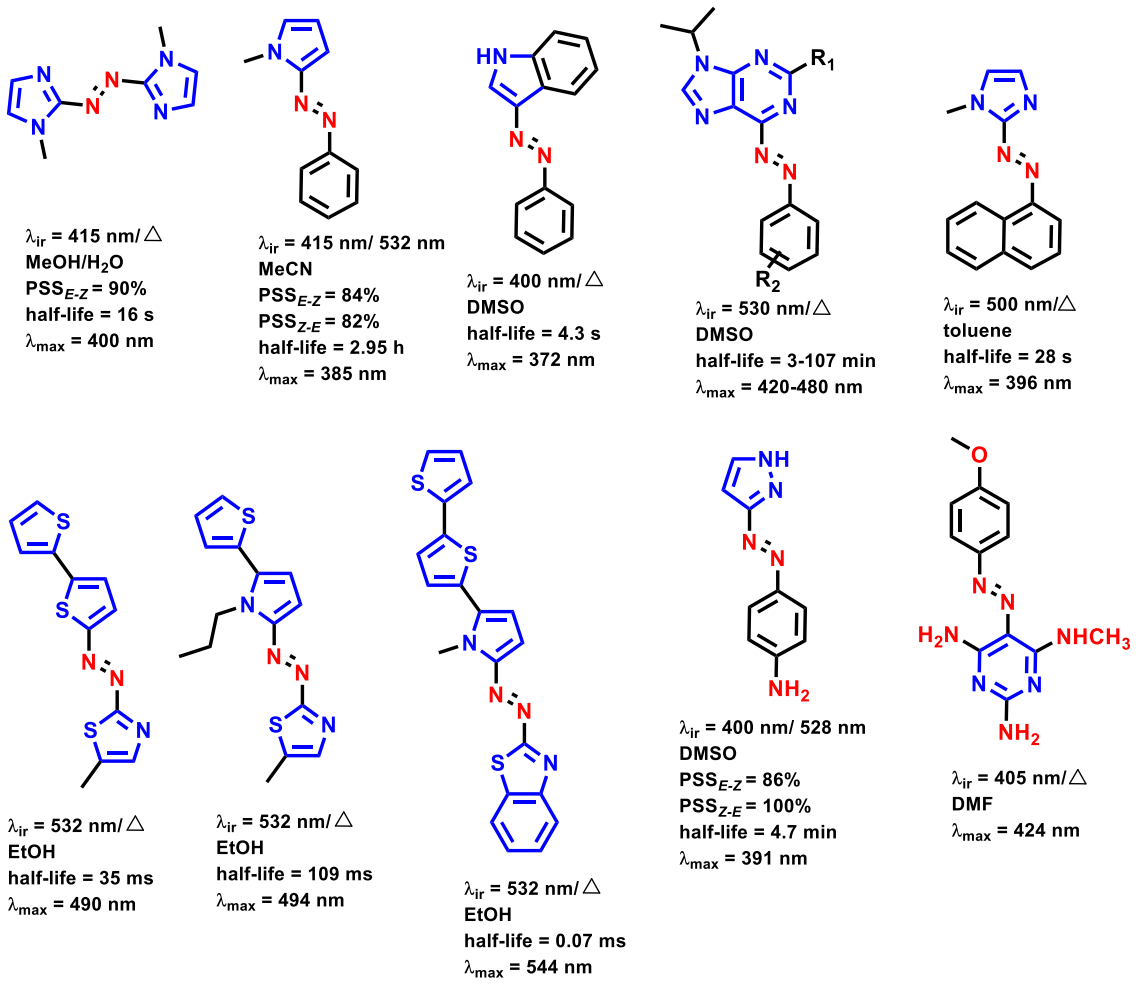

Figure 1.5.1G. Examples of extended π-conjugated and electron rich azo(hetero)arenes.

1.5.1G Extended π-conjugated and electron rich azo(hetero)arenes

Introducing the electron rich ring or extended the conjugation in the azobenzene extend the π-π* band towards red side but decrease the half-life of photoswitches (**Figure 1.5.1G**). [54]

1.6 Azobenzene in aqueous media

Water is one of the crucial components of living beings. Azo photoswitches are lipophilic in nature, so water solubility of azobenzene is very restricted. However, to apply azobenzene switch in biological medium, photoswitching in aqueous medium is essential. There are many general strategies to successfully dissolve azobenzene in water soluble but water can influence the photoswitching efficiency and thermal stability of *Z*-isomer.

1.6.1 General strategies for creating water soluble photoswitches

There are many chemical and physical approaches possible to make water soluble azo photoswitches. The most common method to make the azobenzene water soluble is by

introducing additional ionic or polar units.[55] An alternate possibility is to form the salt of an acid or basic functional groups attached to azobenzene moiety.[56] Interestingly, *Z*-isomer of azobenzene is more polar than its *E*-isomer, which results in increased hydrophilicity.[57] Besides chemical strategies, there are various physical methods also offered to enhance the water solubility like addition of co-solvents, building up of hydrotropes, reducing particle size, and different delivery systems, such as liposomes, micelles, molecular containers, etc.[58] Some of those approaches are discussed in this section with examples.

1.6.2 Solubilizing groups

Introducing solubilizing and polar functional groups, such as amides, carboxylic acids, PEG, etc in azoheteroarene photoswitches can increase the hydrophilicity. Furthermore, solubilizing groups can be categorized into two, namely charged (ionic) and non-ionic groups (**Figure 1.6.2**).

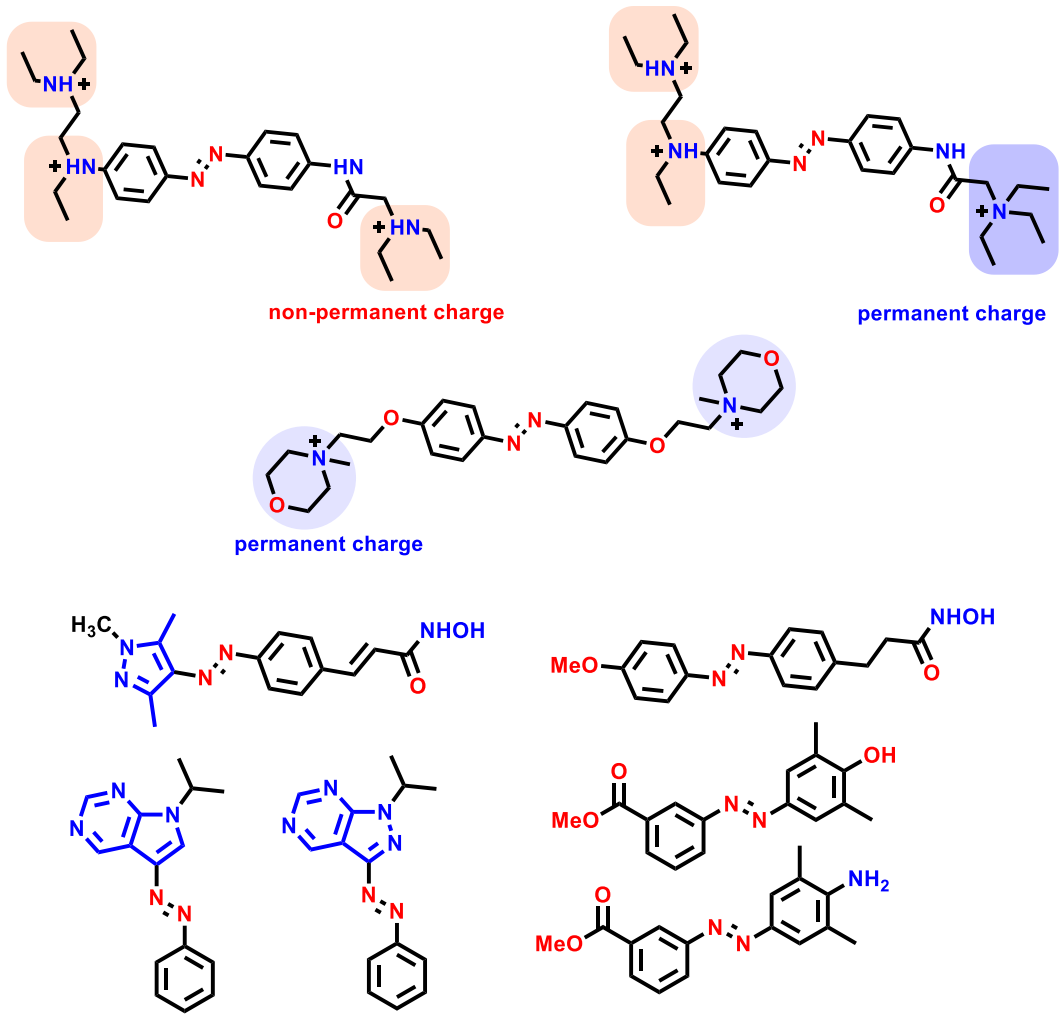

Figure 1.6.2. Selected examples of ionic, and non-ionic approaches for making water soluble azo(hetero)arenes.

1.6.2A Charged or ionic groups

Phosphates, phosphonate, sulfonates, and ammonium are some of the common water-soluble groups.[55] Apart from the choice of cation part of charged groups, the counter anion parts are also crucial for water solubility. Amine group also can be protonated to form ammonium salts under physiological conditions to make them water soluble.[55] However ionic derivative limited the photoswitching effeciecny as well as led to faster *Z-E* thermal isomerization.

1.6.2B Non-ionic groups

Electronegative atoms such as oxygen or nitrogen can increase the dipole moment of the derivative and also interact with water through H-bonding. So, introducing more heteroatoms in azobenzene moieties can also enhance the water solubility. Apart from introducing heteroatoms, various non-ionic groups such as polyethyl glycol (PEG) or oxetanyl sulfoxide groups can also enhance the water solubility.[56]

1.6.3 Salt-formation

Incorporating groups capable forming salts of acidic or basic functional group can also increase the water solubility (**Figure 1.6.3**).[55c]

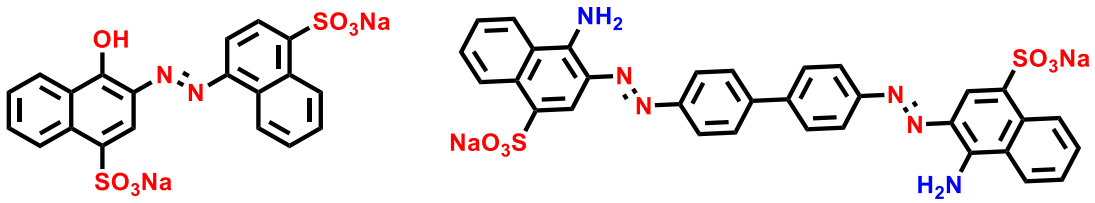

Figure 1.6.3. Selected examples of azo(hetero)arene salts.

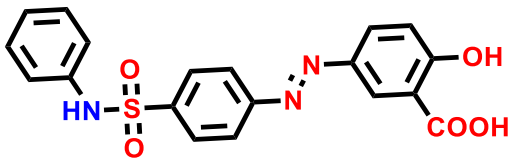

Figure 1.6.4. Selected example of unsymmetrical azo(hetero)arene.

1.6.2A Charged or ionic groups

Phosphates, phosphonate, sulfonates, and ammonium are some of the common water-soluble groups.[55] Apart from the choice of cation part of charged groups, the counter anion

parts are also crucial for water solubility. Amine group also can be protonated to form ammonium salts under physiological conditions to make them water soluble.[55]

1.6.4 Disruption of planarity and symmetry

In general, non-planar molecules makes it more difficult for them to assemble within the crystal lattice and thus disrupting planarity lowers the melting point and results in improved water-solubility. This phenomenon was employed in the design of different systems, where the loss of aromaticity, introduction of a twisted ring or the increase of a dihedral angle of the biaryl systems for increasing the water solubility (**Figure 1.6.4**).[59]

1.6.5 Physical methods

Next to chemical modifications, various physical methods can also be utilized to enhance the water solubility. One simple method is the addition of different water-soluble co-solvents such as DMSO, methanol, acetonitrile, propylene glycol, glycerin, ethanol, etc. The opposite effect, namely ‘‘salting in’’, can be achieved by addition of so-called hydrotropes. Hydrotropes are ionic organic salts, which are added to a poorly water-soluble compound to increase its aqueous solubility in diverse ways, for instance, by forming micellar-like structures. Other physical solubilization methods include, particle size reduction by mechanical micronization[60] to increase the surface of the compound, nanoionisation,[60] dispersion in carriers, such as micelles, or complexation in molecular containers such as cyclodextrins, octa acids, palladium cages.[58]

1.7 Solid state photochromism in azobenzene

Photoswitching in solid-state or bulk is useful for various applications such as energy storage, photomagnetic switching, actuators, litography, photomechanical bending of metal complexes, etc.[61] However, photoswitching in bulk or solid-state is restricted in azobenzene photoswitches compared to those processes in solution phase. This is mainly due to close packing structure of the photoswitch, which is absent in solution state. Compared to other photoswitches like diarylethene, and spiropyran, azobenzenes require more volume for *E-Z* isomerization, which hinders the solid-state photoswitching. In order to overcome such limitations, azobenzene requires the introduction of bulky groups at phenyl ring (**Figure 1.7**). Such approaches can enhance the volume by reducing close packing.[62] In addition, these bulky groups break the planarity in azobenzene and induce effective photoswitching. The alternative approach is incorporation of small photoswitches in three-dimensional geometry possessing minimal or weaker intermolecular interactions.[61]

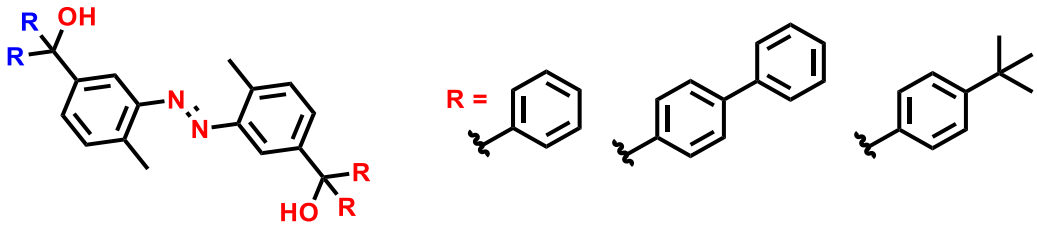

Figure 1.7. Examples of bulky azobenzenes suitable for solid-state photoswitching.

1.8 Motivation and research objectives

Although azobenzene is one of the classical photoswitches, the recent introduction of azoheteroarenes, and their applications in material and biological fields made them more versatile and robust candidates. However, they have some limitations such as the need of UV light for photoisomerization, limition in the solubility particularly in aqueous medium, and poor photoswithcing in bulk state. The motivation of this thesis is to address these short comings of azobenzene and to make azoheteroarenes to undergo photoisomerization under visible light irradiation, and to generate derivatives to exhibit photoswitching in water and solid-state. The second chapter is devoted to design and development of new visible light photoswitchable azoheteroarenes comprising cyclic amines at *ortho* position to the azo group of various azoheteroarenes. The next chapter is mainly focused on the development of new water soluble azoheteroarenes photoswitches with bidirectional photoswitching and *Z*-isomer stability by making them ionic compounds. In the fourth chapter, designing multi azo(hetero)arene-based molecular systems were generated towards making them photochromic in solution and bulk state. This is followed by a chapter on conclusions and perspectives. A dedicated chapter on materials and methods used in the thesis work are presented in chapter six.

1.9 References

1. (a) Hirshberg, Y. *Compt. Rend. Acad. Sci.* **1950**, Paris, *231*, 903; b) Bouas-Laurent, H.; Dürr, H. *Pure Appl. Chem.* **2001**, *73*, 639–665.
2. Fritzsche, J. *Compt. Rend. Acad. Sci.* **1867**, Paris, *69*, 1035.
3. ter Meer, E. *Ann. Chem.* **1876**, *181*, 1.
4. (a) Phipson, T. L. *Chem. News.* **1881**, *43*, 283. (b) Orr, J. B. *Chem. News*. **1881**, *44*, 12.
5. Zhang, J.; Tian, H. Photochromic materials: Preparation, properties and applications. Weinhein: *Wiley-VCH Verlag*, **2016**.
6. (a) Schaudel, B.; Guermeur, C.; Sanchez, C.; Nakatani, K.; Delaire, J.A. *J. Mater. Chem.* **1997**, *7*, 61-65; (b) Koelsch, C. F.; Workman, W. R.; *J. Am. Chem. Soc.* **1952**, *74*, 24, 6288–6289.

7. (a) Cordes, T.; Herzog, T. T.; Malkmus, S.; Draxler, S.; Brust, T.; Digirolamo, J. A.; Lees, W. J.; Braun, M. *Photochem. Photobiol. Sci.* **2009**, *8*, 4, 528; (b)Yokoyama, Y. *Chem. Rev.* **2000**, *100*, 5, 1717–1740.
8. Han, W. G.; Lovell, T.; Liu, T. Q.; Noodleman, L. *ChemPhysChem.* **2002**, *3*, 167.
9. Irie, M. *Chem. Rev.* **2000**, *100*, 1685−1716.
10. Ahmed, S. A.; Tanaka, M.; Ando, H.; Iwamoto, H.; Kimura, K. *Eur. J. Org. Chem.* **2003**, *13*, 2437–2442.
11. (a) Sroda, M. M.; Stricker, F.; Peterson, J. A.; Bernal, A.; Alaniz, J. R. de. *Chem. Eur. J.* **2021**, *27*, 4183-4190; (b) Lerch, M. M.; Hansen, M. J.; Velema, W. A.; Szymanski, W.; Feringa, B. L. *Nat. Commun.* **2016**, *7*, 1-10.
12. Noble, A. *Justus Liebigs Ann. Chem.* **1856**, *98*, 253.
13. Finch, R. G.; Greenwod, D.; Whitley, R. J.; Norrby, S. R. *Antibiotic and Chemotherapy-9th Edition*; 9th ed. *Saunders Elsevier*, **2011**.
14. Hartley, G. S. *Nature*. **1937**, *140*, 281.
15. Fischer, E.; Frankel, M.; Wolovsky, R. *J. Chem. Phys.* **1955**, *23*, 1367- 1367.
16. Hamon, F.; Djedaini F. P.; Barbot, F.; Len, C. *Tetrahedron*, **2009**, *65*, 10105-10123.
17. Merino, E.; Ribagorda, M. *Beilstein J. Org. Chem*. **2012**, *8*, 1071-1090.
18. Le Fèvre, R. J. W.; Worth, C. V. *J. Chem. Soc.* **1951**, 1814-1817.
19. Campbell, N.; Henderson, A. W.; Taylor, D. *J. Chem. Soc.* **1953**, 1281-1285.
20. Wendler, T.; Schütt, C.; Näther, C.; Herges, R. *J. Org. Chem.* **2012**, *77*, 3284-3287.
21. Weston, C. E.; Richardson, R. D.; Haycock, P. R.; White, A. J. P.; Fuchter, M. J. *J. Am. Chem. Soc.* **2014**, *136*, 11878-11881.
22. Simeth, N. A.; Crespi, S.; Fagnoni, M.; König, B. *J. Am. Chem. Soc.* **2018,** *140*, 2940-2946.
23. Calbo, J.; Weston, C. E.; White, A. J. P.; Rzepa, H. S.; Contreras-García, J.; Fuchter, M. J. *J. Am. Chem. Soc.* **2017**, *139*, 1261-1274.
24. Devi, S.; Saraswat, M.; Grewal, S.; Venkataramani, S. *J. Org. Chem.* **2018**, *83*, 4307-4322.
25. Stricker, L.; Böckmann, M.; Kirse, T. M.; Doltsinis, N. L.; Ravoo, B. J. *Chem. Eur. J.* **2018**, 24, 8639-8647.
26. Xu, Y.; Gao, C.; Andréasson, J.; Grøtli, M. *Org. Lett. 2018*, 20, 4875-4879.
27. Diener, H.; Zollinger, H. *Can. J. Chem.* **1986**, *64*, 1102-1107.
28. Diener, H.; Güleç, B.; Skrabal, P.; Zollinger, H. *Helv. Chim. Acta* **1989**, *72*, 800-805.
29. Diener, H.; Güleç, B.; Skrabal, P.; Zollinger, H. *Helv. Chim. Acta.* **1989**, *72*, 800-805.
30. Brown, R. D.; Duffin, H. C.; Maynard, J. C.; Ridd, J. H. *J. Chem. Soc.* **1953**, 3937-3939.
31. Macháčeka, V; Kořínek, J; Kreuzigováb, D; Štěrbaa, V. *Collect. Czech. Chem. Commun.* **1985**, *50*, 658-674.
32. Butler, A. R.; Pogorzelec, P.; Shepherd, P. T. *J. Chem. Soc., Perkin Trans. 2* **1977**, 1452-1457.
33. Anderson, L. M.; Butler, A. R.; Glidewell, C.; Hart, D.; Isaacs, N. *J. Chem. Soc., Perkin Trans. 2* **1989**, 2055-2058.
34. Dommaschk, M.; Peters, M.; Gutzeit, F.; Schütt, C.; Näther, C.; Sönnichsen, F. D.; Tiwari, S.; Riedel, C.; Boretius, S.; Herges, R. *J. Am. Chem. Soc.* **2015**, *137*, 7552-7555.
35. Venkataramani, S.; Jana, U.; Dommaschk, M.; Sönnichsen, F. D.; Tuczek, F.; Herges, R. *Science* **2011**, *331*, 445-448.
36. Herges, R. *Nachrichten aus der Chemie [News from the Chemistry]* **2011**, *59*, 817-821.

37. Dommaschk, M.; Schütt, C.; Venkataramani, S.; Jana, U.; Näther, C.; Sönnichsen, F. D.; Herges, R. *Dalton Trans.* **2014**, *43*, 17395-17405.
38. Heitmann, G.; Schütt, C.; Herges, R. *Eur. J. Org. Chem.* **2016**, *2016*, 3817-3823.
39. Kolarski, D.; Szymanski, W.; Feringa, B. L. *Org. Lett.* **2017**, *19*, 5090-5093.
40. Slavov, C.; Yang, C.; Heindl, A. H.; Wegner, H. A.; Dreuw, A.; Wachtveitl, J. *Angew. Chem. Int. Ed.* **2020**, *59*, 380-387.
41. Kumar, P.; Srivastava, A.; Sah, C.; Devi, S.; Venkataramani, S. *Chem. Eur. J.*, **2019**, *25*, 11924–11932.
42. Beharry, A. A.; Sadovski, O.; Woolley, G. A. *J. Am. Chem. Soc.* **2011**, *133*, 19684-19687.
43. Samanta, S.; McCormick, T. M.; Schmidt, S. K.; Seferos, D. S.; Woolley, G. A. *Chem. Commun.* **2013**, *49* 10314–10316.
44. Bléger, D.; Schwarz, J.; Brouwer, A. M.; Hecth, S. *J. Am. Chem. Soc.* **2012**, *134*, 20597-20600.
45. Konrad, D. B.; Savasci, G.; Allmendinger, L.; Trauner, D.; Ochsenfeld, C.; Ali, A. M. *J. Am. Chem. Soc.* **2020**, *142*, 6538–6547.
46. Siewertsen, R.; Neumann, H.; Buchheim-Stehn, B.; Herges, R.; Nätheret, C.; Renth, F.; Temps, F. *J. Am. Chem. Soc.* **2009**, *131*, 15594–15595.
47. Kerckhoffs, A.; Christensena, K. E; Langton, M. J. *Chem. Sci.* **2022**, 13, 11551-11559.
48. M. Hammerich, C. Schütt, C. Stähler; Lentes P.; Röhricht, F.; Höppner, R.; Herges, R. *J. Am. Chem. Soc.* **2016**, *138*, 13111-13114.
49. Yang, Y.; Hughes, R. P.; Aprahamian, I. *J. Am. Chem. Soc.* **2012**, *134*, 15221–15224.
50. (a) Sadovski, O.; Beharry, A. A.; Zhang, F.; Woolley, G. A. *Angew. Chem. Int. Ed.* 2009, *48*, 1484-1486; (b) Ahmed, Z.; Siiskonen, A.; Virkki, M.; Priimagi, A. *Chem. Commun.* **2017**, *53*, 12520-12523.
51. Dong, M.; Babalhavaeji, A.; Samanta, S.; Beharry, A. A.; Woolley, G. A. *Acc. Chem. Res.* **2015**, *48*, 2662-2670.
52. (a) Samanta, S.; Babalhavaeji, A.; Dong, M. X.; Woolley, G. A. *Angew. Chem. Int. Ed.* **2013**, *52*, 14127–14130; (b) Dong, M.; Babalhavaeji, A.; Collins, C. V.; Jarrah, K.; Sadovski, O.; Dai, Q.; Woolley, G. A. *J. Am. Chem. Soc.* **2017**, *139*, 13483-13486.
53. (a) Weston, C. E.; Richardson, R. D.; Fuchter, M. J. *Chem. Commun.* 2016, 52, 4521-4524; (b) Kennedy, A. D. W.; Sandler, I.; Andréasson, Ho, J.; Beves, J. E. *Chem. Eur. J.* **2020**, *26*, 1103-1110.
54. (a) Bandara, H. M. D.; Burdette, S. C. *Chem. Soc. Rev.* **2012**, 41, 1809.; (b) Chen, H.; Chen, W.; Lin, Y.; Xie, Y.; Sheng, H. L.; Yin, J. *Chin. Chem. Lett.* **2021**, 32, 8, 2359-2368.
55. Merino, E.; R. María. *Beilstein J. Org. Chem.* **2012**, *8*, 1071–1090.
56. (a) Volarić, J.; Szymanski, W.; Simeth, N. A.; Feringa, B. L. *Chem. Soc. Rev.* **2021**, *50*, 12377-12449.; (b) Samanta, D.; Gemen, J.; Chu, Z.; Posner, Y. D.; Shimon, L. J. W.; Klajn, R. *PNAS.* **2018**, *115*, 38, 9379-9384.; (b) Pesce, Luca.; Perego, C.; Grommet, A. B.; Klajn, R.; Pavan, G. M. *J. Am. Chem. Soc.* **2020**, *142*, 21, 9792–9802.; (c) Moscosoa, A. D.; Ballester, P. *Chem. Commun.* **2017**, *53*, 4635-4652. (d) Otolski C. J.; Raj, A. M.; Ramamurthy, V.; Elles, C. G. *J. Phys. Chem. Lett.* **2019**, *10*, 1, 121–127.; (e) Raj A. M.; Ramamurthy, V. *Org. Lett.* **2017**, *19*, 22, 6116–6119.; (f) Otolski C. J.; Raj, A. M.; Ramamurthy, V.; Elles, C. G. *Chem. Sci.* **2020**, *11*, 9513-9523.
57. (a) Hüll, K.; Benster, T.; Manookin, M. B.; Trauner, D.; Van Gelder, R. N.; Laprell, L. *Sci. Rep.* **2019**,*9* ,1-12; (b) O'Hagan, M. P.; Haldar, S.; Duchi, M.; Oliver, T. A. A.; Mulholland, A. J.; Morales, J. C.; Galan, M. C. *Angew. Chem., Int. Ed.* **2019**, *58*, 4334-

4338; (c) Ojala, W. H.; Ojala, C. R.; Gleason, W. B.; *Antivir. Chem. Chemother.* **1995**, *6*, 25-33; (d) Barber, D. M.; Liu, S. A.; Gottschling, K.; Sumser, M.; Hollmann, M.; Trauner, D. *Chem. Sci.* **2016**, *8*, 611-615.
58. (a) Weston, C. E.; Krämer, A.; Colin, F.; Yildiz, Ö.; Baud, M. G. J.; Meyer-Almes, F. J.; Fuchter, M. J. *ACS Infect. Dis.* **2017**, *3*, 152-161; (b) Ferreira, R.; Nilsson, J. R.; Solano, C.; Andréasson, J.; Grøtli, M. *Sci. Rep.* **2015**, *5*, 9769; (c) Blevins, A. A.; Blanchard, G. J. *J. Phys. Chem. B.* **2004**, *108*, 4962-4968.
59. Merlo, E.; Freudenthal, R.; Romano, A.; Neuroscience. **2002**, *112*, 161-172.
60. Khadka, P.; Ro, J.; Kim, H.; Kim, I.; Kim, J. T.; Kim, H.; Cho, J. M.; Yun, G.; Lee, J. *Asian J. Pharm. Sci.* **2014**, *9*, 304-316.
61. Da Silva, F. L. O.; Marques, M. B. D. F.; Kato, K. C.; Carneiro, G. *Expert Opin. Drug Discovery*. **2020**, *15*, 853-864.
62. Gonzalez, A.; Kengmana, E. S.; Fonseca, M. V.; Han, G. G. D. *Mater. Today Adv.* **2020**, *6*, 100058.

Chapter 2. Visible light azoheteroarenes photoswitches

2.1 Introduction

Molecular photoswitch such as azobenzene can toggle between two geometrical isomer planar *E*- (*trans*) and non-planar *Z*- (*cis*) isomers by light. These two isomeric forms show different physical properties such as melting point, planarity, dipole moments, etc. The changes in the properties associated with them and their utility in controlling certain functions through isomerization led to several applications.[1] Indeed, the chemistry of azobenzenes has attained a new status in recent times. This is mainly attributed to the development of systems where one of the benzene rings has been replaced, in particular, with five-membered heterocycles. The resulting azoheteroarenes are one of the increasingly popular classes of photoswitches.[1c,d] Salient features such as improved light induced photoswitching ability, exceptional half-life of photoswitched states, tunability of the thermal stability, cost-effective synthesis, and versatility as well as excellent bidirectional photoswitching properties play a significant role in the choice of such photoswitches. Such azoheteroarenes impart intriguing properties such as photochromism, light-induced phase transition, etc., whereas diverse functionalization enables them to exhibit widespread application prospects such as in catalysis, molecular adhesives, etc.[2] Moreover, the presence of heterocycles stimulates significant interest in azoheteroarenes in the field of medicinal chemistry. Despite a long history of exploring them as drug candidates, the photoisomerization allowed remarkable advancements in recent times.[2e,3] Indeed, the light control of the pharma can be a unique handle in modulating the therapeutic effects. Such pharma can be propitious if the conditions allow photoswitching in the bio-optical window. Similarly, in yet another domain of developing energy storage molecular materials, photoswitches can be advantageous.[2h] Particularly, charging (accessing high energy state through forward *E*-*Z* isomerization) and release (through thermal *Z*-*E* isomerization) demand high thermal stability of the *Z*-isomer. Such requirements in combination with photoswitching under visible light irradiation can be extremely useful for several futuristic applications. Various approaches[4a] such as diazocines (Herges),[4b] tetra *ortho* substitutions with fluorination (Hecht),[5] alkoxy and *S*-ethyl (Woolley),[6,7] cyclic amine connections (Woolley and Priimagi),[8] push-pull type connections (Woolley and Velasco),[9] azo-BF_2 bridging (Aprahamian),[10] etc. have been successfully employed in bringing longer wavelength (visible and NIR) photoswitchable azoarenes. In addition, extended conjugation and protonation have also been attempted.[11] Mostly, the *ortho* substituents, in particular electron-donating groups, lead to an enhanced n–π* band in

azoarenes,[8a] whereas the substituents at the para positions can be used to tune longer wavelength absorptions.[12] The π–π* and n–π* bands are generally blue-shifted and well-separated in five-membered heterocycle-based azoheteroarenes.[2f,13] Furthermore, the heterocycles, interactions in the transition state and *Z*-isomers, substituent effects, and H-bonding typically influence the halflives of the *Z*-isomer.[13] Recently, visible light photoswitching has been enabled in azopyrazoles using *S*-methyl (Samanta) and cyclic amine (Ravoo) connections at the *ortho* position to the azo group and employing symmetric benzazoles (Beves).[11d,14,15] Motivated by the high demands and limited explorations, we decided to utilize a modular strategy to access azoheteroarenes capable of visible light photoswitching (**Scheme 2.1**). Since it is well known that *ortho* fluorination stabilizes the *Z*-isomer[5a] and *ortho* amination induces enhancement in the n–π* and imparts longer wavelength absorption,[8a] we included them in the design strategies. Besides that, the heterocycles such as isoxazoles (**H1** and **H4**),[2f] *N*-methylpyrazoles (**H2** and **H5**),[2a,13] and *N*-methylpyrroles (**H3**)[13a] have been considered due to their excellent photoswitching with variable *Z*-isomer stability. To bring further variation, we have synthesized 3,5- dimethyl or diphenyl substitutions at the isoxazole and pyrazole units. By varying substitution patterns, we have designed three different classes of azoheteroarenes, namely, (a) **Type A** (with *ortho* amination), (b) **Type B** (the combination of fluorine and amine connections at 2,6-positions), and (c) **Type C** (bis-amination at 2,6- or 2,4-positions). Such variations in the design have been engendered to gain insights into the structure−property relationship toward bidirectional photoswitching and the half-lives of the *Z*-isomers. Herein, we report the synthesis of 22 azoheteroarenes, their photoisomerization, kinetics studies, and the structure-property relationship.

2.2 Synthesis

To access these targets, various mono- and difluorinated azoheteroarenes have been synthesized. To synthesize mono- and difluorinated azopyrazoles and azoisoxazoles, the corresponding anilines have been diazotized and derivatized with the acetylacetone or 1,3-diphenylpropane-1,3-dione (DBM), which were further cyclized with hydroxylaxmine or *N*-methylhydrazine to obtain **A1**, **A2**, **B1**, **B2**, **D**, and **E**.[2f,13b] For accessing arylazopyrroles **C1** and **C2**, the corresponding anilines were diazotized and subjected to a direct electrophilic substitution involving *N*-methylpyrrole.[13a] Using an aromatic nucleophilic substitution-based post functionalization strategy,[8b] both mono and bis cyclic amine connected azoheteroarene targets (**1a-i**, **2a-g**, **3a-d**, **4**, and **5**) have been synthesized in excellent yields (**Scheme 2.1**).

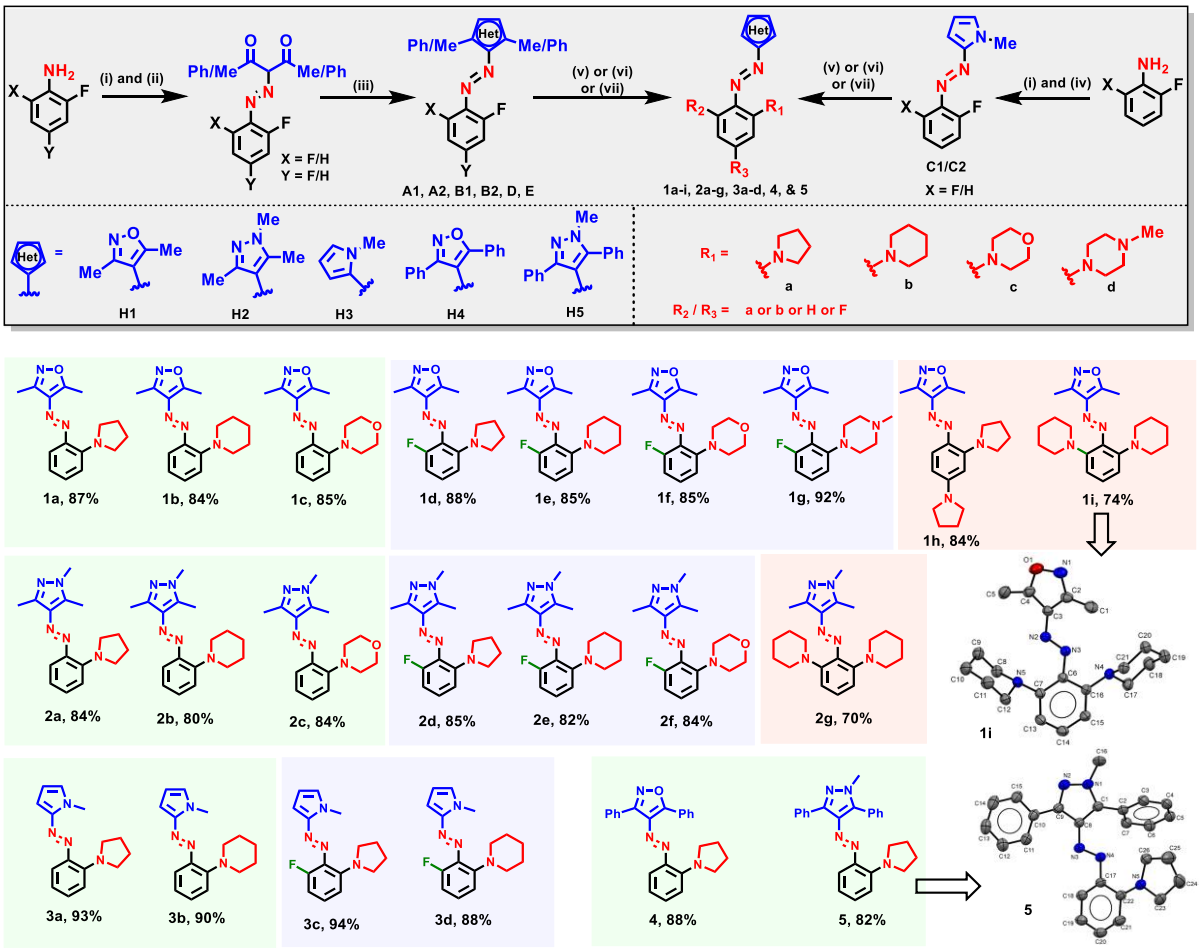

Scheme 2.1. Synthesis of azoheteroarenes (**1a-i**, **2a-g**, **3a-d**, **4** and **5**). Conditions: (i) $NaNO_2$/HCl, H_2O, 0-5 ^oC; (ii) acac or 1,3-diphenylpropane-1,3-dione (DBM), MeOH-H_2O, 0-5 ^oC to rt; (iii) $NH_2OH.HCl$ or $NH_2NHMe.H_2SO_4$, Na_2CO_3, EtOH, reflux; (iv) *N*-methylpyrrole, Na_2CO_3, acetone-H_2O, 0-5 ^oC to rt; (v) pyrrolidine (pyr) or piperidine (pip) or morpholine (mor), neat, 60-80 ^oC, 3-5 hrs; (vi) pyr or pip or mor or *N*-methylpiperazine (Nmpip), MeCN, rt-40 ^oC, 3-5 hrs; (vii) pyr or pip, 100 ^oC, 24 hrs; The crystal structure of **1i** and **5** are depicted.[16] The isolated yields in the final step are indicated.

All the targets were characterized using ^1H, ^{13}C-NMR, HRMS, IR, and UV−vis spectroscopic techniques.

2.3 Photoswitching Studies

The photoswitching studies of all 22 derivatives have been carried out in three different solvents (MeCN, MeOH, and DMSO) and analyzed using UV-vis spectroscopy (**Table 2.1** and **Appendix 2A**). First, we compared the absorption properties of different types of azoheteroarenes in DMSO in their native state (**Table 2.1**). Since the π–π* band ranges

between 288 and 377 nm, the realization of visible light photoswitching can be possible only by considering the n–π* absorption. Interestingly, the bands in the n–π* absorption region showed enhancement in all the cases. The reason for the enhancement in the n–π* region has been recently explored for *ortho*-fluoroaminoazobenzenes by Priimagi and co-workers.[8c,17] To explore the possibilities of visible light photoisomerization, we closely inspected the trends and effects of substituents on it. The following are the generalized observations for redshift of the n–π* band: (a) substitution pattern, **Type A** > **Type B** > **Type C**, (b) heterocycles: **4** > **3a**, **b** (azopyrroles) > **5** > **1a−c** (azoisoxazoles) > **2a−c** (azopyrazoles), and (c) cyclic amines: pyrrolidine > piperidine ≥ morpholine (**Table 2.1** and **Appendix 2A for details**). For analysis of the *E*-*Z* and *Z*-*E* photoisomerization steps, UV−vis spectroscopy has been used (**Appendix 2A**). For instance, the derivatives **2c** and **3a** have been irradiated at 405 nm (blue light) and 505 nm (green light), respectively, for *E*-*Z* isomerization (**Figure 2.1**), whereas at 505 nm, the *Z*-*E* isomerization has taken place in **2c**. However, in **3a**, the reverse isomerization was fast and thermally enabled. Both **2c** and **3a** showed consistency in the test for reversibility that was studied over 5 cycles (**Figure 2.1**). To understand the photoswitching stability of all the derivatives, we subjected them to reversible irradiation sequences in the forward and reverse directions over 5 cycles (**see the Appendix 2A**). Without any visible sign of fatigue, all the derivatives exhibited consistency in reversible photoswitching. Notably, a majority of the compounds except **2b**, **2c**, **2e**, and **5** showed bidirectional photoswitching within a small range. For **3a**, **3b**, **3c**, and **3d**, a reverse isomerization step was performed under thermal conditions as they demand UV light for the corresponding photoisomerization step. The photoswitching effects were quite similar in all three solvents (DMSO, MeCN, and MeOH). In a majority of the cases, the irradiation caused lowering in the intensities of the observed π–π* and n–π* absorption bands with minimal variations for *E*- and *Z*-isomers. The only exceptions are the *N*-methyl pyrrole derivatives **3a−d**, where we observed distinguishable absorption features for the native (*E*-isomer) and photoswitched (*Z*-isomer) states. Almost all of the azoheteroarene derivatives exhibit a shift in the λ_{max} (typically 5 to 10 nm) on changing the solvents from DMSO to MeCN or MeOH. First, we compared the absorption properties of the different types of azoheteroarenes in DMSO in their native state (**Table 2.1**). The λ_{max} values of the π–π* band follow the trend **Type A** ≥ **Type B** > **Type C**, whereas it is pyrrolidine < piperidine ≤ morpholine (in **Type A**) among the cyclic amines attached. As far as the heterocycles are concerned, the λ_{max} has the following trend: **H1** < **H2** < **H5** < **H4** < **H3**.

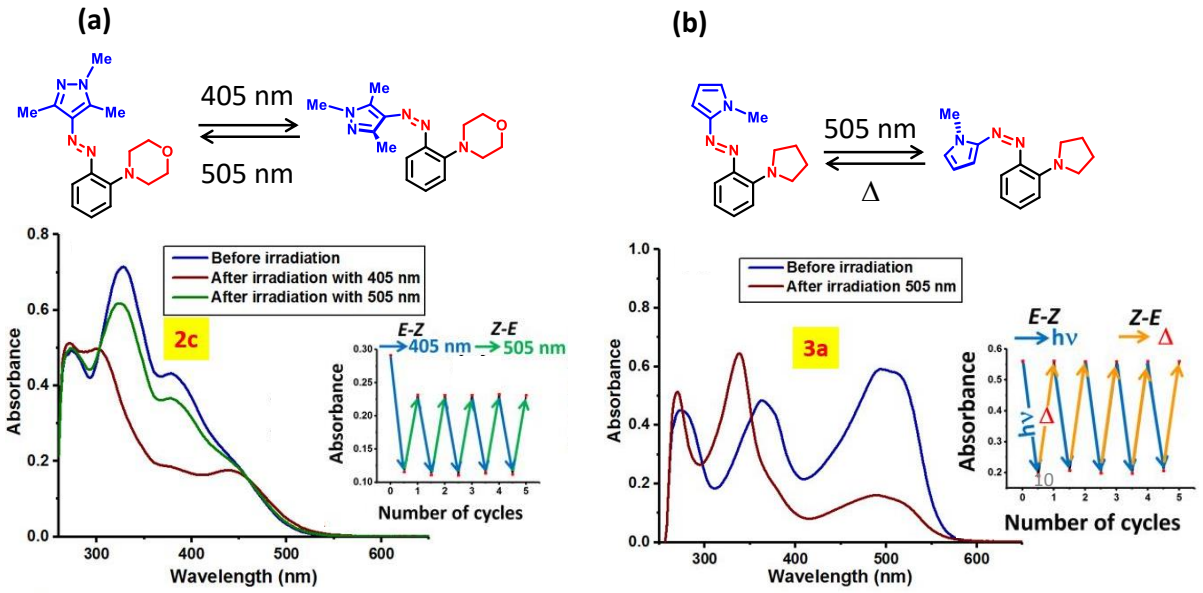

Figure 2.1. Illustration of photoisomerization of selected derivatives. UV-Vis spectroscopic data (DMSO) portraying photoisomerization under indicated conditions in (a) **2c** and (b) **3a**.

Indeed, all the azoheteroarenes except **3b**, **3c**, and **3d**, having *N*-methylpyrrole units, exhibited a well-separated π–π* and n–π* bands along with a hyperchromic effect in the latter. We closely inspected the trends and effect of substituents on the n–π* band. Among the different types, in general, **Type A** photoswitches show a maximum red-shift with intensity enhancement. All the azoheteroarenes follow the same trend irrespective of the heterocycles attached. Notably, all the derivatives exhibit a split in the n–π* signal. However, with *ortho* fluorination, the band at a shorter wavelength gets enhanced, whereas, for all other derivatives, the enhancement appears in the longer wavelength component. Moreover, for the 2,6-disubstituted derivatives, the n–π* absorption is found to be blue shifted, which can be attributed to the non-planar structure as obtained for **1i** (**see Appendix 2A**). Along with the influence of cyclic amines in **Type A** systems, the *ortho* fluorination (**Type B**) and bis amine substitution (**Type C**) showed a serious impact on the n–π* absorption features. For instance, the mono *ortho*-piperidine connected **1b** (**Type A**) shows the n–π* band at 402 nm, whereas the corresponding system with *ortho* fluorinated 1e (**Type B**) exhibits the same at 379 nm. On the other hand, bispiperidine connection in **1i** (**Type C**) exhibits a blue shift (358 nm). A similar pattern was also observed in the case of piperidine connected azopyrazole derivatives **2b** (445 nm), **2e** (430 nm), and **2g** (approx. 450 nm). Even the arylazopyrrole derivatives (**3b**

and **3d**) follow the same trend. Regarding the effect of different aliphatic cyclic amines, pyrrolidine-substituted azoheteroarenes showed the maximum red-shifted n–π* band. The pyrrolidine substituted aryl-3,5- dimethylazoisoxazole **1a** shows the n–π* band at 475 nm, whereas **1b**, with piperidine substitution, shows the band at 402 nm, and morpholine-substituted **1c** shows the band at 392 nm. This trend is valid for all derivatives that fall into the categories **Type A**, **Type B**, and **Type C**, once again irrespective of the heterocycle units attached. For example, **1d**, with both fluoro and pyrrolidine as *ortho* substituents, shows a considerably red-shifted n–π* band (465 nm) compared to **1e** (379 nm) and **1f** (372 nm). Furthermore, the maximum red-shift in the n–π* band and hyperchromic shifts caused by the pyrrolidine ring substitution can be attributed to its relatively higher electron-donating ability among the cyclic amines used.[8c] The reason for such enhancements in the n–π* bands has been attributed to the delocalization of the nitrogen lone pair by Priimagi and co-workers.[8c] This is based on the accumulation of sp^2 hybridization at the amine nitrogen, shortening of the $CPh{-}N_{amine}$ distance, and the steric repulsion of the amine group with the meta hydrogen of the aryl ring. Presumably, such delocalization of the amine lone pair can cause an intramolecular charge transfer (ICT) band, which could be responsible for the enhancements. Since ICT bands are susceptible to the local environments, we performed photoswitching experiments for compound **3a** in a wide range of solvents with different polarities. We observed significant shifts while changing the solvents with different polarities (**Appendix 2A**). Based on these data, we understood that there can be a significant contribution from intramolecular charge transfer in the observed spectral features. This trend is reflected in **Type B** azoheteroarenes also. The same trend can also be felt in the case of *N*-methyl arylazopyrazole derivatives **2a** (461 nm), **2b** (386 nm), and **2c** (380 nm), or **2d** (448 nm), **2e** (420 nm), and **2f** (shoulder). Likewise, pyrrolidine and piperidine connected *N*-methyl arylazopyrrole derivatives **3a** (502 nm), **3b** (423 nm), **3c** (362 nm), and **3d** (344 nm) follow the same trend (**Table 2.1**). Among the different azoheteroarene photoswitches that we prepared, we found that the λ_{max} corresponding to the n–π* band has the following trend: **2a-c** (arylazo-3,5-dimethylpyrazoles) < **1a-c** (arylazo-3,5- dimethylisoxazoles) < **5** (arylazo-3,5-diphenylpyrazole) < **3a, b** (azopyrroles) < **4** (arylazo-3,5-diphenylisoxazole). Within these, the derivatives exhibiting a maximum red shift in the n–π* band are the aryl-3,5-diphenylazoisoxazole derivative **4** (513 nm), *N*-methyl arylazopyrrole derivative **3a** (502 nm), *N*-methyl arylazo-3,5-diphenylpyrazole derivative **5** (492 nm), arylazo-3,5-dimethyl

Table 2.1. UV-Vis spectral data of *E*-/*Z*-isomers, PSS composition (^{1}H-NMR data), and thermal *E*-*Z* isomerization kinetics data.

S. No.	Type	Compound	UV-Vis absorption data[a] λ_{max} in nm				Photoisomerization and PSS composition[b]					*Z*-*E* thermal reverse isomerization[c]	
			E-isomer		*Z*-isomer		$\lambda_{forward}$	*E*-*Z* (%***E***:%***Z***)	$\lambda_{reverse}$	*Z*-*E* (%***E***:%***Z***)	Conc. mM	k, (x 10^{-4}) min^{-1}	$t_{1/2}$
			λ_1	λ_2	λ_1	λ_2							
1	A	**1a**	315	475	270	479	470	53:47	590	76:24	12.1	17.0[d]	6.9 h
2		**1b**	316	402, 440	284	432	405	29:71	435	42:58	11.2	7.2[d]	16.1 h
3		**1c**	319	392	268	432	405	30:70	490	48:52	10.5	4.1[d]	1.2 d
4		**2a**[g]	322	461	271	467	470	45:55	590	76:24	11.3	44.0[d]	8.3 h
5		**2b**[g]	329	379	304	444	405	30:70	535	57:43	10.1	0.95[d]	5.0 d
6		**2c**	328	380	303	438	405	25:75	505	73:27	10.2	3.5[d]	1.4 d
7		**3a**[h]	361	502	338	498	505	34:66	y	y	y	13000[e]	5 min
8		**3b**	377	-	337	-	505	26:74	z	z	11.1	43.0[e]	161 min
9		**4**	332	513	-	513	515	50:50	615	80:20	8.9	12[d]	9.4 h
10		**5**	326	492	-	492	505	68:32	590	83:17	9.2	15[d]	7.6 h
11	B	**1d**	311	465	269	387, 467	x	x	x	x	x	x	x
12		**1e**	310	379	270	376, 433	405	39:61	505	63:37	10.1	0.1[d]	47.8 d
13		**1f**	304	372	272	370, 431	405	40:60	490	54:46	9.8	0.043[d]	112.3 d
14		**1g**	311	378	268	375, 431	405	40:60	535	53:47	9.9	0.06[d]	80.2 d
15		**2d**	312	448	270	452	405	56:44	535	76:24	10.3	9.7[d]	11.9 h
16		**2e**	310	426	297	435	405	49:51	450	76:24	9.4	0.049[d]	98.4 d
17		**2f**	317	-	307	431	405	54:46	470	69:31	9.5	0.072[d]	66.8 d
18		**3c**	362	-	340	-	405	57:43	z	z	10.5	120[d]	56 min
19		**3d**	365	f	340	-	405	23:77	z	z	10.5	7.9[d]	14.6 h
20	C	**1h**	300	400, 480	y	y	y	y	y	y	y	y	y
21		**1i**	-	358	y	y	y	y	y	y	y	y	y
22		**2g**	288	-	y	y	y	y	y	y	y	y	y

[a]in DMSO; [b]in DMSO-d_6; The $\lambda_{forward}$ and $\lambda_{reverse}$ are the wavelengths of light used; [c]in DMSO; [d]estimated at 25 °C using Arrhenius plot, [e]measured at 25 °C; [f]overlapping; [g]Reported in acetonitrile in ref 15; [h]PSS composition was estimated using UV-Vis spectroscopy; [x]Decomposes during photoisomerization; [y]Exhibiting fast thermal relaxation; [z]Requires UV irradiation; λ_1 and λ_2 represents the π–π* and n–π*and/or intramolecular charge transfer (ICT) bands[17], respectively.

isoxazole derivative **1a** (475 nm), and aryl-3,5-dimethylazopyrazole derivative **2a** (461 nm) (**Table 2.1**).Due to fast thermal reverse isomerization rates, the blue shifted π–π* band (below 350 nm), and the overlapping band at the n–π* region, we were unable to induce the reverse isomerization step with visible light in the arylazopyrrole derivatives. However, we were able to perform the thermal reverse isomerization kinetics and deduced the rate constants and half-lives for them.

2.4 Thermal Reverse Isomerization Kinetics

Next, we investigated the thermal reverse isomerization kinetics experiments in DMSO. Except for arylazopyrrole derivatives **3a**, **b** exhibiting fast thermal *Z*-*E* relaxation, all the experiments were performed at higher temperatures and with the help of Eyring plots, and rate constants and half-lives have been deduced at room temperature (25 °C) (**Table 2.2** and **Appendix**). For example, the *Z*-isomers of the derivatives **2c** and **3a** have been subjected to thermal reverse *Z*-*E* isomerization at 50 and 25 °C, respectively (**Figure 2.2**). Among the arylazoisoxazole derivatives, **Type B** showed enhanced thermal stability compared to **Type A** or **Type C**. For instance, the compounds **1e** (47.8 d) and **1f** (112.3 d) showed longer half-lives at 25 °C. Comparatively, the derivatives such as **1b** (16.1 h) and **1c** (1.2 d) exhibited shorter half-lives (**Table 2.1**). Such observations follow the literature trends, where the sigma-withdrawing nature of fluorine has been reported to stabilize the *Z*-isomers.[5,8b] Similarly, arylazopyrazole derivatives exhibit moderate to good thermal stability of the *Z*-isomer; however, they follow similar trends. For instance, **Type A** derivatives **2a** (8.3 h), **2b** (5.0 d), and **2c** (1.4 d) show less thermal stability than the **Type B** derivatives **2d** (11.9 h), **2e** (98.4 d), and **2f** (66.8 d) at 25 °C. Equally, the arylazopyrrole derivative **3a**, with monoamine isoxazole derivative **1a** (475 nm), and aryl-3,5-dimethylazopyrazole derivative **2a** (461 nm) (**Table 2.1**). We observed similar trends in the azopyrazole derivatives also. The pyrrolidine derivative **2a** shows a half-life of 8.3 h, whereas both the piperidine substituted derivative **2b** and the morpholine-substituted derivative **2c** have a half-lives of 5 d and 1.4 d, respectively at rt. Again, the *Z*-isomer of the fluorinated analogue **2d** (11.9 h) is less stable than that of **2e** (98.4 d) and **2f** (66.8 d) upon comparison of their half-lives at rt. This generalization is consistent for arylazopyrroles **3a** (5 min) and **3b** (161 min). Among the different pyrrolidine-substituted azoheteroarene derivatives (**Type A**), arylazo-3,5-diphenylisoxazole **4** showed better thermal stability than other derivatives. The thermal stabilities of arylazo-3,5-dimethylisoxazole **1a** and *N*-methyl arylazo-3,5-dimethylpyrazole **2a** are 6.9 h and 8.3 h, respectively, at 25 °C.

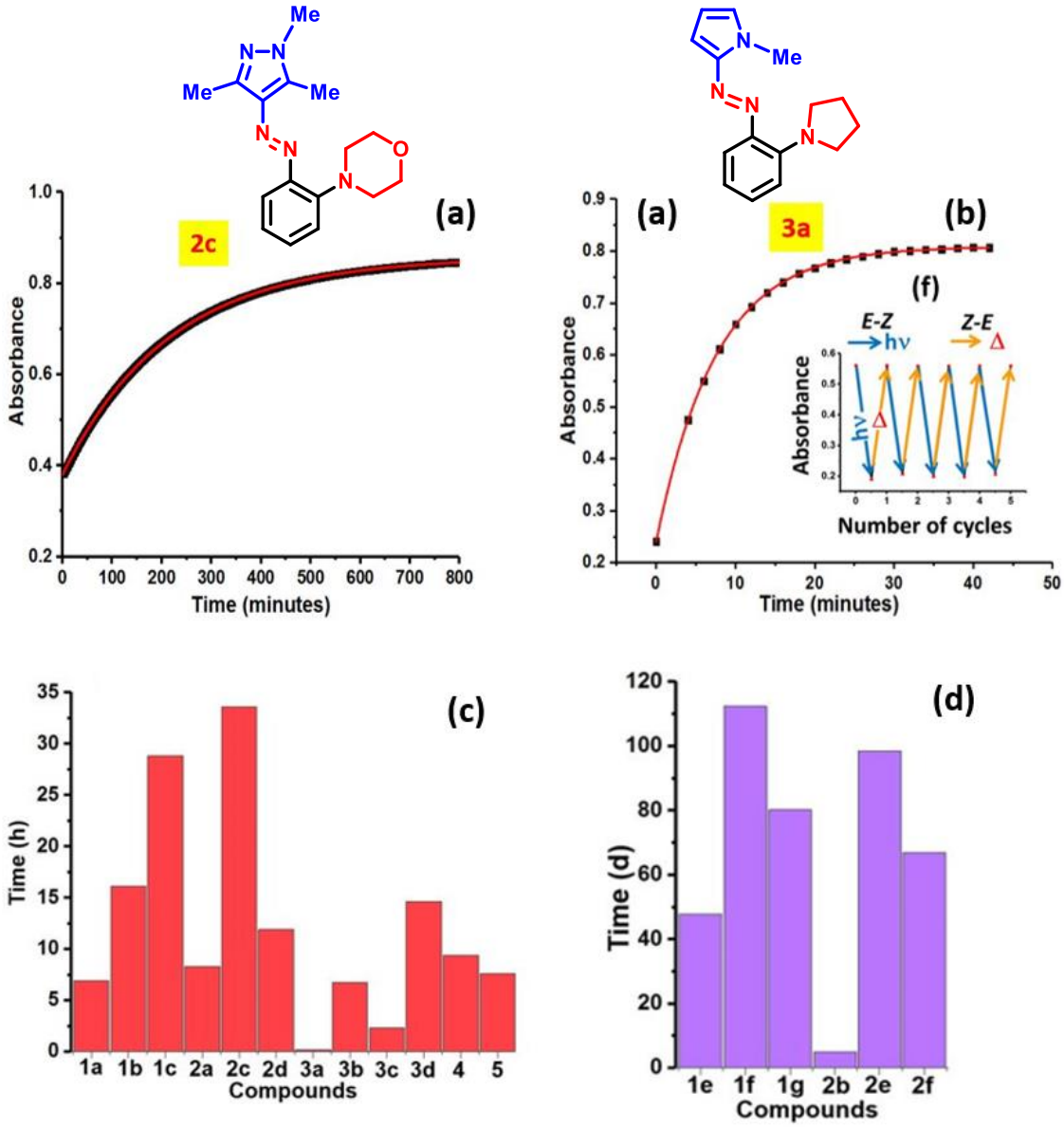

Figure 2.2. Illustration thermal reverse isomerization kinetics in DMSO of UV-Vis spectroscopic data (a) **2c** and (a) **3a**, (c) and (d) overall trends in the half-lives.

Table 2.2. Thermal reverse isomerization kinetics data at 25 °C

S. No.	Compound	Temperature (°C)	Rate constant, k (min^{-1})	Half-life, $t_{1/2}$
1.	**1a**	25	1.7×10^{-3}	6.9 h
2.	**1b**	25	7.2×10^{-4}	16.1 h
3.	**1c**	25	4.1×10^{-4}	1.2 d
4.	**1d**	a	a	a
5.	**1e**	25	1.0×10^{-5}	47.8 d
6.	**1f**	25	4.3×10^{-6}	112.3 d
7.	**1g**	25	6.0×10^{-6}	80.2 d
8.	**1h**	b	b	b

9.	**1i**	b	b	b
10.	**2a**	25	4.4×10^{-3}	8.3 h
11.	**2b**	25	9.5×10^{-5}	5.0 d
12.	**2c**	25	3.5×10^{-4}	1.4 d
13.	**2d**	25	7.9×10^{-4}	11.9 h
14.	**2e**	25	4.9×10^{-6}	98.4 d
15.	**2f**	25	7.2×10^{-6}	66.8 d
16.	**2g**	b	b	b
17.	**3a**	25	1.3×10^{-1}	5 min
18.	**3b**	25	4.3×10^{-3}	161 min
19.	**3c**	25	1.2×10^{-2}	56 min
20.	**3d**	25	7.9×10^{-4}	14.6 h
21.	**4**	25	1.2×10^{-3}	9.4 h
22.	**5**	25	1.5×10^{-3}	7.6 h

[a]The compound decomposed upon irradiation with light; [b]Fast thermal reverse relaxation

As expected, *N*-methyl arylazopyrrole **3a** showed the least thermal stability ($t_{1/2}$ = 5 min at rt).[13a]

2.5 Photoswitching Studies Using ^{1}H NMR Spectroscopy

We estimated the percentage of *E*-and *Z*-isomers in the forward and reverse photoisomerization steps to evaluate the photoswitching ability. All derivatives showed moderate to good forward (32−77%) and reverse photoisomerization (42−83%) conversions (**Table 2.3** and **Appendix 2A**). Due to overlapping absorption spectral features of the *E*- and *Z*-isomers, the PSS could not reach beyond 75% in the majority of cases. However, in the derivatives such as **3a-d**, the distinguishable spectral features allowed us to achieve a higher conversion. The *Z*-isomer of mono pyrrolidine-substituted derivative **3a** was quite unstable even at room temperature and therefore could not be recorded. Although all the derivatives exhibited similar photoisomerization conversions, they differ in the choice of wavelength of light for irradiation in both directions. For arylazo-3,5-dimethylisoxazoles and arylazo-3,5-dimethylpyrazoles, the forward photoisomerization step was induced by blue light (405−470 nm). Maximum conversions were obtained by using blue or green light (405 or 505 nm) for pyrrole derivatives. Among the azoheteroarenes, 3,5-diphenyl derivatives **4** and **5** showed both forward and reverse photoisomerization with green and red to orange lights, respectively, with good conversions. Incidentally, it showed high thermal stability of the *Z*-isomer ($t_{1/2}$ = 9.4 h at 25 °C).

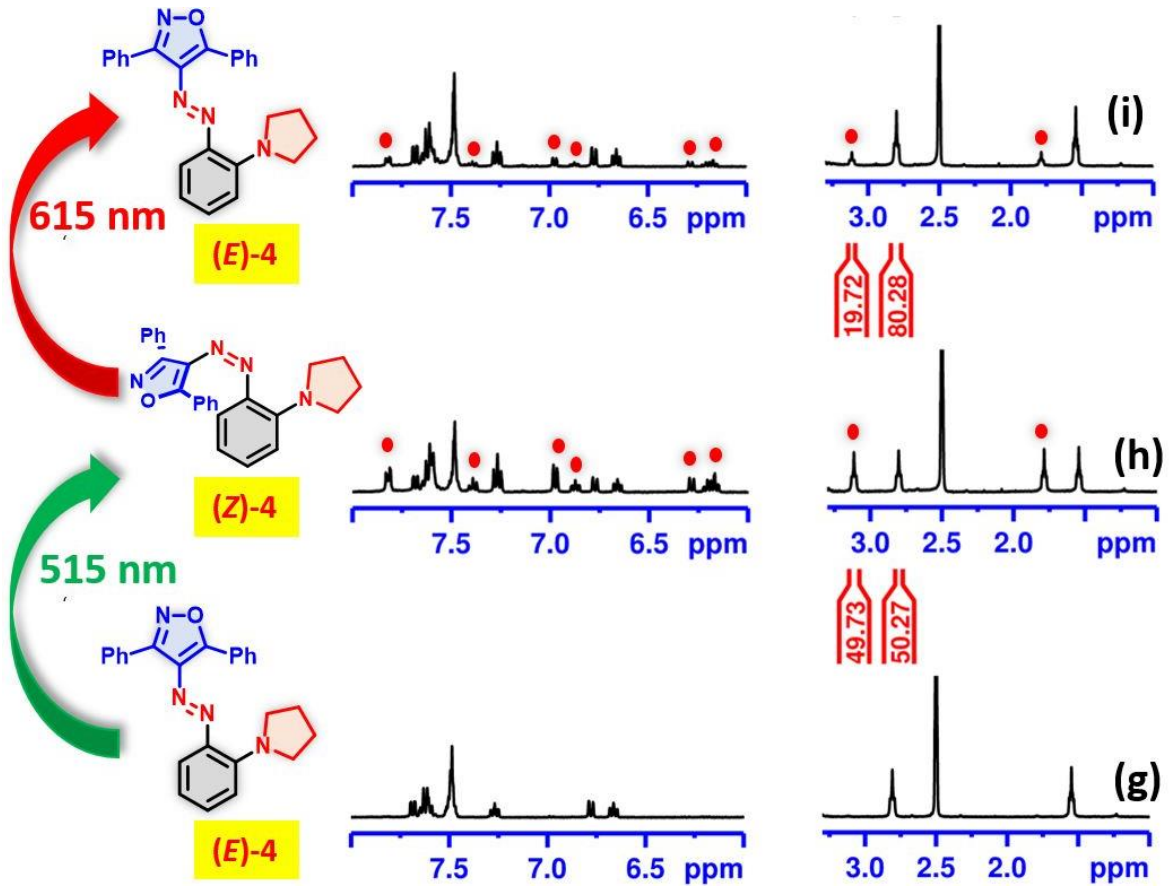

Figure 2.3. (g-i) Estimation of the photostationary state (PSS) composition in **4** under indicated irradiation conditions using ^{1}H-NMR (DMSO-d_6). (Red dots: **(*Z*)-4**).

Based on the UV-vis spectroscopic data, it is clear that pyrrole derivatives with *ortho* fluorination and *ortho* amination **3a−d** do not show any new features or absorptions in the region of 400-800 nm that can be used to distinguish between *E*- and *Z*-isomers. Instead, we observed only the drop in the intensity of bands due to the *E*-isomer upon photoisomerization. Thus, the reverse photoisomerization could not be performed with the help of visible light.

2.6 Experimental Section

All commercially available reagents and solvents were used without further purification. An MBRAUN-SPS solvent purification system was used for dry acetonitrile. Spectroscopic and kinetic studies were performed with HPLC or UV spectroscopy-grade solvents. Aluminum-backed Merck Silica gel 60 F254 TLC plates were used to monitor reactions.

Table 2.3 Quantification of photoisomers by using ^{1}H NMR spectroscopy

Compound	Wavelength (nm)	Irradiation time (min)	%*E*	%*Z*	Proton signal used	Conc. (mM)
1a	470	20	53	47	Isoxazole -Me	12.1
	590	20	76	24		
1b	405	10	29	71	Piperidine -CH_2	11.2
	435	20	42	58		
1c	405	10	30	70	Morpholine -CH_2	10.5
	490	20	48	52		
1d	**a**		**a**	**a**	-	-
	a		**a**	**a**		
1e	405	10	39	61	Isoxazole -Me	10.1
	505	20	63	37		
1f	405	10	40	60	Isoxazole -Me	9.8
	490	20	54	46		
1g	405	10	40	60	Isoxazole -Me	9.9
	535	20	53	47		
1h	**b**		**b**	**b**	-	-
	b		**b**	**b**		
1i	**b**		**b**	**b**	-	-
	b		**b**	**b**		
2a	470	20	45	55	Pyrazole *N*-Me	11.3
	590	20	76	24		
2b	405	10	30	70	Pyrazole *N*-Me	10.1
	535	20	57	43		
2c	405	10	25	75	Pyrazole -Me	10.2
	505	20	73	27		
2d	405	10	56	44	Pyrazole *N*-Me	10.3
	535	20	76	24		
2e	405	10	49	51	Pyrazole *N*-Me	9.4
	450	20	76	24		
2f	405	10	54	46	Pyrazole -Me	9.5
	470	20	69	31		
2g	**b**		**b**	**b**	-	-
	b		**b**	**b**		
3a	**b**		**b**	**b**	-	-
	b		**b**	**b**		
3b	505	20	26	74	Pyrrole *N*-Me	11.1
	c		**c**	**c**		
3c	405	10	57	43	Pyrrolidine -CH_2	10.5
	c		**c**	**c**		
3d	405	10	23	77	Pyrrole *N*-Me	10.5
	c		**c**	**c**		
4	515	20	50	50	Pyrrolidine -CH_2	8.9
	615	20	80	20		
5	505	20	68	32	Pyrazole *N*-Me	9.2
	590	20	83	17		

[a]The compound decomposed upon irradiation with light; [b]Fast photoswitches; [c]No photochemistry was observed in the reverse isomerization with visible light. (Blue-shaded rows represent forward isomerization, and the other rows represent reverse isomerization.

100−200 mesh silica gel or alumina (neutral and basic) was used for column chromatography.[1] H, ^{13}C, and ^{19}F NMR spectra were recorded on a Bruker Avance-III 400 MHz instrument at operational frequencies of 400 MHz (^{1}H NMR), 100 MHz (^{13}C NMR), and 376 MHz (^{19}F NMR). For ^{1}H NMR, residual solvent signals of $CHCl_3$ (7.26 ppm) and DMSO-d_5 (2.50 ppm) have been used for internal calibration. Corresponding signals of $CDCl_3$ (77.16 ppm) and DMSO-d_6 (39.52 ppm) were used for calibrating the spectra for ^{13}C NMR. For ^{19}F spectra, C_6F_6 (10 mM solution in $CDCl_3$) was used as an internal standard for calibration. Chemical shift (δ) values are reported in parts per million (ppm), and coupling constants (J) are reported in Hz. The signal multiplicities are abbreviated as singlet (s), doublet (d), triplet (t), quartet (q), pentet (pt), doublet of doublets (dd), doublet of triplets (dt), triplet of doublets (td), doublet of doublet of doublets (ddd), multiplet (m), broad (br), and overlapping signals (o). High-resolution mass spectra (HRMS) have been recorded and analyzed using a Waters Synapt G2-Si Q-TOF mass spectrometer. The electrospray ionization (ESI) method was used for ionization, and detections were done in both positive and negative modes. FT-IR spectra of the neat solid or neat liquid samples were recorded on a Bruker Alpha ZnSe ATR spectrometer. Single crystal X-ray diffraction data were collected using a Rigaku XtaLAB mini diffractometer equipped with a Mercury375M CCD detector (for details, **Appendix 2A**). (*E*)-4-((2-Fluorophenyl)diazenyl)-3,5-dimethylisoxazole, **(A1)** (yellow solid, yield = 210.0 mg, 96%), (*E*)-4-((2,4-difluorophenyl)- diazenyl)-3,5-dimethylisoxazole, **(A2)** (yellow solid, yield = 180.0 mg, 78%), and (*E*)-4-((2,6-difluorophenyl)diazenyl)-3,5-dimethylisoxazole **(A3)** (yellow solid = 120.0 mg, 53%) were prepared according to a procedure reported in the literature.[2f] (*E*)-4-((2-Fluorophenyl)diazenyl)-1,3,5-trimethyl-1H-pyrazole) **(B1)** (yellow solid, yield = 180.0 mg, 80%) and (*E*)-4-((2,6- difluorophenyl)diazenyl)-1,3,5-trimethyl-1H-pyrazole **(B2)** (yellow solid, yield = 200.0 mg, 80%) were prepared according to a procedure reported in the literature.[2a,13b](*E*)-2-((2-Fluorophenyl)diazenyl)-1-methyl-1H-pyrrole **(C1)** (dark red solid, yield = 0.10 g, 50%) and (*E*)-2-((2,6-difluorophenyl)- diazenyl)-1-methyl-1H-pyrrole **(C2)** (dark red solid, yield = 0.11 g, 50%) were prepared according to a procedure reported in the literature.[13a] General Procedure for Substrates **D** and **E**. To 2-fluoroaniline (3.18 g, 20.0 mmol) kept in a round-bottom flask, 6.5 mL of 37% concentrated HCl was added at 0 °C. A cold aqueous solution of sodium nitrite (1.52 g, 22.0 mmol in 20 mL of water) was slowly added to the reaction mixture. The reaction mixture was allowed to stir for half an hour for completion. Afterward, at 0 °C, a cold aqueous solution of sodium acetate (5.90 g, 70.0 mmol) and 1,3- diphenylpropane-1,3-dione (4.03 g, 18.0 mmol in 100 mL of MeOH) was

added. The reaction was continued at rt and was monitored by TLC. After completion of the reaction, excess water was added to the reaction mixture. The mixture was filtered to obtain a yellow-orange solid product, which was dried under vacuum to yield 2-(2-(2-fluorophenyl)hydrazono)-1,3-diphenylpropane-1,3-dione in 90% yield. A mixture of 2-(2-(2-fluorophenyl)hydrazono)-1,3-diphenylpropane-1,3-dione derivative (0.35 g, 1.0 mmol), sodium carbonate (0.16 g, 1.5 mmol), and hydroxylamine hydrochloride (0.11 g, 1.5 mmol) or methyl hydrazine sulfate (0.07 g, 1.5 mmol) in 10 mL of EtOH was refluxed on an oil bath for 12- 36 h. The reaction was followed using TLC up to the completion. After completion, excess water was added to the reaction mixture and it was extracted multiple times with ethyl acetate. The organic layers were collected and dried over anhydrous sodium sulfate. The distillation of solvent under vacuum led to the crude product. Then, the product was purified by column chromatography (eluent: n-hexane/ethyl acetate = 1:2) to obtain the substrates **D** or **E**, respectively.

(*E*)-4-((2-Fluorophenyl)diazenyl)-3,5-diphenylisoxazole (D). Orange solid, mp = 70−72 °C, Yield = 300.0 mg, 87%. Eluent: n-hexane/ ethyl acetate = 1:2; ^{1}H NMR (400 MHz, $CDCl_3$) δ 8.26 (dd, *J* = 6.4, *J* = 6.4 Hz, 2H), 7.82−7.81 (m, 2H), 7.66−7.62 (m, 1H), 7.58−7.56 (m, 3H), 7.51−7.40 (m, 4H), 7.23−7.19 (m, 2H) ppm; ^{13}C{^{1}H} NMR (100 MHz, $CDCl_3$) δ 166.9, 160.1 (d, *J* = 257.8 Hz), 157.3 (d, *J* = 7.1 Hz), 140.8 (d, *J* = 7.1 Hz), 132.8 (d, *J* = 8.2 Hz), 132.0, 131.5, 130.0, 129.0, 128.9, 128.8, 128.5, 128.1, 127.1, 124.4 (d, *J* = 3.7 Hz), 117.7, 117.5 (d, *J* = 19.5 Hz) ppm; ^{19}F NMR (376.5 MHz, $CDCl_3$) δ −125.79 ppm; HRMS (ESI-TOF) m/z: $[M + H]^+$ Calcd. for $C_{21}H_{15}FN_3O$ 344.1199, obs. 344.1172; IR (KBr, cm^{-1}) 759, 1029, 1078, 1219, 1496, 1609, 2871, 2939.

(*E*)-4-((2-Fluorophenyl)diazenyl)-1-methyl-3,5-diphenyl-1H-pyrazole (E). Orange solid, mp = 89−91 °C, Yield: 290.0 mg, 80%. Eluent: n-hexane/ethyl acetate = 1:2; ^{1}H NMR (400 MHz, $CDCl_3$) δ 8.05 (d, *J* = 6.4 Hz, 2H), 7.55−7.45 (m, 8H), 7.42−7.40 (m, 1H), 7.29 (o, 2H), 7.12−7.07 (m, 2H), 3.87 (s, 2H) ppm; ^{13}C{^{1}H} NMR (100 MHz, $CDCl_3$) δ 159.7 (d, *J* = 255.9 Hz), 147.6, 141.1 (d, *J* = 7.1 Hz), 137.7, 135.2, 132.6, 131.3 (d, *J* = 8.0 Hz), 130.6, 129.3, 129.2, 129.1, 128.43, 128.4, 128.3, 124.1 (d, *J* = 3.7 Hz), 117.5, 116.9 (d, *J* = 19.4 Hz), 37.7 ppm; ^{19}F NMR (376.5 MHz, $CDCl_3$) δ −202.39 ppm; HRMS (ESI-TOF) m/z: $[M + H]^+$ Calcd. for $C_{22}H_{18}FN_4$ 357.1515; Found 357.1512; IR (KBr, cm^{-1}) 810, 1038, 1149, 1446, 1619, 2857, 2919.

General Procedure of Compound 1a-1c

Compound **1a−1c** were synthesized using a modified version of a literature procedure.[8b] The corresponding cyclic amine (10.0 mmol, 50 equiv) was added to **(*E*)-4-((2,6-difluoro)diazenyl)-3,5-dimethylisoxazole** (0.2 mmol, 43.8 mg, 1 equiv). The mixture was stirred at 60 °C for 3−5 h. After checking the TLC for completion of the reaction, it was stopped and quenched with water. The mixture was extracted multiple times with ethyl acetate. The combined organic layers were collected and dried over anhydrous sodium sulfate. The distillation of solvent under vacuum led to the crude product. Further purification of the mixture was done over neutral alumina using a 98:2 mixture of n-hexane: ethyl acetate to give the desired products, **1a-c**.

(*E*)-3,5-Dimethyl-4-((2-(pyrrolidin-1-yl)phenyl)diazenyl)isoxazole (1a). Orange solid, mp = 70−72 °C, Yield = 47.0 mg, 87%. Eluent: n-hexane/ethyl acetate = 98:2; ^{1}H NMR (400 MHz, $CDCl_3$) δ 7.53 (d, *J* = 8.2 Hz, 1H), 7.27−7.24 (o, 1H), 6.82 (d, *J* = 8.5 Hz, 1H), 6.68 (t, *J* = 7.6 Hz, 1H), 3.57−3.54 (m, 4H), 2.69 (s, 3H), 2.47 (s, 3H), 1.99−1.95 (m, 4H) ppm; ^{13}C{^{1}H} NMR (100 MHz, $CDCl_3$) δ 167.0, 153.8, 146.4, 141.5, 133.0, 131.5, 117.6, 116.5, 115.8, 52.3, 25.9, 11.93, 11.90 ppm; HRMS (ESI-TOF) m/z: $[M + H]^+$ Calcd. for $C_{15}H_{18}N_4O$ 271.1559; Found 271.1541; IR (KBr, cm^{-1}) 750, 1045, 1095, 1272, 1496, 1551, 1603, 2865, 2930, 2939.

(*E*)-3,5-Dimethyl-4-((2-(piperidin-1-yl)phenyl)diazenyl)isoxazole (1b). Orange solid, mp = 78−80 °C, Yield = 48.0 mg, 84%. Eluent: nhexane/ethyl acetate = 98:2; ^{1}H NMR (400 MHz, $CDCl_3$) δ 7.52 (d, *J* = 8.0 Hz, 1H), 7.35 (t, *J* = 7.4 Hz, 1H), 7.11 (d, *J* = 8.2 Hz, 1H), 6.99 (t, *J* = 7.6 Hz, 1H), 3.15 (t, *J* = 5.1 Hz, 4H), 2.77 (s, 3H), 2.58 (s, 3H), 1.75 (pt, *J* = 5.7 Hz, 4H), 1.62−1.59 (o, 2H) ppm; ^{13}C{^{1}H} NMR (100 MHz, $CDCl_3$) δ 169.2, 153.7, 151.2, 145.9, 133.0, 131.6, 121.7, 119.2, 116.9, 54.4, 26.6, 24.3, 12.2, 11.9 ppm; HRMS (ESI-TOF) m/z: $[M + H]^+$ Calcd for $C_{16}H_{20}N_4O$ 285.1715; Found 285.1704; IR (KBr, cm^{-1}) 552, 758, 924, 1048, 1229, 1280, 1412, 1483, 1611, 2828, 2861, 2930.

(*E*)-4-(2-((3,5-Dimethylisoxazol-4-yl)diazenyl)phenyl)morpholine (1c). Orange solid, mp = 104−106 °C, Yield = 49.0 mg, 85%. Eluent: n-hexane/ethyl acetate = 98:2; ^{1}H NMR (400 MHz, $CDCl_3$) δ 7.55 (d, *J* = 8.0 Hz, 1H), 7.37 (t, *J* = 7.7 Hz, 1H), 7.08−7.01 (m, 2H), 3.87 (t, *J* = 4.2 Hz, 4H), 3.19 (t, *J* = 4.3 Hz, 4H), 2.74 (s, 3H), 2.52 (s, 3H) ppm; ^{13}C{^{1}H} NMR (100 MHz, $CDCl_3$) δ 169.6, 153.1, 149.8, 145.6, 132.9, 131.7, 122.4, 118.6, 116.9, 67.2, 53.0, 12.1, 11.7 ppm; HRMS (ESI-TOF) m/z: $[M + H]^+$ Calcd $C_{15}H_{18}N_4O_2$ 287.1508; Found 287.1495; IR (KBr, cm^{-1}) 562, 636, 790, 932, 1120, 1252, 1280, 1410, 1482, 1607, 2894, 2938, 2971.

General Procedure of Compound 1d-1g

(*E*)-4-((2,6- Difluorophenyl)diazenyl)-3,5-dimethylisoxazole (0.2 mmol, 47.4 mg, 1 equiv) was added to 2 mL of acetonitrile, and the corresponding cyclic amine (1 mmol, 5 equiv) was added to the mixture. The mixture was stirred at room temperature for 2 to 3 h. After checking the TLC for the completion of reaction, it was stopped and quenched with water. The mixture was extracted multiple times with ethyl acetate. The combined organic layers were collected and dried over anhydrous sodium sulfate. The distillation of solvent under vacuum led to the crude product. Further purification of the mixture was done over neutral alumina using a 98:2 mixture of n-hexane: ethyl acetate to give the required products, **1d-g**.

(*E*)-4-((2-Fluoro-6-(pyrrolidin-1-yl)phenyl)diazenyl)-3,5-dimethylisoxazole (1d). Orange sticky liquid, Yield = 51.0 mg, 88%. Eluent: n-hexane/ethyl acetate = 98:2; ^{1}H NMR (400 MHz, $CDCl_3$) δ 7.09 (td, *J* = 8.3, 6.0 Hz, 1H), 6.60 (d, *J* = 7.4 Hz, 1H), 6.49 (dd, *J* = 11.0, 8.4 Hz, 1H), 3.36 (t, *J* = 6.4 Hz, 4H), 2.70 (s, 3H), 2.46 (s, 3H), 1.95− 1.92 (m, 4H) ppm; ^{13}C{^{1}H} NMR (100 MHz, $CDCl_3$) δ 168.9, 153.4, 152.2 (d, *J* = 252.6 Hz), 145.7 (d, *J* = 3.6 Hz), 133.2, 131.5 (d, *J* = 7.8 Hz), 129.4 (d, *J* = 11.4 Hz), 110.4, (d, *J* = 2.8 Hz) 104.2 (d, *J* = 21.5 Hz) 52.1, 25.8, 11.9, 11.8 ppm; ^{19}F NMR (376.5 MHz, $CDCl_3$) δ −131.53 ppm; HRMS (ESI-TOF) m/z: $[M + H]^+$ Calcd $C_{15}H_{18}FN_4O$ 289.1465, Found 289.1455; IR (KBr, cm^{-1}) 993, 1081, 1387, 1453, 1481, 1621, 2857, 2931.

(*E*)-4-((2-Fluoro-6-(piperidin-1-yl)phenyl)diazenyl)-3,5-dimethylisoxazole (1e). Orange solid, mp = 54−56 °C, Yield = 51.0 mg, 85%. Eluent: n-hexane/ethyl acetate = 98:2; ^{1}H NMR (400 MHz, $CDCl_3$) δ 7.19 (td, *J* = 8.3, 6.1 Hz, 1H), 6.85 (d, *J* = 8.3 Hz, 1H), 6.77 (dd, *J* = 10.0, 8.4 Hz, 1H), 3.01 (t, *J* = 5.0 Hz, 4H), 2.74 (s, 3H), 2.55 (s, 3H), 1.65 (pt, *J* = 5.8, 4H), 1.55 (o, 2H) ppm; ^{13}C{^{1}H} NMR (100 MHz, $CDCl_3$) δ 170.2, 153.3, 152.5 (d, *J* = 254.0 Hz), 150.3 (d, *J* = 2.8 Hz), 136.0 (d, *J* = 6.6 Hz), 133.5, 129.4 (d, *J* = 10.5 Hz), 114.4 (d, *J* = 2.4 Hz), 109.9 (d, *J* = 21.1 Hz), 54.0, 26.4, 24.3, 12.2, 11.8 ppm; ^{19}F NMR (376.5 MHz, $CDCl_3$) δ −131.18 ppm; HRMS (ESI-TOF) m/z: $[M + H]^+$ Calcd for $C_{16}H_{19}FN_4O$ 303.1621; Found 303.1602; IR (KBr, cm^{-1}) 993, 1081, 1387, 1453, 1482, 1621, 2856, 2931.

(*E*)-4-(2-((3,5-Dimethylisoxazol-4-yl)diazenyl)-3-fluorophenyl)- morpholine (1f). Orange solid, mp = 134−136 °C, Yield = 52.0 mg, 85%. Eluent: n-hexane/ethyl acetate = 98:2; ^{1}H NMR (400 MHz, $CDCl_3$) δ 7.27−7.21 (m, 1H), 6.90−6.83 (m, 2H), 3.82−3.80 (m, 4H), 3.11−3.10 (m, 4H), 2.74 (s, 3H), 2.52 (s, 3H) ppm; ^{13}C{^{1}H} NMR (100 MHz, $CDCl_3$) δ 170.7, 152.9, 152.7, (d, *J* = 255.1 Hz), 149.1, (d, *J* = 3.1 Hz), 136.0, (d, *J* = 6.7 Hz), 133.5, 129.8, (d, *J* = 10.4 Hz), 114.1, (d, *J* = 3.0 Hz), 110.9, (d, *J* = 21.0 Hz), 67.2, 52.8, 12.2, 11.8 ppm;. ^{19}F

NMR (376.5 MHz, $CDCl_3$) δ −130.47 ppm; HRMS (ESI-TOF) m/z: $[M + H]^+$ Calcd for $C_{15}H_{17}FN_4O_2$ 305.1414; Found 305.1414; IR (KBr, cm^{-1}) 800, 1001, 1108, 1170, 1235, 1256, 1379, 1412, 1449, 1597, 1617, 2824, 2877, 2931, 2972.

(*E*)-4-((2-Fluoro-6-(4-methylpiperazin-1-yl)phenyl)diazenyl)-3,5- dimethylisoxazole (1g). Orange solid, mp = 89−91 °C, Yield = 58.0 mg, 92%. Eluent: n-hexane/ethyl acetate = 98:2; ^1H NMR (400 MHz, $CDCl_3$) δ 7.21 (td, *J* = 8.3, 5.9 Hz, 1H), 6.88−6.79 (m, 2H), 3.13 (t, *J* = 4.8 Hz, 4H), 2.74 (s, 3H), 2.53 (o, 7H), 2.33 (s, 3H) ppm; $^{13}C\{^1H\}$ NMR (100 MHz, $CDCl_3$) δ 170.5, 153.0, 152.5, (d, *J* = 254.5 Hz), 149.1, (d, *J* = 3.3 Hz), 136.0, (d, *J* = 6.8 Hz), 133.5, 129.6, (d, *J* = 10.5 Hz), 114.3, (d, *J* = 3.0 Hz), 110.5, (d, *J* = 21.0 Hz), 55.4, 52.3, 46.2, 12.3, 11.8 ppm; 19F NMR (376.5 MHz, $CDCl_3$) δ −130.90 ppm; HRMS (ESI-TOF) m/z: $[M + H]^+$ Calcd for $C_{16}H_{21}FN_5O$ 318.1730; Found 318.1730; IR (KBr, cm^{-1}) 804, 1010, 1062, 1379, 1416, 1461, 1617, 1658, 2799, 2853, 2935.

General Procedure of Compound 1h, 1i

To the appropriate isoxazole derivative (0.2 mmol, 1 equiv) in an RB flask, the corresponding cyclic amine, pyrrolidine, or piperidine, (20 mmol, 100 equiv) was added. The mixture was stirred at 100 °C in an oil bath for 24 h. After checking the TLC for completion of the reaction, it was stopped and quenched with water. The mixture was extracted multiple times with ethyl acetate. The combined organic layers were collected and dried over anhydrous sodium sulfate. The distillation of solvent under vacuum led to the crude product. Further purification of the mixture was done over neutral alumina using a 98:2 mixture of n-hexane: ethyl acetate to give the desired products **1h, i**.

(*E*)-4-((2,4-Di(pyrrolidin-1-yl)phenyl)diazenyl)-3,5-dimethylisoxazole (1h). Orange solid, mp = 113−115 °C, Yield = 57.0 mg, 84%. Eluent: n-hexane/ethyl acetate = 98:2; ^1H NMR (400 MHz, $CDCl_3$) δ 7.72 (d, *J* = 8.8 Hz, 1H), 6.05 (d, *J* = 6.8 Hz, 1H), 5.75 (s, 1H), 3.59 (br, 4H), 3.38 (br, 4H), 2.61 (s, 3H), 2.45 (s, 3H), 1.99 (br, 8H) ppm; $^{13}C\{^1H\}$ NMR (100 MHz, $CDCl_3$) δ 163.1, 154.5, 150.6, 148.6, 134.3, 132.8, 118.7, 103.4, 95.8, 52.2, 47.7, 25.8, 25.5, 11.9, 11.6 ppm; HRMS (ESI-TOF) m/z: $[M + H]^+$ Calcd for $C_{19}H_{25}N_5O$ 340.2137, obs; Found 340.2137; IR (KBr, cm^{-1}) 792, 1063, 1116, 1170, 1363, 1461, 1609, 2853, 2931.

(*E*)-4-((2,6-Di(piperidin-1-yl)phenyl)diazenyl)-3,5-dimethylisoxazole (1i). Yellow solid, mp = 107−109 °C, Yield = 54.0 mg, 74%. Eluent: n-hexane/ethyl acetate = 98:2; ^1H NMR (400 MHz, $CDCl_3$) δ 7.16 (t, *J* = 8.1 Hz, 1H), 6.81 (d, *J* = 7.8 Hz, 2H), 2.87 (br, 8H), 2.74 (s, 3H), 2.55 (s, 3H), 1.49 (br, 12H) ppm; $^{13}C\{^1H\}$ NMR (100 MHz, $CDCl_3$) δ 168.8, 153.7, 146.3, 142.9, 133.4, 128.3, 114.1, 54.0, 26.5, 24.4, 12.3, 11.8 ppm; HRMS (ESI-TOF) m/z:

$[M + H]^+$ Calcd for $C_{21}H_{29}N_5O$ 368.2450; Found 368.2437; IR (KBr, cm^{-1}) 667, 730, 989, 1080, 1379, 1449, 1572, 1614, 2795, 2847, 2927. The single crystal of 1i has been grown in methanol by slow evaporation at room temperature.

General Procedure of Compound 2a-2c

The cyclic amines (10 mmol, 50 equiv) were added to (*E*)-4-((2-fluorophenyl)-diazenyl)-1,3,5-trimethyl-1H-pyrazole (0.2 mmol, 46.5 mg, 1 equiv). The mixture was stirred at 80 °C in an oil bath for 4 to 5 h. After checking the TLC for completion of the reaction, it was stopped and quenched with water. The mixture was extracted multiple times with ethyl acetate. The combined organic layers were collected and dried over anhydrous sodium sulfate. The distillation of solvent under vacuum led to the crude product. Further purification of the mixture was done over neutral alumina using a 98:2 mixture of n-hexane:ethyl acetate to give the desired products, **2a-c**.

(*E*)-1,3,5-Trimethyl-4-((2-(pyrrolidin-1-yl)phenyl)diazenyl)-1Hpyrazole (2a). Orange solid, mp = 98−100 °C, Yield = 48.0 mg, 84%. Eluent: n-hexane/ethyl acetate = 98:2; ^{1}H NMR (400 MHz, $CDCl_3$) δ 7.49 (d, *J* = 8.0 Hz, 1H), 7.20 (t, *J* = 7.8 Hz, 1H), 6.80 (d, *J* = 8.4 Hz, 1H), 6.71 (t, *J* = 7.5 Hz, 1H), 3.77 (s, 3H), 3.53 (t, *J* = 6.0 Hz, 4H), 2.54 (s, 3H), 2.45 (s, 3H), 1.96−1.92 (m, 4H) ppm; ^{13}C{^{1}H} NMR (100 MHz, $CDCl_3$) δ 145.8, 142.3, 141.1, 138.2, 135.8, 130.1, 117.6, 116.8, 115.3, 52.2, 36.1, 25.8, 13.9, 10.0 ppm; HRMS (ESI-TOF) m/z: $[M + H]^+$ Calcd for $C_{16}H_{21}N_5$ 284.1875; Found 284.1846; IR (KBr, cm^{-1}) 766, 950, 1274, 1419, 1480, 1613, 2819, 2852, 2936.

(*E*)-1-(2-((1,3,5-Trimethyl-1H-pyrazol-4-yl)diazenyl)phenyl)- piperidine (2b). Yellow solid, mp = 100−102 °C, Yield = 48.0 mg, 80%. Eluent: n-hexane/ethyl acetate = 98:2; ^{1}H NMR (400 MHz, $CDCl_3$) δ 7.54 (dd, *J* = 8.0, 1.1 Hz, 1H), 7.29 (o, 1H), 7.08 (d, *J* = 7.7 Hz, 1H), 6.99 (t, *J* = 7.5 Hz, 1H), 3.79 (s, 3H), 3.15 (br, 4H), 2.61 (s, 3H), 2.54 (s, 3H), 1.76 (br, 4H), 1.61−1.58 (m, 2H) ppm; ^{13}C{^{1}H} NMR (100 MHz, $CDCl_3$) δ 150.4, 146.5, 142.1, 139.0, 135.7, 130.1, 121.8, 118.8, 116.9, 54.3, 36.1, 26.6, 24.4, 14.0, 10.0 ppm; HRMS (ESI-TOF) m/z: $[M + H]^+$ Calcd for $C_{17}H_{23}N_5$ 298.2032; Found 298.2018; IR (KBr, cm^{-1}) 761, 924, 1231, 1413, 1494, 1588, 1617, 2816, 2857, 2936.

(*E*)-4-(2-((1,3,5-Trimethyl-1H-pyrazol-4-yl)diazenyl)phenyl)- morpholine (2c). Yellow solid, mp = 135−137 °C, Yield = 50.0 mg, 84%. Eluent: n-hexane/ethyl acetate = 98:2; ^{1}H NMR (400 MHz, $CDCl_3$) δ 7.57 (dd, *J* = 8.0, 1.6 Hz, 1H), 7.35−7.30 (m, 1H), 7.08− 7.03 (m, 2H), 3.91−3.89 (m, 3H), 3.79 (s, 4H), 3.25−3.22 (m, 4H), 2.60 (s, 3H), 2.51 (s, 3H) ppm; ^{13}C{^{1}H} NMR (100 MHz, $CDCl_3$) δ 149.0, 146.3, 141.7, 139.5, 135.8, 130.3, 122.5, 118.3,

117.0, 67.4, 53.0, 36.2, 14.1, 10.0 ppm; HRMS (ESI-TOF) m/z: $[M + H]^+$ Calcd for $C_{16}H_{21}N_5O$ 300.1813; Found 300.1824; IR (KBr, cm^{-1}) 912, 1112, 1223, 1383, 1403, 1618, 1641, 2861, 2918, 2976.

General Procedure of Compound 2d-2f

The azo derivative (*E*)-4-((2,6-difluorophenyl)diazenyl)-1,3,5-trimethyl-1*H*-pyrazole, **A2** (0.2 mmol, 50.3 mg, 1 equiv), was added to 2 mL of acetonitrile, and the required cyclic amine (1 mmol, 5 equiv) was added to the mixture. The mixture was stirred at 40 °C in an oil bath for 2−3 h. After checking the TLC for completion of the reaction, it was stopped and quenched with water. The mixture was extracted multiple times with ethyl acetate. The combined organic layers were collected and dried over anhydrous sodium sulfate. The distillation of solvent under vacuum led to the crude product. Further purification of the mixture was done over neutral alumina using a 98:2 mixture of n-hexane: ethyl acetate to give required products, **2d-f**.

(*E*)-4-((2-Fluoro-6-(pyrrolidin-1-yl)phenyl)diazenyl)-1,3,5-trimethyl-1*H*-pyrazole (2d). Orange sticky liquid, Yield = 51.0 mg, 85%. Eluent: n-hexane/ethyl acetate = 98:2; ^{1}H NMR (400 MHz, $CDCl_3$) δ 7.03 (td, *J* = 8.4, 6.1 Hz, 1H), 6.54−6.46 (m, 2H), 3.75 (s, 3H), 3.34 (t, *J* = 6.6 Hz, 4H), 2.53 (s, 3H), 2.43 (s, 3H), 1.90−1.87 (m, 4H) ppm; ^{13}C{^{1}H} NMR (100 MHz, $CDCl_3$) δ 153.3, (d, *J* = 249.2 Hz), 145.2 (d, *J* = 3.8 Hz), 141.4, 139.3, 135.9, 132.2 (d, *J* = 8.5 Hz), 128.0 (d, *J* = 11.3 Hz), 110.0 (d, *J* = 2.4 Hz), 104.6 (d, *J* = 21.7 Hz), 52.0, 36.0, 25.7, 13.9, 9.9 ppm; ^{19}F NMR (376.5 MHz, $CDCl_3$) δ −132.67 ppm; HRMS (ESI-TOF) m/z: $[M + H]^+$ Calcd for $C_{16}H_{20}FN_5$ 302.1781; Found 302.1757; IR (KBr, cm^{-1}) 899, 1076, 1666, 1387, 1449, 1597, 1650, 2869, 2923.

(*E*)-1-(3-Fluoro-2-((1,3,5-trimethyl-1*H*-pyrazol-4-yl)diazenyl)- phenyl)piperidine (2e). Orange solid, mp = 74−76 °C, Yield = 52.0 mg, 82%. Eluent: n-hexane/ethyl acetate = 98:2; ^{1}H NMR (400 MHz, $CDCl_3$) δ 7.1 (td, *J* = 8.3, 6.0 Hz, 1H), 6.83−6.73 (m, 2H), 3.78 (s, 3H), 3.02 (t, *J* = 5.1 Hz, 4H), 2.57 (s, 3H), 2.51 (s, 3H), 1.67−1.62 (m, 4H), 1.57−1.50 (o, 2H) ppm; ^{13}C{^{1}H} NMR (100 MHz, $CDCl_3$) δ 152.6 (d, *J* = 251.4 Hz), 149.8 (d, *J* = 3.6 Hz), 141.6, 139.7, 136.6 (d, *J* = 6.9 Hz), 136.1, 128.0 (d, *J* = 10.4 Hz), 114.0 (d, *J* = 2.8 Hz), 109.8 (d, *J* = 21.3 Hz), 53.6, 36.0, 26.3, 24.2, 14.0, 9.9 ppm; ^{19}F NMR (376.5 MHz, $CDCl_3$) δ −132.15 ppm; HRMS (ESI-TOF) m/z: $[M + H]^+$ Calcd for $C_{17}H_{22}FN_5$ 316.1928; Found 316.1937; IR (KBr, cm^{-1}) 778, 997, 1076, 1410, 1461, 1601, 2803, 2861, 2927.

(*E*)-4-(3-Fluoro-2-((1,3,5-trimethyl-1*H*-pyrazol-4-yl)diazenyl)- phenyl)morpholine (2f). Orange solid, mp = 80−82 °C, Yield = 53.0 mg, 84%. Eluent: n-hexane/ethyl acetate = 98:2;

^{1}H NMR (400 MHz, $CDCl_3$) δ 7.16 (td, *J* = 8.2, 6.0 Hz, 1H), 6.83 (t, *J* = 8.8 Hz, 2H), 3.79 (o, 7H), 3.09 (t, *J* = 4.5 Hz, 4H), 2.56 (s, 3H), 2.49 (s, 3H) ppm; ^{13}C{^{1}H} NMR (100 MHz, $CDCl_3$) δ 152.8, (d, *J* = 252.3 Hz) 148.5, (d, *J* = 3.6 Hz) 141.4, 140.2, 136.6 (d, *J* = 7.1 Hz), 136.1, 128.2 (d, *J* = 10.3 Hz), 113.6 (d, *J* = 2.9 Hz), 110.8 (d, *J* = 21.2 Hz), 67.1, 52.5, 36.1, 14.1, 9.8 ppm; ^{19}F NMR (376.5 MHz, $CDCl_3$) δ −131.53 ppm; HRMS (ESI-TOF) m/z: $[M + H]^+$ Calcd for $C_{16}H_{20}FN_5O$ 318.1730; Found 318.1730; IR (KBr, cm^{-1}) 742, 1000, 1118, 1409, 1468, 1514, 1602, 1631, 2857, 2918, 2980, 3054.

Procedure of Compound 2g

Piperidine (20 mmol, 100 equiv, 1.72 mL) was added to (*E*)-4-((2,6-difluorophenyl)diazenyl)-1,3,5- trimethyl-1*H*-pyrazole, **B2** (0.2 mmol, 50.1 mg, 1 equiv). The mixture was stirred at 100 °C in an oil bath for 24 h. After checking the TLC for completion of the reaction, the reaction was stopped and quenched with water. The mixture was extracted multiple times with ethyl acetate. The combined organic layers were collected and dried over anhydrous sodium sulfate. The distillation of solvent under vacuum led to the crude product. Further purification of the mixture was done over neutral alumina using a 98:2 mixture of n-hexane:ethyl acetate to give the desired product.

(*E*)-1,1′-(2-((1,3,5-Trimethyl-1*H*-pyrazol-4-yl)diazenyl)-1,3- phenylene)dipiperidine (2g). Orange solid, mp = 134−136 °C, Yield = 53.0 mg, 70%. Eluent: n-hexane/ethyl acetate = 98:2; ^{1}H NMR (400 MHz, $CDCl_3$) δ 7.10 (t, *J* = 8.1 Hz, 1H), 6.78 (d, *J* = 8.1 Hz, 2H), 3.80 (s, 3H), 2.86 (t, *J* = 4.1 Hz, 8H), 2.57 (s, 3H), 2.52 (s, 3H), 1.51−1.41 (m, 12H), 1.25 (br, 2H) ppm; ^{13}C{^{1}H} NMR (100 MHz, $CDCl_3$) δ 146.1, 143.9, 141.9, 138.3, 136.0, 127.1, 114.2, 53.7, 36.1, 26.5, 24.4, 14.0, 10.1 ppm; HRMS (ESI-TOF) m/z: $[M + H]^+$ Calcd for $C_{22}H_{32}N_6$ 381.2767; Found 381.2766; IR (KBr, cm^{-1}) 730, 1082, 1387, 1457, 1576, 1629, 2849, 2926.

General Procedure of Compound 3a, b

The required cyclic amines, **Am** (10.0 mmol, 50 equiv), was added to (*E*)-2-((2-fluorophenyl)diazenyl)-1-methyl-1*H*-pyrrole, **C1** (0.2 mmol, 40.6 mg). The mixture was stirred at 80 °C in an oil bath for 4 to 5 h. After checking the TLC for completion of the reaction, it was stopped and quenched with water. The mixture was extracted multiple times with ethyl acetate. The combined organic layers were collected and dried over anhydrous sodium sulfate. The distillation of solvent under vacuum led to the crude product. Further purification of the mixture was done over neutral alumina using a 98:2 mixture of n-hexane: ethyl acetate to give the desired products **3a, b**.

(*E*)-1-Methyl-2-((2-(pyrrolidin-1-yl)phenyl)diazenyl)-1*H*-pyrrole (3a). Red gummy solid, mp = 74−76 °C, Yield = 47.0 mg, 93%. Eluent: n-hexane/ethyl acetate = 98:2; ^{1}H NMR (400 MHz, $CDCl_3$) δ 7.71 (dd, *J* = 8.2, 1.6 Hz, 1H), 7.21 (ddd, *J* = 8.5, 6.9, 1.6 Hz, 1H), 6.86−6.80 (m, 2H), 6.70 (ddd, *J* = 8.1, 7.0, 1.2 Hz, 1H), 6.45 (dd, *J* = 4.0, 1.6 Hz, 1H), 6.25 (dd, *J* = 4.0, 2.7 Hz, 1H), 3.98 (s, 3H), 3.62 (m, 4H), 1.98 (m, 4H) ppm; ^{13}C{^{1}H} NMR (100 MHz, $CDCl_3$) δ 147.6, 146.6, 141.1, 130.6, 124.7, 116.6, 116.5, 115.6, 109.4, 97.4, 52.5, 33.2, 26.0 ppm; HRMS (ESI-TOF) m/z: $[M + H]^+$ Calcd for $C_{15}H_{18}N_4$. 255.1610; Found 255.1594; IR (KBr, cm^{-1}) 599, 740, 1050, 1070, 1287, 1491, 1599, 2853, 2925.

(*E*)-1-(2-((1-Methyl-*1H*-pyrrol-2-yl)diazenyl)phenyl)piperidine (3b). Red sticky liquid, Yield = 48.0 mg, 90%. Eluent: n-hexane/ethyl acetate = 98:2; ^{1}H NMR (400 MHz, $CDCl_3$) δ 7.57 (dd, *J* = 8.0, 1.6 Hz, 1H), 7.30−7.27 (o, 1H), 7.05 (dd, *J* = 8.2, 1.0 Hz, 1H), 6.96 (ddd, *J* = 8.3, 7.3, 1.2 Hz, 1H), 6.91−6.90 (m, 1H), 6.69 (dd, *J* = 4.2, 1.6 Hz, 1H), 6.27 (dd, *J* = 4.1, 2.6 Hz, 1H), 3.98 (s, 3H), 3.14 (m, 4H), 1.80 (p, *J* = 6.0 Hz, 4H), 1.63−1.58 (o, 2H) ppm; ^{13}C{^{1}H} NMR (100 MHz, $CDCl_3$) δ 150.6, 147.4, 145.5, 130.2, 126.1, 121.4, 118.6, 116.7, 110.0, 99.5, 54.6, 33.4, 26.5, 24.5 ppm; HRMS (ESI-TOF) m/z: $[M + H]^+$ Calcd for $C_{16}H_{20}N_4$. 269.1766; Found 269.1752; IR (KBr, cm^{-1}) 1062, 1170, 1313, 1387, 1650, 2931.

General Procedure of Compound 3c, d. (*E*)-2-((2,6- Difluorophenyl)diazenyl)-1-methyl-1*H*-pyrrole C2

(0.2 mmol, 44.2 mg, 1 equiv) was added to 2 mL of acetonitrile, and the corresponding cyclic amine (1 mmol, 5 equiv) was added to the mixture. The mixture was stirred at 40 °C in an oil bath for 2 to 3 h. After checking the TLC for completion of the reaction, it was stopped and quenched with water. The mixture was extracted multiple times with ethyl acetate. The combined organic layers were collected and dried over a layer of sodium sulfate. The distillation of solvent under vacuum led to the crude product. Further purification of the mixture was done over neutral alumina using a 98:2 mixture of n-hexane:ethyl acetate to give desired products **3c, d**.

(*E*)-2-((2-Fluoro-6-(pyrrolidin-1-yl)phenyl)diazenyl)-1-methyl-1*H*-pyrrole (3c). Sticky red liquid, Yield = 54.0 mg, 94%. Eluent: n-hexane/ethyl acetate = 98:2; ^{1}H NMR (400 MHz, $CDCl_3$) δ 7.02 (td, *J* = 8.3, 6.0 Hz, 1H), 6.90−6.89 (m, 1H), 6.55−6.53 (m, 1H), 6.50 (dd, *J* = 4.1, 1.6 Hz, 1H), 6.46 (ddd, *J* = 11.8, 8.2, 1.0 Hz, 1H), 6.26 (dd, *J* = 4.1, 2.6 Hz, 1H), 3.93 (s, 3H), 3.48−3.45 (m, 4H), 1.94− 1.90 (m, 4H) ppm; ^{13}C{^{1}H} NMR (100 MHz, $CDCl_3$) δ 153.4, (d, *J* = 254.1 Hz), 147.6, 147.0, (d, *J* = 4.5 Hz), 131.1 (d, *J* = 7.3 Hz), 128.5 (d, *J* = 11.3 Hz), 125.8, 110.3, (d, *J* = 2.8 Hz), 109.7, 104.6, (d, *J* = 21.2 Hz), 97.6, 52.4, 33.3, 25.9 ppm; ^{19}F

NMR (376.5 MHz, $CDCl_3$) δ −130.01 ppm HRMS (ESI-TOF) m/z: $[M+H]^+$ Calcd for $C_{15}H_{17}FN_4$ 273.1515; Found 273.1507; IR (KBr, cm^{-1}) 1170, 1387, 1457, 1473, 1617, 1629, 2861, 2931.

(*E*)-1-(3-Fluoro-2-((1-methyl-1*H*-pyrrol-2-yl)diazenyl)phenyl)- piperidine (3d). Sticky red liquid, Yield = 50.0 mg, 88%. Eluent: n-hexane/ethyl acetate = 98:2; ^1H NMR (400 MHz, $CDCl_3$) δ 7.13 (td, J = 8.2, 6.0 Hz, 1H), 6.94 (br, 1H), 6.81 (d, *J* = 8.3 Hz, 1H), 6.76− 6.71 (m, 2H), 6.29 (dd, *J* = 3.7 Hz, *J* = 2.7 Hz, 1H), 3.94 (s, 3H), 3.04 (t, *J* = 5.2 Hz, 4H), 1.73 (p, *J* = 5.9 Hz, 4H), 1.60−1.54 (pt, *J* = 5.5 Hz, 2H) ppm; $^{13}C\{^1H\}$ NMR (100 MHz, $CDCl_3$) δ 152.7, (d, *J* = 254.8 Hz), 150.8, (d, *J* = 3.8 Hz), 147.4, 135.0, (d, *J* = 6.3 Hz), 128.4, (d, *J* = 10.4 Hz), 126.6, 113.7 (d, *J* = 2.8 Hz), 110.2, 109.5, (d, *J* = 21.0 Hz), 98.9, 54.2, 33.2, 26.3, 24.3 ppm; ^{19}F NMR (376.5 MHz, $CDCl_3$) δ −130.41 ppm; HRMS (ESI-TOF) m/z: $[M + H]^+$ Calcd for $C_{16}H_{19}FN_4$ 287.1672; Found 287.1658; IR (KBr, cm^{-1}) 1170, 1387, 1457, 1473, 1617, 1629, 2861, 2931.

Procedure for Compound 4

Pyrrolidine (10 mmol, 0.8 mL) was added to (*E*)-4-((2-fluorophenyl)diazenyl)-3,5-diphenylisoxazole, **D** (0.2 mmol, 68.7 mg). The mixture was stirred at 70 °C in an oil bath for 4 h. After checking the TLC for completion of the reaction, it was stopped and quenched with water. The mixture was extracted multiple times with ethyl acetate. The combined organic layers were collected and dried over anhydrous sodium sulfate. The distillation of solvent under vacuum led to the crude product. Further purification of the mixture was done over neutral alumina using a 98:2 mixture of n-hexane:ethyl acetate to give the crystalline solid **4**.

(*E*)-3,5-Diphenyl-4-((2-(pyrrolidin-1-yl)phenyl)diazenyl)isoxazole (4). Orange solid, mp = 110−112 °C, Yield = 69.4 mg, 88%. Eluent: n-hexane/ethyl acetate = 98:2; ^1H NMR (400 MHz, $CDCl_3$) δ 8.18 (d, *J* = 7.8 Hz, 2H), 7.79 (d, *J* = 8.4 Hz, 1H), 7.55−7.49 (m, 6H), 7.40 (br, 4H), 6.76 (br, 1H), 2.93 (br, 4H), 1.61 (o, 4H) ppm; $^{13}C\{^1H\}$ NMR (100 MHz, $CDCl_3$) δ 164.5, 156.6, 147.2, 140.1, 132.6, 132.3, 130.4, 129.7, 129.05, 129.00, 128.9, 128.5, 128.0, 127.8, 117.0, 116.4, 115.9, 51.4, 25.7 ppm; HRMS (ESI-TOF) m/z: $[M + H]^+$ Calcd for $C_{25}H_{22}N_4O$ 395.1872; Found 395.1861; IR (KBr, cm^{-1}) 1076, 1166, 1387, 1449, 1560, 1641, 2857, 2927.

Procedure of Compound 5

Pyrrolidine (10 mmol, 0.8 mL) was added to (*E*)-4-((2-fluorophenyl)diazenyl)-1-methyl-3,5-diphenyl1-*H*-pyrazole, **E** (0.2 mmol, 71.2 mg). The mixture was stirred at 70 °C in an oil bath for 4 h. After checking the TLC for completion ofthe reaction, it was stopped

and quenched with water. The mixture was extracted multiple times with ethyl acetate. The combined organic layers were collected and dried over anhydrous sodium sulfate. The distillation of solvent under vacuum led to the crude product. Further purification of the mixture was done over neutral alumina using a 98:2 mixture of n-hexane:ethyl acetate to give a crystalline solid **5**. The single crystal has been grown in methanol by slow evaporation at room temperature.

(*E*)-1-Methyl-3,5-diphenyl-4-((2-(pyrrolidin-1-yl)phenyl)- diazenyl)-1*H*-pyrazole (5). Orange solid, mp = 110−112 °C, Yield = 67.0 mg, 82%. Eluent: n-hexane/ethyl acetate = 98:2; ^{1}H NMR (400 MHz, $CDCl_3$) δ 7.97 (d, *J* = 6.6 Hz, 2H), 7.66 (d, *J* = 7.8 Hz, 1H), 7.44−7.33 (m, 8H), 7.17 (t, *J* = 5.6 Hz, 1H), 6.67−6.59 (m, 2H), 3.82 (s, 3H), 2.84 (br, 4H), 1.59 (o, 4H) ppm; ^{13}C{^{1}H} NMR (100 MHz, $CDCl_3$) δ 146.9, 146.4, 140.6, 135.4, 134.9, 133.2, 131.1, 130.4, 130.0, 128.8, 128.6, 128.4, 128.3, 127.8, 117.2, 115.8, 115.6, 51.2, 37.6, 25.6 ppm; HRMS (ESI-TOF) m/z: $[M + H]^+$ Calcd for $C_{26}H_{25}N_5$ 408.2188; Found 408.2176; IR (KBr, cm^{-1}) 739, 1095, 1170, 1187, 1383, 1476, 1596, 1646, 2861, 2931.

2.7 Conclusions

In summary, we have synthesized 22 visible light photoswitchable azoheteroarenes in high yields through modular synthesis. We have evaluated the structure-property relationships through a systematic variation in the substituents and azoheteroarenes (**Figure 2.4**). The significant outcomes of the studies are as follows: (1) The *ortho* amination in the azoheteroarenes tremendously influenced the n–π* band through enhancement and red-shift, which enables visible light photoswitching. (2) The wavelengths for the forward photoisomerization (*E*-*Z*) solely depend on the heterocycles; in particular, electron-rich *N*-methylpyrrole or highly conjugated diphenyl-substituted pyrazole/isoxazole units can isomerize with longer wavelengths than typical UV/blue light. (3) For the reverse isomerization steps, besides the heterocycles, the substitution pattern equally dictates the choice of wavelength. Again, the diphenyl substituted pyrazole/isoxazole units render isomerization under red light. (4) An additional *ortho* fluorination (**Type B**) or changing the cyclic amine from five-membered to six-membered ring systems (**Type A**) accounts for the need of blue-shifted wavelengths in the reverse isomerization step. (5) Among the heterocycles, only *N*-methylpyrrole derivatives exhibit fast thermal relaxation and in all cases, the additional *ortho* fluorination (**Type B**) can enhance the half-life of the *Z*-isomer irrespective of the heterocycle present.

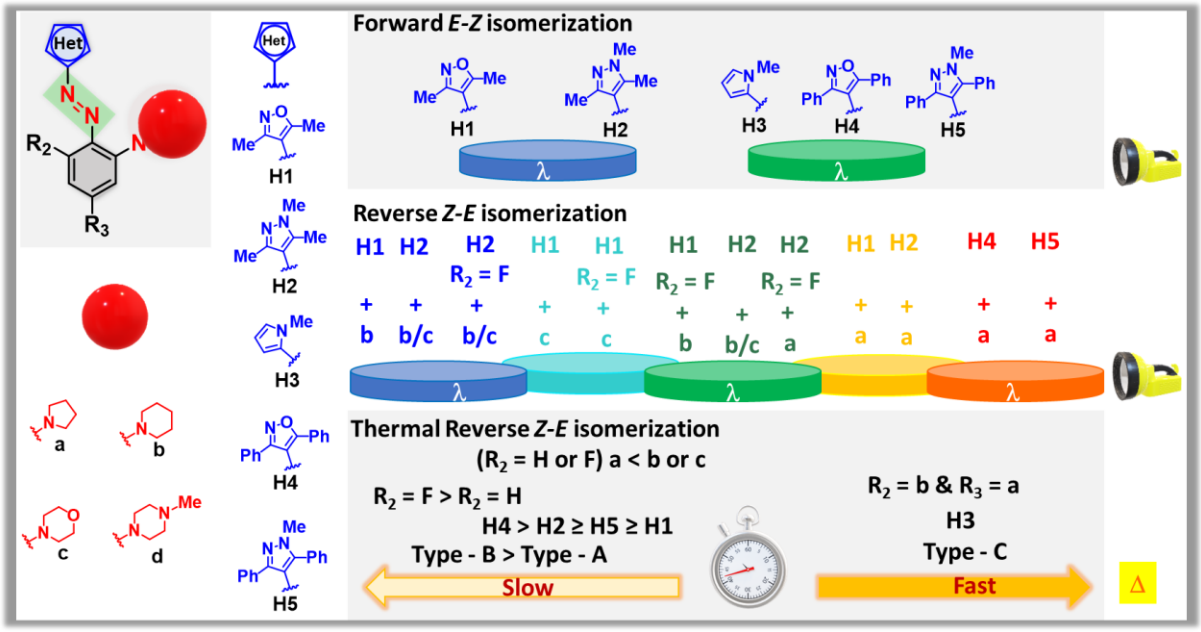

Figure 2.4. Summary depicting the structure-property relationship of azoheteroarene photoswitches.

(6) The thermal relaxation rate of the isomers follows the trend **Type B** < **Type A** < **Type C**.Thus, we deciphered that *ortho* amination and the choice of heterocycle are the critical factors influencing the bidirectional visible light photoswitching, whereas an additional fluorine substitution at *ortho* position can enhance the thermal stability of the *Z*-isomer. Also, the substitution pattern along with heterocycles is vital in tuning the half-lives of the *Z*-isomers. We also unraveled a new class of 3,5-diphenylheteroazoarenes capable of bidirectional visible light photoswitching and possessing longer half-lives of the *Z*-isomer. To the best of our knowledge, there are no reports on azoheteroarene that can switch in both directions under longer wavelengths compared to blue light irradiation conditions and concurrently unveiling extended thermal stability of the photoswitched state.

2.8 References

1. (a) García-Amorós, J.; Velasco, D, Beilstein *J. Org. Chem.* **2012**, *8*, 1003−1017. (b) Blanco, V.; Leigh, D. A.; Marcos, V. *Chem. Soc. Rev.* **2015**, *44*, 5341−5370. (c) Crespi, S.; Simeth, N. A.; König, B. *Nat. Rev. Chem.* **2019**, *3*, 133−146. (d) Grewal, S.; Gupta, D.; Gaur, A. K.; Saraswat, M.; Venkataramani, S. Photoisomerization: Causes, Behavior and Effects; Nova Publishers: New York, 2019.
2. For selected examples, see (a) Weston, C. E.; Richardson, R. D.; Haycock, P. R.; White, A. J. P.; Fuchter, M. J. *J. Am. Chem. Soc.* **2014**, *136*, 11878−11881. (b) Simeth, N. A.; Crespi, S.; Fagnoni, M.; König, B. *J. Am. Chem. Soc.* **2018**, *140*, 2940−2946. (c) Slavov, C.; Yang, C.; Heindl, A. H.; Wegner, H. A.; Dreuw, A.; Wachtveitl, J. *Angew. Chem., Int. Ed.* **2020**, *59*, 380− 387. (d) Tuck, J. R.; Tombari, R. J.; Yardeny, N.; Olson, D. E. *Org. Lett.* **2021**, *23*, 4305−4310. (e) Prischich, D.; Gomila, A. M. J.;

MillaNavarro, S.; Sangüesa, G.; Diez-Alarcia, R.; Preda, B.; Matera, C.; Batlle, M.; Ramírez, L.; Giralt, E.; Hernando, J.; Guasch, E.; Meana, J. J.; de la Villa, P.; Gorostiza, P. *Angew. Chem., Int. Ed.* **2021**, *60*, 3625− 3631. (f) Kumar, P.; Srivastava, A.; Sah, C.; Devi, S.; Vekataramani, S. *Chem. − Eur. J.* **2019**, *25*, 11924−11932. (g) Kortekaas, L.; Simke, J.; Kurka, D. W.; Ravoo, B. J. *ACS Appl. Mater. Interfaces.* **2020**, *12*, 32054−32060. (h) Gerkman, M. A.; Gibson, R. S. L.; Calbo, J.; Shi, Y.; Fuchter, J.; Han, G. G. D. *J. Am. Chem. Soc.* **2020**, *142*, 8688−8695. (i) Nagai, Y.; Ishiba, K.; Yamamoto, R.; Yamada, T.; Morikawa, M.; Kimizuka, N. *Angew. Chem., Int. Ed.* **2021**, *60*, 6333−6338.

3. For example, see: (a) Fuchter, M. J. *J. Med. Chem.* **2020**, *63*, 11436−11447. (b) Velema, W. A.; Szymanski, W.; Feringa, B. L. *J. Am. Chem. Soc.* **2014**, *136*, 2178−2191. (c) Mafy, N. N.; Matsuo, K.; Hiruma, S.; Uehara, R.; Tamaoki, N. *J. Am. Chem. Soc.* **2020**, *142*, 1763−1767.
4. (a) Chen, H.; Chen, W.; Lin, Y.; Xie, Y.; Liu, S. H.; Yin, J *Chin. Chem. Lett.* **2021**, *32*, 2359−2368. (b) Siewertsen, R.; Neurmann, H.; Stehn, B. S.; Herges, R.; Nather, C.; Renth, F.; Temps, F. *J. Am. Chem. Soc.* **2009**, *131*, 15594−15595.
5. For example, see: (a) Bléger, D.; Schwarz, J.; Brouwer, A. M.; Hecht, S. *J. Am. Chem. Soc.* **2012**, *134*, 20597−20600. (b) Bléger, D.; Hecht, S. *Angew. Chem., Int. Ed.* **2015**, *54*, 11338−11349. (c) Calbo, J.; Thawani, A. R.; Gibson, R. S. L.; White, A. J. P.; Fuchter, M. J. *J. Org. Chem.* **2019**, *15*, 2753−2764.
6. (a) Samanta, S.; Beharry, A. A.; Sadovski, O.; McCormick, T. M.; Babalhavaeji, A.; Tropepe, V.; Woolley, G. A. *J. Am. Chem. Soc.* **2013**, *135*, 9777− 9784. (b) Beharry, A. A.; Sadovski, O.; Woolley, G. A. *J. Am. Chem. Soc.* **2011**, *133*, 19684−19687. (c) Dong, M.; Babalhavaeji, A.; Collins, C. V.; Jarrah, K.; Sadovski, O.; Dai, Q.; Woolley, G. A. *J. Am. Chem. Soc.* **2017**, *139*, 13483−13486.
7. Samanta, S.; McCormick, T. M.; Schmidt, S. K.; Seferos, D. S.; Woolley, G. A. *Chem. Commun.* **2013**, *49*, 10314−10316.
8. (a) Sadovski, O.; Beharry, A. A.; Zhang, F.; Woolley, G. A. *Angew. Chem., Int. Ed.* **2009**, *48*, 1484−1486. (b) Ahmed, Z.; Siiskonen, A.; Virkki, M.; Priimagi, A. *Chem. Commun.* **2017**, *53*, 12520−12523. (c) Kuntze, K.; Viljakka, J.; Titov, E.; Ahmed, Z.; Kalenius, E.; Saalfrank, P.; Priimagi, A. *Photochem. Photobiol. Sci.* **2022**, *21*, 159−173.
9. For example, see (a) Dong, M.; Babalhavaeji, A.; Samanta, S.; Beharry, A. A.; Woolley, G. A. *Acc. Chem. Res.* **2015**, *48*, 2662−2670. (b) Garcia-Amorós, J.; Castro, M. C. R.; Coelho, P.; Raposo, M. M. M.; Velasco, D. *Chem. Commun.* **2013**, *49*, 11427−11429.
10. Yang, Y.; Hughes, R. P.; Aprahamian, I. *J. Am. Chem. Soc.* **2014**, *136*, 13190− 13193.
11. (a) Muñoz-Rugeles, L.; Gallardo-Rosas, D.; Durán-Hernández, J.; López-Arteaga, R.; Toscano, R. A.; Esturau-Escofet, N.; LópezCortés, J. G.; Peón, G.; Ortega-Alfaro, M. C. *ChemPhotoChem* **2020**, *3*, 1−12. (b) BalamVillarreal, J. A.; López-Mayorga, B. J.; Gallardo-Rosas, D.; Toscano, R. A.; Carreón-Castro, M. P.; Basiuk, V. A.; Ortega-Alfaro, M. C. *Org. Biomol. Chem.* **2020**, *18*, 1657− 1670. (c) Weston, C. E.; Richardson, R. D.; Fuchter, M. J. *Chem. Commun.* **2016**, *52*, 4521−4524. (d) Kennedy, A. D. W.; Sandler, I.; Andréasson, J.; Ho, J.; Beves, J. E. *Chem. Eur. J.* **2020**, *26*, 1103−1110.
12. Knie, C.; Utecht, M.; Zhao, F.; Kulla, H.; Kovalenko, S.; Brouwer, A. M.; Saalfrank, P.; Hecht, S.; Bléger, D. *Chem. − Eur. J.* **2014**, *20*, 16492−16501.
13. (a) Calbo, J.; Weston, C. E.; White, A. J. P.; Rzepa, H. S.; Contreras-García, J.; Fuchter, M. J. *J. Am. Chem. Soc.* **2017**, *139*, 1261−1274. (b) Devi, S.; Saraswat, M.; Grewal, S.; Venkataramani, S. *J. Org. Chem.* **2018**, *83*, 4307−4322.

14. Bhunia, S.; Dolai, A.; Samanta, S. *Chem. Commun.* **2020**, *56*, 10247−10250.
15. Simke, J.; Bösking, T.; Ravoo, B. J. *Org. Lett.* **2021**, *23*, 19, 7635− 7639.
16. Two products characterized by **1i** and **5** were single-crystal XRD (for details, see Appendix).

Appendix 2A

2A.1. Analysis of photoswitching and thermal stability aspects using UV-vis spectroscopy

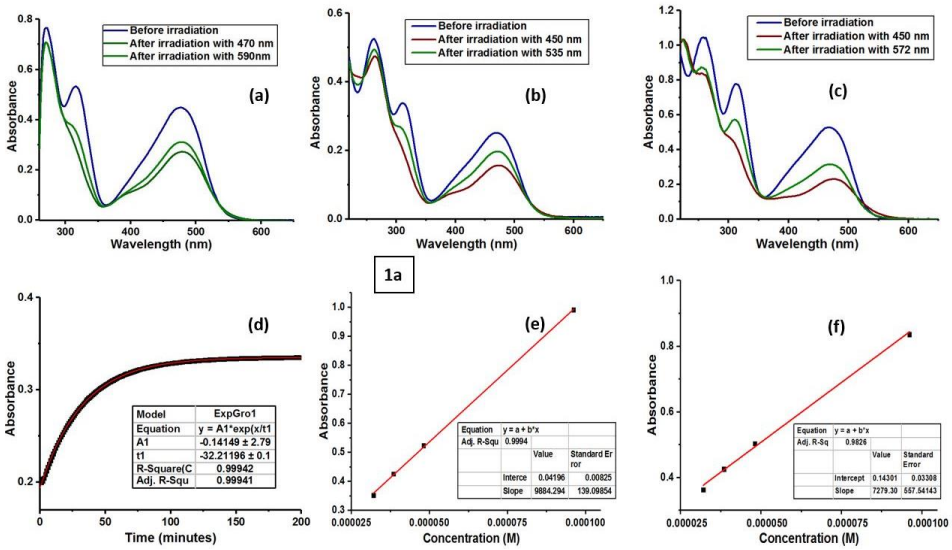

Figure 2A.1.1. Photoswitching behavior of 1a. Forward and reverse isomerization (a) in DMSO (61.9 μM); (b) in MeCN (46.2 μM), and (c) in MeOH (71.4 μM) at the indicated wavelengths; (d) Thermal reverse isomerization kinetics of 1a (DMSO, 50 °C, monitored at λ = 475 nm); Estimation of the molar absorption coefficient of 1a in DMSO at (e) 315 nm, and (f) 475 nm.

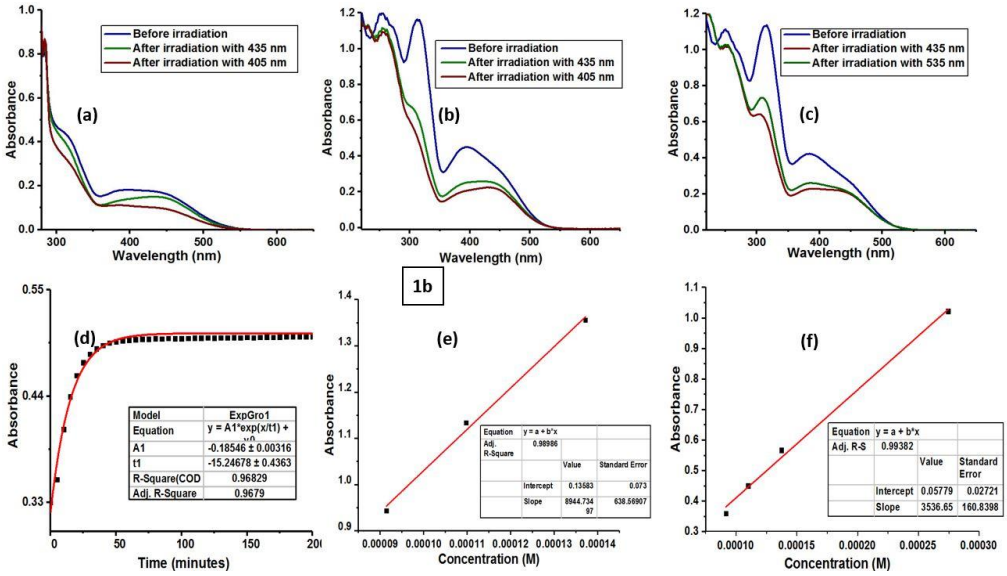

Figure 2A.1.2. Photoswitching behavior of 1b. Forward and reverse isomerization (a) in DMSO (47.0 μM); (b) in MeCN (62.5 μM), and (c) in MeOH (56.2 μM) at the indicated wavelengths; (d) Thermal reverse isomerization kinetics of 1b (DMSO, 80 °C, monitored at λ = 316 nm); Estimation of the molar absorption coefficient of 1b in DMSO at (e) 316 nm, and (f) 402 nm.

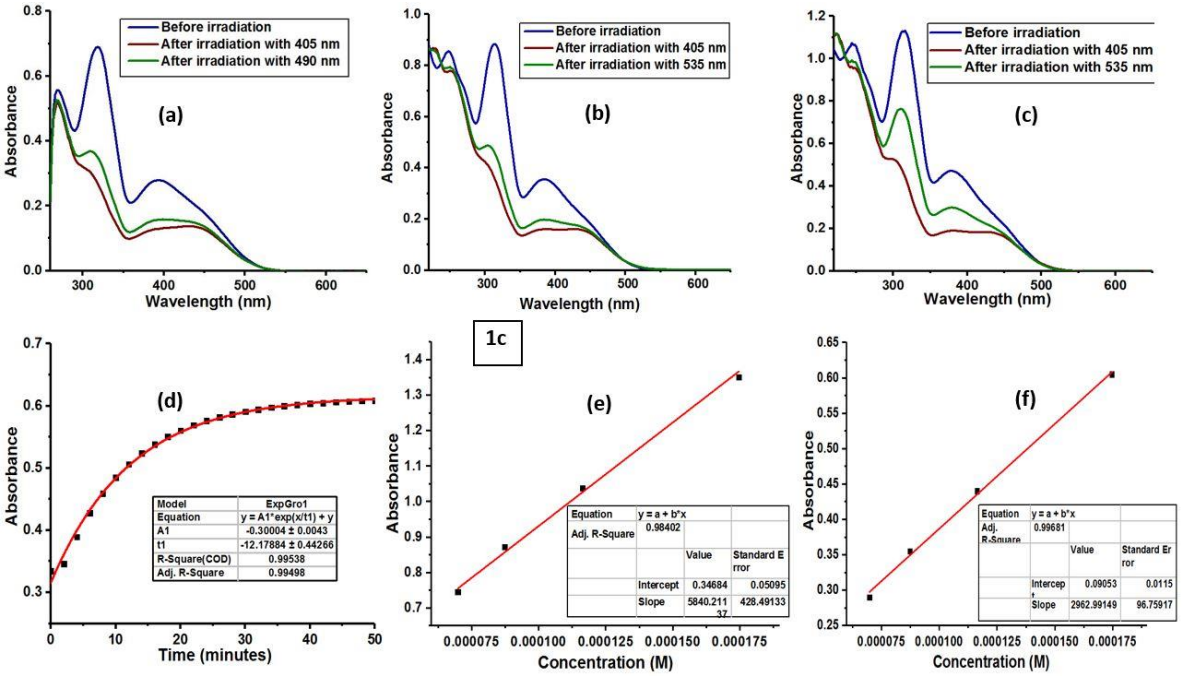

Figure 2A.1.3. Photoswitching behavior of **1c.** Forward and reverse isomerization (a) in DMSO (118.1 μM); (b) in MeCN (129.8 μM), and (c) in MeOH (125.0 μM) at the indicated wavelengths; (d) Thermal reverse isomerization kinetics of **1c** (DMSO, 80 ^{o}C, monitored at λ = 319 nm); Estimation of the molar absorption coefficient of **1c** in DMSO at (e) 319 nm, and (f) 392 nm.

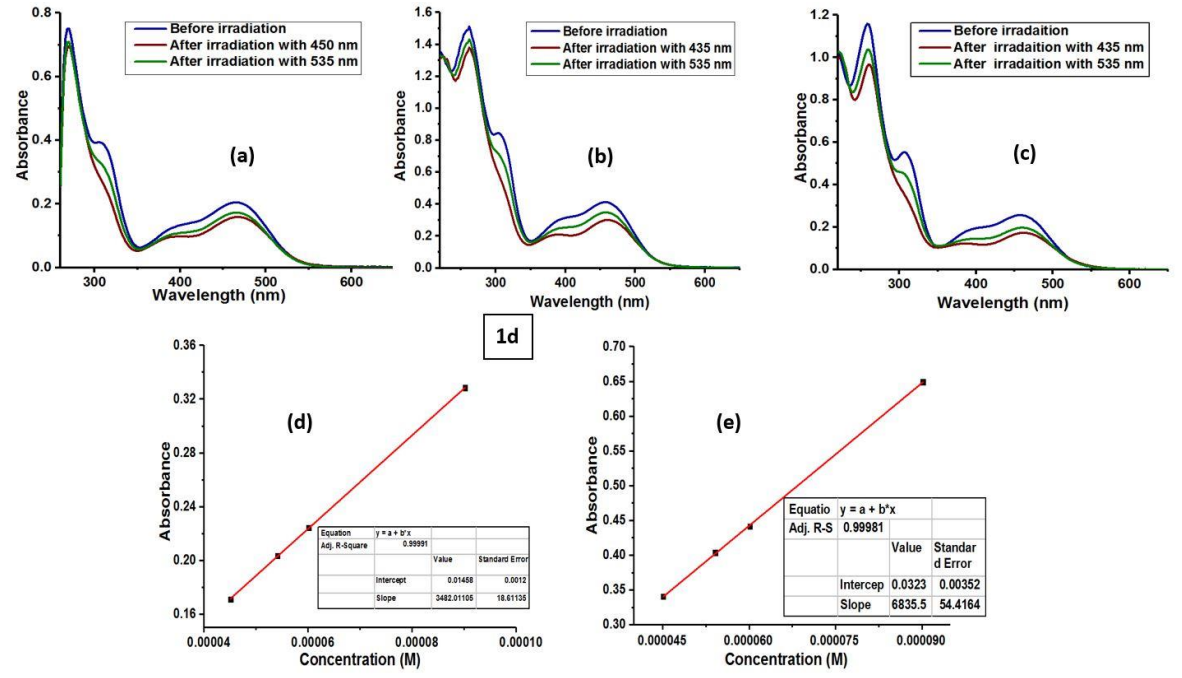

Figure 2A.1.4. Photoswitching behavior of **1d.** Forward and reverse isomerization (a) in DMSO (29.3 μM); (b) in MeCN (66.0 μM), and (c) in MeOH (60.3 μM) at the indicated wavelengths; Estimation of the molar absorption coefficient of **1d** in DMSO at (d) 311 nm, and (e) 465 nm.

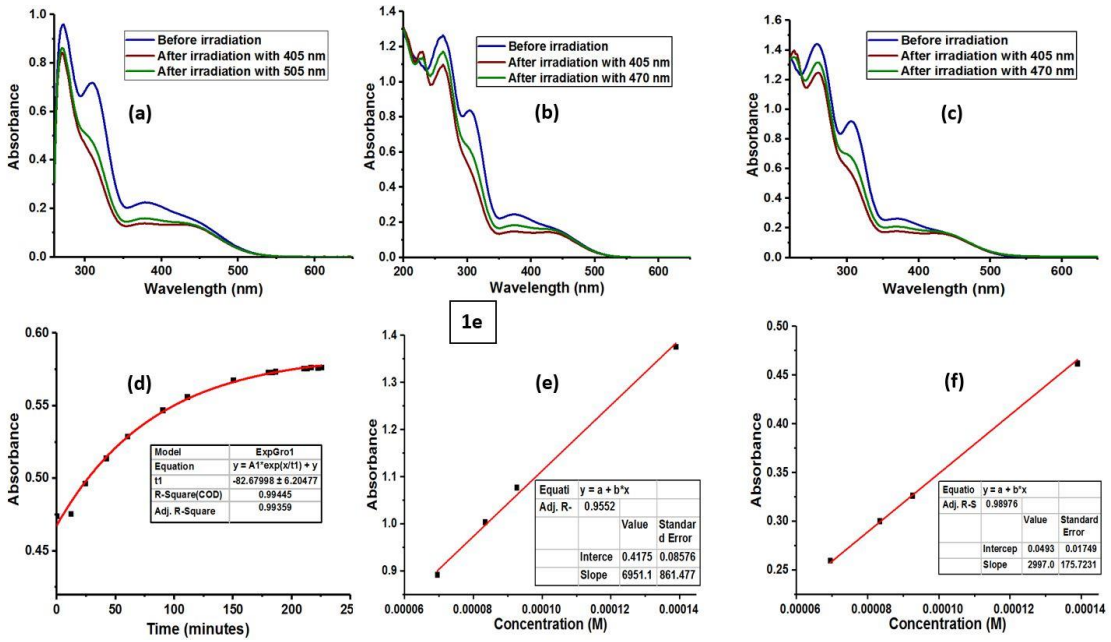

Figure 2A.1.5. Photoswitching behavior of **1e.** Forward and reverse isomerization (a) in DMSO (103.5 μM); (b) in MeCN (116.7 μM), and (c) in MeOH (100.7 μM) at the indicated wavelengths; (d) Thermal reverse isomerization kinetics of **1e** (DMSO, 80 °C, monitored at λ = 310 nm); Estimation of the molar absorption coefficient of **1e** in DMSO at (e) 310 nm, and (f) 379 nm.

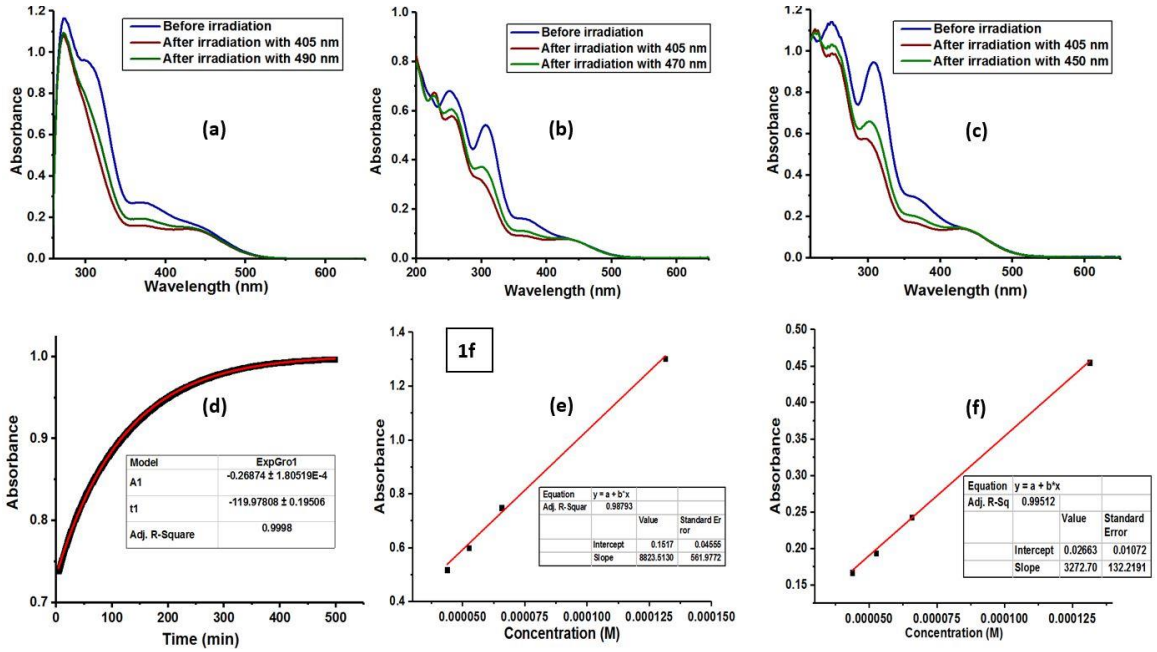

Figure 2A.1.6. Photoswitching behavior of **1f.** Forward and reverse isomerization (a) in DMSO (109.0 μM); (b) in MeCN (120.2 μM), and (c) in MeOH (109.9 μM) at the indicated wavelengths; (d) Thermal reverse isomerization kinetics of **1f** (DMSO, 80 °C, monitored at λ = 304 nm); Estimation of the molar absorption coefficient of **1f** in DMSO at (e) 304 nm, and (f) 372 nm.

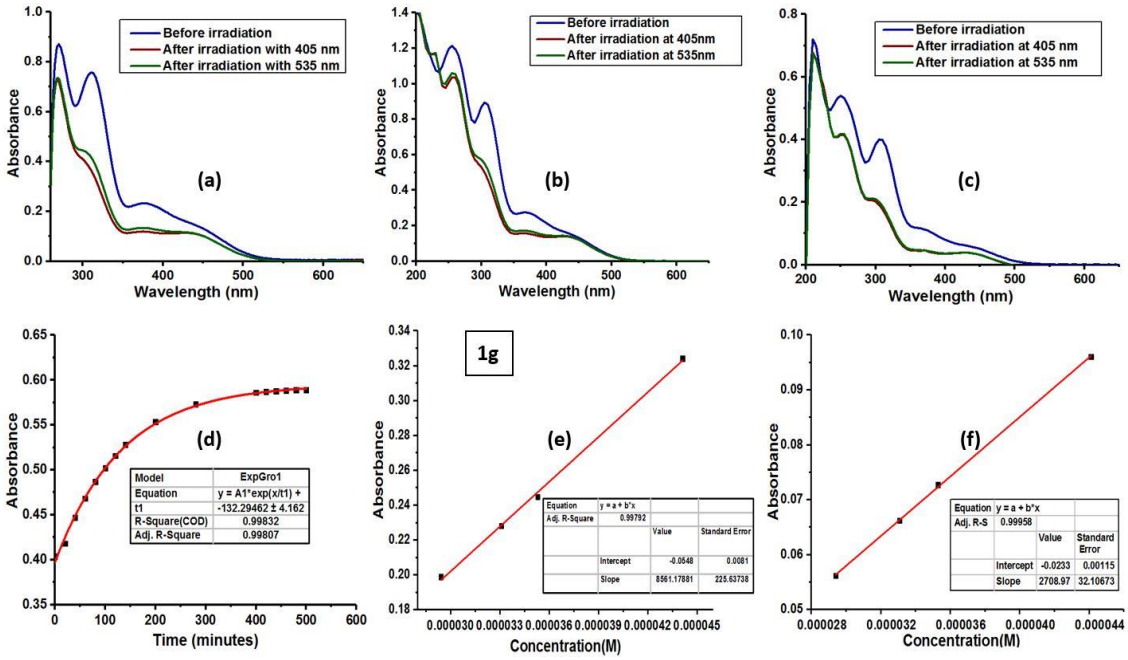

Figure 2A.1.7. Photoswitching behavior of **1g.** Forward and reverse isomerization (a) in DMSO (88.8 μM); (b) in MeCN (95.5 μM), and (c) in MeOH (77.8 μM) at the indicated wavelengths; (d) Thermal reverse isomerization kinetics of **1g** (DMSO, 80 ^{o}C, monitored at λ = 311 nm); Estimation of the molar absorption coefficient of **1g** in DMSO at (e) 311 nm, and (f) 378 nm.

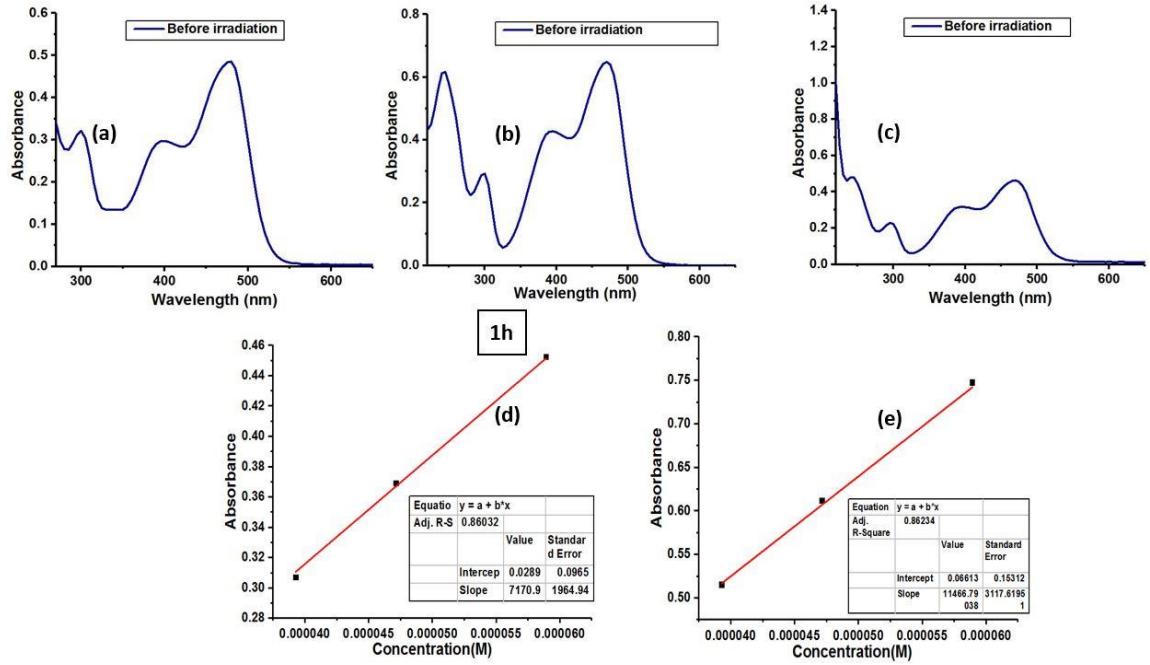

Figure 2A.1.8. Photoswitching behavior of **1h.** Absorption spectra of **1h** (a) in DMSO (42.6 μM); (b) in MeCN (56.7 μM), and (c) in MeOH (69.7 μM) (Note that the sample exhibited no photoisomerization); Estimation of the molar absorption coefficient of **1h** in DMSO at (d) 400 nm, and (e) 480 nm.

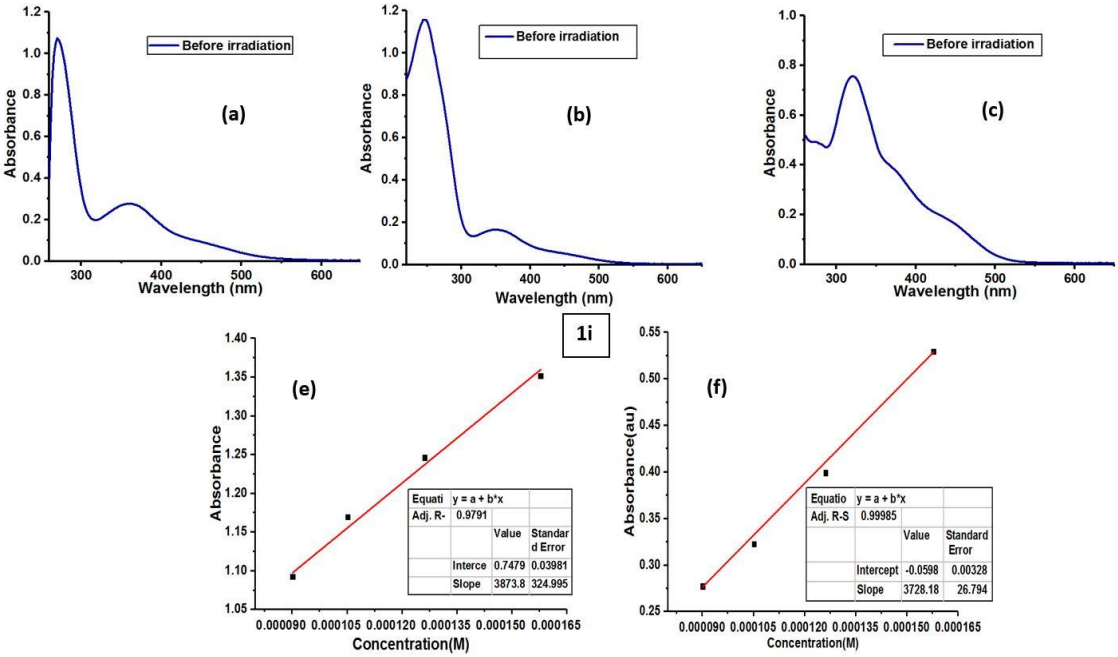

Figure 2A.1.9. Photoswitching behavior of **1i.** Absorption spectra of **1i** (a) in DMSO (73.8 μM); (b) in MeCN (70.8 μM), and (c) in MeOH (87.9 μM) (Note that the sample exhibited no photoisomerization); Estimation of the molar absorption coefficient of **1i** in DMSO at (d) 270 nm, and (e) 358 nm.

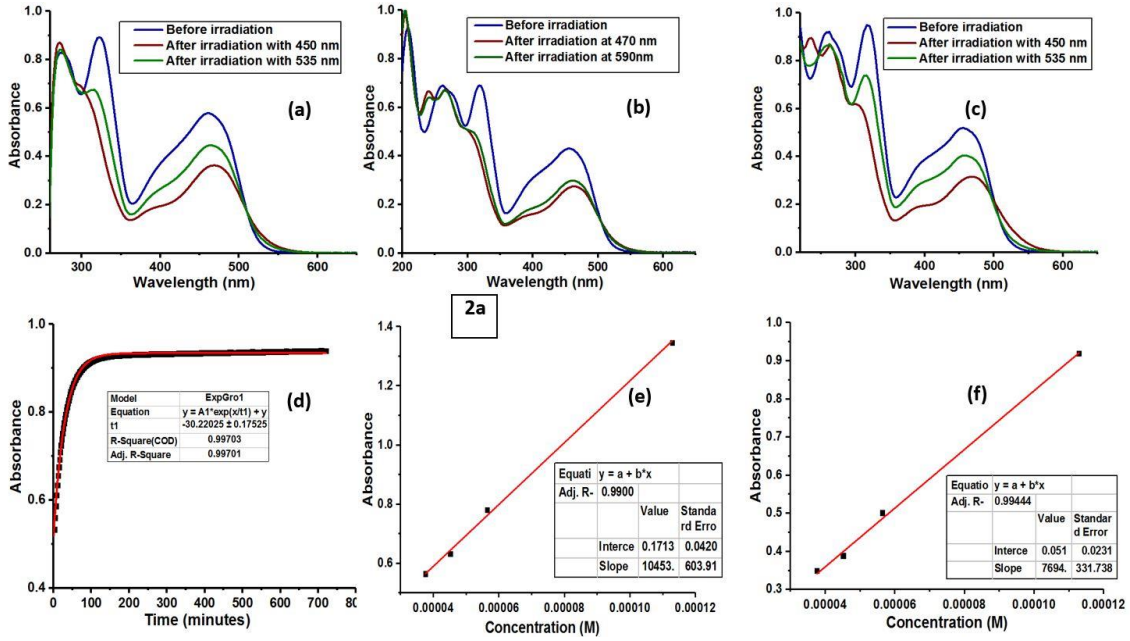

Figure 2A.1.10. Photoswitching behavior of **2a.** Forward and reverse isomerization (a) in DMSO (75.3 μM); (b) in MeCN (67.9 μM), and (c) in MeOH (84.6 μM) at the indicated wavelengths; (d) Thermal reverse isomerization kinetics of **2a** (DMSO, 50 °C, monitored at λ = 461 nm); Estimation of the molar absorption coefficient of **2a** in DMSO at (e) 322 nm, and (f) 461 nm.

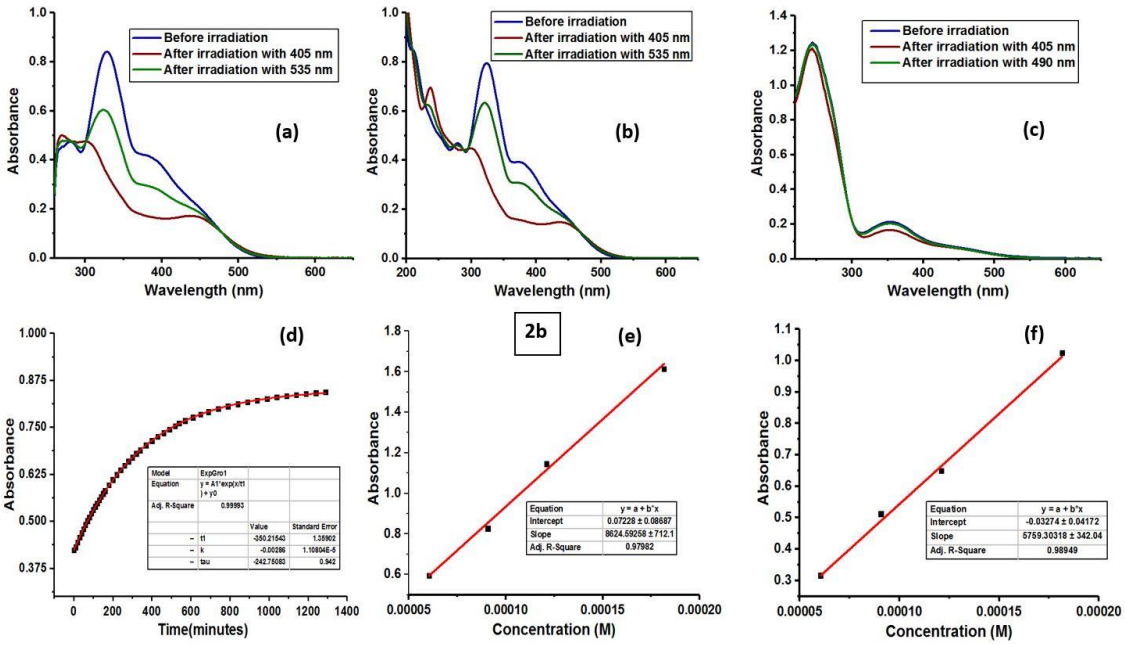

Figure 2A.1.11. Photoswitching behavior of **2b.** Forward and reverse isomerization (a) in DMSO (98.2 μM); (b) in MeCN (90.6 μM), and (c) in MeOH (92.7μM) at the indicated wavelengths; (d) Thermal reverse isomerization kinetics of **2b** (DMSO, 50 °C, monitored at λ = 329 nm); Estimation of the molar absorption coefficient of **2b** in DMSO at (e) 329 nm, and (f) 379 nm.

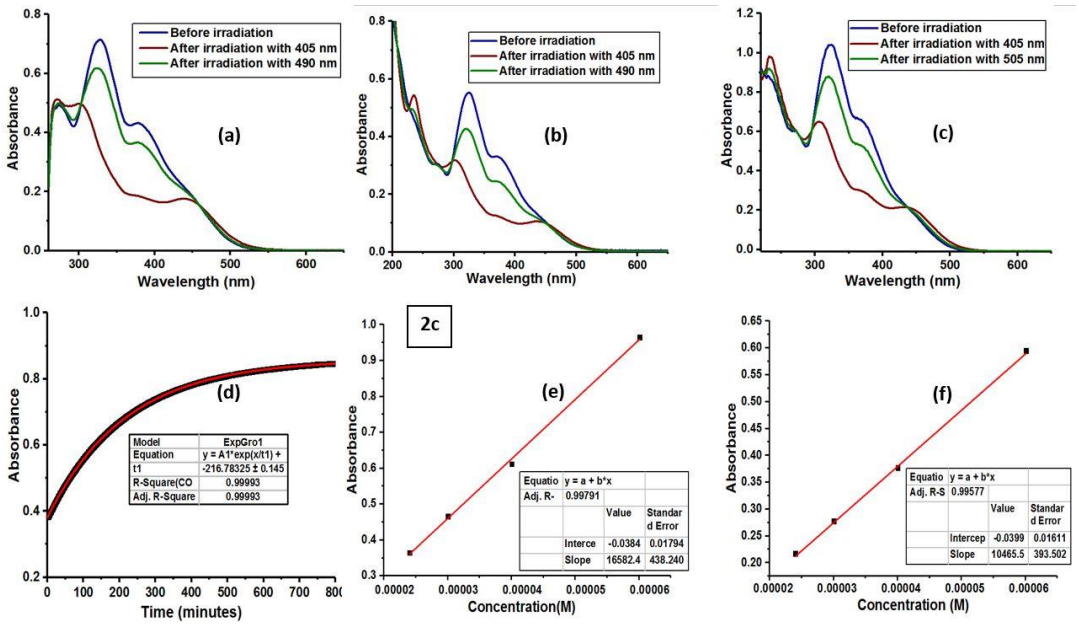

Figure 2A.1.12. Photoswitching behavior of **2c.** Forward and reverse isomerization (a) in DMSO (43.3 μM); (b) in MeCN (60.1 μM), and (c) in MeOH (84.9 μM) at the indicated wavelengths; (d) Thermal reverse isomerization kinetics of **2c** (DMSO, 50 °C, monitored at λ = 328 nm); Estimation of the molar absorption coefficient of **2c** in DMSO at (e) 328 nm, and (f) 380 nm.

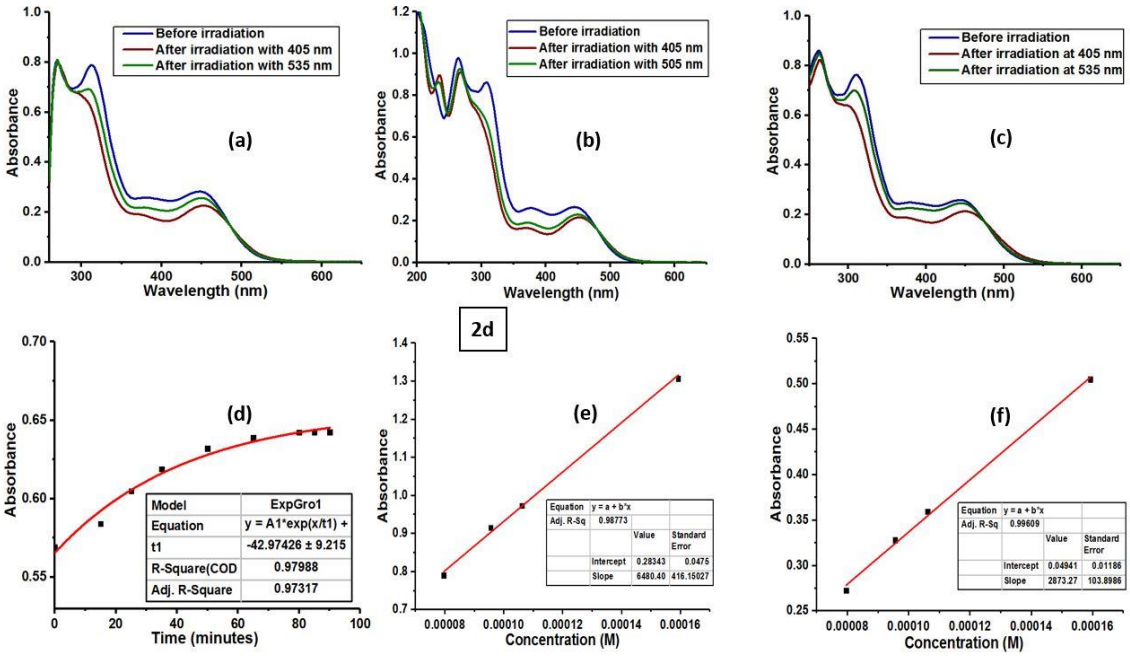

Figure 2A.1.13. Photoswitching behavior of **2d.** Forward and reverse isomerization (a) in DMSO (122.2 μM); (b) in MeCN (100.8 μM), and (c) in MeOH (117.9 μM) at the indicated wavelengths; (d) Thermal reverse isomerization kinetics of **2d** (DMSO, 80 °C, monitored at λ = 312 nm); Estimation of the molar absorption coefficient of **2d** in DMSO at (e) 312 nm, and (f) 448 nm.

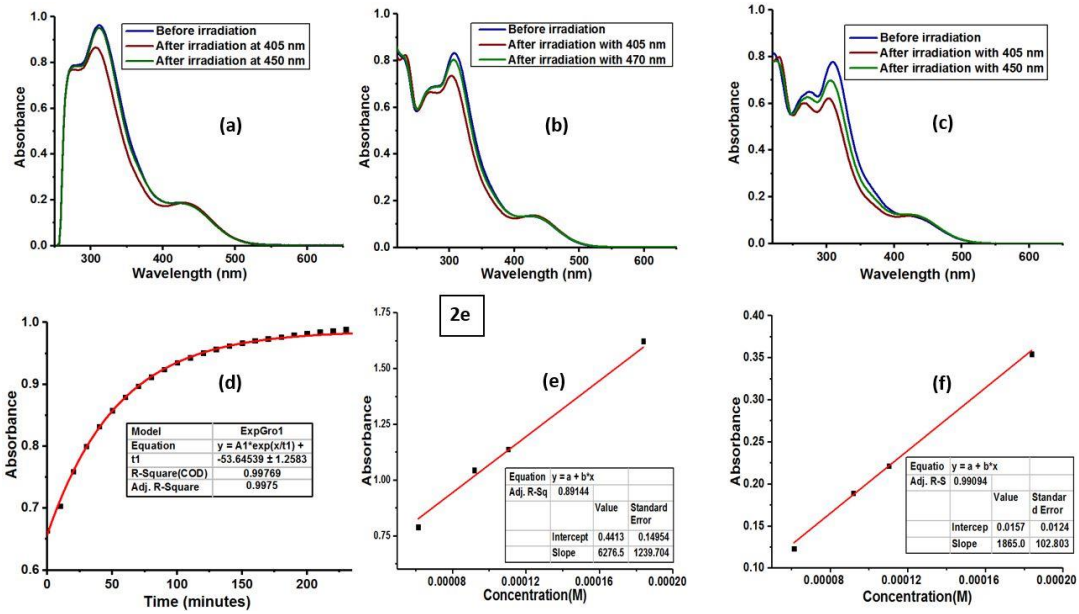

Figure 2A.1.14. Photoswitching behavior of **2e.** Forward and reverse isomerization (a) in DMSO (127.4 μM); (b) in MeCN (111.6 μM), and (c) in MeOH (100.9 μM) at the indicated wavelengths; (d) Thermal reverse isomerization kinetics of **2e** (DMSO, 80 °C, monitored at λ = 310 nm); Estimation of the molar absorption coefficient of **2e** in DMSO at (e) 310 nm, and (f) 426 nm.

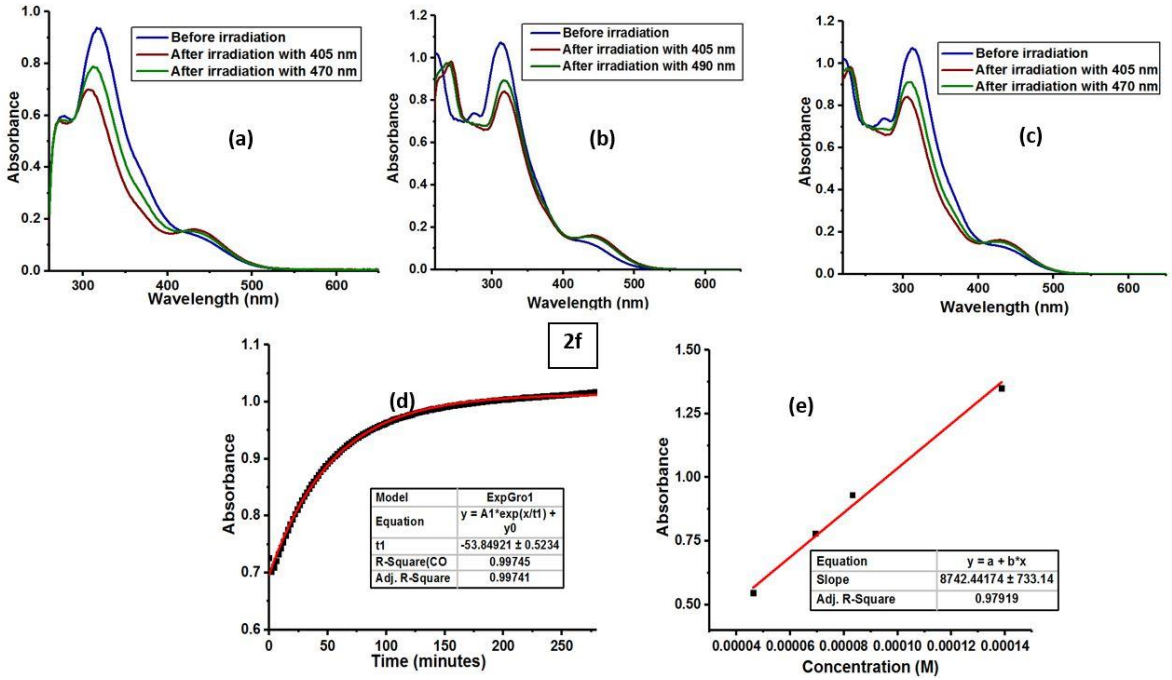

Figure 2A.1.15. Photoswitching behavior of **2f.** Forward and reverse isomerization (a) in DMSO (109.2 μM); (b) in MeCN (100.3 μM), and (c) in MeOH (97.5 μM) at the indicated wavelengths; (d) Thermal reverse isomerization kinetics of **2f** (DMSO, 80 ^{o}C, monitored at λ = 317 nm); Estimation of the molar absorption coefficient of **2f** in DMSO at (e) 317 nm.

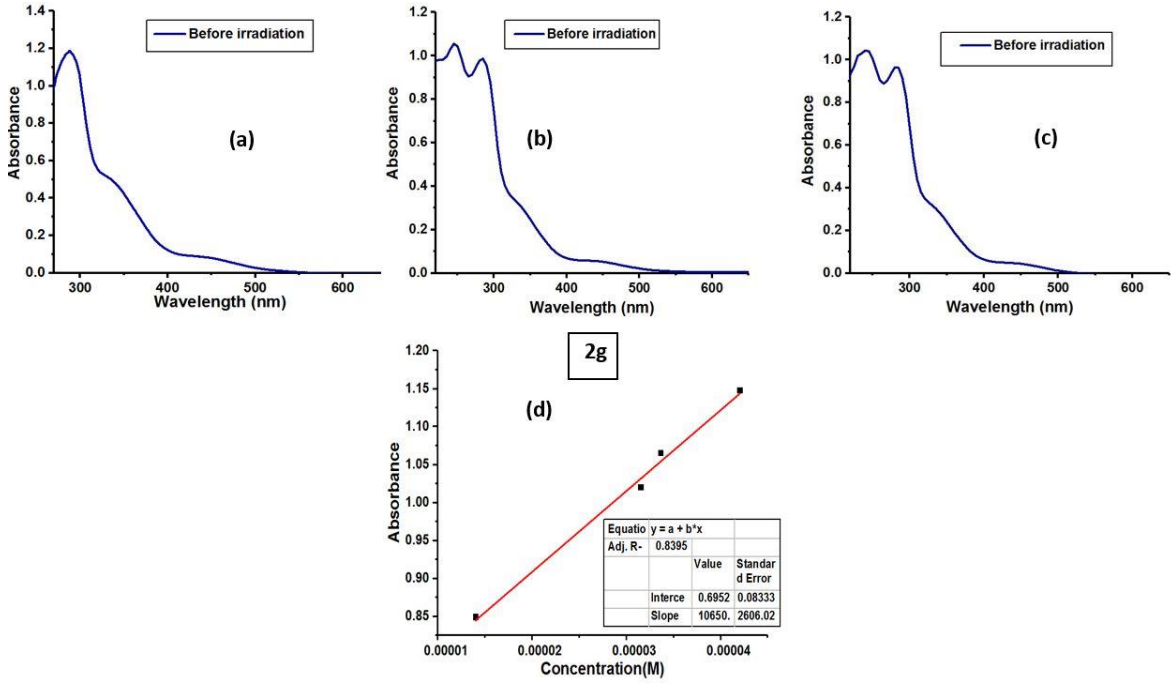

Figure 2A.1.16. Photoswitching behavior of **2g.** Absorption spectra of **2g** (a) in DMSO (111.5 μM); (b) in MeCN (101.2 μM), and (c) in MeOH (99.7 μM) (Note that the sample exhibited no photoisomerization); Estimation of the molar absorption coefficient of **2g** in DMSO at (d) 288 nm.

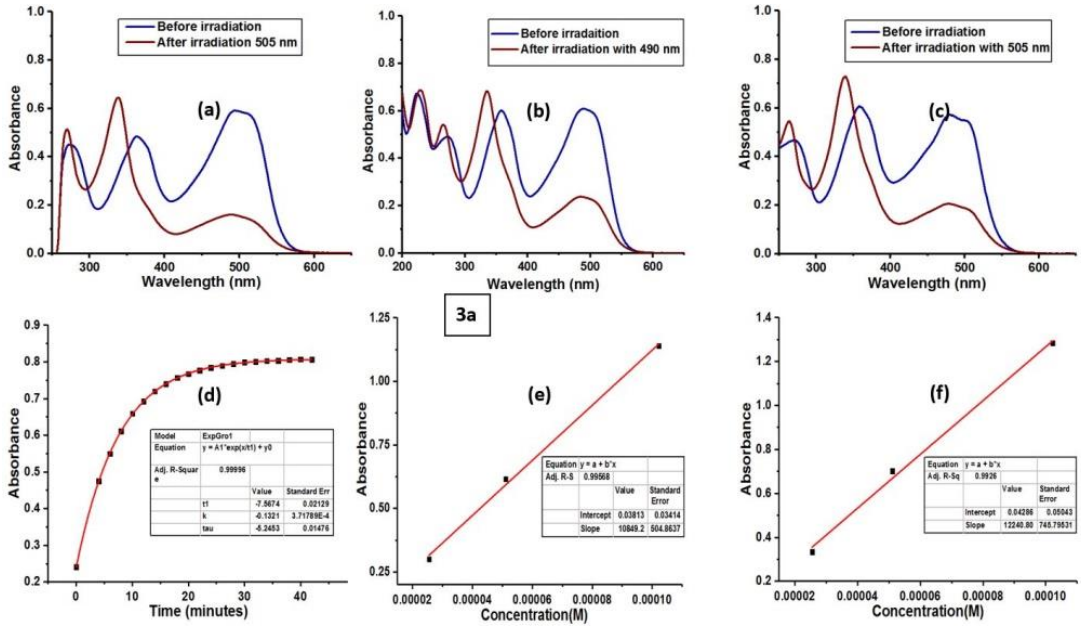

Figure 2A.1.17. Photoswitching behavior of **3a.** Forward and reverse isomerization (a) in DMSO (47.8 μM); (b) in MeCN (67.8 μM), and (c) in MeOH (78.4 μM) at the indicated wavelengths (Note that the reverse photoisomerization could not be carried out with the help of visible light because *E*-and *Z*-isomer bands are non-distinguishable in the visible range of the spectra); (d) Thermal reverse isomerization kinetics of **3a** (DMSO, 25 °C, monitored at λ = 502 nm); Estimation of the molar absorption coefficient of **3a** in DMSO at (e) 361 nm, (f) 502 nm.

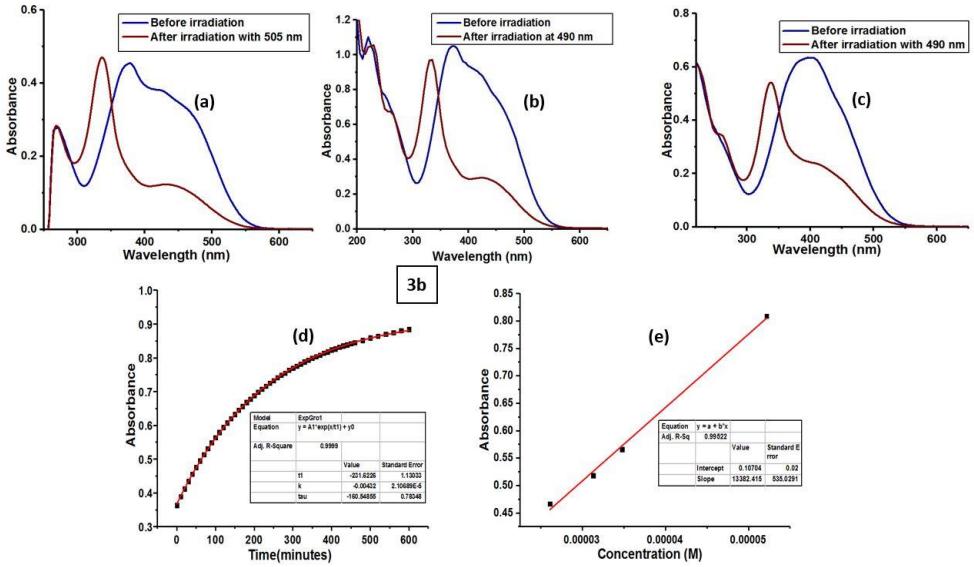

Figure 2A.1.18. Photoswitching behavior of **3b.** Forward and reverse isomerization (a) in DMSO (33.9 μM); (b) in MeCN (52.4 μM), and (c) in MeOH (67.3 μM) at the indicated wavelengths (Note that the reverse photoisomerization could not be carried out with the help of visible light because *E*-and *Z*-isomer bands are non-distinguishable in the visible range of the spectra); (d) Thermal reverse isomerization kinetics of **3b** (DMSO, 25 °C, monitored at λ = 377 nm); Estimation of the molar absorption coefficient of **3b** in DMSO at (e) 377 nm.

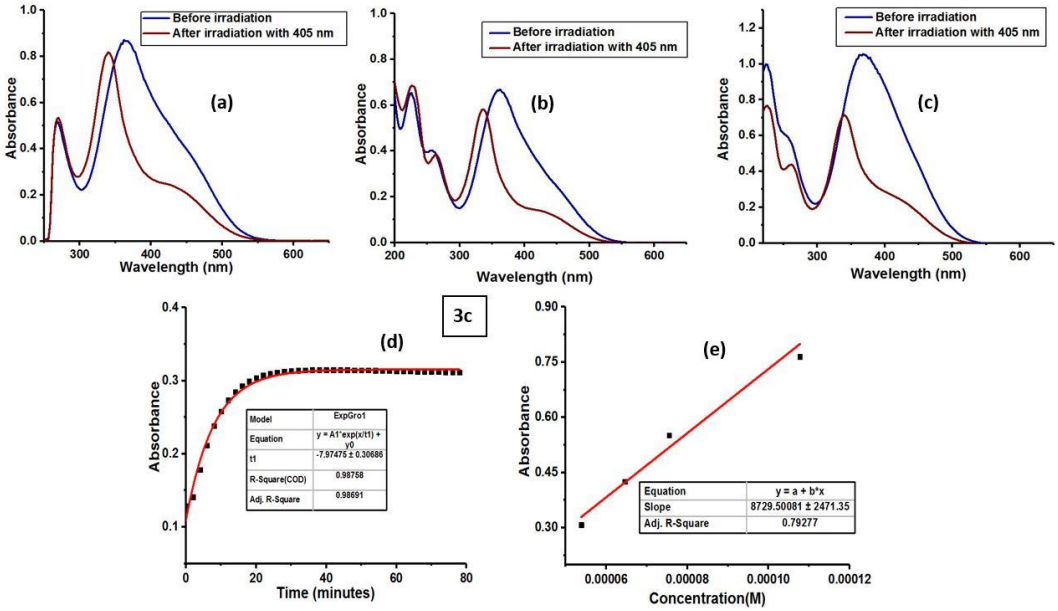

Figure 2A.1.19. Photoswitching behavior of **3c.** Forward and reverse isomerization (a) in DMSO (104.2 μM); (b) in MeCN (100.6 μM), and (c) in MeOH (109.2 μM) at the indicated wavelengths (Note that the reverse photoisomerization could not be carried out with the help of visible light because *E*-and *Z*-isomer bands are non-distinguishable in the visible range of the spectra); (d) Thermal reverse isomerization kinetics of **3c** (DMSO, 80 °C, monitored at λ = 362 nm); Estimation of the molar absorption coefficient of **3c** in DMSO at (e) 362 nm.

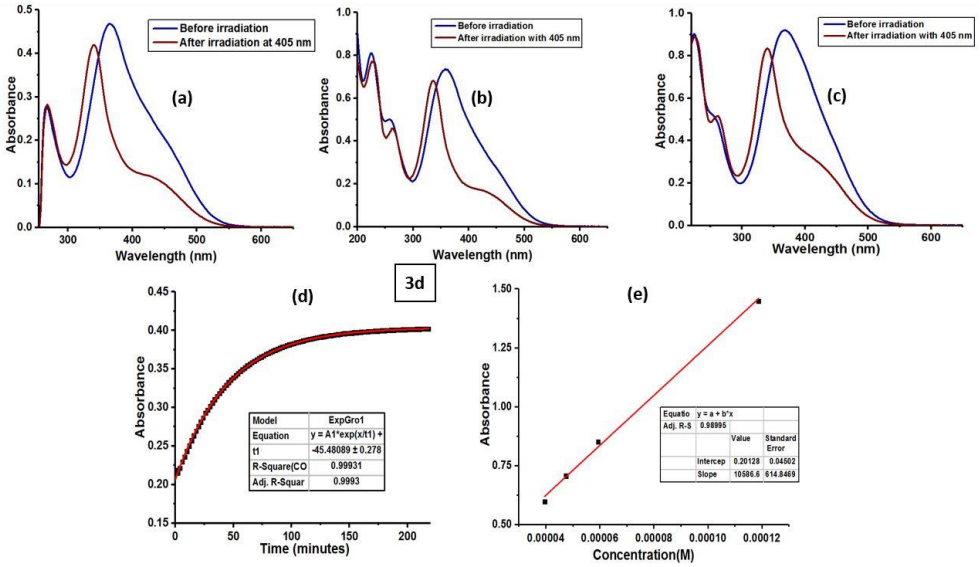

Figure 2A.1.20. Photoswitching behavior of **3d.** Forward and reverse isomerization (a) in DMSO (44.3 μM); (b) in MeCN (66.7 μM), and (c) in MeOH (59.8 μM) at the indicated wavelengths (Note that the reverse photoisomerization could not be carried out with the help of visible light because *E*-and *Z*-isomer bands are non-distinguishable in the visible range of the spectra); (d) Thermal reverse isomerization kinetics of **3d** (DMSO, 80 °C, monitored at λ = 370 nm); Estimation of the molar absorption coefficient of **3d** in DMSO at (e) 370 nm.

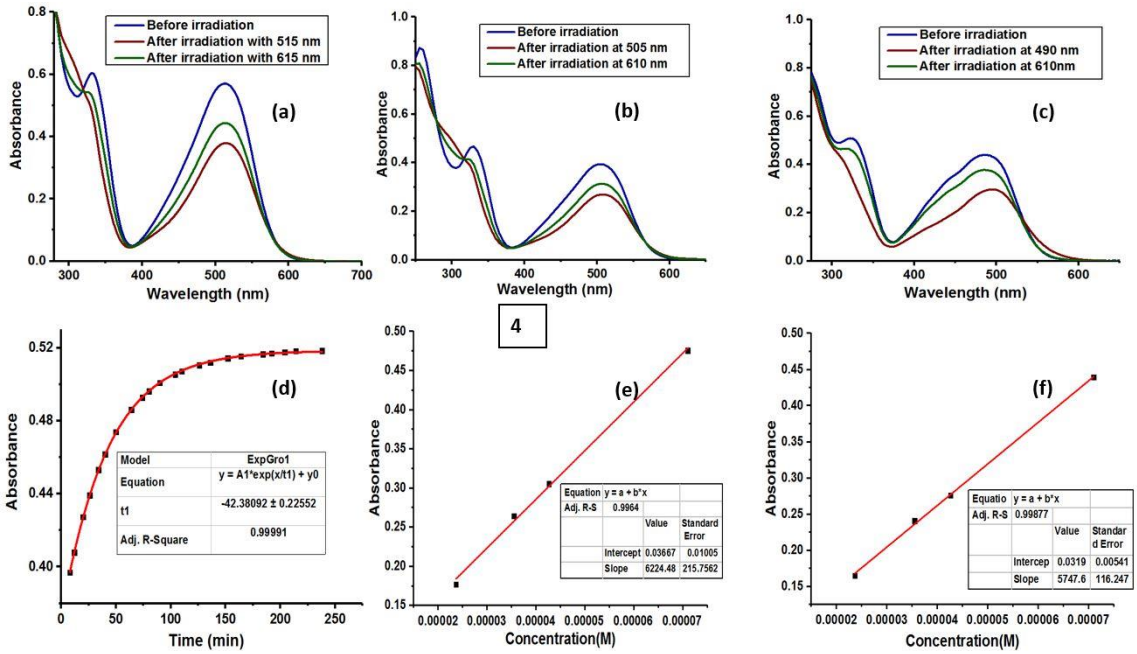

Figure 2A.1.21. Photoswitching behavior of **4.** Forward and reverse isomerization (a) in DMSO (99.9 μM); (b) in MeCN (90.2 μM), and (c) in MeOH (100.3 μM) at the indicated wavelengths; (d) Thermal reverse isomerization kinetics of **4** (DMSO, 50 °C, monitored at λ = 513 nm); Estimation of the molar absorption coefficient of **4** in DMSO at (e) 332 nm, (f) 513 nm.

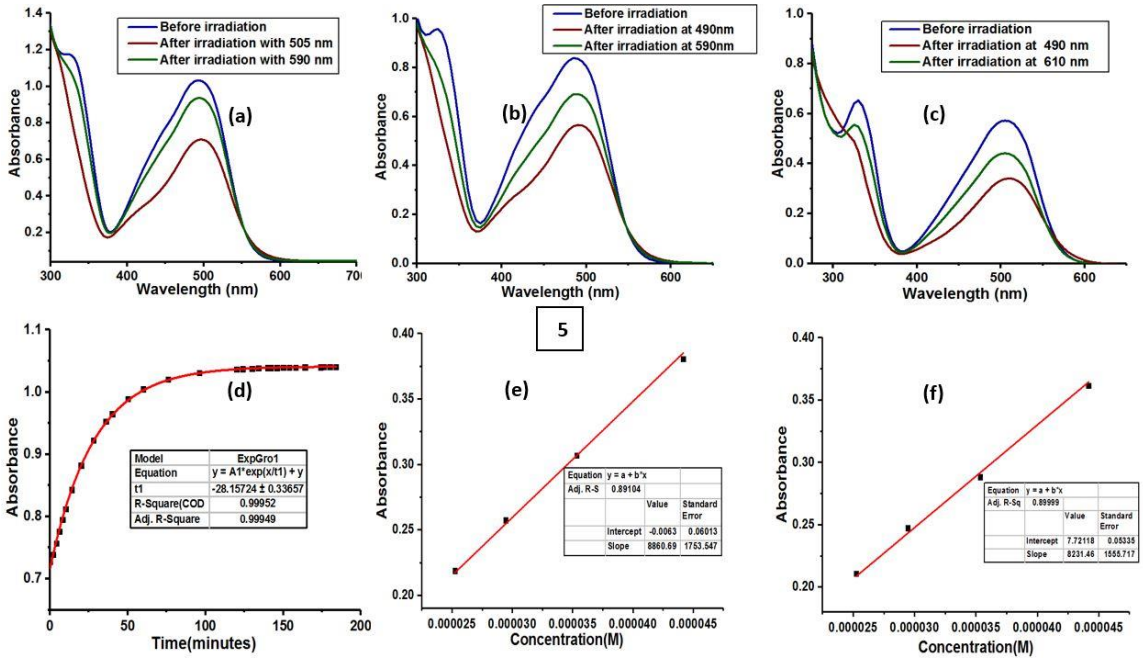

Figure 2A.1.22. Photoswitching behavior of **5.** Forward and reverse isomerization (a) in DMSO (126.0 μM); (b) in MeCN (110.3 μM), and (c) in MeOH (100.9 μM) at the indicated wavelengths; (d) Thermal reverse isomerization kinetics of **5** (DMSO, 50 °C, monitored at λ = 492 nm); Estimation of the molar absorption coefficient of **5** in DMSO at (e) 326 nm, (f) 492 nm.

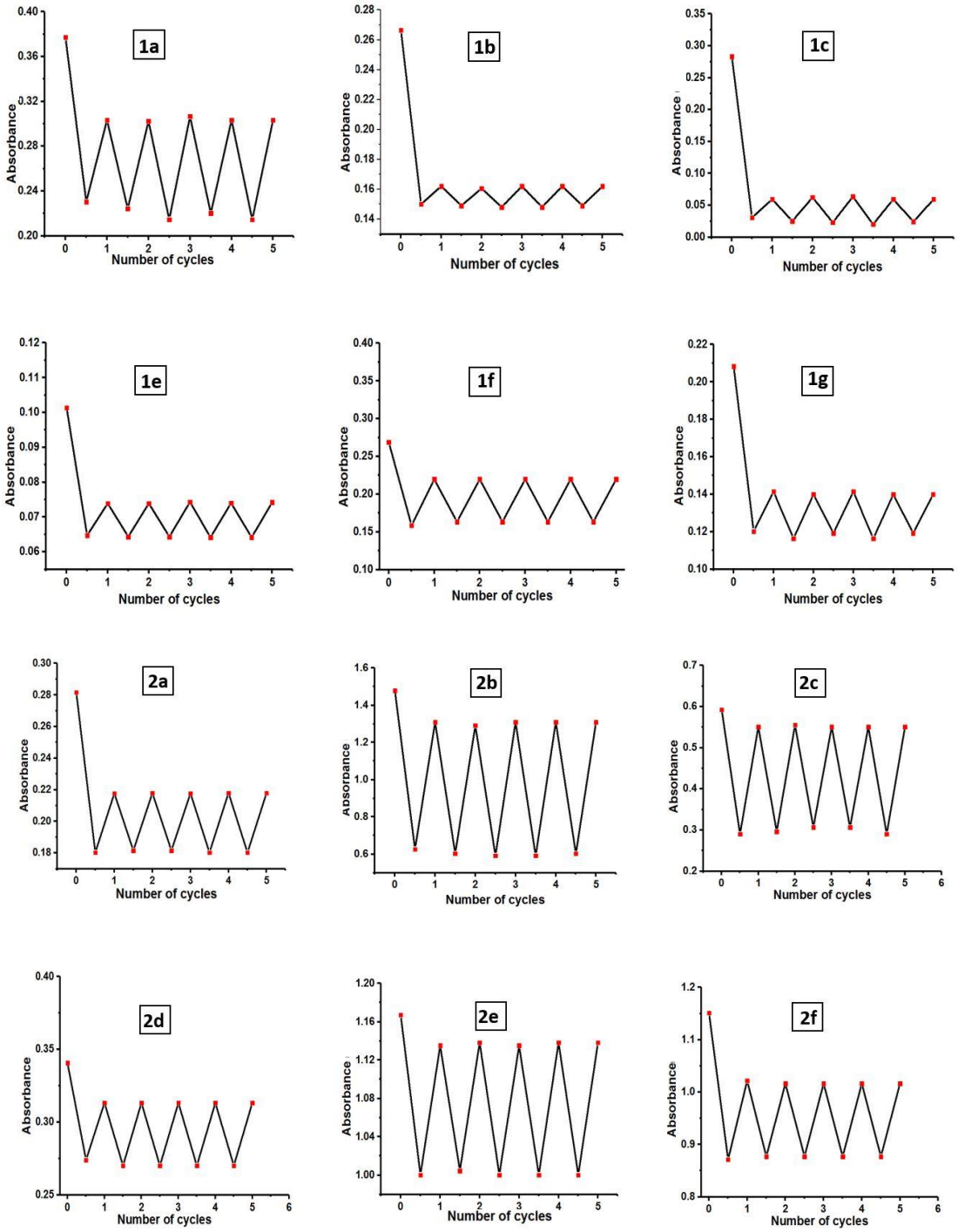

Figure 2A.1.23. Photoswitching stability over five cycles of: **1a** (monitored at 475 nm, Forward 470 nm, reverse 590 nm); **1b** (monitored at 402 nm, Forward 405 nm, reverse 435 nm); **1c** (monitored at 392 nm, Forward 405 nm, reverse 490 nm); **1e** (monitored at 379 nm, Forward 405 nm, reverse 505 nm); **1f** (monitored at 372 nm, Forward 405 nm, reverse 490 nm); **1g** (monitored at 378 nm, Forward 405 nm, reverse 535 nm); **2a** (monitored at 461 nm, Forward 470 nm, reverse 590 nm); **2b** (monitored at 329 nm, Forward 405 nm, reverse 535 nm); **2c** (monitored at 380 nm, Forward 405 nm, reverse 505 nm); **2d** (monitored at 448 nm, Forward 405 nm, reverse 535 nm); **2e** (monitored at 310 nm, Forward 405 nm, reverse 450 nm); **2f** (monitored at 317 nm, Forward 405 nm, reverse 470 nm).

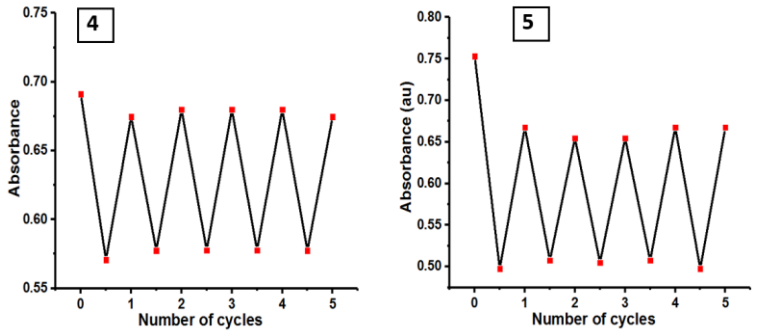

Figure 2A.1.24. Photoswitching stability over five cycles of: **4** (monitored at 513 nm, Forward 515 nm, reverse 615 nm); **5** (monitored at 492 nm, Forward 505 nm, reverse 590 nm).

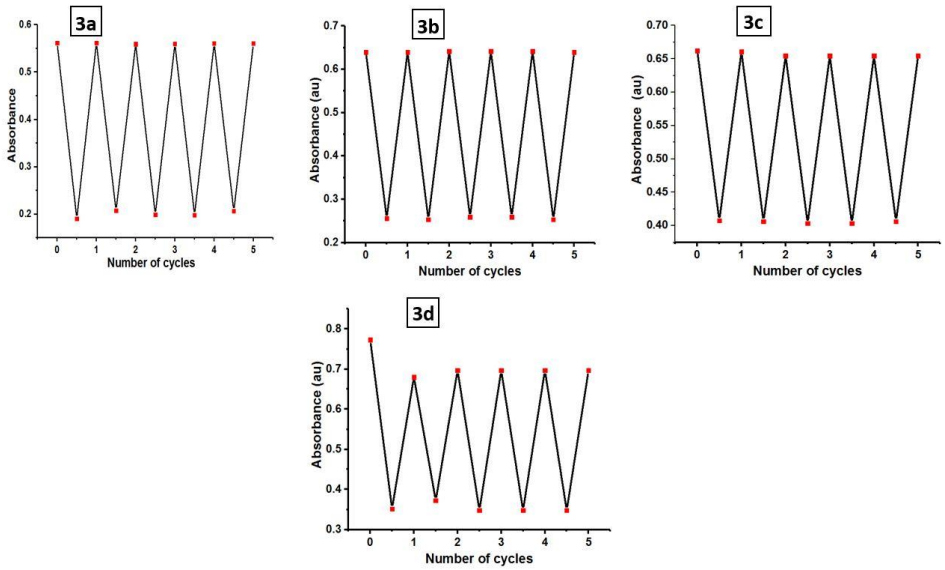

Figure 2A.1.25. Photoswitching stability over five cycles of: **3a** (monitored at 502 nm, Forward 505 nm, reverse at 25 ^{o}C); **3b** (monitored at 377 nm, Forward 505 nm, reverse at 25 ^{o}C); **3c** (monitored at 377 nm, Forward 405 nm, reverse at 80 ^{o}C); **3d** (monitored at 365 nm, Forward 405 nm, reverse at 80 ^{o}C).

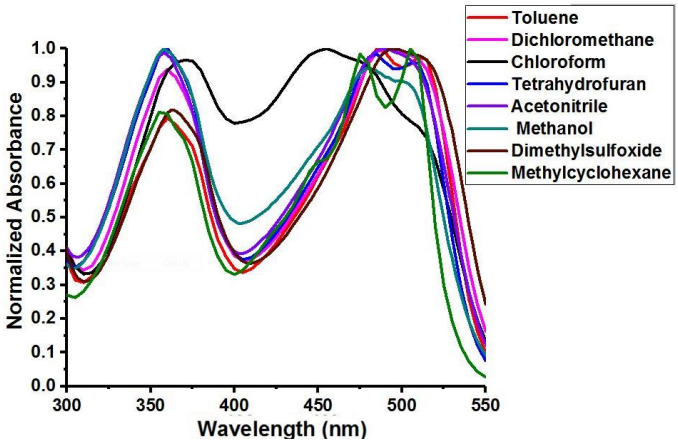

Figure 2A.1.26. UV spectra of *E*-isomer of **3a** in solvents of different polarity.

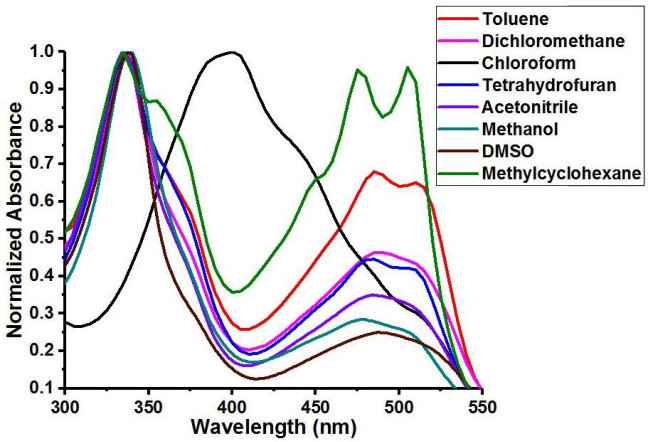

Figure 2A.1.27. UV spectra of *Z*-isomer of **3a** in solvents of different polarity.

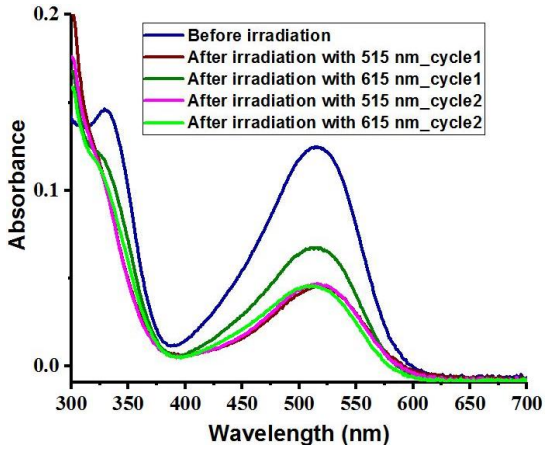

Figure 2A.1.28. Photoswitching behavior of **4** in 70 % DMSO IN PBS buffer (pH=7.4) solution. The solution undergoes efficient forward and reverse photoswitching with 515 and 615 nm, respectively. However, during the second cycle, the solution showed photobleaching.

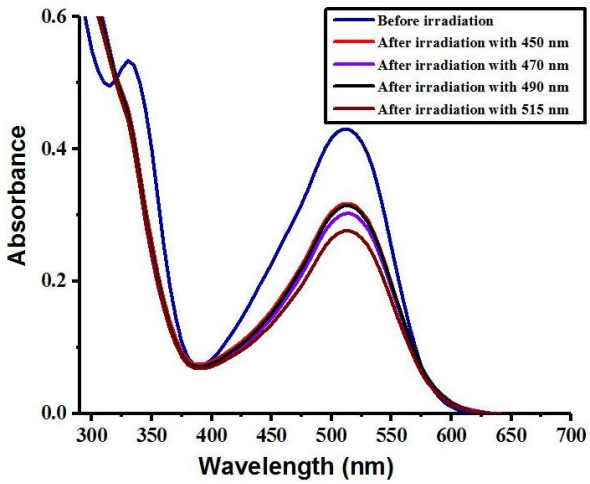

Figure 2A.1.29. Photoswitching behavior of **4** in DMSO with different wavelengths of light. The compound showed most efficient forward photoswitching with the help of 515 nm light.

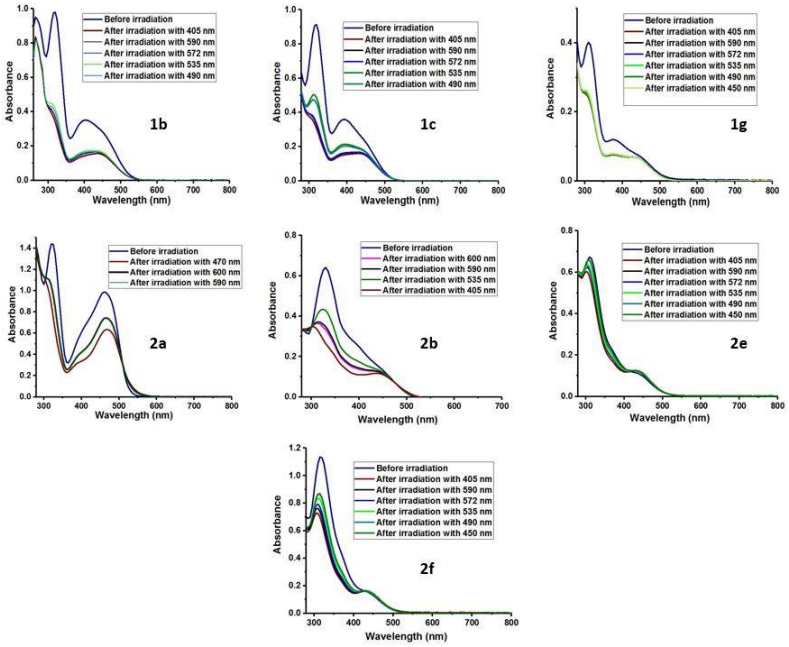

Figure 2A.1.30. Screening of wavelengths for the reverse isomerization in the compounds **1b**, **1c**, **1g**, **2a**, **2b**, **2e** and **2f** (in DMSO) (Each wavelength was screened by irradiating the *Z*-isomer enriched solution for sufficient amount of time (a maximum of 20 min) to attain PSS).

2A.2. Thermal reverse isomerization kinetics data at variable temperature

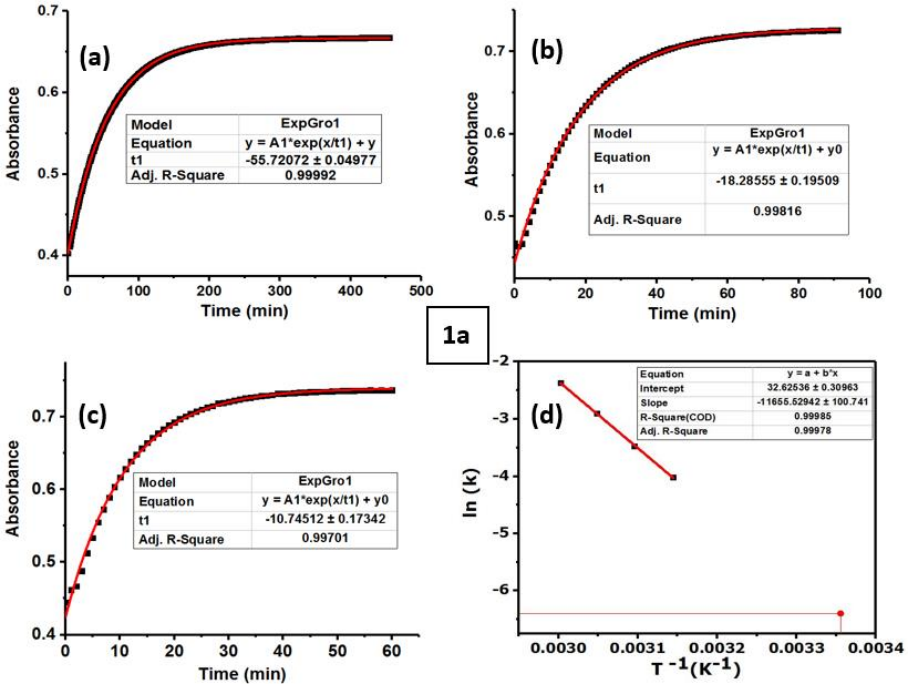

Figure 2A.2.1. Thermal reverse isomerization kinetics of **1a** (DMSO, monitored at λ = 475 nm) at (a) 45 °C, (b) 55 °C, and (c) 60 °C, (d) Arrhenius plot for deducing the rate constant at 25 °C by extrapolation.

.

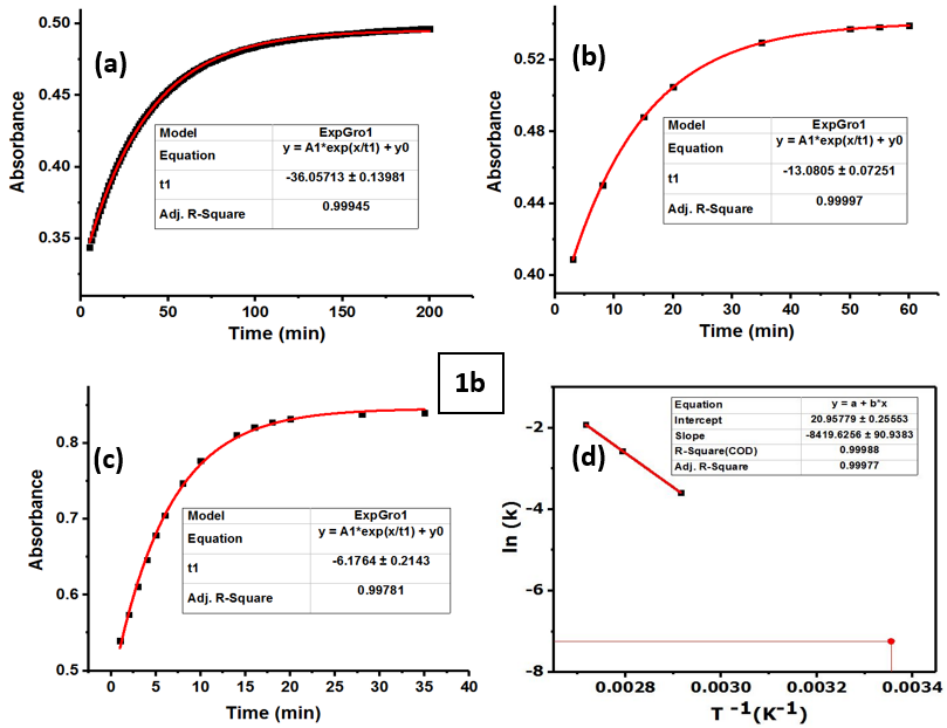

Figure 2A.2.2. Thermal reverse isomerization kinetics of **1b** (DMSO, monitored at λ = 316 nm) at (a) 70 °C, (b) 85 °C, and (c) 90 °C, (d) Arrhenius plot for deducing the rate constant at 25 °C by extrapolation.

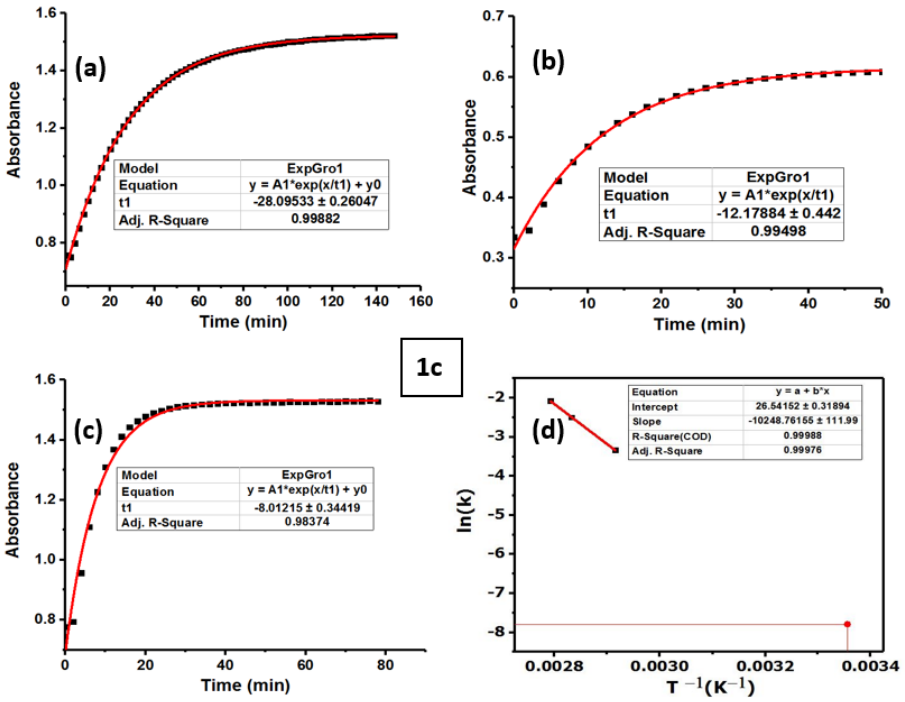

Figure 2A.2.3. Thermal reverse isomerization kinetics of **1c** (DMSO, monitored at λ = 319 nm) at (a) 70 °C, (b) 80 °C, and (c) 85 °C, (d) Arrhenius plot for deducing the rate constant at 25 °C by extrapolation.

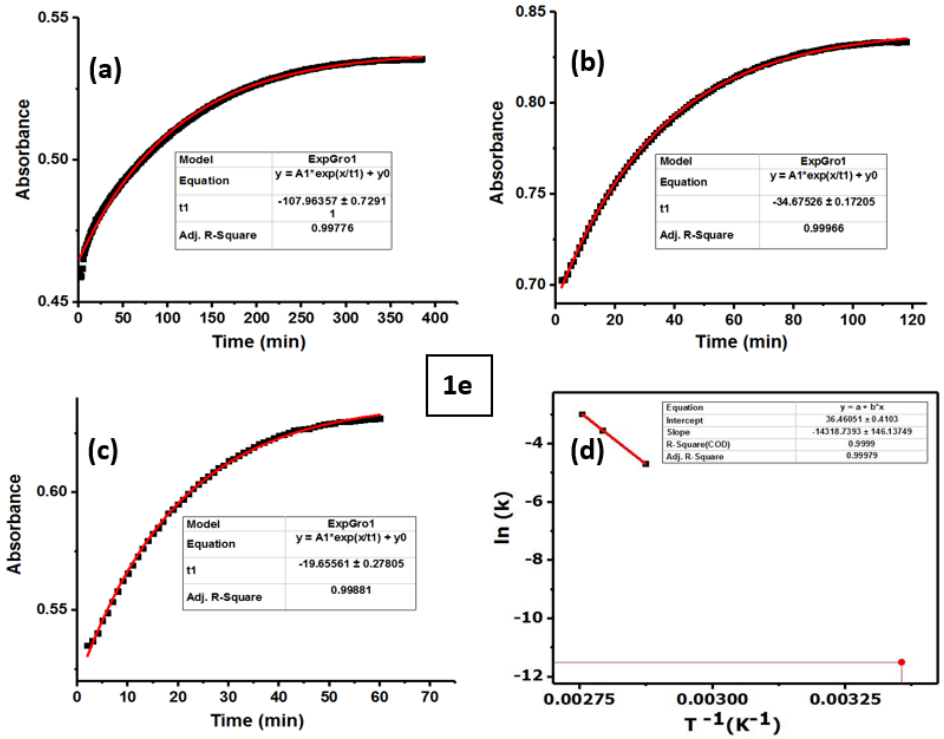

Figure 2A.2.4. Thermal reverse isomerization kinetics of **1e** (DMSO, monitored at λ = 310 nm) at (a) 75 °C, (b) 85 °C, and (c) 90 °C, (d) Arrhenius plot for deducing the rate constant at 25 °C by extrapolation.

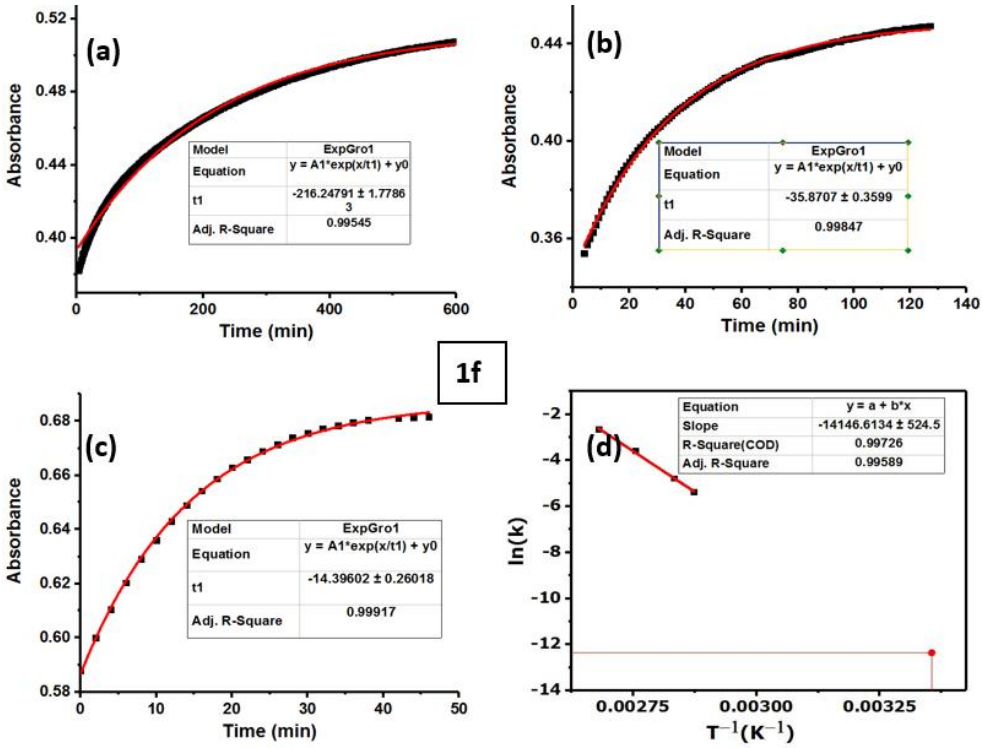

Figure 2A.2.5. Thermal reverse isomerization kinetics of **1f** (DMSO, monitored at λ = 304 nm) at (a) 75 °C, (b) 90 °C, and (c) 100 °C, (d) Arrhenius plot for deducing the rate constant at 25 °C by extrapolation.

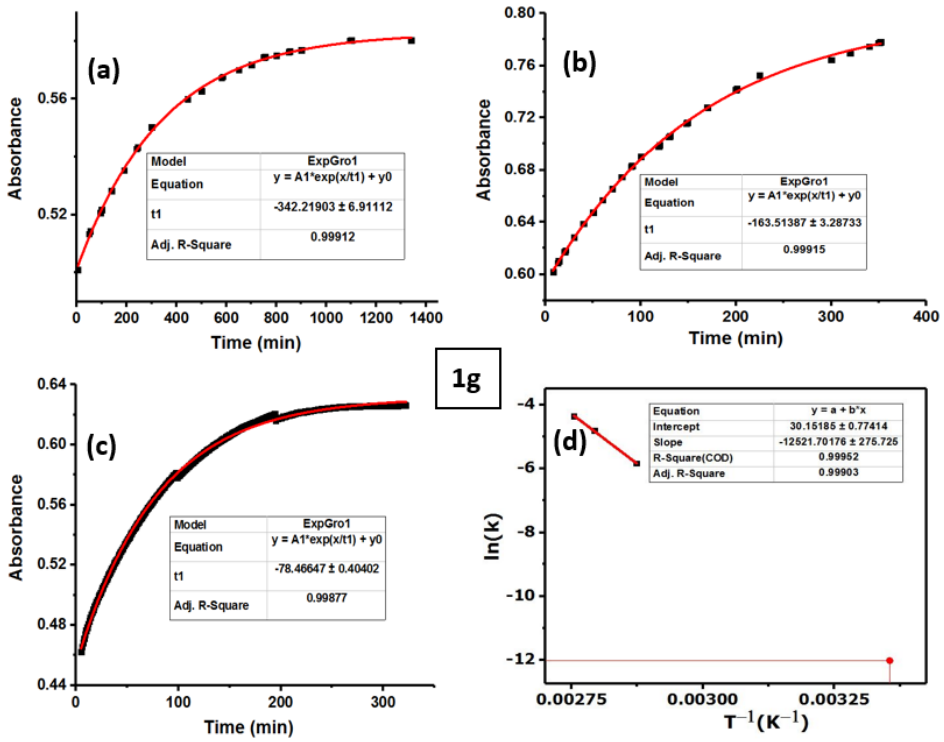

Figure 2A.2.6. Thermal reverse isomerization kinetics of **1g** (DMSO, monitored at λ = 311 nm) at (a) 75 °C, (b) 85 °C, and (c) 90 °C, (d) Arrhenius plot for deducing the rate constant at 25 °C by extrapolation.

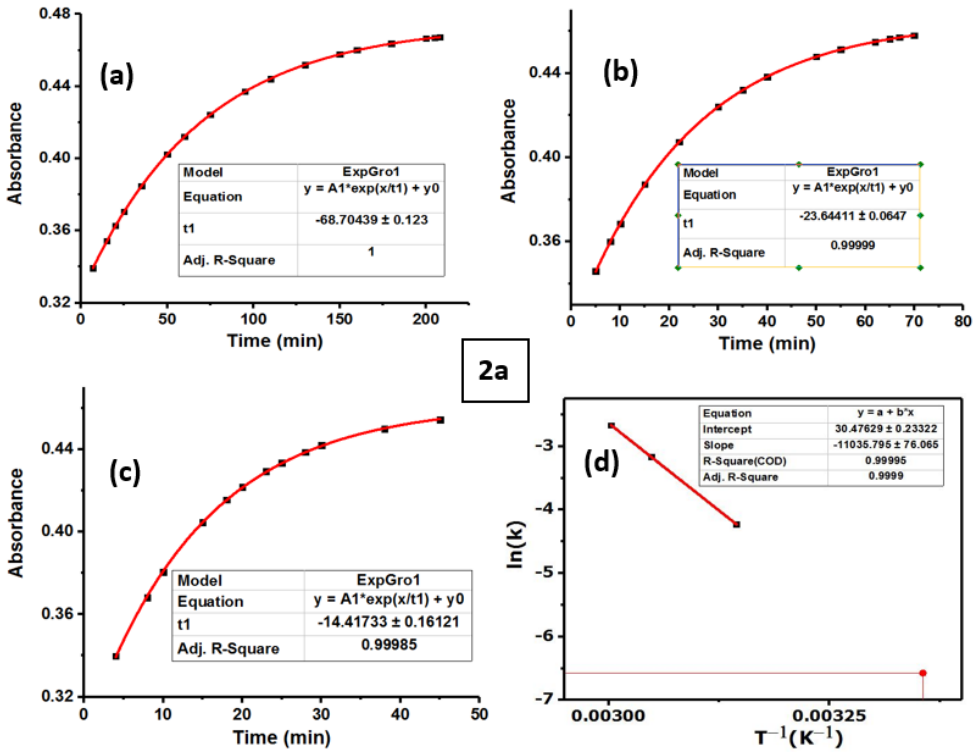

Figure 2A.2.7. Thermal reverse isomerization kinetics of **2a** (DMSO, monitored at λ = 461 nm) at (a) 45 °C, (b) 55 °C, and (c) 60 °C, (d) Arrhenius plot for deducing the rate constant at 25 °C by extrapolation.

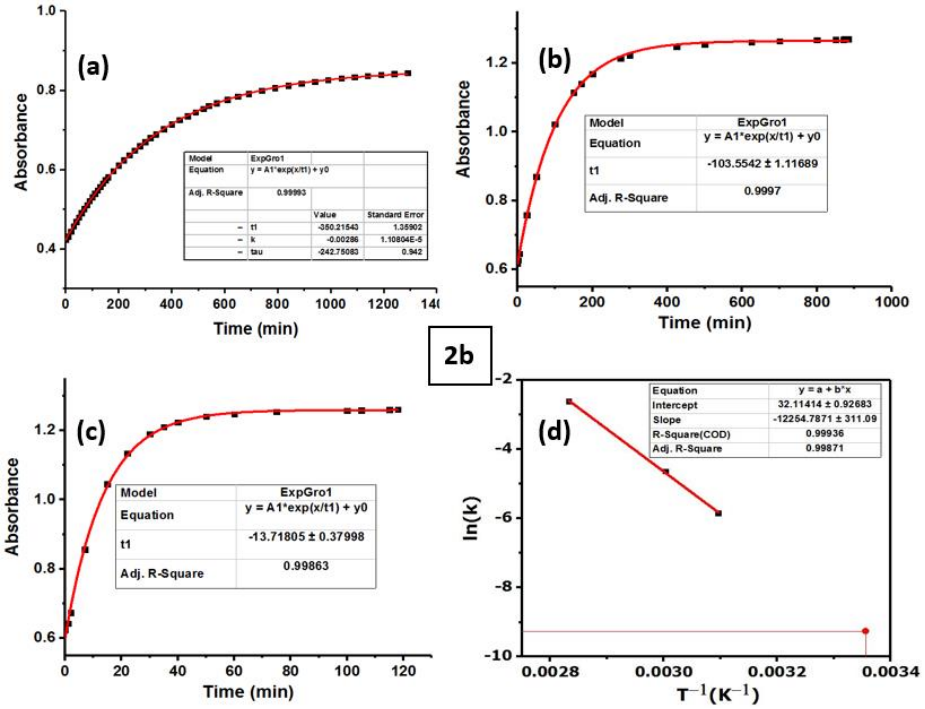

Figure 2A.2.8. Thermal reverse isomerization kinetics of **2b** (DMSO, monitored at λ = 329 nm) at (a) 50 °C, (b) 60 °C, and (c) 80 °C, (d) Arrhenius plot for deducing the rate constant at 25 °C by extrapolation.

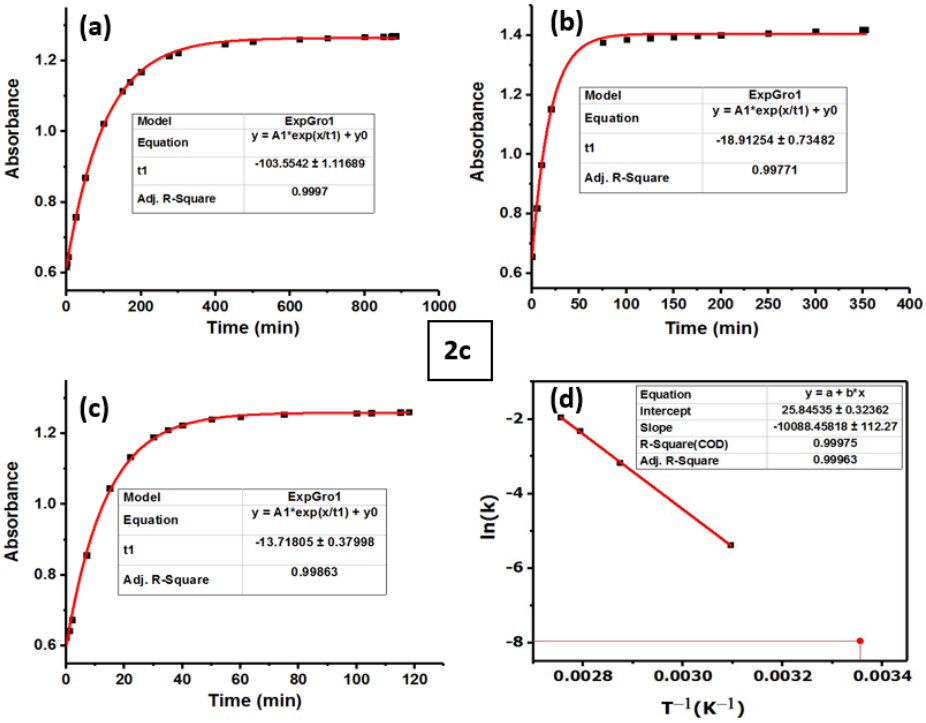

Figure 2A.2.9. Thermal reverse isomerization kinetics of **2c** (DMSO, monitored at λ = 328 nm) at (a) 60 °C, (b) 70 °C, and (c) 80 °C, (d) Arrhenius plot for deducing the rate constant at 25 °C by extrapolation.

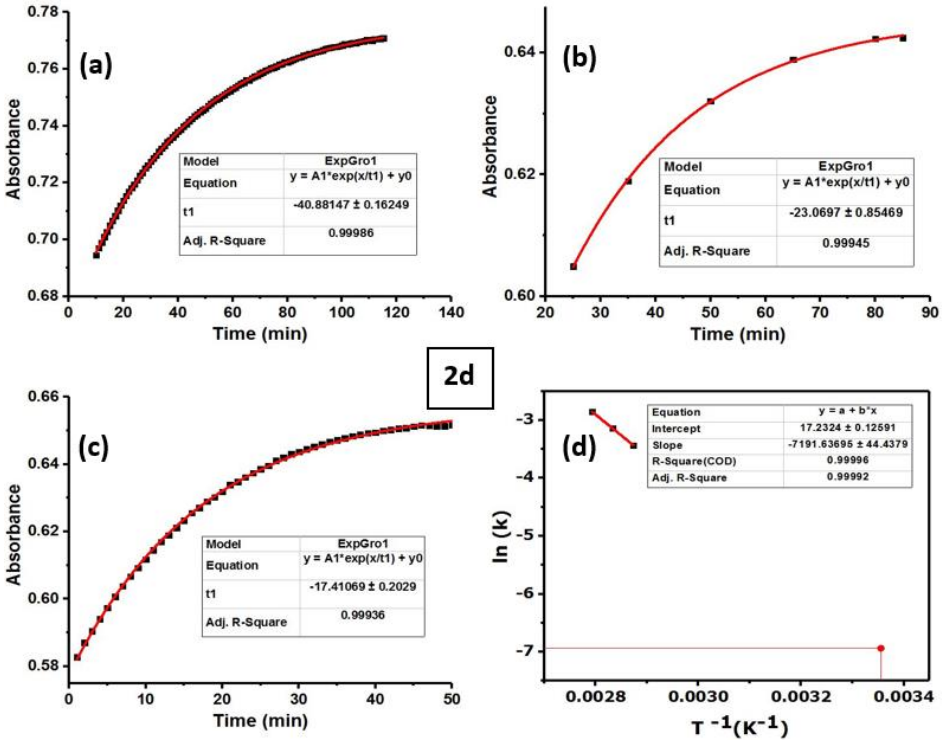

Figure 2A.2.10. Thermal reverse isomerization kinetics of **2d** (DMSO, monitored at λ = 312 nm) at (a) 75 °C, (b) 80 °C, and (c) 85 °C, (d) Arrhenius plot for deducing the rate constant at 25 °C by extrapolation.

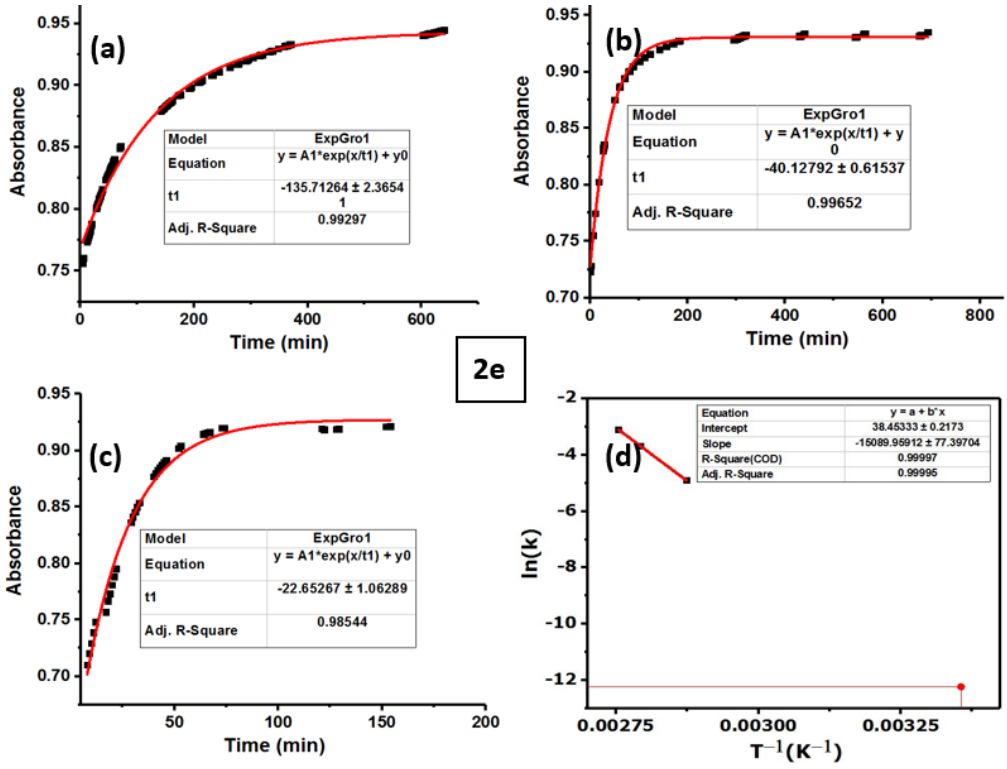

Figure 2A.2.11. Thermal reverse isomerization kinetics of **2e** (DMSO, monitored at λ = 310 nm) at (a) 75 °C, (b) 85 °C, and (c) 90 °C, (d) Arrhenius plot for deducing the rate constant at 25 °C by extrapolation.

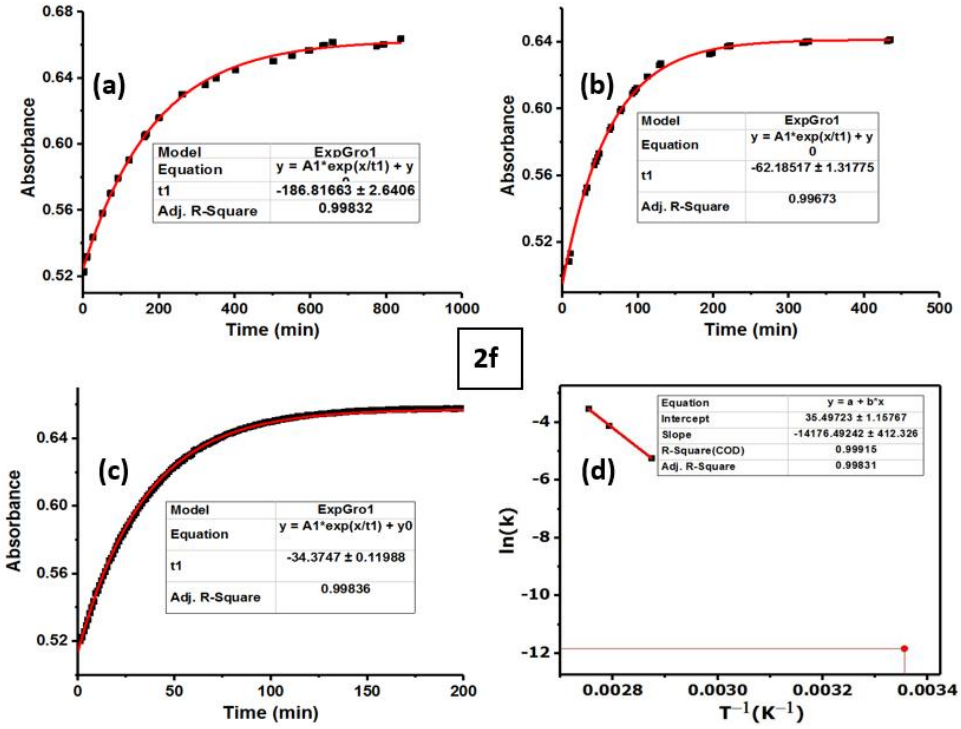

Figure 2A.2.12. Thermal reverse isomerization kinetics of **2f** (DMSO, monitored at λ = 317 nm) at (a) 75 °C, (b) 85 °C, and (c) 90 °C, (d) Arrhenius plot for deducing the rate constant at 25 °C by extrapolation.

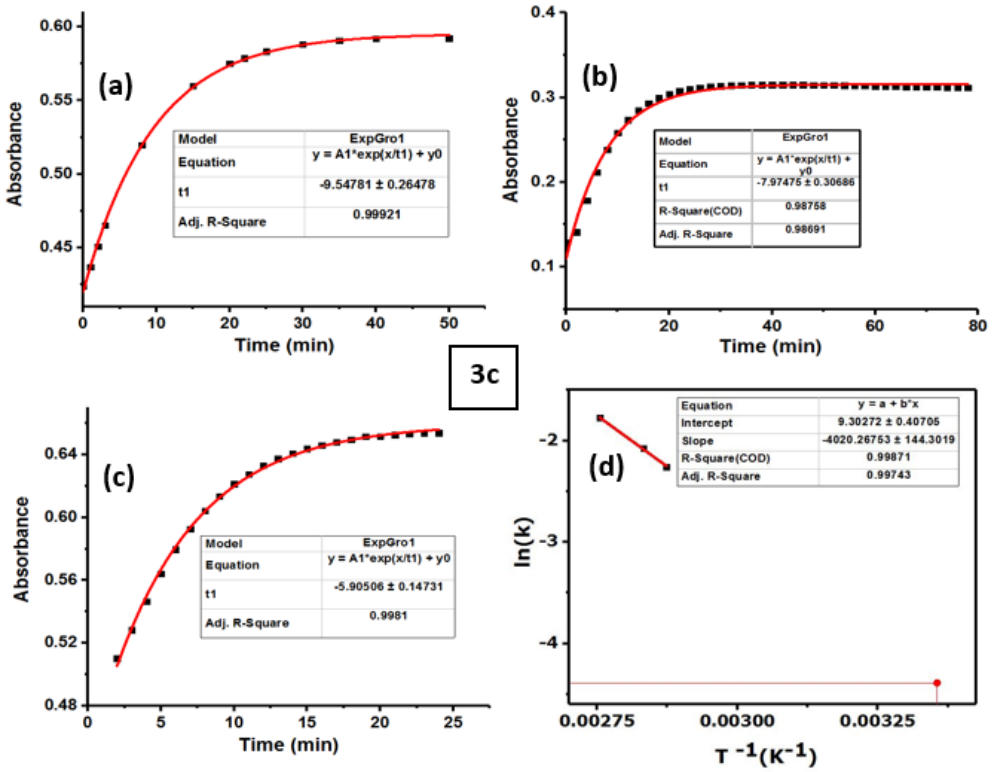

Figure 2A.2.13. Thermal reverse isomerization kinetics of **3c** (DMSO, monitored at λ = 362 nm) at (a) 75 °C, (b) 80 °C, and (c) 90 °C, (d) Arrhenius plot for deducing the rate constant at 25 °C by extrapolation.

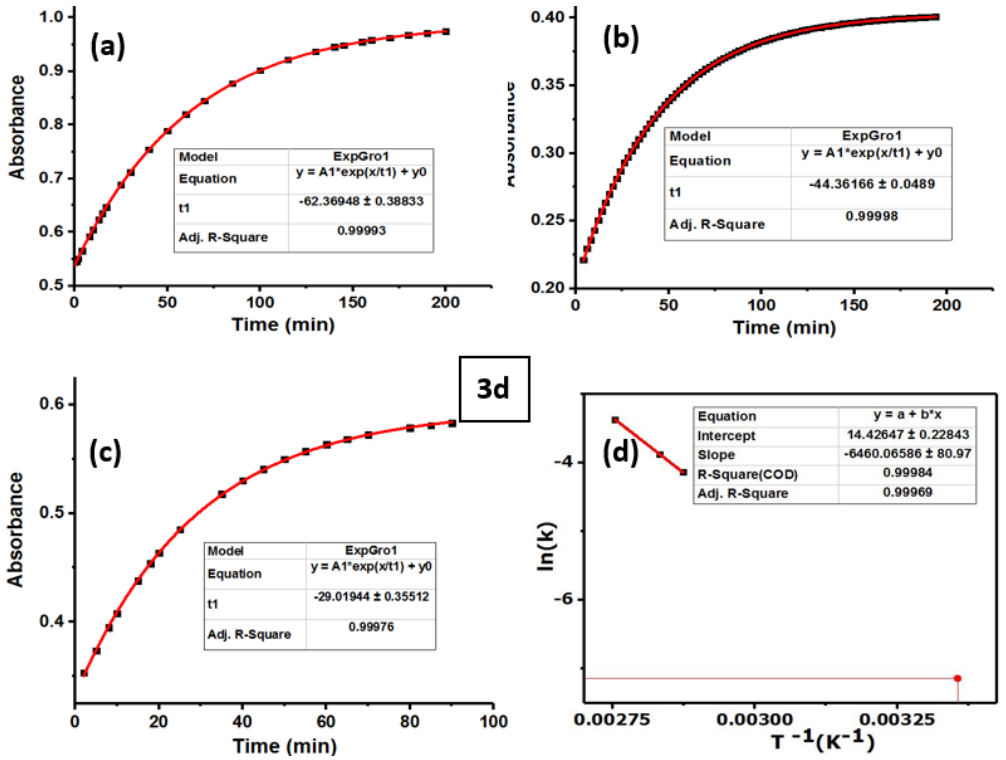

Figure 2A.2.14. Thermal reverse isomerization kinetics of **3d** (DMSO, monitored at λ = 370 nm) at (a) 75 °C, (b) 80 °C, and (c) 90 °C, (d) Arrhenius plot for deducing the rate constant at 25 °C by extrapolation.

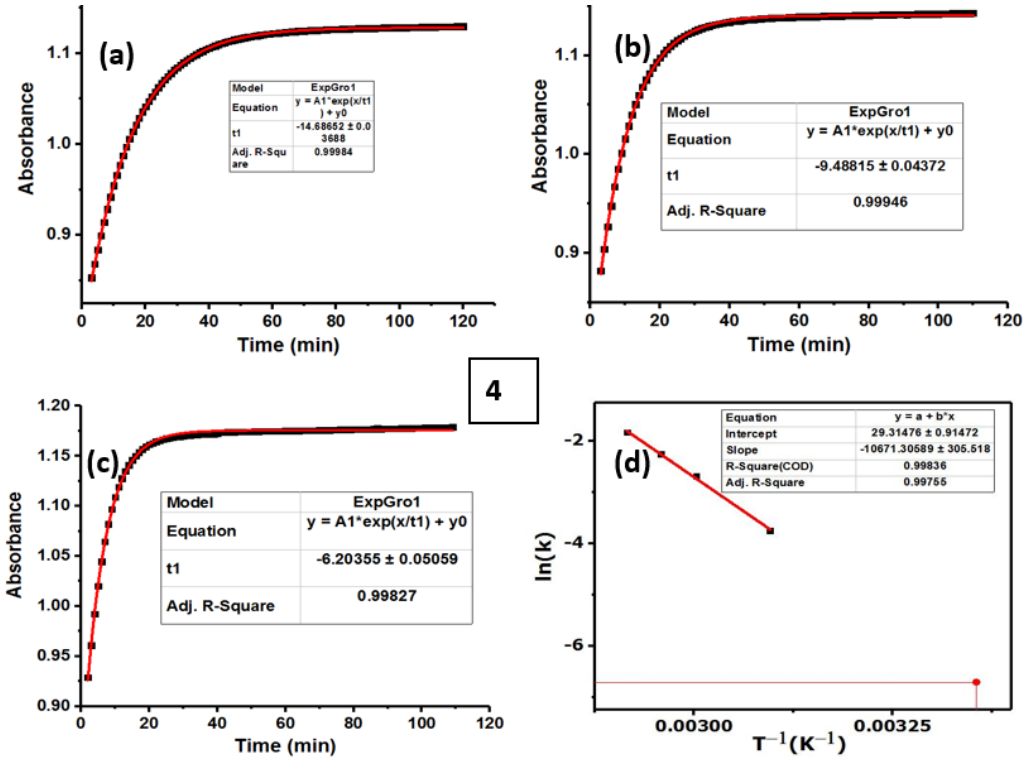

Figure 2A.2.15. Thermal reverse isomerization kinetics of **4** (DMSO, monitored at λ = 513 nm) at (a) 60 °C, (b) 65 °C, and (c) 70 °C, (d) Arrhenius plot for deducing the rate constant at 25 °C by extrapolation.

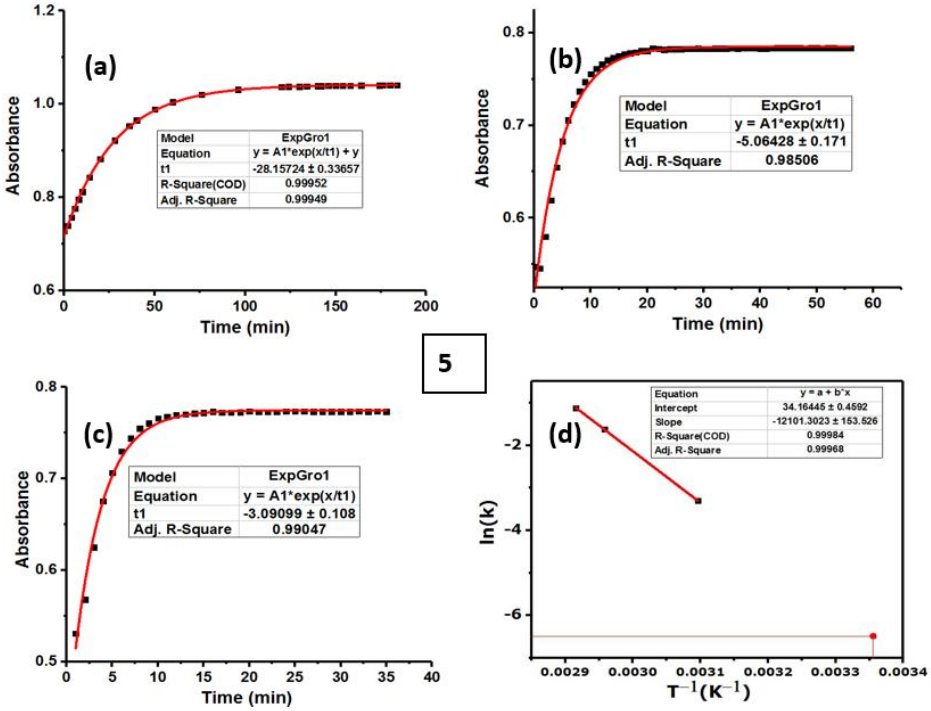

Figure 2A.2.16. Thermal reverse isomerization kinetics of **5** (DMSO, monitored at λ = 492 nm) at (a) 50 °C, (b) 65 °C, and (c) 70 °C, (d) Arrhenius plot for deducing the rate constant at 25 °C by extrapolation.

2A.3. Quantification of photoisomers by using ^{1}H NMR spectroscopy

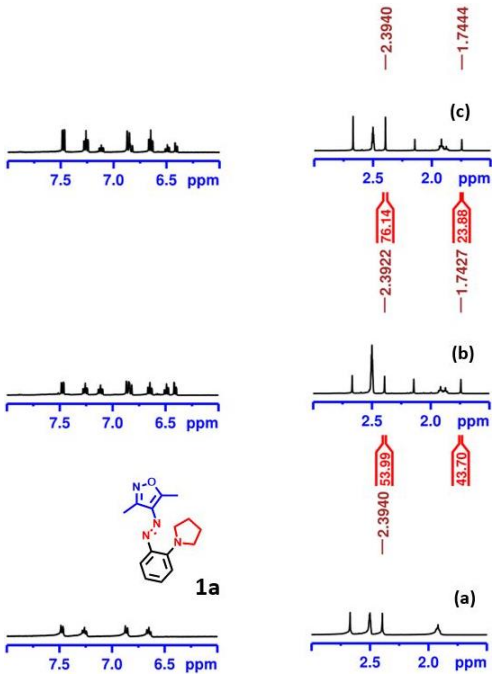

Figure 2A.3.1. Estimation of PSS composition using ^{1}H NMR spectroscopy of **1a** (DMSO-d_6, 12.1 mM) (a) before irradiation; (b) after irradiation at 470 nm; (c) after irradiation at 590 nm. (Normalized integral values of selected protons are indicated for *E*- and *Z*-isomers.

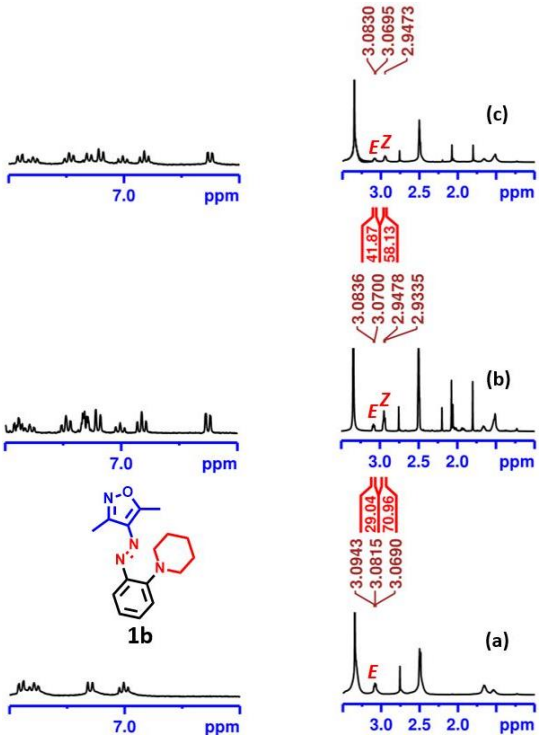

Figure 2A.3.2. Estimation of PSS composition using ^{1}H NMR spectroscopy of **1b** (DMSO-d_6, 11.2 mM) (a) before irradiation; (b) after irradiation at 405 nm; (c) after irradiation at 435 nm. (Normalized integral values of selected protons are indicated for *E*- and *Z*-isomers.)

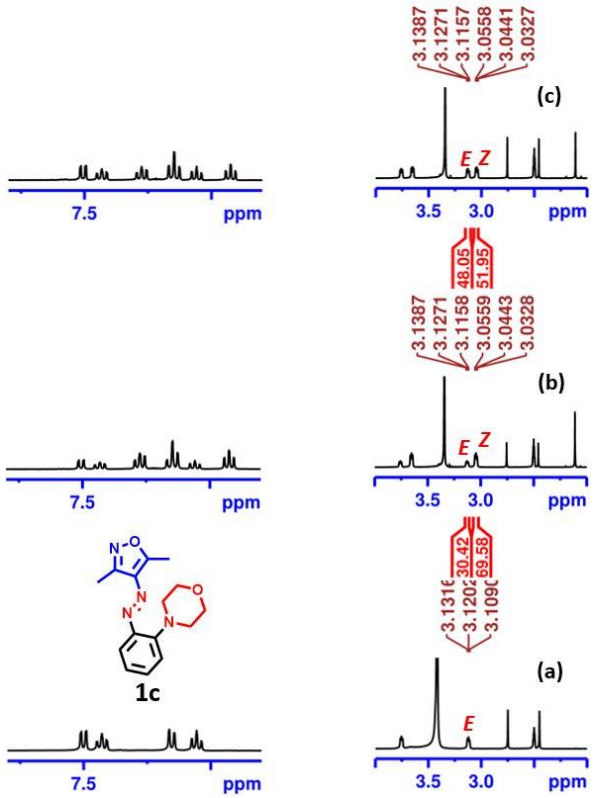

Figure 2A.3.3. Estimation of PSS composition using ^{1}H NMR spectroscopy of **1c** (DMSO-d_6, 10.5 mM) (a) before irradiation; (b) after irradiation at 405 nm; (c) after irradiation at 490 nm. (Normalized integral values of selected protons are indicated for *E*- and *Z*-isomers.)

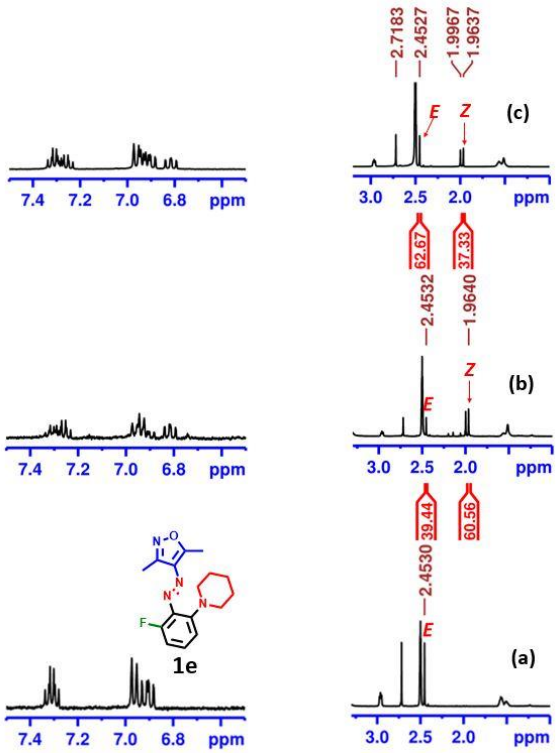

Figure 2A.3.4. Estimation of PSS composition using ^{1}H NMR spectroscopy of **1e** (DMSO-d_6, 10.1 mM) (a) before irradiation; (b) after irradiation at 405 nm; (c) after irradiation at 505 nm. (Normalized integral values of selected protons are indicated for *E*- and *Z*-isomers.)

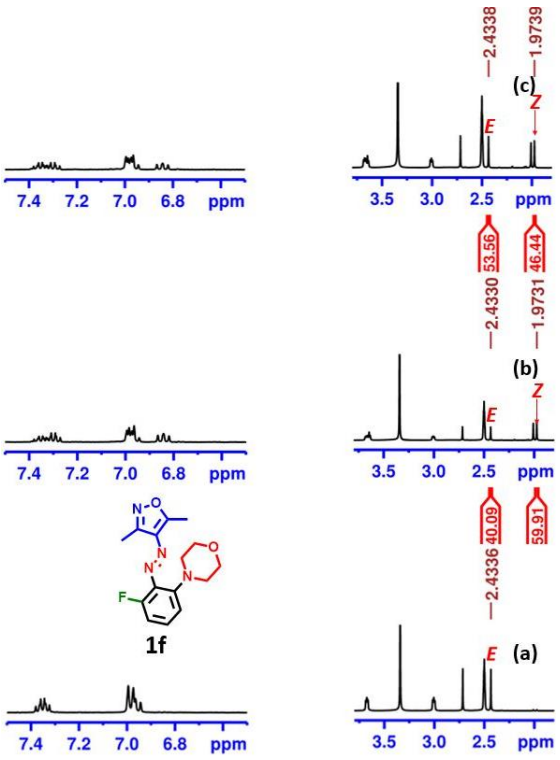

Figure 2A.3.5. Estimation of PSS composition using ^{1}H NMR spectroscopy of **1f** (DMSO-d_6, 9.8 mM) (a) before irradiation; (b) after irradiation at 405 nm; (c) after irradiation at 490 nm. (Normalized integral values of selected protons are indicated for *E*- and *Z*-isomers.)

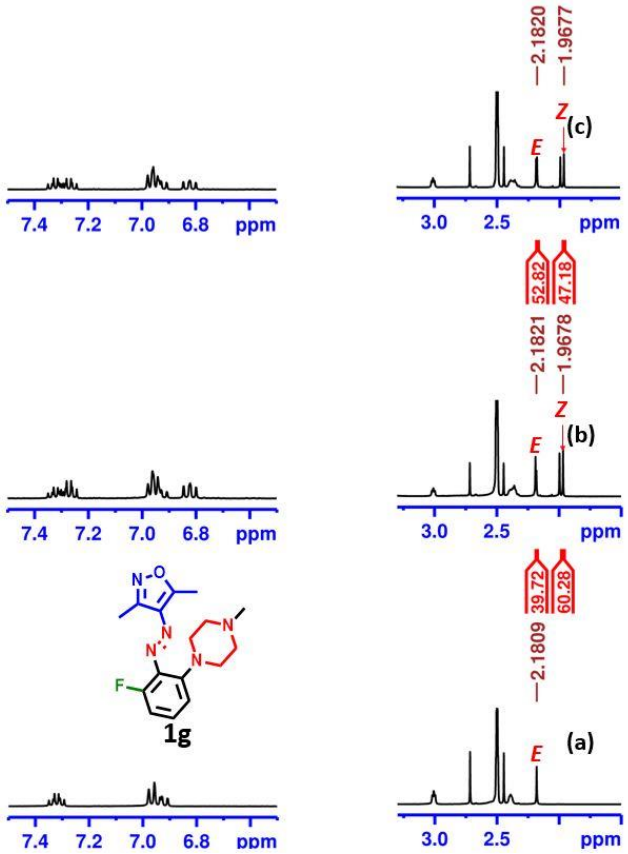

Figure 2A.3.6. Estimation of PSS composition using ^{1}H NMR spectroscopy of **1g** (DMSO-d_6, 9.9 mM) (a) before irradiation; (b) after irradiation at 405 nm; (c) after irradiation at 535 nm. (Normalized integral values of selected protons are indicated for *E*- and *Z*-isomers.)

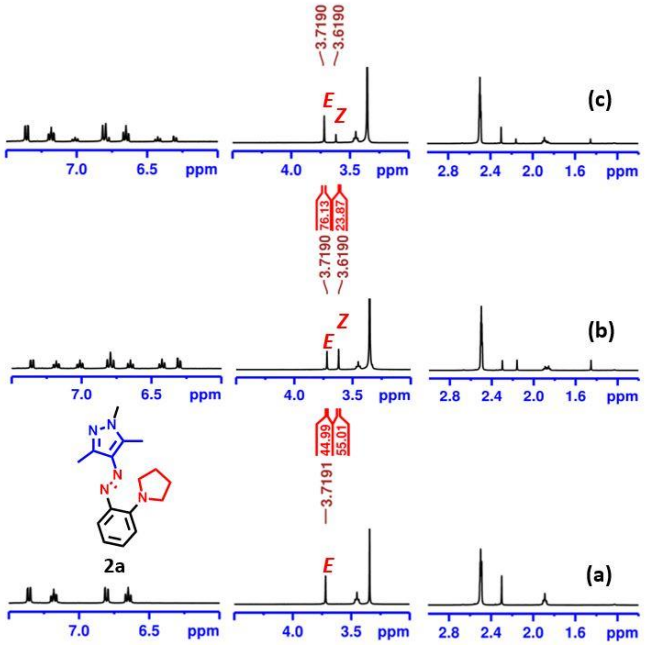

Figure 2A.3.7. Estimation of PSS composition using ^{1}H NMR spectroscopy of **2a** (DMSO-d_6, 11.3 mM) (a) before irradiation; (b) after irradiation at 470 nm; (c) after irradiation at 590 nm. (Normalized integral values of selected protons are indicated for *E*- and *Z*-isomers.)

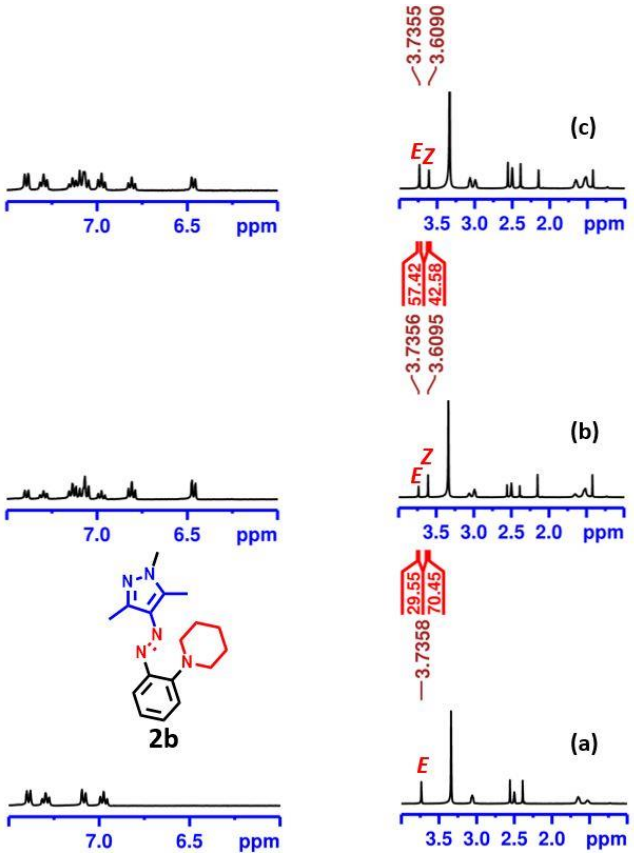

Figure 2A.3.8. Estimation of PSS composition using ^{1}H NMR spectroscopy of **2b** (DMSO-d_6, 10.1 mM) (a) before irradiation; (b) after irradiation at 405 nm; (c) after irradiation at 535 nm. (Normalized integral values of selected protons are indicated for *E*- and *Z*-isomers.)

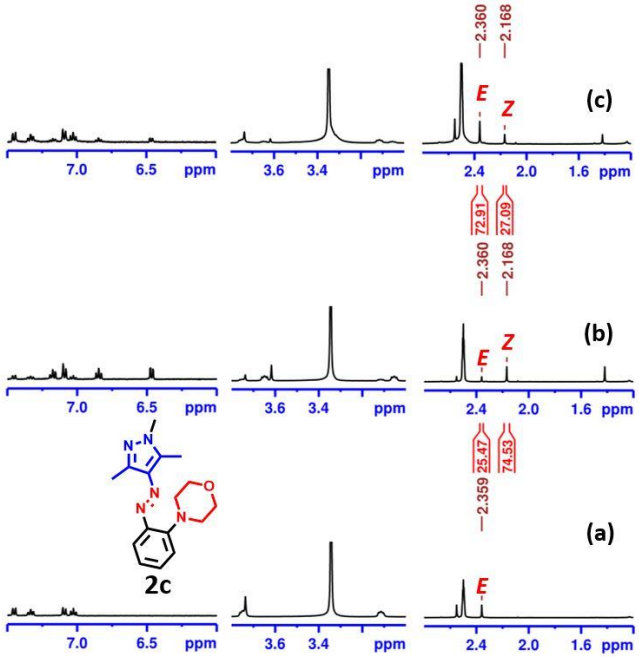

Figure 2A.3.9. Estimation of PSS composition using ^{1}H NMR spectroscopy of **2c** (DMSO-d_6, 10.2 mM) (a) before irradiation; (b) after irradiation at 405 nm; (c) after irradiation at 505 nm. (Normalized integral values of selected protons are indicated for *E*- and *Z*-isomers.)

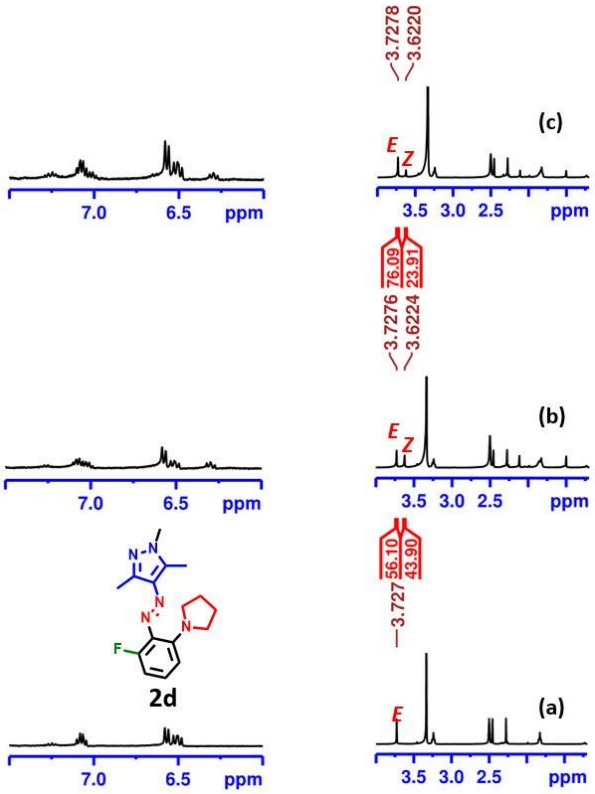

Figure 2A.3.10. Estimation of PSS composition using ^{1}H NMR spectroscopy of **2d** (DMSO-d_6, 10.3 mM) (a) before irradiation; (b) after irradiation at 405 nm; (c) after irradiation at 535 nm. (Normalized integral values of selected protons are indicated for *E*- and *Z*-isomers.)

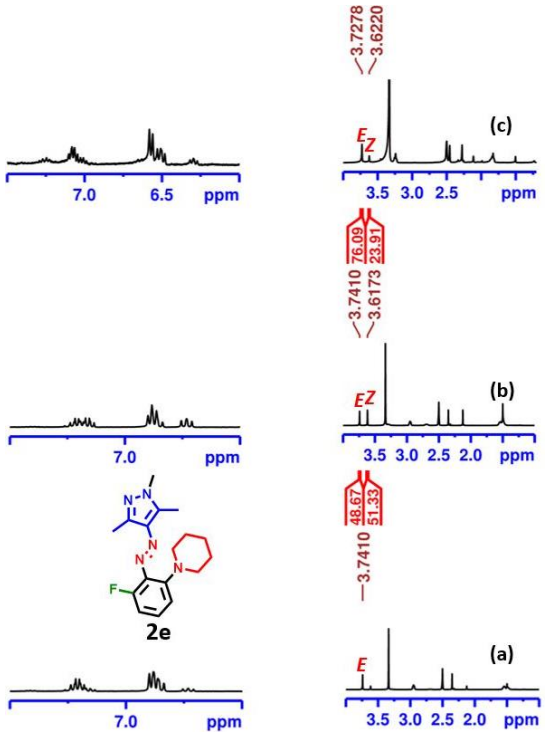

Figure 2A.3.11. Estimation of PSS composition using ^{1}H NMR spectroscopy of **2e** (DMSO-d_6, 9.4 mM) (a) before irradiation; (b) after irradiation at 405 nm; (c) after irradiation at 450 nm. (Normalized integral values of selected protons are indicated for *E*- and *Z*-isomers.)

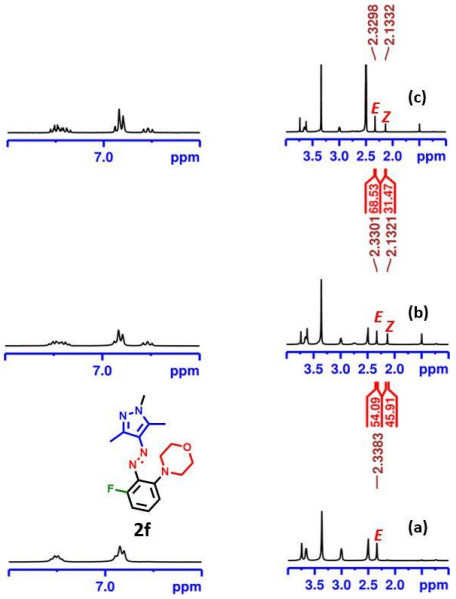

Figure 2A.3.12. Estimation of PSS composition using ^{1}H NMR spectroscopy of **2f** (DMSO-d_6, 9.5 mM) (a) before irradiation; (b) after irradiation at 405 nm; (c) after irradiation at 470 nm. (Normalized integral values of selected protons are indicated for *E*- and *Z*-isomers.)

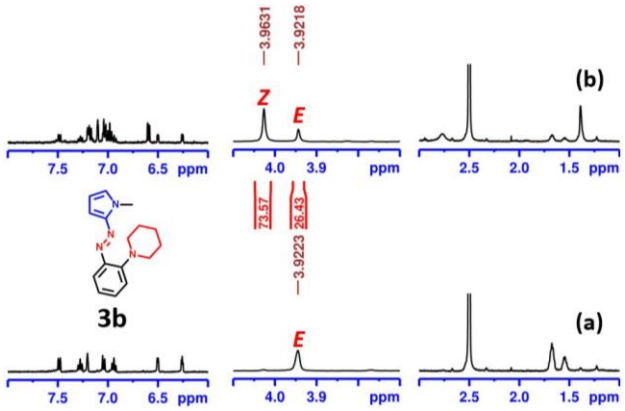

Figure 2A.3.13. Estimation of PSS composition using ^{1}H NMR spectroscopy of **3b** (DMSO-d_6, 11.1 mM) (a) before irradiation; (b) after irradiation at 505 nm.

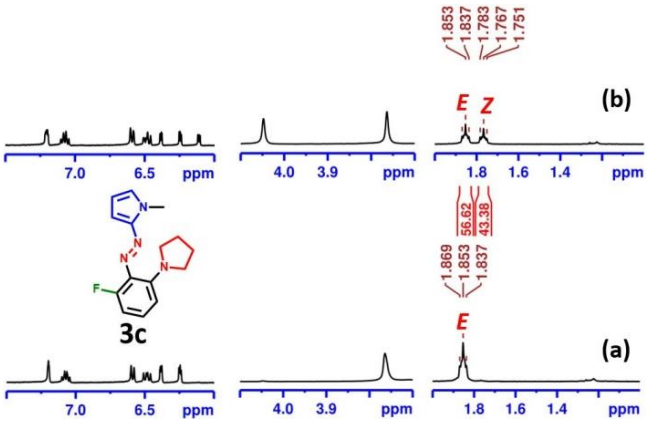

Figure 2A.3.14. Estimation of PSS composition using ^{1}H NMR spectroscopy of **3c** (DMSO-d_6, 10.5 mM) (a) before irradiation; (b) after irradiation at 405 nm.

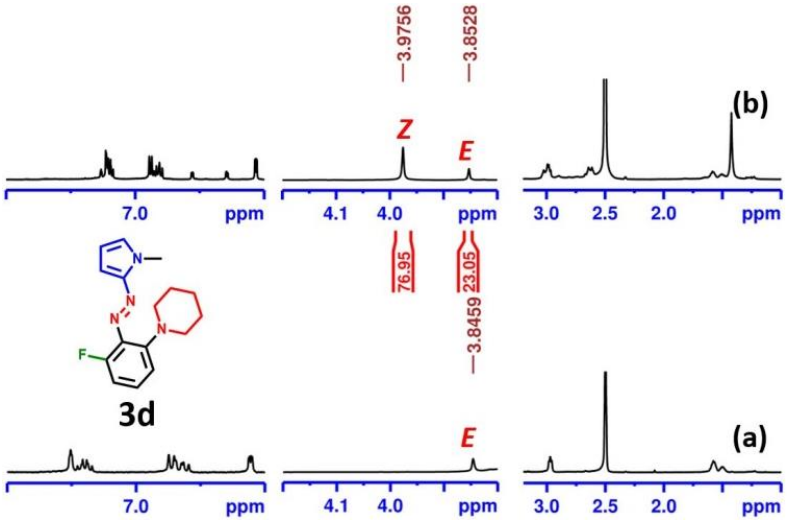

Figure 2A.3.15. ^{1}H NMR photoswitching studies of **3d** in DMSO-d_6 (10.5 mM) (a) before irradiation; (b) after irradiation with 405 nm.

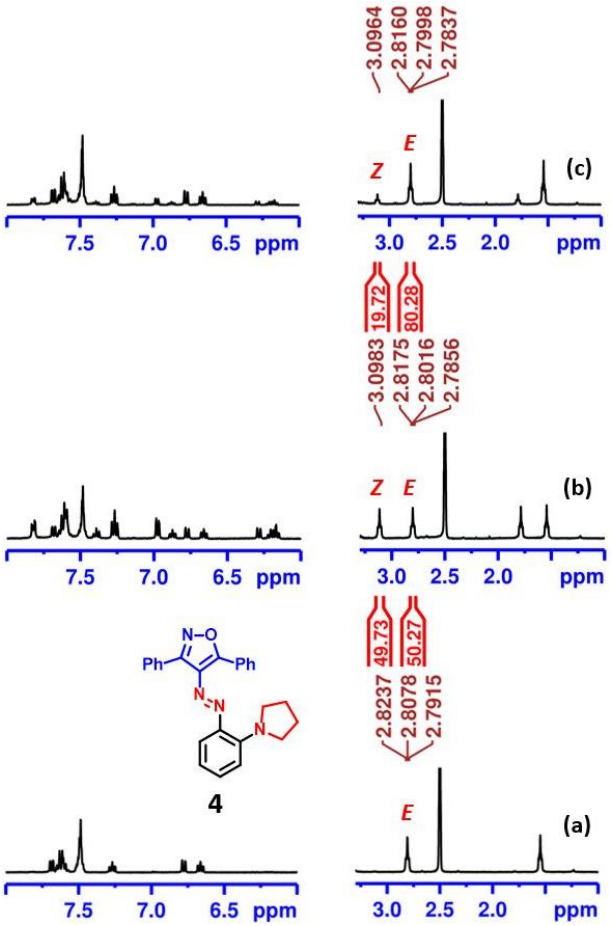

Figure 2A.3.16. Estimation of PSS composition using ^{1}H NMR spectroscopy of **4** (DMSO-d_6, 8.9 mM) (a) before irradiation; (b) after irradiation at 515 nm; (c) after irradiation with 615 nm.

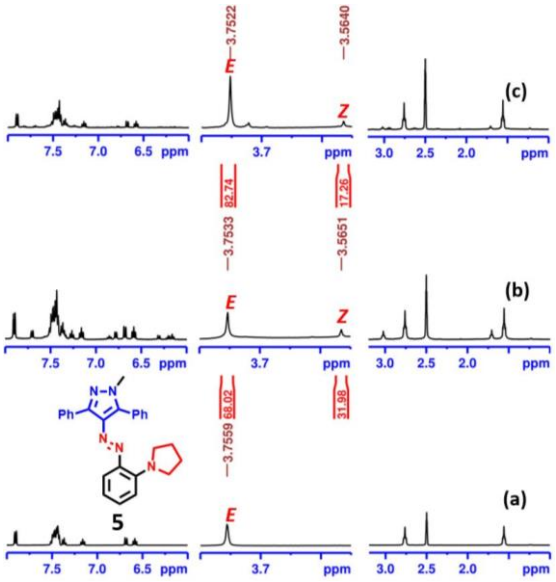

Figure 2A.3.17. Estimation of PSS composition using ^{1}H NMR spectroscopy of **5** (DMSO-d_6, 9.2 mM) (a) before irradiation; (b) after irradiation at 505 nm; (c) after irradiation with 590 nm.

2A.4. Crystallographic details of compound 1i and 5

Single crystal X-ray diffraction data of compound **1i** and **5** was collected using a Rigaku XtaLAB mini diffractometer equipped with Mercury375M CCD detector. The data were collected with MoKα radiation (λ = 0.71073 Å) using omega scans. During the data collection, the detector distance was 49.9 mm (constant) and the detector was placed at 2θ = 29.85° (fixed). The data collection and data reduction were done using CrysAlisPro 1.171.38.46, and crystal structures were solved through OLEX2[1] package using SHELXT[2] and the structures were refined using SHELXL.[3]

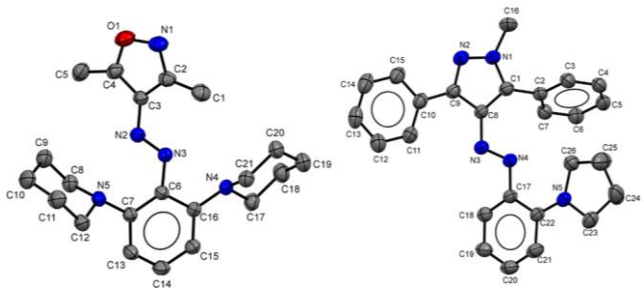

Fig. 2A.4.1 Single crystal X-ray structures of compound **1i** and **5**. Thermal ellipsoids are set at 50% probability. All hydrogen atoms have been omitted for clarity. Selected interatomic distances (Å) and bond angles for compound **1i** (°): O1-N1 = 1.425(3), N2-N3 = 1.258(2), N2-C3 = 1.405(2), N3-C6 = 1.428(2); N3-N2-C3 = 114.15(17), N2-N3-C6 = 114.65(17); Compound **5:** N1-N2 = 1.353(2), N3-C8 = 1.4034(18), N4-N3 = 1.2700(18), N5-C22 = 1.362(2); N4-N3-C8 = 114.00(13), N3-N4-C17 = 113.89(13).

Compound[a]	**1i**	**5**
Chemical Formula	$C_{21}H_{29}N_5O$	$C_{26}H_{25}N_5$
Molar mass	367.49	407.51
Crystal system	triclinic	monoclinic
Space group	$P\bar{1}$	$P2_1/c$
T [K]	200.0(10)	150.01(1)
a [Å]	10.4897(10)	13.3700(7)
b [Å]	11.2575(10)	13.0853(7)
c [Å]	19.1358(10)	12.6475(6)
α [°]	93.114(5)	90
β [°]	103.650(6)	101.442(5)
γ [°]	112.257(8)	90
V [Å^3]	2006.2(3)	2168.7(2)
Z	4	4
D(calcd.) [g·cm^{-3}]	1.217	1.248
μ(Mo-K_α) [mm^{-1}]	0.078	0.076
Reflections collected	44353	29299
Independent reflections	13857	7358
Data/restraints/parameters	13857/0/491	7358/0/281
*R*1, *wR*2[*I*>2*σ*(*I*)][a]	0.0797, 0.1914	0.0730, 0.1886
R1, wR2 (all data)[a]	0.1671, 0.2598	0.1094, 0.2269
GOF	1.023	1.040
CCDC	2114121	2124768

[a] $R1 = \Sigma||Fo| - |Fc||/\Sigma|Fo|$. $wR_2 = [\Sigma w(|Fo^2| - |Fc^2|)^2/\Sigma w|Fo^2|^2]^{1/2}$

1. Dolomanov, O. V.; Bourhis, L. J.; Gildea, R. J.; Howard, J. A. K.; Puschmann, H. *J. Appl. Cryst.* **2009**, *42*, 339-341.
2. Sheldrick, G. M. *Acta Cryst.* **2015**, *A71*, 3-8.
3. Sheldrick, G. M. *Acta Cryst.* **2015**, *C71*, 3-8.)

2A.5. Compound characterization (^{1}H and ^{13}C-NMR) data

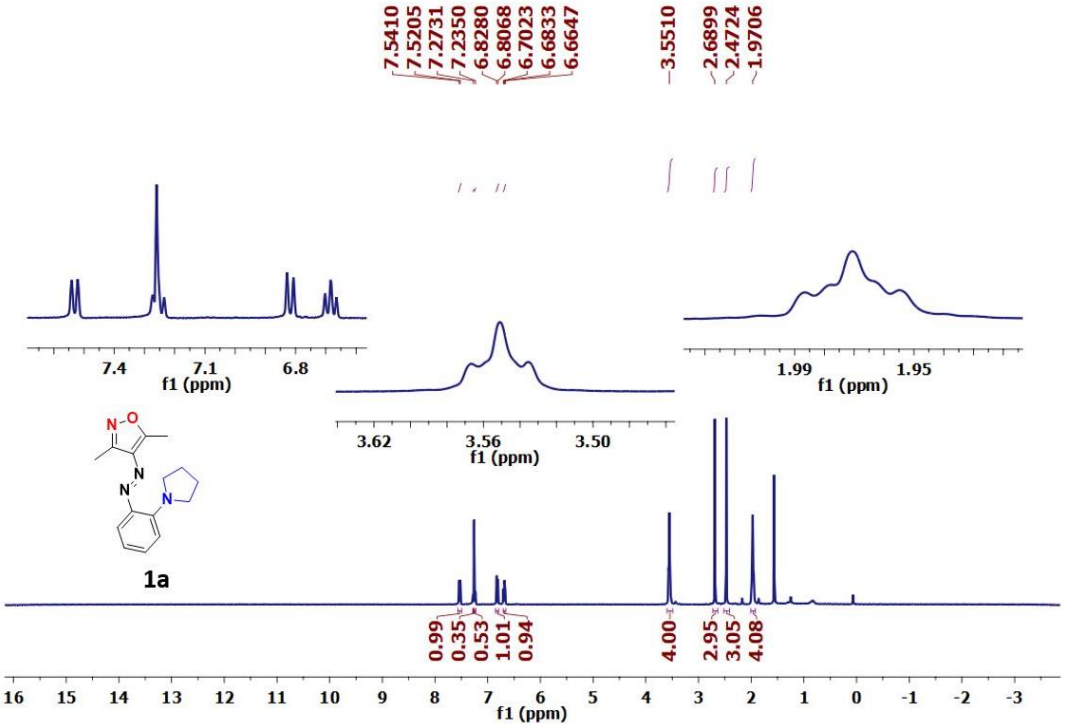

^{1}H NMR spectrum of (*E*)-3,5-dimethyl-4-((2-(pyrrolidin-1-yl)phenyl)diazenyl)isoxazole, **1a** (400 MHz, $CDCl_3$)

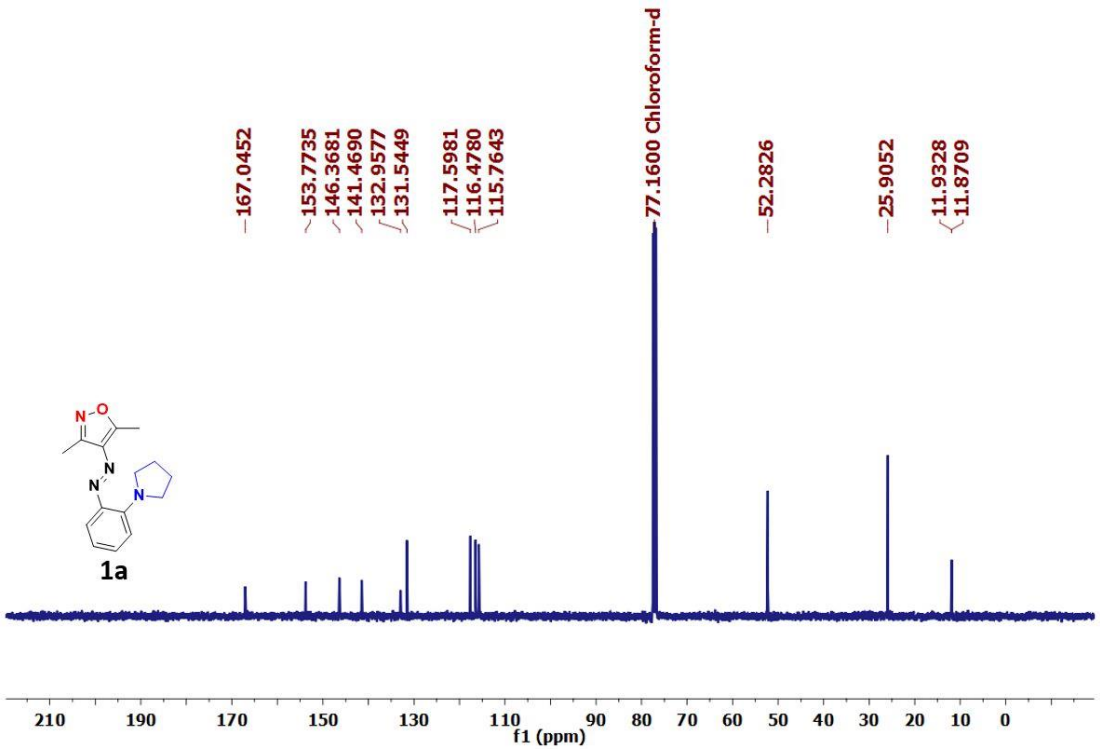

^{13}C{^{1}H} NMR spectrum of (*E*)-3,5-dimethyl-4-((2-(pyrrolidin-1-yl)phenyl)diazenyl)isoxazole, **1a** (100 MHz, $CDCl_3$)

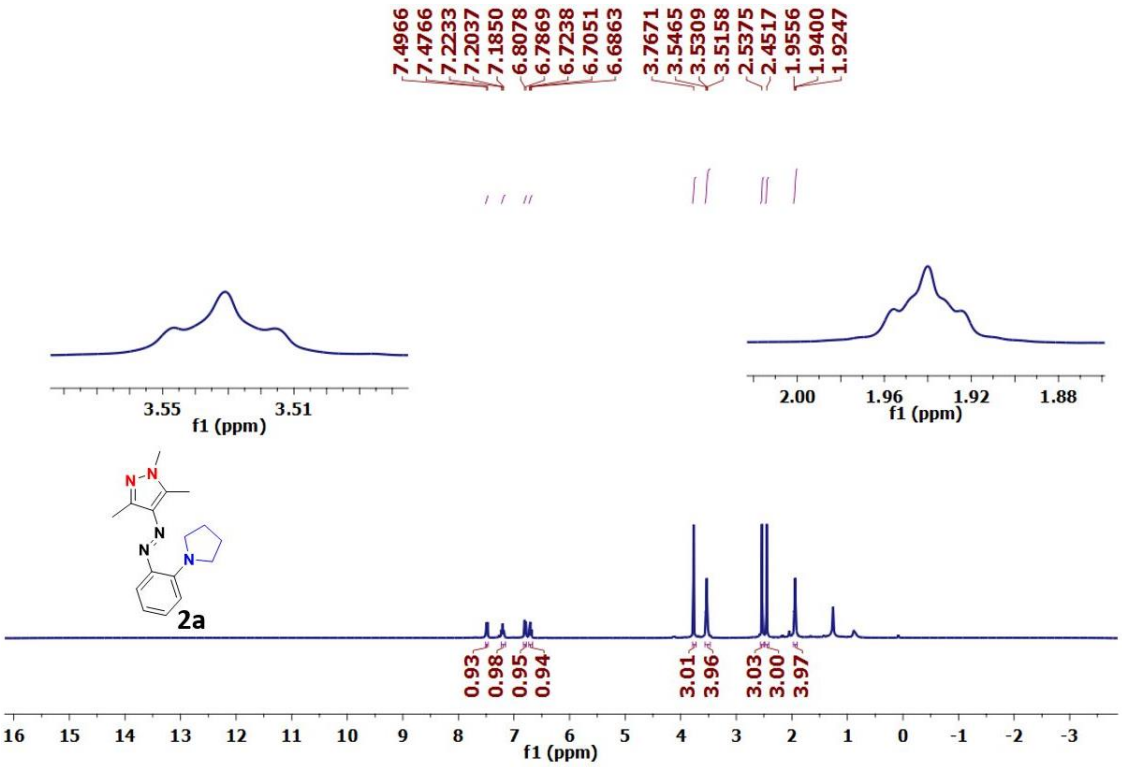

^{1}H NMR spectrum (*E*)-1,3,5-trimethyl-4-((2-(pyrrolidin-1-yl)phenyl)diazenyl)-1H-pyrazole, **2a** (400 MHz, $CDCl_3$)

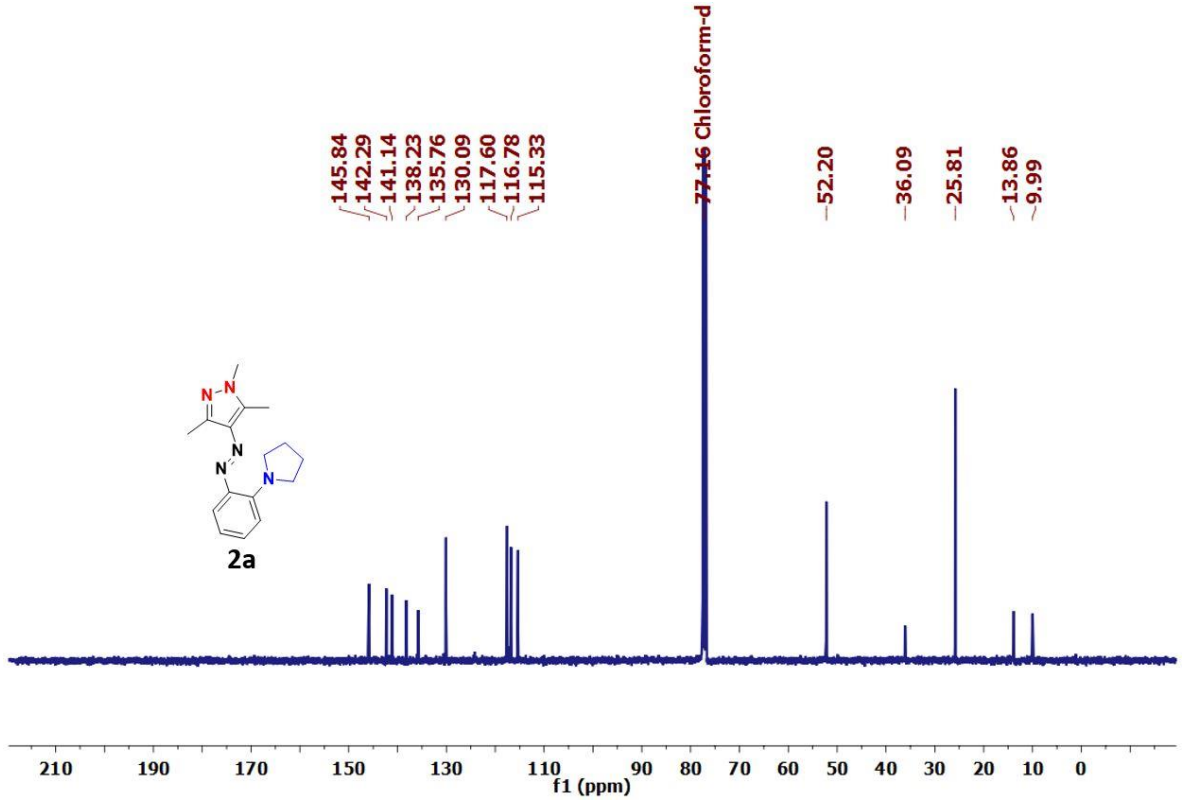

^{13}C{^{1}H} NMR spectrum of (*E*)-1,3,5-trimethyl-4-((2-(pyrrolidin-1-yl)phenyl)diazenyl)-1H-pyrazole, **2a** (100 MHz, $CDCl_3$)

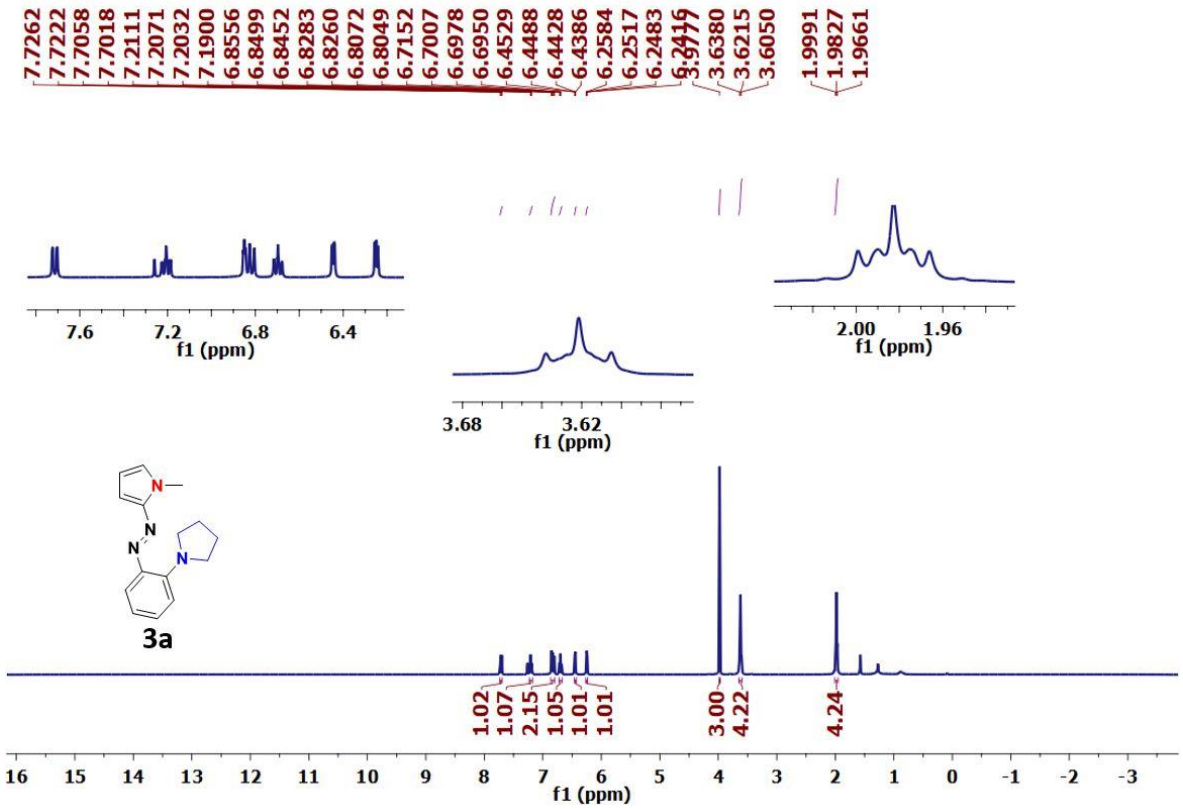

^{1}H NMR spectrum of (*E*)-1-methyl-2-((2-(pyrrolidin-1-yl)phenyl)diazenyl)-1H-pyrrole, **3a** (400 MHz, $CDCl_3$)

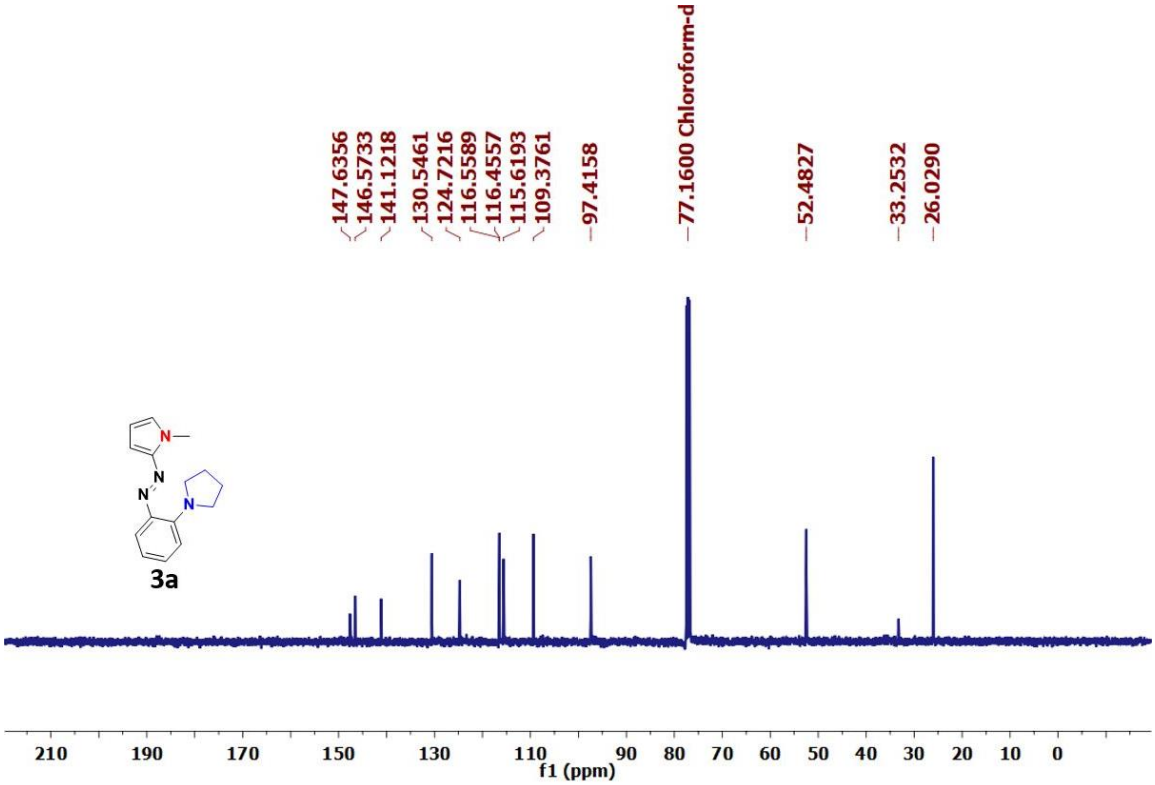

^{13}C{^{1}H} NMR spectrum of (*E*)-1-methyl-2-((2-(pyrrolidin-1-yl)phenyl)diazenyl)-1H-pyrrole, **3a** (100 MHz, $CDCl_3$)

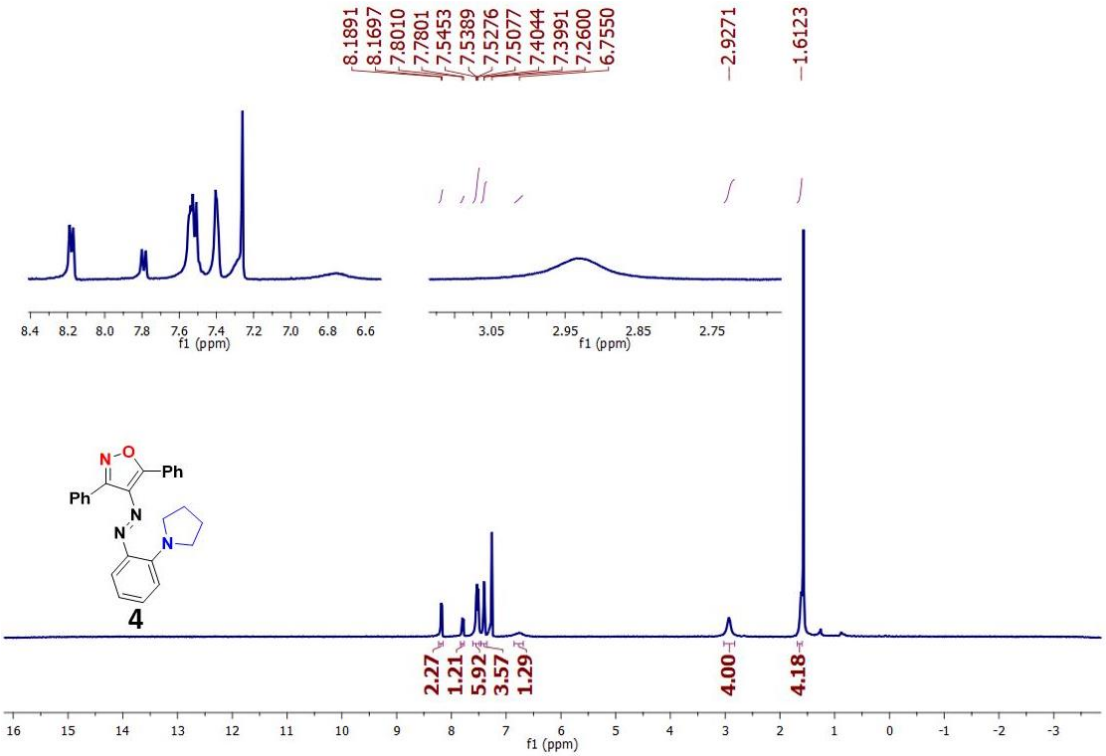

^{1}H NMR spectrum of (*E*)-3,5-diphenyl-4-((2-(pyrrolidin-1-yl)phenyl)diazenyl)isoxazole, **4** (400 MHz, $CDCl_3$)

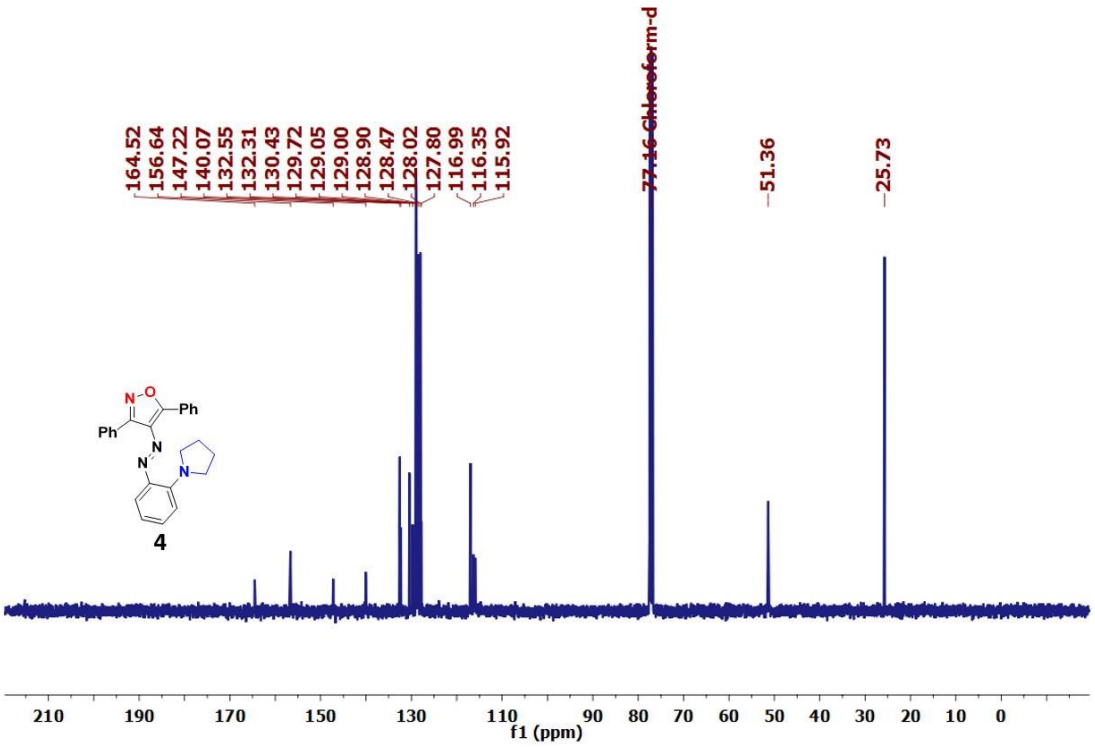

^{13}C{^{1}H} NMR spectrum of (*E*)-3,5-diphenyl-4-((2-(pyrrolidin-1-yl)phenyl)diazenyl)isoxazole, **4** (100 MHz, $CDCl_3$)

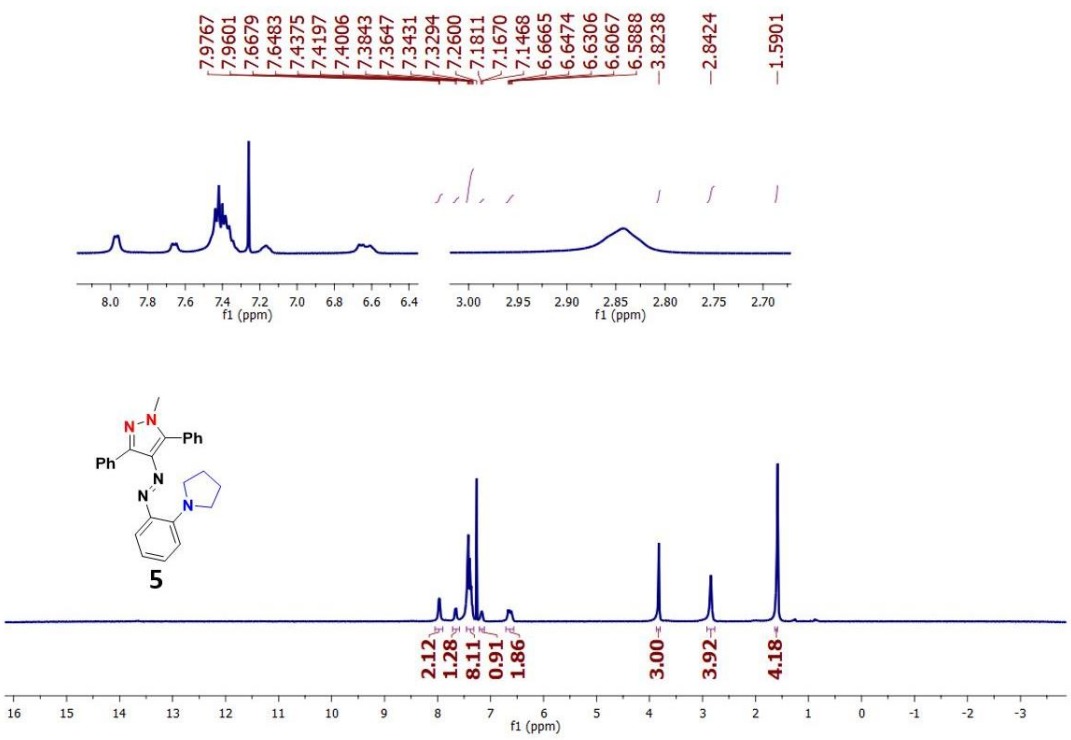

^{1}H NMR spectrum of (*E*)-1-methyl-3,5-diphenyl-4-((2-(pyrrolidin-1-yl)phenyl)diazenyl)-1H-pyrazole, **5** (400 MHz, $CDCl_3$)

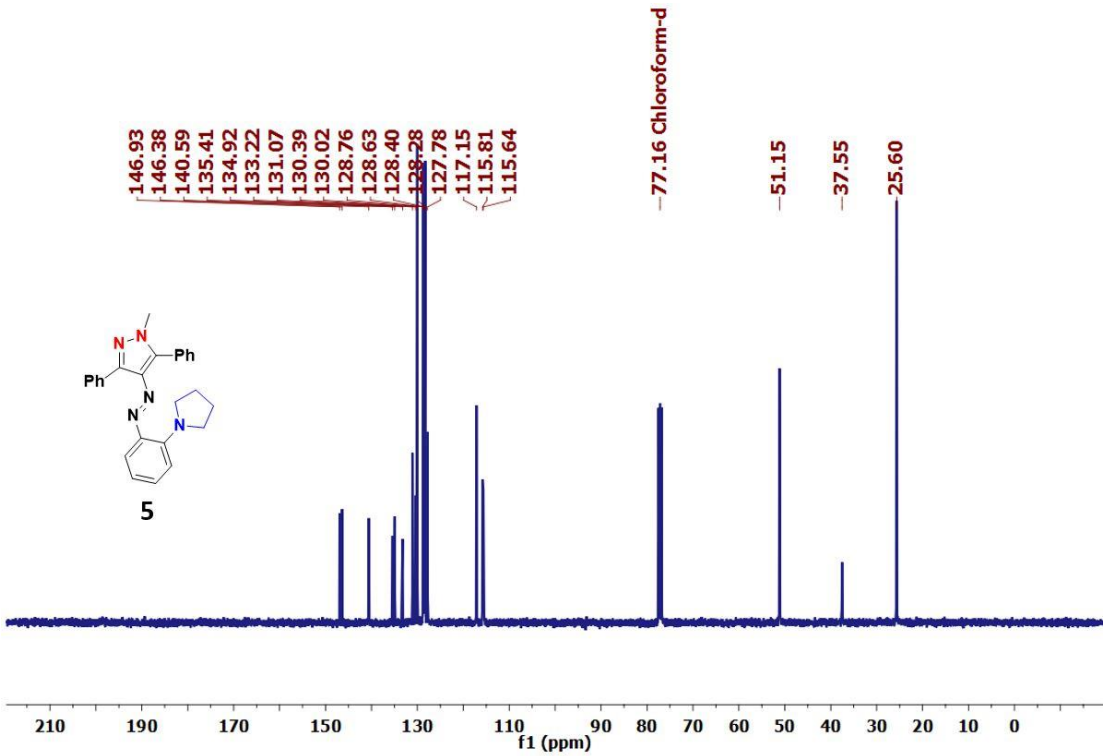

^{13}C{^{1}H} NMR spectrum (*E*)-1-methyl-3,5-diphenyl-4-((2-(pyrrolidin-1-yl)phenyl)diazenyl)-1H-pyrazole, **5** (100 MHz, $CDCl_3$

Chapter 3
Water soluble azoheteroarene photoswitches

Part A. Heteroaryl azopyridinium ionic photoswitches (HAPIPs)

3A.1 Introduction

Azobenzenes are undoubtly versatile molecule which can isomerize between two different geometric isomers by light.[1] In recent times, the introduction of five-membered heterocycle units led to unsymmetrical azoheteroarenes that widens the application potential.[2] This can be attributed to their superior bidirectional photoswitching, and exceptional *Z*-isomer stability. Despite a continuous surge in this direction, photoswitching of azo compounds in aqueous media, in general, remains still as one of the open challenges. Particularly water can destabilize the *Z*-isomer.[3]

Considering the importance of water solubility of photoswitches in the domains of medicinal chemistry and photopharmacology, a few strategies such as, introduction of acidic or basic groups (Woolley and Grøtli),[4] incorporation of polar groups in the rigid ring of the diazocine photoswitches (Herges),[5] manipulation of the polarity by photoswitching (Evans and Yu),[6] etc. have been employed. Alternatively, the photoswitches can be made ionic by connecting a cationic or an anionic group.[7] Using this straight forward approach, a few ionic-based azo photoswitches have been developed by tethering the quaternized ionic centers at a remote location relative to the azo group.[8] However, the best way to exploit and modulate the electrostatic forces of interaction by photoswitching is to create the ionic centre close to the azo group.[9] Direct quarternization of azoheteroarenes, such as, azopyridines, azoimidazoles, etc. can be the possible approach in this regard.[10] Surprisingly, the resulting azopyridinium salts were found to be fast photoswitches (Ogata).[10a] Indeed, such photoswitches were targeted mainly for making real time optical oscillators by exploiting their rapid thermal reverse *Z*-*E* isomerization rates.[10b] Further enhancements in the rates were accomplished by introducing electron donating group at *para* or *ortho* position of the phenyl ring of azopyridinium photoswitch (push-pull type, Valesco).[10b-e]

Notwithstanding such explorations, improving the stability of *Z*-isomers of these compounds in water and bringing tunability have not been attempted yet. At this juncture, we hypothesized that a design comprising five-membered azoheteroarenes[11] (the state-of-the-art

photoswitches, Scheme 1) incorporated with the pyridinium moiety (ionic part) can provide opportunities to achieve the same. To envisage our objectives, we designed 8 heteroaryl azopyridinium ionic photoswitches (HAPIPs) with different five-membered heterocycle units (pyrazole and isoxazole), variation in the alkyl chain (at pyridinium center), changes in the counter ions, and position of the azo relative to the pyridinium center, and substitution at the heterocycle (3,5-dimethyl vs 3,5-diphenyl). Furthermore, the photoswitching and kinetics studies were carried out in different solvents for comparison. The resulting structure-property relationship, effects of solvents and substituents, etc. revealed the tunability of half-lives in the range from seconds to days.

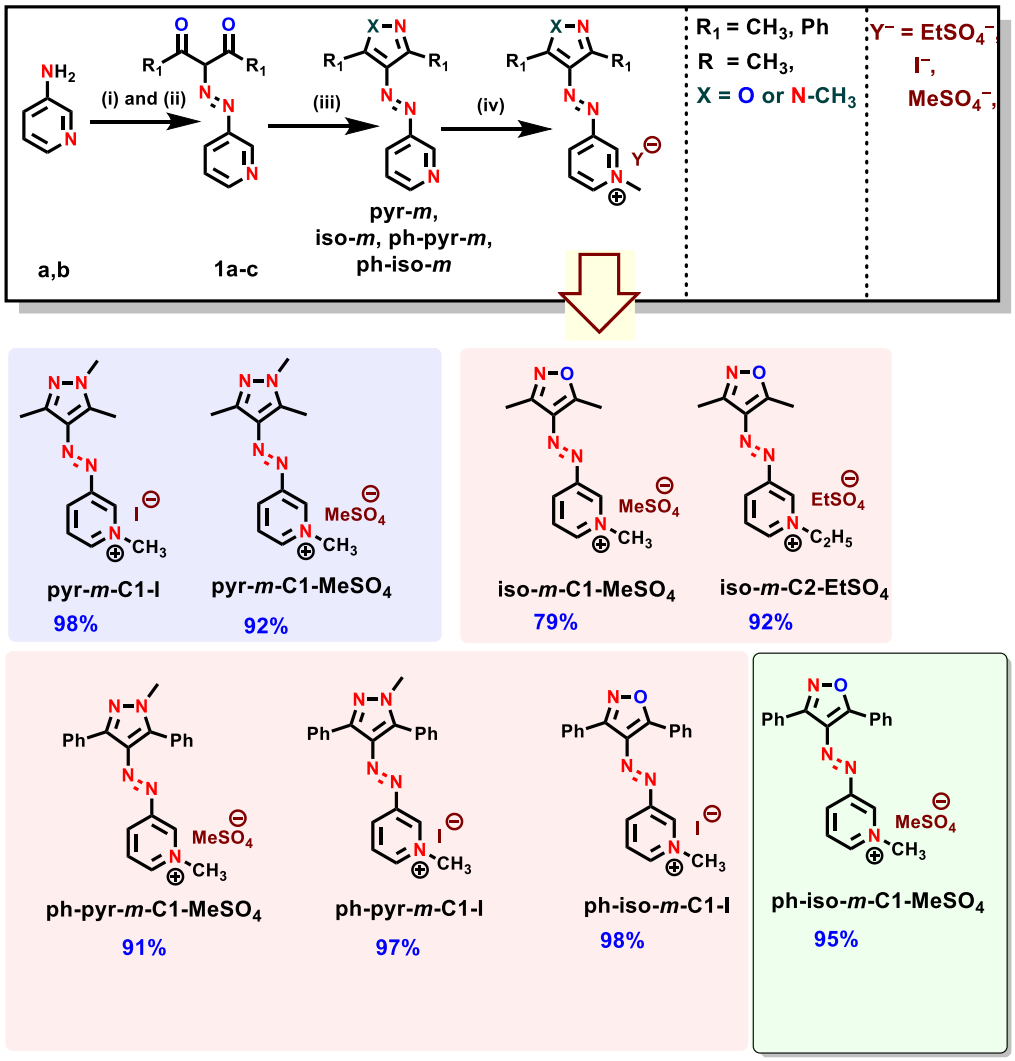

Scheme 3A.1. Synthesis of heteroaryl azopyridinium-based ionic photoswitches (HAPIPs). Conditions: (i) $NaNO_2$/HCl or $NaNO_2$/ HBF_4, H_2O, 0-5 °C; (ii) acac or 1,3-diphenylpropane-1,3-dione, MeOH-H_2O, 0-5 °C to rt, 70-78%; (iii) $NH_2OH.HCl$ or $NH_2NHMe.H_2SO_4$, Na_2CO_3, EtOH, reflux, 8-10 hrs, 60-80%; (iv) alkyl halides or dialkyl sulfate, MeCN, 50-80 °C, 2-5 hrs, 79-98%.

3A.2 Synthesis

To access to the target pyridinium-based azopyrazoles and azoisoxazoles, primarily 3-aminopyridine was diazotized using $NaNO_2$/HCl or $NaNO_2$/HBF_4 conditions, followed by he treatment with acetylacetone (acac) or 1,3-diphenylpropane-1,3-dione (**Scheme 3A.1**). The resulting product was then reacted with *N*-methylhydrazine or hydroxyl amine in the presence of an inorganic base.[2e] The resulting pyridylazopyrazole and pyridylazoisoxazole derivatives were then subjected to quaternization by treating with the corresponding alkyl halides or dialkyl sulfates to obtain our desired heteroaryl azopyridinium ionic photoswitches (**HAPIPs**). In all these targets, either the halides or the alkylsulphates were the counter ions. For the selected compounds, the ion exchange was performed by using sodium tetrafluoroborate, and ammonium hexafluorophosphate.[12] All the targets were characterized using ^{1}H, ^{13}C-NMR, HRMS, IR, and UV-vis spectroscopic techniques (**Appendix 3A**).

3A.3 Photoswitching studies

The photoswitching studies of all 8 HAPIPs were carried out in three different solvents DMSO, MeCN, and H_2O. The thermodynamically stable *E*-isomers of all derivatives exhibited a strong π–π* and a weak n–π* bands. Unlike isoxazole derivatives having a blue shifted π–π* band (320 nm), all the pyrazole-based HAPIPs have shown the π–π* band at or above 348 nm. Such absorption maxima depend on the solvent, where DMSO showed a maximum red shift. All the targets exhibited a maximum forward *E*-*Z* photoisomerization by irradiation at either 365 or 340 nm light. As expected, the enhancement in the intensity of n–π* band and the appearance of blue shifted low intense π–π* transition ascertained the formation of *Z*-isomer. Notably, the n–π* bands of *Z*-isomers of 3,5-dimethyl substituted pyrazole derivatives exhibited a red shift and were separated from the corresponding π–π* bands (**Appendix 3A**).

On the other hand, 3,5-diphenyl substituted pyrazole and all isoxazole (both dimethyl and diphenyl connected) derivatives showed a well separated π–π* and n–π* bands in the spectra of both the *E*- and *Z*-isomers. A representative data on the photoswitching aspects in **pyr-*m*-C1-MeSO$_4$** and **ph-iso-*m*-C1-MeSO$_4$** are included (**Figure 3A.1**). Besides the influences of heterocyclic ring and its substitution, we did not observe any significant changes in the absorption features due to variation in the counter ions (Y^-). All the 3,5-dimethyl substituted pyrazole derivatives, exhibited thermal *Z*-*E* relaxation of *Z*-isomers in seconds, and so the corresponding *Z*-*E* photoisomerization step could not be followed.

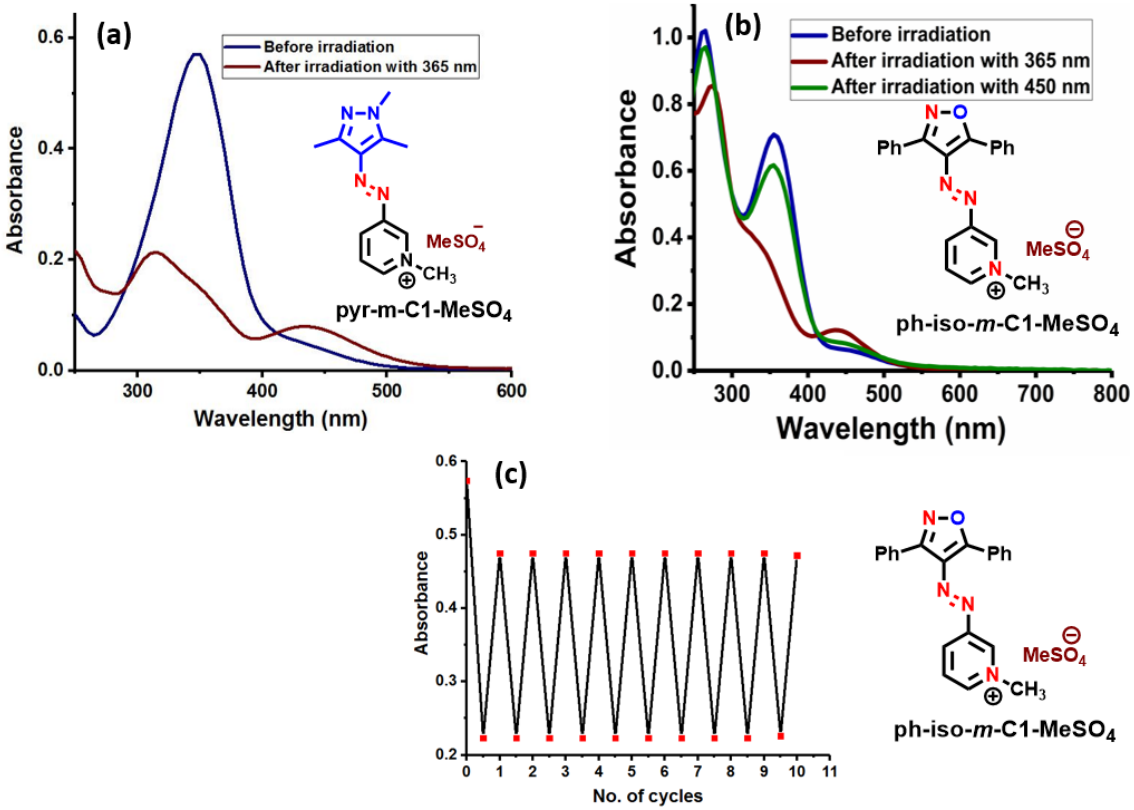

Figure 3A.1. Photoswitching in water: (a) **pyr-*m*-C2-I** and (b) **ph-iso-*m*-C1-MeSO$_4$**; (c) long term stability.

However, the PSS compositions of those derivatives have been estimated using the absorption spectral changes upon forward *E*-*Z* irradiation steps.[3a] Interestingly, the *E*-*Z* photoisomerization conversion in 3,5-dimethyl substituted pyrazole derivatives was maximum (65-75%) in water.

On contrast, the conversion dropped drastically in acetonitrile and DMSO, which could be attributed to faster thermal *Z*-*E* relaxation relative to water. For instance, derivative **pyr-*m*-C1-I** exhibited forward photoisomerization 65% in water while 48% and 7% in DMSO, and MeCN, respectively (**Table 3A.1**). However, all other derivatives showed a moderate to good photoswitching in the forward *E*-*Z* and reverse *Z*-*E* photoisomerization steps in water. Besides that, the stability of *Z*-isomers allowed to follow the photoswitching process by ^{1}H-NMR spectroscopy. Indeed, all isoxazole derivatives and 3,5-diphenyl substituted pyrazole derivatives showed 50-78% forward *E*-*Z* photoisomerization conversion (at 365 or 340 nm, 60 min), whereas the irradiation with blue or green light (60 min) led to the *Z*-*E* photoisomerization with a conversion upto 74-85% in D_2O. For instance, derivative **ph-iso-*m*-C1-MeSO$_4$** showed forward *E*-*Z* photoisomerization upto a maximum of 75% and reverse *Z*-*E* photoisomerization upto 83% in D_2O (**Figure 3A.2**). Furthermore, the photoswitching

stability has been tested for selected derivatives in water over several cycles and they showed fatigue resistance (**Appendix 3A**). Despite exhibiting excellent photoswitching behavior in the forward *E*-*Z* photoisomerization, except a few derivatives several of them showed *Z*-*E* thermal relaxations with half-lives in seconds. To compare the thermal stability of *Z*-isomers of all the 8 targets, we carried out kinetics studies in DMSO, MeCN and H_2O by

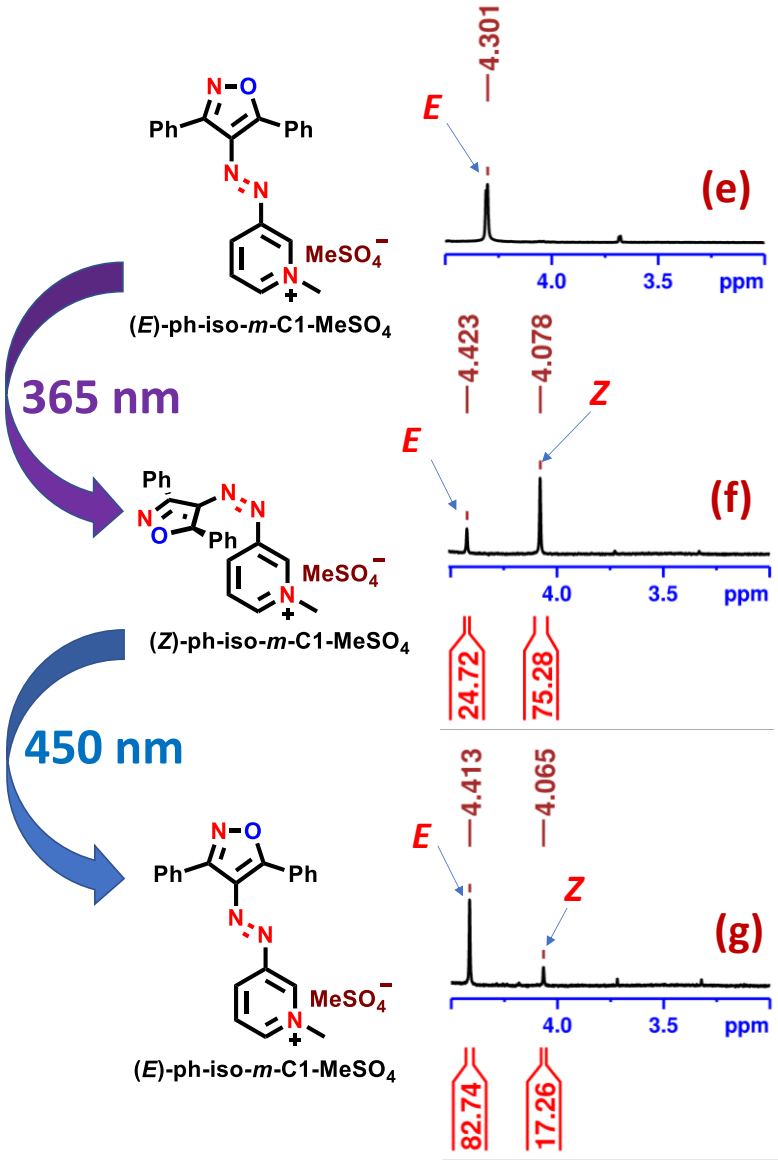

Figure 3A.2. (e-g) partial ^{1}H-NMR data depicting the forward (*E*-*Z*) and reverse (*Z*-*E*) photoisomerization steps in **ph-iso-*m*-C1-MeSO$_4$** (D_2O, 1.3 mM). The normalized integral values due to the pyridinium methyl proton signals are included for the estimation of PSS composition.

following absorption changes in UV-vis spectroscopy. Notably, all 3,5-dimethyl pyrazole derivatives showed a shorter half-life (in seconds to minutes). For instance, the derivative **pyr-**

***m*-C1-I** showed a half-life of *Z*-isomer 47 s, 18 s, and 5 s in water, DMSO, and MeCN, respectively (**Table 3A.1**). Whereas the corresponding 3,5-dimethyl isoxazole derivates showed higher thermal half-lives (in hours) in water. The derivatives **iso-*m*-C1-MeSO$_4$** and **iso-*m*-C2-EtSO$_4$** showed half-lives 2.3 and 2.6 h, respectively in water (**Table 3A.1**). By incorporating 3,5-diphenyl substitution in pyrazole or isoxazole derivatives, the half-lives can further be improved in the order of hours to days. Remarkably, **ph-iso-*m*-C1-MeSO$_4$** exhibited the maximum half-life of 6.3 d in water, which has been estimated based on the extrapolation of an Eyring plot to 25 ^{o}C (**Appendix 3A**). Moreover, the kinetics experiments performed using all pyrazole derivatives were consistently showed a trend, where the rates are varying in the order: water < DMSO < MeCN. For instance, pyrazole derivative **pyr-*m*-C1-I** in water exhibited nine- and three-times slower rate of thermal reverse *Z*-*E* isomerization compared to MeCN and DMSO, respectively (**Table 3A.1**). On the other hand, such rates of the isoxazole derivatives exhibited a slightly different trend: DMSO < water < MeCN. For example, **ph-iso-*m*-C1-I** exhibited a half-life of 6.6 h in MeCN, whereas, it was 8.8 h and 3.9 d in water and DMSO, respectively. Presumably, the solvation of such species or polar transition states play a significant role in the observed trends.[13]

Although *N*-methyl phenylazo-3,5-dimethylpyrazole and phenylazo-3,5-dimethylisoxazole have been reported to be stable photoswitches with long half-lives for *Z*-isomers,[3c,2e] upon generating the corresponding pyridinium derivatives showed contrasting behavior with a wider range of half-lives from seconds to hours. The shorter half-life in pyrazole derivatives of HAPIPs can be attributed to the relatively electron rich *N*-methylpyrazole ring and electron deficient pyridinium ring that makes a pseudo push-pull type azophotoswitch. The stability of the *Z*-isomer further enhanced upon replacing 3,5-dimethyl group with 3,5-diphenyl, which can be attributed to a π-π interaction between the phenyl group and pyridinium moiety.

3A.4 Experimental section

(***E*)-3-(pyridin-3-yldiazenyl)pentane-2,4-dione**, **1a** were prepared according to a procedure reported in literatures.[1,2]

(***E*)-3-(pyridin-4-yldiazenyl)pentane-2,4-dione**, **1b** were prepared according to a procedure reported in literatures.[1,2]

(*E*)-3-((1,3,5-trimethyl-1*H*-pyrazol-4-yl)diazenyl)pyridine, **pyr-*m*** were prepared according to a procedure reported in literatures.[1,2]

(*E*)-3,5-dimethyl-4-(pyridin-3-yldiazenyl)isoxazole, **iso-*m*** were prepared according to a procedure reported in literature.[2]

3A.3.1. General procedure for the synthesis of ph-pyr-*m* or ph-iso-*m*

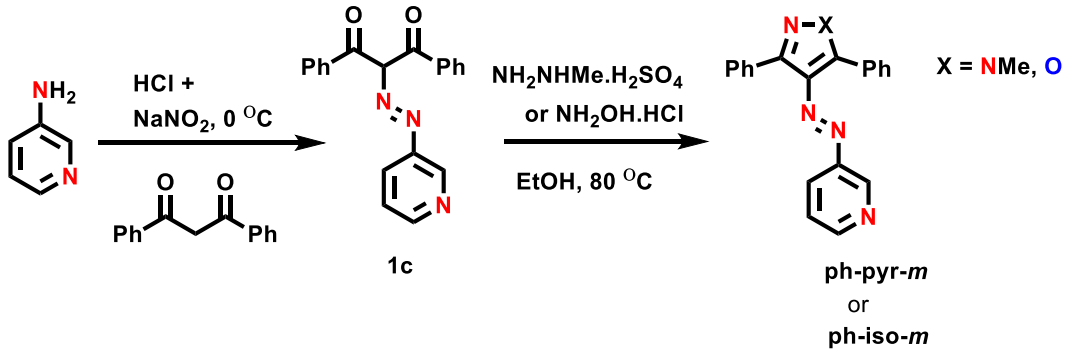

3A.3.2. General procedure for the synthesis of pyr-*m*-C1-I, ph-pyr-*m*-C1-I, ph-iso-*m*-C1-I

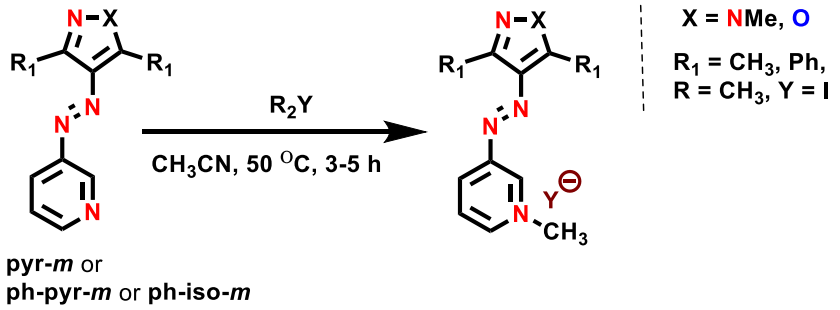

To a solution of **pyr-*m*** (1.0 mmol, 1 eq.) in 10 ml dry acetonitrile in RB flask, the corresponding alkyl bromide or iodide (2.0 mmol, 2 eq.) was added. The mixture was stirred at 80 °C for 3-5 h. After checking TLC for completion of the reaction, it was stopped and cooled down to room temperature. To the reaction mixture diethyl ether was added to generate a crude solid product, which was filtered, washed with excess ether and dried to yield the desired product.

3A.3.3. Synthesis of pyr-*m*-C1-$MeSO_4$ and pyr-*m*-C18-Br or pyr-*p*-C1-I

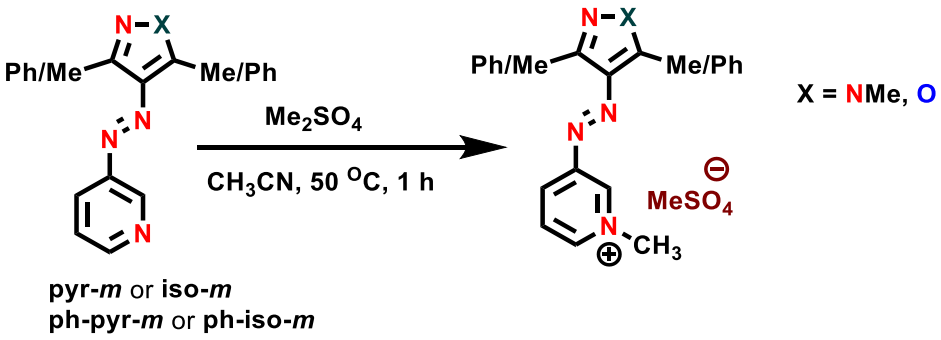

To a solution of **pyr-*m*** or **iso-*m*** or **ph-pyr-*m*** or **ph-iso-*m*** (1.0 mmol, 1 eq.) in 10 ml dry acetonitrile in a RB flask, dimethyl sulphate or diethyl sulphate (2.0 mmol, 2 eq.) was

Table 3A.1. UV-Vis absorption spectroscopic data, PSS compositions and kinetics data in DMSO, MeCN and H_2O

	Compound	Solvent	UV-Vis absorption data λ_{max} in nm				PSS composition UV-Vis spectroscopic data			Kinetics data UV-Vis spectroscopic data	
			E-isomer		*Z*-isomer		*E*-*Z*	*Z*-E	Conc.	k, (x 10^{-2})	$t_{1/2}$
			π–π*	n–π*	π–π*	n–π*	(%*E*:%*Z*)	(%*E*:%*Z*)	(μM)	s^{-1}	
1	**pyr-*m*-C1-I**	DMSO	358	a	355	435	52:48	b	8.7	3.9 ± 0.01	18 s
		MeCN	358	a	358	-	93:07	b	6.3	13.9 ± 0.01	5 s
		H_2O	352	a	323	433	35:65	b	4.4	1.5 ± 0.08	47 s
2	**pyr-*m*-C1-MeSO$_4$**	DMSO	358	a	320	441	22:78	b	32.2	2.9 ± 0.03	23 s
		MeCN	357	a	357	-	98:02	b	21.9	15.5 ± 1.2	4 s
		H_2O	355	a	315	435	25:75	b	10.1	1.9 ± 0.001	37 s
3	**iso-*m*-C1-MeSO$_4$**	DMSO	325	430	295	420	33:67	66:34	40.2	0.2 ± 0.0003 [d]	6.7 h
		MeCN	325	-	305	430	32:68	63:37	50.6	1.2 ± 0.006 [d]	57 min
		H_2O	320	420	305	420	33:67	37:63	38.3	0.5 ± 0.0007 [d]	2.3 h
4	**iso-*m*-C2-EtSO$_4$**	DMSO	327	412	300	427	27:73	68:32	39.3	0.3 ± 0.0003	4.3 h
		MeCN	325	-	305	-	46:54	33:67	30.6	0.7± 0.004 [d]	1.5 h
		H_2O	320	420	305	420	45:55	48:52	43.2	0.5 ± 0.003 [d]	2.6 h
5	**ph-pyr-*m*-C1-MeSO$_4$**	DMSO	365	-	-	444	32:68	62:38	61.8	0.4 [d]	2.7 h [e]
		MeCN	365	-	338	444	32:68	65:35	64.6	1.0 ± 0.0008 [d]	71 min
		H_2O	355	-	-	434	36:64	59:31	86.8	0.1 [d]	9.8 h [e]
6	**ph-pyr-*m*-C1-I**	DMSO	365	-	-	445	33:67	59:41	61.5	0.4 [d]	3.1 h [e]
		MeCN	365	-	345	445	32:68	59:41	55.3	0.6 [d]	1.9 h [e]

		H_2O	355	-	327	440	33:67	59:41	59.9	0.08 [d]	14.9 h[e]
7	**ph-iso-*m*-C1-MeSO$_4$**	DMSO	360	-	-	435	44:56	50:50	142.1	0.004 [d]	13.3 d[e]
		MeCN	360	-	345	445	30:70	64:36	45.1	0.03 [d]	1.9 d[e]
		H_2O	355	-	327	443	43:57	51:49	446.9	0.008 [d]	6.4 d[e]
8	**ph-iso-*m*-C1-I**	DMSO	360	-	-	435	40:60	59:41	37.9	0.01 [d]	3.9 d[e]
		MeCN	360	-	345	445	39:61	56:44	37.1	0.2 ± 0.0008 [d]	6.6 h
		H_2O	355	-	327	443	33:67	59:41	25.9	0.1 [d]	1.8 d[e]

[a]π–π* and n–π* are overlapping; [b]due to fast *Z-E* thermal relaxation, light induced reverse isomerization could not be per-formed; [c]forward *E-Z* photoisomerization was not detected possibly due to fast reverse isomerization. [d] Rate constant in 10^{-2} min^{-1}.[e]Rate constant at 25 ^oC

added. The mixture was stirred at 50 °C for 1 h. After checking TLC for completion of the reaction, it was stopped and cooled down to room temperature. To the mixture diethyl ether was added to generate a crude solid product, which was filtered, washed with excess ether and dried to yield the desired product.

(*E*)-1-methyl-3-((1,3,5-trimethyl-1*H*-pyrazol-4-yl)diazenyl)pyridin-1-ium iodide, **pyr-*m*-C1-I**, 98%, yellow solid, mp = 256-258 °C

^{1}H NMR (400 MHz, DMSO-d_6) δ 9.44 (s, 1H), (b, 8.97 (d, *J* = 8 Hz, 1H), 8.79-8.77 (m, 1H), 8.20 (dd, *J* = 4 Hz, *J* = 8 Hz, 1H), 4.44 (s, 3H), 3.79 (s, 3H), 2.63 (s, 3H), 2.42 (s, 3H) ppm; ^{13}C NMR (100 MHz, $CDCl_3$) δ 151.6, 144.7, 143.1, 141.4, 140.9, 135.3, 134.5, 128.2, 48.2, 36.4, 14.0, 9.7 ppm; HRMS-ESI: *m*/*z* $C_{16}H_{21}N_5$ $[M+H]^+$ calc. 230.1400, obs. 230.1411, *m*/*z* I $[M]^-$ calc. 126.9050, obs. 126.9028; IR (KBr, cm^{-1}) 766, 950, 1274, 1419, 1480, 1613, 2819, 2852, 2936.

(*E*)-1-methyl-3-((1,3,5-trimethyl-1*H*-pyrazol-4-yl)diazenyl)pyridin-1-ium methyl sulfate, **pyz-*m*-C1-MeSO$_4$**, 92%, brown solid, mp = 135-137 °C

^{1}H NMR (400 MHz, $CDCl_3$) δ 9.17 (d, *J* = 5.7 Hz, 1H), 9.13 (s, 1H), 8.62 (d, *J* = 8.3 Hz, 1H), 8.12 (t, *J* = 7.0 Hz, 1H), 4.68 (s, 3H), 3.80 (s, 3H), 3.66 (s, 3H), 2.62 (s, 3H), 2.46 (s, 3H) ppm; ^{13}C NMR (100 MHz, $CDCl_3$) δ 151.8, 145.42, 145.16, 139.99, 139.97, 136.3, 135.3, 128.7, 54.5, 49.4, 36.5, 14.4, 10.4 ppm; HRMS-ESI: *m*/*z* $C_{16}H_{21}N_5$ $[M+H]^+$ calc. 468.4061, obs. 468.4079. *m*/*z* CH_3O_4S $[M]^-$ calc. 126.9050, obs. 126.9028; IR (KBr, cm^{-1}) 769, 950, 1260, 1419, 1480, 1630, 2819, 2852, 2934.

(*E*)-3-((3,5-dimethylisoxazol-4-yl)diazenyl)-1-methylpyridin-1-ium methyl sulfate, **iso-*m*-C1-MeSO$_4$**, 79%, redish-brown solid, mp = 121 °C

^{1}H NMR (400 MHz, CD_3OD) δ 9.48 (s, 1H), 8.98 (s, 1H), 8.91 (d, *J* = 8.4 Hz 1H), 8.22 (t, *J* = 8.6 Hz, 1H), 4.54 (s, 3H), 3.68 (s, 3H), 2.86 (s, 3H), 2.55 (s, 2H) ppm; ^{13}C NMR (100 MHz, CD_3OD) δ 176.0, 154.2, 152.0, 147.2, 143.2, 136.7, 134.4, 129.6, 55.1, 12.2, 11.7 ppm; HRMS-ESI: *m*/*z* $C_{16}H_{21}N_5$ $[M+H]^+$ calc. . 217.1084, obs. 217.1087. *m*/*z* CH_3O_4S $[M]^-$ calc. 110.9752, obs. 110.9745; IR (KBr, cm^{-1}) 775, 950, 1274, 1419, 1480, 1622, 2819, 2852, 2936.

(*E*)-3-((3,5-dimethylisoxazol-4-yl)diazenyl)-1-ethylpyridin-1-ium ethyl sulfate, **iso-*m*-C2-EtSO$_4$**, 92%, reddish orange sticky liquid

^{1}H NMR (400 MHz, $CDCl_3$) δ 9.39-9.36 (m, 2H), 8.69 (d, *J* = 8.0 Hz, 1H), 8.26 (dd, *J* = 8.0 Hz, *J* = 4.0 Hz, 1H), 5.01 (q, *J* = 8.0 Hz, 2H), 4.02 (q, *J* = 8.0 Hz, 2H), 2.84 (s, 3H), 2.52 (s, 3H), 1.75 (t, *J* = 8.0 Hz, *3*H), 1.22 (t, *J* = 8.0 Hz, 3H) ppm; ^{13}C NMR (100 MHz, $CDCl_3$) δ 174.7, 153.1, 150.8, 146.0, 140.2, 135.5, 133.6, 129.4, 63.5, 58.4 17.2, 15.3, 12.25, 12.23

ppm; HRMS-ESI: *m*/*z* $C_{16}H_{21}N_5$ $[M+H]^+$ calc. 231.1240, obs. 231.1237. *m*/*z* $C_2H_5O_4S$ $[M]^-$ calc. 124.9909, obs. 124.9993; IR (KBr, cm^{-1}) 770, 954, 1270, 1419, 1480, 1623, 2819, 2852, 3036.

(*E*)-1-methyl-3-((1-methyl-3,5-diphenyl-1*H*-pyrazol-4-yl)diazenyl)pyridin-1-ium methyl sulfate, ph-pyr-*m*-C1-MeSO$_4$, 91%, **m.p.** = 110-112 ^oC

^1H NMR (400 MHz, DMSO-d_6) δ 9.07 (s, 1H), 8.96 (d, *J* = 6.0 Hz, 1H), 8.43 (d, *J* = 8.6 Hz, 1H) 8.18-8.15 (m, 1H), 7.96-7.94 (m, 2H), 7.68-7.65 (m, 2H), 7.62-7.6 (m, 3H), 7.53-7.48 (m, 3H), 4.39 (s, 3H), 3.88 (s, 3H) ppm; ^{13}C NMR (100 MHz, DMSO-d_6) δ 155.9, 149.3, 147.6, 147.0, 145.3, 142.6, 134.8, 132.6, 131.0, 130.5, 130.3, 129.6, 129.5, 129.0, 128.6, 128.5, 128.3, 127.5, 125.6, 48.43, 48.40 ppm; HRMS-ESI: *m*/*z* $C_{22}H_{20}N_5$ $[M]^+$ calc. 354.1713, obs. 354.1705. *m*/*z* CH_3O_4S $[M]^-$ calc. 110.9752, obs. 110.9745; IR (KBr, cm^{-1}) 620, 834, 1103, 1222, 1385, 1464, 1636, 2846, 2921, 3023, 3449.

(*E*)-1-methyl-3-((1-methyl-3,5-diphenyl-1*H*-pyrazol-4-yl)diazenyl)pyridin-1-ium Iodide, ph-pyr-*m*-C1-I, 97%, **m.p.** = 130-132 ^oC

^1H NMR (400 MHz, DMSO-d_6) δ 9.06 (s, 1H), 8.95 (d, *J* = 5.9 Hz, 1H), 8.43 (d, *J* = 8.3 1H), 8.17-8.14 (m, 1H), 7.95-7.93 (m, 2H), 7.67-7.65 (m, 2H), 7.59-7.57 (m, 3H), 7.53-7.46 (m, 3H), 4.38 (s, 3H), 3.87 (s, 3H); ^{13}C NMR (100 MHz, DMSO-d_6) δ 150.1, 146.5, 145.5, 141.7, 139.8, 134.2, 134.0, 131.7, 130.4, 129.8, 128.9, 128.6, 128.4, 128.3, 127.9, 48.3, 38.0 ppm; HRMS-ESI: *m*/*z* $C_{22}H_{20}N_5$ $[M]^+$ calc. 354.1713, obs. 354.1707, *m*/*z* I $[M]^-$ calc. 126.9050, obs. 126.9028; IR (KBr, cm^{-1}) 626, 834, 1101, 1225, 1387, 1469, 1639, 2847, 2921, 3028, 3449.

(*E*)-3-((3,5-diphenylisoxazol-4-yl)diazenyl)-1-methylpyridin-1-ium methyl sulfate, ph-iso-*m*-C1-MeSO$_4$, 95%, **m.p.** = 172-174 ^oC

^1H NMR (400 MHz, DMSO-d_6) δ 9.30 (s, 1H), 9.10 (d, *J* = 5.6 Hz, 1H), 8.68 (d, *J* = 8.1 Hz, 1H), 8.28-8.21 (m, 3H), 7.75-7.68 (m, 5H), 7.58-7.52 (m, 3H), 4.46 (s, 3H) ppm; ^{13}C NMR (100 MHz, DMSO-d_6) δ 169.3, 155.8, 149.4, 147.0, 142.6, 134.8, 132.6, 131.0, 130.5, 129.6, 129.5, 129.0, 128.6, 128.3, 127.5, 125.6, 48.43 ppm; HRMS-ESI: *m*/*z* $C_{21}H_{17}N_4O$ $[M]^+$ calc. 341.1397, obs. 341.1395, *m*/*z* CH_3O_4S $[M]^-$ calc. 110.9752, obs. 110.9745.; IR (KBr, cm^{-1}) 629, 824, 1109, 1232, 1385, 1469, 1639, 2846, 2921, 3028, 3443.

(*E*)-3-((3,5-diphenylisoxazol-4-yl)diazenyl)-1-methylpyridin-1-ium Iodide, ph-iso-*m*-C1-I, 98%, **m.p.** = 230-232 ^oC

^1H NMR (400 MHz, DMSO-d_6) δ 9.32 (s, 1H), 9.10 (d, *J* = 5.8 Hz, 1H), 8.70 (d, *J* = 8.4 Hz, 1H), 8.30-8.23 (m, 3H), 7.76-7.68 (m, 5H), 7.61-7.53 (m, 3H), 4.63 (s, 3H) ppm; ^{13}C NMR

(100 MHz, DMSO-d_6) δ 169.2, 155.8, 149.3, 146.8, 142.5, 134.8, 132.6, 131.0, 130.4, 129.5, 129.4, 128.9, 128.5, 127.4, 125.5, 48.42 ppm; HRMS-ESI: *m*/*z* $C_{21}H_{17}N_4O$ $[M]^+$ calc. 341.1397, obs. 341.1395. *m*/*z* I $[M]^-$ calc. 126.9050, obs. 126.9028.; IR (KBr, cm^{-1}) 620, 838, 1123, 1242, 1387, 1468, 1635, 2816, 2941, 3026, 3449.

(*E*)-1,3-diphenyl-2-(pyridin-3-yldiazenyl)propane-1,3-dione, 1c, 70%**, m.p.** = 125-127 °C ^{1}H NMR (400 MHz, $CDCl_3$) δ 13.33 (s, 1H), 8.58 (d, *J* = 2.5 Hz, 1H), 8.37 (dd, *J* = 4.7 Hz, *J* = 1.2 Hz, 1H), 8.10-8.07 (m, 2H), 7.69-7.63 (m, 3H), 7.59-7.51 (m, 4H), 7.42-7.38 (m, 2H), 8.28 (dd, *J* = 8.3 Hz, *J* = 4.7 Hz, 1H); ^{13}C NMR (100 MHz, $CDCl_3$) δ 192.9, 191.2, 145.9, 138.4, 138.2, 137.6, 136.6, 135.4, 133.2, 133.1. 130.7, 128.6, 128.51, 128.46, 124.2, 122.6 ppm; HRMS-ESI: *m*/*z* $C_{20}H_{16}N_3O$ $[M+H]^+$ calc. 330.1243, obs. 330.1225; IR (KBr, cm^{-1}) 627, 833, 1103, 1222, 1388, 1467, 1636, 2845, 2921, 3028, 3449.

(*E*)-3-((1-methyl-3,5-diphenyl-1H-pyrazol-4-yl)diazenyl)pyridine, ph-pyr-*m*, 75% **m.p.** = 155-157 °C

^{1}H NMR (400 MHz, $CDCl_3$) δ 8.73 (d, *J* = 2.0 Hz, 1H), 8.55 (dd, *J* = 4.7 Hz, *J* = 1.5 Hz, 1H), 8.02-7.99 (m, 2H) 7.82-7.79 (m, 1H), 7.52-7.40 (m, 8H), 7.30 (ddd, *J* = 8.2 Hz, *J* = 4.7 Hz, *J* = 0.5 Hz, 1H), 3.86 (s, 3H)ppm; ^{13}C NMR (100 MHz, $CDCl_3$) δ 150.7, 148.3, 147.7, 146.8, 137.7, 134.8, 132.5, 130.4, 129.4, 129.1, 128.6, 128.5, 128.3, 126.5, 123.9, 37.7 ppm; HRMS-ESI: *m*/*z* $C_{21}H_{18}N_5$ $[M+H]^+$ calc. 340.1562, obs. 340.1543.; IR (KBr, cm^{-1}) 620, 834, 1103, 1222, 1385, 1464, 1638, 2857, 2925, 3023, 3450.

(*E*)-3,5-diphenyl-4-(pyridin-3-yldiazenyl)isoxazole, ph-iso-*m*, 68%, **m.p.** = 139-141 °C

^{1}H NMR (400 MHz, $CDCl_3$) δ 8.73 (d, *J* = 2.0 Hz, 1H), 8.35 (dd, *J* = 4.8 Hz, *J* = 1.6 Hz, 1H), 7.92-7.88 (m, 2H) 7.65-7.61 (m, 1H), 7.41-7.39 (m, 2H), 7.26-7.24 (m, 2H), 7.20-7.08 (m, 5H) ppm; ^{13}C NMR (100 MHz, $CDCl_3$) δ 167.7, 156.7, 151.9, 147.9, 146.7, 131.6, 131.5, 129.0, 128.7, 128.1, 127.0, 124.1 ppm; HRMS-ESI: *m*/*z* $C_{20}H_{15}N_4O$ $[M+H]^+$ calc. . 327.1246, obs. 327.1227.; IR (KBr, cm^{-1}) 610, 874, 1109, 1226, 1388, 1464, 1639, 2846, 2931, 3028, 3448.

3A.5 Conclusions

In summary, we have synthesized 8 heteroaryl azopyridinium-based HAPIPs in high yields. Variation in heterocycles (pyrazole vs isoxazole moiety), changing position of azopyridinium nitrogen relative to azo group (3- vs 4-), alteration in alkyl chain lengths connected at the pyridinium center, and counter ion exchanges (I^-, Br^-, $MeSO_4^-$, BF_4^-, PF_6^-, and $EtSO_4^-$) and variation in the substitution at heterocycle (3,5-dimethyl vs 3,5-diphenyl

substitution) have been investigated in detail.[14] Through this study, we found (a) the remarkable effect of isoxazole moiety in the stability of *Z*-isomers of 3-azopyridinium systems; (b) tunability in rate of thermal relaxations between seconds and days by means of changing solvent, counterions, heterocycle unit and its substitution; (c) More importantly, efficient and bidirectional photoswitching in water (**Figure 3A.1**). All these results are quite valuable in the exploration of azoaheteroarene based systems for various applications pertaining aqueous media.

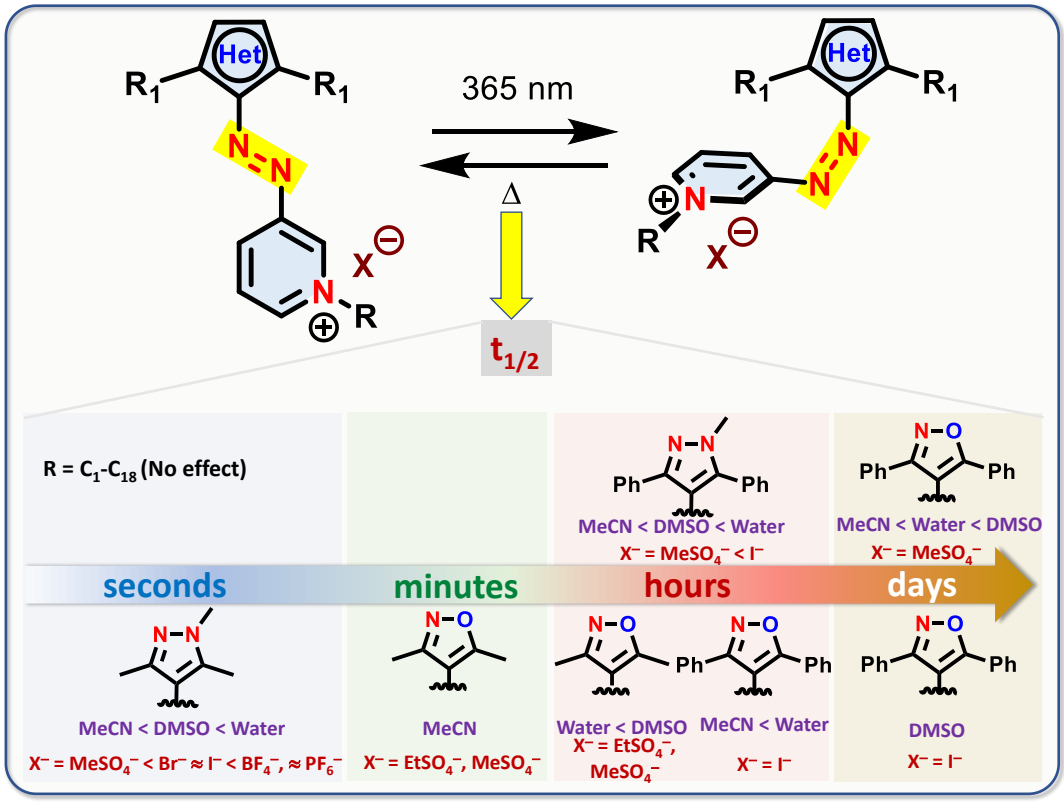

Figure 3A.3. Summary of HAPIPs.

3A.6 References

1. (a) Jerca, F. A.; Jerca, V. V.; Hoogenboom, R. *Nat. Rev. Chem.* **2022**, *6*, 51-69. (b) Trads, J. B.; Hüll, K.; Matsuura, B. S.; Laprell, L.; Fehrentz, T.; Görldt, N.; Kozek , K. A.; Weaver, C. D.; Klöcker, N.; Barber, D. M.; Trauner, *Angew. Chem. Int. Ed.* **2019**, *58*, 43, 15421-15428.
2. For example, (a) Crespi, S.; Simeth, N. A.; König, B. *Nat. Rev. Chem.*, **2019**, *3*, 133−146. (b) Grewal, S.; Gupta, D.; Gaur, A. K.; Saraswat, M.; Venkataramani, S. Nova Publishers: New York, **2019**. (c) Gerkman, M. A.; Gibson, R. S. L.; Calbo, J.; Shi, Y.; Fuchter, J.; Han, G. G. D. *J. Am. Chem. Soc*. **2020**, *142*, 8688-8695. (d) Kortekaas, L.; Simke, J.; Kurka, D. W.; Ravoo, B. J. *ACS Appl. Matter. Interfaces.*, **2020**, *12*, 32054-32060. (e) Kumar, P.; Srivastava, A. Sah, C.; Devi, S.; Vekataramani, S. *Chem. Eur. J.* **2019**, *25*, 11924-11932. (f) Nagai, Y.; Ishiba, K.;

Yamamoto, R.; Yamada, T.; Morikawa, M.; Kimizuka, N. *Angew. Chem. Int. Ed*. **2021**, *60*, 6333-6338. (g) Weston, C. E.; Kramer, A.; F. Collin, O. Yildiz, F. J. M. Almes, M. J. Fuchter, *ACS infect. Dis.*, 2017, **3**, 152-161. (h) Mafy, N.; Matsuo, K.; Hiruma, S.; Uehara, R.; Tamaoki, N.; *J. Am. Chem. Soc*. **2020**, *142*, 1763−1767.

3. (a) Weston, C. E.; Richardson, R. D.; Haycock, P. R.; White, A. J. P.; Fuchter, M. J.; *J. Am. Chem. Soc*. **2014**, *136*, 11878-11881. (b) Devi, S.; Saraswat, M.; Grewal, S.; Venkataramani, S. *J. Org. Chem*. **2018**, *83*, 8, 4307-4322.
4. (a) Zhang, Z.; Burns, D. C., Kumita, J. R.; Smart, O. S.; Woolley, G. A. A. *Bioconjugate Chem*. **2003**, *14*, 4, 824–829. (b) Ferreira, R.; Nilsson, J. R.; Solano, C.; Andréasson, J.; Grøtli, M. *Sci. Rep*. **2015**, *5*, 9769.
5. (a) Lentes, P.; Frühwirt, P.; Freißmuth, H.; Moormann, W.; Kruse, F.; Gescheidt, G.; Herges, R. *J. Org. Chem*. **2021**, *86*, 4355−4360. (b) Lentes, P.; Stadler, E.; Röhricht, F.; Brahms, A.; Gröbner, J.; Sönnichsen F. D., Gescheidt, G.; Herges, R. *J. Am. Chem. Soc*. **2019**, *141*, 13592−13600.
6. (a) Blayo, C.; Kelly, E. A.; Houston, J. E.; Khunti, N.; Cowieson, N. P.; Evans, R. C. *Soft Matter*. **2020**, *16*, 9183-9187. (b) Liu, Y.; Zhu, C.; Zhao, Y.; Qing, X.; Wang, F.; Deng, D.; Wei, J.; Yu, Y. *J. Adv. Mater. Interfaces*. **2019**, *6*, 1901158.
7. (a) Xia, D.; Yu, G.; Li., J.; Huang, F. *Chem. Commun*. **2014**, *50*, 3606-3608. (b) Kang, N.; Li, P.; Tan, S.; Wang, C.; *Soft Matter*. **2019**, *15*, 7992-7995.
8. (a) Wuckert, E.; Harjung, M. D.; Kapernaum, N.; Mueller, C.; Frey, W.; Baro, A.; Giesselmann, F.; Laschat, S. *Phys. Chem. Chem. Phys*. **2015**, *17*, 8382-8392. (b) Mogaki, R.; Okuro, K.; Aida, T. *J. Am. Chem. Soc*. **2017**, *139*, 10072-10078.
9. (a) Yoshida, T.; Monji, T.; Kawamori, D.; Akai, N.; Shibuya, K.; Kawai, A. *Chem. Lett*. **2013**, *42*, 1490-1492. (b) Lin, C.; Yang, L.; Xu, M.; An, Q.; Xiang, Z.; Liu, X. *RSC Adv*. **2016**, *6*, 51552–51561.
10. (a) Nakagawa, M.; Rikukawa, M.; Watanabe, M.; Sanui, K.; Ogata, N. *Bull. Chem. Soc. Jpn*. **1997**, *70*, 737-744. (b) Amorós, J. G.; Massad, W. A.; Nonell, S.; Velasco, D. *Org. Lett*. **2010**, *12*, 15, 3514-3517. (c) Amorós, J. G.; Nonell, S.; Velasco, D. *Chem. Commun*. **2012**, *48*, 3421–3423. (d) Amorós, J. G.; Gómez, E. ; Vallés, E.; Velasco, D. *Chem. Commun*. **2012**, *48*, 9080-9082. (e) Amorós, J. G.; Gómez, E.; Velasco, D. *Beilstein J. Org. Chem.* **2012**, *8*, 1003-1017.
11. For example, (a) Calbo, J.; Weston, C. E.; White, A. J. P.; Rzepa, H. S.; Contreras-García, J.; Fuchter, M. J. *J. Am. Chem. Soc*. **2017**, *139*, 1261-1274. (b) Slavov, C.; Yang, C.; Heindl, A. H.; Wegner, H. A.; Dreuw, A.; Wachtveitl, J. *Angew. Chem. Int. Ed*. **2020**, *59*, 380-387. (c) Tuck, J. R.; Tombari, R. J.; Yardeny, N.; Olson, D. E. *Org. Lett*. **2021**, *23*, 4305-4310.
12. Dai, J.; Zhao, K. Q.; Wang, B. Q.; Hu, P.; Heinrich, B.; Donnio, B. *J. Mater. Chem. C*. **2020**, *8*, 4215-4225.
13. Presumably, the polarity of the solvent and mode of solvation influences the thermal stability of *Z*-isomers. Besides that, the polar transition states are sensitive to the solvent polarity, and so the thermal relaxation rates may vary depending on the solvents used. For example, see: Dokić, J.; Gothe, M.; Wirth, J.; Peters, M. V.; Schwarz, J.; Hecht, S.; Saalfrank, P. *J. Phys. Chem. A*. **2009**, *113*, 24, 6763-6773.
14. Synthesis, Characterization and Photoswitching Studies of Photoswitchable Azopyridine Based Ionic Compounds (http://hdl.handle.net/123456789/3904).

Appendix 3A

3A.1. Analysis of photoswitching and thermal stability using UV-Vis spectroscopy

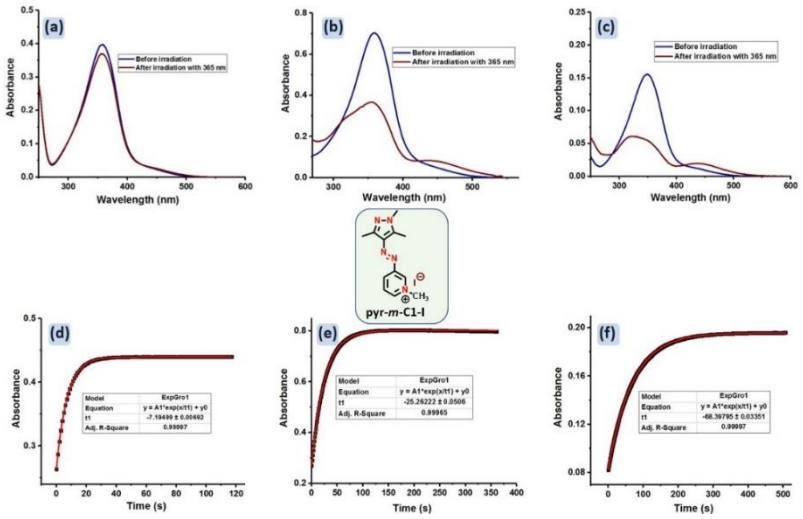

Figure 3A.1. Photoswitching behavior of **pyr-*m*-C1-I**. Forward photoisomerization of **pyr-*m*-C1-I** in (a) MeCN (6.3 μM); (b) DMSO (8.7 μM), and (c) H_2O (4.4 μM); Thermal reverse isomerization kinetics at rt (d) in MeCN (monitored at λ= 358 nm, 7.1 μM), (e) in DMSO (monitored at λ= 358 nm, 9.6 μM), and (f) in H_2O (monitored at λ= 352 nm, 4.4 μM). (The first order rate constants have been estimated using an exponential fit).

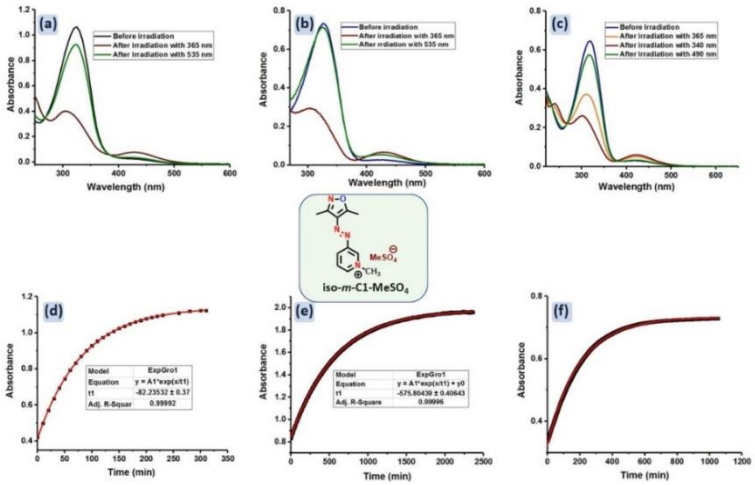

Figure 3A.2. Photoswitching behavior of **iso-*m*-C1-MeSO$_4$**. Reversible photoisomerization of **iso-*m*-C1-MeSO$_4$** in (a) MeCN (50.6 μM); (b) in DMSO (40.2 μM), and (c) in H_2O (38.3 μM) at the indicated wavelengths; Thermal reverse isomerization kinetics at rt in (d) MeCN (monitored at λ = 325 nm, 50.6 μM), (e) DMSO (monitored at λ = 325 nm, 96.5 μM), and (f) H_2O (monitored at λ = 320 nm, 38.3 μM). (The first order rate constants have been estimated using an exponential fit).

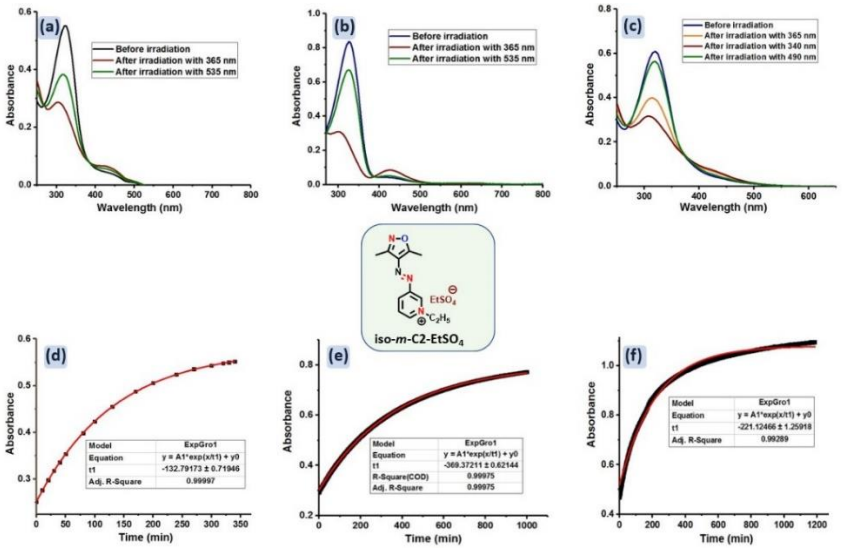

Figure 3A.3. Photoswitching behavior of **iso-*m*-C2-EtSO$_4$**. Reversible photoisomerization of **iso-*m*-C2-EtSO$_4$** in (a) MeCN (30.6 μM); (b) DMSO (39.3 μM), and (c) H_2O (43.2 μM); Thermal reverse isomerization kinetics at rt in (d) MeCN (monitored at λ = 325 nm, 30.6 μM), (e) DMSO (monitored at λ = 327 nm, 39.3 μM) and (f) H_2O (monitored at λ = 320 nm, 43.2 μM). (The first order rate constants have been estimated using an exponential fit).

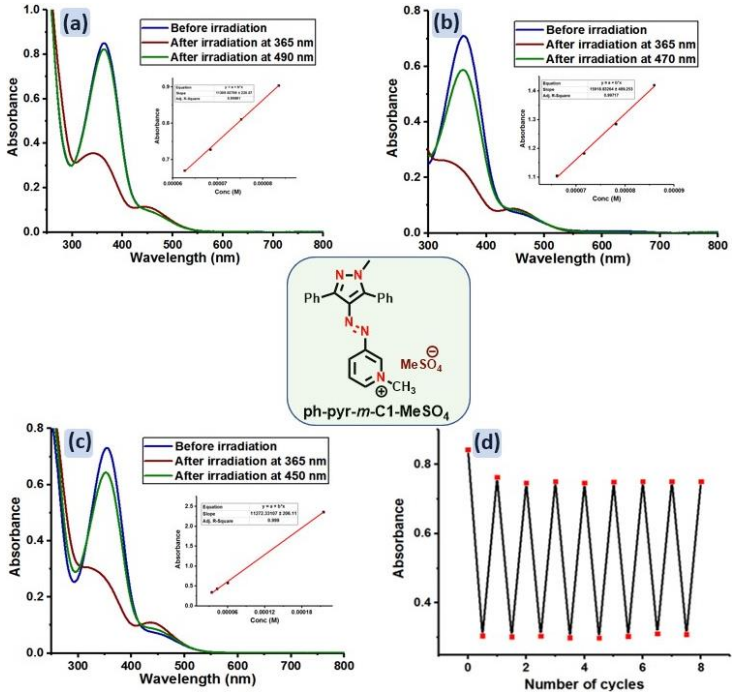

Figure 3A.4. Photoswitching behavior of **ph-pyr-*m*-C1-MeSO$_4$**. Reversible photoisomerization of **ph-pyr-*m*-C1-MeSO$_4$**in (a) MeCN (75.2 μM); (b) DMSO (45.6 μM), and (c) H_2O (64.9 μM); (d) Cyclic experiment in H_2O (monitored at λ = 355 nm, 74.8 μM).

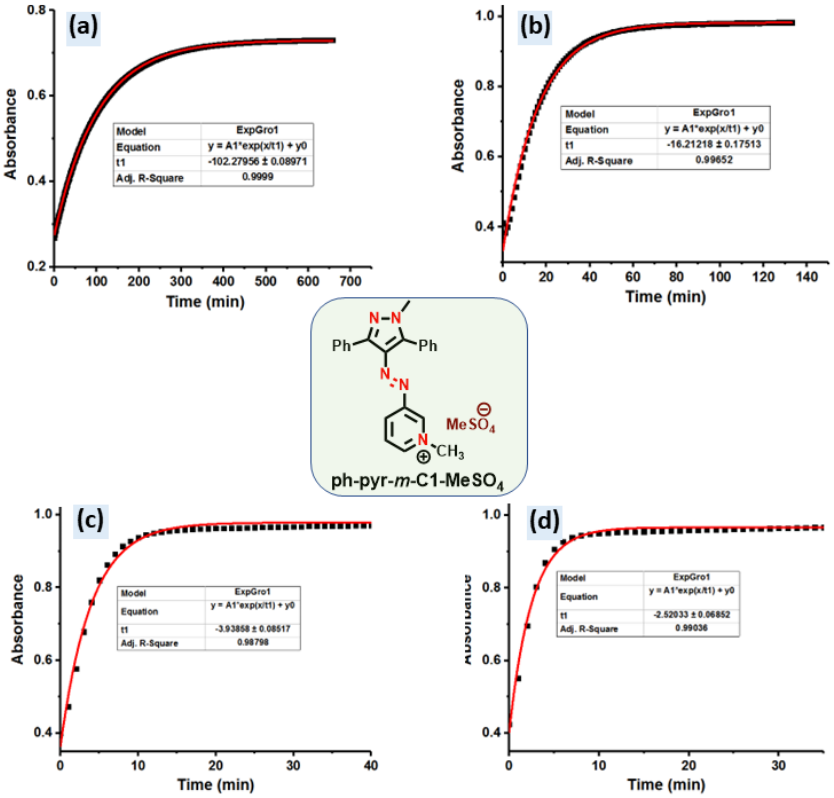

Figure 3A.5. Thermal reverse isomerization kinetics of **ph-pyr-*m*-C1-MeSO₄** in (a) MeCN (64.6 μM) at rt; In DMSO (61.8 μM) (b), (c), and (d) at 50 °C, 65 °C, and 70 °C respectively.

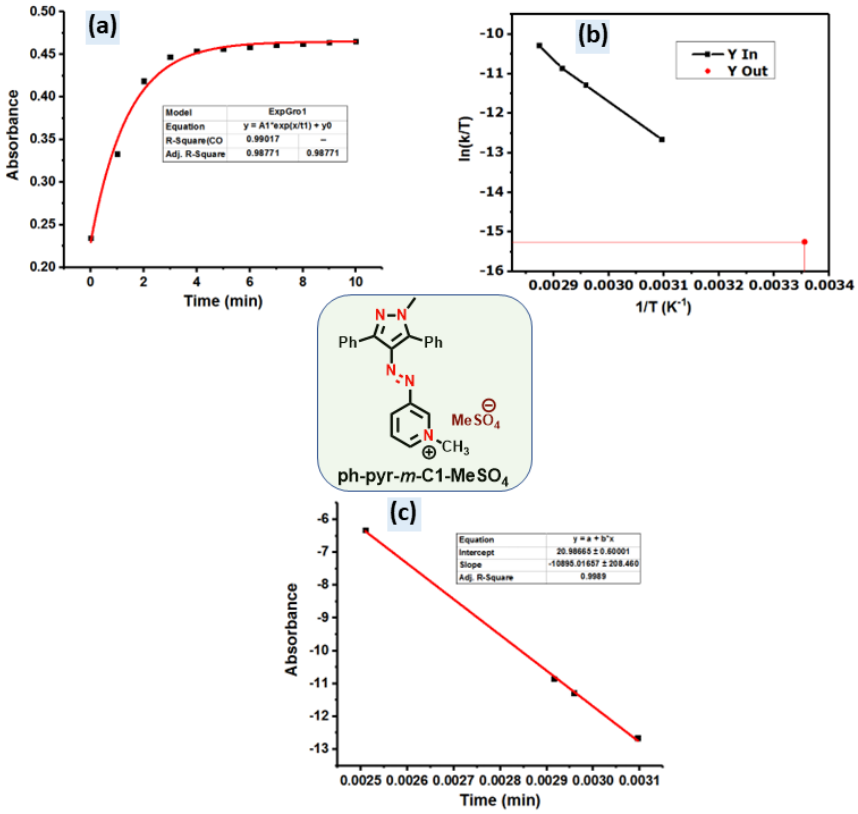

Figure 3A.6. Thermal reverse isomerization kinetics of **ph-pyr-*m*-C1-MeSO₄** in DMSO (61.8 μM)) (a) 75 °C (b) Erying plot and (c) Erying plot extrapolated to 25 °C.

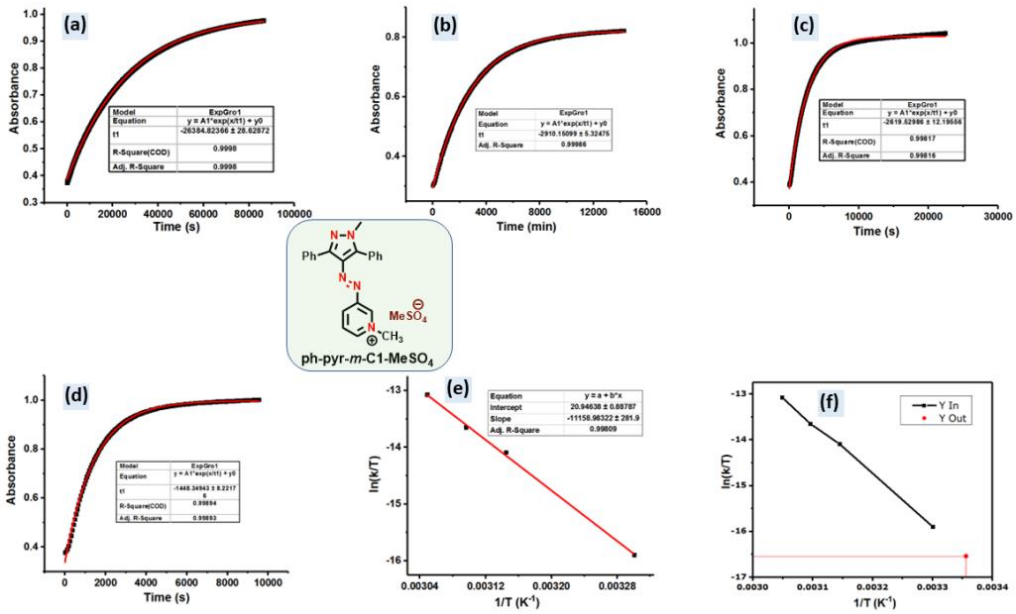

Figure 3A.7. Thermal reverse isomerization kinetics of **ph-pyr-*m*-C1-MeSO$_4$** in H_2O (86.8 μM) (a), (b), (c), and (d) at 30 °C, 45 °C, 50 °C and 55 °C respectively, (e) Erying plot and (f) Erying plot extrapolated to 25 °C.

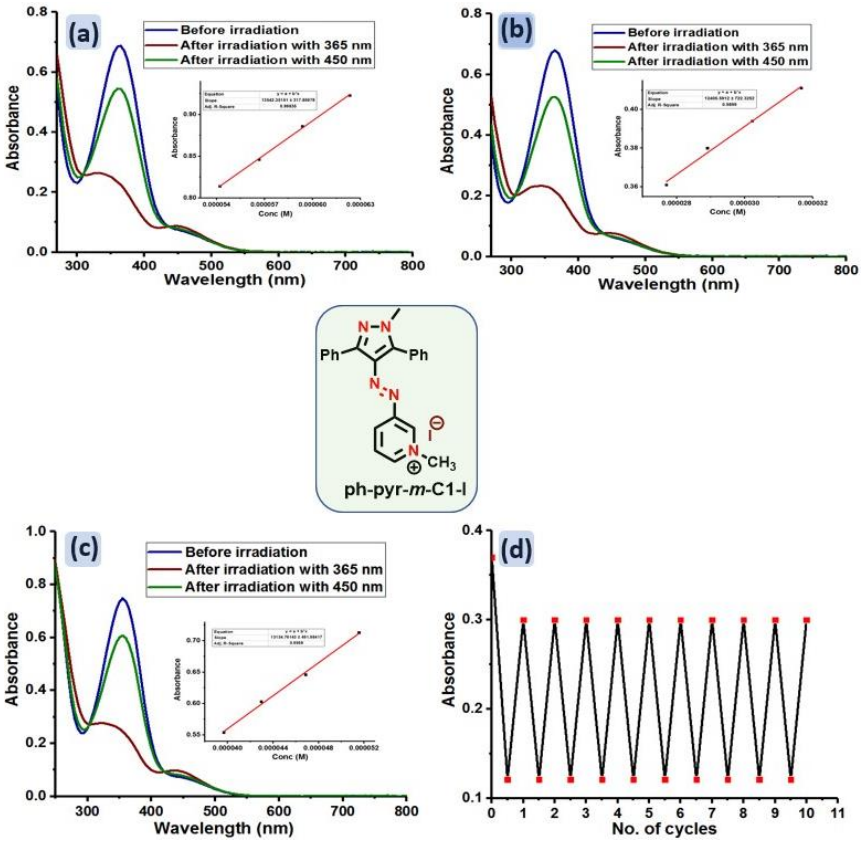

Figure 3A.8. Photoswitching behavior of **ph-pyr-*m*-C1-I**. Reversible photoisomerization of **ph-pyr-*m*-C1-I** in (a) MeCN (50.2 μM); (b) DMSO (54.3 μM), and (c) H_2O (57.0 μM); (d) Cyclic experiment in H_2O (monitored at λ = 355 nm, 28.2 μM).

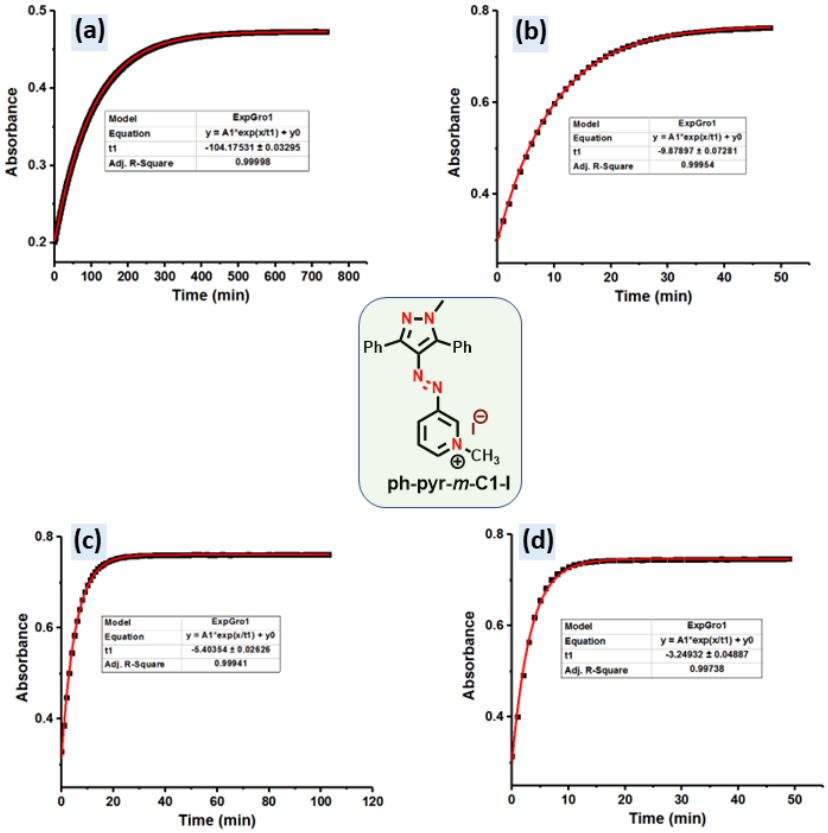

Figure 3A.9. Thermal reverse isomerization kinetics of **ph-pyr-*m*-C1-MeSO$_4$** (a) in MeCN (55.3 μM); In DMSO (b), and (c), (d) at 50 °C, 55 °C, and 60 °C respectively.

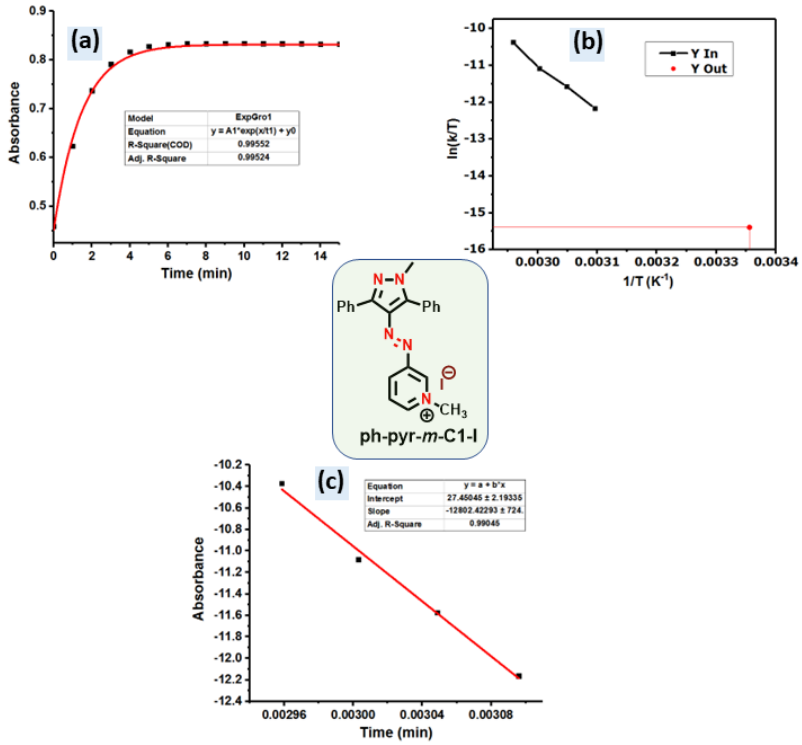

Figure 3A.10. Thermal reverse isomerization kinetics of **ph-pyr-*m*-C1-MeSO$_4$** in DMSO (61.5 μM) (a) 65 °C (b) Erying plot and (c) Erying plot extrapolated to 25 °C.

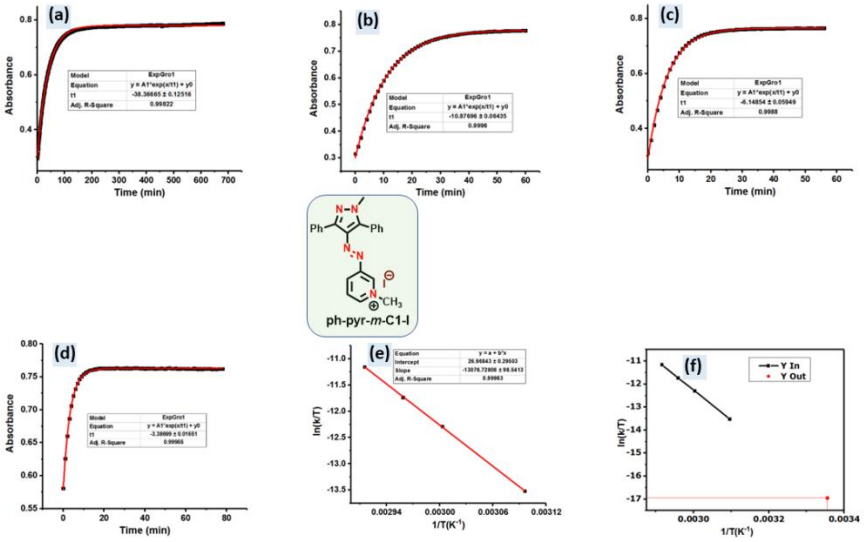

Figure 3A.11. Thermal reverse isomerization kinetics of **ph-pyr-*m*-C1-MeSO$_4$** in H_2O (59.9 μM) (a), (b), (c), and (d) at 55 °C, 60 °C, and 65 °C, and 70 °C respectively, (d) Erying plot and (e) Erying plot extrapolated to 25 °C.

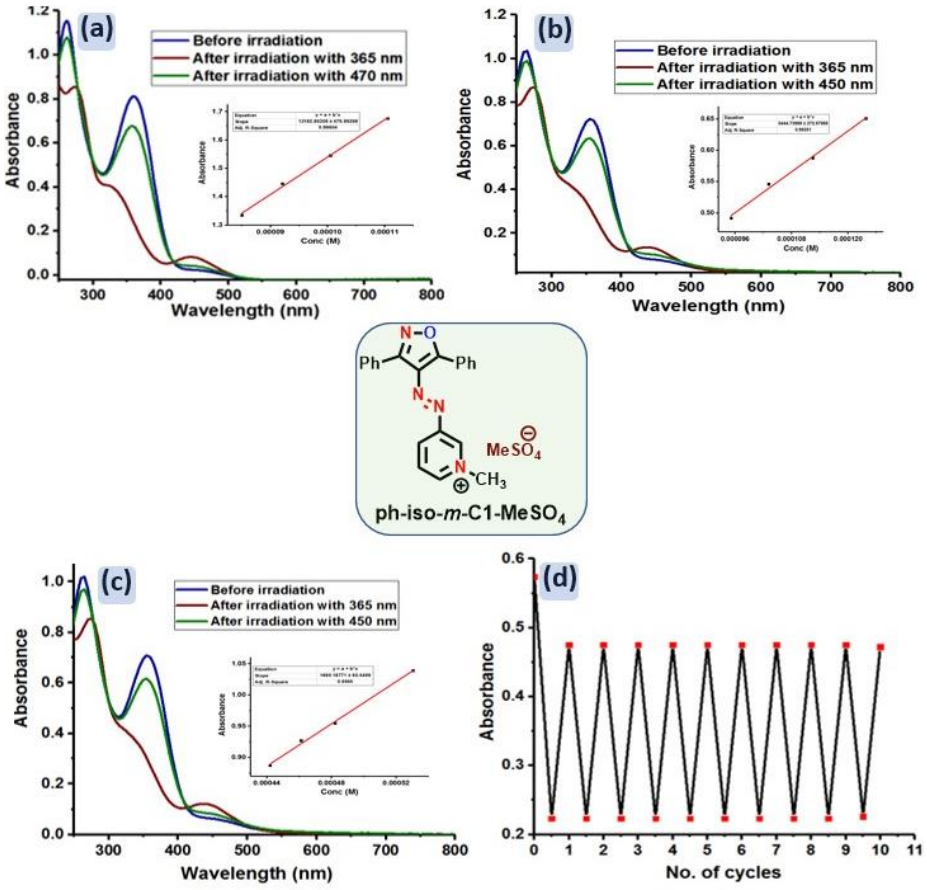

Figure 3A.12. Photoswitching behavior of **ph-iso-*m*-C1-MeSO$_4$**. Reversible photoisomerization of **ph-iso-*m*-C1-MeSO$_4$** in (a) MeCN (61.6 μM); (b) DMSO (133.0 μM), and (c) H_2O (414.7 μM); (d) Cyclic experiment in H_2O (monitored at λ = 355 nm, 339.6 μM).

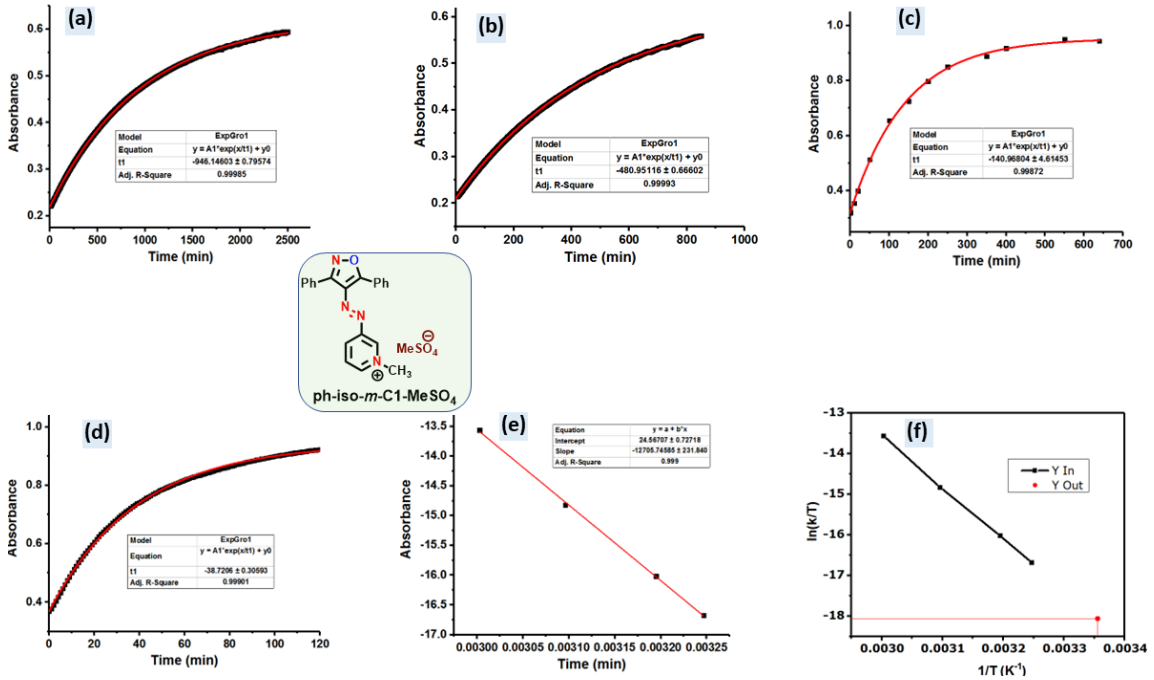

Figure 3A.13. Thermal reverse isomerization kinetics of **ph-iso-*m*-C1-MeSO$_4$** in MeCN (45.1 μM) (a), (b), (c), and (d) at 35 °C, 40 °C, and 50 °C, 60 °C respectively, (d) Erying plot and (e) Erying plot extrapolated to 25 °C.

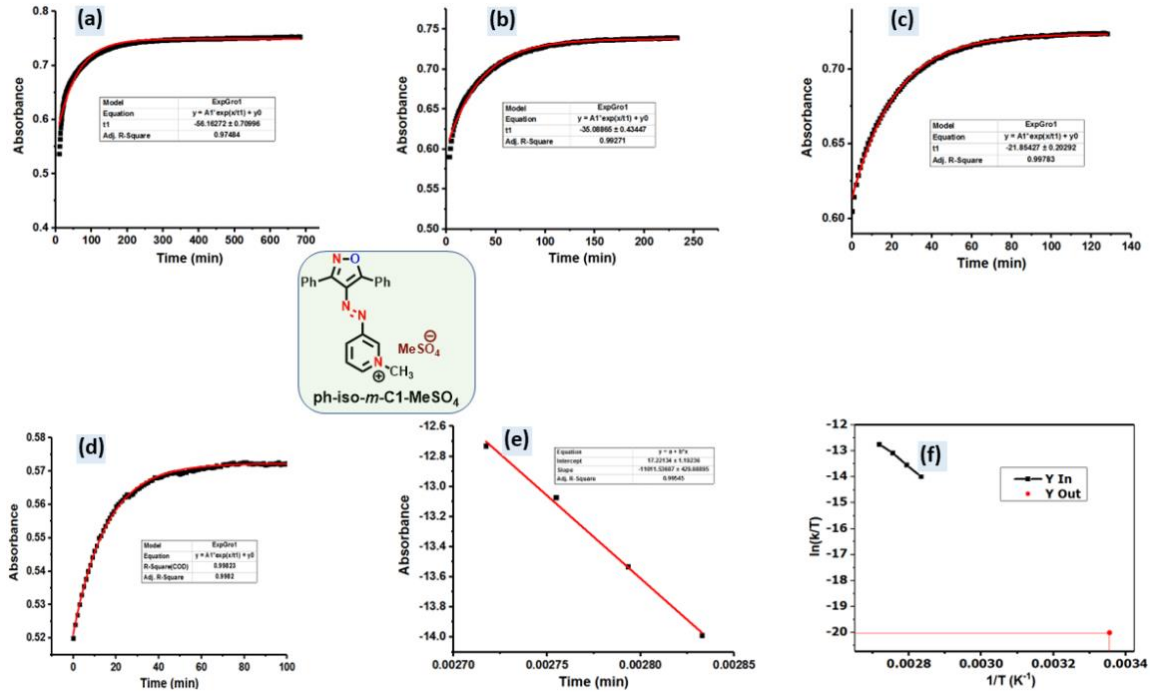

Figure 3A.14. Thermal reverse isomerization kinetics of **ph-iso-*m*-C1-MeSO$_4$** in DMSO (142.1 μM) (a), (b), (c), and (d) at 80 °C, 85 °C, 90 °C, and 95 °C respectively, (d) Erying plot and (e) Erying plot extrapolated to 25 °C.

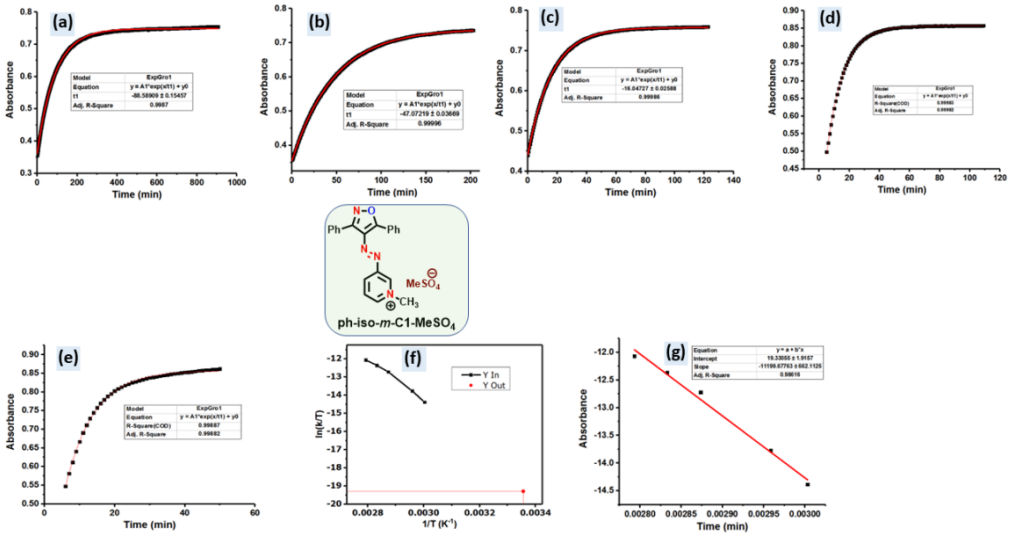

Figure 3A.15. Thermal reverse isomerization kinetics of **ph-iso-*m*-C1-MeSO$_4$** in H_2O (446.9 μM) (a), (b), (c), (d), and (e) at 60 °C, 65 °C, 75 °C, 80 °C, and 85 °C respectively, (f) Erying plot ,and (g) Erying plot extrapolated to 25 °C.

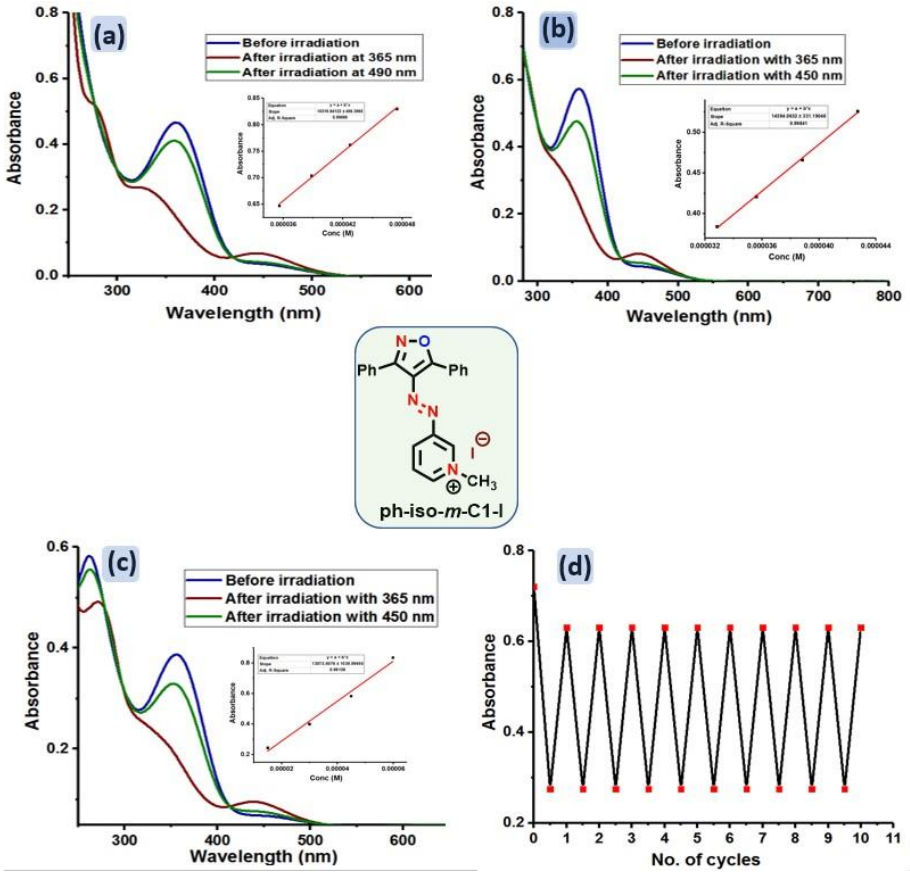

Figure 3A.16. Photoswitching behavior of **ph-iso-*m*-C1-I**. Reversible photoisomerization of **ph-iso-*m*-C1-I** in (a) MeCN (30.6 μM); (b) DMSO (39.8 μM), and (c) H_2O (29.6 μM); (d) Cyclic experiment in H_2O (monitored at λ = 355 nm, 55.2 μM).

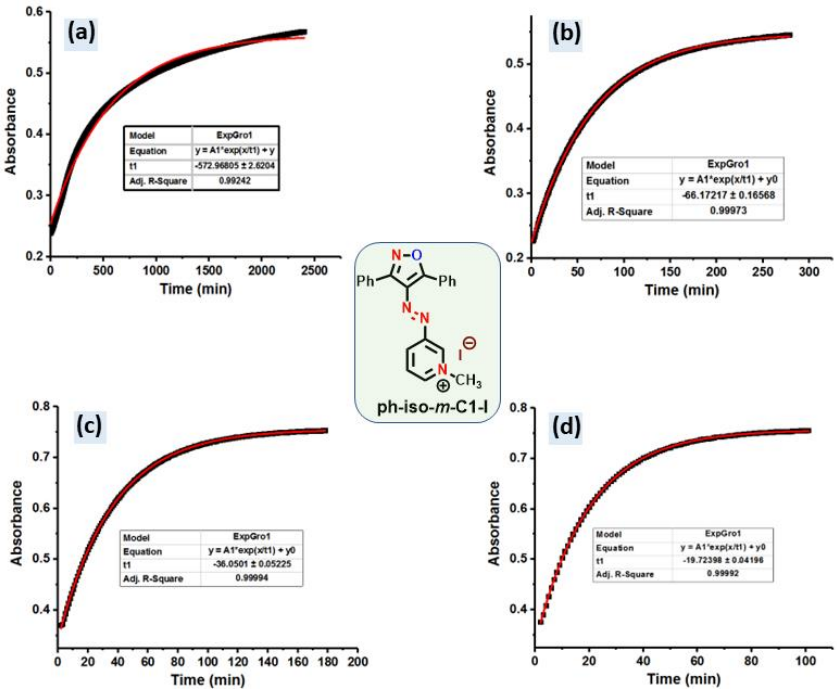

Figure 3A.17. Thermal reverse isomerization kinetics of **ph-iso-*m*-C1-I** in (a) **MeCN** (37.1 μM) at rt; (b), and (c), (d) in DMSO (37.9 μM) at 60 °C, 65 °C, and 70 °C respectively.

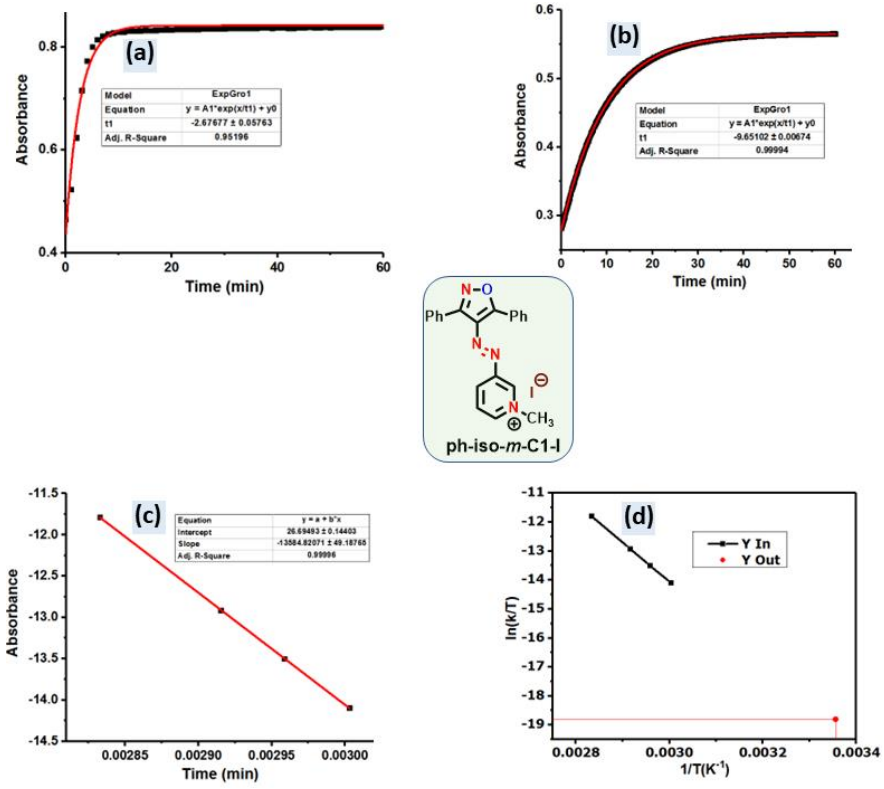

Figure 3A.18. Thermal reverse isomerization kinetics of **ph-iso-*m*-C1-I** in DMSO (37.9 μM) (a) at 75 °C, (b) 80 °C; (c) Erying plot, and (d) Erying plot extrapolated to 25 °C.

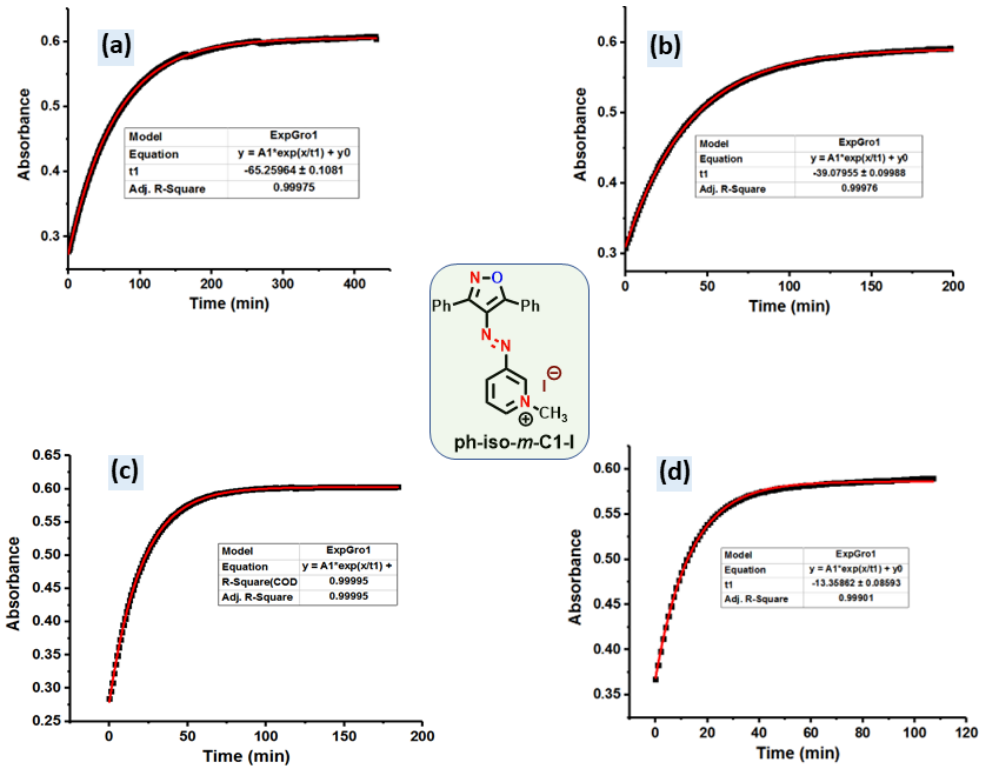

Figure 3A.19. Thermal reverse isomerization kinetics of **ph-iso-*m*-C1-I** in H_2O (25.9 μM) (a)60 °C, (b) 65 °C, (c) 70 °C,and (d) at 75 °C.

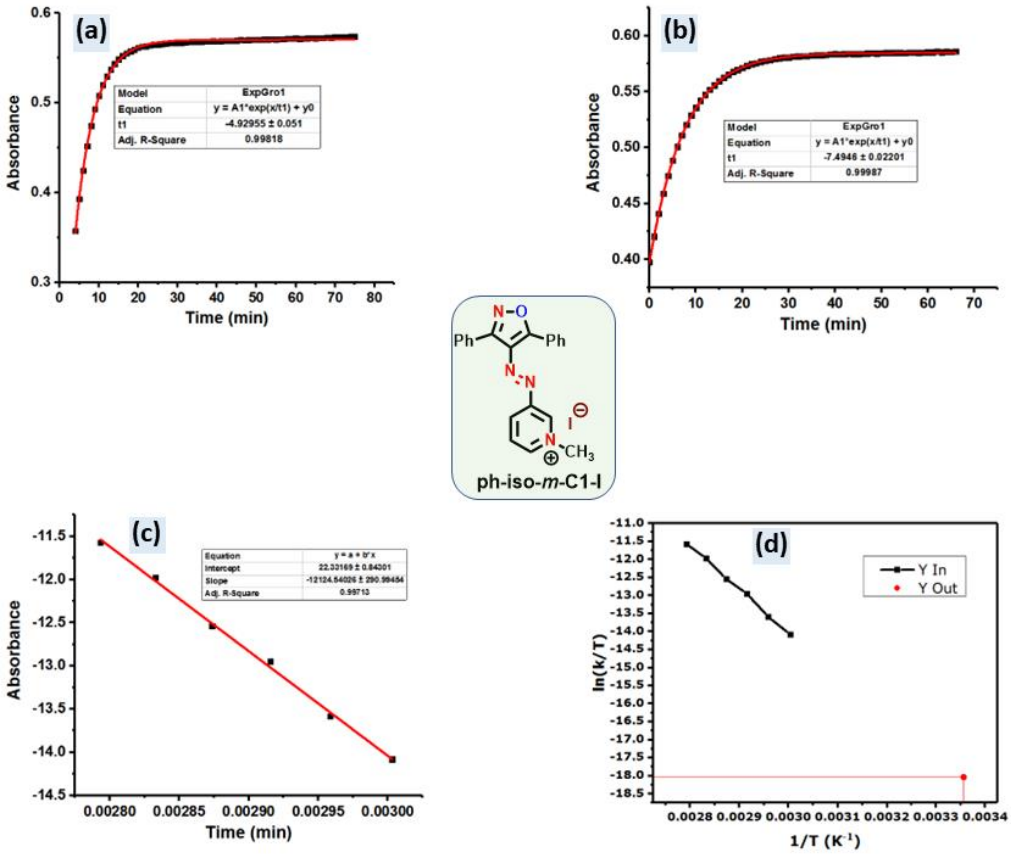

Figure 3A.20. Thermal reverse isomerization kinetics of **ph-iso-*m*-C1-I** in H_2O (25.9 μM) (a) 80 °C, (b) 85 °C; (c) Erying plot, and (d) Erying plot extrapolated to 25 °C.

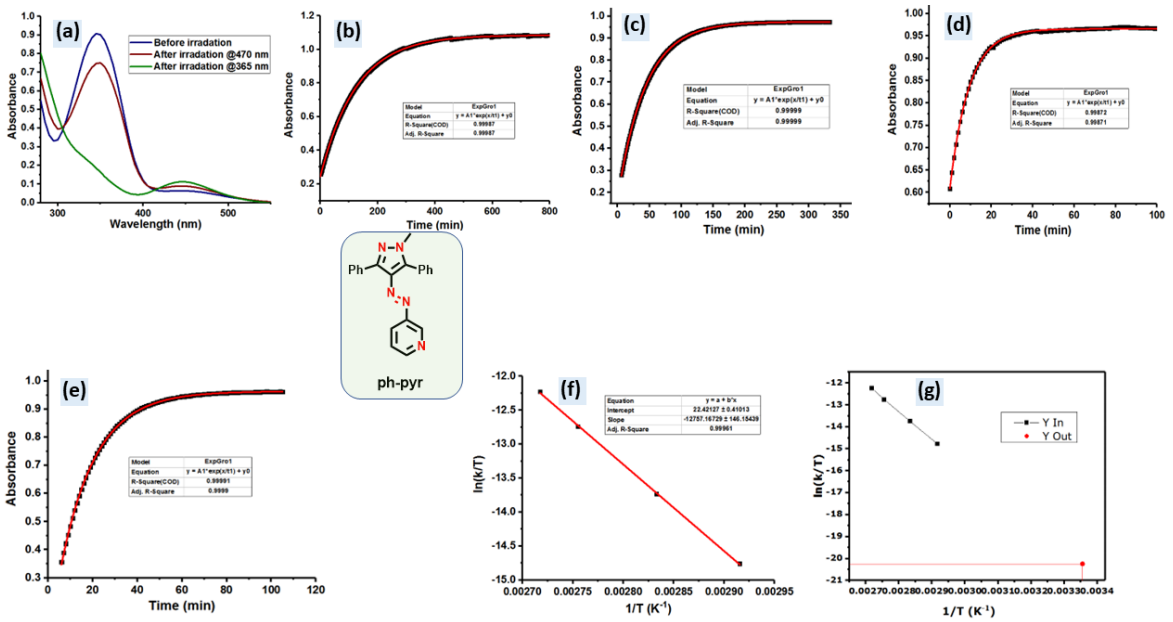

Figure 3A.21. Photoswitching behavior and thermal reverse isomerization kinetics of **ph-pyr** in DMSO (a) reversible photoisomerization; thermal reverse kinetics at (b) 70 °C, (b) 80 (c) 90, and (d) 95; (e) Erying plot, and (f) Erying plot extrapolated to 25 °C.

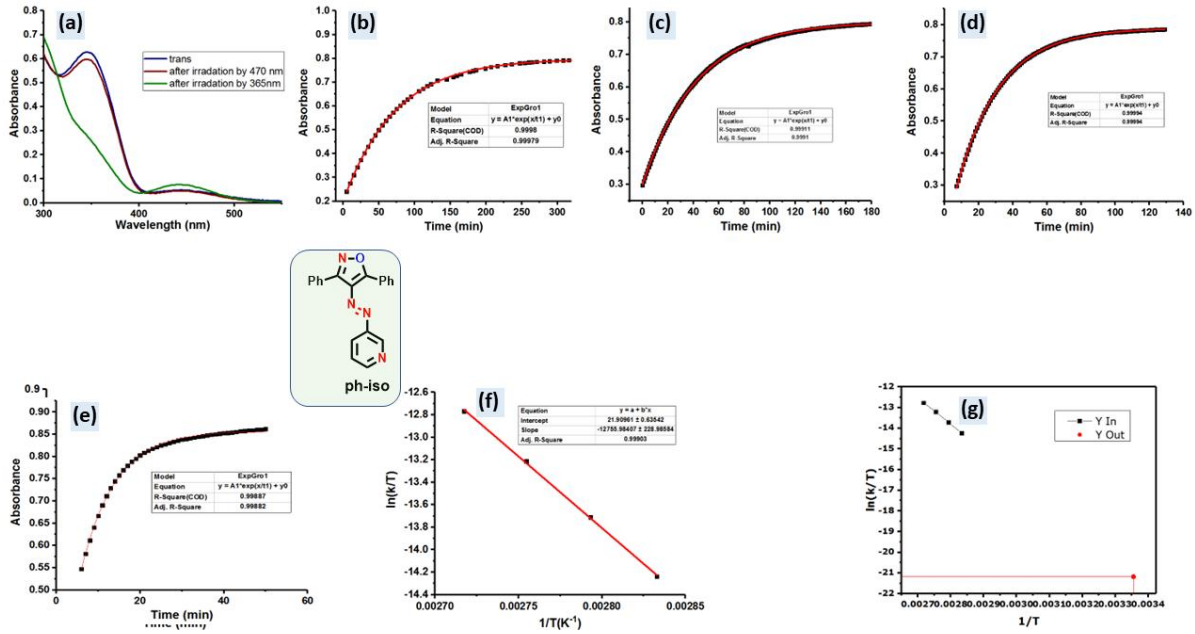

Figure 3A.22. Photoswitching behavior and thermal reverse isomerization kinetics of **ph-iso** in DMSO (a) reversible photoisomerization; thermal reverse kinetics at (a) 80 °C, (b) 85 °C (c) 90 °C, and (d) 95 °C; (e) Erying plot, and (f) Erying plot extrapolated to 25 °C.

3A.2. Quantification of photoisomers using ^{1}H NMR spectroscopy

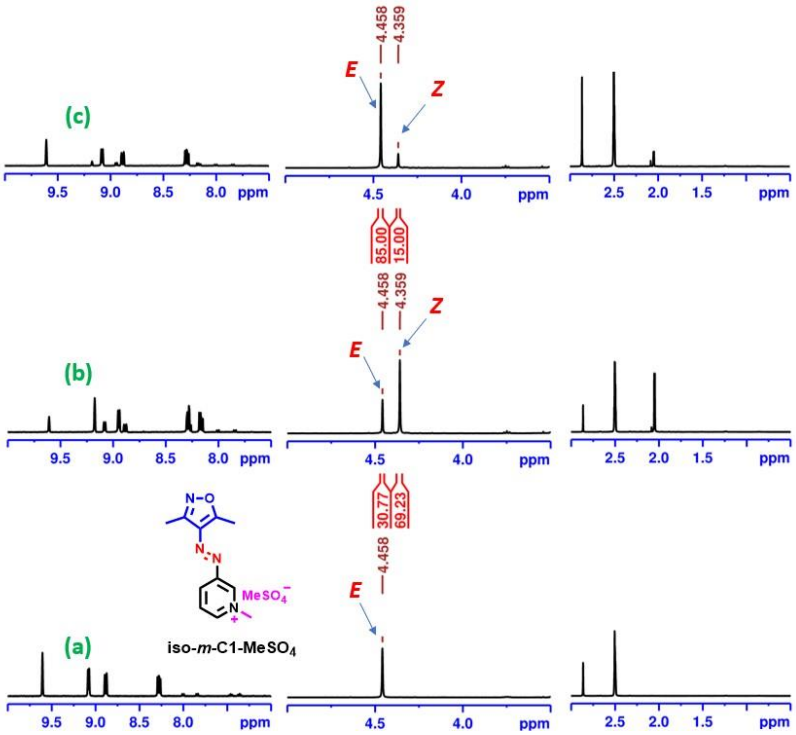

3A.2.1. Quantification of photoisomers of **iso-*m*-C1-MeSO$_4$** by ^{1}H NMR (2.2 mM, DMSO-d_6); (a) before irradiation, (b) forward *E*-*Z* isomerization at 365 nm, and (c) reverse *Z*-*E* isomerization at 535 nm.

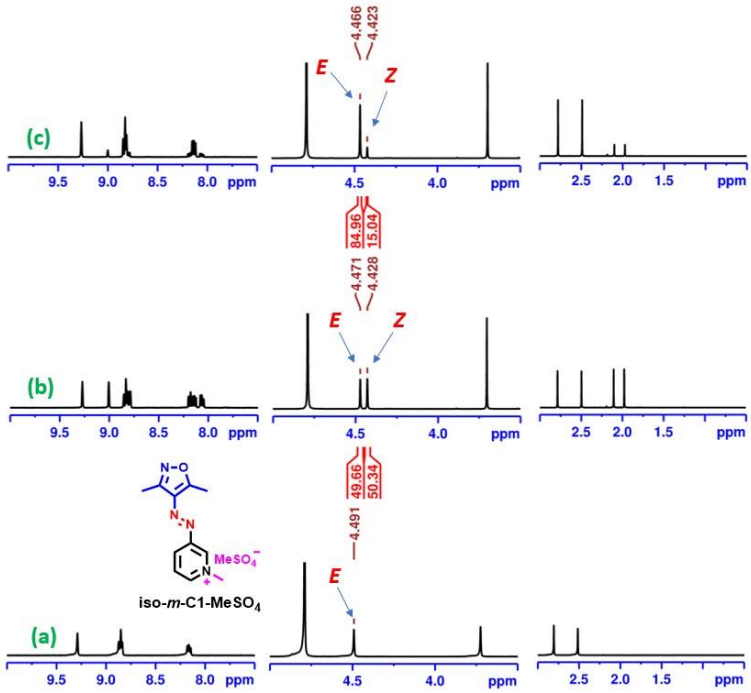

3A.2.1. Quantification of photoisomers of **iso-*m*-C1-MeSO$_4$** by ^{1}H NMR (2.1 mM, D_2O); (a) before irradiation, (b) forward *E*-*Z* isomerization at 365 nm, and (c) reverse *Z*-*E* isomerization at 490 nm.

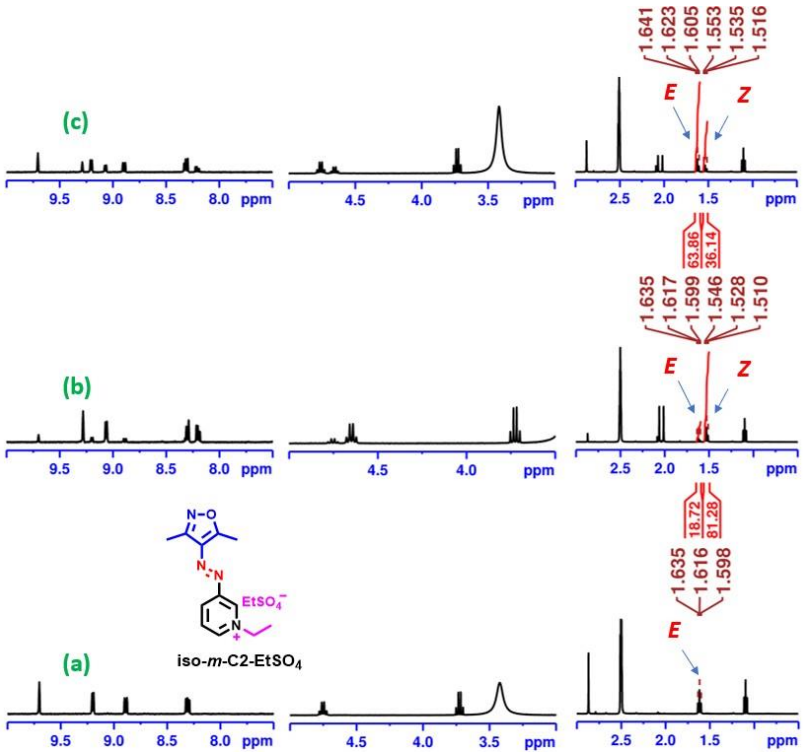

3A.2.3. Quantification of photoisomers of **iso-*m*-C1-MeSO₄** by ^{1}H NMR (1.9 mM, DMSO-d_6); (a) before irradiation, (b) forward *E*-*Z* isomerization at 365 nm, and (c) reverse *Z*-*E* isomerization at 535 nm.

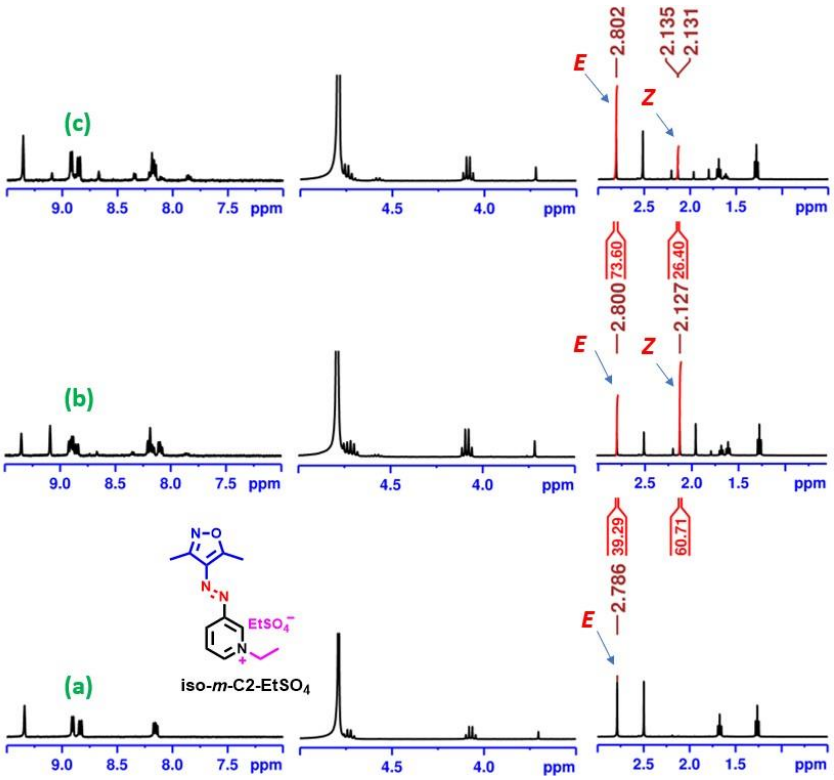

3A.2.4. Quantification of photoisomers of **iso-*m*-C1-MeSO₄** by ^{1}H NMR (2.2 mM, DMSO-d_6); (a) before irradiation, (b) forward *E*-*Z* isomerization at 365 nm, and (c) reverse *Z*-*E* isomerization at 490 nm.

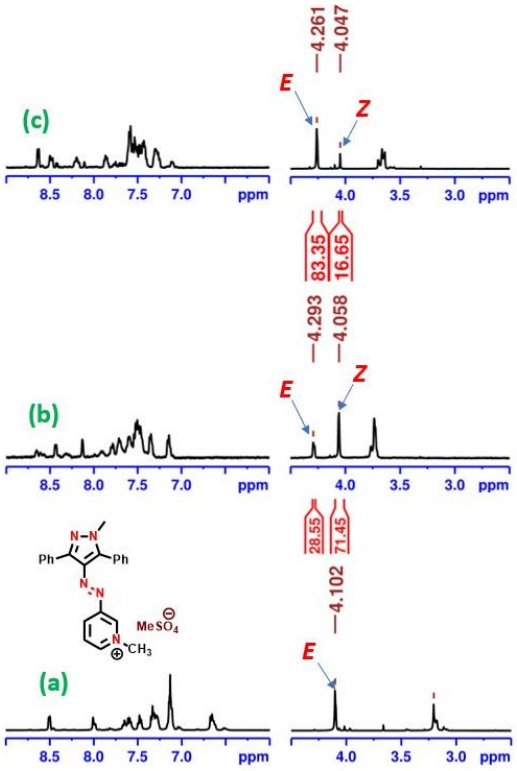

3A.2.5. Quantification of photoisomers of **ph-pyr-*m*-C1-MeSO₄** by ^{1}H NMR (1.2 mM, D_2O); (a) before irradiation, (b) forward *E*-*Z* isomerization at 365 nm, and (c) reverse *Z*-*E* isomerization at 450 nm.

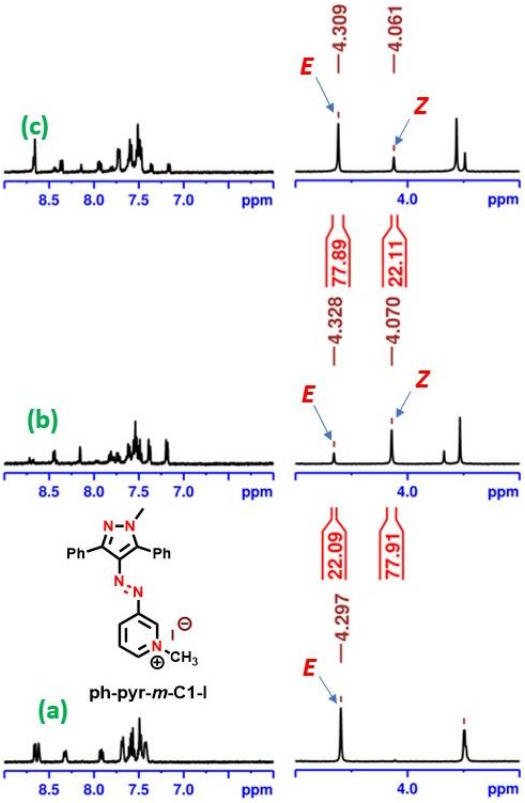

3A.2.6. Quantification of photoisomers of **ph-pyr-*m*-C1-I** by ^{1}H NMR (1.3 mM, D_2O); (a) before irradiation, (b) forward *E*-*Z* isomerization at 365 nm, and (c) reverse *Z*-*E* isomerization at 450 nm.

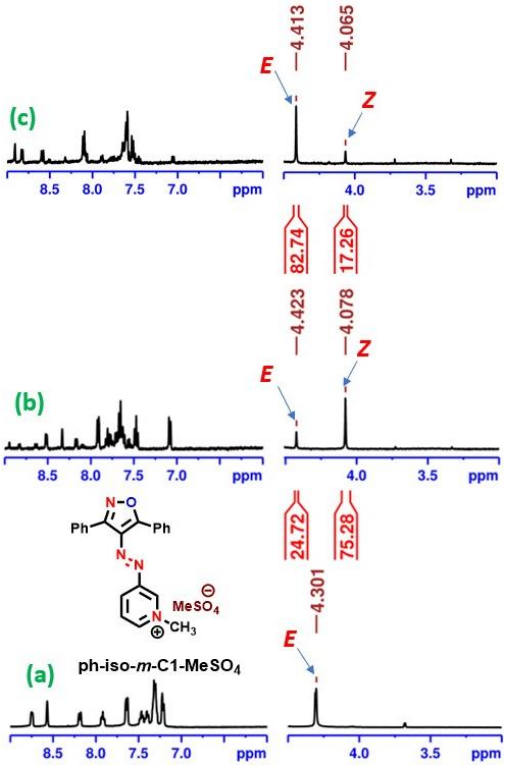

3A.2.7. Quantification of photoisomers of **ph-iso-*m*-C1-MeSO₄** by ^{1}H NMR (1.3 mM, D_2O); (a) before irradiation, (b) forward *E*-*Z* isomerization at 365 nm, and (c) reverse *Z*-*E* isomerization at 450 nm.

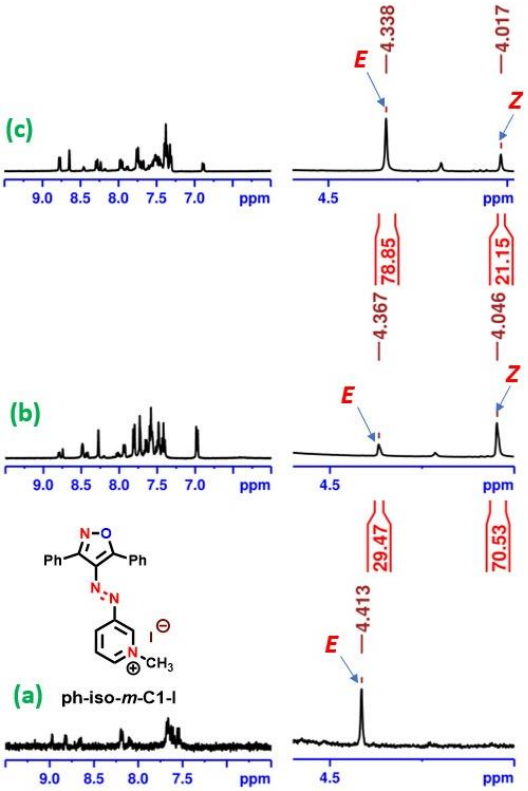

3A.2.8. Quantification of photoisomers of **ph-pyr-*m*-C1-I** by ^{1}H NMR (1.0 mM, D_2O); (a) before irradiation, (b) forward *E*-*Z* isomerization at 365 nm, and (c) reverse *Z*-*E* isomerization at 450 nm.

3A.4. Compound characterization (^{1}H and ^{13}C{^{1}H}-NMR) data

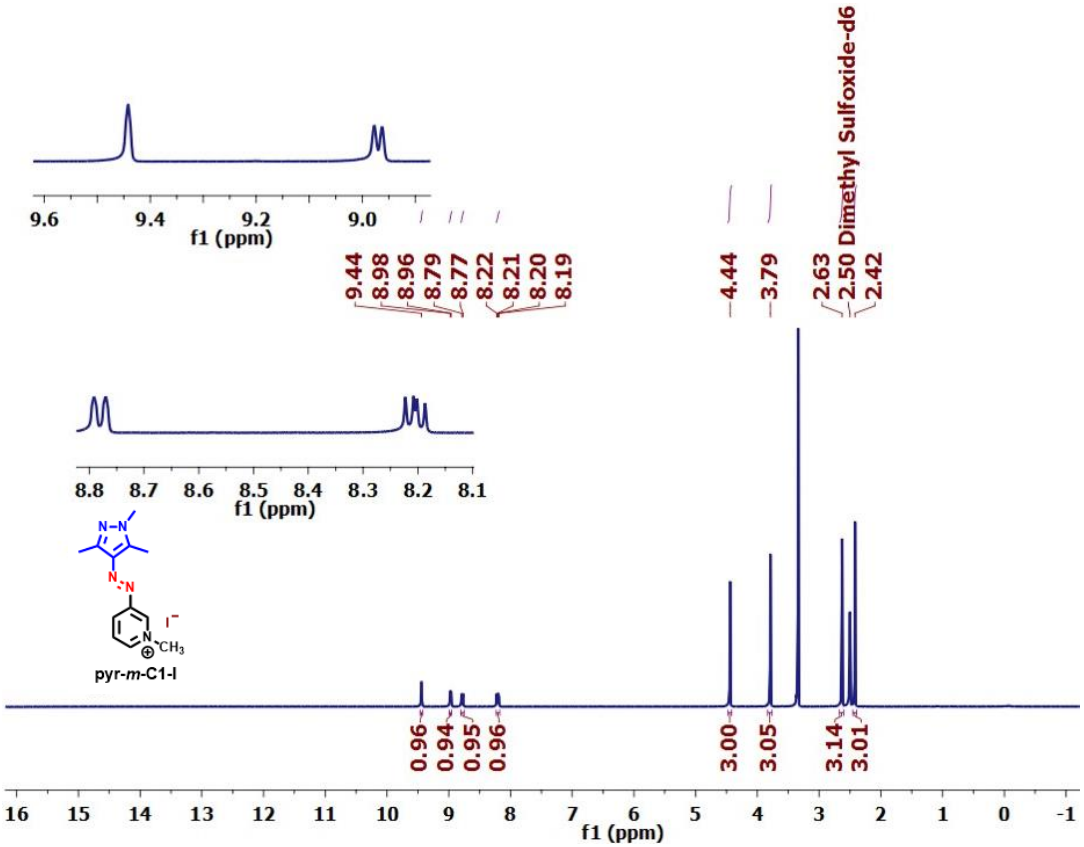

^{1}H NMR spectrum of (*E*)-1-methyl-3-((1,3,5-trimethyl-1H-pyrazol-4-yl)diazenyl)pyridin-1-ium iodide, **pyr-*m*-C1-I** (400 MHz, $CDCl_3$).

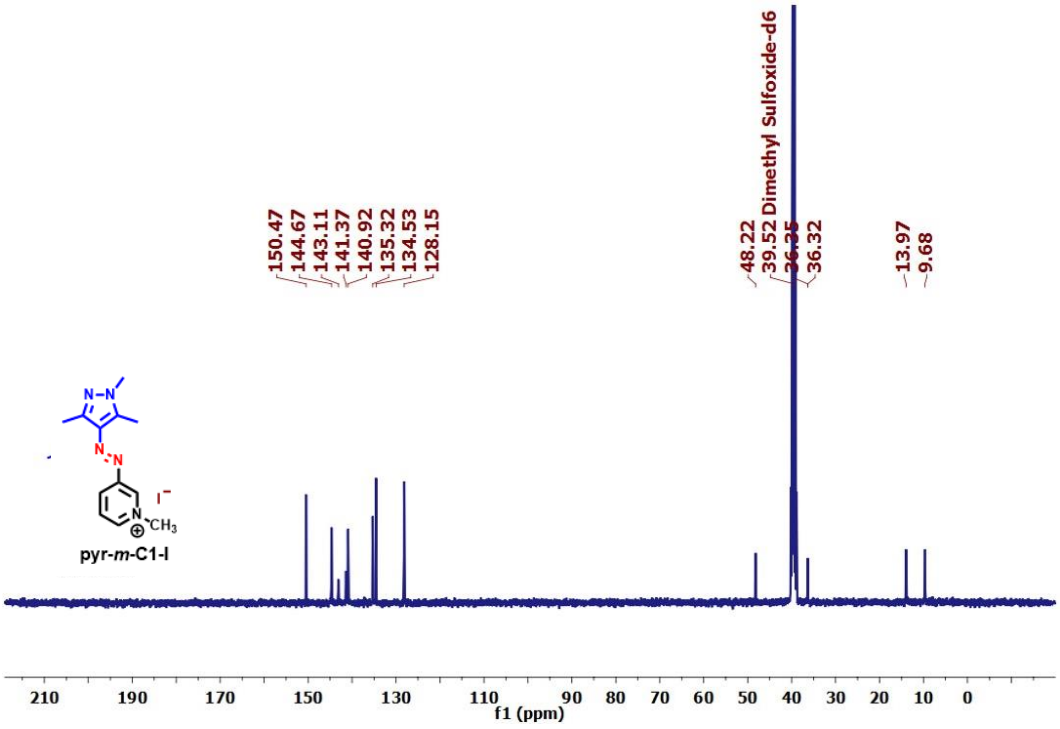

^{13}C{^{1}H} NMR spectrum of (*E*)-1-methyl-3-((1,3,5-trimethyl-1H-pyrazol-4-yl)diazenyl)pyridin-1-ium iodide, **pyr-*m*-C1-I** (100 MHz, $CDCl_3$).

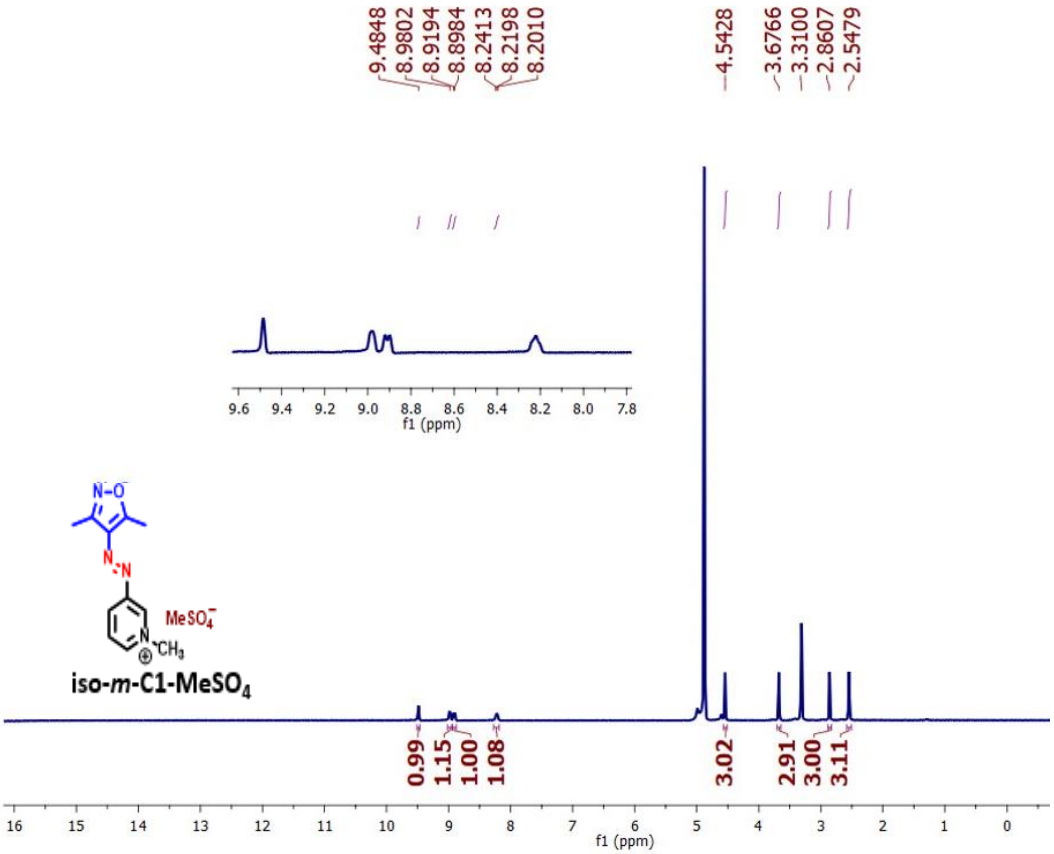

^{1}H NMR spectrum of (*E*)-3-((3,5-dimethylisoxazol-4-yl)diazenyl)-1-methylpyridin-1-ium methyl sulfate, **iso-*m*-C1-MeSO$_4$** (400 MHz, $CDCl_3$).

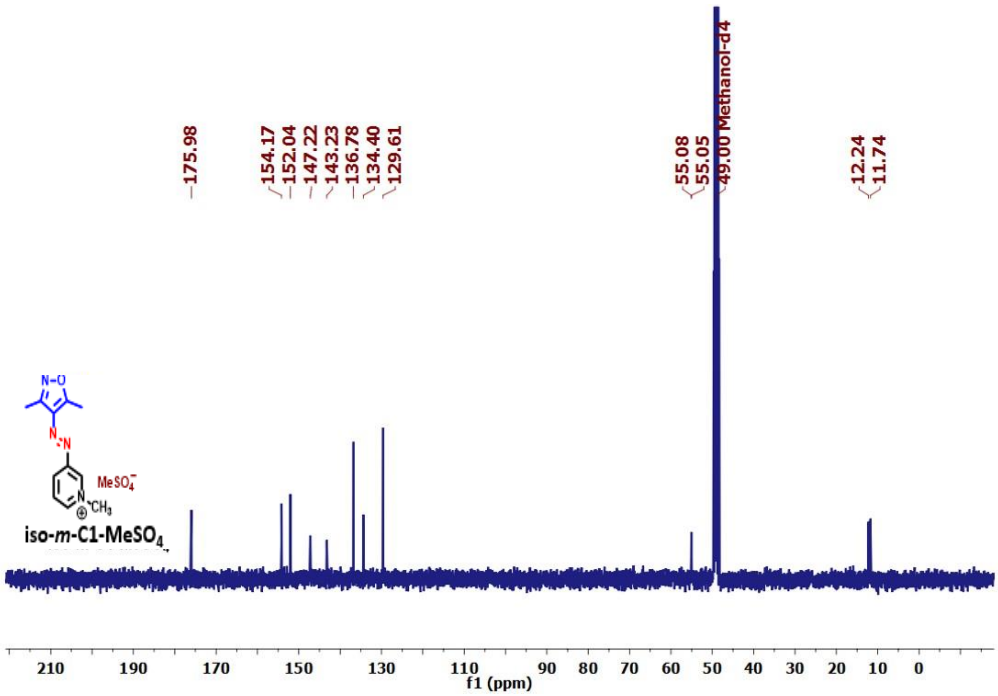

^{13}C{^{1}H} NMR spectrum of (*E*)-3-((3,5-dimethylisoxazol-4-yl)diazenyl)-1-methylpyridin-1-ium methyl sulfate, **iso-*m*-C1-MeSO$_4$** (100 MHz, $CDCl_3$).

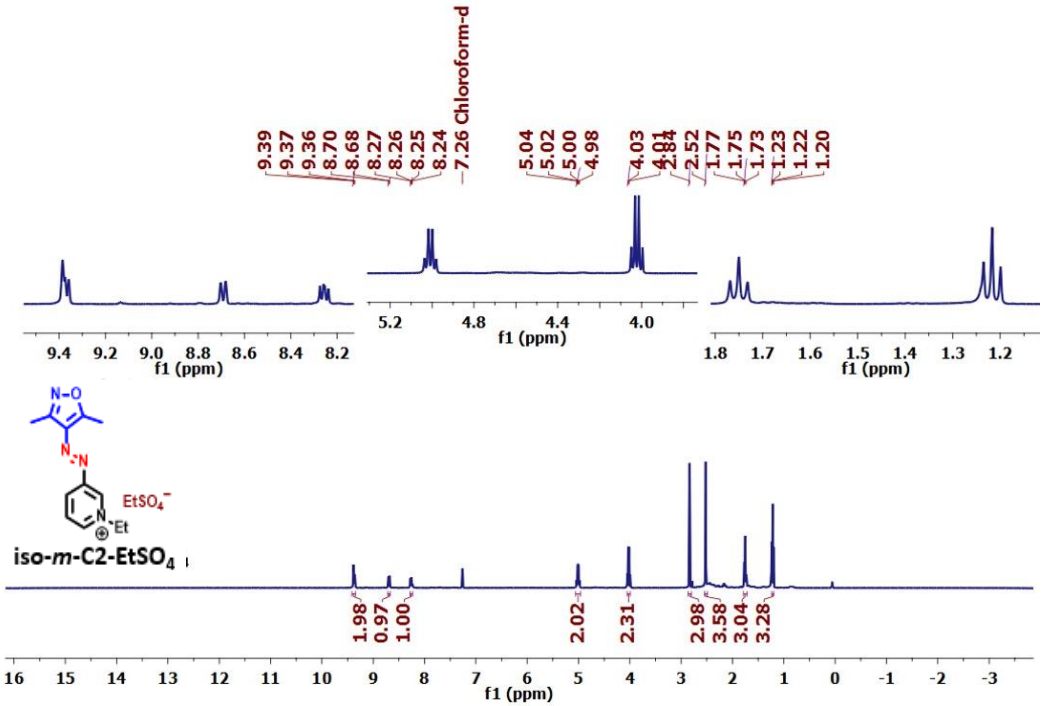

^{1}H NMR spectrum of (*E*)-3-((3,5-dimethylisoxazol-4-yl)diazenyl)-1-ethylpyridin-1-ium methyl sulfate, **iso-*m*-C2-EtSO$_4$** (400 MHz, $CDCl_3$).

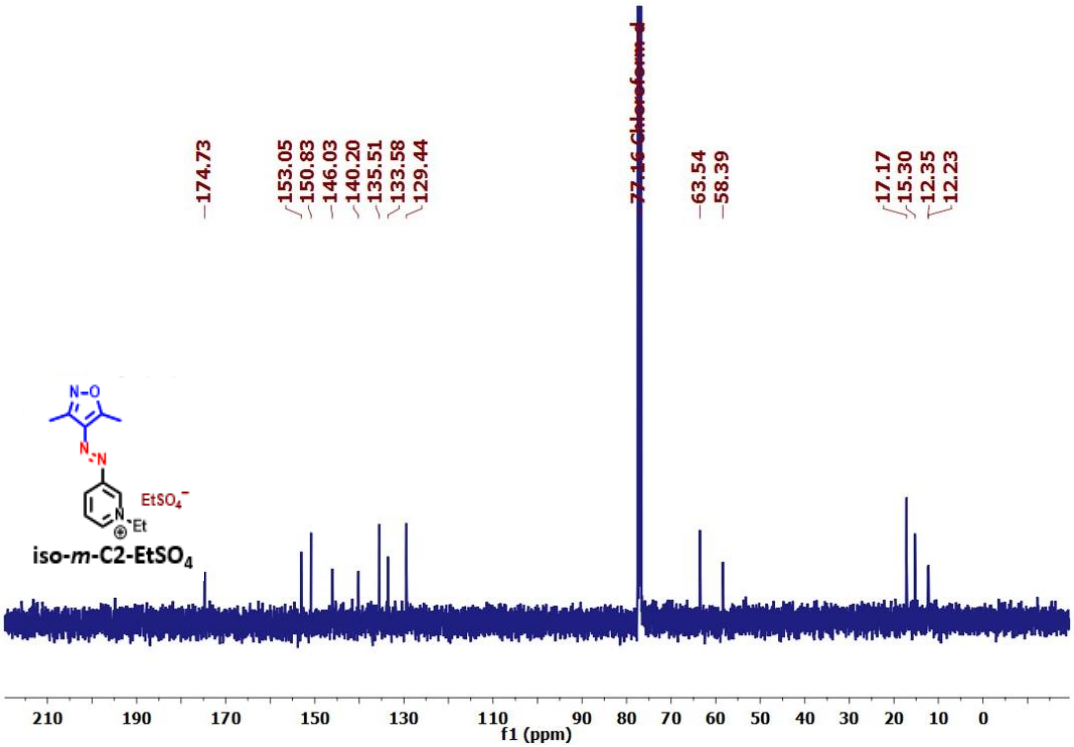

^{13}C{^{1}H} NMR spectrum of (*E*)-3-((3,5-dimethylisoxazol-4-yl)diazenyl)-1-ethylpyridin-1-ium methyl sulfate, **iso-*m*-C2-EtSO$_4$** (100 MHz, $CDCl_3$).

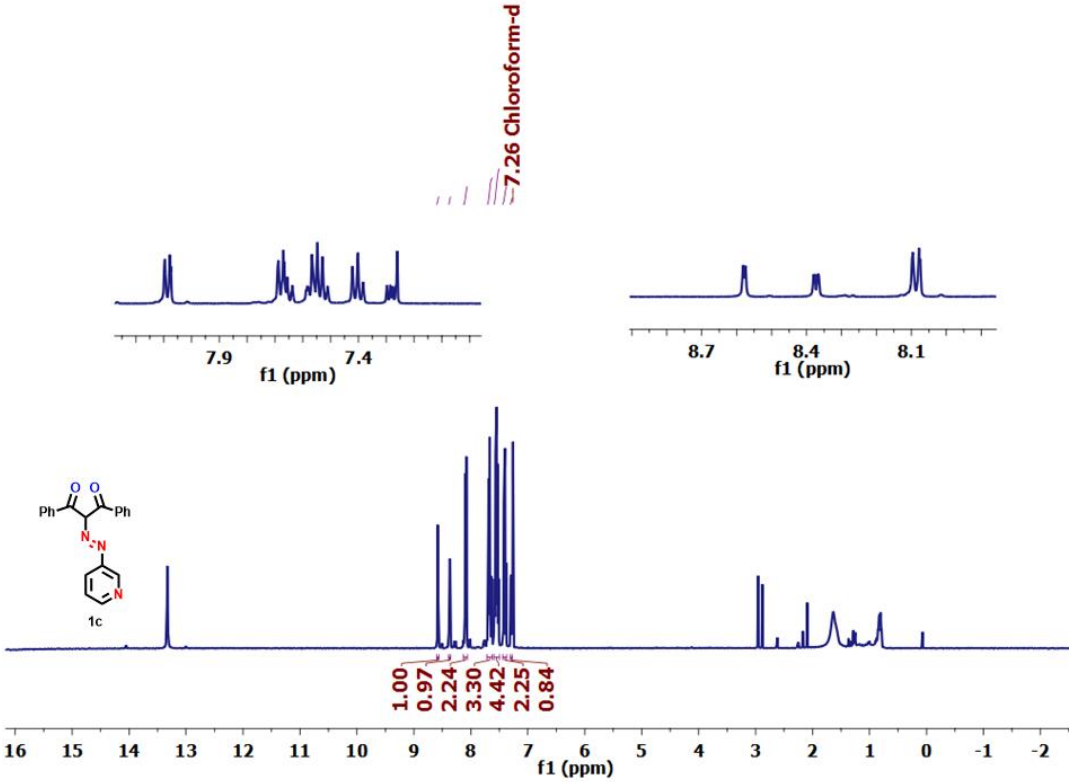

^{1}H NMR spectrum of (*E*)-1,3-diphenyl-2-(pyridin-3-yldiazenyl)propane-1,3-dione, **1c** (400 MHz, $CDCl_3$).

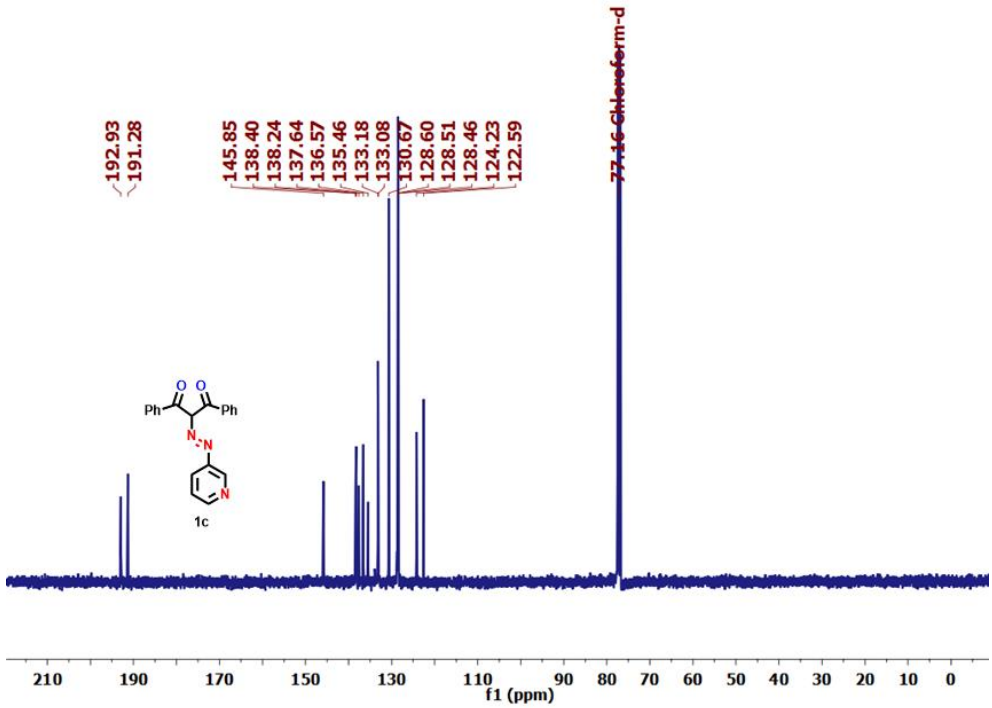

^{13}C{^{1}H} NMR spectrum of (*E*)-1,3-diphenyl-2-(pyridin-3-yldiazenyl)propane-1,3-dione, **1c** (100 MHz, $CDCl_3$).

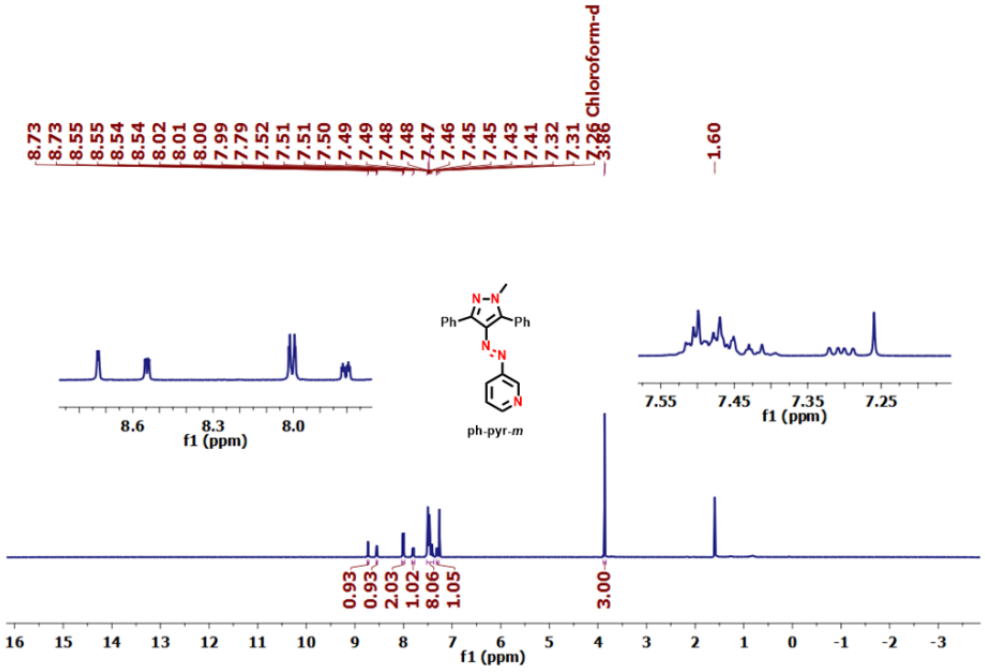

^{1}H NMR spectrum of (*E*)-3-((1-methyl-3,5-diphenyl-1H-pyrazol-4-yl)diazenyl)pyridine, **ph-pyr-*m*** (400 MHz, $CDCl_3$).

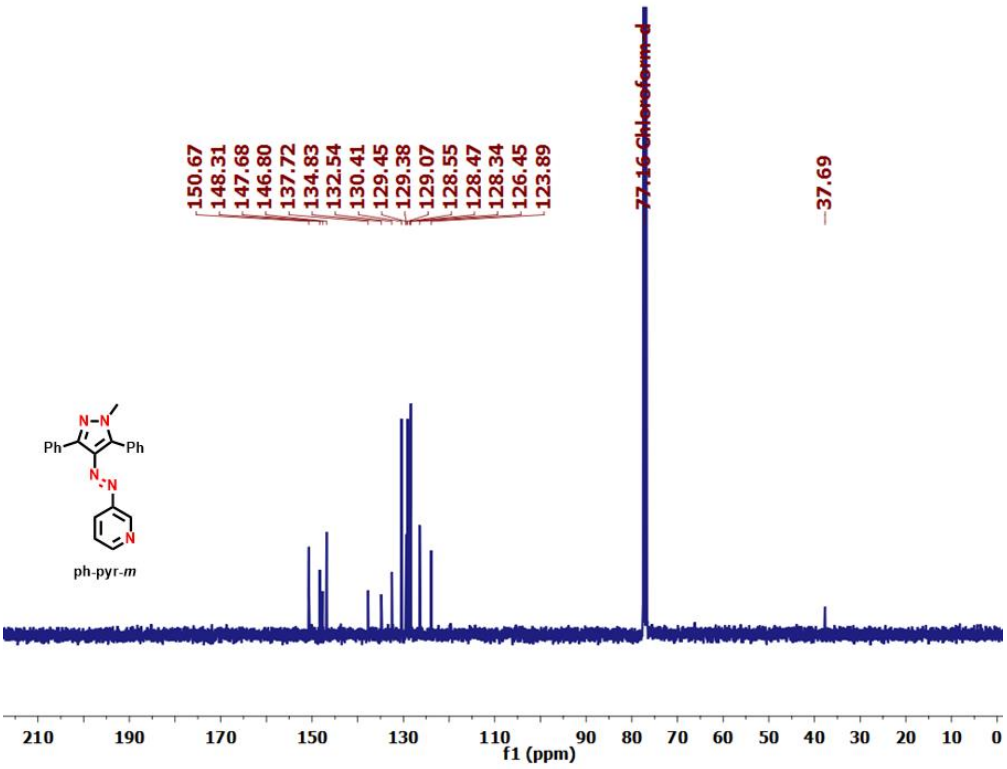

^{13}C{^{1}H} NMR spectrum of (*E*)-3-((1-methyl-3,5-diphenyl-1H-pyrazol-4-yl)diazenyl)pyridine, **ph-pyr-*m*** (100 MHz, $CDCl_3$).

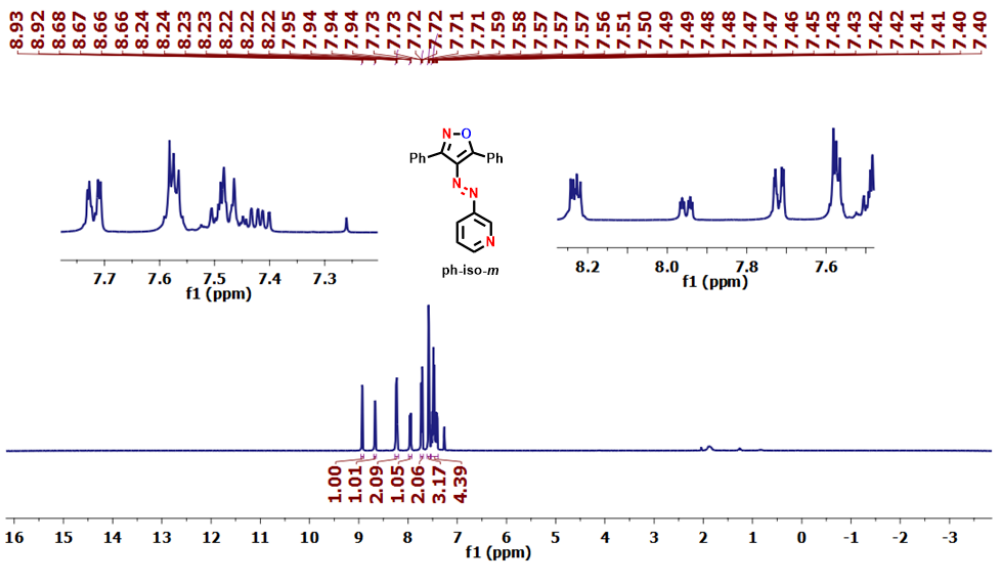

^{1}H NMR spectrum of (*E*)-3,5-diphenyl-4-(pyridin-3-yldiazenyl)isoxazole, **ph-iso-*m*** (400 MHz, $CDCl_3$).

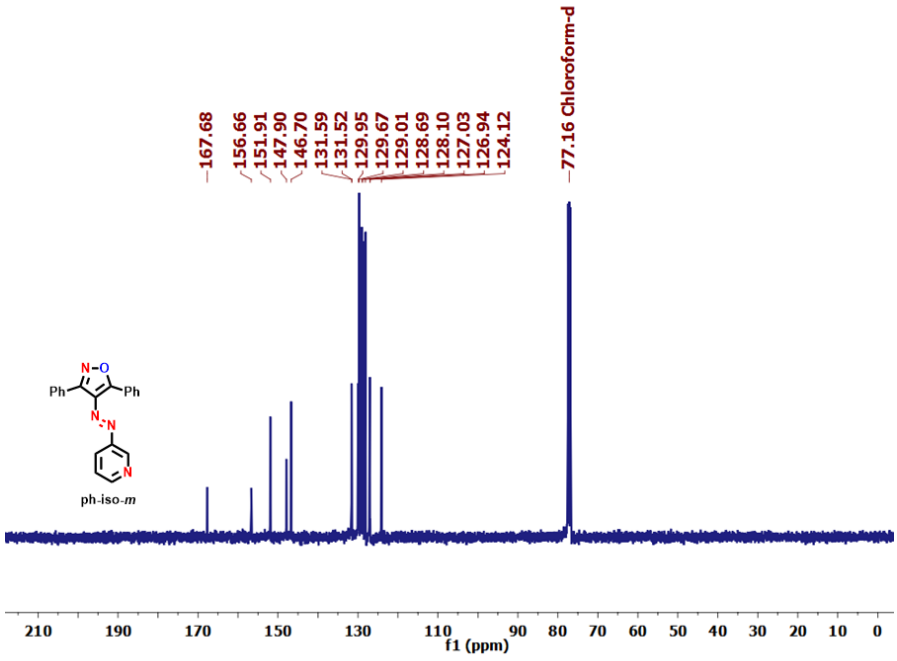

^{13}C{^{1}H} NMR spectrum of (*E*)-3,5-diphenyl-4-(pyridin-3-yldiazenyl)isoxazole, **ph-iso-*m*** (100 MHz, $CDCl_3$).

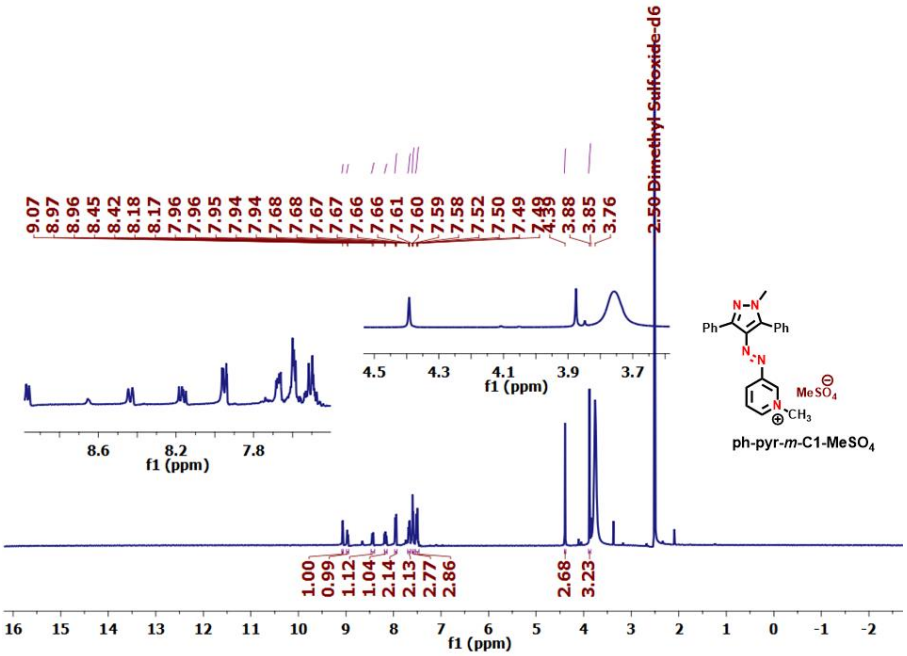

^{1}H NMR spectrum of (*E*)-3-((3,5-diphenylisoxazol-4-yl)diazenyl)-1-methylpyridin-1-ium methyl sulfate, **ph-pyr-*m*-C1-MeSO$_4$** (400 MHz, DMSO-d$_6$).

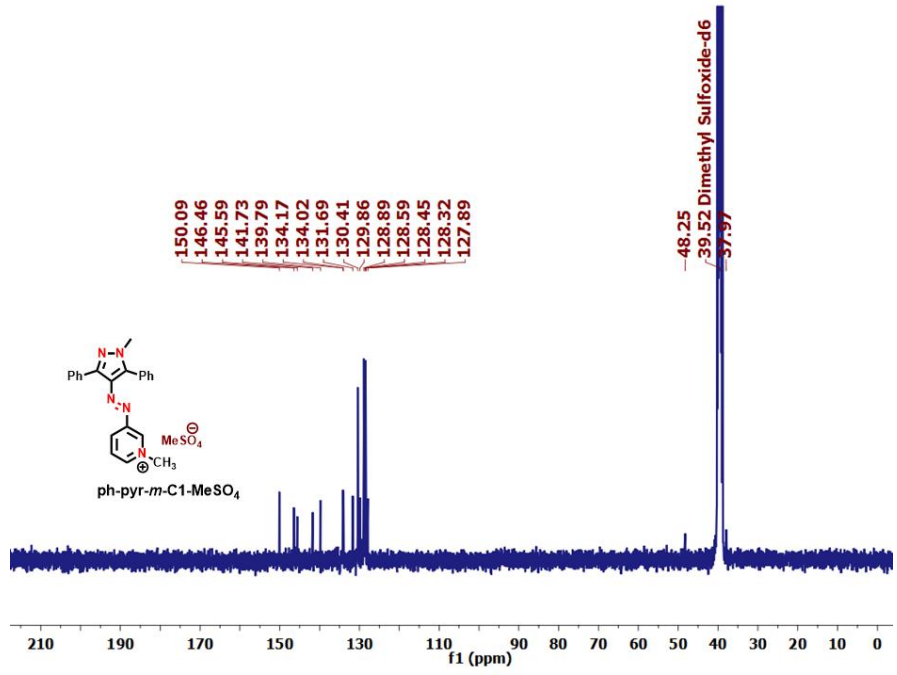

^{13}C{^{1}H} NMR spectrum of (*E*)-3-((3,5-diphenylisoxazol-4-yl)diazenyl)-1-methylpyridin-1-ium methyl sulfate, **ph-pyr-*m*-C1-MeSO$_4$** (100 MHz, DMSO-d$_6$)

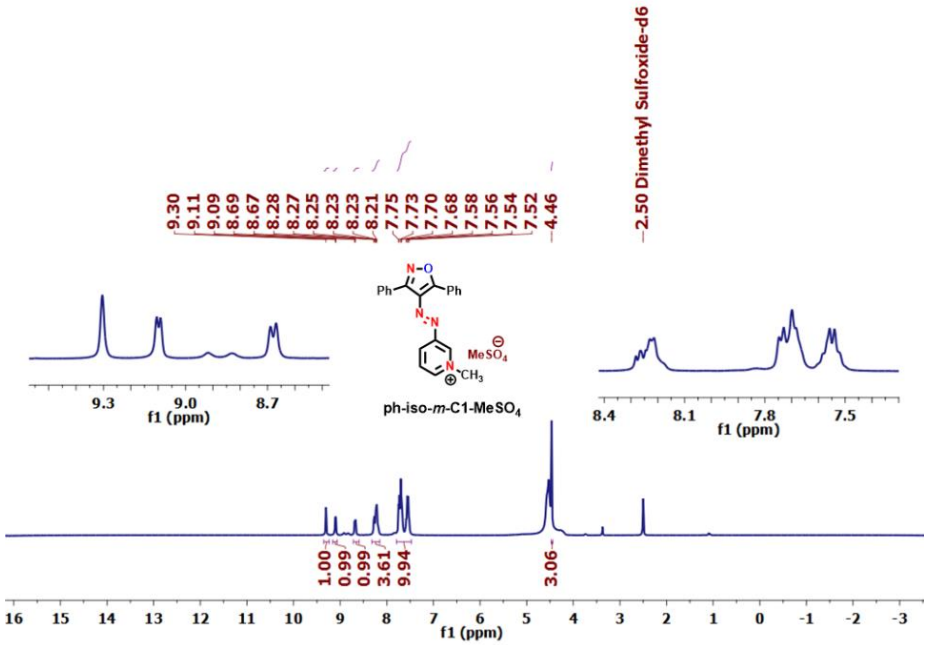

^{1}H NMR spectrum of (*E*)-3-((3,5-diphenylisoxazol-4-yl)diazenyl)-1-methylpyridin-1-ium methyl sulfate, **ph-iso-*m*-C1-MeSO$_4$** (400 MHz, DMSO-d$_6$).

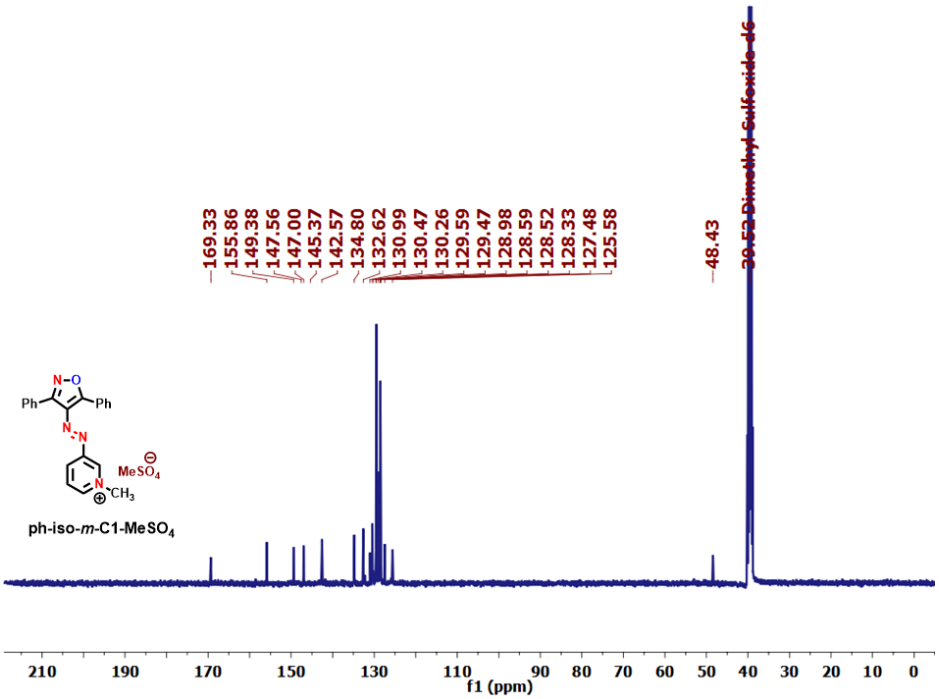

^{13}C{^{1}H} NMR spectrum of (*E*)-3-((3,5-diphenylisoxazol-4-yl)diazenyl)-1-methylpyridin-1-ium methyl sulfate, **ph-iso-*m*-C1-MeSO$_4$** (100 MHz, DMSO-d$_6$).

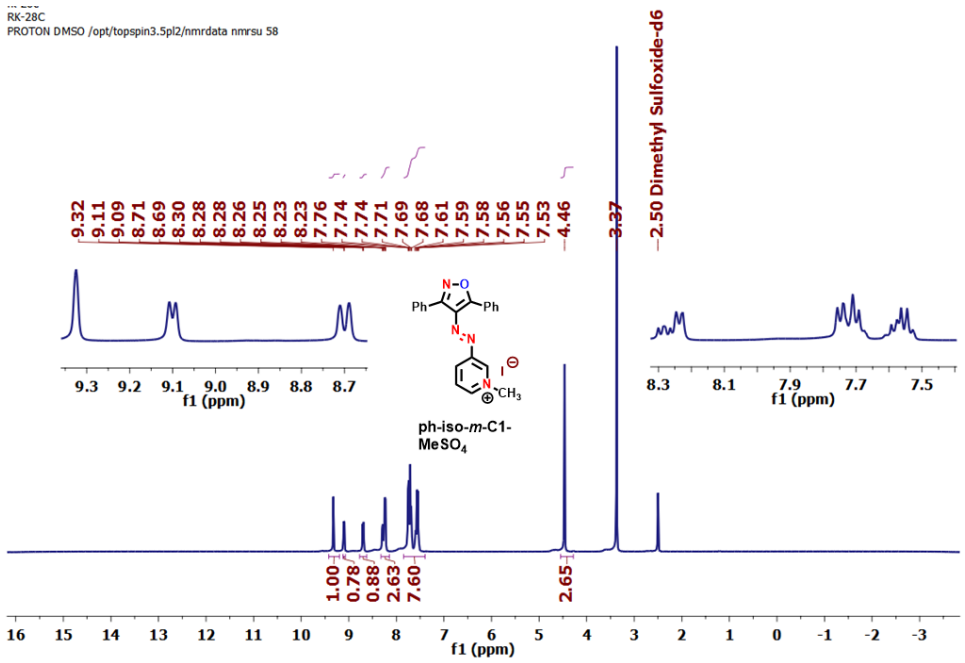

^{1}H NMR spectrum of (*E*)-3-((3,5-diphenylisoxazol-4-yl)diazenyl)-1-methylpyridin-1-ium Iodide, **ph-iso-*m*-C1-I** (400 MHz, DMSO-d_6).

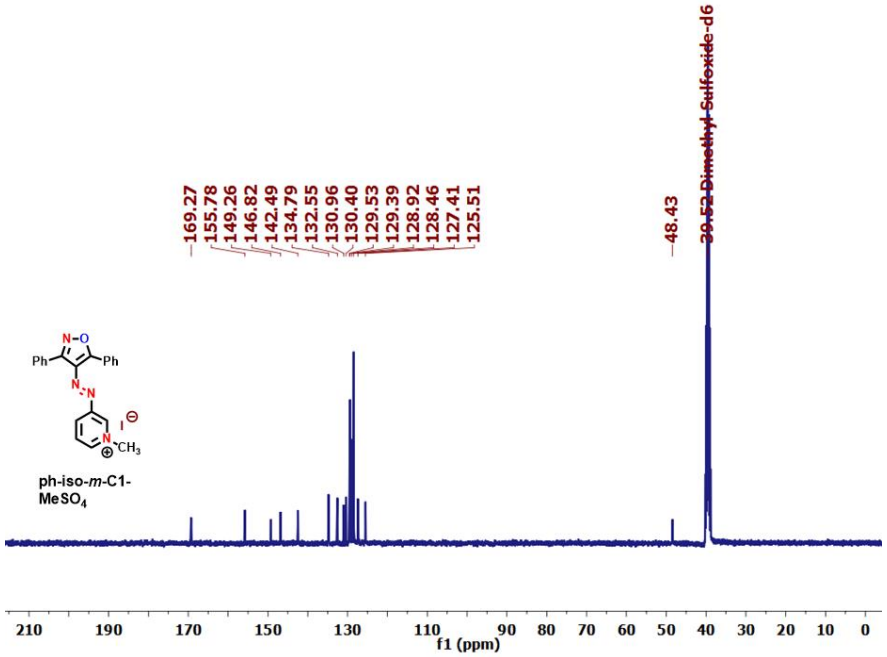

^{13}C{^{1}H} NMR spectrum of (*E*)-3-((3,5-diphenylisoxazol-4-yl)diazenyl)-1-methylpyridin-1-ium Iodide**, ph-iso-*m*-C1-I** (100 MHz, DMSO-d_6).

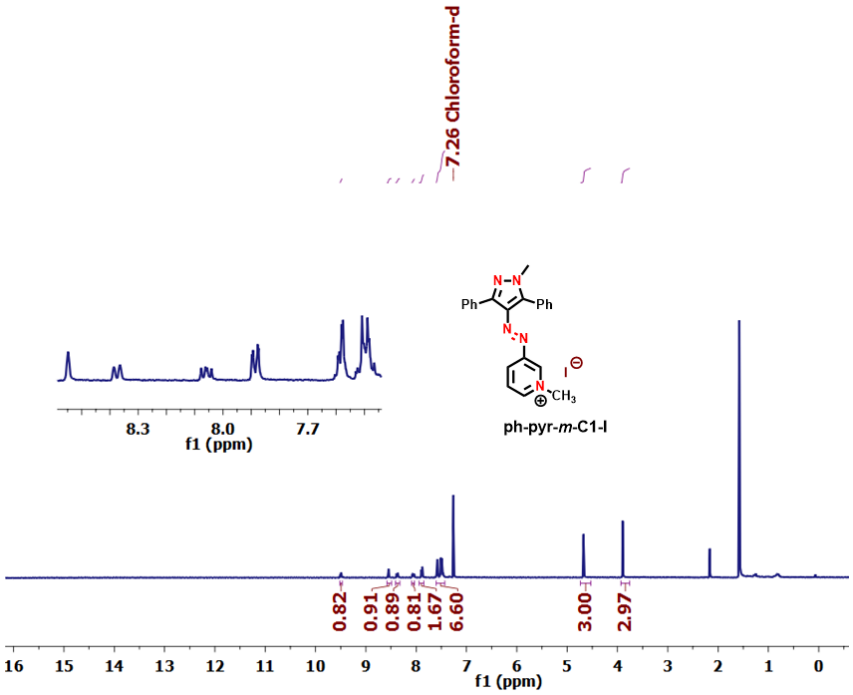

^{1}H NMR spectrum of (*E*)-1-methyl-3-((1-methyl-3,5-diphenyl-1H-pyrazol-4-yl)diazenyl)pyridin-1-ium Iodide, **ph-pyr-*m*-C1-I** (400 MHz, $CDCl_3$).

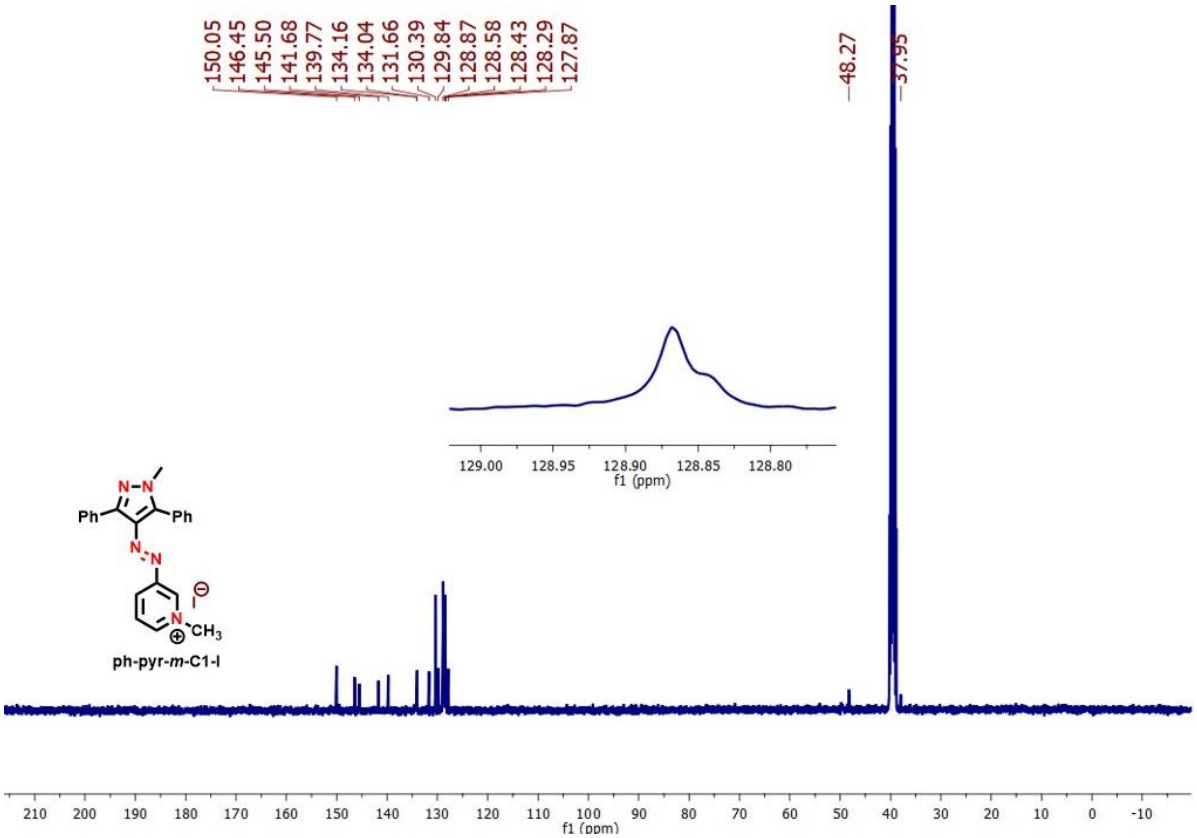

^{13}C{^{1}H} NMR spectrum of (*E*)-1-methyl-3-((1-methyl-3,5-diphenyl-1H-pyrazol-4-yl)diazenyl)pyridin-1-ium Iodide, **ph-pyr-*m*-C1-I** (100 MHz, DMSO-d_6).

Part B

Arylazopyrazolium ionic photoswitches (AAPIPs)

3B.1 Introduction

Azoarenes are intriguing class of photoswitches exhibiting light modulated bistability.[1] Designing new derivatives with improved performance is one of the recent areas of research due to the increasing demand for photoswitchable molecules in widespread applications.[2,3] Particularly, the advent of azoheteroarenes and their role in photopharmocology tremendously widens their scope. Likewise, it also necessitates to strike a balance between photoswitching ability and medicinal effects.[4] Introducing photoresponsiveness to the existing drug molecules, and exploring the photoswitches decorated with suitable drug-like moieties are the most profoundly adopted strategies to gain light controlled therapeutic effects.[5,6] Considering the importance of structural features of drugs and their influence in pharmacokinetics and pharmacodynamics, the following characteristics are essential in the utilization of azoheteroarenes in this domain: (a) robust and bidirectional photoswitching, (b) long life-time in hours to days at physiological temperature of the photoswitched state, (c) tolerance to the substituents exhibiting pharmacological effects towards photoswitching, (d) stability of photoswitched states in a wide range of pH, and more importantly, (e) water solubility and balanced lipophilicity, and (f) differential pharmacological effects of the *E*- and *Z*-isomers.

Many of these characteristics have been separately addressed by different research groups. Among them, the introduction of azopyrazoles with excellent bidirectional photoswitching, and long-lived *Z*-isomers by Fuchter and co-workers (**Scheme 3B.1**) are an important milestone (**Scheme 3B.1**).[7]Since then, several heteroacyclic-based azoarenes have been reported with various properties and utilities.[8] However, the number of azoheteroarenes exhibiting photoswitching in aqueous conditions is limited (**Scheme 3B.1**).[9] Herges and co-workers introduced bridged diazocines showing remarkable photoswitching in water (**Scheme 3B.1**).[10] Recently, the utility of azo(hetero)arenes with specific substitutions undergoing photoswitching in buffer solutions was reported by Woolley's and Samanta's groups.[11]

However, such approaches mandate the presence of organic co-solvent. Incorporation of PEG to the photoswitches can also bring light responsiveness in aqueous solution.[12] The groups of Klajn, Ramamurthy and Ravoo have successfully demonstated photoswitching of azo compounds in water by means of utilizing molecular containers or capsules.[9a-b,13]

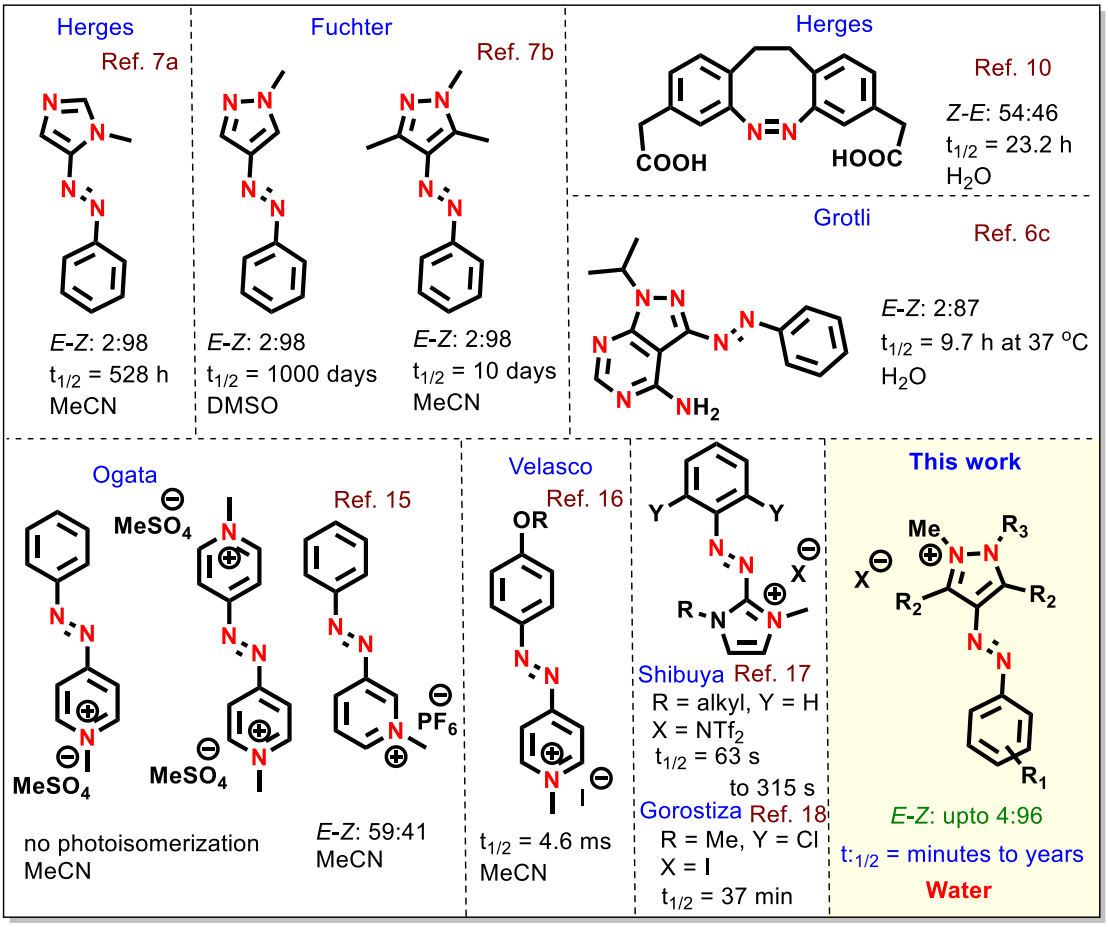

Scheme 3B.1. Azoheteroarene and water soluble photoswitches.

Despite the presence of such varied approaches, one of the most profoundly attempted strategies is to introduce groups that can impart ionic character to the photoswitches to increase water solubility. In this regard, simple azobenzenes have been functionalized with imidazolium, and piperidinium groups and derivatized into ionic photoswitches. However, their photoswitching abilities in water were found to be moderate.[14] Likewise, the direct quaternization of azopyridines has been explored by Ogate and co-workers (**Scheme 3B.1**).[15] Apparently, such approach led to fast thermal relaxation of their *Z*-isomers, which was also demonstrated by Valesco and co-workers (**Scheme 3B.1**).[16] Similarly, Kawai and co-workers have made azoimidazolium salts that exhibited *Z*-isomer half-life in the order of seconds to minutes (**Scheme 3B.1**).[17] In a recent study, Gorostiza and co-workers have reported an azoimidazolium ionic compound as adrenoswitch with *Z*-isomer's half-life of 37 min at rt under physiological pH.[18]

Motivated by these reports, we decided to develop ionic photoswitches that can fulfil the criteria mentioned previously. To achieve this, we envisioned to quaternize the five-

membered pyrazole ring of the azopyrazole photoswitches having different electronic substitution (R_1 and R_2) and to vary their lipophilic character (R_3). The resulting arylazopyrazolium ionic photoswitches (AAPIPs) not only showed exceptional photoswitching but also exhibited very slow thermal relaxation of *Z*-isomers in water. To gain the structure-property relationship, the effect of solvents, counter ions, substitutions, concentration, pH and glutathione have been studied. Herein, we report a systematic investigation of these new class of ionic and water soluble photoswitches.

3B.2 Synthesis

To access the target arylazopyrazolium ionic photoswitches (AAPIPs), several attempts have been made with different alkylation reagents and conditions**.** The desired ionic photoswitch **1-C1-MeSO$_4$** was obtained in excellent yields when the corresponding *N*-methyl-phenylazo-3,5-dimethylpyrazole 1-C1 was treated with dimethyl sulfate in dry MeCN under reflux conditions. Taking advantage of this method, many other AAPIPs with methyl sulphate as a counter ion **1-24-Cn-MeSO$_4$** have been synthesized (**Scheme 3B.2**). In this regard, the corresponding arylazopyrazoles **1-24-Cn** have been accessed through K_2CO_3 mediated N-alkylation strategy, for which the N-H azopyrazoles **1-24** were synthesized using the literature methods.[8h] For chloride ion exchange, the AAPIPs were treated with the Amberlite® ion exchange resin, whereas other counter ions have been introduced by exchanging chloride ions with sodium or ammonium salts of the desired anions.[19] All the target molecules have been characterized by ^{1}H, ^{13}C, HRMS, IR and UV-Vis spectroscopic techniques.

3B.3 Photophysical studies

The photophysical properties of the ionic photoswitches were evaluated in water and DMSO primarily using UV-vis spectroscopy (**Table 3B.1** and **Appendix 3B**). After screening and standardization of conditions, experiments were also conducted and analyzed using ^{1}H-NMR spectroscopy. All the AAPIPs reported in this manuscript exhibit a strong absorption band between 315 and 350 nm ($\pi-\pi^*$), and a weak band at 420-450 ($n-\pi^*$) in water (**Table 3B.1**). A representative absorption spectral data of (*E*)**-1-C1-MeSO$_4$** is depicted (**Figure 3B.1**). The $\pi-\pi^*$ band of all these AAPIPs showed a slight bathochromic shift (5-10 nm) in DMSO in comparison to water because the excited state is more stabilized than the ground state.[20] More importantly, the absorption maxima of $\pi-\pi^*$ and $n-\pi^*$ bands are independent of variation in the alkyl chain at pyrazolium nitrogen (R_3, the group rendering lipophilic character) or the counter ions; whereas the substitution at 3,5 positions of the pyrazolium unit

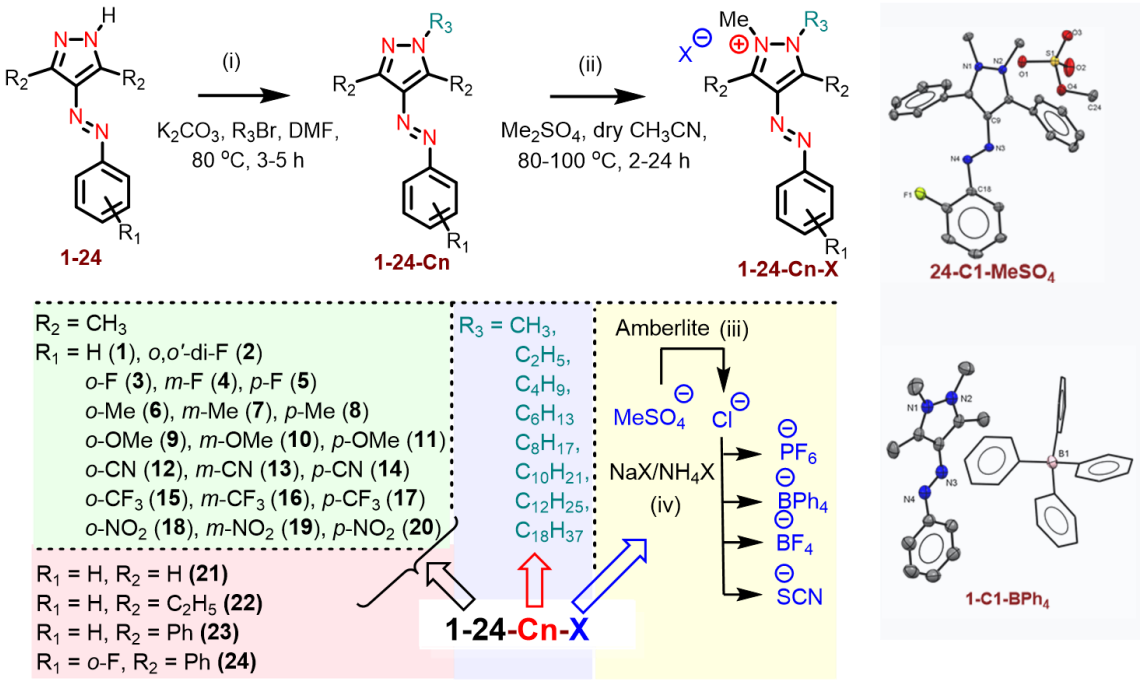

Scheme 3B.2. Synthesis of the target ionic photoswitches (AAPIPs) and generalized numbering scheme. Crystal structures depict the AAPIPs, **24-C1-MeSO₄** (top) and **1-C1-BPh₄** (bottom).

(R_2) and/or at the phenyl ring (R_1) showed a significant influence depicting the impact of electronic and steric factors. Especially, the 4-methoxy derivative **11-C10-MeSO₄** showed a maximum bathochromic shift in the π–π* band upto 345 nm (**Table 3B.4**). Upon subjecting to UV irradiation, majority of the targets showed excellent *E*-*Z* photoisomerization (near quantitative conversion based on ^{1}H-NMR data) involving isosbestic points in UV-vis spectra (**Table 3B.4**). The only exception is *ortho* nitro derivative **18-C10-MeSO₄**, which could possibly undergo fast thermal reverse *Z*-*E* isomerization. In general, a moderate to excellent conversion (49-89%) was achieved for the reverse *Z*-*E* photoisomerization by irradiating the solution at a wavelength corresponding to the n–π* band of the *Z*-isomer (**Table 3B.4**). The moderate conversion in the reverse *Z*-*E* photoisomerization of certain AAPIPs is attributed to the overlapping nature of absorption features of both *E*- and *Z*-isomers. However, several derivatives including 4-methoxy (**11-C10-MeSO₄**) were found to exhibit excellent bidirectional photoswitching in water with an isomerization conversion above 90% in forward and >75% in the reverse directions. Particularly, for electron donating substituted derivatives absorbing at longer wavelengths the non-overlapping part of n–π* band between *Z*- and *E*-isomers (at 490 nm light) allowed maximal *Z*-*E* photoisomerization.

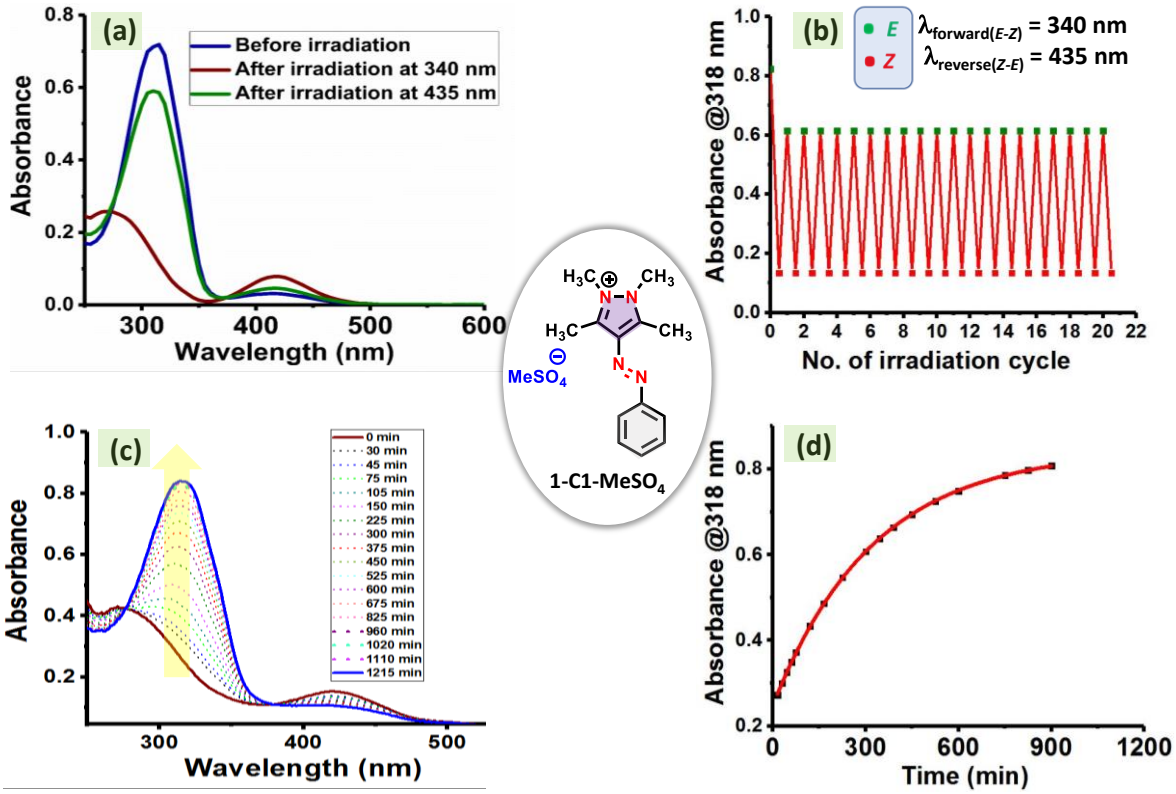

Figure 3B.1. Photoisomerization and thermal reverse isomerization kinetics in **1-C1-MeSO$_4$**. (a) Bidirectional photoisomerization {Forward: 340 nm for 15 min, and reverse: 435 nm for 15 min} in water (61.9 μM); (b) Photoswitching stability test over 20 cycles in water; (c & d) Thermal reverse isomerization kinetics and its exponential fit for the formation of *E*-isomer at 80 °C in water (λ_{max} (π–π^*) = 318 nm).

Table 3B.1. Quantum yield calculation of forward photoisomerization of derivatives of **1-C1-MeSO$_4$**, **21-C1-MeSO$_4$**, and **23-C1-MeSO$_4$** in MeCN.

Compound	Wavelength (nm)	Extinction coefficient, $\mathcal{E}$ ($L^{-1}mol^{-1}cm^{-1}$)	Rate kinetics (10^{-3}) s^{-1}	Power (10^{-4})	Photon Flux (10^{-10})	Quantum yield
1-C1-MeSO$_4$	340	10915 ± 187	3.48	1.99	5.69	0.24
	340	10915 ± 187	4.34	2.53	7.23	0.24
	340	10915 ± 187	4.89	2.48	7.09	0.28
	355	1887 ± 43	1.31	1.54	4.60	0.67
	355	1887 ± 43	0.98	1.74	5.20	0.43
	355	1887 ± 43	1.89	2.53	7.00	0.62
21-C1-MeSO$_4$	340	7936 ± 71	3.18	2.67	7.61	0.23
	340	7936 ± 71	3.40	2.67	7.61	0.24
	340	7936 ± 71	3.62	2.67	7.63	0.26
	355	1047 ± 75	0.72	1.86	5.53	0.55

	355	1047 ± 75	1.09	1.94	5.77	0.78
	355	1047 ± 75	0.83	1.90	5.67	0.60
23-C1-MeSO$_4$	355	6498 ± 180	2.56	1.96	5.85	0.65
	355	6498 ± 180	2.25	1.59	4.73	0.65
	355	6498 ± 180	2.55	1.66	4.95	0.65
	365	2024 ± 57	1.50	2.64	8.09	0.40
	365	2024 ± 57	1.83	3.41	10.46	0.38
	365	2024 ± 57	2.39	3.41	10.46	0.49

For **1-C1-MeSO$_4$**, the forward *E*-*Z* photoisomerization quantum yield in MeCN was 0.25 ± 0.02 at 340 nm and 0.57 ± 0.13 at 355 nm. Similarly, the quantum yields of derivatives **9-C1-MeSO$_4$**, and **11-C1-MeSO$_4$** were also determined (see **Table 3B.1**). For **9-C1-MeSO$_4$**, and **11-C1-MeSO$_4$** the quantum yields were 0.24 ± 0.06 and 0.42 ± 0.06 at 340 nm, respectively. Meanwhile at 355 nm, the values were found to be 0.64 ± 0.1 and 0.65 ± 0.00), respectively. Such high photoswitching stability and moderate quantum yields are comparable to the aryazopyrazoles.[8c]

Thermal reverse isomerization kinetics and *Z*-isomer stability

Bidirectional photoswitching is crucial for many practical applications of the photoswitches, which depends mainly on the thermal lifetime of the *Z*-isomers. In applications related to the photopharmocolgy, such bidirectional photoswitching in aqueous conditions is highly desirable. However, water as a medium can inhibit the photoswitching and induce fast thermal *Z*-*E* relaxation.[7,8h] Taking advantages of their ionic nature and high solubility, we explored the thermal reverse *Z*-*E* isomerization behavior of the AAPIPs in water. In this regard, the kinetics studies were performed for **1-C1-MeSO$_4$** in aqueous conditions with and without buffer medium (pH = 2-13) and followed by UV-vis spectroscopy. Except the three nitro derivatives **18-C10-MeSO$_4$**, and **20-C10-MeSO$_4$**, almost all AAPIPs were found to have slow rate of thermal reverse *Z*-*E* isomerization (**Table 3B.3**). Hence, a few selected derivatives were subjected to kinetics studies in water at 80 ^{o}C. For instance, the pyrazolium derivative **1-C1-MeSO$_4$** showed a half-life of 224 min at 80 ^{o}C. Similar experiments were performed also in DMSO. Surprisingly, the half-life has dropped by a factor of three to 84 min. Such lowering in the half-life was consistent for the other derivatives except the derivative with C_{18} alkyl chain **1-C18-MeSO$_4$**.

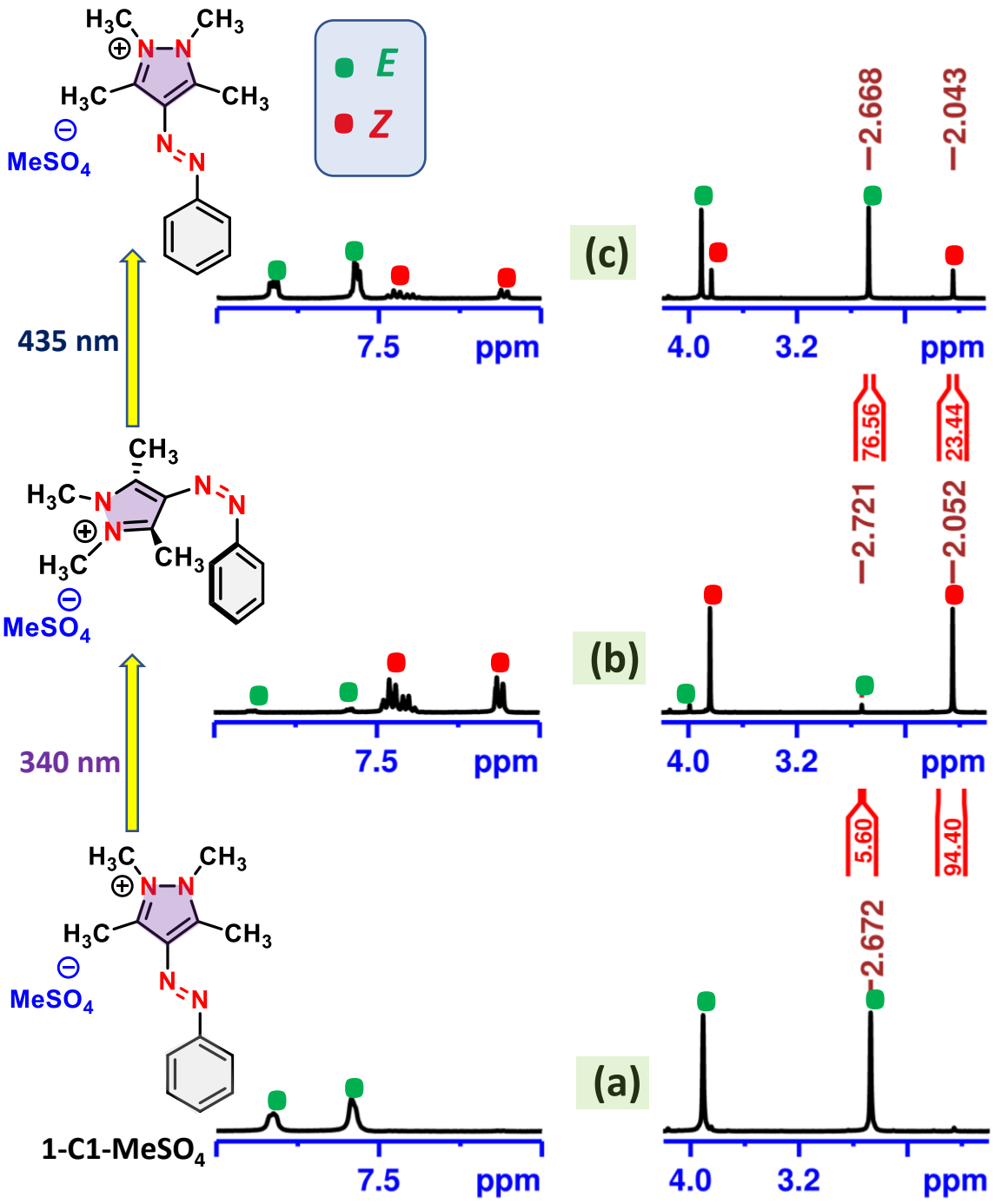

Figure 3B.2. Partial ^{1}H-NMR spectral data of IP **1-C1-MeSO$_4$** (25.4 mM, D_2O) depicting photoisomerization: (a) before irradiation (*E*-isomer); (b) after irradiation at 340 nm (2 h); (c) after irradiation at 435 nm (45 min); PSS compositions were estimated using the normalized integral values corresponding to the selected proton signals (R_3 = Me) of *E*- and *Z*-isomers at 2.72 and 2.05 ppm, respectively.

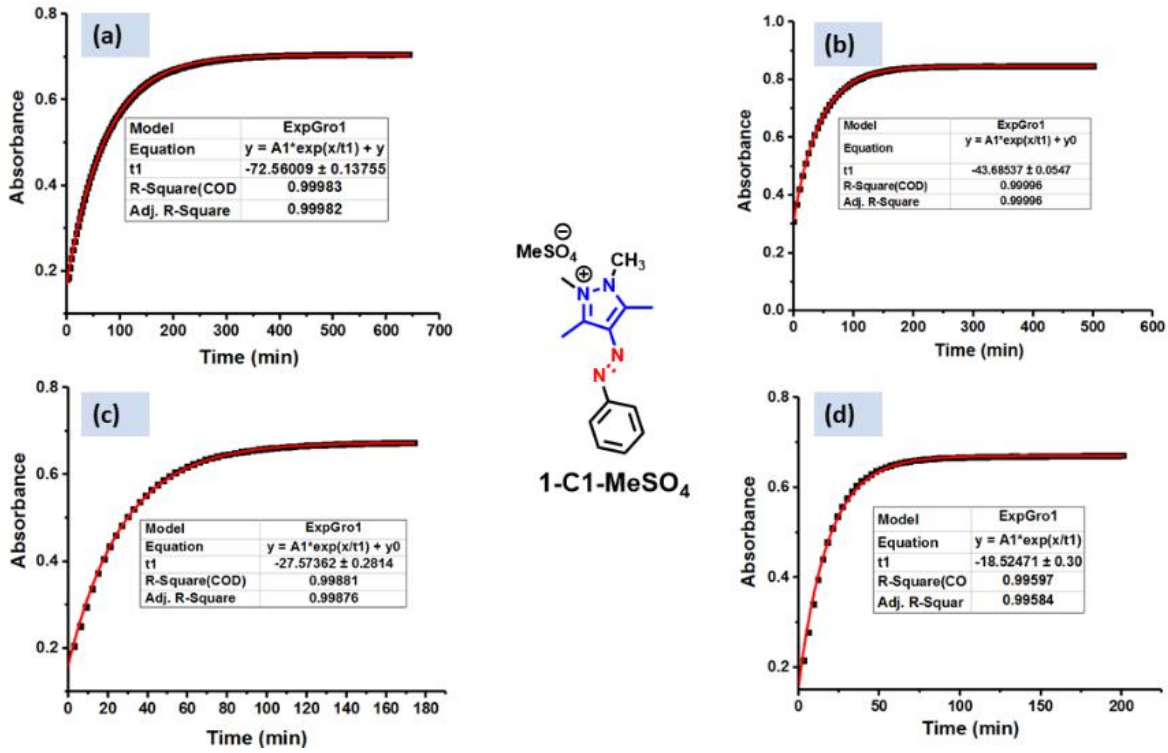

Figure 3B.3. Variable temperatures reverse *Z-E* isomerization kinetics of **1-C1-MeSO$_4$** in DMSO at (a) 85 ^oC; (b) 90 ^oC; (c) 95 ^oC, and (d) 100 ^oC.

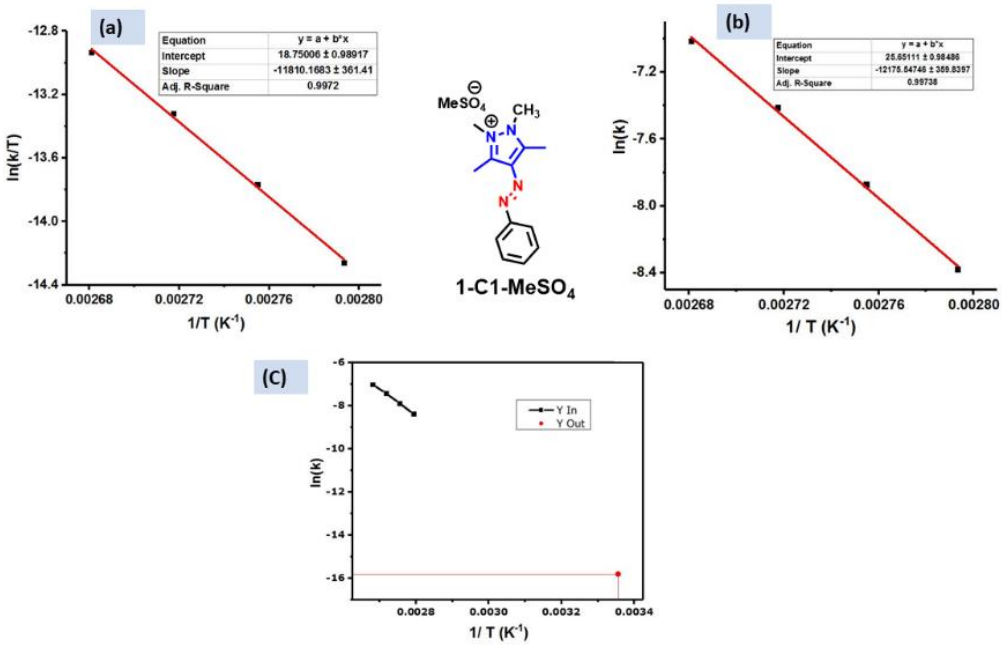

Figure 3B.4. (a) Eyring plot, and (b) Arrhenius plot for **1-C1-MeSO$_4$** in DMSO; (c) Extrapolation of Arrhenius plot for **1-C1-MeSO$_4$** in DMSO to room temperature (298 K).

Similar experiments were performed also in DMSO. Surprisingly, the half-life has dropped by a factor of three to 84 min. Such lowering in the half-life was consistent for the other derivatives except the derivative with C_{18} alkyl chain **1-C18-MeSO$_4$**.

Table 3B.2. Activation parameters deduced from the variable temperature kinetics studies, Arrhenius and Eyring plots

S. No.	Compound	E_a (kJ/mol)	$\Delta H^{\ddagger}$ (kJ/mol)	$\Delta S^{\ddagger}$ (J/K mol)	$\Delta G^{\ddagger}$ (kJ/mol)	k^a (s^{-1})
1.	**1-C1-MeSO$_4$**	101.2 ± 3.0	98.2 ± 3	-41.6 ± 8.2	110.6 ± 5.4	1.4 x 10^{-7}
2.	**1-C10-MeSO$_4$**	104.1 ± 4.7	101.1 ± 4.7	-35.4 ± 12.8	111.6 ± 8.5	1.3 x 10^{-7}
3.	**1-C12-MeSO$_4$**	110.9 ± 1.6	108.1 ± 1.7	-16.2 ± 4.7	112.9 ± 3.1	1.2 x 10^{-7}
4.	**2-C10-MeSO$_4$**	116.3 ± 1.3	113.3 ± 1.3	-12.4 ± 3.6	117.0 ± 2.4	1.4 x 10^{-8}
5.	**22-C1-MeSO$_4$**	96.2 ± 3.8	93.1 ± 3.8	-51.1 ± 10.5	108.3 ± 6.9	3.2 x 10^{-7}
6.	**23-C1-MeSO$_4$**	104.9 ± 3.1	101.9 ± 3.1	-32.0 ± 8.5	111.4 ± 5.6	1.4 x 10^{-7}

[a]The rate constants (k) at room temperature (25 °C) were estimated based on extrapolation.

Table 3B.3. Rate constants of azopyrazolium derivatives in water (at 80 °C) and DMSO (at 90 °C)

S.No.	Compound	R_1	Rate constant (s^{-1}) in water	Rate constant (s^{-1}) in DMSO
1.	**1-C1-MeSO$_4$**	H	5.1 x 10^{-5} ± 5.2 x 10^{-7}	3.8 x 10^{-4} ± 4.8 x 10^{-7}
2.	**1-C2-MeSO$_4$**	H	5.9 x 10^{-5} ± 2.9 x 10^{-6}	3.5 x 10^{-4} ± 5.1 x 10^{-7}
3.	**1-C4-MeSO$_4$**	H	4.7 x 10^{-5} ± 1.5 x 10^{-6}	3.3 x 10^{-4} ± 7.8 x 10^{-7}
4.	**1-C6-MeSO$_4$**	H	3.6 x 10^{-5} ± 9.0 x 10^{-7}	3.2 x 10^{-4} ± 1.5 x 10^{-6}
5.	**1-C8-MeSO$_4$**	H	9.8 x 10^{-5} ± 4.0 x 10^{-7}	3.2 x 10^{-4} ± 1.7 x 10^{-6}
6.	**1-C10-MeSO$_4$**	H	5.0 x 10^{-5} ± 5.0 x 10^{-6}	2.9 x 10^{-4} ± 1.7 x 10^{-6}
7.	**1-C12-MeSO$_4$**	H	3.2 x 10^{-5} ± 2.3 x 10^{-8}	3.1 x 10^{-4} ± 7.2 x 10^{-7}
8.	**1-C18-MeSO$_4$**	H	4.0 x 10^{-4} ± 2.2 x 10^{-6}	3.1 x 10^{-4} ± 1.6 x 10^{-6}
9.	**1-C1-BF$_4$**	H	insoluble	3.4 x 10^{-4} ± 2.4 x 10^{-6}
10.	**1-C1-PF$_6$**	H	insoluble	4.3 x 10^{-4} ± 1.7 x 10^{-6}
11.	**1-C1-BPh$_4$**	H	insoluble	4.1 x 10^{-4} ± 2.9 x 10^{-7}
12.	**1-C1-SCN**	H	5.8 x 10^{-5} ± 6.9 x 10^{-8}	3.9 x 10^{-4} ± 2.5 x 10^{-6}
13.	**1-C1-Cl**	H	5.8 x 10^{-5} ± 1.1 x 10^{-6}	3.7 x 10^{-4} ± 1.2 x 10^{-7}
14.	**2-C1-MeSO$_4$**	2,6-diF	-	9.1 x 10^{-5} ± 1.6 x 10^{-7}
15.	**3-C1-MeSO$_4$**	2-F	-	2.6 x 10^{-4} ± 6.8 x 10^{-7}
16.	**4-C1-MeSO$_4$**	3-F	-	4.3 x 10^{-4} ± 1.5 x 10^{-6}
17.	**5-C1-MeSO$_4$**	4-F	-	3.2 x 10^{-4} ± 1.4 x 10^{-6}
18.	**6-C1-MeSO$_4$**	2-Me	-	5.5 x 10^{-4} ± 2.4 x 10^{-6}
19.	**7-C1-MeSO$_4$**	3-Me	-	3.6 x 10^{-4} ± 1.5 x 10^{-6}
20.	**8-C1-MeSO$_4$**	4-Me	-	4.6 x 10^{-4} ± 2.2 x 10^{-6}
21.	**9-C1-MeSO$_4$**	2-OMe	-	8.7 x 10^{-5} ± 1.2 x 10^{-7}
22.	**10-C1-MeSO$_4$**	3-OMe	-	3.7 x 10^{-4} ± 1.6 x 10^{-6}
23.	**11-C1-MeSO$_4$**	4-OMe	-	7.9 x 10^{-4} ± 3.5 x 10^{-6}
24.	**12-C1-MeSO$_4$**	2-CN	-	4.1 x 10^{-4} ± 1.4 x 10^{-6}
25.	**13-C1-MeSO$_4$**	3-CN	-	2.6 x 10^{-3} ± 2.0 x 10^{-4}
26.	**14-C1-MeSO$_4$**	4-CN	-	3.5 x 10^{-3} ± 1.8 x 10^{-4}
27.	**15-C1-MeSO$_4$**	2-CF_3	-	2.7 x 10^{-3} ± 2.0 x 10^{-4}
28.	**16-C1-MeSO$_4$**	3-CF_3	-	3.7 x 10^{-4} ± 1.7 x 10^{-6}
29.	**17-C1-MeSO$_4$**	4-CF_3	-	1.0 x 10^{-3} ± 1.3 x 10^{-5}
30.	**18-C1-MeSO$_4$**	2-NO_2	-	2.4 x 10^{-3} ± 2.9 x 10^{-5a}
31.	**19-C1-MeSO$_4$**	3-NO_2	-	4.7 x 10^{-4} ± 2.7 x 10^{-6}
32.	**20-C1-MeSO$_4$**	4-NO_2	-	1.4 x 10^{-2} ± 5.5 x 10^{-4}
33.	**21-C1-MeSO$_4$**	H	8.0 x 10^{-5} ± 4.2 x 10^{-8}	6.6 x 10^{-4} ± 1.8 x 10^{-7}

34.	**22-C1-MeSO$_4$**	H	$1.0 \times 10^{-5} \pm 2.4 \times 10^{-7}$	$1.1 \times 10^{-4} \pm 1.3 \times 10^{-7}$
35.	**23-C1-MeSO$_4$**	H	$5.2 \times 10^{-5} \pm 4.3 \times 10^{-7}$	$3.6 \times 10^{-4} \pm 1.6 \times 10^{-6}$
36.	**24-C1-MeSO$_4$**	2-F	-	$3.3 \times 10^{-4} \pm 1.3 \times 10^{-7}$

The choice of DMSO is also due to the possibility of performing the experiments at a wider temperature range, which are restricted in water, due to the slow kinetics at lower temperature. Variable temperature kinetics measurements were also performed, and by extrapolation of Arrhenius plot to 25 ^{o}C, we estimated the half-life of **1-C1-MeSO$_4$** to be 58 days (in DMSO) and 157 days (in water) at 25 ^{o}C (**Appendix**). Interestingly, the half-life is nearly seven times higher than that of *N*-methyl-3,5-dimethyl azoarylpyrazole reported by Fuchter and co-workers (10 days in MeCN; 8.7 days in DMSO).[7a] Next, we compared the thermal half-lives in DMSO of all the 36 AAPIPs having different substituents (R_1 and R_2), alkyl chains (R_3) and counterions (X). *N*-alkyl chain length has a weak effect on the half-lives (30-39 minutes at 90 ^{o}C). Similarly, the counter ions also showed a negligible influence on the *Z*-isomer stability, presumably attributed to the solvent separated ion pairing of the pyrazolium and counter ions (**Table 3B.3** and **Figure 3B.5a-b**). Indeed, an independent thermal *Z*-*E* isomerization kinetics experiment of **1-C1-MeSO$_4$** was also performed using a saturated sodium chloride solution that showed no impact on the photoswitching or kinetics. (Appendix). On contrast, variation in the substitutions at the 3,5-positions of the pyrazolium ring, and the substitutions at the phenyl ring led to significant changes in the half-lives. All these results confirm the presence of a strong electronic and/or steric influence of substituents on the *Z*-isomer stability of AAPIPs.

Electronic and steric effects of substituents in the stability of *Z*-Isomers

To understand the substituent effects at the pyrazolium ring, we have installed H, Et and Ph groups at 3,5-positions by replacing the two methyl groups in **1-C1-MeSO$_4$**. Next, photoswitching and kinetics of the systems have been investigated (**Table 3B.3** and **Figure 3B.5c**). Although the R2 substitutions impacted the π–π^* and n–π^* absorption features, the photoswitching was almost identical after the substitution. However, remarkable changes in the thermal stability of the *Z*-isomers were observed. The order of *Z*-isomer stabilization upon changing the substitution at 3,5-positions is H (**21-C1-MeSO$_4$**) > Me (**1-C1-MeSO$_4$**) > Ph (**23-C1-MeSO$_4$**) > Et (**22-C1-MeSO$_4$**). This trend is consistent in DMSO and water (**Table 3B.2**). Presumably the absence of steric hinderance and a possible H–π interaction in a highly symmetric T-shaped geometry of the *Z*-isomer (based on the computational studies) can be attributed to the exceptional stabilization in **21-C1-MeSO$_4$** (vide infra).[8c] Despite a similar

twisted geometry, the π–π stacking in 3,5-diphenyl substituted **23-C1-MeSO$_4$** enhances the stabilization of its *Z*-isomer. Based on these studies, it is apparent that the steric factor at the 3,5-positions of pyrazolium IPs is critical in influencing the stability of *Z*-isomers. At this juncture, the exceptional *Z*-isomer stability of majority of the AAPIPs can be attributed to the electrostatic interactions between the pyrazolium cationic part and the aryl group in their *Z*-isomeric state and electronic effects of the latter. To unravel the electronic and steric influence of the substituents at the phenyl ring, we decided to utilize the linear free energy relationships (LFER) using Taft[20a-b] (for *ortho* substitution) and Hammett[20c] (for meta and para substitutions) constants.[8h] As far as the electronic effects due to meta substitution is concerned, the Hammett relationship {log(k_R/k_H) vs substituent constants σ_m} revealed a positive trendline albeit a non-linear relationship (**Figure 3B.5d**). This is an indicative of a possible complex interplay of resonance, inductive effects and field effects in influencing the stabilization of *Z*-isomers, apart from the possible mechanistic changes in the thermal reverse isomerization.[21] Contrary to this, such Hammett plot for the para substituents signifies once again a non-linear relationship (**Figure 3B.5e**). Indeed, the electron donating substituents did not influence much and so the log(k_R/k_H) was nearly the same, however, the electron withdrawing groups at the para positions strongly destabilize the *Z*-isomers. This effect is maximal for para nitro derivative **20-C10-MeSO$_4$**, which undergoes thermal relaxation at faster rate even at rt. Based on these Hammett relationships, it is evident that the *Z*-isomers of the AAPIPs gain stabilization through electro-static interaction between the cationic pyrazolium ring and the π-cloud of the phenyl ring. Since the electron donating substituents enhance such interactions, they stabilize the *Z*-isomers nearly equally. On the contrary, the electron with-drawing groups diminish the electron density on the phenyl ring leading to weakening of such electrostatic interactions that shortens the half-life of the *Z*-isomers. Similarly, the substituent effects at the *ortho* position through the Taft plot between the log(k_R/k_{Me}) and the steric substituent constant (Es) revealed a linear correlation with a negative slope (**Figure 3B.5f**). Such trend confirms the release of steric factor at the transition state relative to the *Z*-isomer. Thus, the steric factor destabilizes the *Z*-isomeric species, which is consistent with the studies on azoheteroarenes.[8h]

Solvent and Concentration Effects

For all the derivatives, the PSS composition in the forward (*E*-*Z*) and reverse (*Z*-*E*) photoisomerization steps, were determined in D_2O using ^{1}H-NMR spectroscopy (Table 1). The observed near quantitative isomerization conversion in forward and moderate to excel-

lent recovery in the reverse steps were tested for solvent effects. Indeed, a significant difference in the half-life of *Z*-isomer was observed upon changing the solvent from water to DMSO (vide supra). This necessitates to explore the effects of solvents on both photoswitching ability and thermal relaxations. In this regard, a series of experiments was carried out for **1-C1-MeSO$_4$** in different solvents such as MeOH, $CHCl_3$, toluene, MeCN, and THF, in addition to DMSO and water, and the studies were followed by UV-vis spectroscopy. To estimate the PSS compositions, we have also performed ^{1}H-NMR spectroscopic studies in DMSO-d_6, CD_3OD, $CDCl_3$, and CD_3CN. We found that the isomerization conversions are consistent (forward: >90% and reverse: >70%) and are independent of the solvents used (**Figure 3B.6**). However, the thermal reverse isomerization of the *Z*-isomers was strongly influenced by the solvent polarity (**Figure 3B.5**). At this stage, we have tested the concentration dependency of the photoswitching ability to enumerate the role of intermolecular interactions. In this regard, photoswitching experiments were carried out using **1-C1-MeSO$_4$** in D_2O and DMSO-d_6.

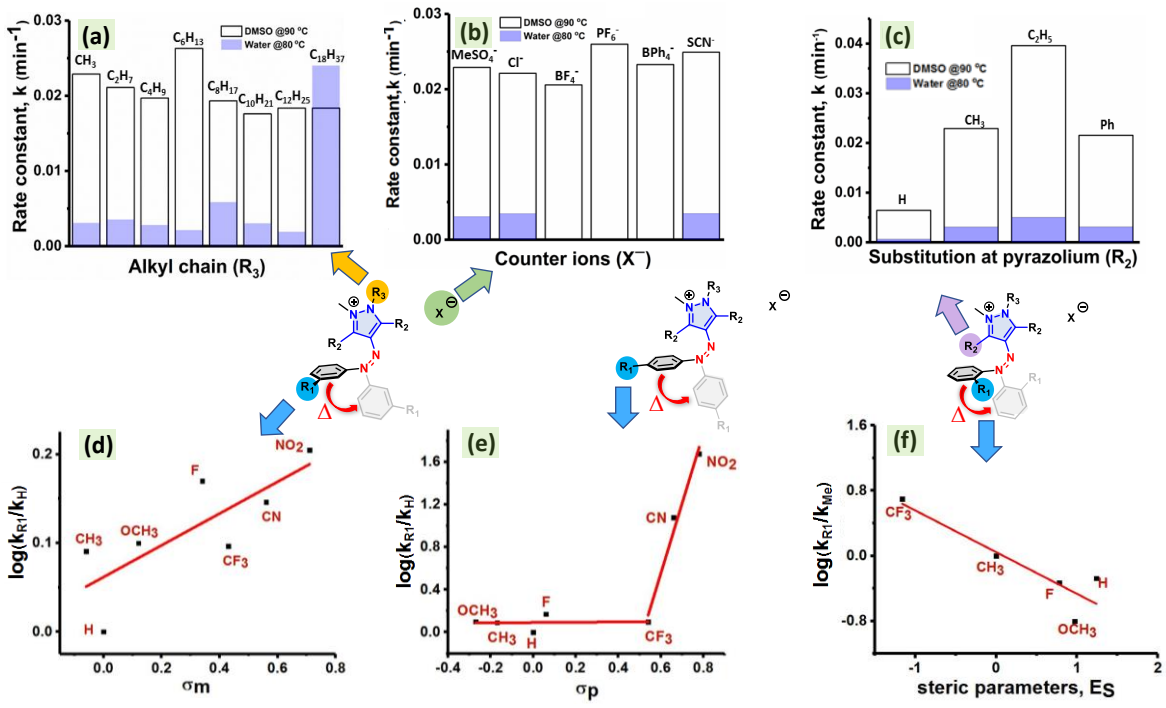

Figure 3B.5. Substituent and counter ion effects in the thermal *Z*-*E* relaxation rates of AAPIPs. Effect of (a) alkyl chain (R_3), (b) counter ions (X^-) and (c) substitution at pyrazolium (R_2) on the rate of thermal *Z*-*E* isomerization of AAPIPs; Electronic and steric effects of the substituents (R_1): Hammett plots of (d) *meta*, (e) *para* substituents, and (f) Taft plot depicting the effect of *ortho* substituents. (For Hammett and Taft plots, the rate constants have been measured in DMSO at 90 °C and followed by UV-Vis spectroscopy)

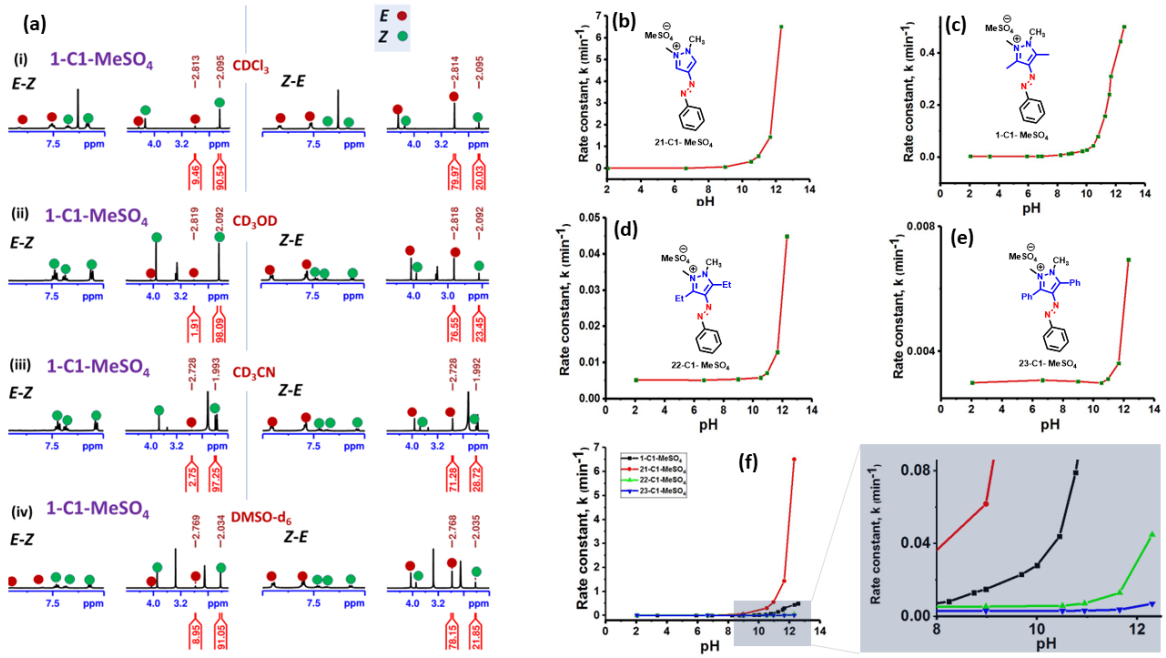

Figure 3B.6. (a) Effect of solvent on the photoisomerization of **1-C1-MeSO$_4$** (15-30 mM): Photoswitching experiments and PSS estimation in the forward *E*-*Z* (340 nm, 2 h or 365 nm, 45 min) and reverse *Z*-*E* photoisomerization (435 nm, 45 min) steps followed by ^{1}H-NMR in (i) $CDCl_3$, (ii) CD_3OD, (iii) CD_3CN, and DMSO-d_6. (The normalized integral values corresponding to *C*-Me signals of the pyrazolium for *E*- and *Z*-isomers are depicted) Effect of pH (2-13) on the thermal reverse (*Z*-*E*) isomerization kinetics (at 80 ^{o}C) followed by UV-Vis spectroscopy in: (b) **21-C1-MeSO$_4$**; (c) **1-C1-MeSO$_4$**; (d) **22-C1-MeSO$_4$**; (e) **23-C1-MeSO$_4$**; (f) Comparison of the b-e; The zoomed part depicts the rate changes due to the effect of basic pH 8-12 in differently substituted azopyrazolium derivatives. (The pH titrations were performed in phosphate buffer (pH 6.65, 25 mM) by adding either 12 M HCl or 10 M NaOH in H_2O and the details are available in **Appendix 3B**.)

Remarkably, at a wide range of concentrations between 8 and 227 mM, we did not see any significant difference in the PSS compositions (**Apendix 3B**). Moreover, independent kinetics experiments on **1-C1-MeSO$_4$** followed by UV-Vis spectroscopy (in H_2O, 68.5 μM) and ^{1}H-NMR spectroscopy (in D_2O, 20.5 mM) exhibited almost identical rates of thermal *Z*-*E* relaxations, 0.3 x 10^{-2} ± 0.003 x 10^{-2} and 0.2 x 10^{-2} ± 0.01 x 10^{-2}, respectively. Similar rates have been estimated for the derivatives **21-C1-MeSO$_4$**, **22-C1-MeSO$_4$** and **23-C1-MeSO$_4$** also (**Appendix 3B**). The similarity in the rates is an indication of exceptional thermal stability of *Z*-isomers of these photoswitches in a wide concentration range.

Effect of pH

In general, azobenzene photoisomerization and the thermal stability of *Z*-isomers aresensitive to pH of the medium.

Table 3B.4. Electronic absorption properties of *E*- and *Z*-isomers (in water), PSS composition for the forward (*E*-*Z*) and reverse (*Z*-*E*) photoisomerization steps (in D_2O) and solvent-dependent thermal reverse (*Z*-*E*) isomerization kinetics data of arylazopyrazolium ionic photoswitches (AAPIPs)

S. No.	Compound	R_1	R_2	UV-vis data[a]				^{1}H-NMR PSS data (%)[b]		Kinetics data ($t_{1/2}$, min)[c]	
				E-isomer		*Z*-isomer					
				π– π* (nm)	n–π* (nm)	π– π* (nm)	n– π* (nm)	*E*-*Z* (%*Z*)	*E*-*Z* (%*E*)	Water at 80 ºC	DMSO at 90 ºC
1.	**1-C1-MeSO$_4$**	H	Me	320	420	o	425	97	79	224	30
2.	**1-C2-MeSO$_4$**	H	Me	320	420	o	425	98	76	196	33
3.	**1-C4-MeSO$_4$**	H	Me	320	420	o	425	89	75	247	35
4.	**1-C6-MeSO$_4$**	H	Me	320	420	o	425	86	76	324	36
5.	**1-C8-MeSO$_4$**	H	Me	320	420	o	425	88	76	118	36
6.	**1-C10-MeSO$_4$**	H	Me	320	420	o	425	87	72	228	39
7.	**1-C12-MeSO$_4$**	H	Me	320	420	o	425	93	81	364	38
8.	**1-C18-MeSO$_4$**[e]	H	Me	320	420	o	425	90	76	29	38
9.	**1-C1-BF$_4$**	H	Me	320	420	o	425	92	73	x	34
10.	**1-C1-PF$_6$**	H	Me	320	420	o	425	91	71	x	27
11.	**1-C1-BPh$_4$**[e]	H	Me	320	420	o	425	89	72	x	28
12.	**1-C1-SCN**	H	Me	320	420	o	425	90	73	198	30
13.	**1-C1-Cl**	H	Me	320	420	o	425	92	76	200	31
14.	**2-C10-MeSO$_4$**	2,6-diF	Me	310	422	281	412	93	76	x	127
15.	**3-C10-MeSO$_4$**	2-F	Me	321	419	274	416	88	72	x	45
16.	**4-C10-MeSO$_4$**	3-F	Me	316	420	271	424	93	80	x	27
17.	**5-C10-MeSO$_4$**	4-F	Me	322	415	271	422	93	75	x	36
18.	**6-C10-MeSO$_4$**	2-Me	Me	325	425	275	425	94	69	x	21
19.	**7-C10-MeSO$_4$**	3-Me	Me	320	420	270	420	85	78	x	32
20.	**8-C10-MeSO$_4$**	4-Me	Me	330	415	250	425	76	80	x	25

21.	**9-C10-MeSO$_4$**	2-OMe	Me	316	o	256	424	87	49	x	133
22.	**10-C10-MeSO$_4$**	3-OMe	Me	315	o	o	425	84	69	x	31
23.	**11-C10-MeSO$_4$**	4-OMe	Me	345	o	324	430	94	89	x	15
24.	**12-C10-MeSO$_4$**	2-CN	Me	310	425	255	425	91	77	x	28
25.	**13-C10-MeSO$_4$**	3-CN	Me	325	425	260	430	95	75	x	4
26.	**14-C10-MeSO$_4$**	4-CN	Me	320	435	230	425	98	70	x	3
27.	**15-C10-MeSO$_4$**	2-CF_3	Me	315	425	245	425	97	76	x	4
28.	**16-C10-MeSO$_4$**	3-CF_3	Me	310	420	o	420	97	74	x	32
29.	**17-C10-MeSO$_4$**	4-CF_3	Me	310	425	345	420	81	74	x	12
30.	**18-C10-MeSO$_4$**	2-NO_2	Me	320	420	320	420	f	f	x	5[g]
31.	**19-C10-MeSO$_4$**	3-NO_2	Me	309	420	265	422	50	68	x	25
32.	**20-C10MeSO$_4$**	4-NO_2	Me	329	431	300	430	62	f	x	1
33.	**21-C1-MeSO$_4$**	H	H	315	410	o	410	80	67	1100	108
34.	**22-C1-MeSO$_4$**	H	Et	320	425	273	425	86	78	144	18
35.	**23-C1-MeSO$_4$**[d]	H	Ph	325	434	280	430	86	83	223	32
36.	**24-C1-MeSO$_4$**[d]	2-F	Ph	335	435	290	430	89	78	x	35

[a]All UV-Vis spectral data were recorded in H_2O in the concentration range 27-106 μM; [b]To estimate PSS composition, ^{1}H-NMR spectral data were recorded in D_2O in the concentration range 6.1-27.8 mM; [c]Thermal reverse (*Z*-*E*) isomerization kinetics were followed by UV-Vis spectroscopy; Unless specified, *E*-*Z* forward photoisomerization was performed at 340 nm (xenon lamp with a monochromator) or [d]365 nm (LED light source); conversely, 435 nm or [e]490 nm (LED light sources) were used for *Z*-*E* reverse photoisomerization; the irradiation was continued until achieving PSS. [g]The kinetics analysis was performed at 25 °C. (o-overlapping; f-fast thermal relaxation; x-not performed in water.

The effect of acid medium and pH have also been explored for different azoheteroarenes. Typically, the protonation of azo nitrogen in acidic conditions (low pH) destabilizes the *Z*-isomers, which makes them to undergo fast thermal relaxation.[9c]
In contrast, hydroxy or amino substituted azo compounds are known for their fast thermal *Z*-*E* relaxation in basic medium (higher pH).[22] Since the azo compounds are desired to tolerate a wide range of pH towards the applications in photopharmolocogy, we intended to study the behaviour of our compounds at different pH.

In this regard, we systematically investigated the effect of a wide range of pH (2 to 13) on photoswitching ability and thermal relaxations using selected pyrazolium derivatives **1-C1-MeSO$_4$**, **21-C1-MeSO$_4$**, **22-C1-MeSO$_4$**, and **21-C1-MeSO$_4$** that were carried out using phosphate buffers. Firstly, the inspection of the absorption features revealed no shifts in the λ_{max} or changes in the absorption profile of the derivatives over a wide range of pH (2-13) indicating the stability of the native *E*-isomeric state. Similarly, the irradiation in the forward and reverse isomerization steps also did not exhibit any significant impact on the absorption profiles of *Z*- or *E*-isomers. Indeed, the photoswitching stability study over five cycles was also conducted that revealed no photobleaching or fatigueness at different pH. Notably, the PSS composition was also estimated to be the same at different pH. For comparison, these experiments were also followed using ^{1}H-NMR in D_2O and phosphate buffer (60:40) at specific pH that includes 2.04, 5.90, and 11.30.

Table 3B.5. Thermal *Z*-*E* isomerization kinetics data at 80 ^oC obtained from UV-Vis spectroscopic studies at different pH of the compounds **21-C1-MeSO$_4$**, **22-C1-MeSO$_4$**, and **23-C1-MeSO$_4$**

S. No.	pH	Rate constant (s^{-1}) @ 80 °C		
		21-C1-MeSO$_4$	**22-C1-MeSO$_4$**	**23-C1-MeSO$_4$**
1	2.04	$2.5 \times 10^{-5} \pm 5.0 \times 10^{-7}$	$8.7 \times 10^{-5} \pm 3.3 \times 10^{-8}$	$5.0 \times 10^{-5} \pm 5.0 \times 10^{-9}$
2	6.65	$2.7 \times 10^{-5} \pm 5.0 \times 10^{-9}$	$8.7 \times 10^{-5} \pm 3.3 \times 10^{-8}$	$5.0 \times 10^{-5} \pm 5.0 \times 10^{-8}$
3	8.98	$1.0 \times 10^{-3} \pm 6.7 \times 10^{-7}$	$9.0 \times 10^{-5} \pm 3.3 \times 10^{-8}$	$5.0 \times 10^{-5} \pm 1.7 \times 10^{-8}$
4	10.51	$5.2 \times 10^{-3} \pm 8.3 \times 10^{-5}$	$9.7 \times 10^{-5} \pm 5.0 \times 10^{-8}$	$5.0 \times 10^{-5} \pm 1.0 \times 10^{-7}$
5	10.91	$9.3 \times 10^{-3} \pm 1.5 \times 10^{-4}$	$1.2 \times 10^{-4} \pm 5.0 \times 10^{-8}$	$5.0 \times 10^{-5} \pm 3.3 \times 10^{-8}$
6	11.65	$1.4 \pm 1.8 \times 10^{-1}$	$2.2 \times 10^{-4} \pm 5.0 \times 10^{-7}$	$6.7 \times 10^{-5} \pm 8.3 \times 10^{-7}$
7	12.30	6.5[a]	$7.5 \times 10^{-4} \pm 5.0 \times 10^{-6}$	$1.2 \times 10^{-4} \pm 3.3 \times 10^{-6}$

[a]rate constant evaluated from extrapolation of Arrhenius plot to 353 K.

Table 3B.6 Thermal *Z-E* isomerization kinetics data obtained from UV-Vis spectroscopic studies at different pH of the compound **1-C1-MeSO$_4$**

S. No.	pH	Rate constant (s^{-1}) @ 80 °C (**1-C1-MeSO$_4$**)
1.	2.04	$5.0 \times 10^{-5} \pm 5.0 \times 10^{-9}$
2.	3.36	$5.0 \times 10^{-5} \pm 5.0 \times 10^{-9}$
3.	5.90	$5.0 \times 10^{-5} \pm 1.0 \times 10^{-8}$
4.	6.65	$5.0 \times 10^{-5} \pm 1.2 \times 10^{-8}$
5.	6.93	$5.0 \times 10^{-5} \pm 6.7 \times 10^{-7}$
6.	8.20	$1.3 \times 10^{-4} \pm 1.5 \times 10^{-6}$
7.	8.74	$2.0 \times 10^{-4} \pm 1.7 \times 10^{-7}$
8.	8.98	$2.5 \times 10^{-4} \pm 1.7 \times 10^{-7}$
9.	9.69	$3.8 \times 10^{-4} \pm 1.7 \times 10^{-6}$
10.	10.00	$4.7 \times 10^{-4} \pm 1.7 \times 10^{-6}$
11.	10.45	$7.3 \times 10^{-4} \pm 1.5 \times 10^{-6}$
12.	10.77	$1.3 \times 10^{-3} \pm 3.3 \times 10^{-6}$
13.	11.24	$2.7 \times 10^{-3} \pm 1.0 \times 10^{-5}$
14.	11.54	$4.0 \times 10^{-3} \pm 1.7 \times 10^{-5}$
15.	11.65	$5.2 \times 10^{-3} \pm 1.7 \times 10^{-5}$
16.	12.30	$7.5 \times 10^{-3} \pm 1.4 \times 10^{-4}$
17.	12.56	$8.3 \times 10^{-3} \pm 3.3 \times 10^{-4}$
18.	sat. NaCl	$5.0 \times 10^{-5} \pm 6.7 \times 10^{-9}$

Neither changes in the chemical shifts before and after irradiation nor the isomerization conversions at the expense of variation in the pH of the medium were obseved. These experiments demonstrated the bidirectional phototoisomerization ability and tolerance of **1-C1-MeSO$_4$** in a wide range of pH. The salient feature of this photoswitch is the remarkable stability of its *Z*-isomer at a wide range of pH. Towards this, the *Z-E* thermal reverse isomerization kinetics experiments have been carried out at a different pH and followed by UV-vis spectroscopy. The results revealed no influence of acidic or neutral pH on the *Z*-isomer stability, however, if the pH was increased further above pH = 8, it induced a fast relaxation. Such rate jumps due to basic pH was also observed in the derivatives **21-C1-MeSO$_4$**, **22-C1-MeSO$_4$**, and **23-C1-MeSO$_4$** (**Figure 3B.3**). The di-H derivative **21-C1-MeSO$_4$**, showed an inflexion point around 8, whereas, **1-C1-MeSO$_4$**, and **22-C1-MeSO$_4$** exhibited such rate changes at a slightly higher pH, 8.5 and 11, respectively. Notably, the di-phenyl derivative **23-C1 MeSO$_4$** showed the maximum stability with a pH jump around 12. Based on the results, Similar rates have been estimated for the derivatives **21-C1-MeSO$_4$**, **22-C1-MeSO$_4$** and **23-C1-MeSO$_4$** also (**Appendix 3B**). The similarity in the rates is an indication of exceptional thermal stability of *Z*-isomers of these photoswitches in a wide concentration range. This showed pyrazolium derivatives are stable under wide range of pH that has been confirmed by ^{1}H NMR spectroscopy (**Appedix 3B**).

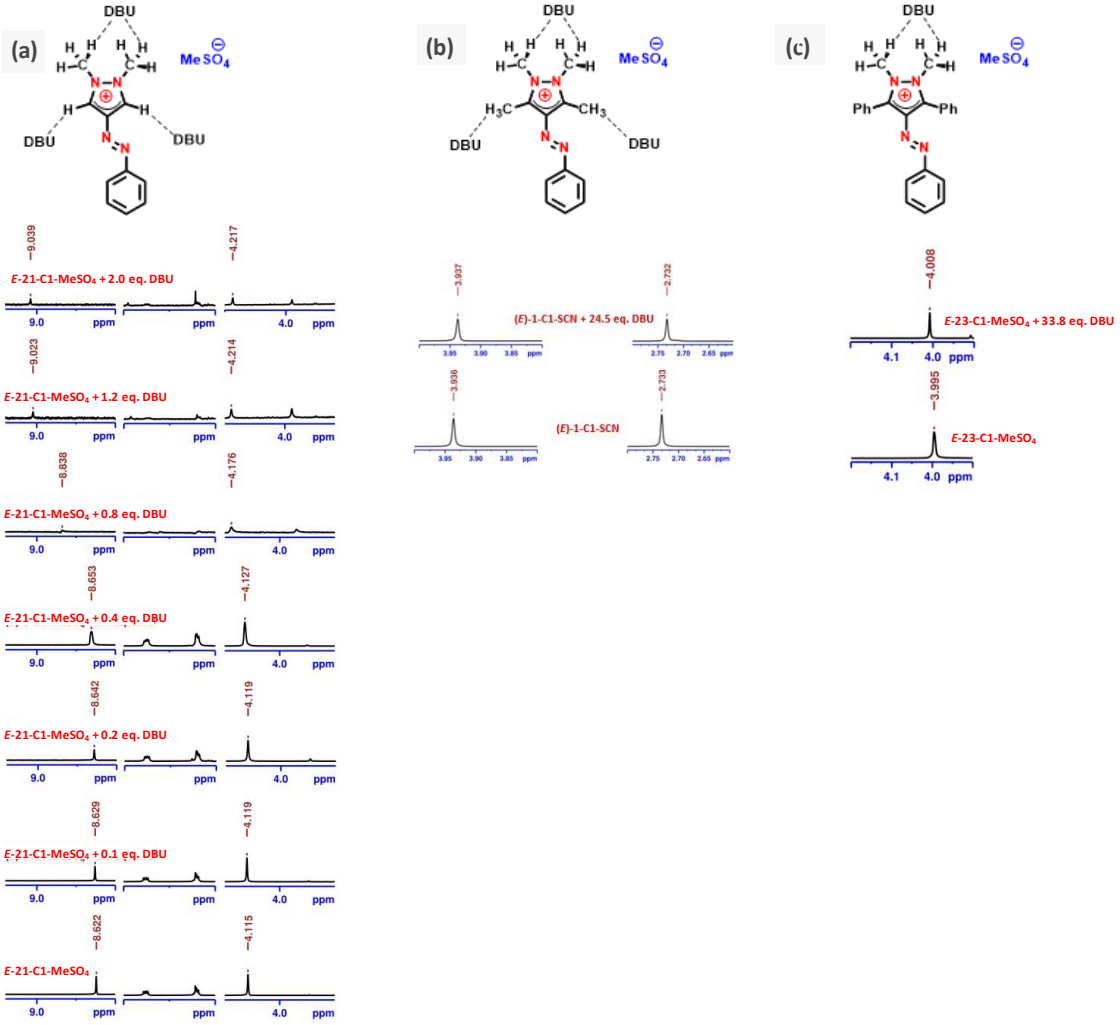

Figure 3B.7. Titration experiment with increasing amounts of DBU as a base in CD_3CN of (a) (*E*)-**21-C1-MeSO4** (R_2=H), (b) (*E*)-**1-C1-SCN** (R_2=Me) and (c) (*E*)-**23-C1-MeSO4** (R_2=Ph). The protons influenced by the possible interaction with DBU exhibit downfield shifts in ^{1}H-NMR, which are depicted in the chemical structures.

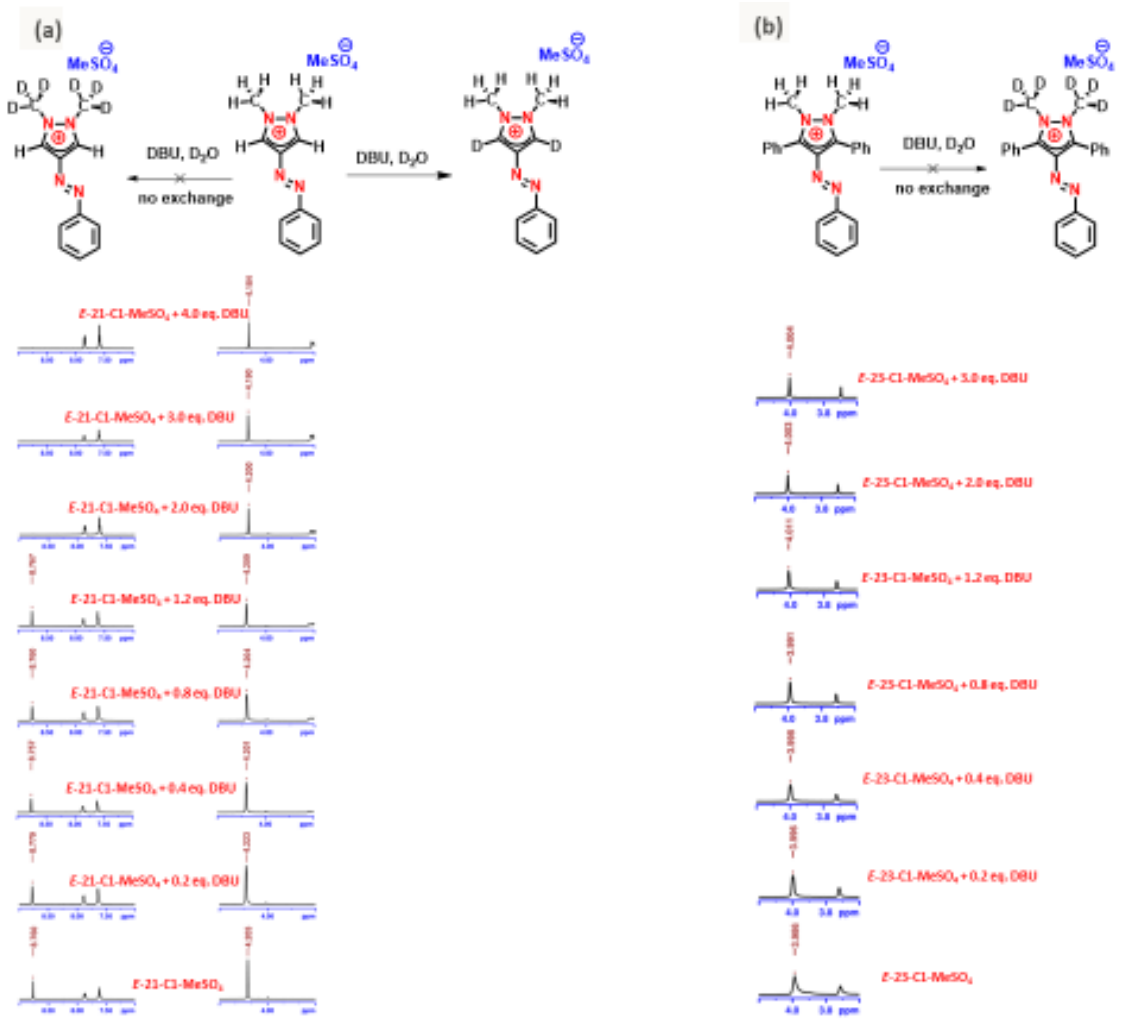

Figure 3B.8. Titration experiment with increasing amounts of DBU as a base in D_2O of (a) (*E*)-**21-C1-MeSO$_4$** (R_2=H) and (b) (*E*)-**23-C1-MeSO$_4$** (R_2=Ph) indicating deuterium exchange at pyrazolium ring protons (R_2=H) in (*E*)-**21-C1-MeSO$_4$**.

Stability towards GSH

Furthermore, the stability of **1-C1-MeSO$_4$** in *E*- and *Z*-isomeric forms with the highest physiologically relevant concentration of GSH (10 mM) was tested. Both *E*- and *Z*-isomers were found stable towards GSH-induced reduction of the azo group. We tested five cycles of reversible photoswitching in the presence of GSH, and the derivative was stable under these conditions (**Figure 3B.9**). These results demonstrate that AAPIPs are as stable as other known azopyrazole derivatives.[11b]

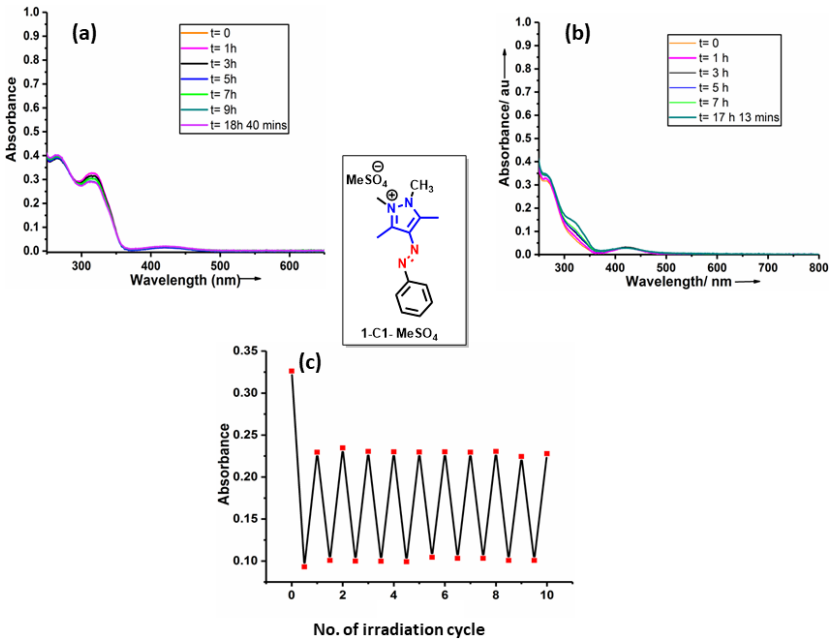

Figure 3B.9. Stability of **1-C1-MeSO$_4$** under the possible maximum biological concentration of glutathione (GSH) (10 mM) in phosphate buffer (pH = 7.4). (a) The UV-Vis spectral data of *E*- isomer of **1-C1-MeSO$_4$** in the presence of GSH; The spectra were recorded at different time intervals (o min, 1 h, 3 h, 5 h, 7 h, 9 h, 18 h 40 min), (b) The UV-Vis spectral data of *Z*-isomer of **1-C1-MeSO$_4$** in the presence of GSH; The spectra were recorded at different time intervals (o, 1 h, 3 h, 5 h, 7 h 17 h 13 min), (c) Photoisomerization stability of **1-C1-MeSO$_4$** in presence of GSH (The forward *E-Z* and the reverse *Z-E* photoisomerzation steps were alternatively carried out at 340 and 435 nm, respectively over 10 cyclesof **1-C1-MeSO$_4$** under the possible maximum biological concentration of glutathione (GSH) (10 mM) in phosphate buffer (pH = 7.4).

3B.4 Expeimental section

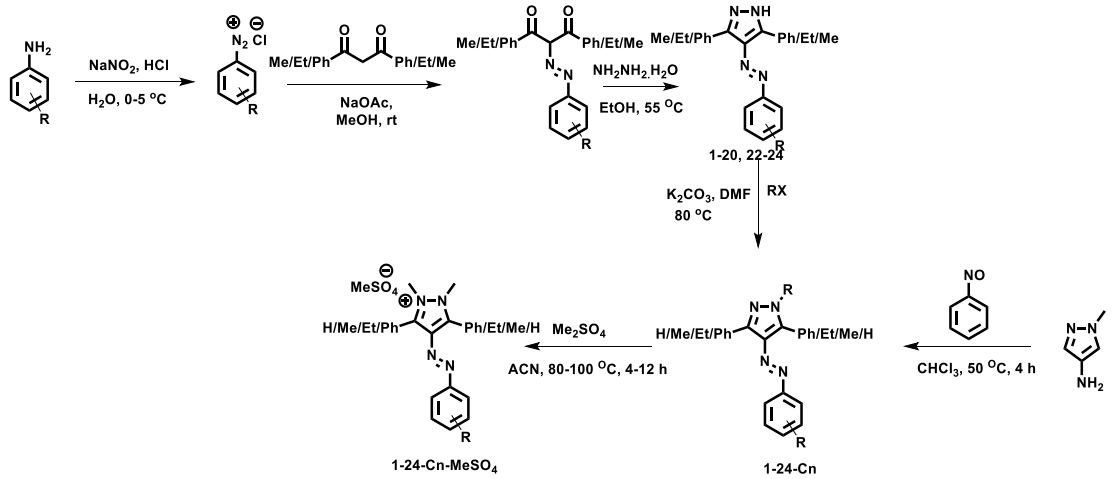

Scheme 3B.3. Synthesis of **c**ompounds **1-24 -Cn**

General procedure for synthesis of compound 1-24-Cn-MeSO$_4$

The solution of the compounds **1-24-Cn** (1 mmol, 1 eq) in dry MeCN has been charged in to an RB flask. Dimethyl sulfate (3 mmol, 3 eq.) was added to the solution and the reaction mixture was then heated at 80-100 ^{o}C for 4-12 hrs. Reaction was monitored with TLC. After completion, the reaction was cooled to room temperature and diethyl ether was added to the reaction mixture and the resulting suspension was kept in refrigerator overnight. Afterwards, the precipitate was filtered and thoroughly washed with excess amount of diethyl ether. The filtered solid was either dried and directly utilized for characterization or passed through a neutral alumina column using MeOH-ethyl acetate (20:80) as eluent, on distillation gave the pure product.

General procedures for ion exchange

The compound **1-C1-MeSO$_4$** (500 mg) was dissolved in 10 ml MeOH in an RB flask. About 500 mg Amberlite® IRA402 chloride form resin was added into the above solution and stirred for overnight.

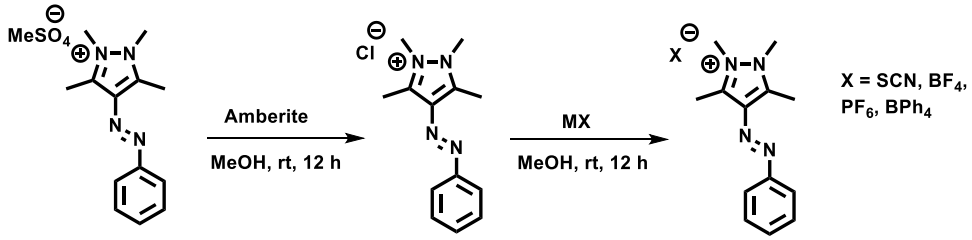

Scheme 3B.4. Synthesis of **c**ompounds **1-24 -Cn-X**

After 12 h the solution was filtered and the solution was evaporated to dryness to give the desired products **1-C1-Cl**. The complete replacement was confirmed by the NMR spectroscopy and HRMS. For exchanging with the other counter ions, the compound **1-C1-Cl** (500 mg) was dissolved in methanol. Ammonium or sodium or potassium salt of corresponding anion has been added in excess (3 to 5 eq.) into the above solution and stirred for 12 h at room temperature. After 12 h this solution was filtered through a filter paper and the solution was evaporated to dryness. The resulting solid compound was dissolved in DCM and kept in refrigerator for overnight. Afterwards, the solid precipitate of excess amount of ammonium or sodium or potassium salt used was filtered at cold condition. The remaining solution of DCM was evaporated to dryness yielding the desired products, which were further characterized.

(*E*)-1,2,3,5-tetramethyl-4-(phenyldiazenyl)-1*H*-pyrazol-2-ium methanesulfonate, 1-C1-MeSO$_4$, yellow solid, mp = 273-275 ^{o}C, yield = 98%.

^{1}H NMR (400 MHz, DMSO-d_6) δ 7.90 -7.87 (m, 2H), 7.63-7.58 (m, 3H), 4.06 (s, 6H), 3.36 (s, 3H), 2.77 (s, 6H) ppm; ^{13}C NMR (100 MHz, DMSO-d_6) δ 152.0, 141.2, 132.3, 131.9, 129.6, 122.3, 33.9, 10.6 ppm; HRMS (ESI^+) m/z: calcd. for $C_{13}H_{17}N_4$ $[M]^+$ 229.1448, Found 229.1447; (ESI^-) m/z: calcd. for CH_3O_4S $[M]^-$ 110.9758, Found 110.9751; IR (KBr, cm^{-1}) 780, 1020, 1090, 1230, 1250, 1460, 2850, 2928.

(*E*)-1-ethyl-2,3,5-trimethyl-4-(phenyldiazenyl)-1*H*-pyrazol-2-iummethanesulfonate, 1-C2-MeSO$_4$, yellow solid, mp = 74-76 ^{o}C, yield = 98%.

^{1}H NMR (400 MHz, $CDCl_3$) δ 7.83 -7.82 (m, 2H), 7.52-7.51 (m, 3H), 4.73 (q, *J* = 6.9 Hz, 2H), 4.23 (s, 6H), 3.64 (s, 3H), 3.64 (s, 3H), 2.81-2.80 (s, 6H), 1.51 (t, *J* = 7 Hz, 3H) ppm; ^{13}C NMR (100 MHz, DMSO-d_6) δ 152.1, 142.1, 140.8, 132.5, 131.9, 129.6, 122.3, 42.1, 33.9, 13.7, 10.6, 10.3 ppm; HRMS (ESI^+) m/z: calcd. For $C_{14}H_{19}N_4$ $[M]^+$ 243.1604, Found 243.1604; (ESI^-) m/z: calcd. for CH_3O_4S $[M]^-$ 110.9758, Found 110.9750; IR (KBr, cm^{-1}) 780, 1028, 1090, 1238, 1250, 1460, 2849, 2920.

(*E*)-1-butyl-2,3,5-trimethyl-4-(phenyldiazenyl)-1*H*-pyrazol-2-ium methanesulfonate, 1-C4-MeSO$_4$, yellow solid, mp = 78-80 ^{o}C, yield = 98%.

^{1}H NMR (400 MHz, $CDCl_3$) δ 7.84 -7.82 (m, 2H), 7.53-7.51 (m, 3H), 4.72 (t, *J* = 7.8 Hz, 2H), 4.27 (s, 3H), 3.64 (s, 3H), 2.82 (s, 3H), 2.80 (s, 3H), 1.82-1.79 (pt, *J* = 6.2 Hz, 2H), 1.53-1.45 (m, 2H), 1.02 (t, *J* = 7.3 Hz, 3H) ppm; ^{13}C NMR (100 MHz, $CDCl_3$) δ 152.3, 142.4, 141.2, 133.4, 131.9, 129.3, 122.6, 54.3, 47.5, 34.70, 34.68, 31.2, 19.8, 13.6, 11.1 ppm; HRMS (ESI^+) m/z: calcd. for $C_{16}H_{23}N_4$ $[M]^+$ 271.1917**,** Found 271.1937; (ESI^-) m/z: calcd. for CH_3O_4S $[M]^-$ 110.9758, Found 110.9741; IR (KBr, cm^{-1}) 780, 1010, 1090, 1230, 1220, 1460, 2840, 2915.

(*E*)-1-hexyl-2,3,5-trimethyl-4-(phenyldiazenyl)-1*H*-pyrazol-2-ium methanesulfonate, 1-C6-MeSO$_4$, dark red, sticky liquid, yield = 98%.

^{1}H NMR (400 MHz, $CDCl_3$) δ 7.72 -7.70 (m, 2H), 7.41-7.40 (m, 3H), 4.85 (t, *J* = 8.0 Hz, 2H), 4.37 (s, 3H), 2.82 (s, 3H), 2.80 (s, 3H), 1.82-1.79 (m, 2H), 1.53-1.45 (m, 2H), 1.02 (t, *J* = 7.3 Hz, 3H) ppm; ^{13}C NMR (100 MHz, $CDCl_3$) δ 152.4, 142.9, 141.2, 133.0, 131.4, 129.2, 122.5, 47.3, 34.42, 34.39, 31.2, 29.0, 25.8, 22.4, 14.0, 11.1, 10.9 ppm; HRMS (ESI^+) m/z: calcd. for $C_{18}H_{27}N_4$ $[M]^+$ 299.2236, Found 299.2232; (ESI^-) m/z: calcd. for CH_3O_4S $[M]^-$ 110.9758, Found 110.9751; IR (KBr, cm^{-1}) 780, 1020, 1090, 1210, 1250, 1460, 2830, 2915.

(*E*)-2,3,5-trimethyl-1-octyl-4-(phenyldiazenyl)-1*H*-pyrazol-2-ium methanesulfonate, 1-C8-MeSO$_4$, red-brown, solid, mp = 143-145 ^{o}C, yield = 97%.

^{1}H NMR (400 MHz, $CDCl_3$) δ 7.84 -7.81 (m, 2H), 7.52-7.50 (m, 3H), 4.62 (t, *J* = 7.6 Hz, 2H), 4.20 (s, 3H), 3.63 (s, 3H), 2.81 (s, 3H), 2.81 (s, 3H), 2.79 (s, 3H), 1.82-1.78 (m, 2H), 1.41-1.26 (m, 10H), 0.87 (t, *J* = 6.4 Hz, 3H) ppm; ^{13}C NMR (100 MHz, $CDCl_3$) δ 152.5, 142.6, 141.3, 133.3, 131.8, 129.3, 122.6, 54.5, 47.5, 34.5, 31.8, 29.25, 29.16, 29.12, 26.5, 22.6, 14.1, 11.2, 11.1 ppm; HRMS (ESI^+) m/z: calcd. for $C_{20}H_{31}N_4$ $[M]^+$ 327.2543, Found 327.2549; (ESI^-) m/z: calcd. for CH_3O_4S $[M]^-$ 110.9758, Found 110.9718; IR (KBr, cm^{-1}) 790, 1020, 1090, 1200, 1220, 1430, 2830, 2918.

(*E*)-1-decyl-2,3,5-trimethyl-4-(phenyldiazenyl)-1*H*-pyrazol-2-ium methanesulfonate, 1-C10-MeSO$_4$, yellow solid, mp = 108-110 °C, yield = 97%**.**

^{1}H NMR (400 MHz, $CDCl_3$) δ 7.84 -7.81 (m, 2H), 7.52-7.50 (m, 3H), 4.63 (t, *J* = 7.6 Hz, 2H), 4.20 (s, 3H), 3.64 (s, 3H), 2.81 (s, 3H), 2.79 (s, 3H), 1.80 (pt, *J* = 8.0 Hz, 2H), 1.41-1.25 (m, 14H), 0.87 (t, *J* = 6.5 Hz, 3H) ppm; ^{13}C NMR (100 MHz, $CDCl_3$) δ 152.4, 142.5, 141.2, 133.3, 131.9, 129.3, 122.6, 54.4, 47.5, 34.5, 31.9, 29.51, 29.45, 29.39, 29.30, 29.24, 29.18, 26.5, 22.7, 14.2, 11.2, 11.1 ppm; HRMS (ESI^+) m/z: calcd. For $C_{22}H_{35}N_4$ $[M]^+$ (ESI^-) m/z: calcd. for CH_3O_4S $[M]^-$ 110.9758, Found 110.9796; IR (KBr, cm^{-1}) 789, 1020, 1090, 1215, 1250, 1460, 2850, 2918.

(*E*)-1-dodecyl-2,3,5-trimethyl-4-(phenyldiazenyl)-1*H*-pyrazol-2-ium methanesulfonate, 1-C12-MeSO$_4$, red-brown, solid, mp = 64-66 °C, yield = 98%.

^{1}H NMR (400 MHz, $CDCl_3$) δ 7.84 -7.81 (m, 2H), 7.52-7.50 (m, 3H), 4.64 (t, *J* = 7.7 Hz, 2H), 4.20 (s, 3H), 3.64 (s, 3H), 2.81 (s, 3H), 2.79 (s, 3H), 1.79 (pt, *J* = 8.2 Hz, 2H), 1.42-1.25 (m, 18H), 0.87 (t, *J* = 6.4 Hz, 3H) ppm; ^{13}C NMR (100 MHz, $CDCl_3$) δ 152.3, 142.7, 141.1, 133.1, 131.6, 129.1, 122.4, 54.4, 47.3, 34.4, 31.8, 29.58, 29.56, 29.52, 29.39, 29.29, 29.13, 29.05, 26.3, 22.6, 14.1, 11.0, 10.9 ppm; HRMS (ESI^+) m/z: calcd. for $C_{24}H_{39}N_4$ $[M]^+$ 383.3169, Found 383.3181; (ESI^-) m/z: calcd. for CH_3O_4S $[M]^-$ 110.9758, Found 110.9749; IR (KBr, cm^{-1}) 780, 1020, 1090, 1230, 1250, 1460, 2839, 2908.

(*E*)-2,3,5-trimethyl-1-octadecyl-4-(phenyldiazenyl)-1*H*-pyrazol-2-ium methanesulfonate, 1-C18-MeSO$_4$, yellow solid, mp = 135-137 °C, yield = 95%**.**

^{1}H NMR (400 MHz, $CDCl_3$) δ 7.84 -7.81 (m, 2H), 7.53-7.50 (m, 3H), 4.64 (t, *J* = 7.7 Hz, 2H), 4.20 (s, 3H), 3.64 (s, 3H), 2.82 (s, 3H), 2.80 (s, 3H), 1.80 (pt, *J* = 6.6 Hz, 2H), 1.42-1.24 (m, 30H), 0.87 (t, *J* = 6.4 Hz, 3H) ppm; ^{13}C NMR (100 MHz, $CDCl_3$) δ 152.5, 142.4, 141.2, 133.4, 131.9, 129.3, 122.6, 54.4, 47.6, 34.6, 32.0, 29.77, 29.73, 29.67, 29.58, 29.48, 29.43, 29.28, 29.20, 26.5, 22.8, 14.2, 11.20, 11.18, 11.14 ppm; HRMS (ESI^+) m/z: calcd.

for $C_{30}H_{51}N_4$ $[M]^+$ 467.4108, Found 467.4108; (ESI^-) m/z: calcd. for CH_3O_4S $[M]^-$ 110.9758, Found 110.9749; IR (KBr, cm^{-1}) 780, 1020, 1090, 1210, 1250, 1460, 2860, 2928.

(*E*)-1,2,3,5-tetramethyl-4-(phenyldiazenyl)-1*H*-pyrazol-2-ium thiocyanate chloride, 1-C1-Cl, light yellow solid, mp = 225-227 °C, yield = 99%.

^1H NMR (400 MHz, DMSO-d_6) δ 7.91 -7.88 (m, 2H), 7.64-7.58 (m, 3H), 4.05 (s, 6H), 2.77 (s, 6H) ppm; ^{13}C NMR (100 MHz, DMSO-d_6) δ 152.0, 141.2, 132.3, 131.9, 129.6, 122.3, 33.9, 10.5 ppm; HRMS (ESI^+) m/z: calcd. for $C_{13}H_{17}N_4$ $[M]^+$ 229.1448, Found 229.1464; (ESI^-) m/z: calcd. for Cl $[M]^-$ 34.9689, Found 34.9708; IR (KBr, cm^{-1}) 780, 1035, 1090, 1230, 1250, 1460, 2850, 2928.

(*E*)-1,2,3,5-tetramethyl-4-(phenyldiazenyl)-1*H*-pyrazol-2-ium tetrafluoroborate, 1-C1-BF_4, light yellow solid, mp = 240-242 °C, yield = 99%.

^1H NMR (400 MHz, DMSO-d_6): δ 7.91 -7.89 (m, 2H), 7.64-7.58 (m, 3H), 4.04 (s, 6H), 2.76 (s, 6H) ppm; ^{13}C NMR (100 MHz, DMSO-d_6) δ 152.1, 141.3, 132.3, 131.9, 129.6, 122.3, 33.8, 10.6 ppm; ^{19}F NMR (376.5 MHz, DMSO-d_6) δ -148.3 ppm; ^{11}B NMR (128.3 MHz, DMSO-d_6) δ -1.30 ppm. HRMS (ESI^+) m/z: calcd. for $C_{13}H_{17}N_4$ $[M]^+$ 229.1448, Found 229.1455; (ESI^-) m/z: calcd. for BF_4 $[M]^-$ 87.0029, Found 87.0009; IR (KBr, cm^{-1}) 780, 835, 1020, 1090, 1230, 1250, 1460, 2850, 2928.

(*E*)-1,2,3,5-tetramethyl-4-(phenyldiazenyl)-1*H*-pyrazol-2-ium hexafluorophosphate, 1-C1-PF_6, light yellow solid, mp = 210-212 °C, yield = 99%.

^1H NMR (400 MHz, CD_3CN) δ 7.92 -7.90 (m, 2H), 7.59-7.57 (m, 3H), 3.92 (s, 6H), 2.73 (s, 6H) ppm; ^{13}C NMR (100 MHz, CD_3CN) δ 153.5, 142.9, 134.1, 132.9, 130.4, 123.4, 34.7, 11.2 ppm; ^{19}F NMR (376.5 MHz, CD_3CN) δ -73.0 (d, *J* = 707.8 Hz) ppm; ^{31}P NMR (162.1 MHz, CD_3CN) δ -144.65 (sept, *J* = 706.7 Hz) ppm. HRMS (ESI^+) m/z: calcd. for $C_{13}H_{17}N_4$ $[M]^+$ 229.1448, Found 229.1447; (ESI^-) m/z: calcd. for PF_6 $[M]^-$ 144.9642, Found 144.9621; IR (KB r, cm^{-1}) 780, 1030, 1090, 1230, 1250, 1460, 2054, 2850, 2928.

(*E*)-1,2,3,5-tetramethyl-4-(phenyldiazenyl)-1*H*-pyrazol-2-ium thiocyanate, 1-C1-SCN, light yellow solid, mp = 255-257 °C, yield = 99%.

^1H NMR (400 MHz, DMSO-d_6) δ 7.91 -7.88 (m, 2H), 7.63-7.58 (m, 3H), 7.18-7.17 (m, 8H), ,6.91 (t, *J* = 7.3 Hz, 8H), 6.88-6.77 (m, 4H), 4.02 (s, 6H), 2.76 (s, 6H) ppm; ^{13}C NMR (100 MHz, DMSO-d_6) δ 152.0, 141.2, 132.3, 131.8, 129.71, 129.54, 122.3, 33.9, 10.6 ppm; HRMS (ESI^+) m/z: calcd. for $C_{13}H_{17}N_4$ $[M]^+$ 229.1448, Found 229.1447; (ESI^-) m/z: calcd. for SCN $[M]^-$ 57.9751, Found 57.9751; IR (KBr, cm^{-1}) 780, 1020, 1090, 1230, 1250, 1460, 2054, 2850, 2928.

(*E*)-1,2,3,5-tetramethyl-4-(phenyldiazenyl)-1*H*-pyrazol-2-ium tetraphenyl-l4-borane, 1-C1-BPh$_4$, Light yellow solid, mp = 260-262 ^{o}C, yield = 99%.

^{1}H NMR (400 MHz, DMSO-d$_6$) δ 7.90 -7.88 (m, 2H), 7.62-7.58 (m, 3H), 4.05 (s, 6H), 2.76 (s, 6H) ppm; ^{13}C NMR (100 MHz, DMSO-d$_6$) δ 163.4 (q, *J* = 50 Hz), 152.0, 141.2, 135.5, 132.3, 131.9, 129.5, 125.3, 122.3, 121.5, 33.7, 10.5 ppm; ^{11}B NMR (128.3 MHz, DMSO-d$_6$) δ 92.67 ppm. HRMS (ESI$^+$) m/z: calcd. for $C_{13}H_{17}N_4$ $[M]^+$ 229.1448, Found 229.1463; (ESI$^-$) m/z: calcd. for $C_{24}H_{20}B$ $[M]^-$ 319.1658, Found 319.1689; IR (KBr, cm^{-1}) 780, 1013, 1090, 1230, 1259, 1461, 2850, 2918, 3055.

(*E*)-1-decyl-4-((2,6-difluorophenyl)diazenyl)-2,3,5-trimethyl-1*H*-pyrazol-2-ium methanesulfonate, 2-C10- MeSO$_4$ yellow solid, mp = 133-135 ^{o}C, yield = 96%.

^{1}H NMR (400 MHz, $CDCl_3$) δ 7.42 -7.34 (m, 1H), 7.06 (t, *J* = 9.0 Hz, 3H), 4.69 (t, *J* = 7.6 Hz, 2H), 4.26 (s, 3H), 3.62 (s, 3H), 2.80 (s, 3H), 2.77 (s, 3H), 1.81 (pt, *J* = 8.2 , 2H), 1.45-1.25 (m, 14H), 0.87 (t, *J* = 5.9 Hz, 3H) ppm; ^{13}C NMR (100 MHz, $CDCl_3$) δ 156.0 (dd, *J* = 260.0 Hz, *J* = 3.8 Hz), 142.8, 141.4, 134.4, 131.7 (t, *J* = 10.5 Hz) 130.6 (t, *J* = 9.0 Hz), 112.7 (dd, *J* = 20.3 Hz, *J* = 3.4 Hz), 54.2, 47.8, 34.74, 34.72 31.8, 29.46, 29.40, 29.25, 29.19, 29.12, 26.5, 22.7, 14.1, 11.10, 11.07 ppm; ^{19}F NMR (376.5 MHz, $CDCl_3$) δ -120.2 HRMS (ESI$^+$) m/z: calcd. for $C_{22}H_{33}F_2N_4$ $[M]^+$ 391.2673, Found 391.2675; (ESI$^-$) m/z: calcd. for CH_3O_4S $[M]^-$ 110.9758, Found 110.9781; IR (KBr, cm^{-1}) 782, 1015, 1090, 1230, 1250, 1460, 2850, 2928.

(*E*)-1-decyl-4-((2-fluorophenyl)diazenyl)-2,3,5-trimethyl-1*H*-pyrazol-2-ium methanesulfonate, 3-C10-MeSO$_4$, yellow solid, mp = 128-130 ^{o}C, yield = 96%.

^{1}H NMR (400 MHz, $CDCl_3$) δ 7.68 (dt, *J* = 7.3 Hz, 1.4 Hz, 3H), 7.53-7.46 (m, 1H), 7.30-7.21 (o, 2H), 4.70 (t, *J* = 7.7 Hz, 2H), 4.27 (s, 3H), 3.63 (s, 3H), 2.83 (s, 3H), 2.80 (s, 3H), 1.81-1.78 (o, 2H), 1.44-1.25 (m, 14H), 0.87 (t, *J* = 6.5 Hz, 3H) ppm; ^{13}C NMR (100 MHz, $CDCl_3$) δ 160.1 (d, *J* = 257.7 Hz), 142.9, 141.2, 140.2 (d, *J* = 6.6 Hz), 133.8, 133.5 (d, *J* = 8.3 Hz), 124.4 (d, *J* = 3.5 Hz), 117.2 (d, *J* = 19.8 Hz), 116.7, 54.1, 47.6, 34.64, 34.61, 31.7, 29.38, 29.33, 29.17, 29.07, 29.03, 26.4, 22.6, 14.0, 11.1, 11.0 ppm; ^{19}F NMR (376.5 MHz, $CDCl_3$) δ -123.7 ppm; HRMS (ESI$^+$) m/z: calcd. for $C_{22}H_{34}FN_4$ $[M]^+$ 373.2762, Found 373.2763; (ESI$^-$) m/z: calcd. for CH_3O_4S $[M]^-$ 110.9758, Found 110.9751; IR (KBr, cm^{-1}) 780, 1020, 1090, 1230, 1250, 1593, 2859, 2927.

(*E*)-1-decyl-4-((3-fluorophenyl)diazenyl)-2,3,5-trimethyl-1*H*-pyrazol-2-ium methanesulfonate, 4-C10- MeSO$_4$, redish brown solid, mp = 102-104 ^{o}C, yield = 96%.

^{1}H NMR (400 MHz, $CDCl_3$) δ 7.68 -7.66 (m, 1H), 7.53-7.48 (m, 2H), 7.22 (dt, *J* = 8.2 Hz, *J* = 2.2 Hz, 1H), 4.64 (t, *J* = 7.6 Hz, 2H), 3.64 (s, 3H), 3.34 (s, 3H), 2.82 (s, 3H), 2.80 (s, 3H), 1.81 (pt, *J* = 7.1 Hz, 2H), 1.44-1.29 (m, 14H), 0.87 (t, *J* = 6.5 Hz, 3H) ppm; ^{13}C NMR (100 MHz, $CDCl_3$) δ 163.3 (d, *J* = 246.5 Hz), 154.0 (d, *J* = 6.8 Hz), 143.0, 141.8, 133.1, 130.5 (d, *J* = 8.6 Hz), 120.4 (d, *J* = 2.7 Hz), 118.3 (d, *J* = 21.7 Hz), 107.6 (d, *J* = 22.8 Hz), 47.6, 34.67, 34.64, 31.9, 29.57, 29.47, 29.34, 29.26, 29.23, 26.4, 22.7, 14.2, 11.25, 11.18 ppm; ^{19}F NMR (376.5 MHz, $CDCl_3$) δ -123.7; HRMS (ESI^+) m/z: calcd. for $C_{22}H_{34}FN_4$ $[M]^+$ 373.2762, Found 373.2766; (ESI^-) m/z: calcd. for CH_3O_4S $[M]^-$ 110.9758, Found 110.9774; IR (KBr, cm^{-1}) 780, 1005, 1080, 1230, 1250, 1460, 2850, 2926.

(*E*)-1-decyl-4-((4-fluorophenyl)diazenyl)-2,3,5-trimethyl-1*H*-pyrazol-2-ium methanesulfonate, 5-C10- MeSO$_4$, dark red sticky liquid, yield = 96%.

^{1}H NMR (400 MHz, $CDCl_3$) δ 7.86 -7.83 (m, 2H), 7.22-7.17 (m, 2H), 4.64 (t, *J* = 7.6 Hz, 2H), 4.23 (s, 3H), 3.62 (s, 3H), 2.81 (s, 3H), 2.78 (s, 3H), 1.80 (pt, *J* = 7.5 Hz, 2H), 1.41-1.25 (m, 14H), 0.87 (t, *J* = 6.6 Hz, 3H) ppm; ^{13}C NMR (100 MHz, $CDCl_3$) δ 163.4 (d, *J* = 252.0 Hz), 148.9 (d, *J* = 3.0 Hz), 142.4, 141.0, 133.1, 124.6 (d, *J* = 9.0 Hz), 116.2 (d, *J* = 22.9 Hz), 54.1, 47.5, 34.46, 34.42, 31.8, 29.39, 29.34, 29.18, 29.08, 29.04, 26.4, 22.6, 14.1, 11.07, 11.00 ppm; ^{19}F NMR (376.5 MHz, $CDCl_3$) δ -107.6; HRMS (ESI^+) m/z: calcd. for $C_{22}H_{34}FN_4$ $[M]^+$ 373.2762, Found 373.2772; (ESI^-) m/z: calcd. for CH_3O_4S $[M]^-$ 110.9758, Found 110.9751; IR (KBr, cm^{-1}) 780, 1020, 1090, 1230, 1250, 1460, 2850, 2930.

(*E*)-1-decyl-2,3,5-trimethyl-4-(o-tolyldiazenyl)-1*H*-pyrazol-2-ium methanesulfonate, 6-C10- MeSO$_4$, red-brown, solid, mp = 88-90 ^{o}C, yield = 98%.

^{1}H NMR (400 MHz, $CDCl_3$) δ 7.58 (d, *J* = 8.1 Hz, 1H), 7.40-7.33 (m, 2H), 7.27-7.23 (o, 1H), 4.61 (t, *J* = 7.5 Hz, 2H), 4.21 (s, 3H), 3.59 (s, 3H), 2.80 (s, 3H), 2.77 (s, 3H), 2.62 (s, 3H), 1.80 (pt, *J* = 7.3 Hz, 2H), 1.42-1.31 (m, 14H), 0.85 (t, *J* = 6.6 Hz, 3H) ppm; ^{13}C NMR (100 MHz, $CDCl_3$) δ 150.7, 142.2, 141.0, 138.5, 134.0, 132.1, 131.6, 126.7, 114.8, 54.4, 47.6, 34.56, 34.53, 31.9, 29.51, 29.45, 29.32, 29.30, 29.18, 26.5, 22.7, 18.03, 18.01, 14.2, 11.25, 11.20 ppm; HRMS (ESI^+) m/z: calcd. for $C_{23}H_{37}N_4$ $[M]^+$ 369.3013, Found 369.3015; (ESI^-) m/z: calcd. for CH_3O_4S $[M]^-$; IR (KBr, cm^{-1}) 787, 1020, 1061, 1230, 1250, 1460, 2854, 2925.

(*E*)-1-decyl-2,3,5-trimethyl-4-(m-tolyldiazenyl)-1*H*-pyrazol-2-ium methanesulfonate, 7-C10-MeSO$_4$,yellow solid, mp = 83-85 ^{o}C, yield = 96%.

^{1}H NMR (400 MHz, $CDCl_3$) δ 7.62-7.61 (br, 2H), 7.39 (t, *J* = 7.7 Hz, 1H), 7.32-7.30 (m, 1H), 4.61 (t, *J* = 7.6 Hz, 2H), 4.20 (s, 3H), 3.60 (s, 3H), 2.81 (s, 3H), 2.78 (s, 3H), 2.44 (s,

3H), 1.80 (pt, *J* = 7.6 Hz, 2H), 1.42-1.34 (m, 14H), 0.86 (t, *J* = 6.5 Hz, 3H) ppm; ^{13}C NMR (100 MHz, $CDCl_3$) δ 152.1, 142.1, 140.6, 138.8, 132.8, 132.2, 128.7, 122.6, 119.4, 53.7, 47.0, 34.0, 33.97, 31.4, 29.07, 29.04, 28.85, 28.69, 28.65, 26.1, 22.2, 21.0, 13.7, 10.70, 10.60 ppm; HRMS (ESI^+) m/z: calcd. for $C_{23}H_{37}N_4$ $[M]^+$ 369.3013, Found 369.3013; (ESI^-) m/z: calcd. for CH_3O_4S $[M]^-$ 110.9758, Found 110.9751; IR (KBr, cm^{-1}) 780, 1020, 1090, 1230, 1250, 1460, 2852, 2923.

(*E*)-1-decyl-2,3,5-trimethyl-4-(p-tolyldiazenyl)-1*H*-pyrazol-2-ium methanesulfonate, 8-C10- $MeSO_4$, yellow solid, mp = 93-95 °C, yield = 96%.

^{1}H NMR (400 MHz, $CDCl_3$) δ 7.73 (d, *J* = 8.2 Hz, 2H), 7.31 (d, *J* = 8.2 Hz, 2H), 4.65 (t, *J* = 7.6 Hz, 2H), 4.22 (s, 3H), 3.63 (s, 3H), 2.80 (s, 3H), 2.78 (s, 3H), 2.44 (s, 3H), 1.80 (pt, *J* = 7.2 Hz, 2H), 1.45-1.20 (m, 14H), 0.87 (t, *J* = 7.0 Hz, 3H) ppm; ^{13}C NMR (100 MHz, $CDCl_3$) δ 150.4, 142.5, 142.1, 140.7, 133.1, 129.8 122.4, 54.0, 47.3, 34.29, 34.24, 31.7, 29.30, 29.26, 29.08, 28.95, 28.93, 26.3, 22.5, 21.43, 21.40, 14.0, 10.93, 10.83 ppm; HRMS (ESI^+) m/z: calcd. for $C_{23}H_{37}N_4$ $[M]^+$ 369.3013, Found 369.3015; calcd. CH_3O_4S 110.9758, Found 110.9751; (ESI^-) m/z: calcd. for CH_3O_4S $[M]^-$ 110.9758, Found 110.9751; IR (KBr, cm^{-1}) 780, 1020, 1072, 1236, 1250, 1460, 2850, 2928.

(*E*)-1-decyl-4-((2-methoxyphenyl)diazenyl)-2,3,5-trimethyl-1*H*-pyrazol-2-ium methanesulfonate, 9-C10- $MeSO_4$, yellow solid, mp = 140-142 °C, yield = 96%.

^{1}H NMR (400 MHz, $CDCl_3$) δ 7.60 (dd, *J* = 8.0 Hz, , *J* = 1.4 Hz, 1H), 7.51-7.47 (m, 1H), 7.10 (d, *J* = 8.2 Hz, 1H), 7.01 (t, *J* = 7.8 Hz, 1H), 4.70 (t, *J* = 7.7 Hz, 2H), 4.26 (s, 3H), 3.99 (s, 3H), 3.65 (s, 3H), 2.81 (s, 3H), 2.79 (s, 3H), 1.83-1.76 (o, 2H), 1.40-1.21 (m, 14H), 0.87 (t, *J* = 6.6 Hz, 3H) ppm; ^{13}C NMR (100 MHz, $CDCl_3$) δ 157.4, 142.2, 141.7, 140.8, 134.2, 133.7, 120.7, 115.8, 112.8, 56.2, 54.2, 47.6, 34.59, 31.8, 29.44, 29.38, 29.23, 29.20, 29.11, 26.4, 22.6, 14.1, 11.1, 11.0 ppm; HRMS (ESI^+) m/z: calcd. for $C_{23}H_{37}N_4O$ $[M]^+$ 385.2962, Found 385.2967; (ESI^-) m/z: calcd. for CH_3O_4S $[M]^-$ 110.9758, Found 110.9751; IR (KBr, cm^{-1}) 780, 1020, 1090, 1230, 1240, 1460, 2850, 2932.

(*E*)-1-decyl-4-((3-methoxyphenyl)diazenyl)-2,3,5-trimethyl-1*H*-pyrazol-2-ium methanesulfonate, 10-C10- $MeSO_4$, yellow solid, mp = 80-82 °C, yield = 96%.

^{1}H NMR (400 MHz, $CDCl_3$) δ 7.46-7.39 (m, 2H), 7.31 (m, 1H), 7.01--7.04 (m, 1H), 4.61 (t, *J* = 7.4 Hz, 2H), 4.21 (s, 3H), 3.87 (s, 3H), 3.60 (s, 3H), 2.81 (s, 3H), 2.78 (s, 3H), 1.80 (pt, *J* = 7.6 Hz, 2H), 1.40-1.24 (m, 14H), 0.86 (t, *J* = 6.3 Hz, 3H) ppm; ^{13}C NMR (100 MHz, $CDCl_3$) δ 160.1, 153.3, 142.3, 140.8, 132.9, 129.7, 117.8, 116.4, 105.6, 55.3, 53.9, 47.2, 34.2, 31.6, 29.20, 29.16, 28.98, 28.83, 26.2, 22.4, 13.9, 10.86, 10.79 ppm; HRMS (ESI^+)

m/z: calcd. for $C_{23}H_{37}N_4O$ $[M]^+$ 385.2962, Found 385.2961; (ESI^-) m/z: calcd. for CH_3O_4S $[M]^-$ 110.9758, Found 110.9751; IR (KBr, cm^{-1}) 780, 1020, 1090, 1230, 1250, 1460, 2850, 2928.

(*E*)-1-decyl-4-((4-methoxyphenyl)diazenyl)-2,3,5-trimethyl-1*H*-pyrazol-2-ium methanesulfonate, 11-C10- $MeSO_4$, yellow solid, mp = 106-108 °C, yield = 96%.

^1H NMR (400 MHz, $CDCl_3$) δ 7.82 (d, *J* = 8.8 Hz, 2H), 7.00 (d, *J* = 8.9 Hz, 2H), 4.67 (t, *J* = 7.3 Hz, 2H), 4.24 (s, 3H), 3.90 (s, 3H), 3.64 (s, 3H), 2.79 (s, 3H), 2.77 (s, 3H), 1.80 (pt, *J* = 6.9 Hz, 2H), 1.41-1.25 (m, 14H), 0.87 (t, *J* = 6.5 Hz, 3H) ppm; ^{13}C NMR (100 MHz, $CDCl_3$) δ 162.7, 146.7, 141.8, 140.5, 133.2, 124.4, 114.3, 55.6, 54.0, 47.4, 34.4, 31.7, 29.32, 29.28, 29.11, 29.07, 28.98, 26.3, 22.5, 14.00, 10.93, 10.90 ppm; HRMS (ESI^+) m/z: calcd. for $C_{23}H_{37}N_4O$ $[M]^+$ 385.2962, Found 385.2961; (ESI^-) m/z: calcd. for CH_3O_4S $[M]^-$ 110.9758, Found 110.9751; IR (KBr, cm^{-1}) 780, 1020, 1064, 1216, 1253, 1323, 2855, 2926.

(*E*)-4-((2-cyanophenyl)diazenyl)-1-decyl-2,3,5-trimethyl-1*H*-pyrazol-2-ium methanesulfonate, 12-C10- $MeSO_4$, yellow solid, mp = 86-88 °C, yield = 96%.

^1H NMR (400 MHz, $CDCl_3$) δ 8.07 -8.04 (m, 2H), 7.77-7.75 (m, 1H), 7.66-7.26 (m, 1H), 4.61 (t, *J* = 7.2 Hz, 2H), 4.21 (s, 3H), 3.58 (s, 3H), 2.83 (s, 3H), 2.80 (s, 3H), 1.80 (pt, *J* = 7.1 Hz, 2H), 1.40-1.34 (m, 14H), 0.86 (t, *J* = 6.4 Hz, 3H) ppm; ^{13}C NMR (100 MHz, $CDCl_3$) δ 152.1, 143.0, 141.5, 134.3, 132.9, 130.1, 126.9, 125.5 117.8, 113.2, 54.0, 47.5, 34.4, 31.6, 29.26, 29.22, 29.04, 28.88, 28.86, 26.3, 22.4, 13.9, 11.06, 11.03 ppm; HRMS (ESI^+) m/z: calcd. for $C_{23}H_{34}N_5$ $[M]^+$ 380.2809, Found 380.2810; (ESI^-) m/z: calcd. for CH_3O_4S $[M]^-$ 110.9758, Found 110.9751; IR (KBr, cm^{-1}) 788, 1017, 1061, 1222, 1252, 1465, 1533, 2232, 2854, 2925.

(*E*)-4-((3-cyanophenyl)diazenyl)-1-decyl-2,3,5-trimethyl-1*H*-pyrazol-2-ium methanesulfonate, 13-C10- $MeSO_4$, yellow solid, mp = 158-160 °C, yield = 96%.

^1H NMR (400 MHz, $CDCl_3$) δ 7.80 -7.78 (m, 2H), 7.69 (t, *J* = 7.4 Hz, 1H), 7.58-7.55 (m, 1H), 4.55 (br, 2H), 4.18 (s, 3H), 3.52 (s, 3H), 2.84 (s, 3H), 2.80 (s, 3H), 1.79 (bs, 2H), 1.35-1.14 (m, 14H), 0.81 (br, 3H) ppm; ^{13}C NMR (100 MHz, $CDCl_3$) δ 153.2, 143.9, 141.8, 133.6, 133.5, 133.4 131.8, 116.8, 116.5, 112.6, 54.1, 47.6, 34.5, 31.7, 29.46, 29.33, 29.29, 29.12, 28.97, 26.4, 22.5, 14.0, 11.45, 11.17 ppm; HRMS (ESI^+) m/z: calcd. for $C_{23}H_{34}N_5$ $[M]^+$ 380.2809, Found 380.2809; (ESI^-) m/z: calcd. for CH_3O_4S $[M]^-$ 110.9758, Found 110.9751; IR (KBr, cm^{-1}) 788, 1017, 1061, 1222, 1252, 1465, 1533, 2232, 2854, 2925.

(*E*)-4-((4-cyanophenyl)diazenyl)-1-decyl-2,3,5-trimethyl-1*H*-pyrazol-2-ium methanesulfonate, 14-C10-$MeSO_4$, yellow-orange solid, mp = 108- 110 °C, yield = 96%.

^{1}H NMR (400 MHz, $CDCl_3$): δ 7.91 (d, *J* = 8.3 Hz, 2H), 7.77 (d, *J* = 8.4 Hz, 2H), 4.62 (t, *J* = 7.6 Hz, 2H), 4.22 (s, 3H), 3.60 (s, 3H), 2.84 (s, 3H), 2.81 (s, 3H), 1.81 (pt, *J* = 7.4 Hz, 2H), 1.45-1.28 (m, 14H), 0.86 (t, *J* = 6.6 Hz, 3H) ppm; ^{13}C NMR (100 MHz, $CDCl_3$): δ 154.1, 143.2, 141.6, 133.21, 133.17, 122.9, 118.1, 114.3, 54.0, 47.5, 34.5, 34.4, 31.6, 29.3, 29.2, 29.1, 29.0, 28.9, 26.3, 22.5, 14.0, 11.0 ppm; HRMS (ESI^+) m/z: calcd. for $C_{23}H_{34}N_5$ $[M]^+$380.2809, Found 380.2809; (ESI^-) m/z: calcd. for CH_3O_4S $[M]^-$ 110.9758, Found 110.9751; IR (KBr, cm^{-1}) 788, 1017, 1061, 1222, 1252, 1465, 1533, 2232, 2854, 2925.

(*E*)-1-decyl-2,3,5-trimethyl-4-((2-(trifluoromethyl)phenyl)diazenyl)-1*H*-pyrazol-2-ium methanesulfonate, 15-C10- $MeSO_4$, yellow solid, mp = 144-146 °C, yield = 96%. ^{1}H NMR (400 MHz, $CDCl_3$) δ 7.90 (d, *J* = 7.7 Hz, 2H), 7.78-76 (m, 2H), 7.67 (t, *J* = 7.3 Hz, 2H), 7.62-7.58 (m, 2H), 4.64 (t, *J* = 7.8 Hz, 2H), 4.22 (s, 3H), 3.62 (s, 3H), 2.83 (s, 3H), 2.80 (s, 3H), 1.81 (pt, *J* = 7.9 Hz, 2H), 1.42-1.36 (m, 14H), 0.87 (t, *J* = 6.4 Hz, 3H) ppm; ^{13}C NMR (100 MHz, $CDCl_3$) δ 148.9, 143.5, 141.6, 133.6, 132.8, 126.1 (q, *J* = 20 Hz), 126.7 (q, *J* = 20 Hz), 125.2, 122.5, 115.6, 54.2, 47.6, 34.4, 31.6, 29.27, 29.23, 29.05, 28.89, 28.86, 26.3, 22.5, 13.9, 11.10, 11.04 ppm; ^{19}F NMR (376.5 MHz, $CDCl_3$) δ -58.0; HRMS (ESI^+) m/z: calcd. for $C_{23}H_{34}F_3N_4$ $[M]^+$ 423.2730, Found 423.2738; (ESI^-) m/z: calcd. for CH_3O_4S $[M]^-$ 110.9758, Found 110.9780; IR (KBr, cm^{-1}) 780, 1020, 1090, 1230, 1250, 1460, 2857, 2929.

(*E*)-1-decyl-2,3,5-trimethyl-4-((3-(trifluoromethyl)phenyl)diazenyl)-1*H*-pyrazol-2-ium methanesulfonate, 16-C10- $MeSO_4$, yellow solid, mp = 83-85 °C, yield = 96%. ^{1}H NMR (400 MHz, $CDCl_3$) δ 8.05 (s, 1H), 8.00 (d, *J* = 8.0 Hz, 1H), 7.76-7.74 (m, 1H), 7.67-7.63 (m, 1H), 4.62 (t, *J* = 7.8 Hz, 2H), 4.22 (s, 3H), 3.59 (s, 3H), 2.84 (s, 3H), 2.81 (s, 3H), 1.81 (pt, *J* = 7.7 Hz, 2H), 1.39-1.24 (m, 14H), 0.86 (t, *J* = 6.6 Hz, 3H) ppm; ^{13}C NMR (100 MHz, $CDCl_3$) δ 151.8, 142.6, 141.0, 132.6, 131.1 (q, *J* = 32.4 Hz), 129.6, 127.3, 125.1, 124.6, 121.8, 118.8, 53.4, 47.1, 34.0, 31.2, 28.89, 28.68, 28.51, 28.41, 25.9, 22.1, 13.5, 10.63, 10.56 ppm; ^{19}F NMR (376.5 MHz, $CDCl_3$) δ -62.8; HRMS (ESI^+) m/z: calcd. for $C_{23}H_{34}F_3N_4$ $[M]^+$ 423.2730, Found 423.2733; (ESI^-) m/z: calcd. for CH_3O_4S $[M]^-$ 110.9758, Found 110.9751; IR (KBr, cm^{-1}) 780, 1020, 1090, 1230, 1293, 1460, 2850, 2928.

(*E*)-1-decyl-2,3,5-trimethyl-4-((4-(trifluoromethyl)phenyl)diazenyl)-1*H*-pyrazol-2-ium methanesulfonate, 17-C10- $MeSO_4$, yellow solid, mp = 98-100 °C, Yield = 96%. ^{1}H NMR (400 MHz, $CDCl_3$) δ 7.90 (d, *J* = 8.5 Hz, 2H), 7.81 (d, *J* = 8.4 Hz, 2H), 4.62 (t, , *J* = 7.4 Hz, 2H), 4.22 (s, 3H), 3.59 (s, 3H), 2.84 (s, 3H), 2.81 (s, 3H), 1.81 (pt, *J* = 7.2 Hz, 2H), 1.41-1.19 (m, 14H), 0.86 (t, *J* = 6.4 Hz, 3H) ppm; ^{13}C NMR (100 MHz, $CDCl_3$) δ

153.2, 143.2, 141.6, 133.21, 133.17, 122.9 118.1, 114.3, 54.0, 47.5, 34.4, 31.6, 29.27, 29.23, 29.05, 28.89, 28.86, 26.3, 22.5, 13.9, 11.10, 11.04 ppm; ^{19}F NMR (376.5 MHz, $CDCl_3$) δ -62.8; HRMS (ESI^+) m/z: $[M]^+$ calcd. for $C_{23}H_{34}F_3N_4$ 423.2730, Found 423.2733; (ESI^-) m/z: calcd. for CH_3O_4S $[M]^-$ 110.9758, Found 110.9751; IR (KBr, cm^{-1}) 780, 1020, 1090, 1230, 1250, 1460, 2850, 2928.

(*E*)-1-decyl-2,3,5-trimethyl-4-((2-nitrophenyl)diazenyl)-1*H*-pyrazol-2-ium methanesulfonate, 18-C10- $MeSO_4$, yellow solid, mp = 173-175 °C, yield = 96%.

^{1}H NMR (400 MHz, $CDCl_3$) δ 7.94 (d, *J* = 7.8 Hz, 1H), 7.73-7.70 (m, 1H), 7.65-7.61 (m, 2H), 4.63 (t, *J* = 7.5 Hz, 2H), 4.22 (s, 3H), 3.62 (s, 3H), 2.80 (s, 3H), 2.77 (s, 3H), 1.81 (pt, *J* = 8.4 Hz, 2H), 1.44-1.22 (m, 14H), 0.87 (t, *J* = 6.3 Hz, 3H) ppm; ^{13}C NMR (100 MHz, $CDCl_3$) δ 147.5, 144.8, 143.7, 141.9, 133.6, 133.3, 131.6, 1214.1, 117.8, 54.1, 47.7, 34.6, 31.8, 29.39, 29.34, 29.18, 29.02, 26.4, 22.6, 14.1, 11.19, 11.04 ppm; HRMS (ESI^+) m/z: calcd. for $C_{22}H_{34}N_5O_2$ $[M]^+$ 400.2707, Found 400.2714; (ESI^-) m/z: calcd. for CH_3O_4S $[M]^-$ 110.9758, Found 110.9751; IR (KBr, cm^{-1}) 796, 1019, 1061, 1225, 1252, 1376, 1535, 2854, 2924.

(*E*)-1-decyl-2,3,5-trimethyl-4-((3-nitrophenyl)diazenyl)-1*H*-pyrazol-2-ium methanesulfonate, 19-C10- $MeSO_4$, yellow solid, mp = 63-65 °C, yield = 96%.

^{1}H NMR (400 MHz, $CDCl_3$) δ 8.61 (m, 1H), 8.17 (d, *J* = 7.9 Hz, 1H), 7.72 (t, *J* = 8.0 Hz, 1H), 4.60 (t, *J* = 7.3 Hz, 2H), 4.21 (s, 3H), 3.61 (s, 3H), 2.85 (s, 3H), 2.82 (s, 3H), 1.81 (pt, *J* = 8.4 Hz, 2H), 1.42-1.24 (m, 14H), 0.86 (t, *J* = 6.5 Hz, 3H), ppm; ^{13}C NMR (100 MHz, $CDCl_3$) δ 152.8, 148.8, 142.2, 133.1, 130.5, 128.8, 125.3, 116.8, 47.6, 34.6, 31.9, 29.57, 29.47, 29.33, 29.26, 29.16, 26.4, 22.7, 14.2, 11.38, 11.25 ppm; HRMS (ESI-TOF) m/z: calcd. for $C_{22}H_{34}N_5O_2$ $[M]^+$ 400.2707, Found 400.2708; (ESI^-) m/z: calcd. for CH_3O_4S $[M]^-$ 110.9758, Found 110.9751; IR (KBr, cm^{-1}) 790, 1019, 1061, 1225, 1252, 1372, 1534, 2856, 2923.

(*E*)-1-decyl-2,3,5-trimethyl-4-((4-nitrophenyl)diazenyl)-1*H*-pyrazol-2-ium methanesulfonate, 20-C10- $MeSO_4$, yellow solid, mp = 152-154 °C, yield = 96%.

^{1}H NMR (400 MHz, $CDCl_3$) δ 8.39-8.34 (m, 2H), 7.96-7.92 (m, 2H), 4.65-4.61 (m, 2H), 4.22 (s, 3H), 3.62-3.57 (s, 3H), 2.85-2.82 (s, 3H), 2.82 (s, 3H), 1.82 (pt, *J* = 8.4 Hz, 2H), 1.42-1.25 (m, 14H), 0.88-0.85 (m, 3H) ppm; ^{13}C NMR (100 MHz, $CDCl_3$) δ 155.5, 149.0, 143.5, 142.0, 133.5, 124.9, 123.0, 54.2, 47.8, 34.7, 31.8, 29.46, 29.42, 29.25, 29.11, 26.5, 22.7, 14.1, 11.36, 11.32 ppm; HRMS (ESI^+) m/z: calcd $C_{22}H_{34}N_5O_2$ $[M]^+$ 400.2707, Found

400.2704; (ESI^-) m/z: calcd. for CH_3O_4S $[M]^-$ 110.9758, Found 110.9751; IR (KBr, cm^{-1}) 796, 1019, 1061, 1225, 1252, 1378, 1535, 2854, 2922.

(*E*)-1,2-dimethyl-4-(phenyldiazenyl)-1*H*-pyrazol-2-ium methanesulfonate, 21-C10-MeSO$_4$, reddish brown solid, mp = 234-236 °C, yield = 97%.

^1H NMR (400 MHz, DMSO-d_6) δ 9.21 (s, 2H), 7.87-7.84 (s, 2H), 7.64-7.61 (s, 3H), 4.19 (s, 6H); ^{13}C NMR (100 MHz, DMSO-d_6) δ 151.6, 137.8, 132.5, 131.5, 13 129.8, 122.6, 37.3 ppm; HRMS (ESI^+) m/z: calcd. for $C_{11}H_{13}N_4$ $[M]^+$ 201.1140, Found 201.1140, (ESI^-) m/z: calcd. for CH_3O_4S $[M]^-$ 110.9758, Found 110.9751; IR (KBr, cm^{-1}) 780, 1020, 1090, 1230, 1250, 1460, 2850, 2928.

(*E*)-3,5-diethyl-1,2-dimethyl-4-(phenyldiazenyl)-1*H*-pyrazol-2-ium methanesulfonate, 22-C1-MeSO$_4$, reddish brown solid, mp = 227-229 °C, yield = 97%.

^1H NMR (400 MHz, DMSO-d_6) δ 7.87 -7.85 (m, 2H), 7.64-7.58 (m, 3H), 4.08 (s, 6H), 3.36 (s, 3H), 3.19 (q, *J* = 8 Hz, 4H), 1.23 (t, *J* = 8 Hz, 6H) ppm; ^{13}C NMR (100 MHz, DMSO-d_6) δ 152.2, 145.4, 131.9, 131.5, 129.6, 122.3, 33.75, 33.71, 17.6, 12.2 ppm; HRMS (ESI^+) m/z: calcd. for $C_{15}H_{21}N_4$ $[M]^+$ 257.1766, Found 257.1764, (ESI^-) m/z: calcd. for CH_3O_4S $[M]^-$ 110.9758, Found 110.9751; IR (KBr, cm^{-1}) 780, 1020, 1094, 1230, 1250, 1465, 2850, 2925.

(*E*)-1,2-dimethyl-3,5-diphenyl-4-(phenyldiazenyl)-1*H*-pyrazol-2-ium methanesulfonate, 23-C1-MeSO$_4$, reddish solid, mp = 247-245 °C, yield = 97%.

^1H NMR (400 MHz, DMSO-d_6) δ 7.70 (m, 10H), 7.47-7.45 (m, 3H), 7.35-7.33 (m, 2H), 4.10 (s, 6H), 3.36 (s, 3H) ppm; ^{13}C NMR (100 MHz, DMSO-d_6) δ 151.5, 141.4, 132.8, 132.2, 131.2, 130.6, 129.5, 128.9, 124.8, 122.0, 52.9, 35.5 ppm; HRMS (ESI^+) m/z: calcd. for $C_{23}H_{21}N_4$ $[M]^+$353.1766, Found 353.1764, (ESI^-) m/z: calcd. for CH_3O_4S $[M]^-$ 110.9758, Found 110.9751; IR (KBr, cm^{-1}) 780, 1020, 1090, 1230, 1250, 1460, 2852, 2928, 2957.

(*E*)-4-((2-fluorophenyl)diazenyl)-1,2-dimethyl-3,5-diphenyl-1*H*-pyrazol-2-ium methanesulfonate, 24-C1-MeSO$_4$, reddish brown solid, mp = 254-256 °C, yield = 97%.

^1H NMR (400 MHz, DMSO-d_6) δ 7.67-7.71 (m, 10H), 7.56-7.49 (m, 1H), 7.35-7.28 (m, 2H), 7.24-7.20 (m, 1H), 4.08 (s, 6H), 3.36 (s, 3H) ppm; ^{13}C NMR (100 MHz, DMSO-d_6) δ 160.4 (d, *J* =257 Hz), 141.8, 139.5 (d, *J* = 7 Hz), 134.4 (d, *J* = 8 Hz), 133.3, 131.4, 130.6, 129.1, 125.1 (d, *J* = 19 Hz), 124.7, 117.4 (d, *J* = 19 Hz), 116.8, 53.0, 35.7 ppm; ^{19}F NMR (376.5 MHz, DMSO-d_6): δ -123.4 ppm; HRMS (ESI^+) m/z: calcd. for $C_{23}H_2N_4F$ $[M]^+$ 371.1672, Found 371.1679, (ESI^-) m/z: calcd. for CH_3O_4S $[M]^-$ 110.9758, Found 110.9751; IR (KBr, cm^{-1}) 780, 1020, 1090, 1230, 1250, 1460, 2852, 2928, 2957.

3B.5 Conclusions

We have developed a new class of highly water soluble arylazopyrazolium-based ionic photoswitches (AAPIPs). The AAPIPs exhibit excellent bidirectional photoswitching in both organic and aqueous media along with long term photoswitching stability. More interestingly, the photoswitching ability and thermal stability of *Z*-isomers can be tuned by electronic and/or steric substitutions at the aryl group and the pyrazolium ring, solvents, and pH. The quantitative forward photoisomerization, moderate to good reverse photoisomerization, the resulting bistability and bidirectional photoswitching, tolerance towards lipophilic groups at the pyrazolium nitrogen, exceptional *Z*-isomer stability, tolerance to a wide range of pH, scope for various substitutions, and stability towards azo reductase glutathione (GSH) are some of the important salient features of this AAPIPs. All these features make this class of photoswitches a suitable candidate for variety of applications including photopharmocology. By a structure-activity relationship, we identified key features improving both photochemical switching and thermal stability of the *Z*-form. These factors were synergically combined to develop AAPIPs with exceptionally stable *Z*-form (up to 573 days in DMSO) with high photostationary states of forward (*E*-*Z*, up to 98%) and reverse (*Z*-*E*, up to 89%) photoisomerization.

3B.6 References

1. (a) Bandara, H. M. D.; Burdette, S. C. *Chem*. *Soc*. *Rev*. **2012**, *41*, 1809-1825. (b) Jerca, F. A.; Jerca, V. V.; Hoogenboom, R. *Nature Reviews Chemistry.* **2022**, *6*, 51–69. (c) Crespi, S.; Simeth, N. A.; König, B. *Nat. Rev. Chem.* **2019**, *3*, 133−146.
2. (a) Dong, L.; Feng, Y.; Wang, L.; Feng, W. *Chem*. *Soc*. *Rev*. **2018**, *47*, 7339. (b) Kortekaas, L.; Simke, J.; Kurka, D. W.; Ravoo, B. J. *ACS Appl. Matter. Interfaces*. **2020**, *12*, 32054-32060. (c) Larik, F. A.; Fillbrook, L. L.; Nurttila, S. S.; Martin, A. D.; Kuchel, R. P.; Taief, K. A.; Bhadbhade, M.; Beves, J. E.; Thordarson, P. *Angew. Chem. Int. Ed*. **2021**, *60*, 6764-6770. (d) Nagai, Y.; Ishiba, K.; Yamamoto, R.; Yamada, T.; Morikawa, M.; Kimizuka, N. *Angew. Chem. Int. Ed*. **2021**, *60*, 6333-6338.
3. (a) Gerkman, M. A.; Gibson, R. S. L.; Calbo, J.; Shi Y.; Fuchter, J.; Han, G. G. D. *J. Am. Chem. Soc*. **2020**, *142*, 8688-8695. (b) Le, M.; Han, G. G. D. *Acc*. *Mater*. *Res*. **2022**, *3*, 6, 634–643.
4. (a) Weston, C. E.; Kramer, A.; Collin, F.; Yildiz, O.; Almes, F. J. M.; Fuchter, M. J. *ACS infect. Dis.* **2017**, *3*, 152-161. (b) Mafy, N.; Matsuo, K.; Hiruma, S.; Uehara, R.; Tamaoki, Nobuyuki. *J. Am*. *Chem*. *Soc*. **2020**, *142*, 1763−1767. (c) Lam, P. Y.; Thawani, A. R.; Balderas, E.; White, A. J. P.; Chaudhuri, D.; Fuchter, M. J; Peterson, R. T. *J*. *Am*. *Chem*. *Soc*. **2020**, *142*, 17457−17468.
5. (a) Fuchter, M. J. *J. Med*. *Chem*. **2020**, *63*, 20, 11436–11447. (b) Kabauri, P.; Galenkamp, N. S.; Schulte, A. M.; Vries, J. D.; Simeth, N. A.; Maglia, G.; Thallmair S.; Kolarski, D.; Szymanski, W.; Feringa, B. L. *J. Med*. *Chem*. **2022**, *65*, 6, 4798–4817.

6. (a) Müller, M.; Niemeyer, K.; Urban, N.; Ojha, N. K.; Zufall, F.; Zufall, T. L.; Schaefer, M.; Seshold, O. T. *Angew*. *Chem*. *Int*. *Ed*. **2022**, *61*, 36, e202201565. (b) Trads, J. B.; Hüll, K.;. Matsuura, B. S.; Laprell, L.; Fehrentz, T.; Görldt, N.; Kozek , K. A.; Weaver, C. D.; Klöcker, N.; Barber, D. M.; Trauner, D. *Angew*. *Chem*. *Int*. *Ed*. **2019**, *58*, 43, 15421-15428. (c) Ferreira, R.; Nilsson, J. R.; Solano C.; Andre´asson, J.; Grøtli, M. *Sci*. *Rep*. **2015**, *5*, 9769.
7. (a) Wendler, T.; Schütt, C.; Näther, C.; Herges, R. *J. Org. Chem.* **2012**, *77*, 7, 3284–3287. (b) Weston, C. E.; Richardson, R. D.; Haycock, P. R.; White, A. J. P.; Fuchter, M. J. *J. Am. Chem. Soc*. **2014**, *136*, 11878−11881.
8. (a) Crespi, S.; Simeth, N. A.; König, B. *Nat*. *Rev*. *Chem*. **2019**, *3*, 133−146. (b) Grewal, S.; Gupta, D.; Gaur, A. K.; Saraswat, M.; Venkataramani, S. Nova Publishers: New York, **2019**. (c) Calbo, J.; Weston, C. E.; White, A. J. P.; Rzepa, H. S.; Contreras-García, J.; Fuchter, M. J. *J*. *Am*. *Chem*. *Soc*. **2017**, *139*, 1261−1274. (d) Simeth, N. A.; Crespi, S.; Fagnoni, M.; Konig, B. *J*. *Am*. *Chem*. *Soc*. **2018**, *140*, 2940-2946. (e) Slavov, C.; Yang, C.; Heindl, A. H.; Wegner, H. A.; Dreuw, A.; Wachtveitl, J. *Angew*. *Chem*. *Int*. *Ed*. **2020**, *59*, 380-387. (f) Tuck, J. R.; Tombari, R. J.; Yardeny, N.; Olson, D. E. *Org*. *Lett*. **2021**, *23*, 4305-4310. (g) Pfaff, P.; Anderl, F.; Fink, M.; Balkenhohl, M.; Carreira, E. M. *J*. *Am*. *Chem*. *Soc*., **2021**, *143*, 36, 14495-14501. (h) Devi, S.; Saraswat, M.; Grewal, S.; Venkataramani, S. *J*. *Org*. *Chem*. **2018**, *83*, 8, 4307-4322
9. (a) Stricker, L.; Fritz, E. C.; Peterlechner, M.; Doltsinis, N. L.; Ravoo, B. J. *J*. *Am*. *Chem*. *Soc*. **2016**, *138*, 13, 4547–4554. (b) Stricker, L.; Böckmann, M.; Kirse, T. M.; Doltsinis, N. L.; Ravoo, B. J. *Chem*. *Eur*. *J*. **2018**, *24*, 34, 8639-8647. (c) Ludwanowski, S.; Ari, M.; Parison, K.; Kalthoum, S.; Straub, P.; Pompe, N.; Weber, S.; Walter, M.; Walther, A. *Chem*. *Eur*. *J*. **2020**, *26*, 58, 13203-13212. (d) Volarić, J.; Szymanski, W.; Simeth, N. A.; Feringa, B. L. *Chem*. *Soc*. *Rev*. **2021**, *50*, 12377-12449. (e) Kortekaas, R.; Simke, J.; Arndt, N. B.; Böckmann, M.; Doltsinis, N. L.; Ravoo, B. J. *Chem. Sci.*, **2021**,*12*, 11338-11346. (f) Gibson, R. S. L.; Calbo, J.; Fuchter, M. J. *ChemPhotoChem*, **2019**, *3*, 372-377.
10. (a) Lentes, P.; Frühwirt, P.; Freißmuth, H.; Moormann, W.; Kruse, F.; Gescheidt, G.; Herges, R. Photoswitching of Diazocines in Aqueous Media. *J*. *Org*. *Chem*. **2021**, *86*, 4355−4360. (b) Lentes, P.; Stadler, E.; Röhricht, F.; Brahms, Arne.; Gröbner, J.; Sönnichsen, F. D.; Gescheidt, G.; Herges, R. *J*. *Am*. *Chem*. *Soc*. **2019**, *141*, 13592−13600.
11. (a) Dong, M.; Babalhavaeji, A.; Hansen, M. J.; Ka'lma'n, L.; Woolley, G. A*Chem*. *Commun*. **2015**, *51*, 12981. (b) Bhunia, S.; Dolai, A.; Samanta, S. *Chem. Commun*. **2020**, *56*, 10247−10250.
12. (a) Greenwald, R. B.; Choe, Y. H.; McGuire, J.; Conover, C. D. *Adv*. *Drug Delivery Rev*. **2003**, *55*, 217–250. (b) Mogaki, R.; Okuro, K.; Aida, T. *J. Am. Chem. Soc.* **2017**, *139*, 29, 10072–10078.
13. (a) Samanta, D.; Gemen, J.; Chu, Z.; Posner, Y. D.; Shimon, L. J. W.; Klajn, R. *PNAS*. **2018**, *115*, 38, 9379-9384. (b) Pesce, Luca.; Perego, C.; Grommet, A. B.; Klajn, R.; Pavan, G. M. *J*. *Am*. *Chem*. *Soc*. **2020**, *142*, 21, 9792–9802. (c) Moscosoa, A. D.; Ballester, P. *Chem*. *Commun*., **2017**, *53*, 4635-4652. (d) Otolski C. J.; Raj, A. M.; Ramamurthy, V.; Elles, C. G. *J*. *Phys*. *Chem*. *Lett*. **2019**, *10*, 1, 121–127. (e) Raj A. M.; Ramamurthy, V. *Org*. *Lett*. **2017**, *19*, 22, 6116–6119. (f) Otolski C. J.; Raj, A. M.; Ramamurthy, V.; Elles, C. G. *Chem*. *Sci*. **2020**, *11*, 9513-9523.
14. (a) Wang, X.; Huang, J.; Zhou, Y.; Yan, S.; Weng, X.; Wu, X.; Deng, M.; Zhou, X.; *Angew*. *Chem*. *Int*. *Ed*. **2010**, *122*, 31, 5433-5437. (b) Wu, A.; Lu, F.; Sun, P.; Gao, X.; Shi, L.; Zheng, L. *Langmuir*, **2016**, *32*, 32, 8163–8170. (c) Wang, C.; Hashimoto, K.; Tamate, R.; Kokubo, H.; Watanabe, M. *Angew. Chem. Int. Ed.* **2018**, *57*, 227–230.

15. Nakagawa, M.; Rikukawa, M.; Watanabe, M.; Sanui, K.; Oga-ta, N. *Bull*. *Chem*. *Soc*. *Jpn*. **1997**, *70*, 737–744.
16. (a) Amorós, J. G.; Massad, W. A.; Non-ell, S.; Velasco, D. *Org*. *Lett*. **2010**, *12*, 15, 3514–3517. (b) Amorós, J. G.; Nonell, S.; Velasco, D. *Chem*. *Commun*. **2012**, *48*, 3421–3423. (c) Amorós, J. G.; Gómez, E.; Vallés, E.; Velasco, D. *Chem*. *Commun*. **2012**, *48*, 9080-9082.
17. Yoshida, T.; Monji, T.; Kawamori, D.; Akai, N.; Shibuya, K.; Kawai, A*Chem*. *Lett*. **2013**, *42*, 1490-1492.
18. Prischich, D.; Gomila, A. M. J.; Milla-Navarro, S.; Sangüesa, G.; Diez-Alarcia, R.; Preda, B.; Matera, C.; Batlle, M.; Ramírez, L.; Giralt, E.; Hernando, J.; Guasch, E.; Meana, J. J.; de la Villa, P.; Gorostiza, P. *Angew. Chem. Int. Ed.* **2021**, *60*, 3625–3631.
19. Dai, J.; Zhao, K. Q.; Wang, B. Q.; Hu, P.; Heinrich, B. Donnio, B. *J*. *Mater*. *Chem*. *C*. **2020**, *8*, 4215-4225.
20. (a) Taft, R. W. *J. Am. Chem. Soc.* **1952**, *74*, 2729−2732. (b) Fujita, T.; Takayama, C.; Nakajima, M. *J. Org. Chem.* **1973**, *38*, 1623−1630. (c) Hammett, L. P. *J. Am. Chem. Soc.* **1937**, *59*, 96−103. J.
21. Dokić, M. Gothe, J. Wirth, M. V. Peters, J. Schwarz, S. Hecht, Saalfrank P. *J. Phys. Chem. A*, **2009**, *113*, 24, 6763-6773.
22. Angelini, G.; Canilho, N.; Emo, M.; Kingsley, M.; Gasbarri, C. *J*. *Org*. *Chem*. **2015**, *80*, 15, 7430–7434.

Appendix 3B

3B.1. Analysis of photoswitching and thermal stability: UV-Vis spectroscopy

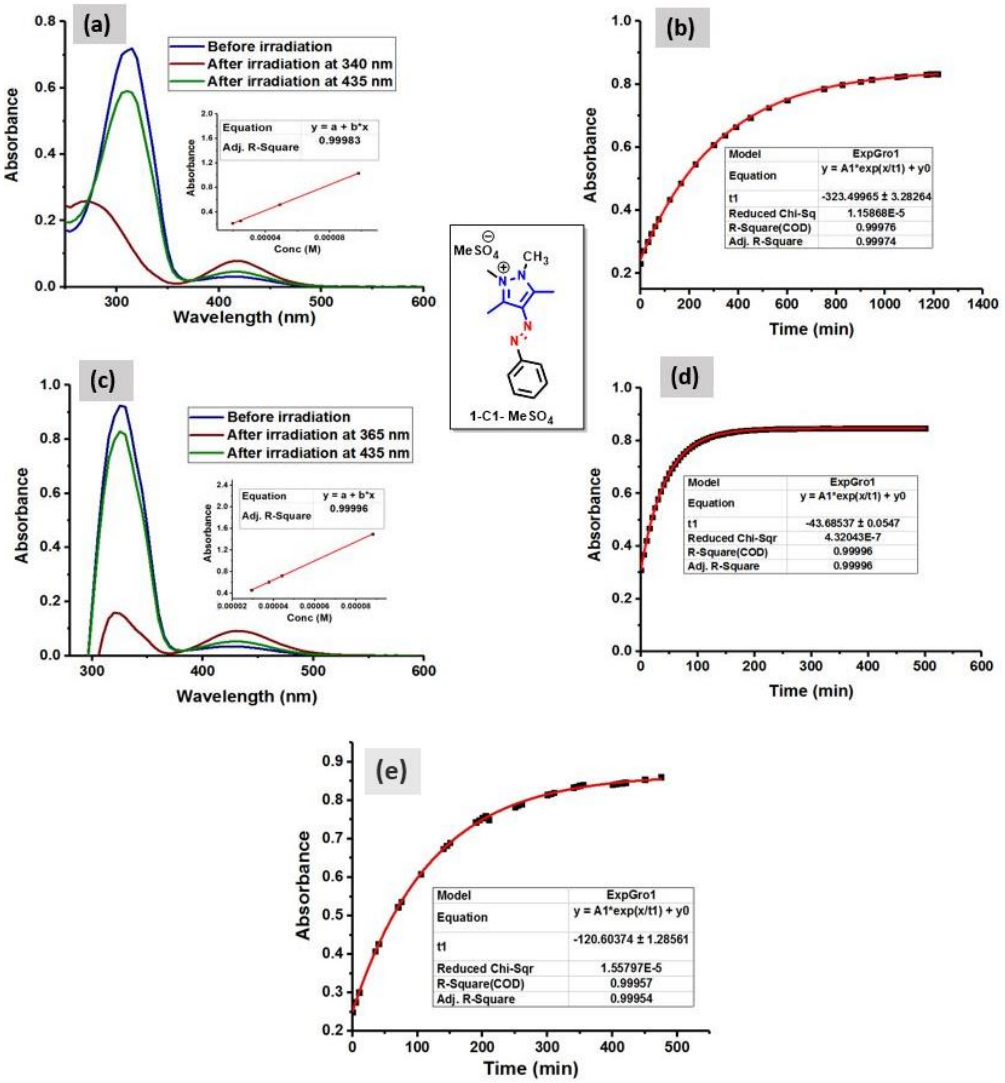

Figure 3B.1. Photoswitching behaviour of **1-C1-MeSO$_4$.** (a) Forward and reverse photoisomerization (61.9 μM in H_2O) and the insert plot depicts estimation of molar absorption coefficient; (b) Thermal *Z-E* isomerization kinetics at 80 °C in H_2O (68.5 μM, monitored at λ=315 nm); (c) Forward and reverse photoisomerization (52.3 μM) and the insert plot depicts estimation of molar absorption coefficient in DMSO; (d Thermal *Z-E* isomerization kinetics at 90 °C in DMSO (48.0 μM, monitored at λ=325 nm), (e) Thermal *Z-E* isomerization kinetics at 80 °C in DMSO (48.0 μM, monitored at λ=325 nm).

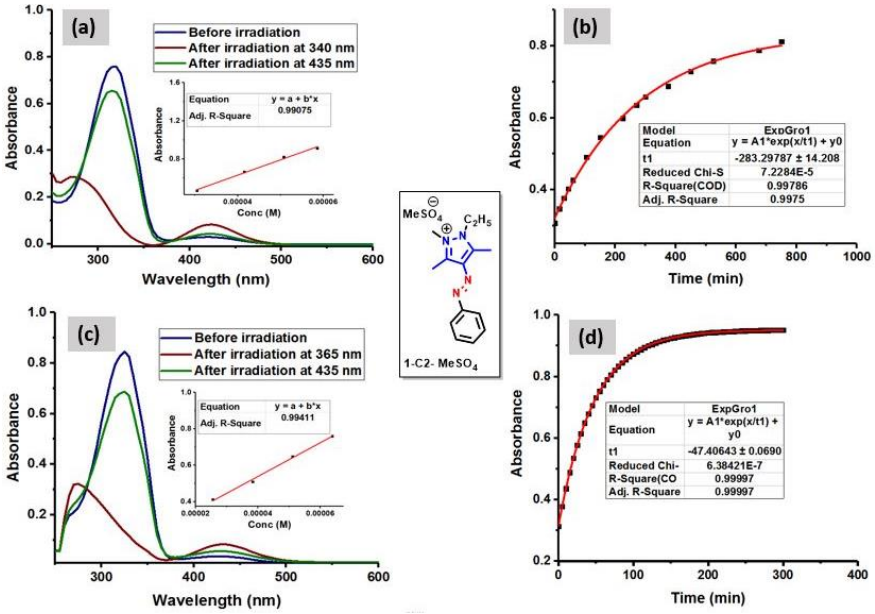

Figure 3B.2. Photoswitching behaviour of **1-C2-MeSO$_4$.** (a) Forward and reverse photoisomerization (47.3 μM in H_2O) and the insert plot depicts estimation of molar absorption coefficient; (b) Thermal *Z-E* isomerization kinetics at 80 °C in H_2O (50.7 μM, monitored at λ=320 nm); (c) Forward and reverse photoisomerization (102.7 μM) and the insert plot depicts estimation of molar absorption coefficient in DMSO; (d) Thermal *Z-E* isomerization kinetics at 90 °C in DMSO (102.7μM, monitored at λ=325 nm).

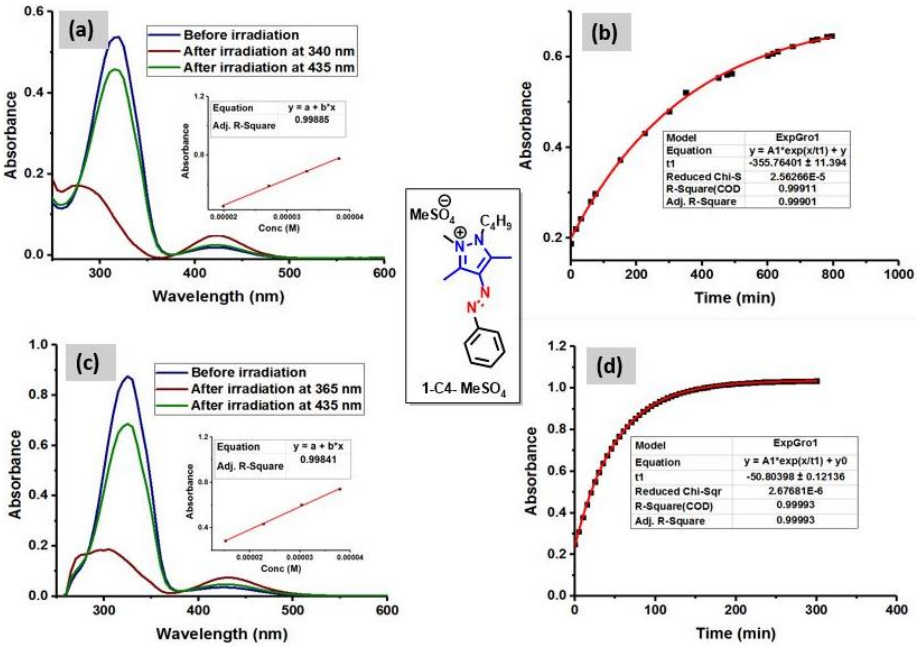

Figure 3B.3. Photoswitching behaviour of **1-C4-MeSO$_4$** (a) Forward and reverse photoisomerization (30.4 μM in H_2O) and the insert plot depicts estimation of molar absorption coefficient; (b) Thermal *Z-E* isomerization kinetics at 80 °C in H_2O (36.6 μM, monitored at λ=320 nm); (c) Forward and reverse photoisomerization (43.2 μM) and the insert plot depicts estimation of molar absorption coefficient in DMSO; (d) Thermal *Z-E* isomerization kinetics at 90 °C in DMSO (50.0 μM, monitored at λ=325 nm).

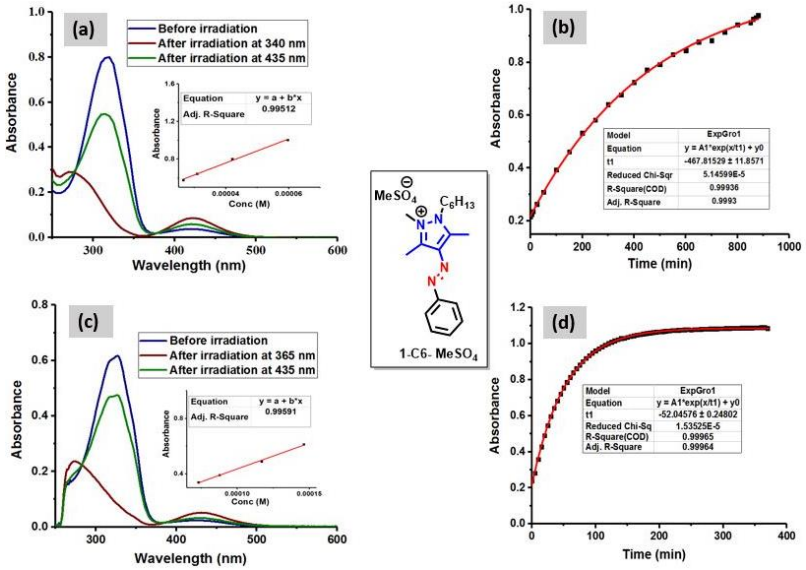

Figure 3B.4. Photoswitching behaviour of **1-C6-MeSO4.** (a) Forward and reverse photoisomerization (60.6 μM in H_2O) and the insert plot depicts estimation of molar absorption coefficient; (b) Thermal *Z-E* isomer stability at 80 °C in H_2O (76.5 μM, monitored at λ=320 nm); (c) Forward and reverse photoisomerization (165.6 μM) and the insert plot depicts estimation of molar absorption coefficient in DMSO; (d) Thermal *Z-E* isomerization kinetics at 90 °C (185.3 μM, monitored at λ=325 nm).

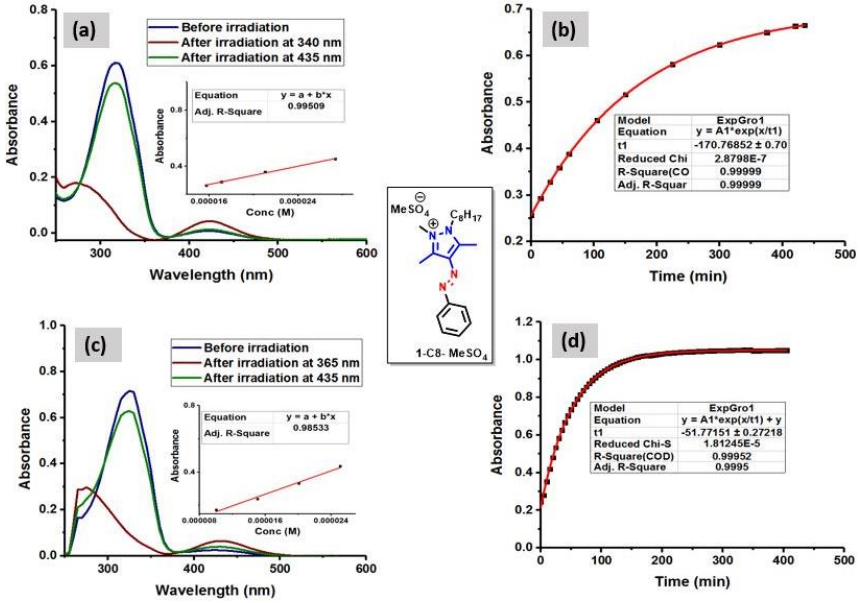

Figure 3B.5. Photoswitching behaviour of **1-C8-MeSO4.** (a) Forward and reverse photoisomerization (37.6 μM in H_2O), and the insert plot depicts estimation of molar absorption coefficient; (b) Thermal *Z-E* isomer stability at 80 °C in H_2O (40.9 μM, monitored at λ=320 nm); (c) Forward and reverse photoisomerization (40.8 μM) and the insert plot depicts estimation of molar absorption coefficient in DMSO; (d) Thermal *Z-E* isomerization kinetics at 90 °C in DMSO (59.7 μM, monitored at λ=325 nm).

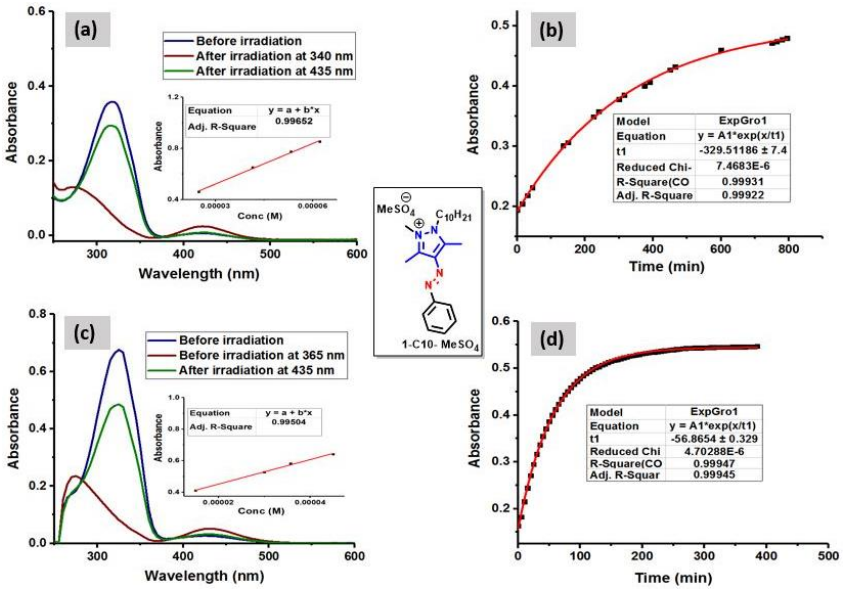

Figure 3B.6. Photoswitching behaviour of **1-C10-MeSO$_4$.** (a) Forward and reverse photoisomerization (33.9 μM in H_2O) and the insert plot depicts estimation of molar absorption coefficient; (b) Thermal *Z-E* isomer stability at 80 ^oC in H_2O (45.4 μM, monitored at λ=320 nm); (c) Forward and reverse photoisomerization (86.9 μM) and the insert plot depicts estimation of molar absorption coefficient in DMSO; (d) Thermal *Z-E* isomerization kinetics at 90 ^oC in DMSO (70.3 μM, monitored at λ=320 nm).

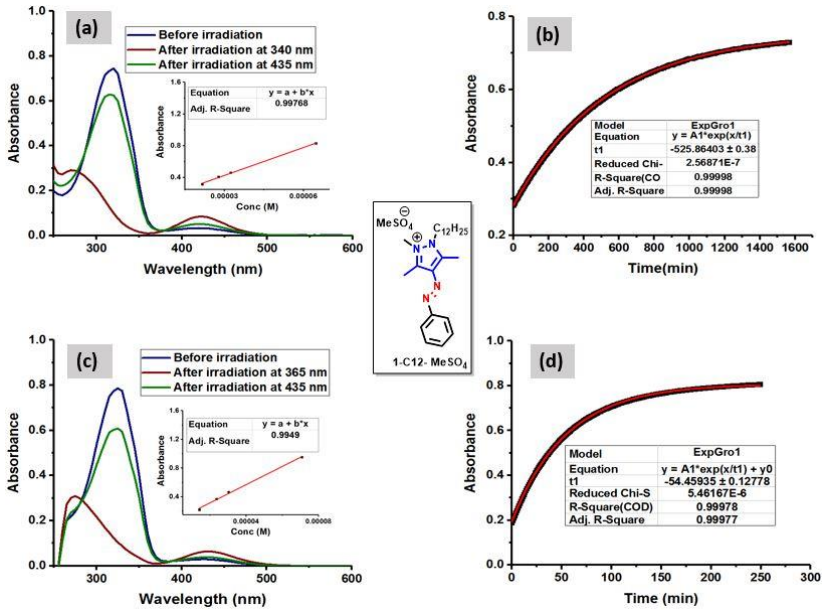

Figure 3B.7. Photoswitching behaviour of **1-C12-MeSO$_4$.** (a) Forward and reverse photoisomerization (63.5 μM in H_2O) and the insert plot depicts estimation of molar absorption coefficient; (b) Thermal *Z-E* isomer stability at 80 ^oC in H_2O (62.3 μM, monitored at λ=320 nm); (c) Forward and reverse photoisomerization (61.9 μM) and the insert plot belongs to estimation of molar absorption coefficient in DMSO; (d) Thermal *Z-E* isomerization at 90 ^oC in DMSO (63.6 μM, monitored at λ=325 nm).

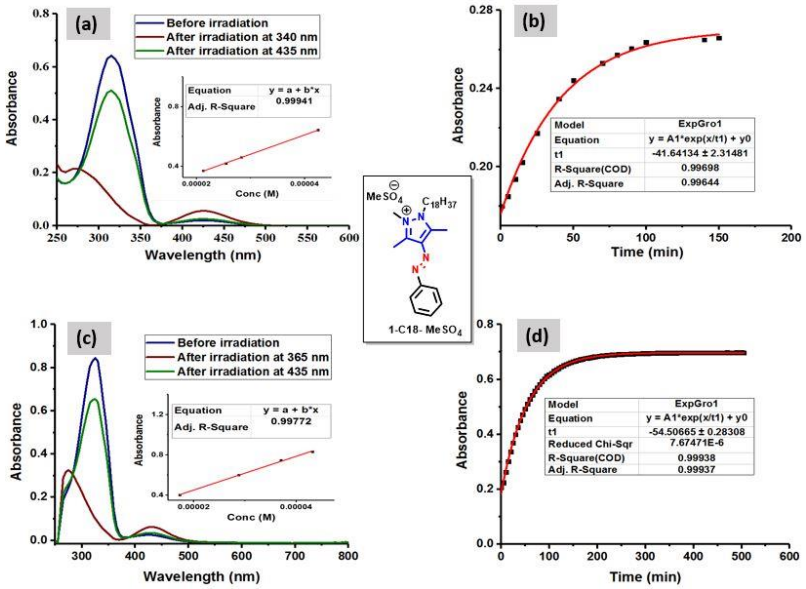

Figure 3B.8. Photoswitching behaviour of **1-C18-MeSO$_4$** (a) Forward and reverse photoisomerization (49.7 μM in H_2O) and the insert plot depicts estimation of molar absorption coefficient; (b) Thermal *Z-E* isomer stability at 80 ^oC in H_2O (20.6 μM, monitored at λ=320 nm); (c) Forward and reverse photoisomerization (50.5 μM) and the insert plot depicts estimation of molar absorption coefficient in DMSO; (d) Thermal *Z-E* isomerization at 80 ^oC in DMSO (21.7 μM, monitored at λ=325 nm).

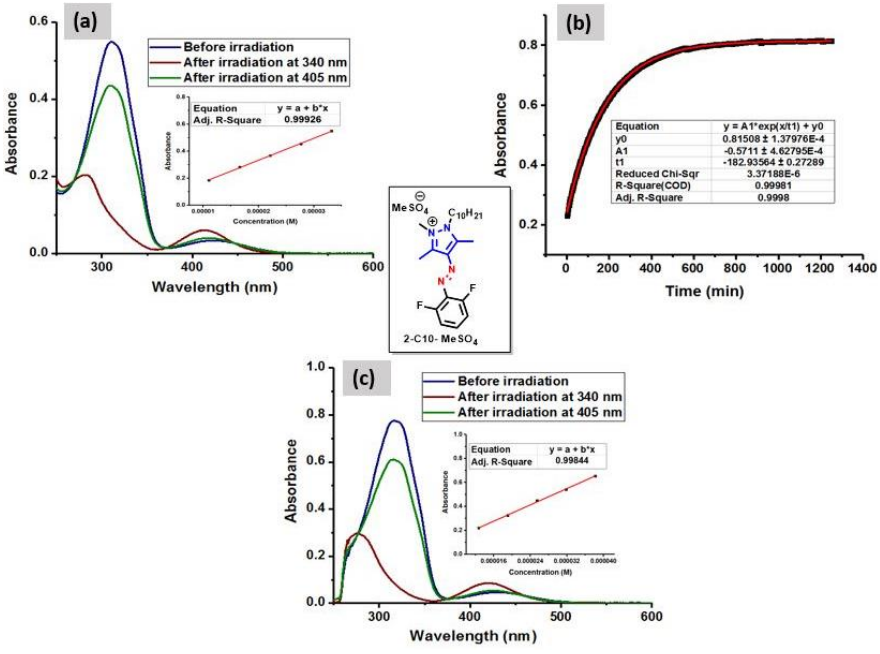

Figure 3B.9. Photoswitching behaviour of **2-C10-MeSO$_4$.** (a) Forward and reverse photoisomerization (45.6 μM in DMSO) and the insert plot depicts estimation of molar absorption coefficient; (b) Thermal *Z-E* isomer stability at 90 ^oC in DMSO (47.9 μM, monitored at λ=317 nm); (c) Forward and reverse photoisomerization (33.9 μM) and the insert plot depicts estimation of molar absorption coefficient in H_2O.

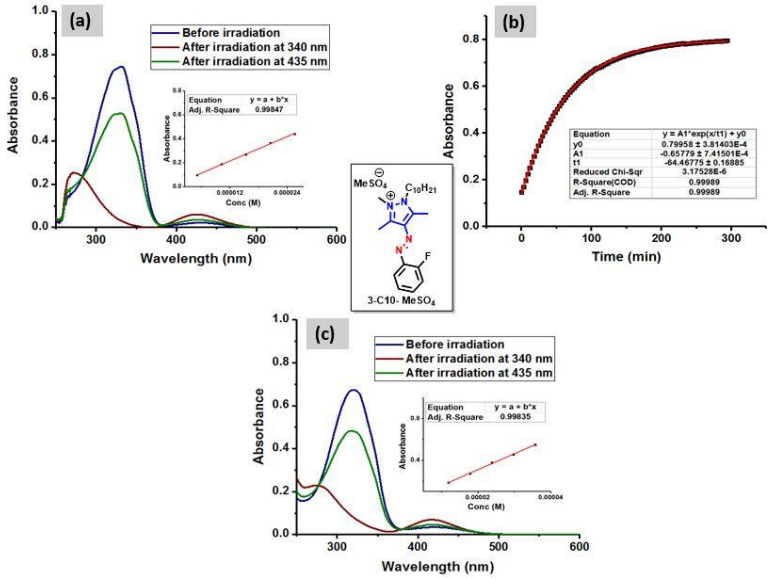

Figure 3B.10. Photoswitching behaviour of **3-C10-MeSO$_4$.** (a) Forward and reverse photoisomerization (41.0 μM in DMSO), and the insert plot depicts estimation of molar absorption coefficient; (b) Thermal *Z-E* isomer stability at 90 ^{o}C in DMSO (46.9 μM, monitored at λ=333 nm); (c) Forward and reverse photoisomerization (47.1 μM) and the insert plot depicts estimation of molar absorption coefficient in H_2O.

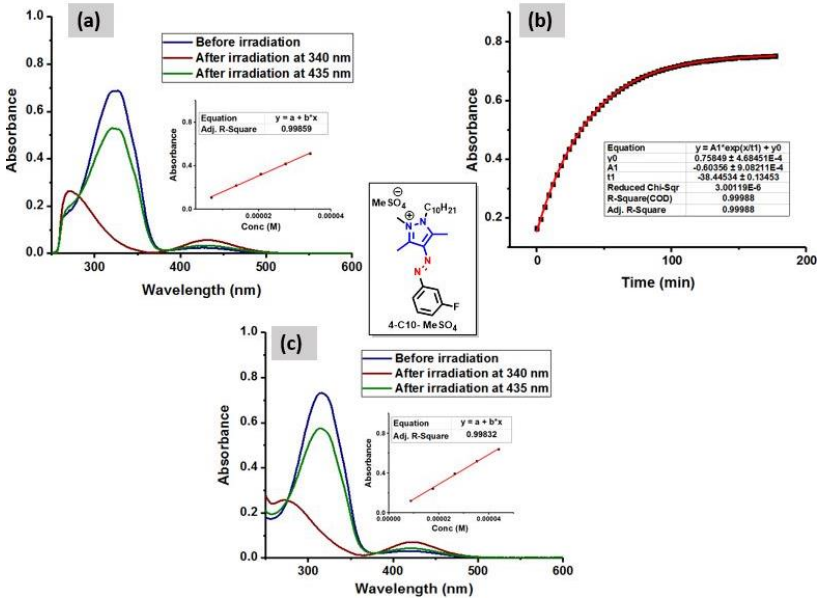

Figure 3B.11. Photoswitching behaviour of **4-C10-MeSO$_4$.** (a) Forward and reverse photoisomerization (40.5 μM in DMSO) and the insert plot depicts estimation of molar absorption coefficient; (b) Thermal *Z-E* isomer stability at 90 ^{o}C in DMSO (51.2 μM, monitored at λ=325 nm); (c) Forward and reverse photoisomerization (49.0 μM) and the insert plot depicts estimation of molar absorption coefficient in H_2O.

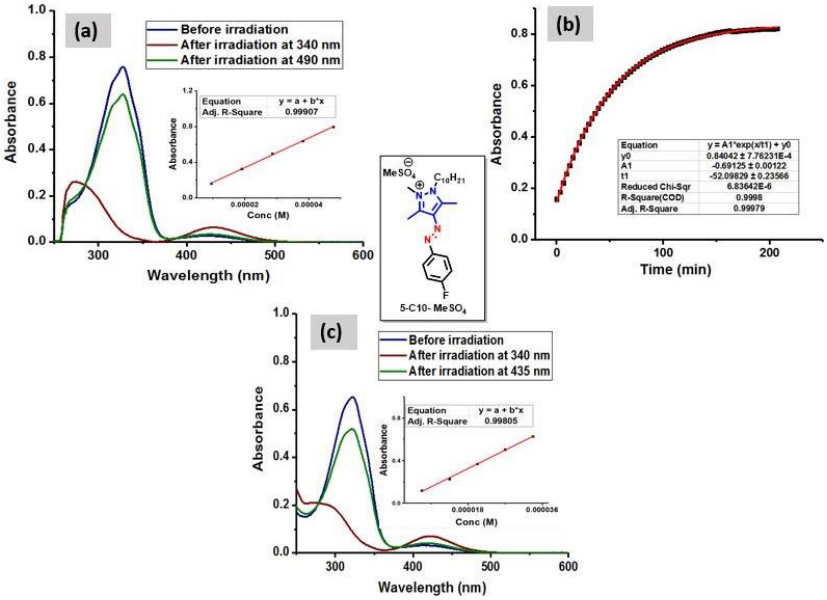

Figure 3B.12. Photoswitching behaviour of **5-C10-MeSO$_4$.** (a) Forward and reverse photoisomerization (51.6 μM in DMSO) and the insert plot depicts estimation of molar absorption coefficient; (b) Thermal *Z-E* isomer stability at 90 ^{o}C in DMSO (49.4 μM, monitored at λ=327 nm); (c) Forward and reverse photoisomerization and the insert plot depicts estimation of molar absorption coefficient in H_2O (33.9 μM).

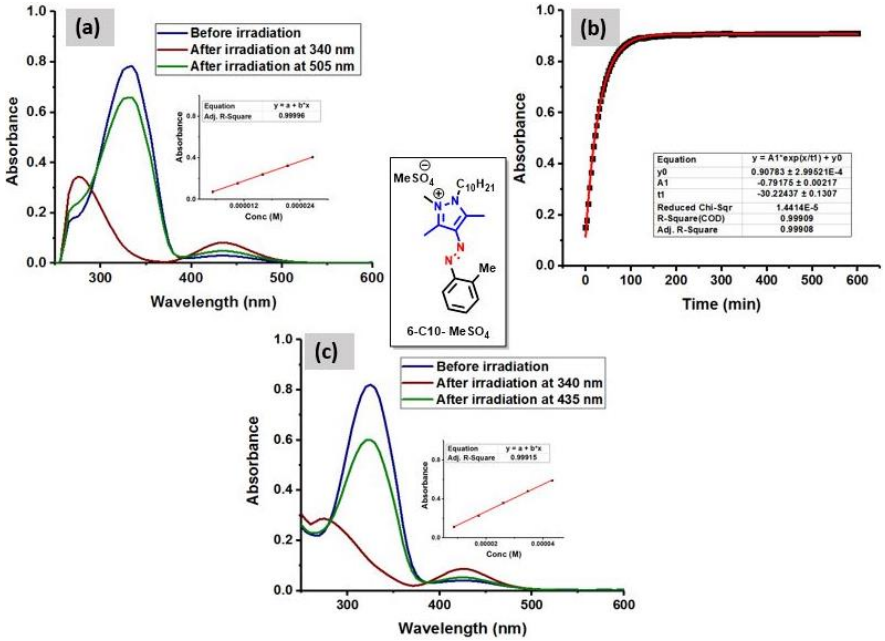

Figure 3B.13. Photoswitching behaviour of **6-C10-MeSO$_4$.** (a) Forward and reverse photoisomerization (49.7 μM in DMSO) and the insert plot depicts estimation of molar absorption coefficient; (b) Thermal *Z-E* isomerization at 90 ^{o}C in DMSO (57.8 μM, monitored at λ=335 nm); (c) Forward and reverse photoisomerization (60.2 μM) and the insert plot depicts estimation of molar absorption coefficient in H_2O.

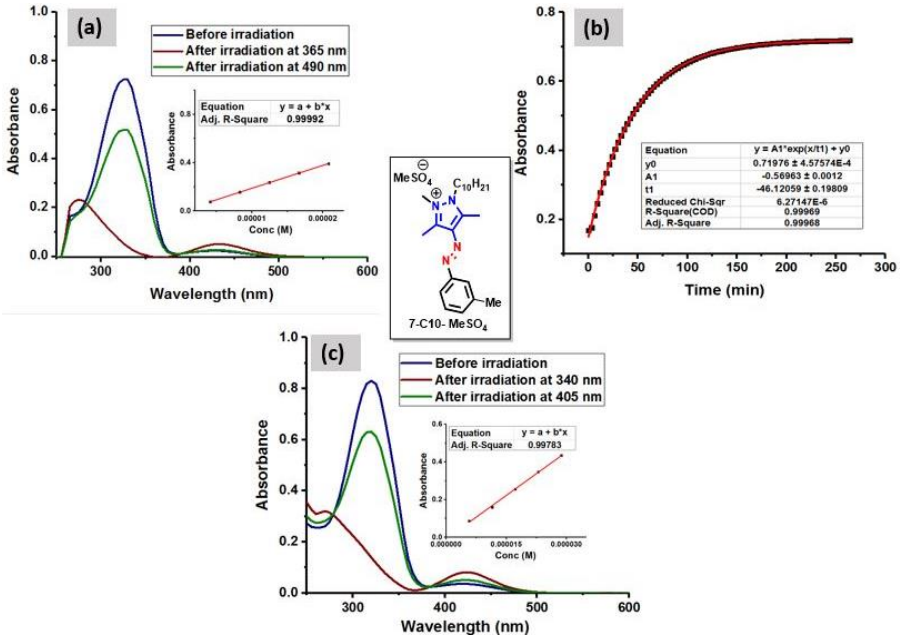

Figure 3B.14. Photoswitching behaviour of **7-C10-MeSO$_4$.** (a) Forward and reverse photoisomerization (38.3 μM in DMSO) and the insert plot depicts estimation of molar absorption coefficient; (b) Thermal *Z-E* isomerization at 90 ^{o}C in DMSO (37.8 μM, monitored at λ=330 nm); (c) Forward and reverse photoisomerization (54.0 μM) and the insert plot depicts estimation of molar absorption coefficient in H_2O.

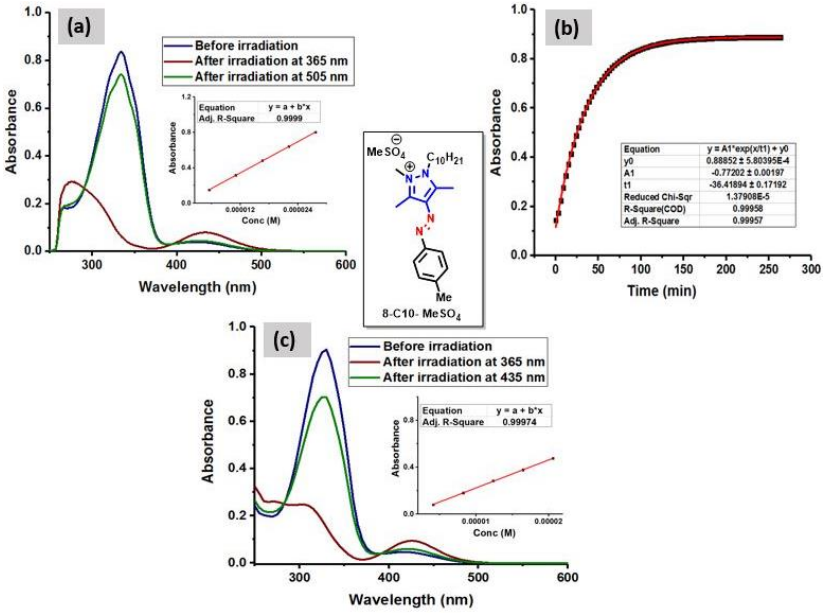

Figure 3B.15. Photoswitching behaviour of **8-C10-MeSO$_4$.** (a) Forward and reverse photoisomerization (28.5 μM in DMSO) and the insert plot depicts estimation of molar absorption coefficient; (b) Thermal *Z-E* isomerization at 90 ^{o}C in DMSO (30.2 μM, monitored at λ=334 nm); (c) Forward and reverse photoisomerization (37.9 μM) and the insert plot depicts estimation of molar absorption coefficient in H_2O.

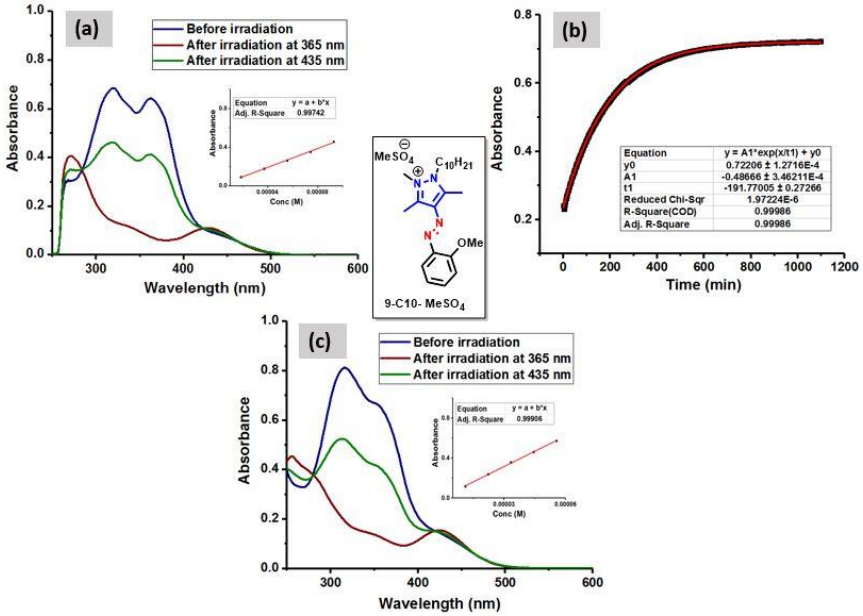

Figure 3B.16. Photoswitching behaviour of **9-C10-MeSO$_4$.** (a) Forward and reverse photoisomerization (38.7 μM in DMSO) and the insert plot depicts estimation of molar absorption coefficient; (b) Thermal *Z-E* isomerization at 90 ^{o}C in DMSO (47.5 μM, monitored at λ=363 nm); (c) Forward and reverse photoisomerization (67.2 μM) and the insert plot depicts estimation of molar absorption coefficient in H_2O.

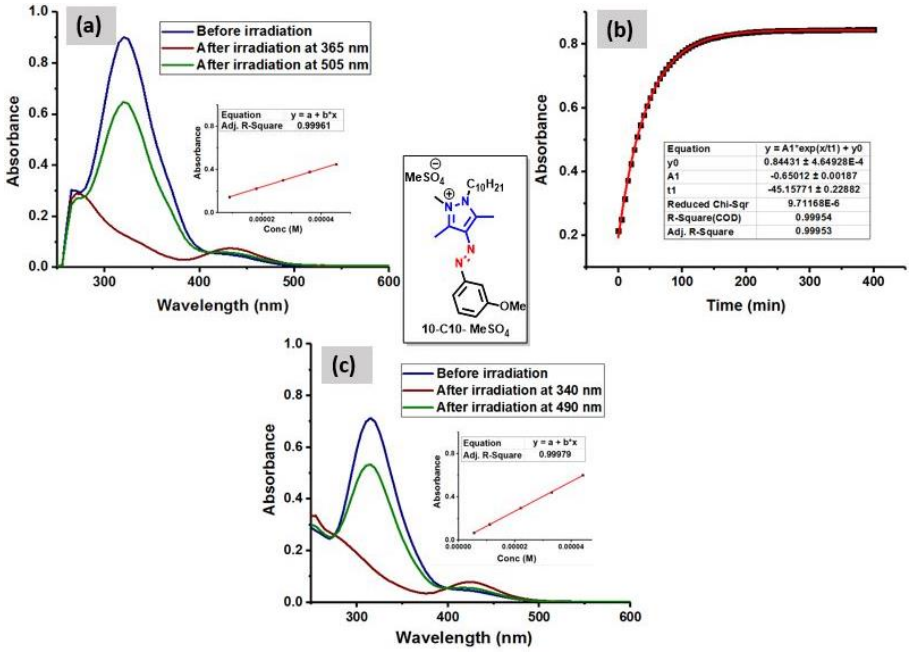

Figure 3B.17. Photoswitching behaviour of **10-C10-MeSO$_4$.** (a) Forward and reverse photoisomerization (106.6 μM in DMSO) and the insert plot depicts estimation of molar absorption coefficient; (b) Thermal *Z-E* isomerization at 90 ^{o}C in DMSO (100.2 μM, monitored at λ=320 nm); (c) Forward and reverse (52.2 μM) photoisomerization and the insert plot depicts estimation of molar absorption coefficient in H_2O.

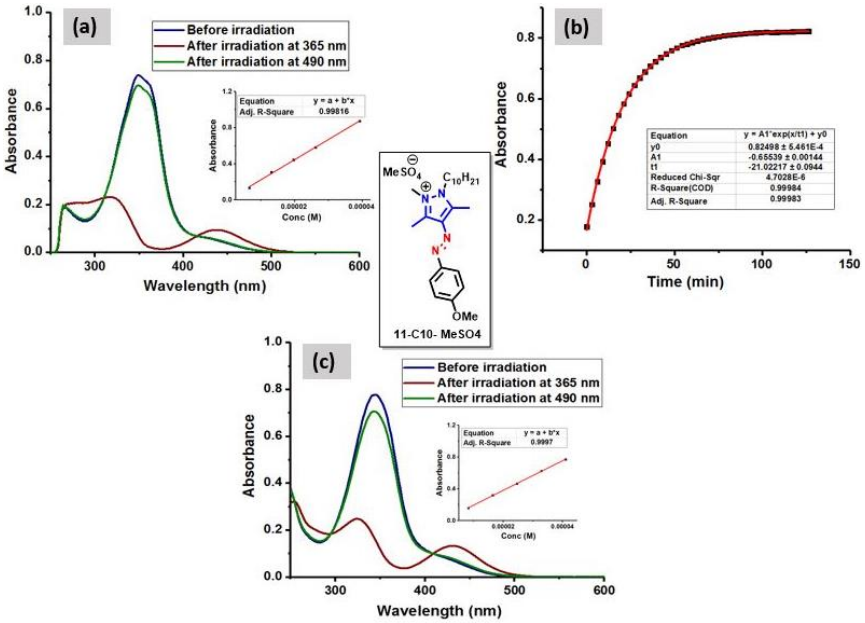

Figure 3B.18. Photoswitching behaviour of **11-C10-MeSO$_4$.** (a) Forward and reverse photoisomerization (31.1 μM in DMSO) and the insert plot depicts estimation of molar absorption coefficient; (b) Thermal *Z*-*E* isomerization at 90 ^{o}C in DMSO (36.9 μM, monitored at λ=349 nm); (c) Forward and reverse photoisomerization (43.9 μM). and the insert plot depicts estimation of molar absorption coefficient in H_2O.

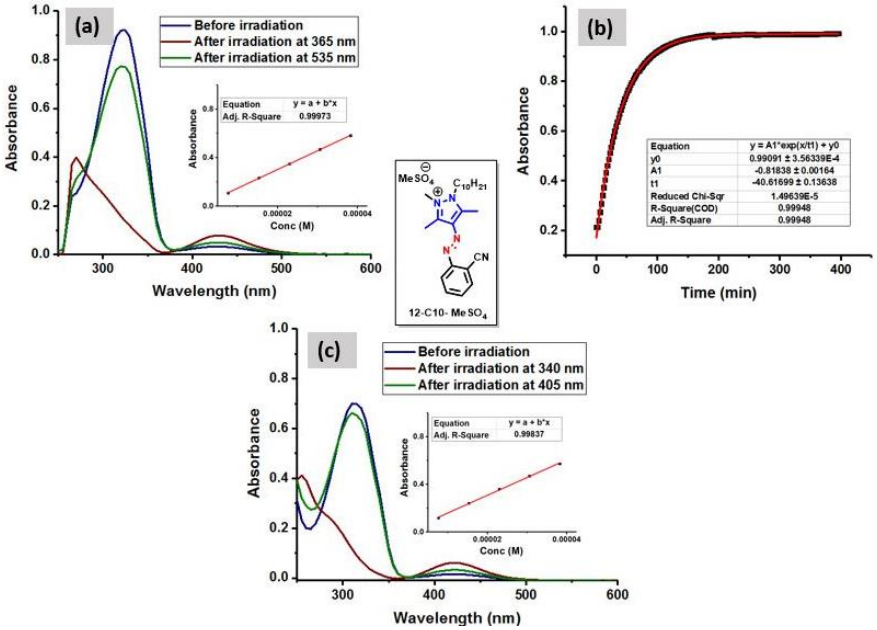

Figure 3B.19. Photoswitching behaviour of **12-C10-MeSO$_4$.** (a) Forward and reverse photoisomerization (59.8 μM in DMSO) and the insert plot depicts estimation of molar absorption coefficient; (b) Thermal *Z*-*E* isomerization at 90 ^{o}C in DMSO (64.2 μM, monitored at λ=325 nm); (c) Forward and reverse photoisomerization (47.0 μM) and the insert plot depicts estimation of molar absorption coefficient in H_2O.

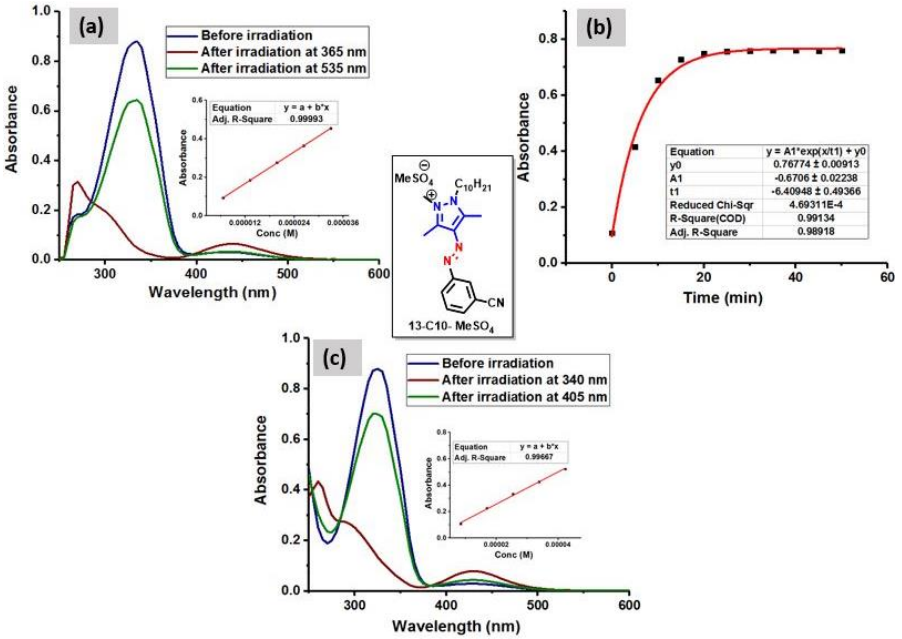

Figure 3B.20. Photoswitching behaviour of **13-C10-MeSO$_4$.** (a) Forward and reverse photoisomerization (64.5 μM in DMSO) and the insert plot depicts estimation of molar absorption coefficient; (b) Thermal *Z-E* isomerization at 90 °C in DMSO (55.5 μM, monitored at λ=335 nm); (c) Forward and reverse photoisomerization (72.2 μM) and the insert plot depicts estimation of molar absorption coefficient in H_2O.

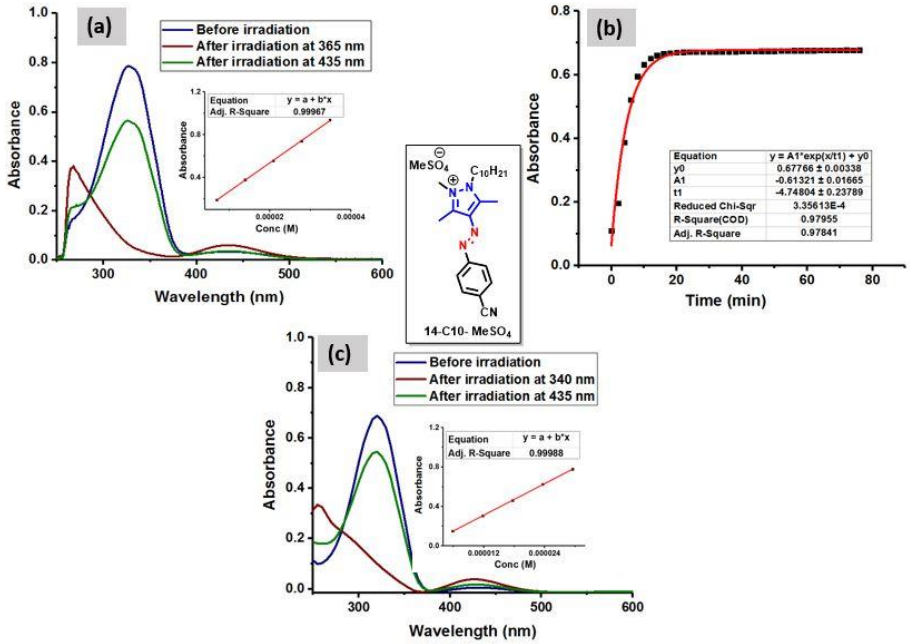

Figure 3B.21. Photoswitching behaviour of **14-C10-MeSO$_4$.** (a) Forward and reverse photoisomerization (29.7 μM in DMSO) and the insert plot depicts estimation of molar absorption coefficient; (b) Thermal *Z-E* isomerization at 90 °C in DMSO (25.5 μM, monitored at λ=327 nm); (c) Forward and reverse photoisomerization (25.8 μM) and the insert plot depicts estimation of molar absorption coefficient in H_2O.

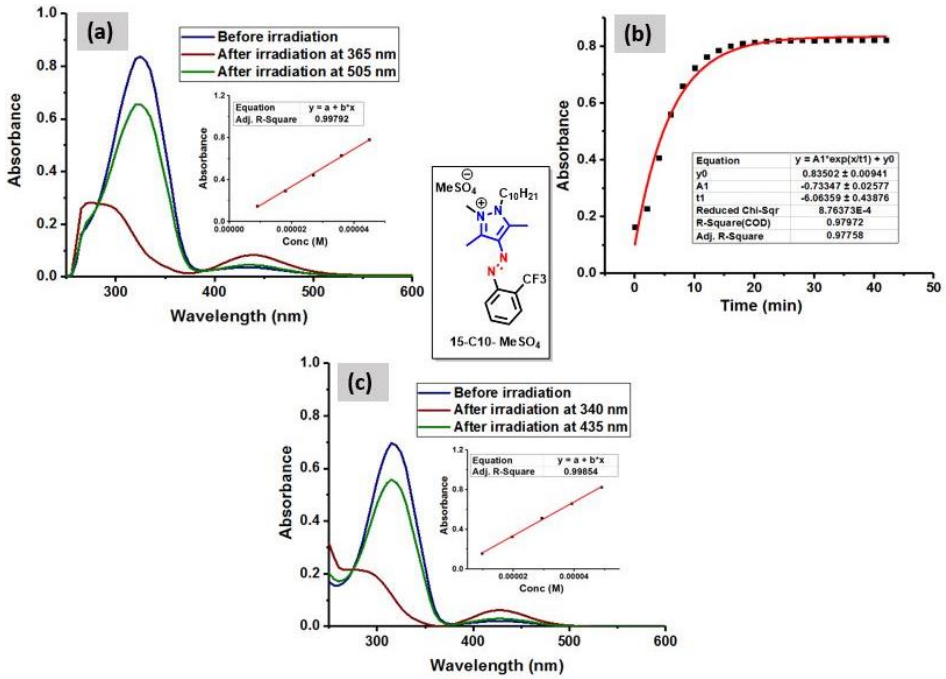

Figure 3B.22. Photoswitching behaviour of **15-C10-MeSO₄** (a) Forward and reverse photoisomerization (47.0 μM in DMSO) and the insert plot depicts estimation of molar absorption coefficient; (b) *Z*-isomer stability at 90 °C in DMSO (46.1 μM, monitored at λ=325 nm); (c) Forward and reverse photoisomerization (41.1 μM) and the insert plot depicts estimation of molar absorption coefficient in H_2O.

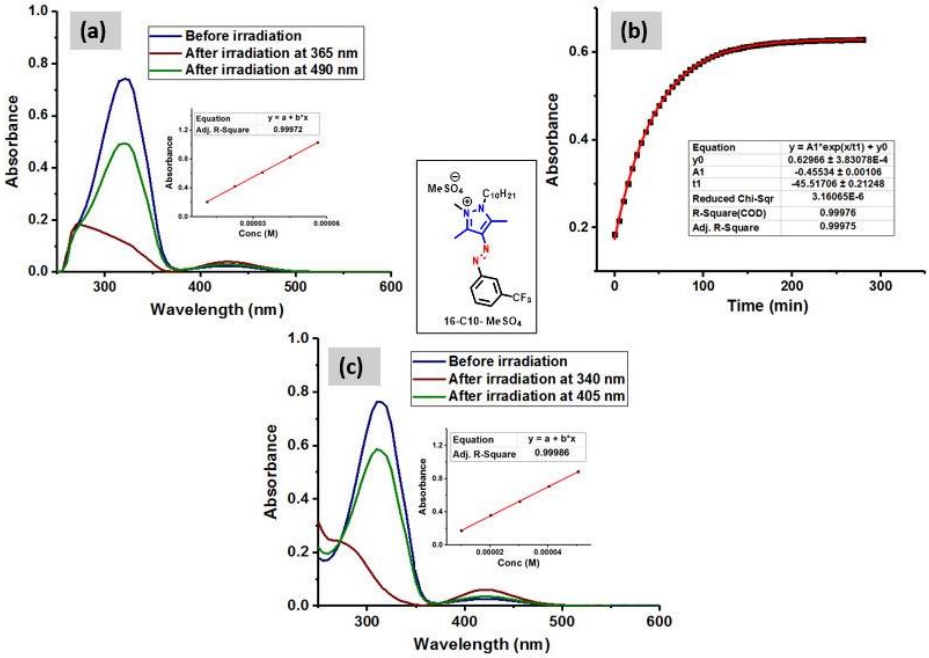

Figure 3B.23. Photoswitching behaviour of **16-C10-MeSO₄.** (a) Forward and reverse photoisomerization (40.9 μM in DMSO) and the insert plot depicts estimation of molar absorption coefficient; (b) Thermal *Z-E* isomerization at 90 °C in DMSO (34.6 μM, monitored at λ=320 nm); (c) Forward and reverse photoisomerization (44.9 μM) and the insert plot depicts estimation of molar absorption coefficient in H_2O.

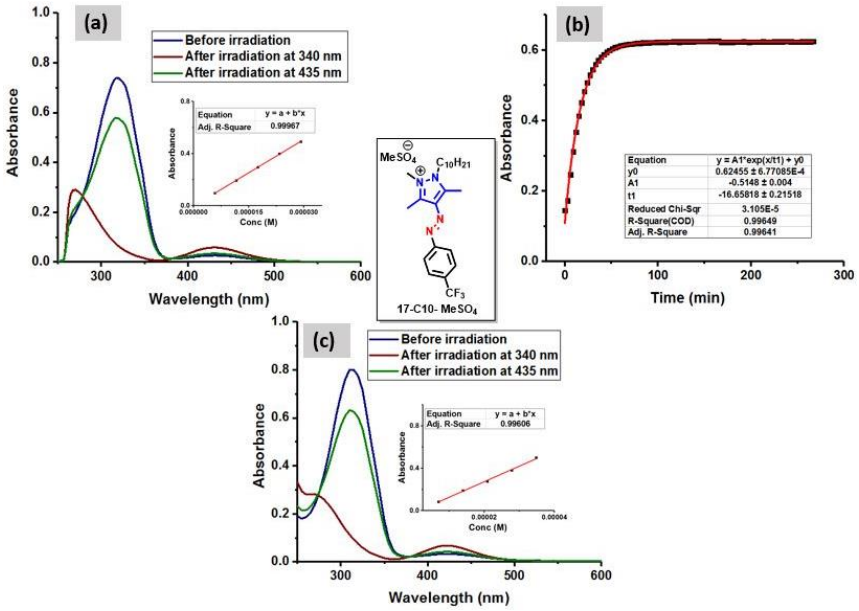

Figure 3B.24. Photoswitching behaviour of **17-C10-MeSO$_4$.** (a) Forward and reverse photoisomerization (43.5 μM in DMSO) and the insert plot depicts estimation of molar absorption coefficient; (b) Thermal *Z*-*E* isomerization at 90 ^{o}C in DMSO (36.6 μM monitored at λ=320 nm); (c) Forward and reverse photoisomerization (54.4 μM) and the insert plot depicts estimation of molar absorption coefficient in H_2O.

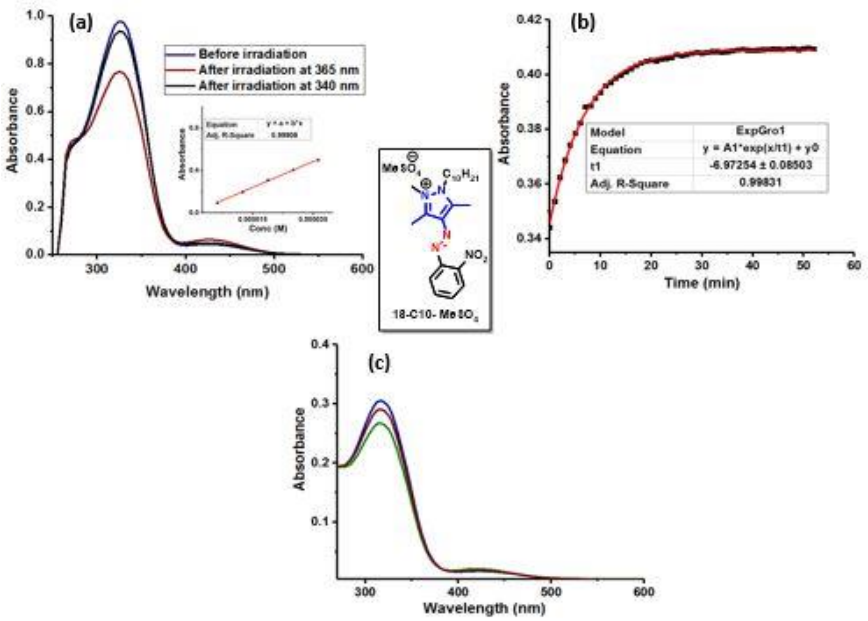

Figure 3B.25. Photoswitching behaviour of **18-C10-MeSO$_4$.** (a) Forward and reverse photoisomerization (27.0 μM in DMSO) and the insert plot depicts estimation of molar absorption coefficient; (b) Thermal *Z*-*E* isomerization at 25 ^{o}C in DMSO (25.5 μM, monitored at λ=325 nm); (c) Forward and reverse photoisomerization (21.1 μM) and the insert plot depicts estimation of molar absorption coefficient in H_2O.

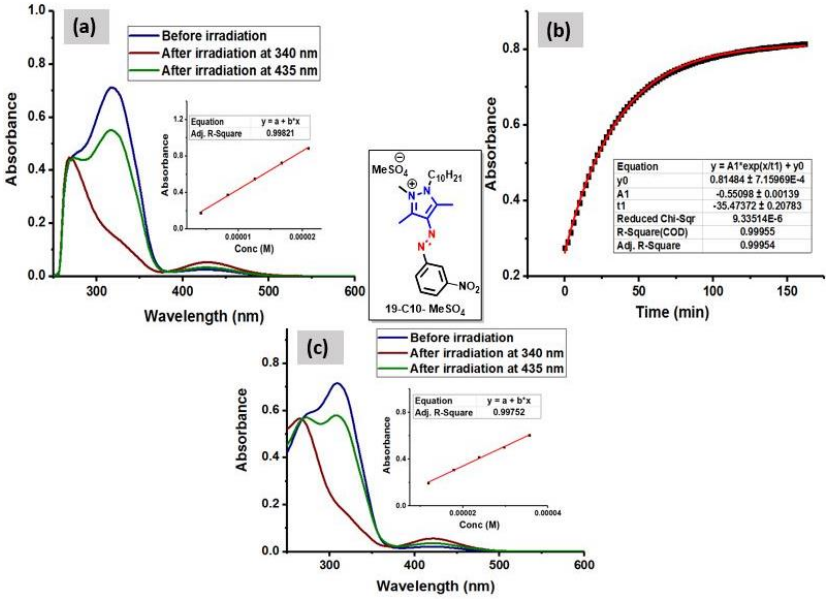

Figure 3.26. Photoswitching behaviour of **19-C10-MeSO$_4$.** (a) Forward and reverse isomerization (16.9 μM in DMSO) and the insert plot depicts estimation of molar absorption coefficient; (b) Thermal *Z-E* isomerization at 90 ^oC in DMSO (19.3 μM, monitored at λ=318 nm); (c) Forward and reverse photoisomerization (31.5 μM and the insert plot depicts estimation of molar absorption coefficient in H_2O).

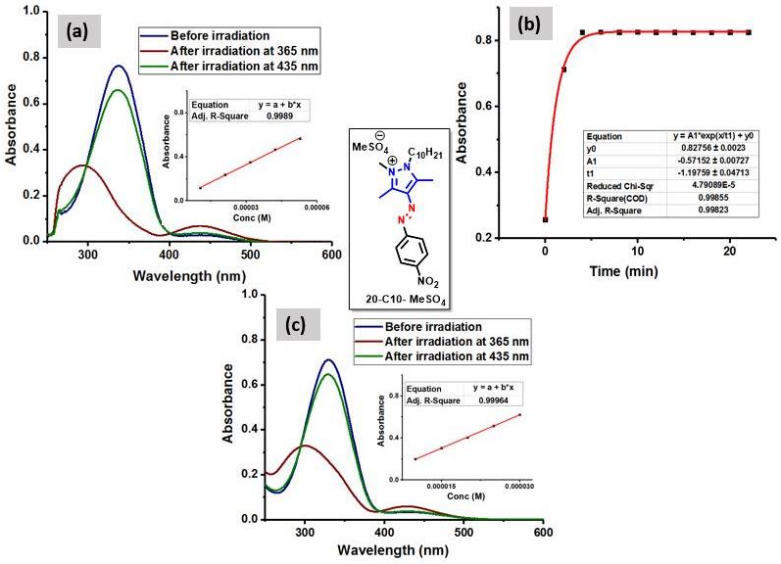

Figure 3B.27. Photoswitching behaviour of **20-C10-MeSO$_4$.** (a) Forward and reverse photoisomerization (71.6 μM in DMSO) and the insert plot depicts estimation of molar absorption coefficient; (b) Thermal *Z-E* isomerization at 90 ^oC in DMSO (80.2 μM monitored at λ=337 nm); (c) Forward and reverse photoisomerization (72.6 μM) and the insert plot depicts estimation of molar absorption coefficient in w H_2O.

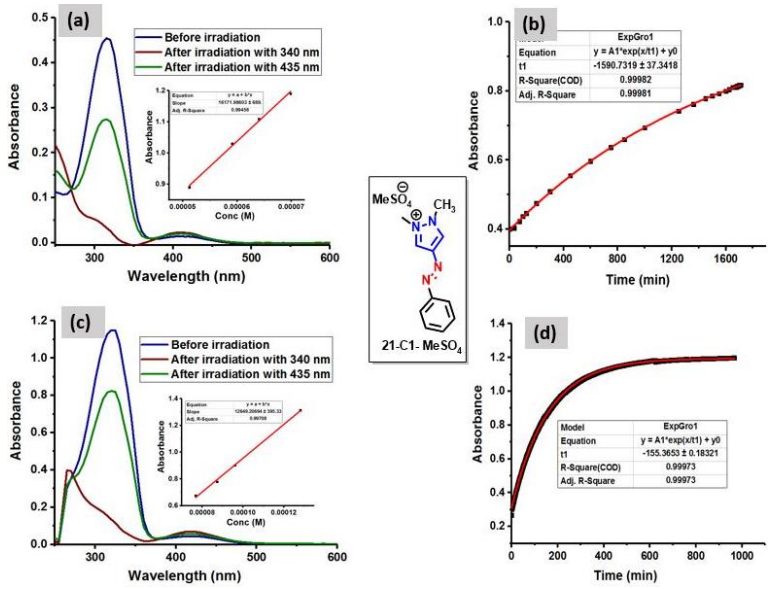

Figure 3B.28. Photoswitching behaviour of **21-C10-MeSO4.** (a) Forward and reverse photoisomerization (28.1 μM in H_2O) and the insert plot depicts estimation molar absorption coefficient; (b) Thermal *Z-E* isomerization at 80 °C in H_2O (50.6 μM, monitored at λ=315 nm); (c) Forward and reverse photoisomerization (28.1 μM) and the insert plot depicts estimation of molar absorption coefficient in DMSO; (d) *Z*-isomer stability at 90 °C in DMSO (94.7 μM, monitored at λ=315 nm).

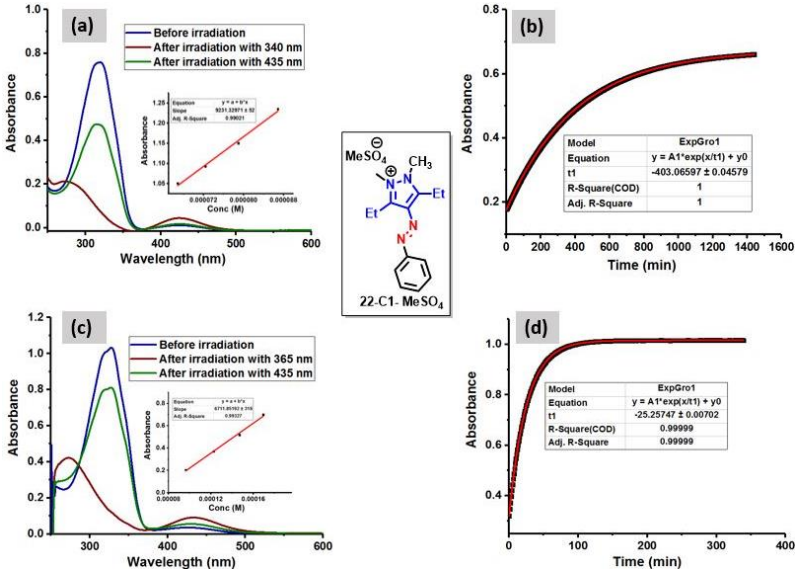

Figure 3B.29. Photoswitching behaviour of **22-C10-MeSO4.** (c) Forward and reverse photoisomerization (82.2 μM in H_2O) and the insert plot depicts estimation of molar absorption coefficient; (b) Thermal *Z-E* isomerization at 80 °C in H_2O (71.6 μM, monitored at λ=320 nm); (c) Forward and reverse photoisomerization (153.8 μM) and the insert plot depicts estimation of molar absorption coefficient in DMSO; (d) Thermal *Z-E* isomerization kinetics at 90 °C in DMSO (151.4 μM, monitored at λ=328 nm).

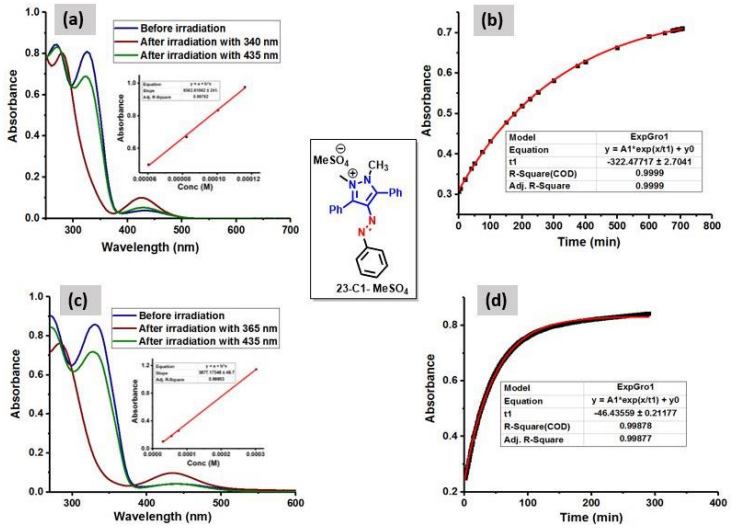

Figure 3B.30. Photoswitching behaviour of **23-C10-MeSO$_4$.** (a) Forward and reverse photoisomerization (94.6 μM in H_2O) and the insert plot depicts estimation of molar absorption coefficient; (b) Thermal *Z-E* isomerization at 80 °C in H_2O (83.0 μM, monitored at λ=325 nm); (c) Forward and reverse photoisomerization and the insert plot depicts estimation of molar absorption coefficient (221.3 μM) in DMSO; (d) Thermal *Z-E* isomerization kinetics at 90 °C in DMSO (217.4 μM, monitored at λ=330 nm).

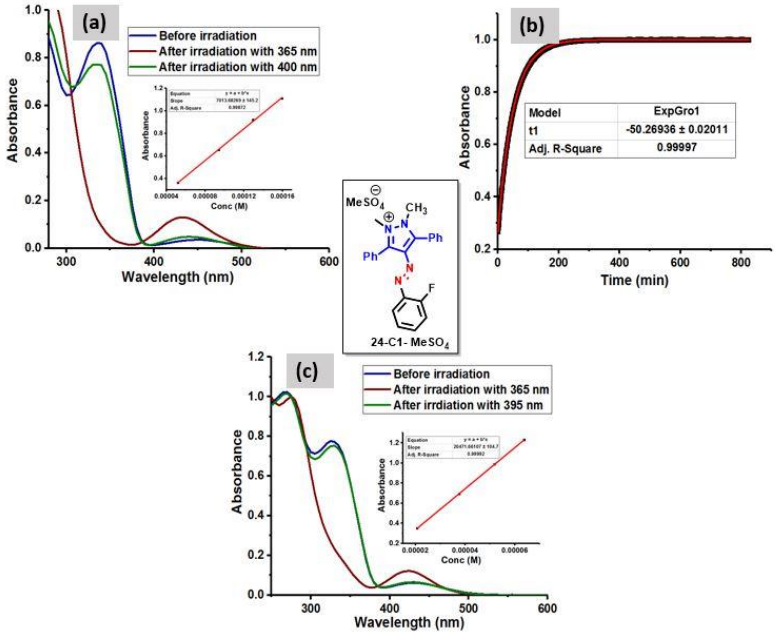

Figure 3B.31. Photoswitching behaviour of **24-C10-MeSO$_4$.** (a) Forward and reverse photoisomerization (122.7 μM in DMSO) and inserted plot depcits estimation of molar absorption coefficient; (b) Thermal *Z-E* isomerization at 90 °C in DMSO (142.7 μM, monitored at λ=340 nm); (c) Forward and reverse photoisomerization (37.9 μM) and the insert plot depicts estimation of molar absorption coefficient in H_2O.

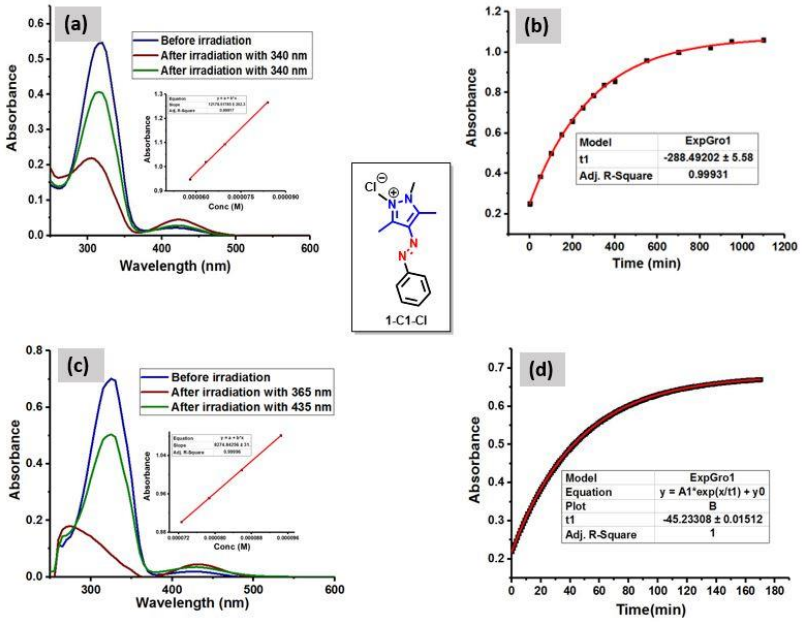

Figure 3B.32. Photoswitching behaviour of **1-C1-Cl.** (a) Forward and reverse photoisomerization (71.4 μM in H_2O) and the insert plot depicts molar absorption coefficient in; (b) Thermal *Z-E* isomerization at 80 °C in H_2O (81.0 μM, monitored at λ=320 nm). (c) Forward and reverse photoisomerization (84.8 μM) and the insert plot depicts estimation of molar absorption coefficient in DMSO; (d) Thermal *Z-E* isomerization stability at 90 °C in DMSO (81.0 μM, monitored at λ=320 nm).

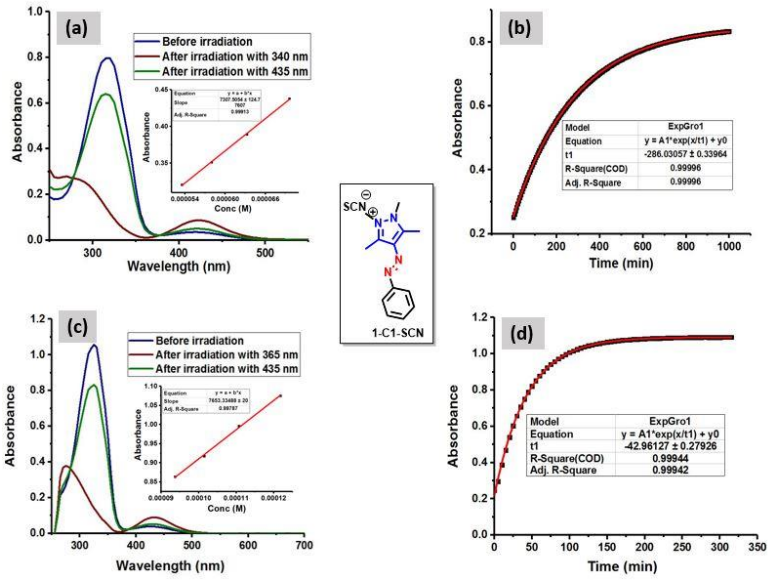

Figure 3B.33. Photoswitching behaviour of **1-C1-SCN.** (a) Forward and reverse photoisomerization (104.1 μM in H_2O) and the insert plot depicts estimation of molar absorption coefficient; (b) Thermal *Z-E* isomerization at 80 °C in H_2O (108.9 μM, monitored at λ=320 nm); (c) Forward and reverse photoisomerization (144.6 μM) and the insert plot depicts estimation of molar absorption coefficient in DMSO; (d) Thermal *Z-E* isomerization stability at 90 °C in DMSO (149.3 μM, monitored at λ=325 nm).

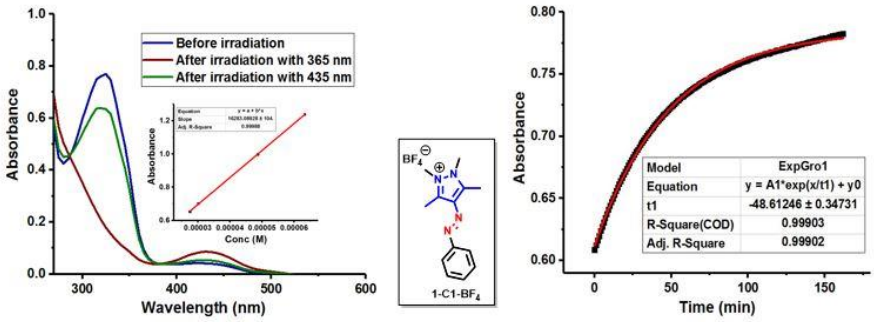

Figure 3B.34. Photoswitching behaviour of **1-C1-BF$_4$.** (a) Forward and reverse photoisomerization (47.3 μM in DMSO) and the insert plot depicts estimation of molar absorption coefficient; (b) Thermal *Z*-*E* isomerization at 90 °C in DMSO (48.1 μM, monitored at λ=325 nm).

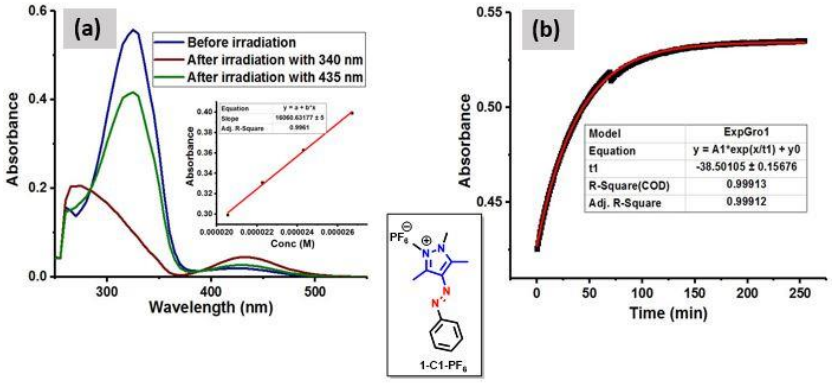

Figure 3B.35. Photoswitching behaviour of **1-C1-PF$_6$.** (a) Forward and reverse photoisomerization (34.7 μM in DMSO) and the insert plot depicts estimation of molar absorption coefficient; (b) Thermal *Z*-*E* isomerization at 90 °C in DMSO (33.3 μM, monitored at λ=325 nm).

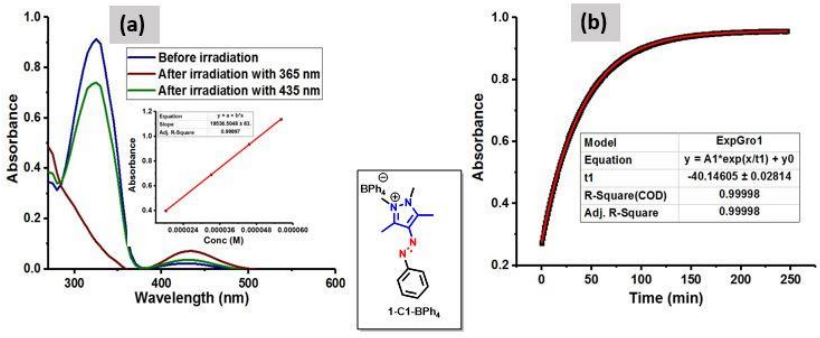

Figure 3B.36. Photoswitching behaviour of **1-C1-BPh$_4$.** (a) Forward and reverse photoisomerization (46.8 μM in DMSO) and the insert plot depicts estimation of molar absorption coefficient; (b) Thermal *Z*-*E* isomerization at 90 °C in DMSO (49.0 μM, monitored at λ=325 nm).

3B.2. Variable temperature kinetics studies and evaluation of activation parameters

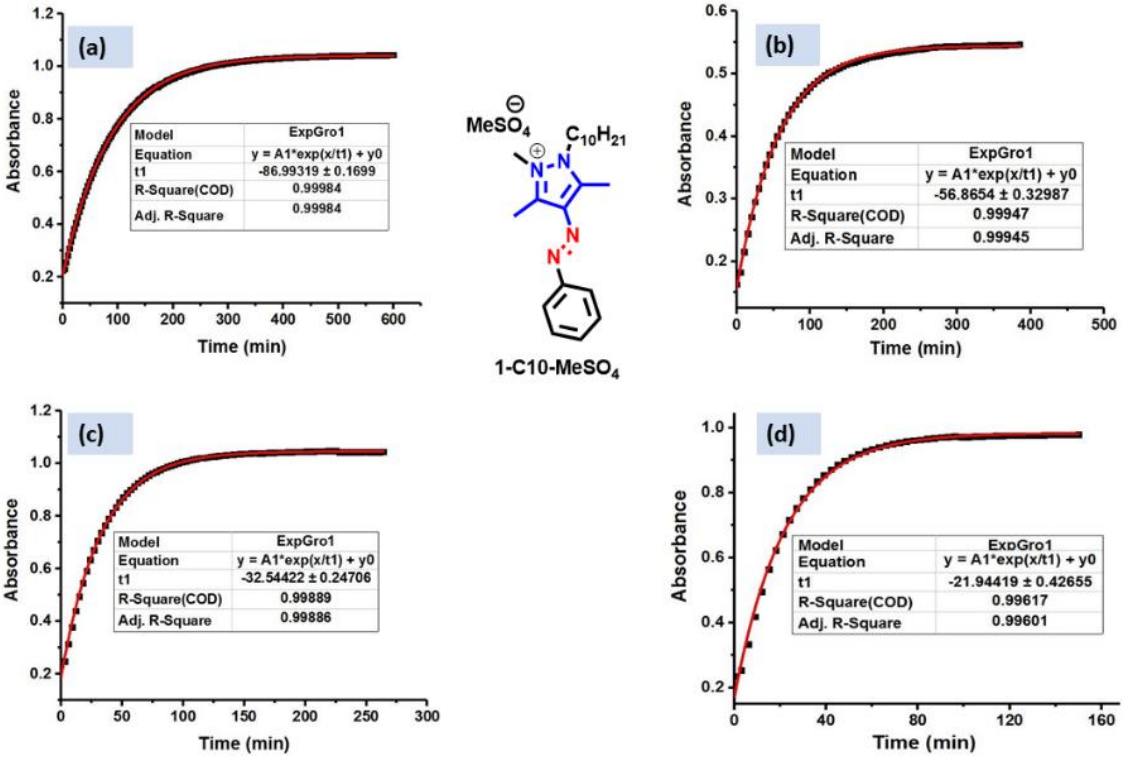

Figure 3B.2.1. Variable temperatures reverse *Z-E* isomerization kinetics of **1-C10-MeSO$_4$** in DMSO at (a) 85 ^oC; (b) 90 ^oC; (c) 95 ^oC, and (d) 100 ^oC.

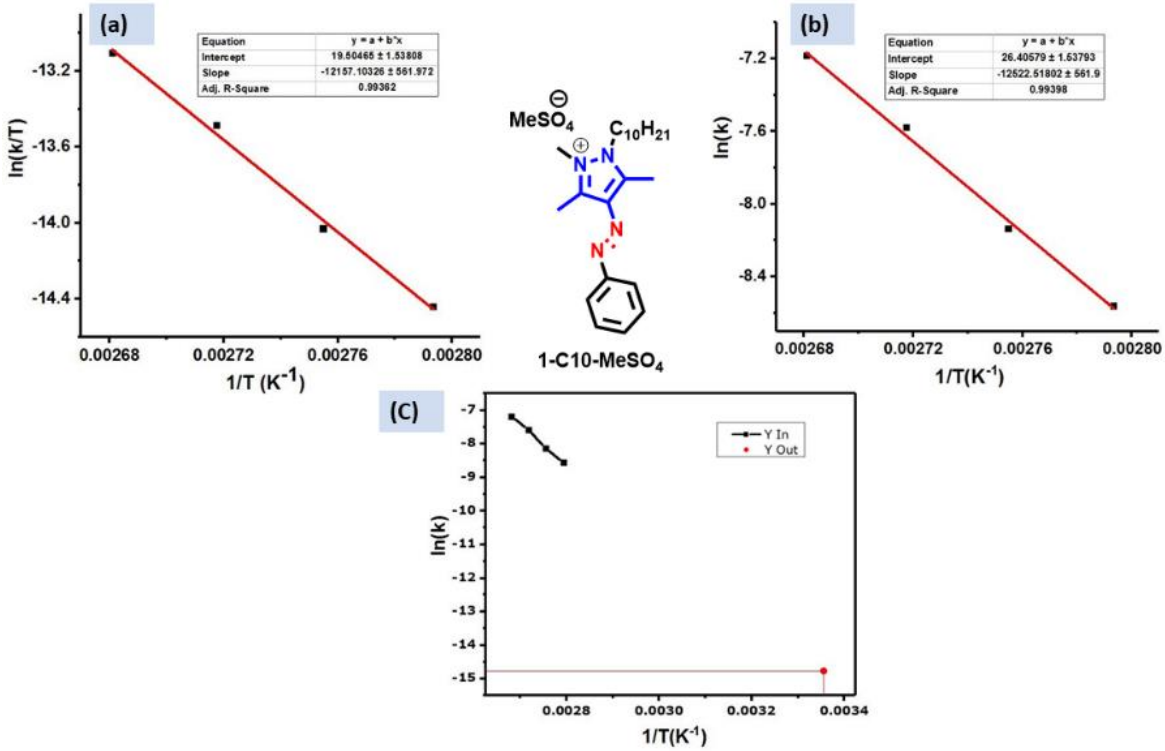

Figure 3B.2.2. (a) Eyring plot, and (b) Arrhenius plot for **1-C10-MeSO$_4$** in DMSO**;** (c) Extrapolation of Arrhenius plot for **1-C10-MeSO$_4$** in DMSO to room temperature (298 K).

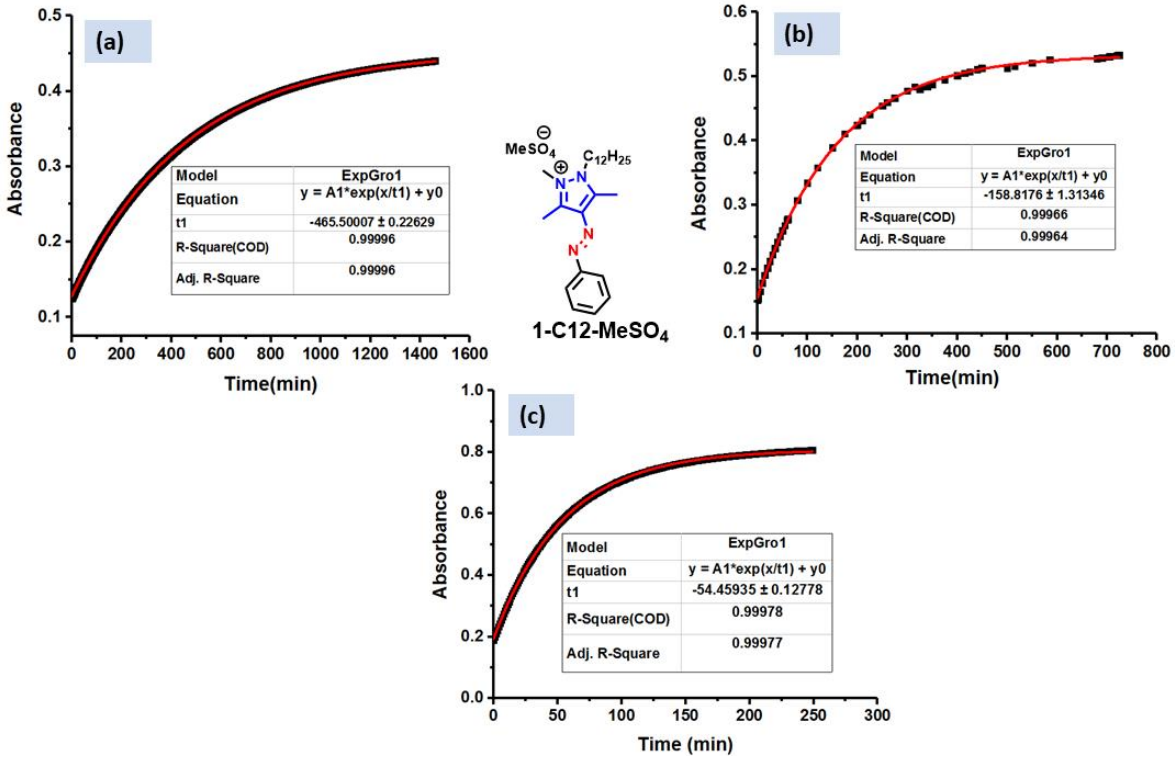

Figure 3B.2.3. Variable temperatures reverse *Z-E* isomerization kinetics of **1-C12-MeSO4** in DMSO at (a) 85 °C; (b) 90 °C; (c) 95 °C, and (d) 100 °C.

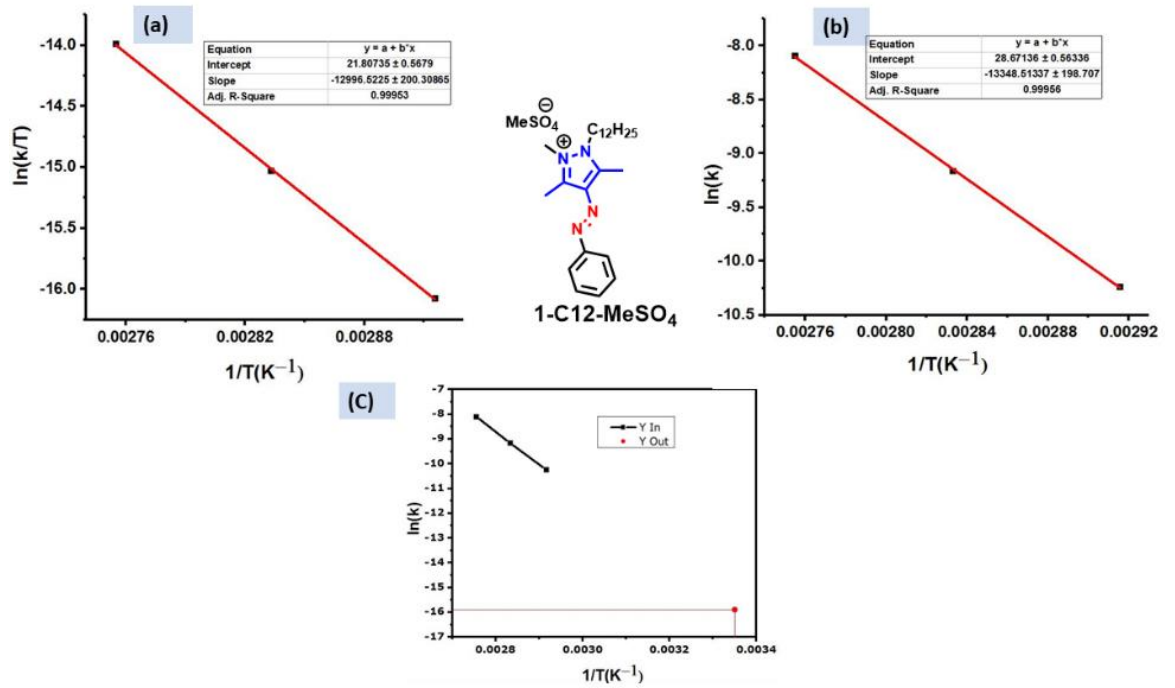

Figure 3B.2.4. (a) Eyring plot, and (b) Arrhenius plot for **1-C12-MeSO4** in DMSO, (c) Extrapolation of Arrhenius plot for **1-C12-MeSO4** in DMSO to room temperature (298 K).

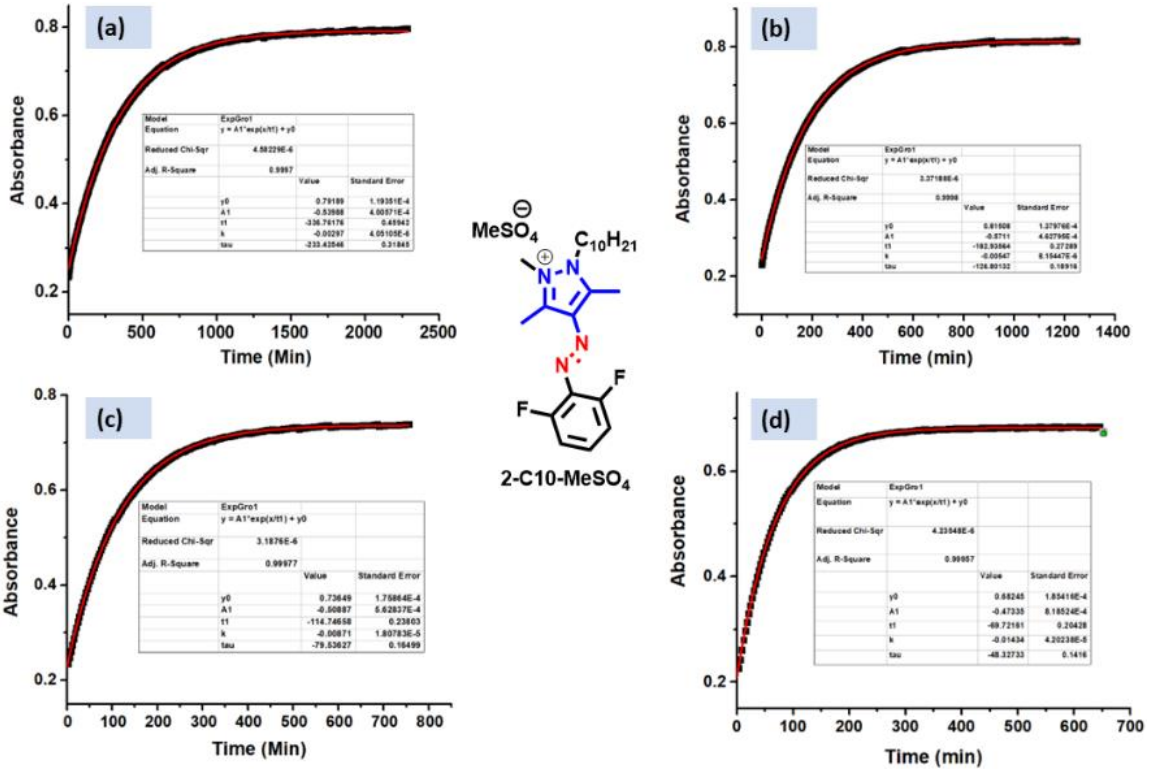

Figure 3B.2.5. Variable temperatures reverse *Z-E* isomerization kinetics of **1-C12-MeSO$_4$** in DMSO**.** (a) 85 ^oC; (b) 90 ^oC; (c) 95 ^oC, and (d) 100 ^oC.

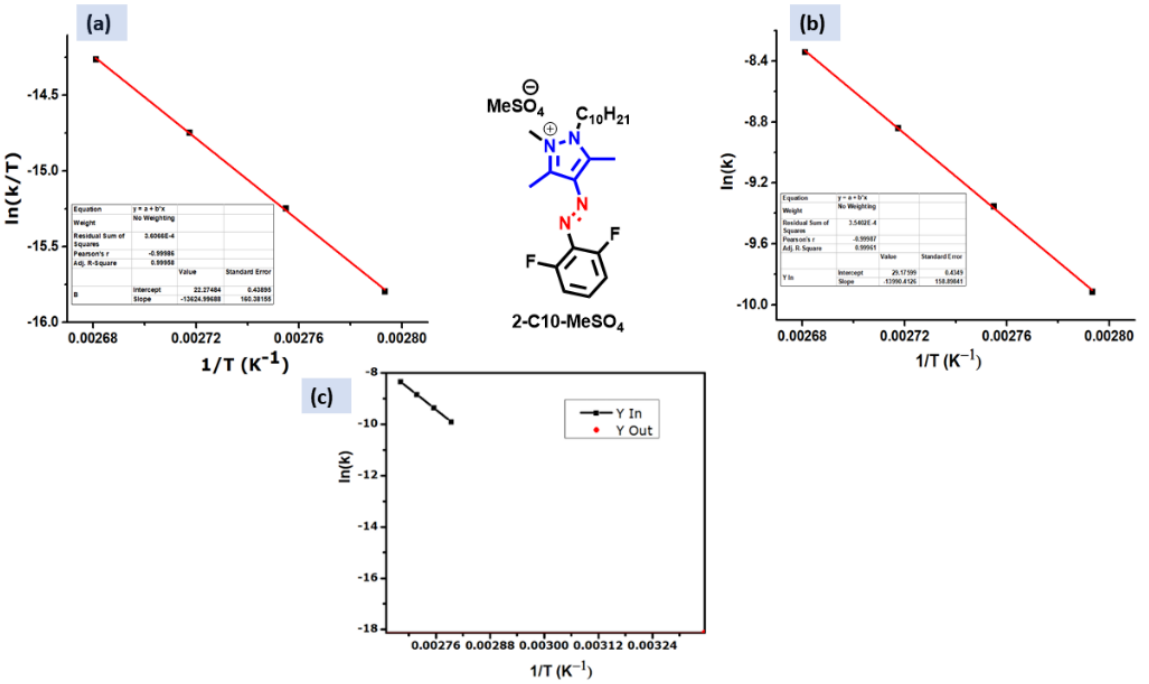

Figure 3B.2.6. (a) Eyring plot, and (b) Arrhenius plot for **1-C12-MeSO$_4$** in DMSO, (c) Extrapolation of Arrhenius plot for **2-C10-MeSO$_4$** in DMSO to room temperature (298 K).

3B.3. Solvent effects and long-term stability

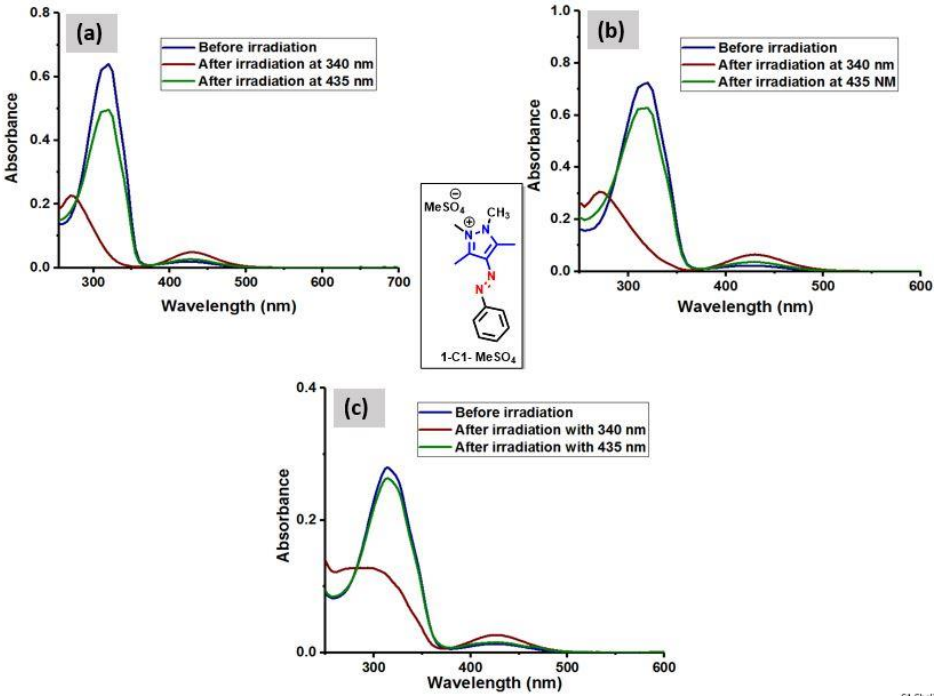

Figure 3B.3.1. Photoswitching behaviour of **1-C1-MeSO$_4$** in (a) MeCN (52.6 μM), (b) MeOH (60.4 μM), and (c) $CHCl_3$ (28.1 μM). {For forward *E*-*Z* photoisomerization: 340 nm (15 min) and for reverse *Z*-*E* photoisomerization: 435 nm (15 min)}.

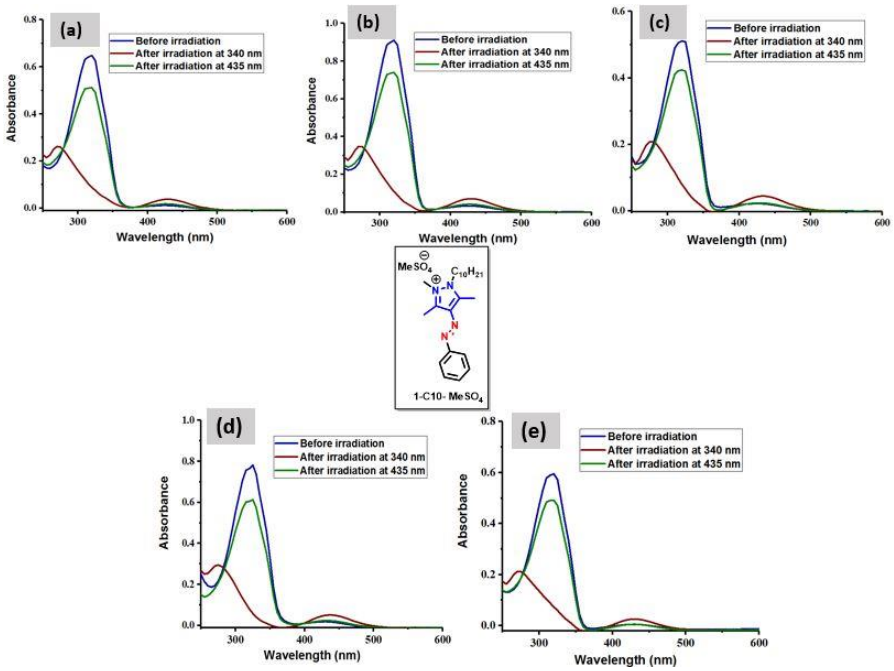

Figure 3B.3.2. Photoswitching behaviour of **20-C10-MeSO$_4$** (a) in MeCN (50.7 μM), (b) in MeOH (63.9 μM), (c) in $CHCl_3$ (43.1 μM), (d) in THF (52.6 μM), (e) in Toluene (47.6 μM). {For forward *E*-*Z* photoisomerization: 340 nm (15 min) and for reverse *Z*-*E* photoisomerization: 435 nm (15 min)}.

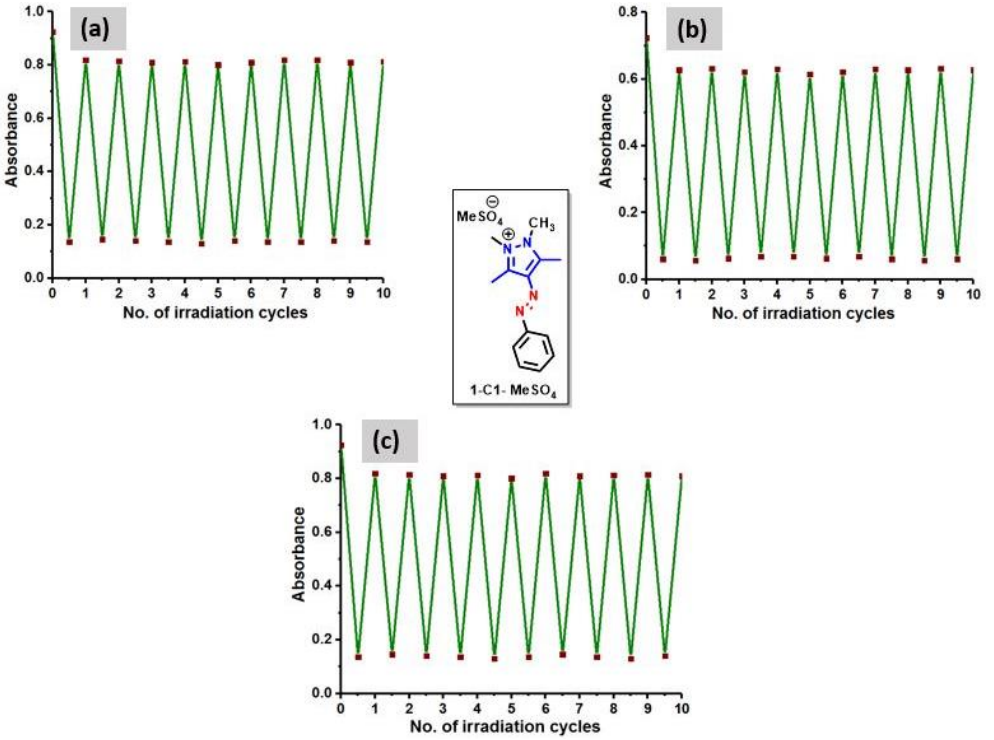

Figure 3B.3.3. Long-term stability of **1-C1-MeSO$_4$** in (a) DMSO (52.3 μM), (b) MeCN (52.6 μM), and (c) MeOH (65.9 μM). {For forward *E*-*Z* photoisomerization: 340 nm (15 min) or 365 nm (2 min, in DMSO only) and for reverse *Z*-*E* photoisomerization: 435 nm (15 min); Both the steps were alternatively performed over 10 cycles}.

3B.4. Photoisomerization quantum yields

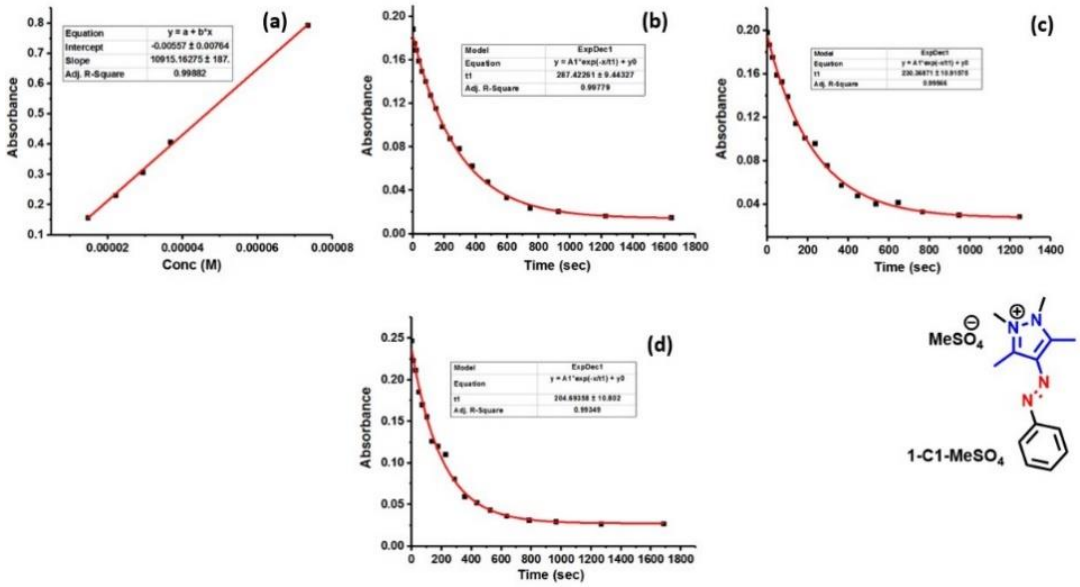

Figure 3B.4.1. UV-Vis studies for quantum yield of derivative **1-C1-MeSO4** in MeCN (a) Estimation of molar absorption coefficient at 340 nm; (b), (c), and (d) Kinetics plot of forward isomerization at 340 nm irradiation.

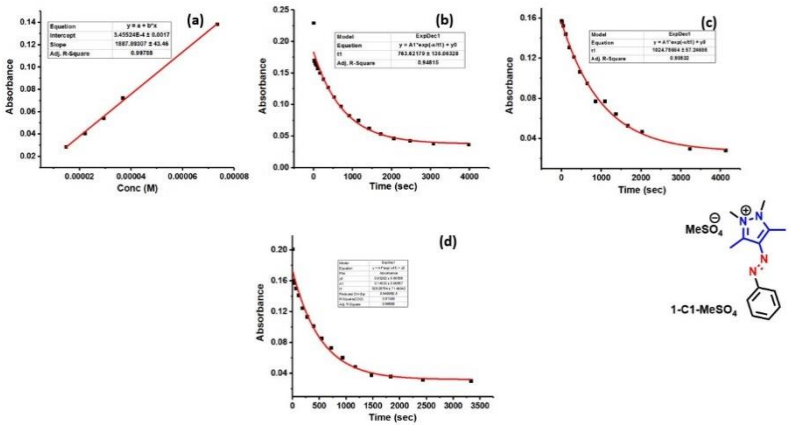

Figure 3B.4.2. UV-Vis studies for quantum yield of derivative **1-C1-MeSO4** in MeCN (a) Estimation of molar absorption coefficient at 355 nm; (b), (c), and (d) Kinetics plot of forward isomerization at 355 nm irradiation.

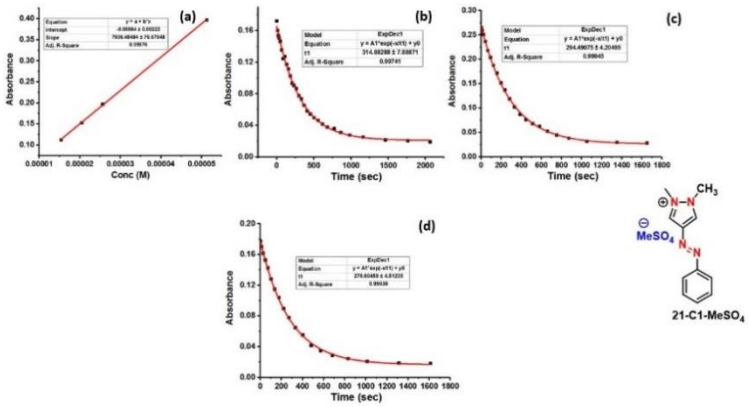

Figure 3B.4.3. UV-Vis studies for quantum yield of derivative **21-C1-MeSO4** in MeCN (a) Estimation of molar absorption coefficient at 340 nm; (b), (c), and (d) Kinetics plot of forward isomerization at 340 nm irradiation.

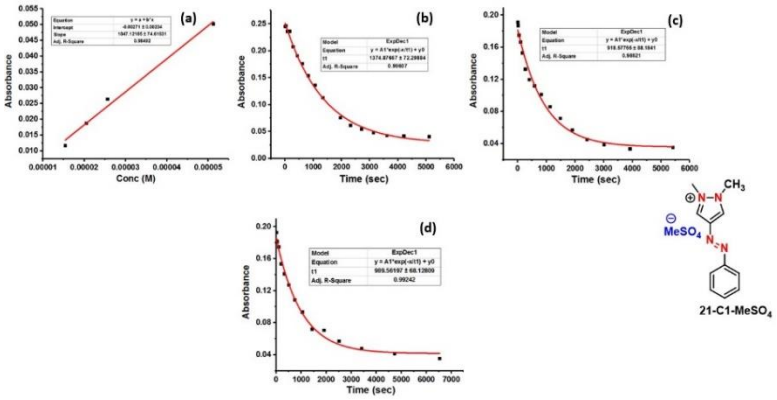

Figure 3B.4.4. UV-Vis studies for quantum yield of derivative **1-C1-MeSO4** in MeCN (a) Estimation of molar absorption coefficient at 355 nm; (b), (c), and (d) Kinetics plot of forward isomerization at 355 nm irradiation.

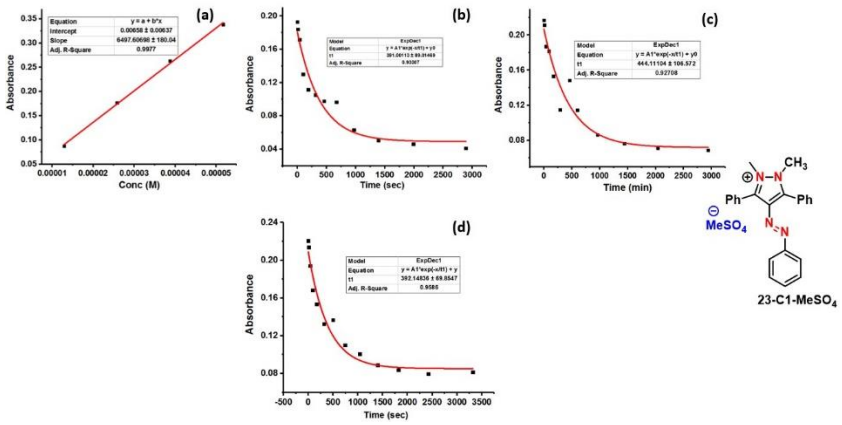

Figure 3B.4.5. UV-Vis studies for quantum yield of derivative **23-C1-MeSO4** in MeCN (a) Estimation of molar absorption coefficient at 355 nm; (b), (c), and (d) Kinetics plot of forward isomerization at 355 nm irradiation.

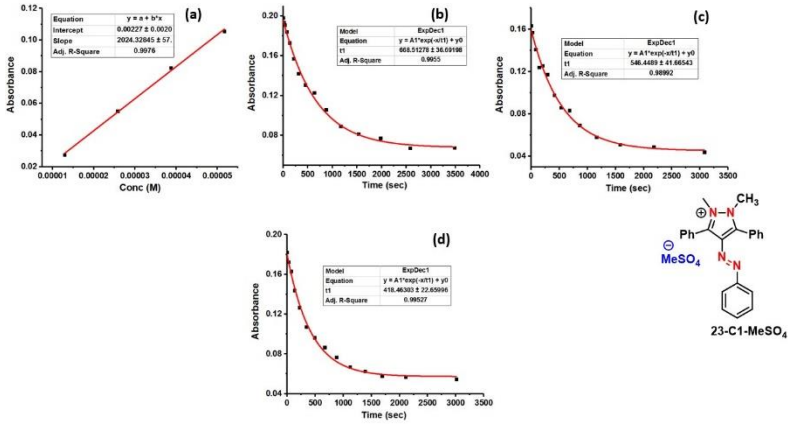

Figure 3B.4.6. UV-Vis studies for quantum yield of derivative **23-C1-MeSO4** in MeCN (a) Estimation of molar absorption coefficient at 365 nm; (b), (c), and (d) Kinetics plot of forward isomerization at 365 nm irradiation.

3B.5. Kinetics studies: ^{1}H-NMR Spectroscopy

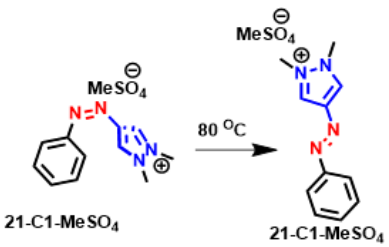

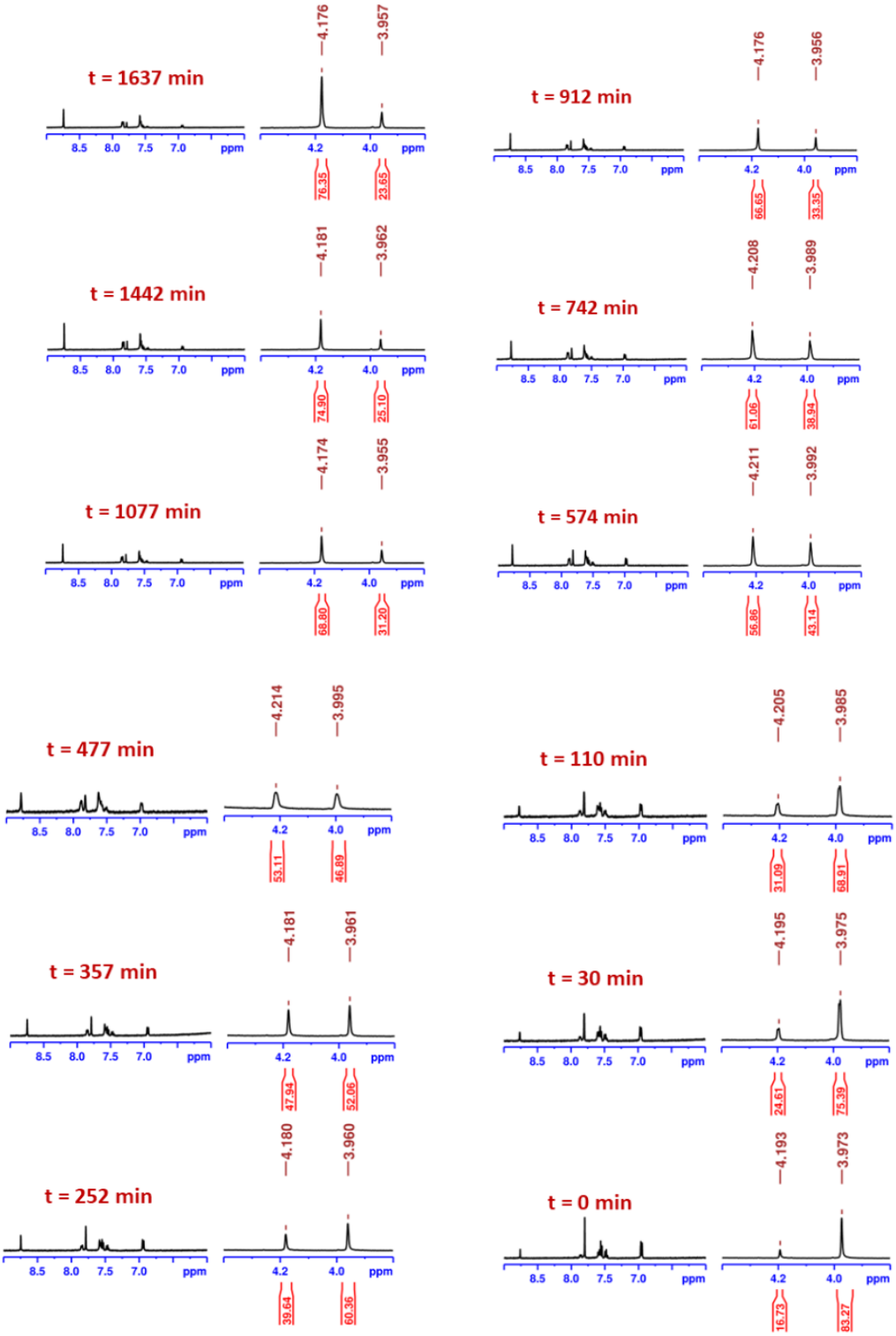

Figure 3B.5.1. Thermal reverse (*Z*-*E*) isomerization kinetics of **21-C1-MeSO$_4$** in D_2O (27.8 mM) at 80 °C followed by ^{1}H-NMR spectroscopy (The normalized integral values corresponding to the *N*-methyl protons were used for deducing the composition of *E*- and *Z*-isomers; The corresponding time of measurements are indicated.).

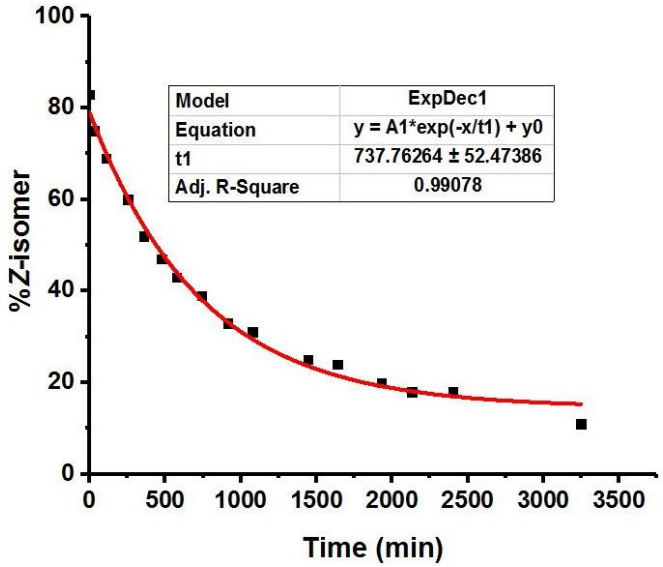

Figure 3B.5.2. Thermal reverse (*Z*-*E*) isomerization kinetics of **21-C1-MeSO$_4$** in D_2O (27.8 mM) at 80 ^oC fitted to first order decay with an exponential fit.

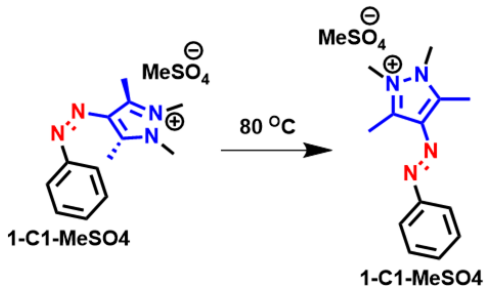

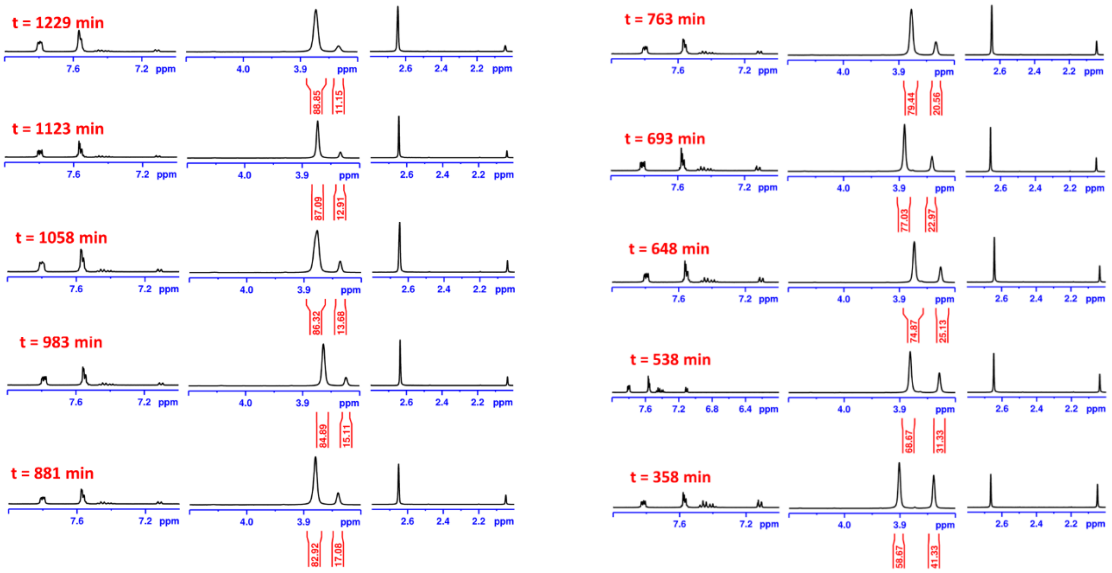

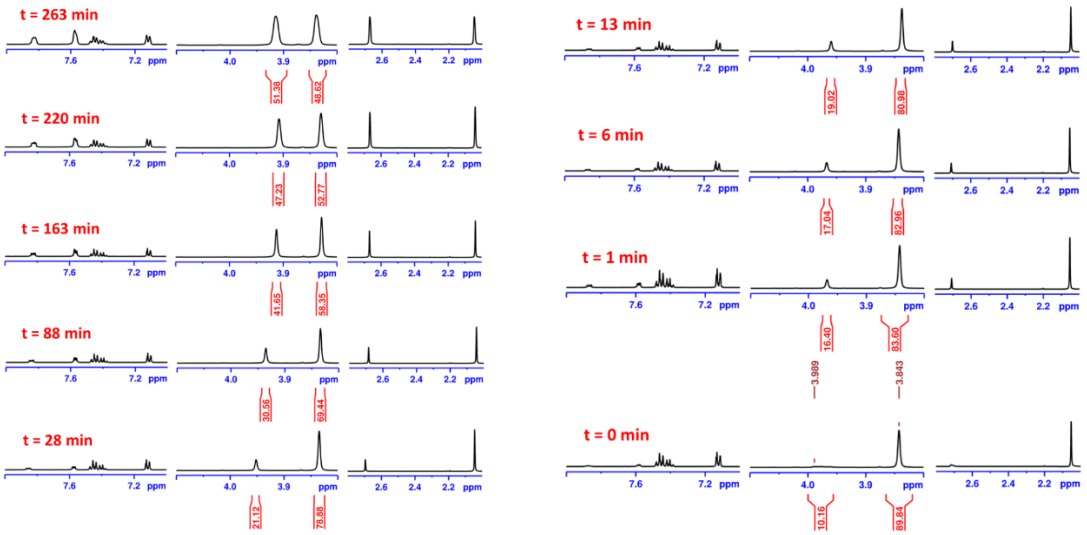

Figure 3B.5.3. Thermal reverse (*Z*-*E*) isomerization kinetics of **1-C1-MeSO$_4$** in D_2O (25.4 mM) at 80 ^oC followed by ^{1}H-NMR spectroscopy. (The normalized integral values corresponding to the *N*-methyl protons were used for deducing the composition of *E*- and *Z*-isomers; The corresponding time of measurements are indicated.).

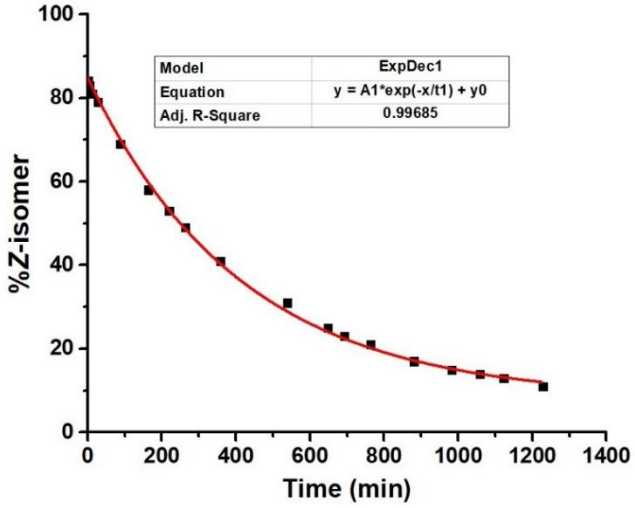

Figure 3B.5.4. ^{1}H NMR kinetics study fitted to first order decay of **21-C1-MeSO$_4$** at 80 ^oC (25.4 mM).

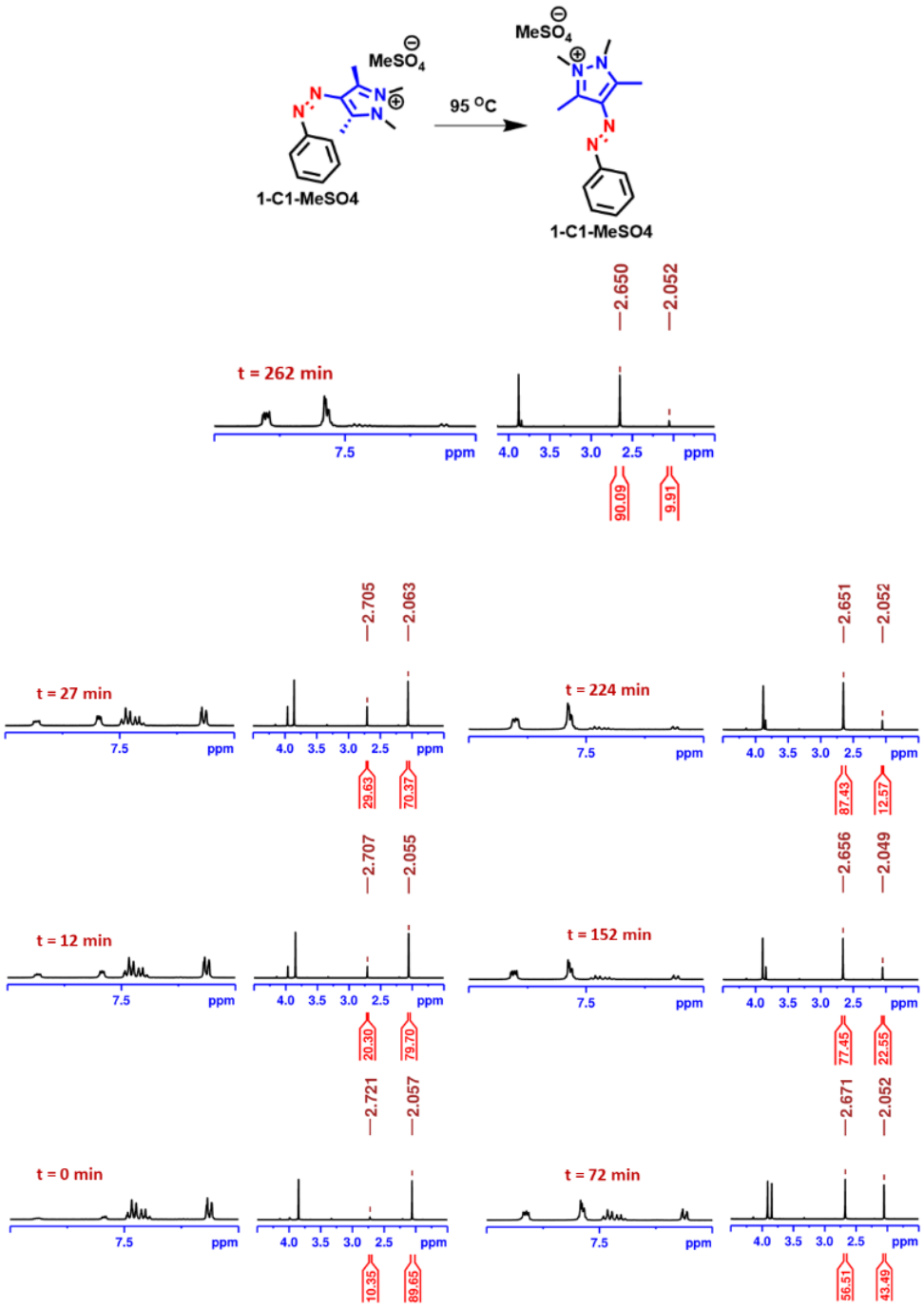

Figure A5.5. Thermal reverse (*Z*-*E*) isomerization kinetics of **1-C1-MeSO₄** in D_2O (25.4 mM) at 95 °C followed by ^{1}H-NMR spectroscopy. (The normalized integral values corresponding to the *N*-methyl protons were used for deducing the composition of *E*- and *Z*-isomers; The corresponding time of measurements are indicated.)

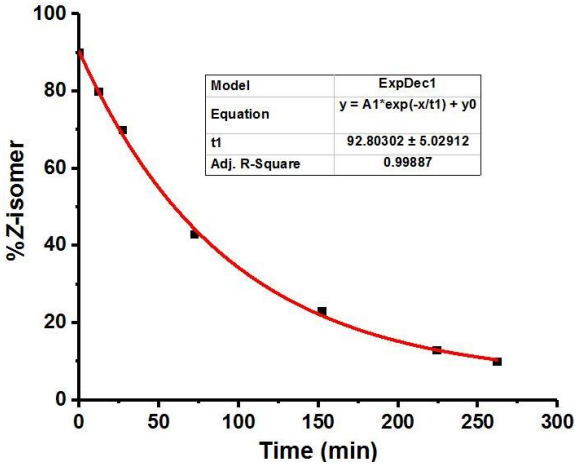

Figure 3B.5.6. ^{1}H NMR kinetics study fitted to first order decay of **1-C1-MeSO$_4$** at 95 ^{o}C (25.4 mM).

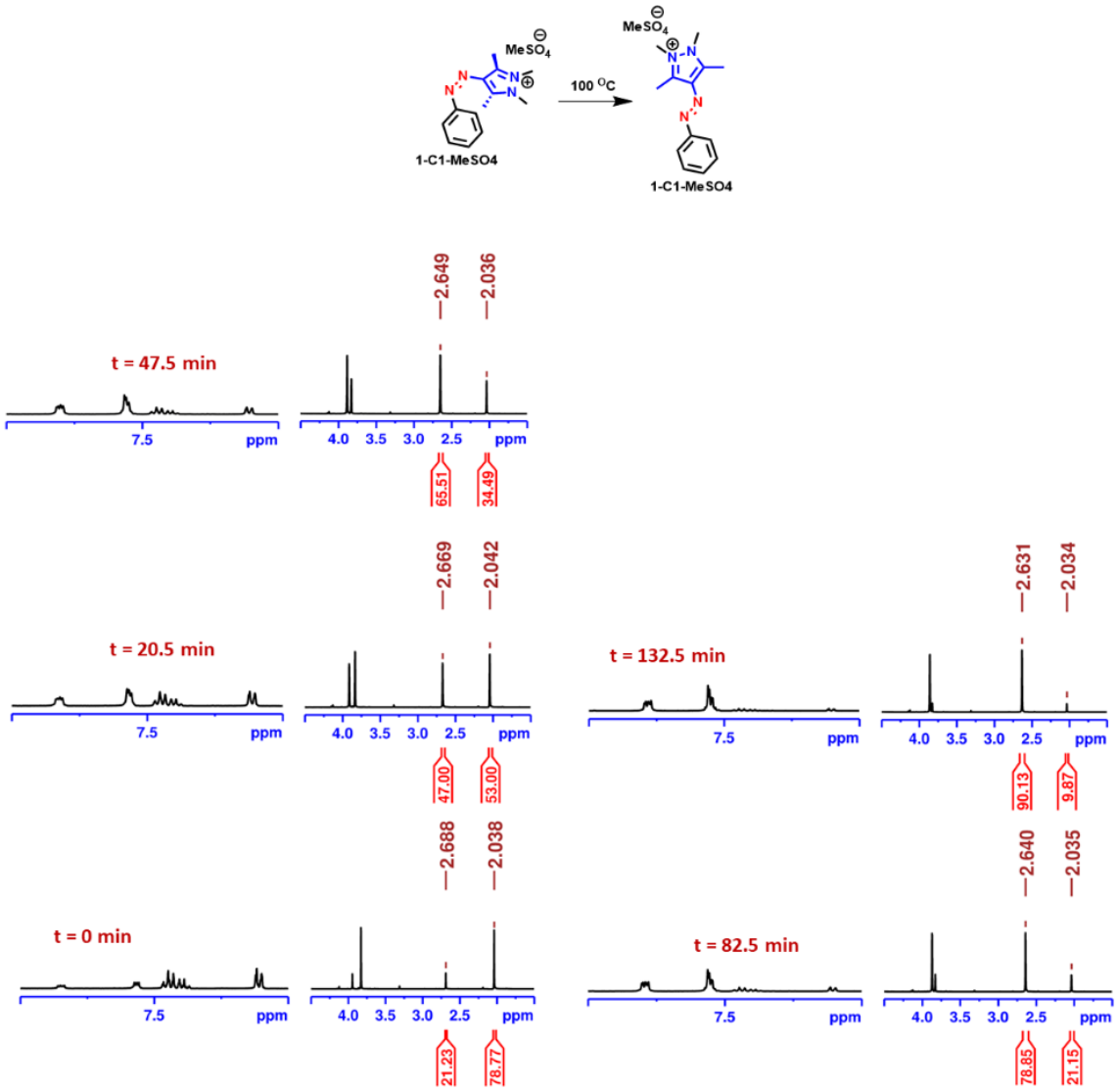

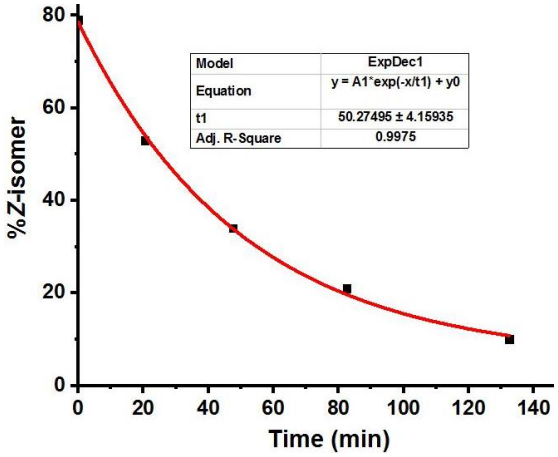

Figure 3B.5.7: Thermal reverse (*Z*-*E*) isomerization kinetics of **1-C1-MeSO$_4$** in D_2O (25.4 mM) at 100 ^oC followed by ^{1}H-NMR spectroscopy. (The normalized integral values corresponding to the *N*-methyl protons were used for deducing the composition of *E*- and *Z*-isomers; The corresponding time of measurements are indicated.).

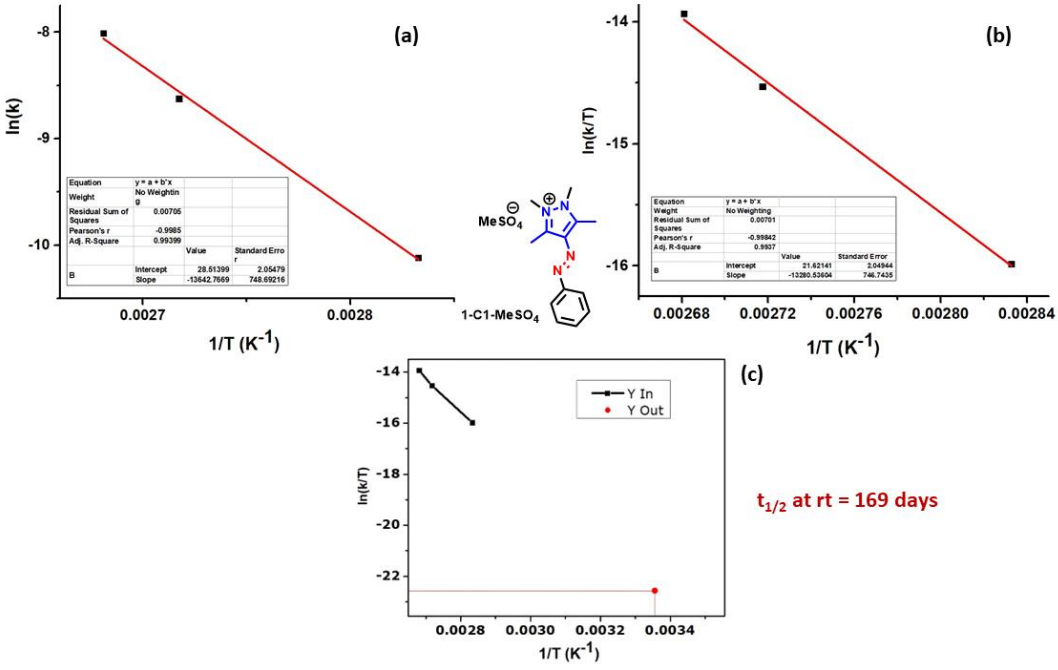

Figure 3B.5.8: (a) Arrhenius plot for **1-C1-MeSO$_4$** in D_2O; (b) Eyring plot; (c) Extrapolation of Erying plot for **1-C1-MeSO$_4$** in D_2O to room temperature (298 K).

Table 3B.5.1. Activation parameters and room temperature rate constant for the *Z*-*E* thermal reverse isomerization of **1-C1-MeSO$_4$** in DMSO

S.No.	**Compound**	***E**$_a$* (kJ/mol)	**$\Delta H^{\ddagger}$** (kJ/mol)	**$\Delta S^{\ddagger}$** (J/K mol)	**$\Delta G^{\ddagger}$** (kJ/mol)	**Rate constants, k (s^{-1})**
1.	**1-C1-MeSO$_4$**	113.4 ± 6.2	110.4 ± 6.2	-17.8 ± 17.0	118.7 ± 11.3	4.7 x 10^{-8}

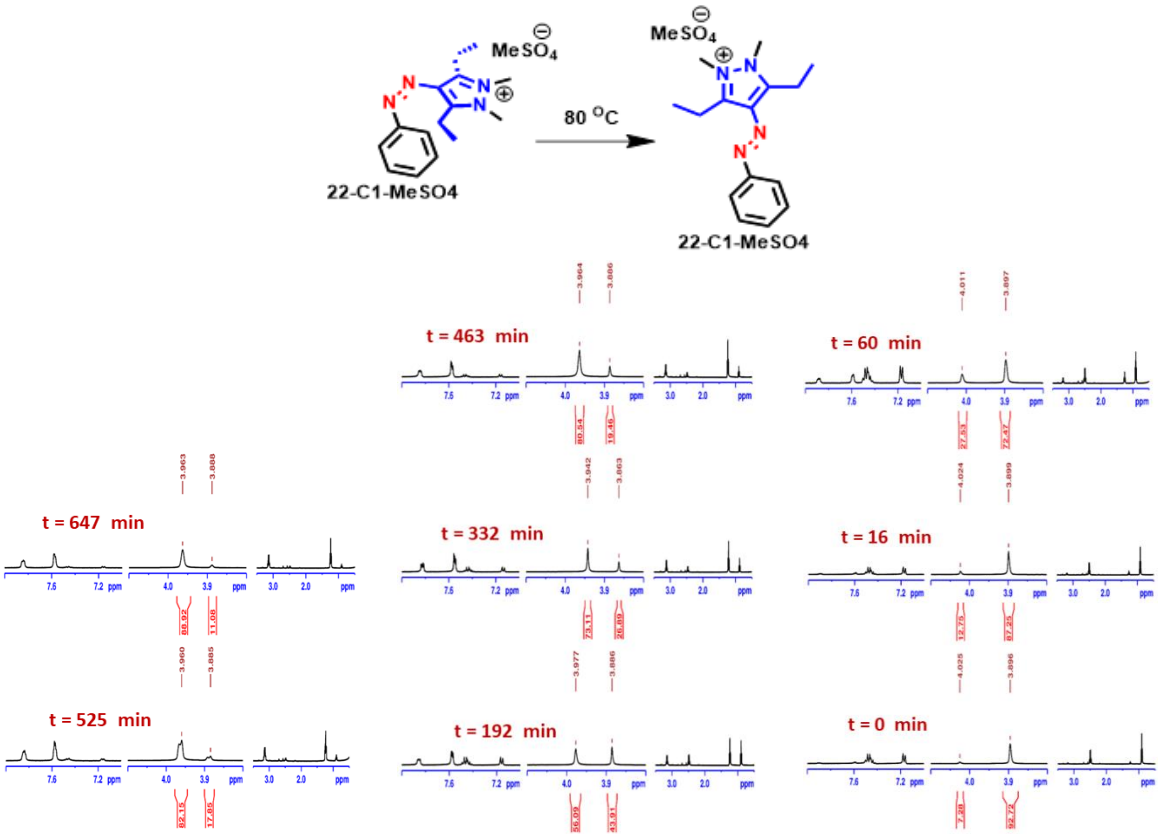

Figure 3B.5.9. Thermal reverse (Z-E) isomerization kinetics of **22-C1-MeSO$_4$** in D_2O (23.8 mM) at 80 °C followed by ^{1}H-NMR spectroscopy. (The normalized integral values corresponding to the *N*-methyl protons were used for deducing the composition of *E*- and *Z*-isomers; The corresponding time of measurements are indicated.)

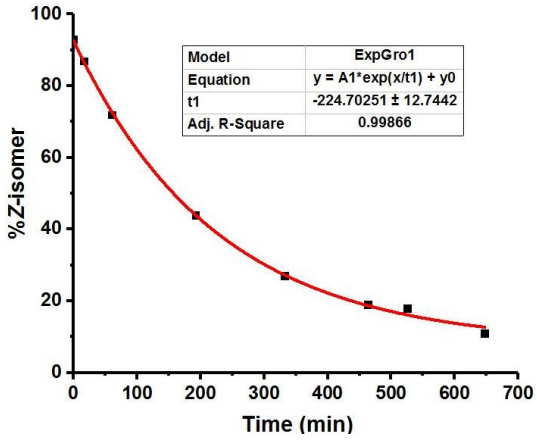

Figure 3B.5.10. ^{1}H NMR kinetics study fitted to first order decay of **22-C1-MeSO$_4$** at 80 °C (23.8 mM).

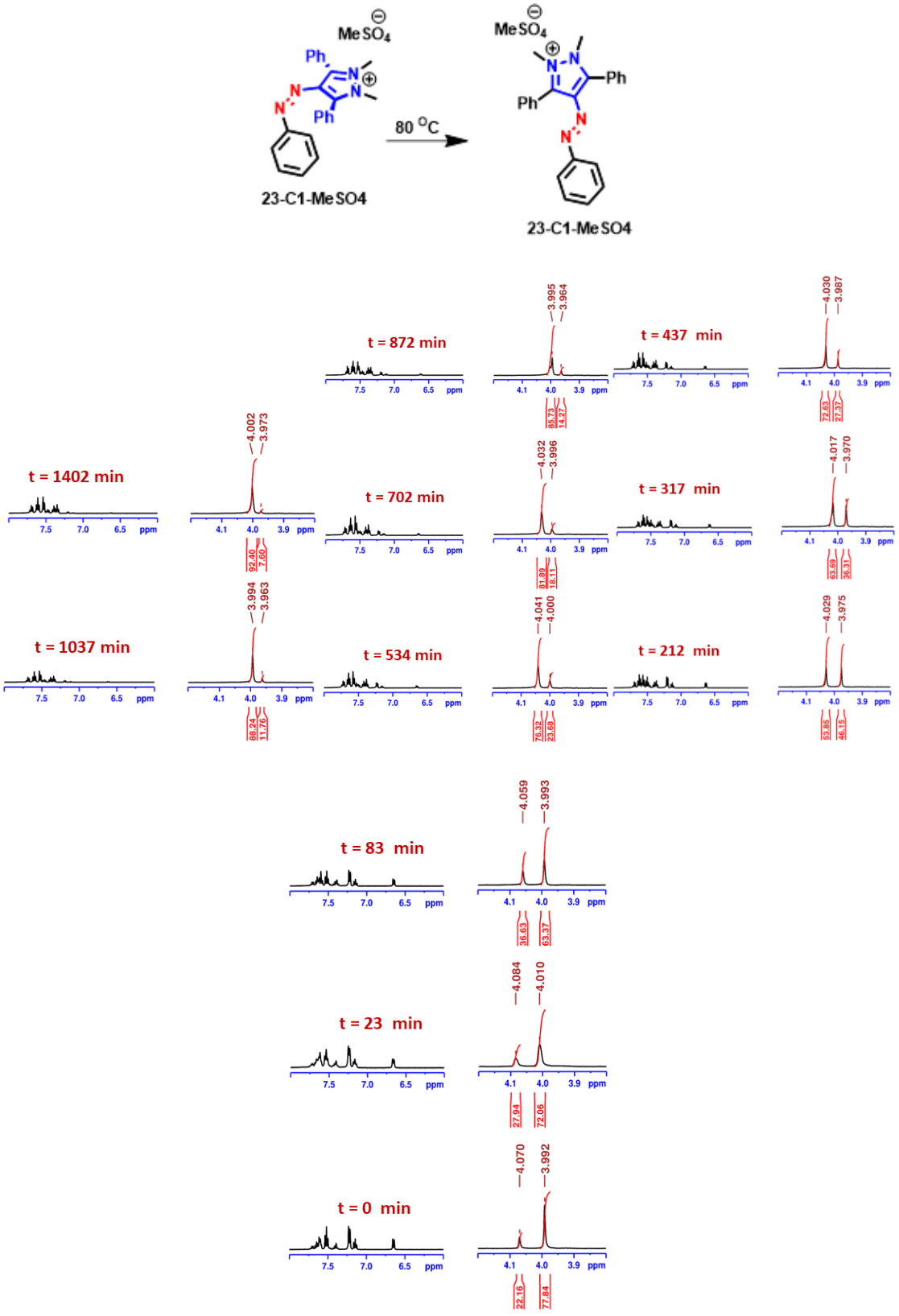

Figure 3B.5.11. Thermal reverse (*Z*-*E*) isomerization kinetics of **23-C1-MeSO$_4$** in D_2O (19.5 mM) at 80 °C followed by ^{1}H-NMR spectroscopy. (The normalized integral values corresponding to the *N*-methyl protons were used for deducing the composition of *E*- and *Z*-isomers; The corresponding time of measurements are indicated.)

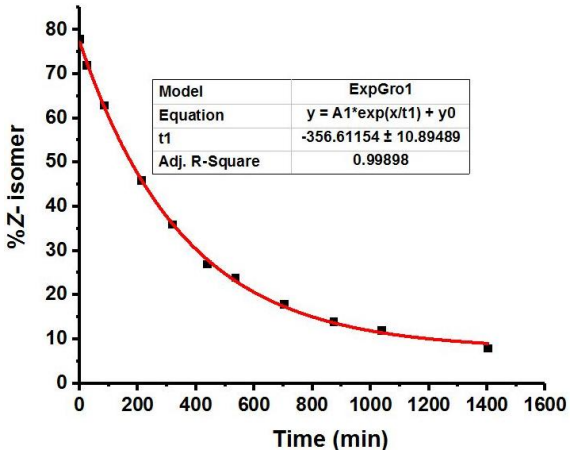

Figure 3B.5.12. ^{1}H NMR kinetics study of **23-C1-MeSO$_4$** at 80 ^{o}C (19.5 mM)

Table 3B.5.2.

S.No.	Compound	Temperature (^{o}C)	Rate constant (10^{-2} min^{-1})
1.	**1-C1-MeSO$_4$**	80	0.2 ± 0.01
2.	**21-C1-MeSO$_4$**	80	0.1 ± 0.01
3.	**22-C1-MeSO$_4$**	80	0.4 ± 0.01
4.	**23-C1-MeSO$_4$**	80	0.3 ± 0.01

3B.6. Quantification of photoisomers: ^{1}H NMR spectroscopy

Table 3B.6.1. The PSS composition of *E*- and *Z*- isomers of AAPIPs at the forward and reverse photoisomerization steps estimated by ^{1}H-NMR spectroscopy.

Compound	Wavelength (nm)	%*E*	%*Z*	Conc. (mM)	Protons for integration
1-C1-MeSO$_4$	340	3	97	25.4	*N-Me*
	435	79	21		
1-C2-MeSO$_4$	340	2	98	27.2	*N-Me*
	435	76	24		
1-C4-MeSO$_4$	340	11	89	18.5	*N-Me*
	435	75	25		
1-C6-MeSO$_4$	340	14	86	19.1	*N-Me*
	435	76	24		
1-C8-MeSO$_4$	340	12	88	16.2	*N-Me*
	435	76	24		
1-C10-MeSO$_4$	340	13	87	16.4	*N-Me*
	435	72	28		
1-C12-MeSO$_4$	340	7	93	17.3	*N-Me*
	435	81	19		

1-C18-MeSO$_4$	340	10	90	8.1	*N-Me*
	435	76	24		
2-C1-MeSO$_4$	340	6	93	20.1	*N-Me*
	435	76	31		
3-C1-MeSO$_4$	340	12	88	22.4	*N-Me*
	435	77	23		
4-C1-MeSO$_4$	340	7	93	20.1	*N-Me*
	435	80	20		
5-C1-MeSO$_4$	340	7	93	14.6	*N-Me*
	435	75	25		
6-C1-MeSO$_4$	340	6	94	24.1	*N-Me*
	435	69	31		
7-C1-MeSO$_4$	340	15	85	19.7	*N-Me*
	435	78	22		
8-C1-MeSO$_4$	365	24	76	20.1	*N-Me*
	490	80	20		
9-C1-MeSO$_4$	340	13	87	17.3	*O-Me*
	435	51	49		
10-C1-MeSO$_4$	340	6	84	16.1	*O-Me*
	435	69	31		
11-C1-MeSO$_4$	365	6	94	18.1	*O-Me*
	490	89	11		
12-C1-MeSO$_4$	340	9	91	21.2	*N-Me*
	435	77	23		
13-C1-MeSO$_4$	340	5	95	13.1	*N-Me*
	435	75	25		
14-C1-MeSO$_4$	340	2	98	16.4	*N-Me*
	435	70	30		
15-C1-MeSO$_4$	340	3	97	13.7	*N-Me*
	435	77	23		
16-C1-MeSO$_4$	340	3	97	14.6	*N-Me*
	435	74	26		
17-C1-MeSO$_4$	340	19	81	6.1	*N-Me*
	435	74	26		
18-C1-MeSO$_4$	340	a	a	a	*a*
	435	a	a		
19-C1-MeSO$_4$	340	68	32	18.1	*N-Me*
	435	70	30		
20-C1-MeSO$_4$	340	38	62	7.1	*N-Me*

	435	b	b		
21-C1-MeSO$_4$	340	12	88	27.8	*N-Me*
	435	67	33		
22-C1-MeSO$_4$	340	7	93	23.8	*N-Me*
	435	78	22		
23-C1-MeSO$_4$	365	15	85	19.5	*N-Me*
	435	77	23		
24-C1-MeSO$_4$	365	11	89	18.1	*N-Me*
	435	24	76		
1-C1-Cl	340	10	90	25.3	*N-Me*
	435	73	27		
1-C1-SCN	340	13	87	23.1	*N-Me*
	435	75	25		
1-C1-BF$_4$[c]	340	10	90	27.4	*N-Me*
	435	76	24		
1-C1-PF$_6$[c]	340	10	90	20.2	*N-Me*
	435	25	75		
1-C1-BPh$_4$[c]	340	11	89	17.7	*N-Me*
	435	75	25		

Blue-shaded rows represent forward (*E*-*Z*) photoisomerization steps, whereas the rows without shading represent that of reverse (*Z*-*E*) photoisomerization step; [a]No photoisomerization; [b]Not determined due to fast thermal relaxation; [c]Photoswitching studies performed in DMSO-d$_6$.

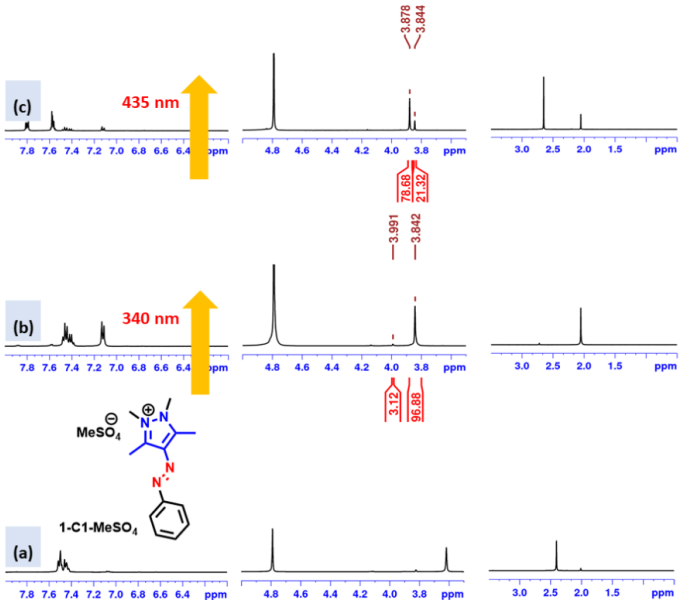

Figure 3B.6.1. Estimation of PSS composition using ^{1}H NMR spectroscopy of **1-C1-MeSO$_4$** (D$_2$O, 25.4 mM). (a) before irradiation; (b) after irradiation at 340 nm (2 h); (c) after irradiation at 435 nm (45 min). (Normalized integral values of selected protons are indicated for *E*- and *Z*-isomers.)

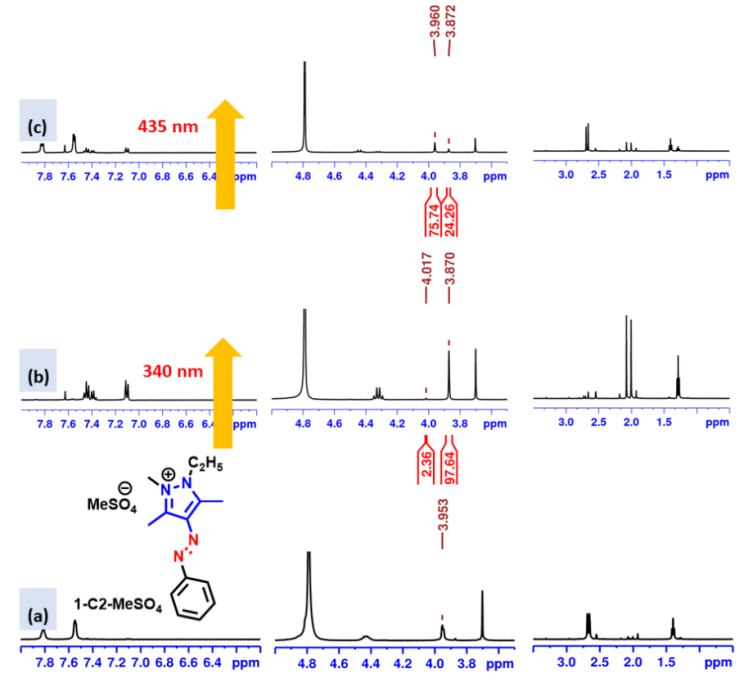

Figure 3B.6.2. Estimation of PSS composition using ^{1}H NMR spectroscopy of **1-C2-MeSO$_4$** (D_2O, 27.2 mM). (a) before irradiation; (b) after irradiation at 340 nm (2 h); (c) after irradiation at 435 nm (45 min); (Normalized integral values of selected protons are indicated for *E*- and *Z*-isomers.)

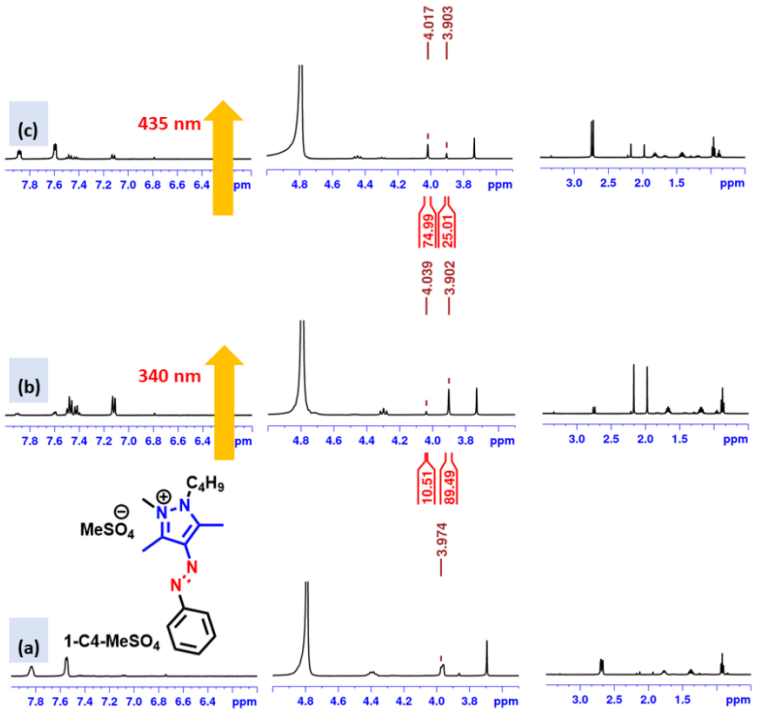

Figure 3B.6.3. Estimation of PSS composition using ^{1}H NMR spectroscopy of **1-C4-MeSO$_4$** (D_2O, 18.5 mM) (a) before irradiation; (b) after irradiation at 340 nm (2 h); (c) after irradiation at 435 nm (45 min); (Normalized integral values of selected protons are indicated for *E*- and *Z*-isomers.)

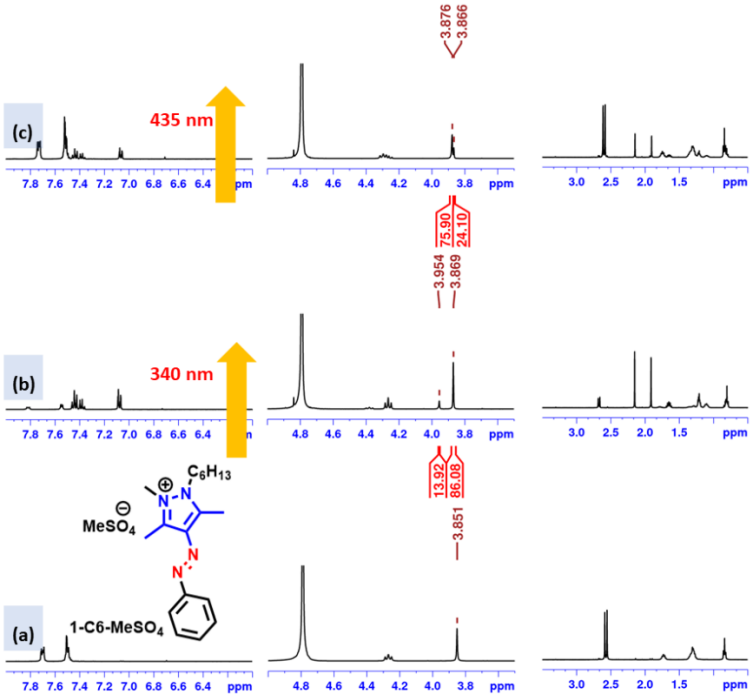

Figure 3B.6.4. Estimation of PSS composition using ^{1}H NMR spectroscopy of **1-C6-MeSO$_4$** (D_2O, 19.1 mM) (a) before irradiation; (b) after irradiation at 340 nm (2 h); (c) after irradiation at 435 nm (45 min); (Normalized integral values of selected protons are indicated for *E*- and *Z*-isomers.)

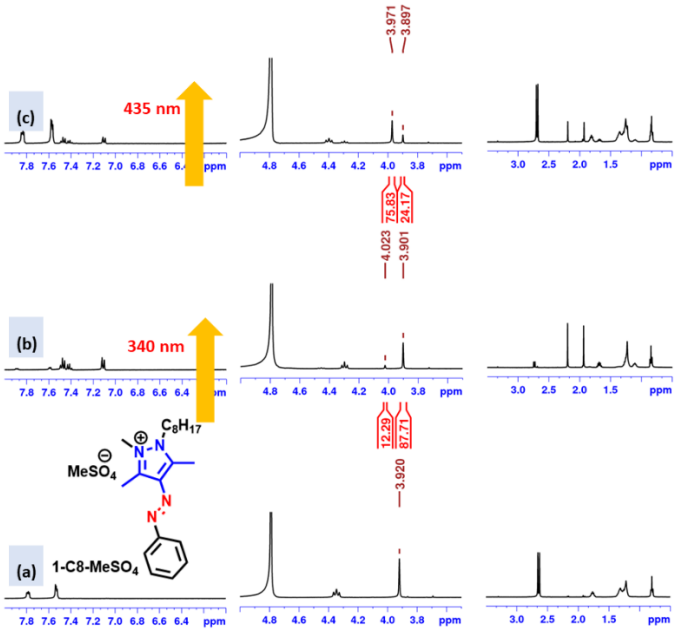

Figure 3B.6.5. Estimation of PSS composition using ^{1}H NMR spectroscopy of **1-C8-MeSO$_4$** (D_2O, 16.2 mM) (a) before irradiation; (b) after irradiation at 340 nm (2 h); (c) after irradiation at 435 nm (45 min); (Normalized integral values of selected protons are indicated for *E*- and *Z*-isomers.)

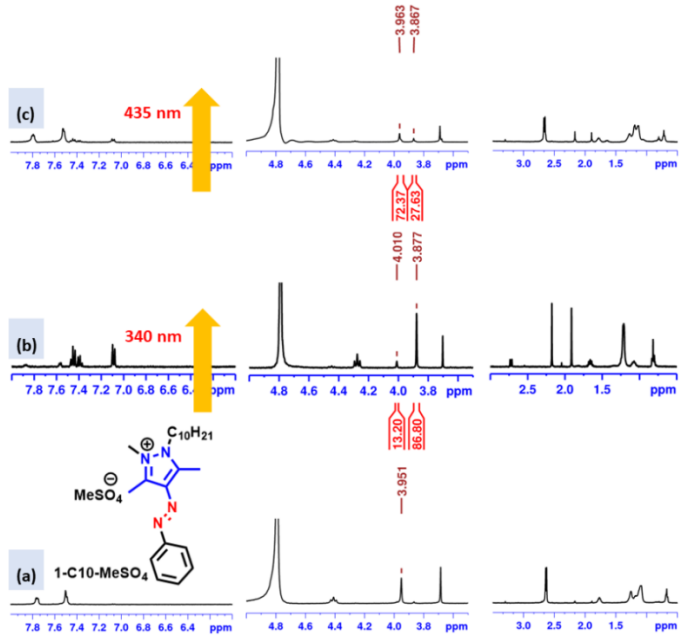

Figure 3B.6.6. Estimation of PSS composition using ^{1}H NMR spectroscopy of **1-C10-MeSO$_4$** (D_2O, 16.4 mM) (a) before irradiation; (b) after irradiation at 340 nm (2 h); (c) after irradiation at 435 nm (45 min); (Normalized integral values of selected protons are indicated for *E*- and *Z*-isomers.)

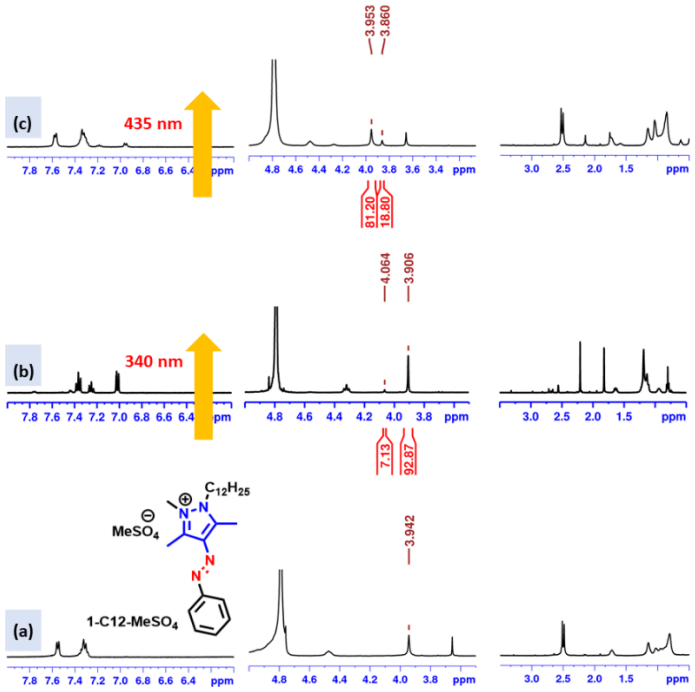

Figure 3B.6.7. Estimation of PSS composition using ^{1}H NMR spectroscopy of **1-C12-MeSO$_4$** (D_2O, 17.3 mM) (a) before irradiation; (b) after irradiation at 340 nm (2 h); (c) after irradiation at 435 nm (45 min); (Normalized integral values of selected protons are indicated for *E*- and *Z*-isomers.)

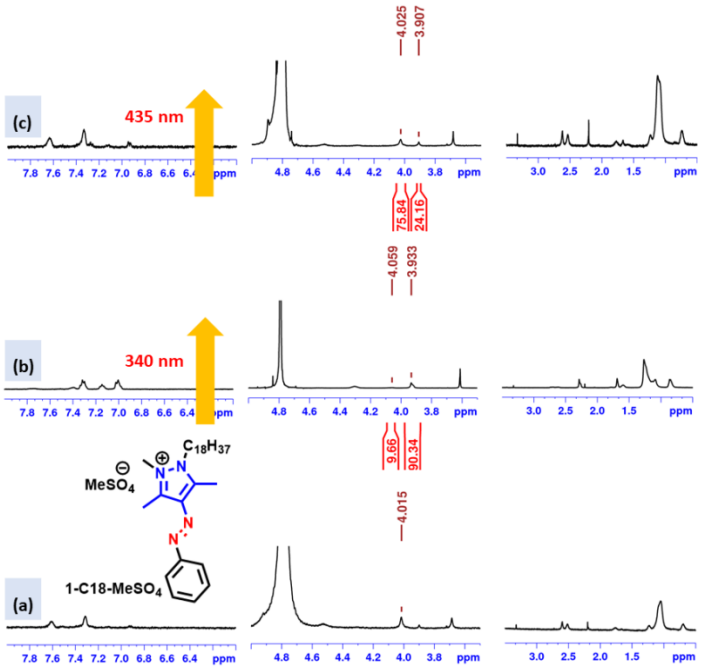

Figure 3B.6.8. Estimation of PSS composition using ^{1}H NMR spectroscopy of **1-C18-MeSO$_4$** (D_2O, 8.1 mM) (a) before irradiation; (b) after irradiation at 340 nm (2 h); (c) after irradiation at 435 nm (45 min); (Normalized integral values of selected protons are indicated for *E*- and *Z*-isomers.)

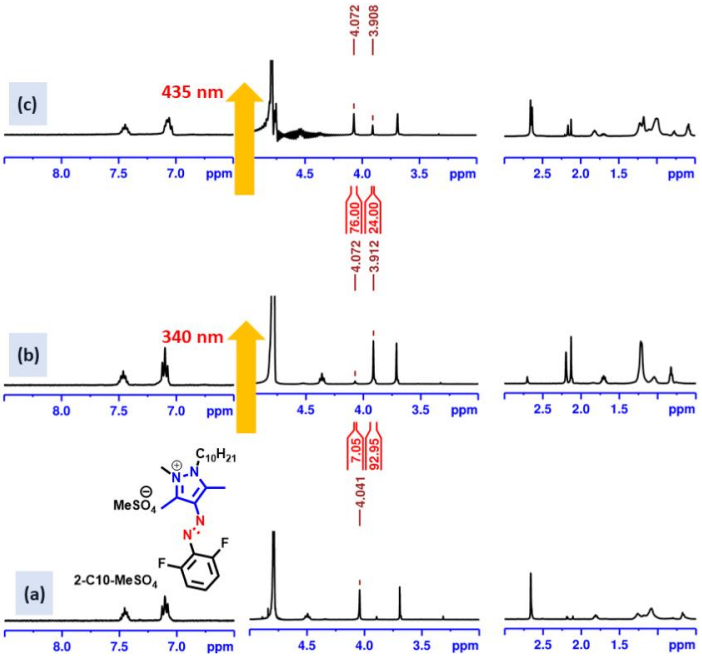

Figure 3B.6.9. Estimation of PSS composition using ^{1}H NMR spectroscopy of **2-C10-MeSO$_4$** (D_2O, 20.1 mM) (a) before irradiation; (b) after irradiation at 340 nm (2 h); (c) after irradiation at 435 nm (45 min); (Normalized integral values of selected protons are indicated for *E*- and *Z*-isomers.)

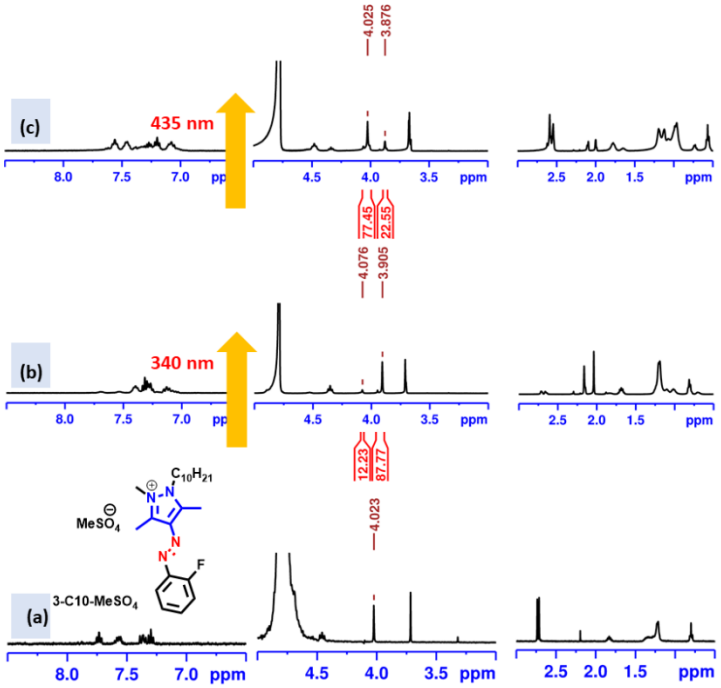

Figure 3B.6.10. Estimation of PSS composition using ^{1}H NMR spectroscopy of **3-C10-MeSO$_4$** (D_2O, 22.4 mM) (a) before irradiation; (b) after irradiation at 340 nm (2 h); (c) after irradiation at 435 nm (45 min); (Normalized integral values of selected protons are indicated for *E*- and *Z*-isomers.)

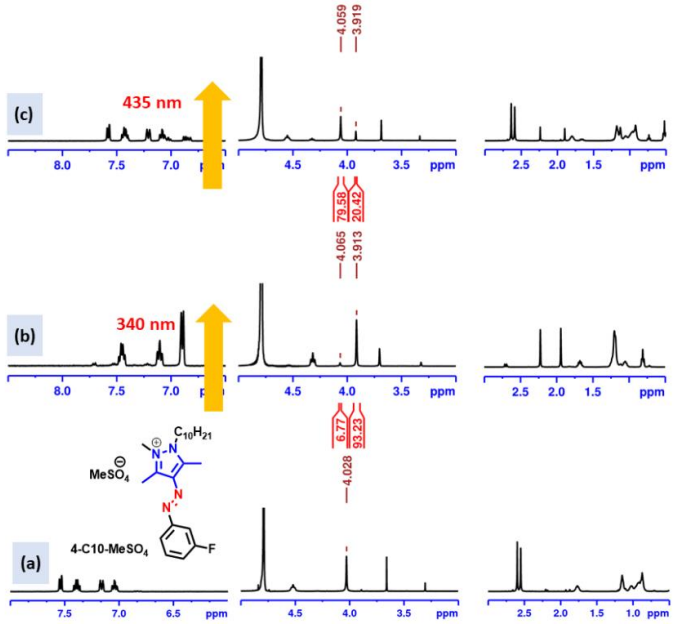

Figure 3B.6.11. Estimation of PSS composition using ^{1}H NMR spectroscopy of **4-C10-MeSO$_4$** (D_2O, 20.1 mM) (a) before irradiation; (b) after irradiation at 340 nm (2 h); (c) after irradiation at 435 nm (45 min); (Normalized integral values of selected protons are indicated for *E*- and *Z*-isomers.)

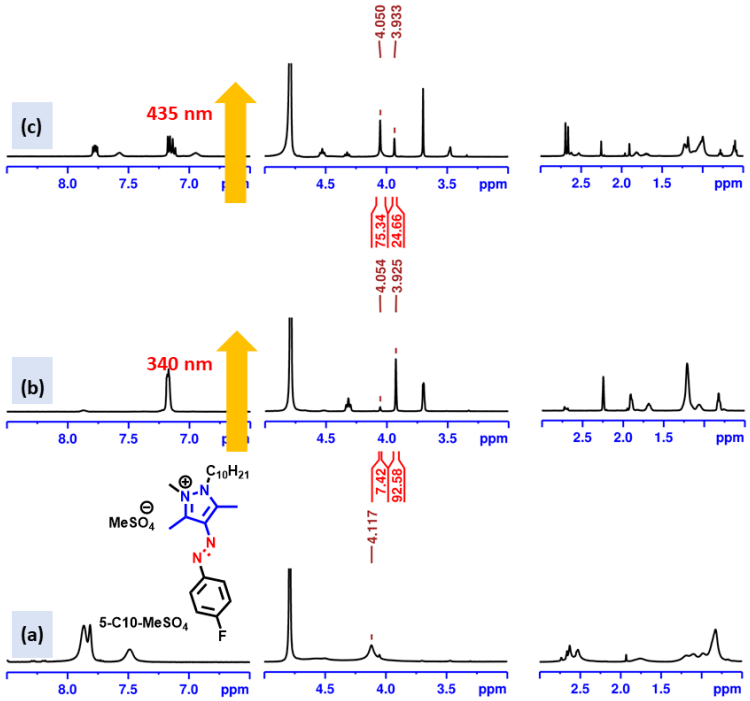

Figure 3B.6.12. Estimation of PSS composition using ^{1}H NMR spectroscopy of **5-C10-MeSO$_4$** (D_2O, 14.6 mM) (a) before irradiation; (b) after irradiation at 340 nm (2 h); (c) after irradiation at 435 nm (45 min); (Normalized integral values of selected protons are indicated for *E*- and *Z*-isomers.)

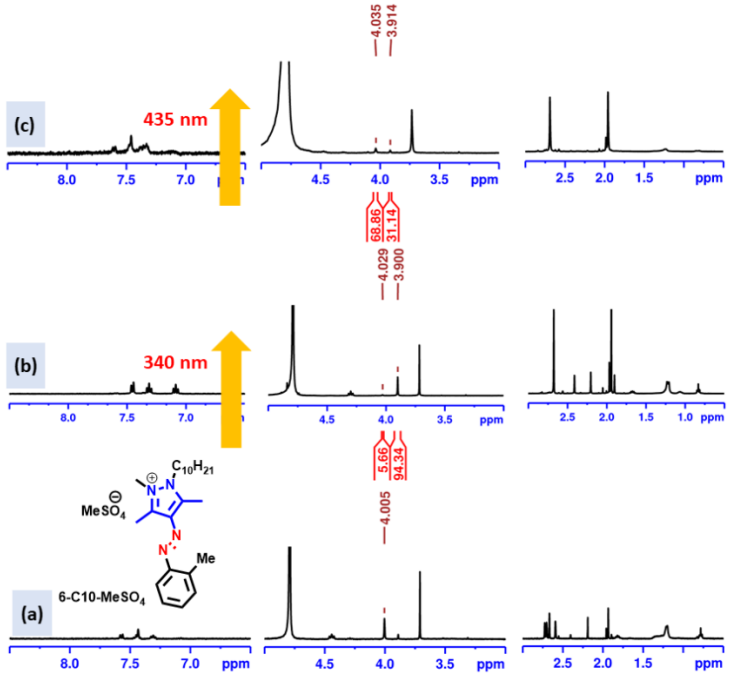

Figure 3B.6.13: Estimation of PSS composition using ^{1}H NMR spectroscopy of **6-C10-MeSO$_4$** (D_2O, 24.1 mM) (a) before irradiation; (b) after irradiation at 340 nm (2 h); (c) after irradiation at 435 nm (45 min); (Normalized integral values of selected protons are indicated for *E*- and *Z*-isomers.)

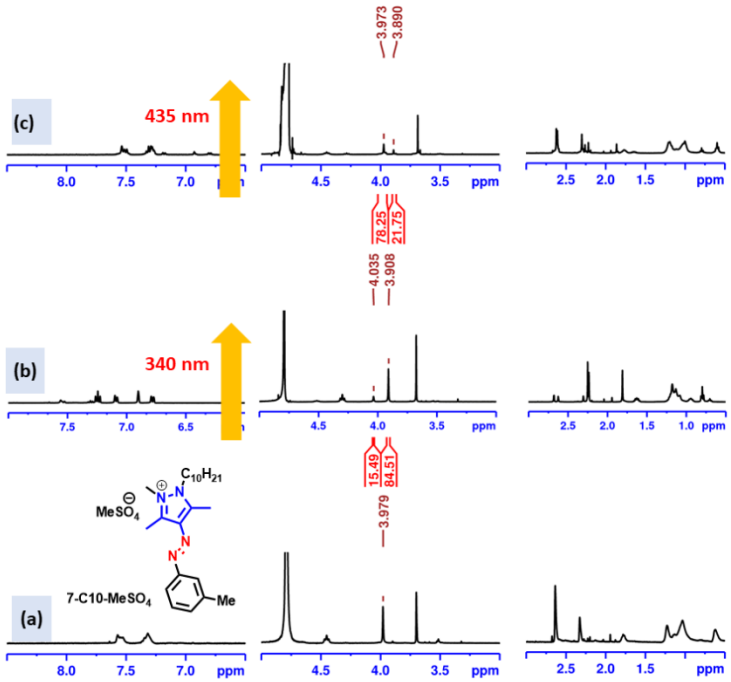

Figure 3B.6.14. Estimation of PSS composition using ^{1}H NMR spectroscopy of **7-C10-MeSO$_4$** (D_2O, 19.7 mM) (a) before irradiation; (b) after irradiation at 340 nm (2 h); (c) after irradiation at 435 nm (45 min). (Normalized integral values of selected protons are indicated for *E*- and *Z*-isomers.)

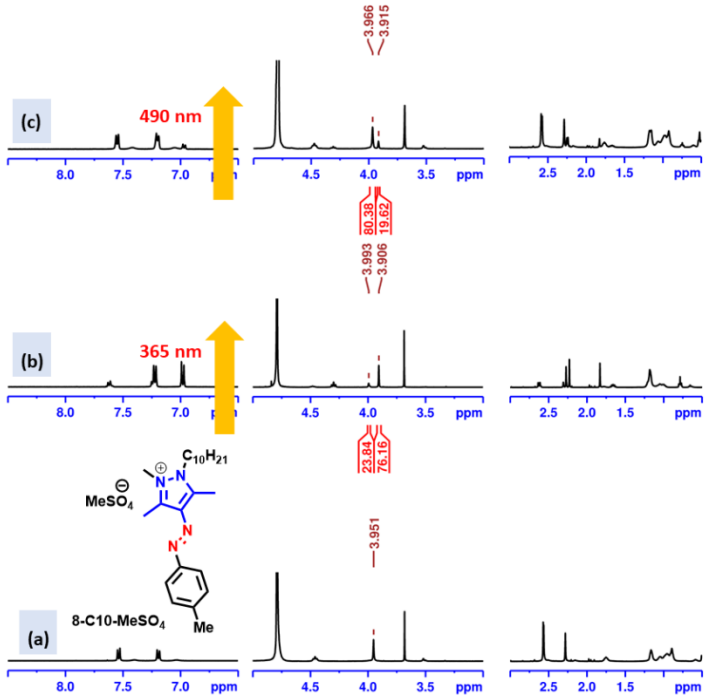

Figure 3B.6.15. Estimation of PSS composition using ^{1}H NMR spectroscopy of **8-C10-MeSO$_4$** (D_2O, 20.1 mM) (a) before irradiation; (b) after irradiation at 365 nm (1 h); (c) after irradiation at 490 nm (45 min); (Normalized integral values of selected protons are indicated for *E*- and *Z*-isomers.)

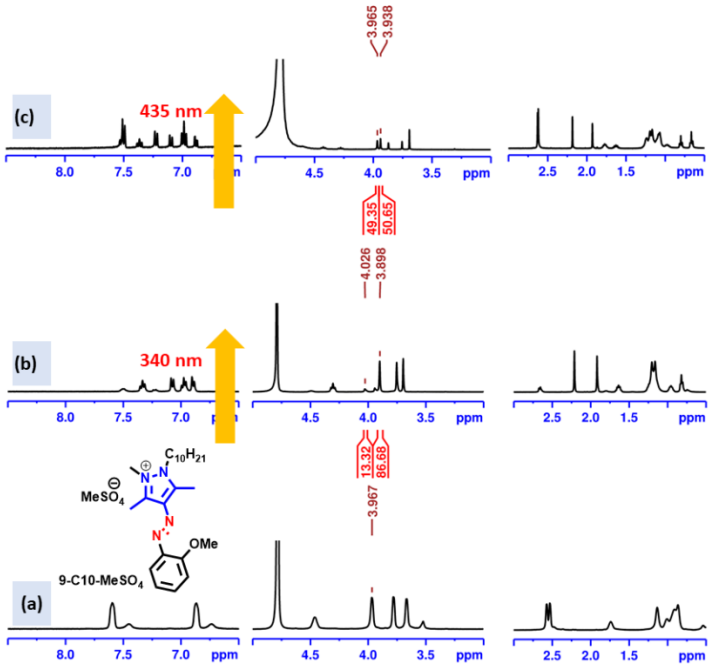

Figure 3B.6.16. Estimation of PSS composition using ^{1}H NMR spectroscopy of **9-C10-MeSO$_4$** (D_2O, 17.3 mM) (a) before irradiation; (b) after irradiation at 340 nm (2 h); (c) after irradiation at 435 nm (45 min); (Normalized integral values of selected protons are indicated for *E*- and *Z*-isomers.)

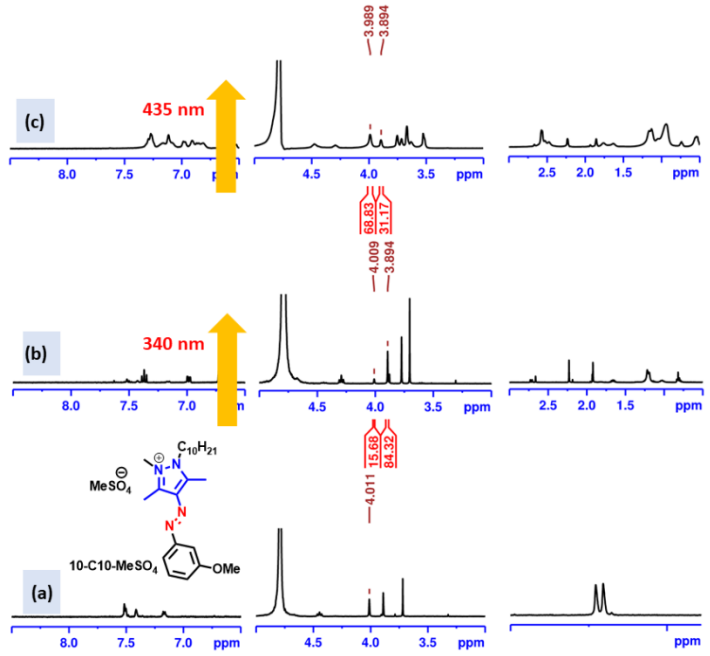

Figure 3B.6.17. Estimation of PSS composition using ^{1}H NMR spectroscopy of **10-C10-MeSO$_4$** (D_2O, 16.1 mM) (a) before irradiation; (b) after irradiation at 340 nm (2 h); (c) after irradiation at 435 nm (45 min); (Normalized integral values of selected protons are indicated for *E*- and *Z*-isomers.)

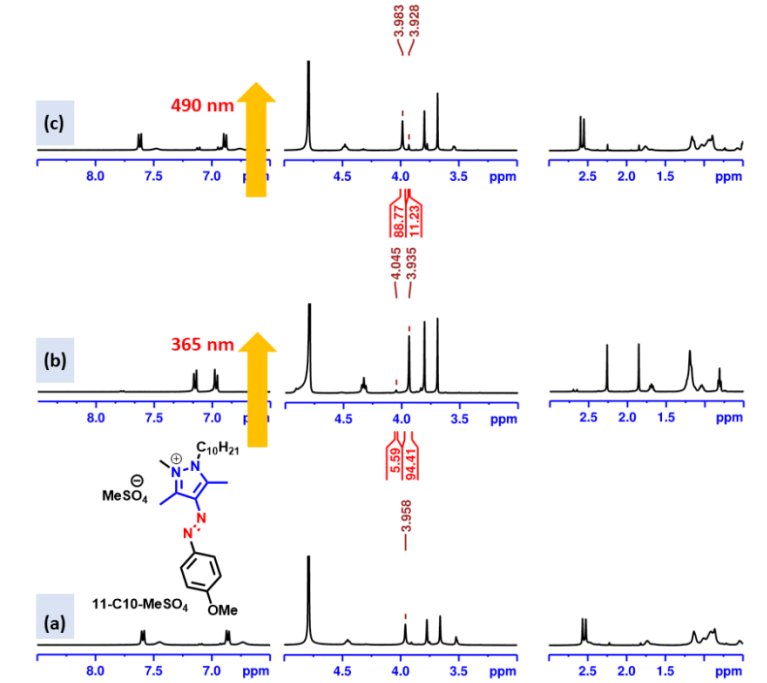

Figure 3B.6.18. Estimation of PSS composition using ^{1}H NMR spectroscopy of **11-C10-MeSO$_4$** (D_2O, 18.1 mM) (a) before irradiation; (b) after irradiation at 365 nm (1 h); (c) after irradiation at 490 nm (45 min); (Normalized integral values of selected protons are indicated for *E*- and *Z*-isomers.)

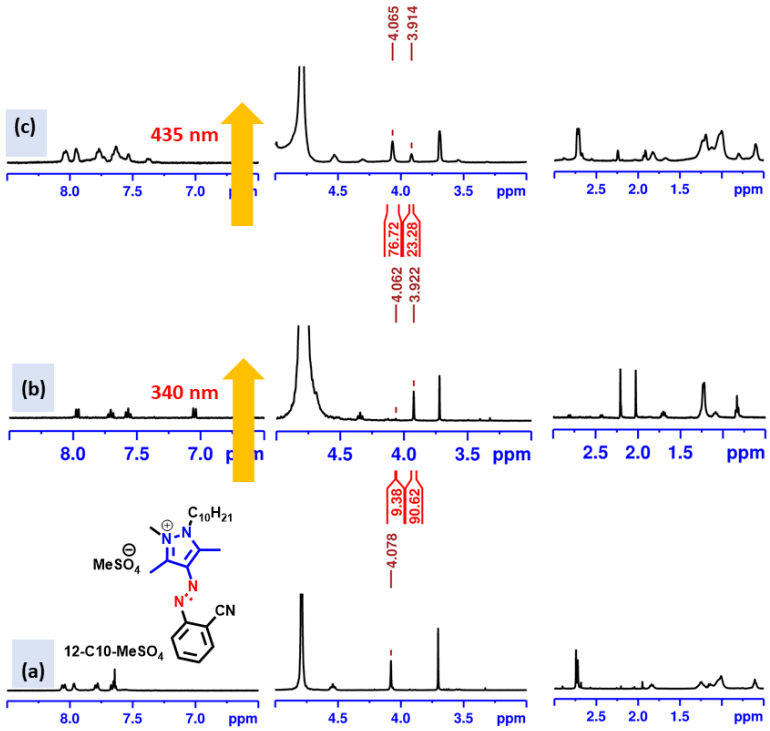

Figure 3B.6.19. Estimation of PSS composition using ^{1}H NMR spectroscopy of **12-C10-MeSO$_4$** (D_2O, 21.2 mM) (a) before irradiation; (b) after irradiation at 340 nm (2 h); (c) after irradiation at 435 nm (45 min); (Normalized integral values of selected protons are indicated for *E*- and *Z*-isomers.)

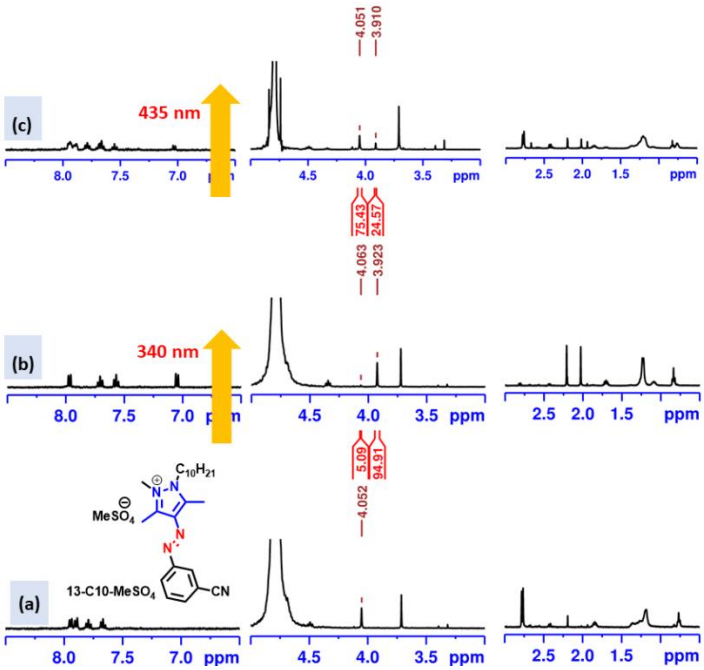

Figure 3B.6.20. Estimation of PSS composition using ^{1}H NMR spectroscopy of **13-C10-MeSO$_4$** (D_2O, 13.1 mM) (a) before irradiation; (b) after irradiation at 340 nm (2 h); (c) after irradiation at 435 nm (45 min); (Normalized integral values of selected protons are indicated for *E*- and *Z*-isomers.)

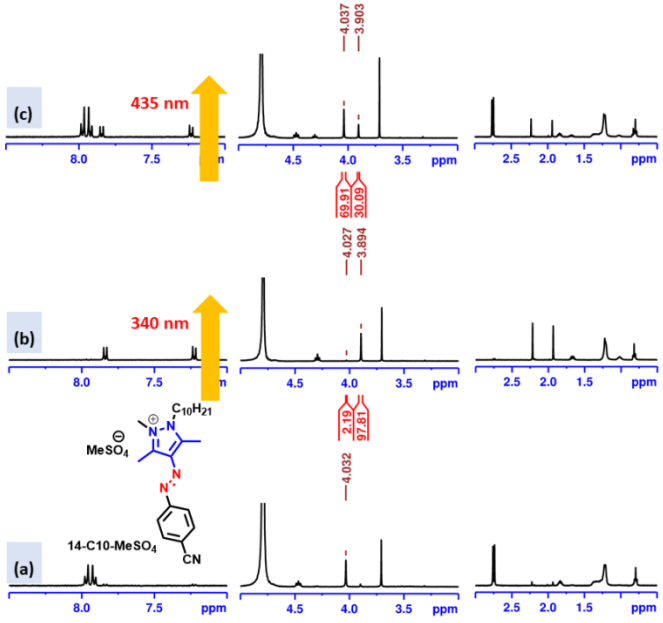

Figure 3B.6.21. Estimation of PSS composition using ^{1}H NMR spectroscopy of **14-C10-MeSO$_4$** (D_2O, 16.4 mM) (a) before irradiation; (b) after irradiation at 340 nm (2 h); (c) after irradiation at 435 nm (45 min); (Normalized integral values of selected protons are indicated for *E*- and *Z*-isomers.)

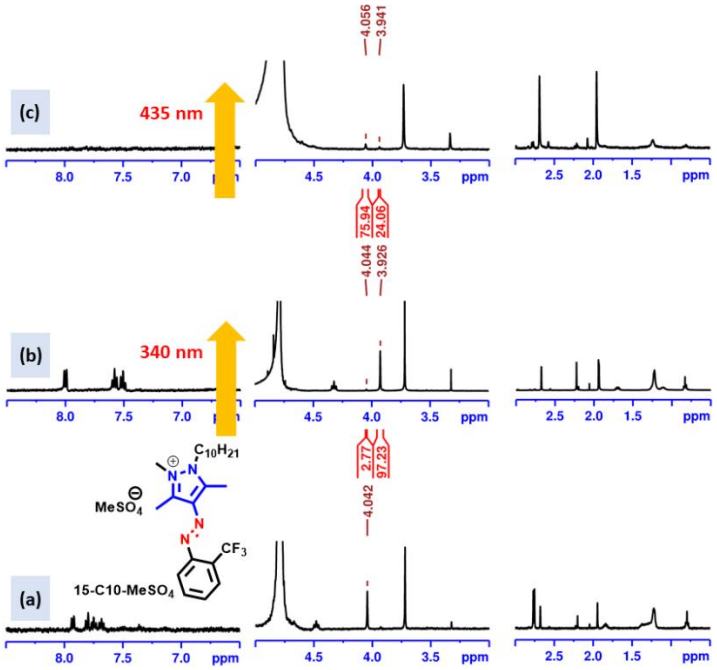

Figure 3B.6.22. Estimation of PSS composition using ^{1}H NMR spectroscopy of **15-C18-MeSO$_4$** (D_2O, 13.7 mM) (a) before irradiation; (b) after irradiation at 340 nm (2 h); (c) after irradiation at 435 nm (45 min); (Normalized integral values of selected protons are indicated for *E*- and *Z*-isomers

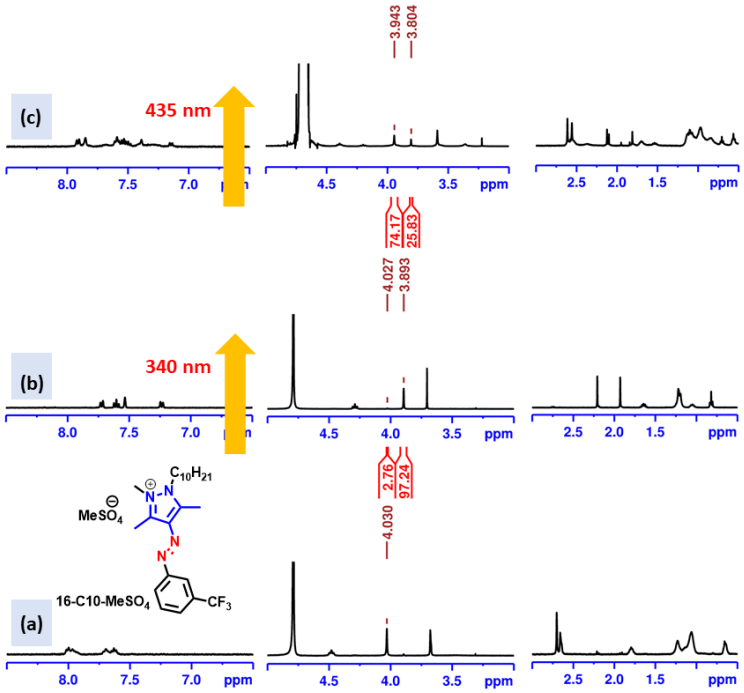

Figure 3B.6.23. Estimation of PSS composition using ^{1}H NMR spectroscopy of **16-C10-MeSO$_4$** (D_2O, 14.6 mM) (a) before irradiation; (b) after irradiation at 340 nm (2 h); (c) after irradiation at 435 nm (45 min); (Normalized integral values of selected protons are indicated for *E*- and *Z*-isomers.)

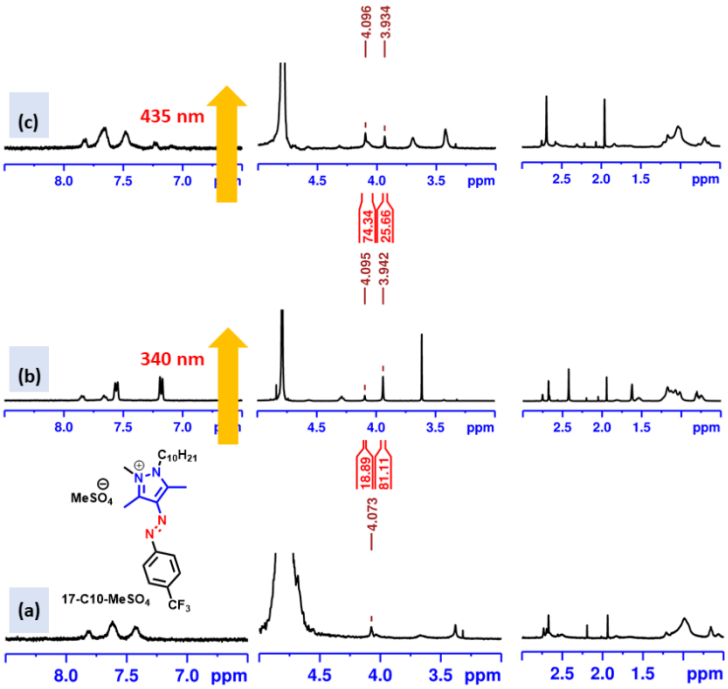

Figure 3B.6.24. Estimation of PSS composition using ^{1}H NMR spectroscopy of **17-C10-MeSO$_4$** (D_2O, 6.1 mM) (a) before irradiation; (b) after irradiation at 340 nm (2 h); (c) after irradiation at 435 nm (45 min); (Normalized integral values of selected protons are indicated for *E*- and *Z*-isomers.)

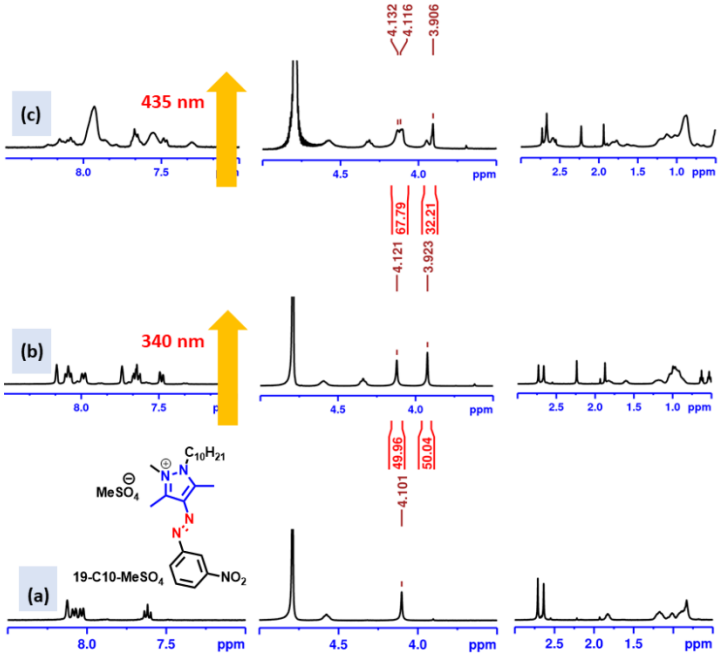

Figure 3B.6.25. Estimation of PSS composition using ^{1}H NMR spectroscopy of **19-C10-MeSO$_4$** (D_2O, 18.1 mM) (a) before irradiation; (b) after irradiation at 340 nm (2 h); (c) after irradiation at 435 nm (45 min); (Normalized integral values of selected protons are indicated for *E*- and *Z*-isomers.)

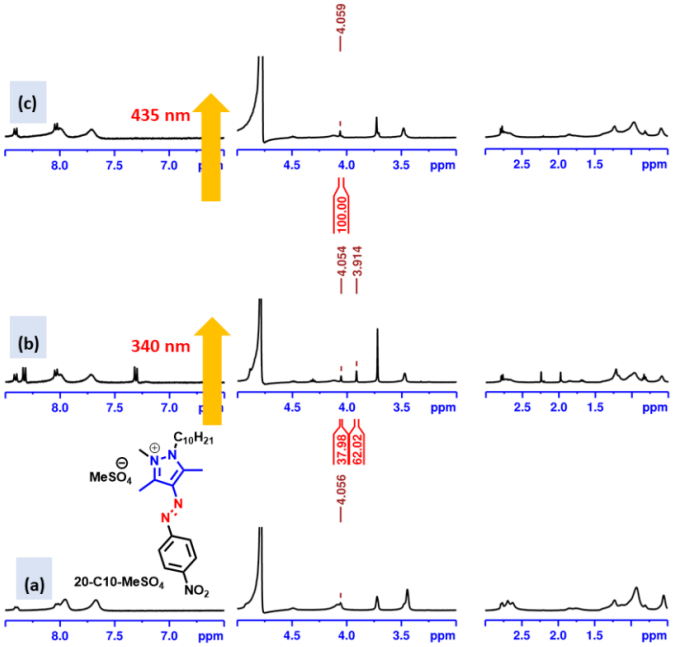

Figure 3B.6.26. Estimation of PSS composition using ^{1}H NMR spectroscopy of **20-C10-MeSO$_4$** (D_2O, 7.1 mM) (a) before irradiation; (b) after irradiation at 340 nm (2 h); (c) after irradiation at 435 nm (45 min); (Normalized integral values of selected protons are indicated for *E*- and *Z*-isomers.)

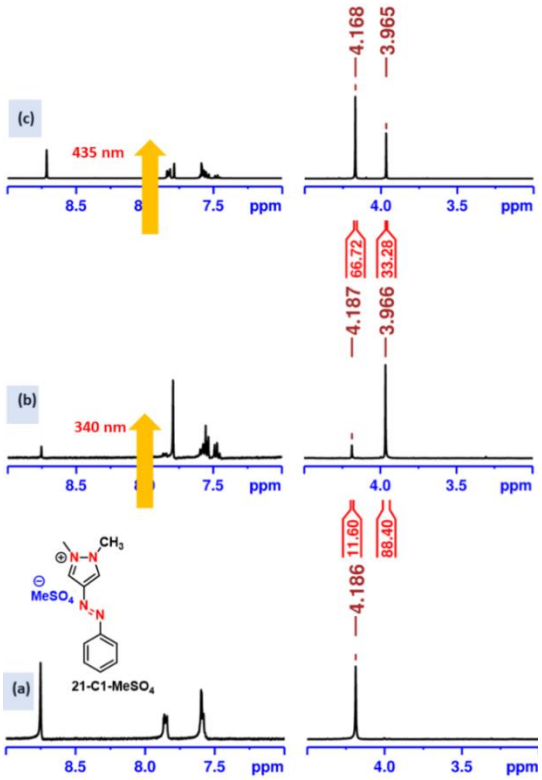

Figure 3B.6.27. Estimation of PSS composition using ^{1}H NMR spectroscopy of **21-C10-MeSO$_4$** (D_2O, 27.8 mM) (a) before irradiation; (b) after irradiation at 340 nm (2 h); (c) after irradiation at 435 nm (45 min); (Normalized integral values of selected protons are indicated for *E*- and *Z*-isomers.)

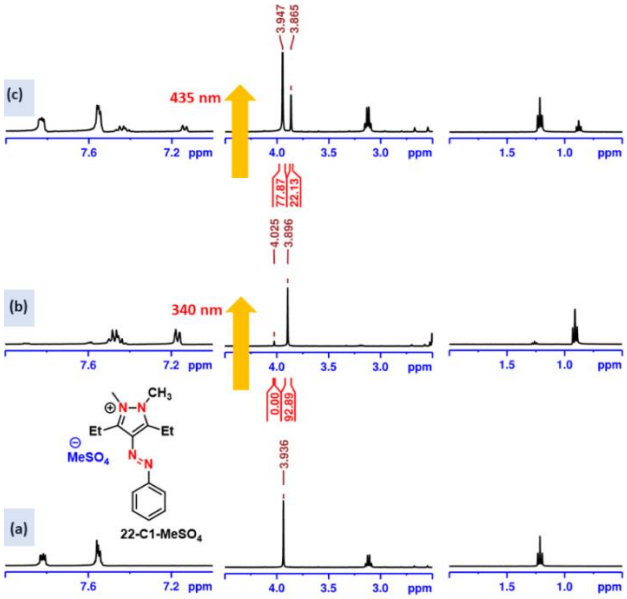

Figure 3B.6.28. Estimation of PSS composition using ^{1}H NMR spectroscopy of **22-C10-MeSO$_4$** (D_2O, 23.8 mM) (a) before irradiation; (b) after irradiation at 340 nm (2 h); (c) after irradiation at 435 nm (45 min); (Normalized integral values of selected protons are indicated for *E*- and *Z*-isomers.)

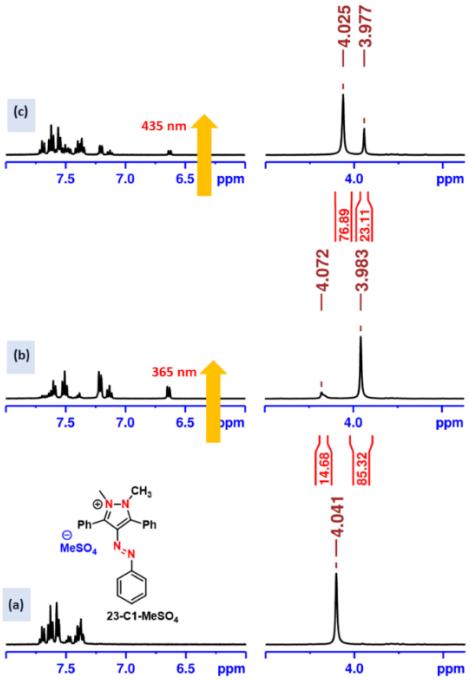

Figure 3B.6.29. Estimation of PSS composition using ^{1}H NMR spectroscopy of **23-C10-MeSO$_4$** (D_2O, 19.5 mM) (a) before irradiation; (b) after irradiation at 365 nm (1 h); (c) after irradiation at 435 nm (45 min); (Normalized integral values of selected protons are indicated for *E*- and *Z*-isomers.)

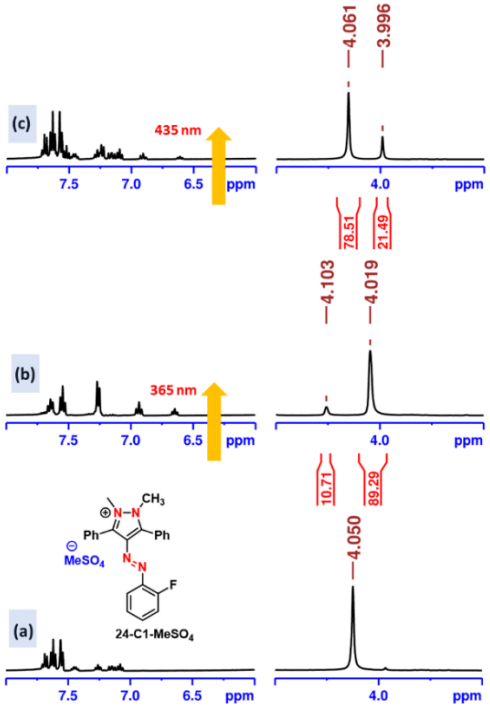

Figure 3B.6.30. Estimation of PSS composition using ^{1}H NMR spectroscopy of **24-C10-MeSO$_4$** (D_2O, 18.1 mM) (a) before irradiation; (b) after irradiation at 365 nm (1 h); (c) after irradiation at 435 nm (45 min); (Normalized integral values of selected protons are indicated for *E*- and *Z*-isomers.)

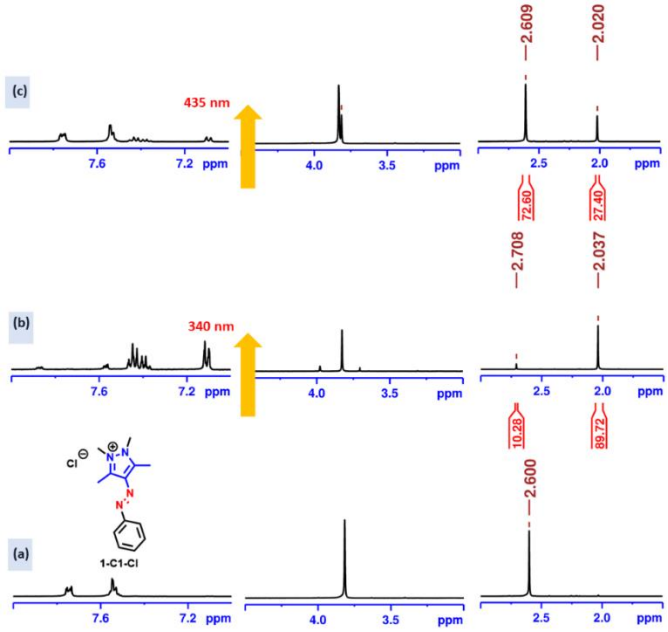

Figure 3B.6.31. Estimation of PSS composition using ^{1}H NMR spectroscopy of **1-C1-Cl** (D_2O, 25.3 mM) (a) before irradiation; (b) after irradiation at 340 nm (2 h); (c) after irradiation at 435 nm (45 min); (Normalized integral values of selected protons are indicated for *E*- and *Z*-isomers.)

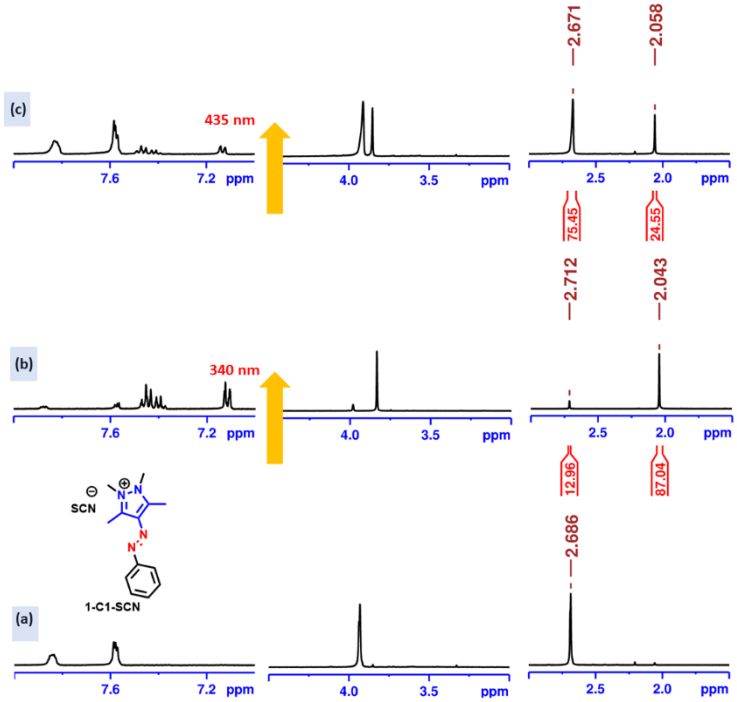

Figure 3B.6.32. Estimation of PSS composition using ^{1}H NMR spectroscopy of **1-C1-SCN** (D_2O, 23.1 mM) (a) before irradiation; (b) after irradiation at 340 nm (2 h); (c) after irradiation at 435 nm (45 min); (Normalized integral values of selected protons are indicated for *E*- and *Z*-isomers.)

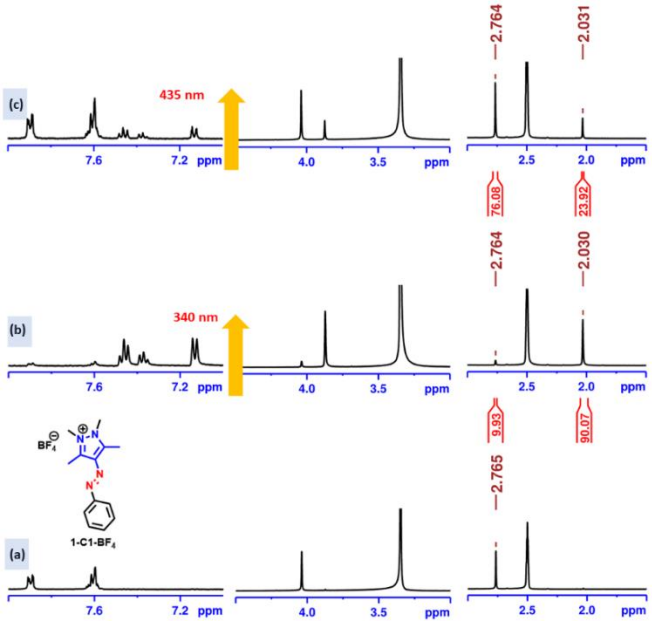

Figure 3B.6.33. Estimation of PSS composition using ^{1}H NMR spectroscopy of **1-C1-BF$_4$** (DMSO-d_6, 27.4 mM) (a) before irradiation; (b) after irradiation at 340 nm (2 h); (c) after irradiation at 435 nm (45 min); (Normalized integral values of selected protons are indicated for *E*- and *Z*-isomers.)

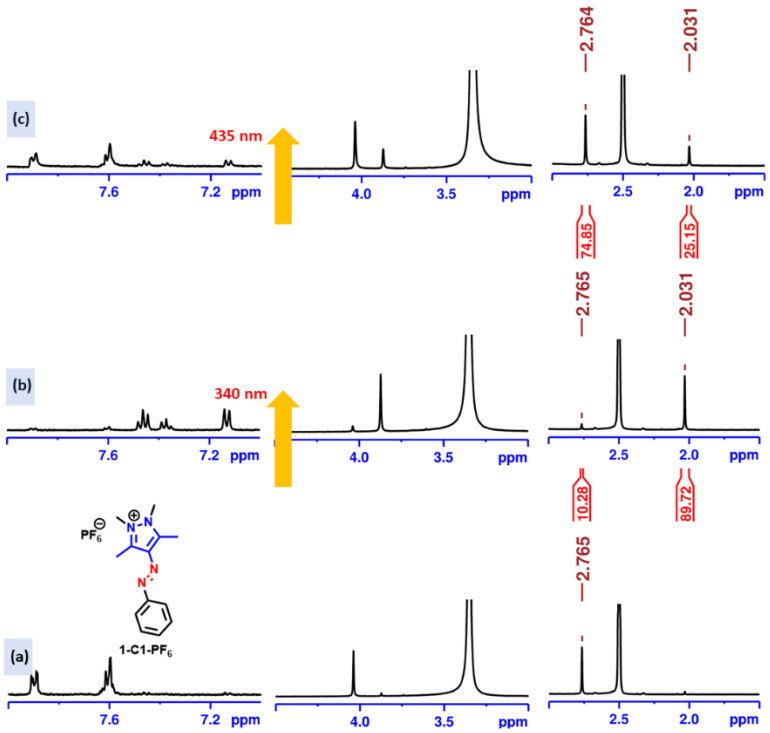

Figure 3B.6.34. Estimation of PSS composition using ^{1}H NMR spectroscopy of **1-C1-PF$_6$** (DMSO-d$_6$, 20.2 mM)) (a) before irradiation; (b) after irradiation at 340 nm (2 h); (c) after irradiation at 435 nm (45 min); (Normalized integral values of selected protons are indicated for *E*- and *Z*-isomers.)

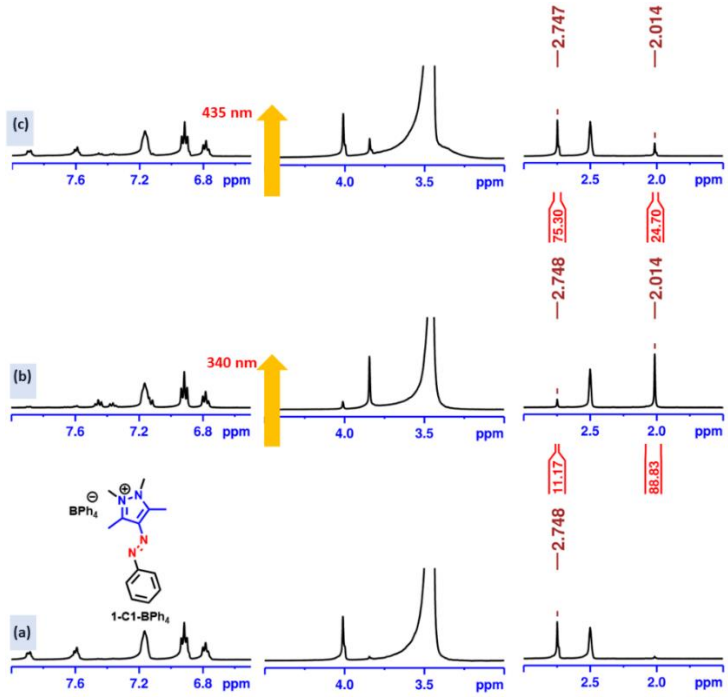

Figure 3B.6.35. Estimation of PSS composition using ^{1}H NMR spectroscopy of **1-C1-BPh$_4$** (DMSO-d$_6$, 17.7 mM)) (a) before irradiation; (b) after irradiation at 340 nm (2 h); (c) after irradiation at 435 nm (45 min); (Normalized integral values of selected protons are indicated for *E*- and *Z*-isomers.)

3B.7. Concentration dependency on photoisomerization: ^{1}H NMR spectroscopy

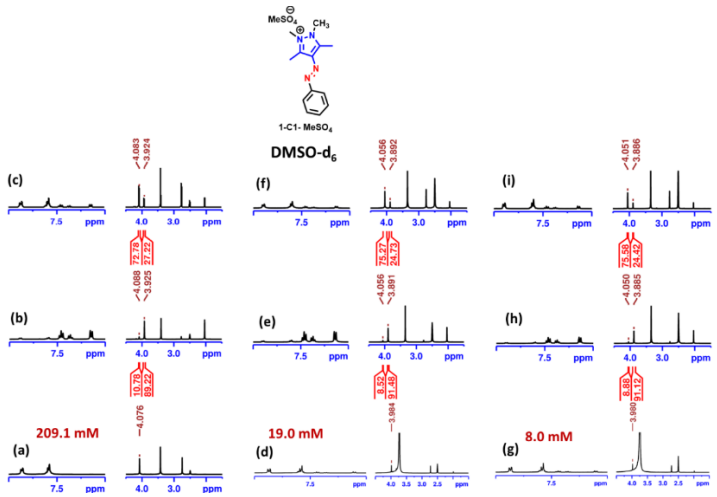

Figure 3B.7.1. Estimation of PSS composition using ^{1}H NMR spectroscopy of **1-C1-MeSO$_4$** (DMSO-d$_6$) at different concentrations: (a) before irradiation (209.1 mM), (b) after irradiation at 365 nm (209.1 mM), (c) after irradiation at 435 nm (209.1 mM); (d) before irradiation (19.0 mM), (e) after irradiation at 365 nm (19.0 mM); (f) after irradiation at 435 nm (19.0 mM); (g) before irradiation (8.0 mM), (h) after irradiation at 365 nm (8.0 mM); (i) after irradiation at 435 nm (8.0 mM). (Normalized integral values of selected protons are indicated for *E*- and *Z*-isomers.)

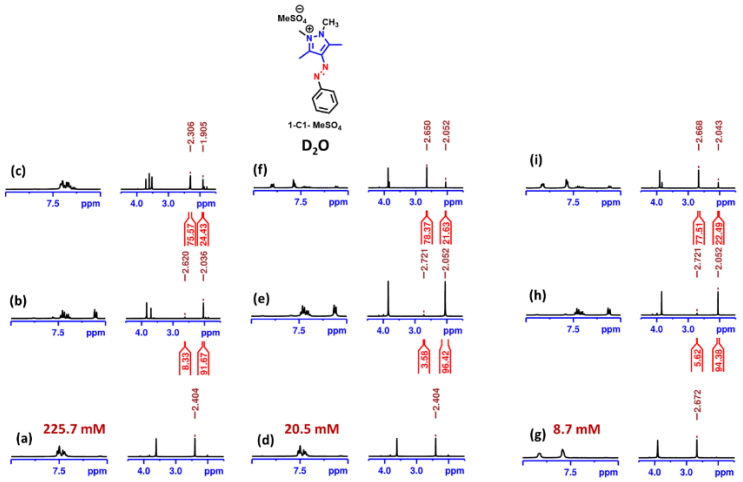

Figure 3B.7.2: Estimation of PSS composition using ^{1}H NMR spectroscopy of **1-C1-MeSO$_4$** (D$_2$O) at different concentrations: (a) before irradiation (225.7 mM), (b) after irradiation at 340 nm (225.7 mM), (c) after irradiation at 435 nm (225.7 mM); (d) before irradiation (20.5 mM), (e) after irradiation at 340 nm (20.5 mM); (f) after irradiation at 435 nm (20.5 mM); (g) before irradiation (8.7 mM), (h) after irradiation at 340 nm (8.7 mM); (i) after irradiation at 435 nm (8.7 mM). (Normalized integral values of selected protons are indicated for *E*- and *Z*-isomers.)

3B.8. Effect of pH: UV-Vis spectroscopic studies

Buffer solutions ranging from pH 6-13 were prepared by adding NaOH (10 M) to solutions of phosphate buffer (pH = 6.65) and from pH 2-6 by adding standard HCl. The pH of the prepared

solutions was measured with a Oaklon PH550 Benchtop pH Meter. All solution were prepared in Milli-Q water.

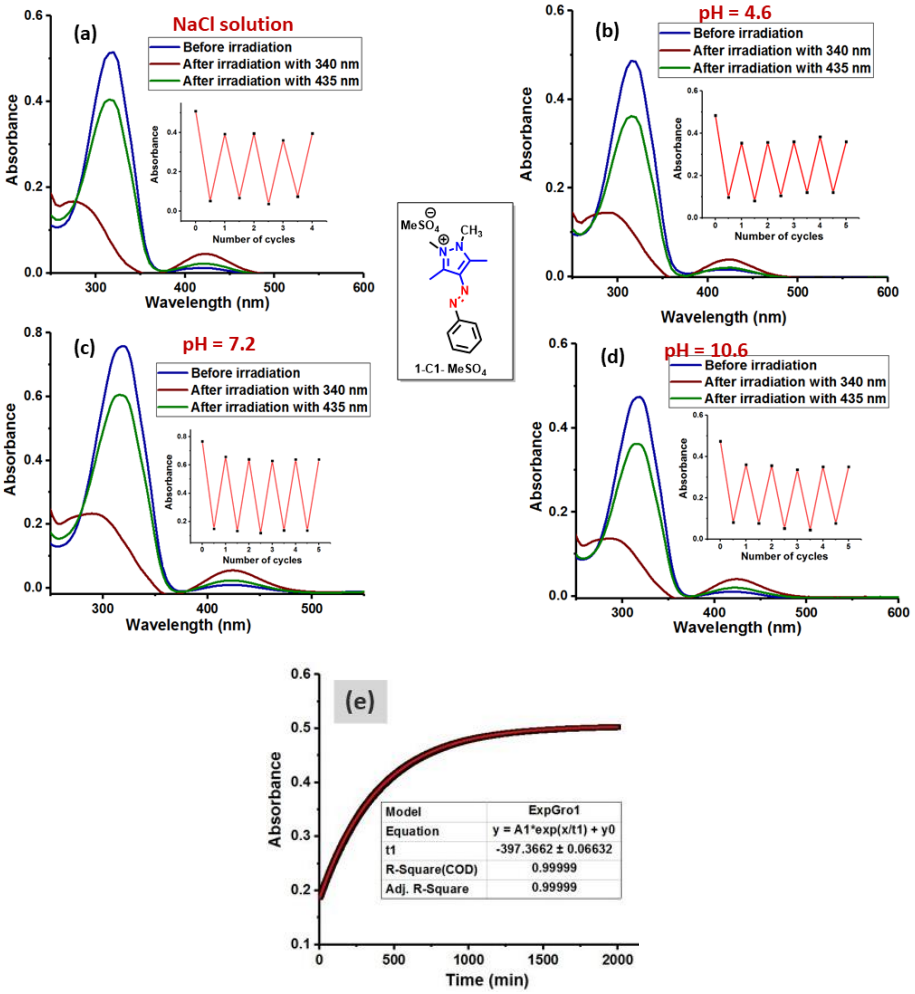

Figure 3B.8.1. UV-Vis photoswitching studies of compound **1-C1-MeSO4** in (a) saturated solution of NaCl, and in the buffer solutions at various pH (b) at pH = 4.6; (c) at pH = 7.2 and (d) at pH = 10.6; {for forward photoisomerization step, 365 nm and for the reverse isomerization 435 nm wavelengths of light were used; The inserts correspond to photoswitching stability test over five cycles in the forward and reverse isomerization sequences}; (e) Kinetcis studies at 80 ^{o}C in saturated NaCl solution.

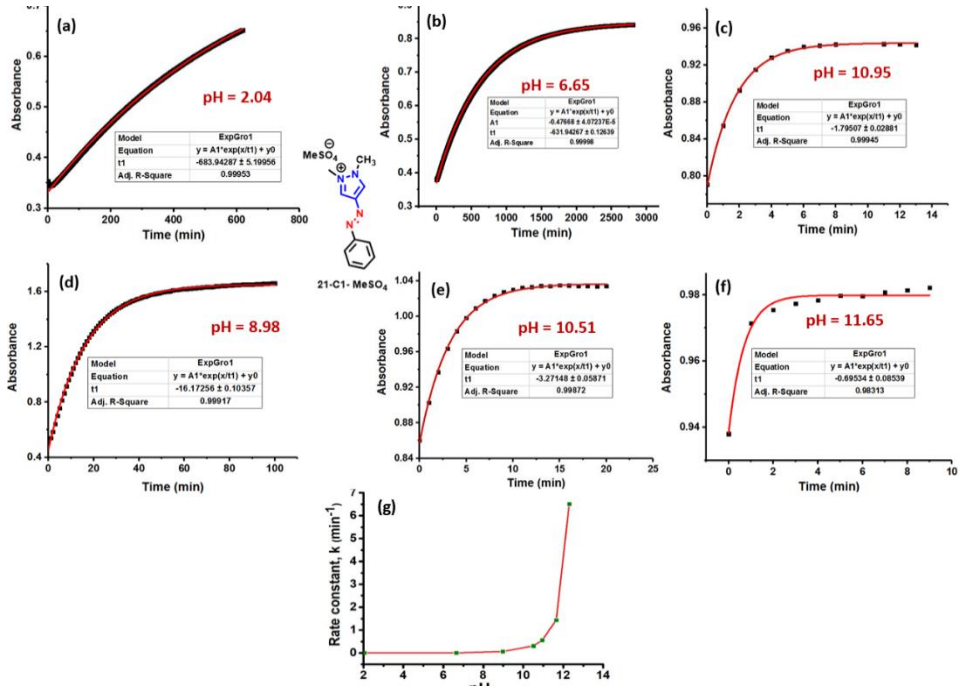

Figure 3B.8.2. Thermal *Z-E* isomerization kinetics studies followed by UV-Vis spectroscopy of compound **21-C1-MeSO4** at (a) pH = 2.04, (b) pH = 6.65, (c) pH = 8.98, (d) pH = 11.65, (e) pH = 10.95, (f) pH = 11.65, (g) plot between rate constant, k vs pH.

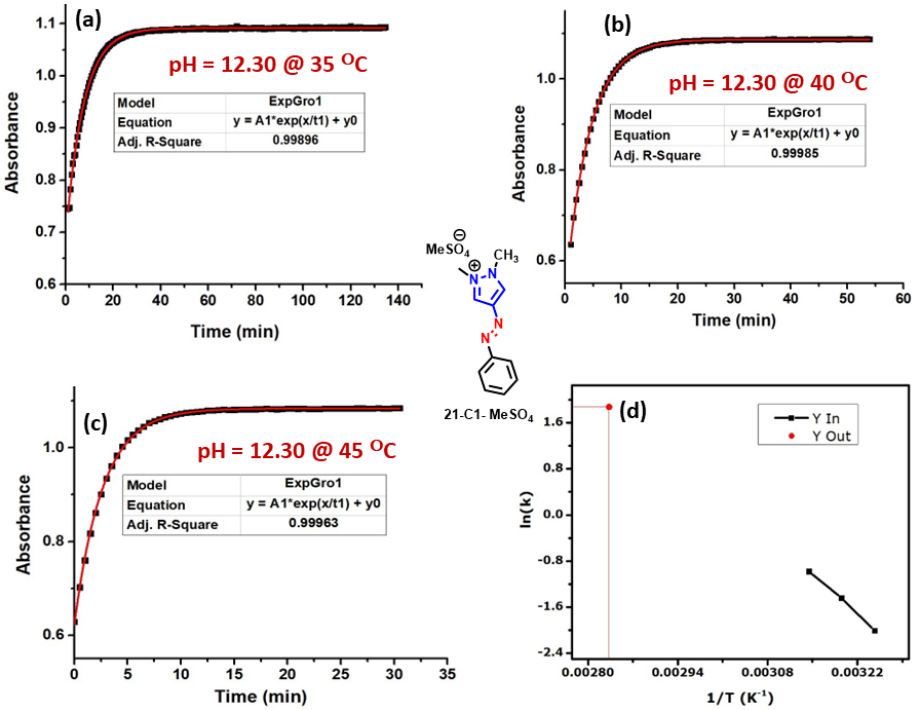

Figure 3B.8.3. Variable temperature thermal *Z-E* isomerization kinetics studies followed by UV-Vis spectroscopy of compound **21-C1-MeSO4** at pH = 12.30; (a) at 35 °C, (b) at 40 °C, and (c) at 45 °C; (d) Extrapolation of the data to obtain the rate constant at 80 °C at pH = 12.30.

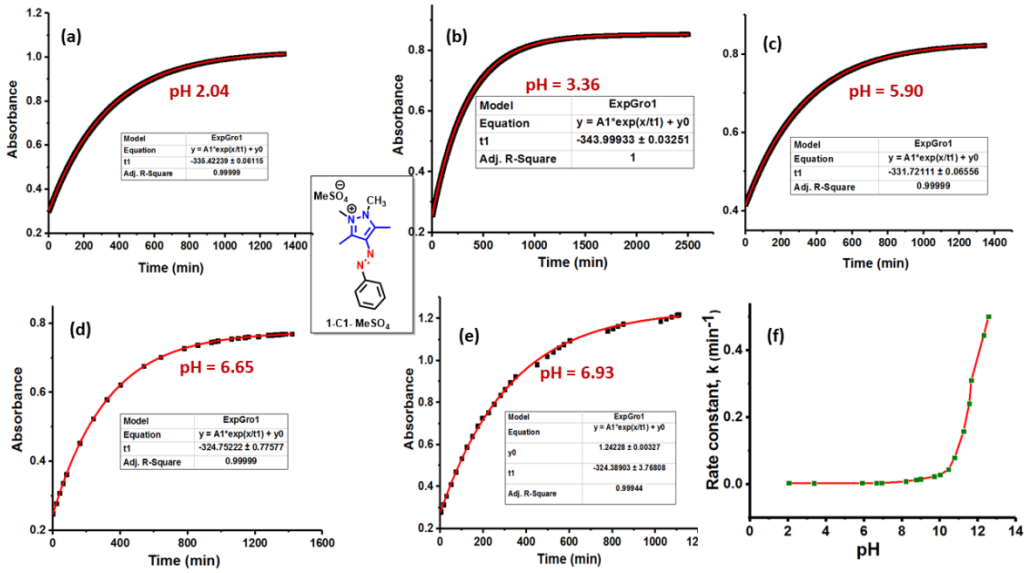

Figure 3B.8.4. Thermal *Z-E* isomerization kinetics studies followed by UV-Vis spectroscopy of compound **1-C1-MeSO4** at pH (a) = 2.04, (b) = 3.36, (c) = 5.90, (d) = 6.65, (d) = 6.93, (e) = pH 6.93, (f) plot between rate constant, k vs pH.

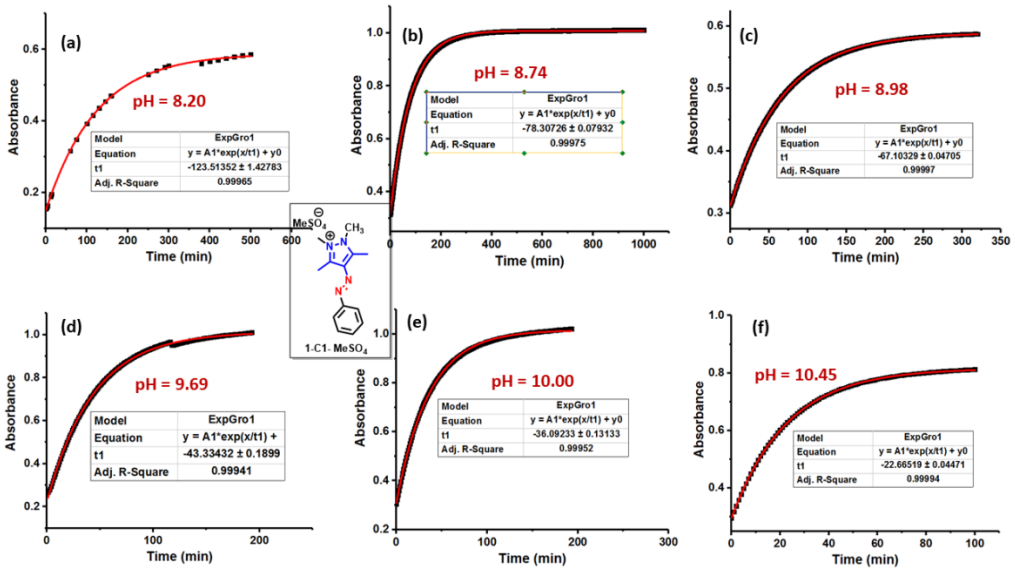

Figure 3B.8.5. Thermal *Z-E* isomerization kinetics studies followed by UV-Vis spectroscopy of compound **1-C1-MeSO4** at pH (a) = 8.20, (b) = 8.74, (c) = 8.98, (d) = 9.69, (e) = 10.00, (f) = 10.45.

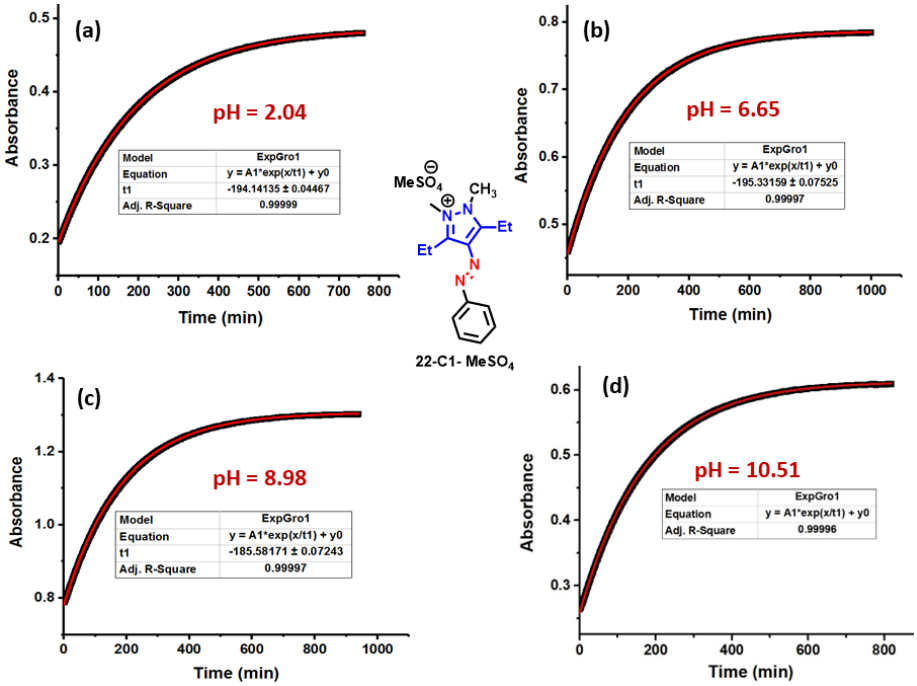

Figure 3B.8.7. Thermal *Z*-*E* isomerization kinetics studies followed by UV-Vis spectroscopy of compound **22-C1-MeSO4** at pH (a) = 2.04, (b) = 6.65, (c) = 8.98, (d) = 10.51.

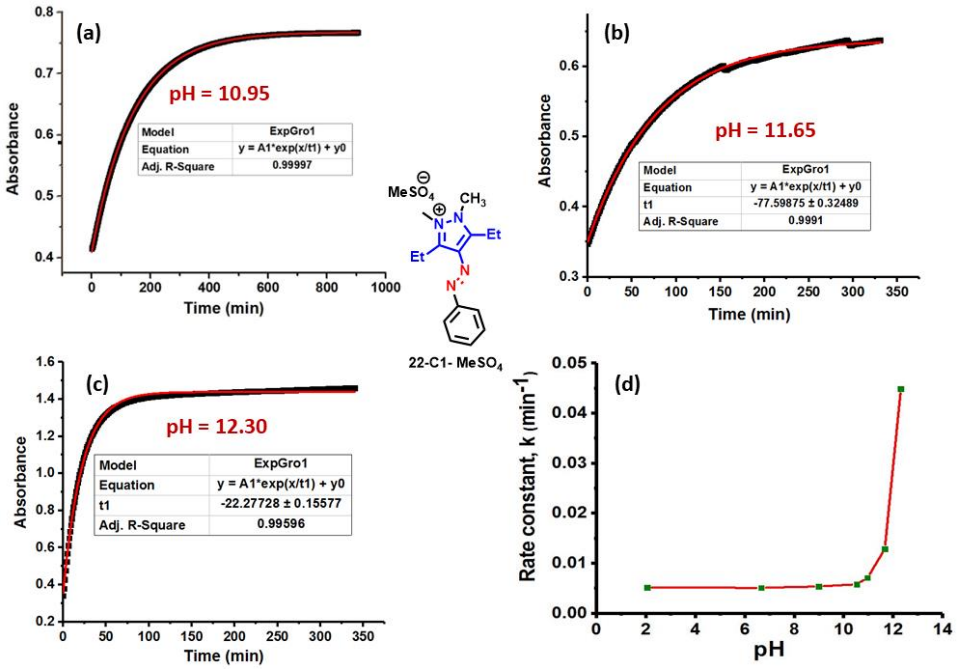

Figure 3B.8.8. Thermal *Z*-*E* isomerization kinetics studies followed by UV-Vis spectroscopy of compound **22-C1-MeSO4** at pH (a) = 10.95, (b) = 11.65, (c) = 12.30, (d) plot between rate constant, k vs pH.

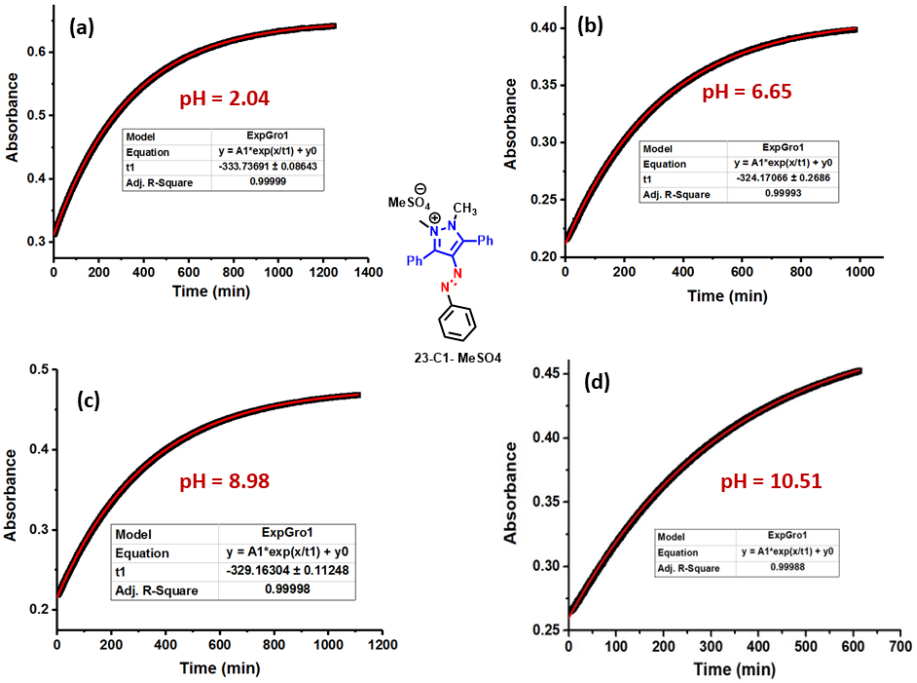

Figure 3B.8.9. Thermal *Z-E* isomerization kinetics studies followed by UV-Vis spectroscopy of compound **23-C1-MeSO4** at pH (a) = 2.04, (b) = 6.65, (c) = 8.98, (d) = 10.51.

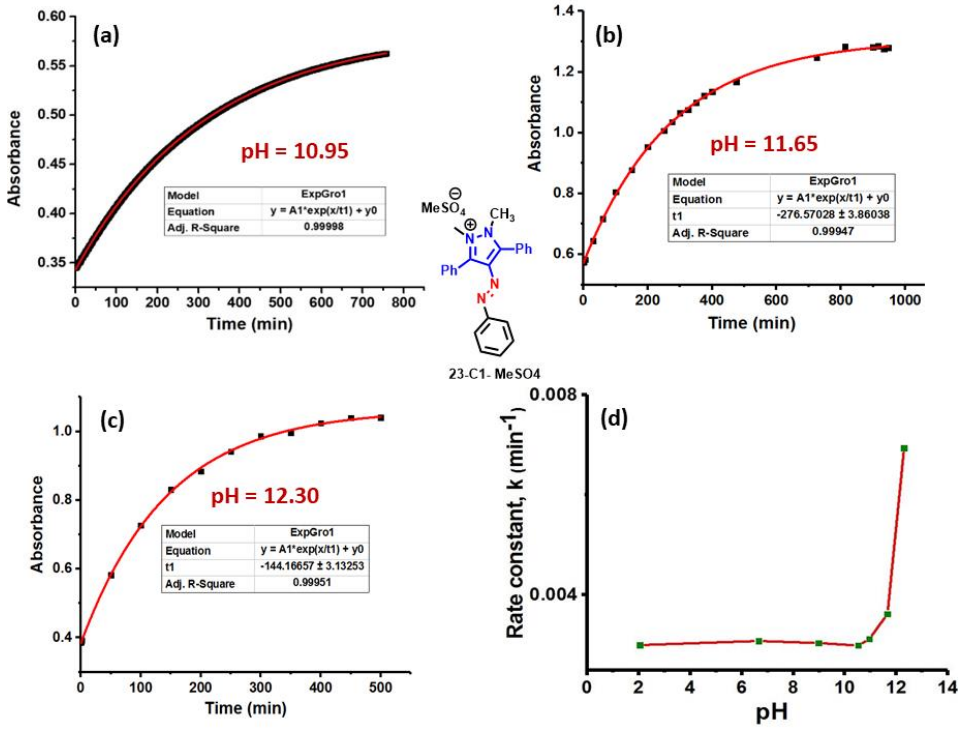

Figure 3B.8.10. UV-Vis photoswitching studies of compound **23-C1-MeSO4** at pH (a) = 10.95, (b) = 11.65, (c) = 12.30, (d) plot between rate constant, k vs pH.

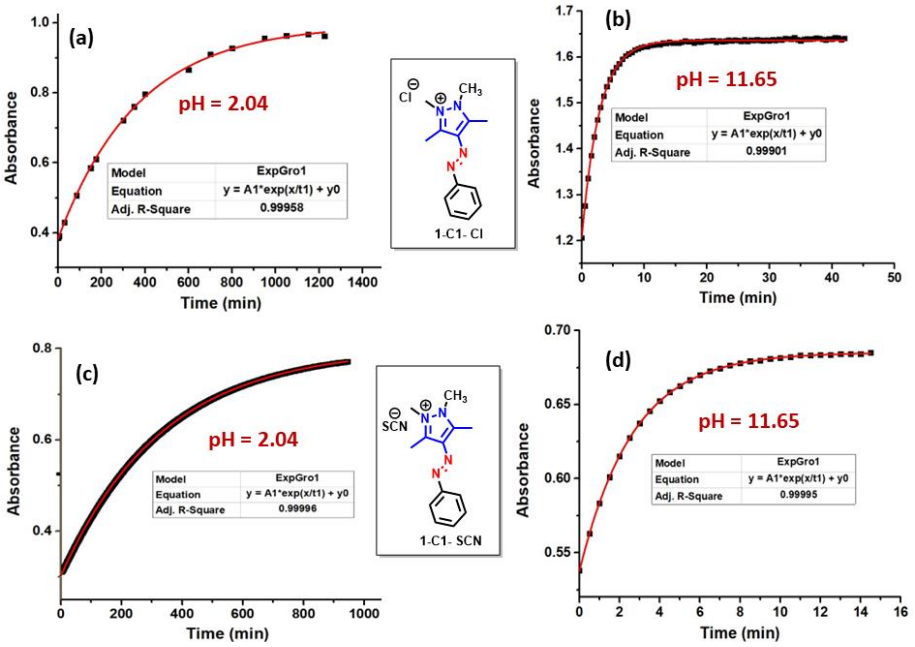

Figure 3B.8.11. Thermal *Z-E* isomerization kinetics studies followed by UV-Vis spectroscopy of compound (a) compound **1-C1-Cl** at pH 2.04, (b) compound **1-C1-Cl** at pH 11.65, (c) compound **1-C1-SCN** at pH 2.04, (d) compound **1-C1-SCN** at pH 11.65.

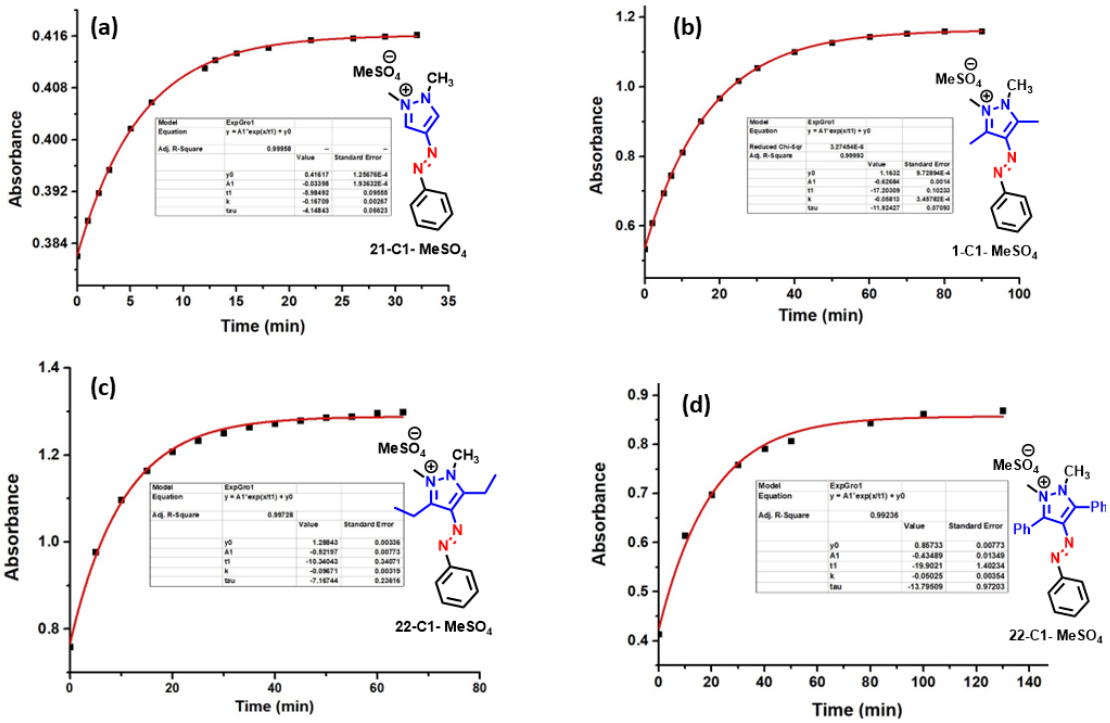

Figure 3B.8.12: Thermal *Z-E* isomerization kinetics studies followed by UV-Vis spectroscopy in excess amount of **DBU** (a) derivative **21-C1-MeSO4** at rt; (b) derivative **1-C1-MeSO4** at rt; (c) derivative **23-C1-MeSO4** at 80 ^{o}C; (d) derivative **23-C1-MeSO4** at 80 ^{o}C.

3B.9. Quantification of photoisomers in different pH: ^{1}H NMR spectroscopy

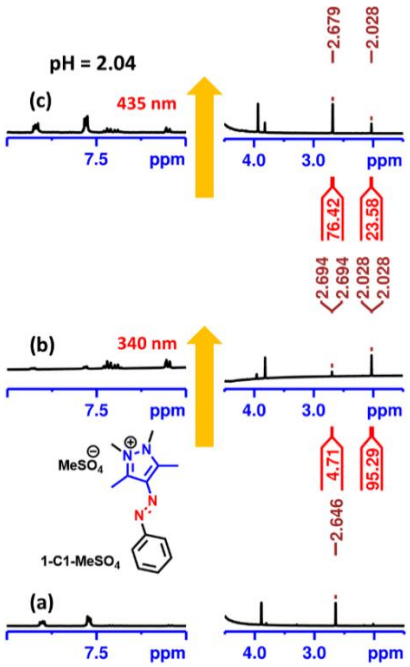

Figure 3B.9.1. Estimation of PSS composition using ^{1}H NMR spectroscopy of **1-C1-MeSO$_4$** (60% D_2O: buffer, pH = 2.04). (a) before irradiation; (b) after irradiation at 340 nm (2 h); (c) after irradiation at 435 nm (45 min). (Normalized integral values of selected protons are indicated for *E*- and *Z*-isomers.)

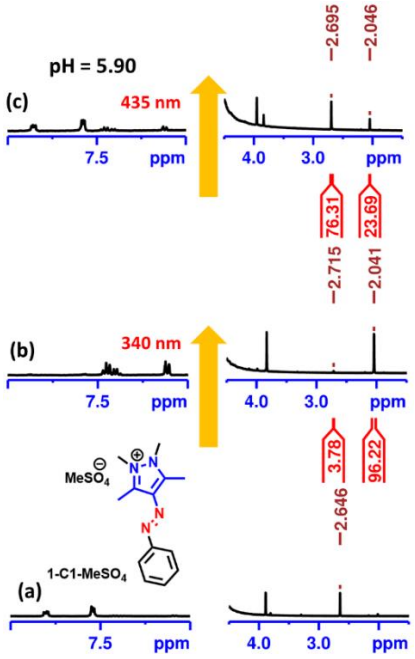

Figure 3B.9.2. Estimation of PSS composition using ^{1}H NMR spectroscopy of **1-C1-MeSO$_4$** (60% D_2O: buffer, pH = 5.90). (a) before irradiation; (b) after irradiation at 340 nm (2 h); (c) after irradiation at 435 nm (45 min). (Normalized integral values of selected protons are indicated for *E*- and *Z*-isomers.)

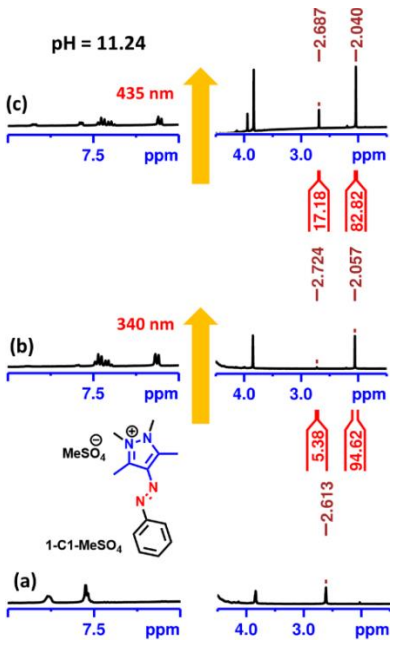

Figure 3B.9.3. Estimation of PSS composition using ^{1}H NMR spectroscopy of **1-C1-MeSO$_4$** (60% D_2O: buffer, pH = 11.24). (a) before irradiation; (b) after irradiation at 340 nm (2 h); (c) after irradiation at 435 nm (45 min). (Normalized integral values of selected protons are indicated for *E*- and *Z*-isomers.)

3B.10. Photoswitching and long-term stability of 1-C1-MeSO$_4$ in presence of GSH

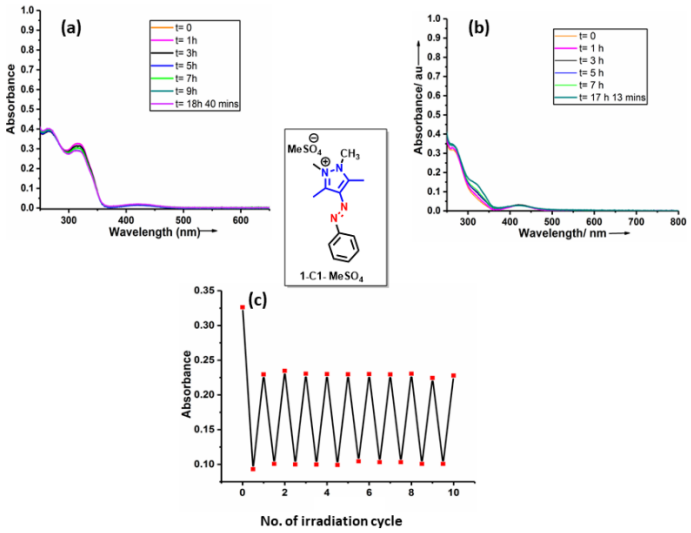

Figure 3B.10.1: Stability of **1-C1-MeSO$_4$** under the possible maximum biological concentration of glutathione (GSH) (10 mM) in phosphate buffer (pH = 7.4). (a) The UV-Vis spectral data of *E*- isomer of **1-C1-MeSO$_4$** in the presence of GSH; The spectra were recorded at different time intervals (o min, 1 h, 3 h, 5 h, 7 h, 9 h, 18 h 40 min), (b) The UV-Vis spectral data of *Z*- isomer of **1-C1-MeSO$_4$** in the presence of GSH; The spectra were recorded at different time intervals (o, 1 h, 3 h, 5 h, 7 h 17 h 13 min), (c) Photoisomerization stability of **1-C1-MeSO$_4$** in presence of GSH (The forward *E*-*Z* and the reverse *Z*-*E* photoisomerzation steps were alternatively carried out at 340 and 435 nm, respectively over 10 cycles.

3B.11. Crystallographic details of compound **1-C1-BPh$_4$** and **24-C1-MeSO$_4$**

Single crystal X-ray diffraction data of compounds **1-C1-BPh$_4$** and **24-C1-MeSO$_4$** were collected using a Rigaku XtaLAB mini diffractometer equipped with Mercury375M CCD detector. The data were collected with MoKα radiation (λ = 0.71073 Å) using omega scans. During the data collection, the detector distance was 49.9 mm (constant) and the detector was placed at 2θ = 29.85° (fixed). The data collection and data reduction were done using CrysAlisPro 1.171.38.46, and crystal structures were solved through OLEX2 package using SHELXT and the structures were refined using SHELXH-1997 (**1-C1-BPh$_4$**) and SHELXL (**24-C1-MeSO$_4$**) programs.

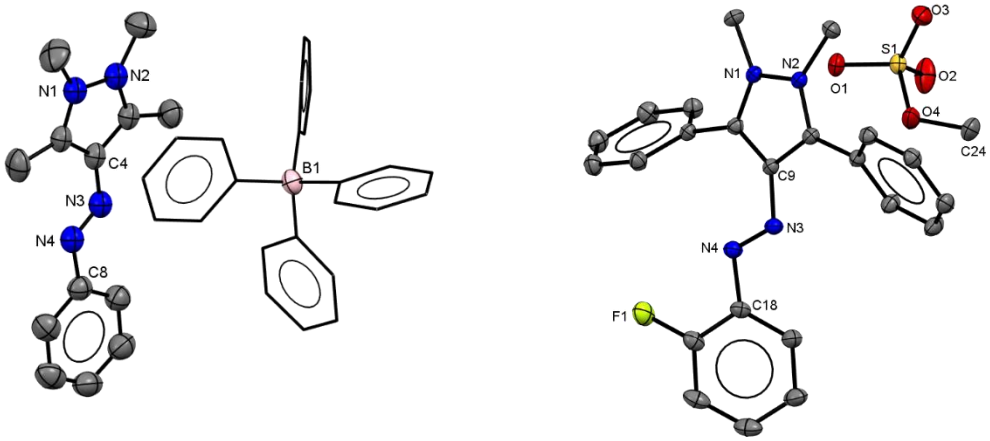

Figure 3B.11. Single crystal X-ray structures of compound **1-C1-BPh$_4$ (Left)** and **24-C1-MeSO$_4$ (Right)**. All hydrogen atoms have been omitted for clarity. Selected interatomic distances (Å) and bond angles for compound **1-C1-BPh$_4$** (°): N1-N2 = 1.375(4), N3-N4 = 1.247(4); N4-N3-C4 = 114.2(3), N3-N4-C8 = 112.8(3). Compound **24-C1-MeSO$_4$:** N1-N2 = 1.3632(14), N4-N3 = 1.2593(15), N3-C9 = 1.3994(15), N4-C18 = 1.4231(16); N4-N3-C9 = 114.90(11), N3-N4-C18 = 112.55(11).

Compound[a]	**1-C1-BPh_4**	**24-C1-$MeSO_4$**
Chemical Formula	$C_{37}H_{37}BN_4$	$C_{24}H_{23}FN_4O_4S$
Molar mass	548.52	482.52
Crystal system	Monoclinic	Monoclinic
Space group	$P2_1/n$	$P2_1/n$
T [K]	298.01(1)	150.00(10)
a [Å]	9.5331(16)	8.1092(3)
b [Å]	16.345(3)	30.1258(10)
c [Å]	19.808(3)	10.0304(4)
α [°]	90.0	90
β [°]	90.774(15)	111.532(4)
γ [°]	90.0	90
V [Å^3]	3086.3(8)	2279.38(16)
Z	4	4
D(calcd.) [g·cm^{-3}]	1.180	1.406
μ(Mo-K_α) [mm^{-1}]	0.069	0.190
Reflections collected	22345	25343
Independent reflections	5469	7921
Data/restraints/parameters	5469/0/353	7921/0/310
$R1$, $wR2[I>2\sigma(I)]$[a]	0.0964, 0.2620	0.0565, 0.1572
R1, wR2 (all data)[a]	0.1339, 0.3312	0.0647, 0.1710
GOF	1.054	1.074
CCDC	2209844	2209843

[a] $R1 = \Sigma||Fo| - |Fc||/\Sigma|Fo|$. $wR_2 = [\Sigma w(|Fo^2| - |Fc^2|)^2/\Sigma w|Fo^2|^2]^{1/2}$

3B.12. Compound characterization (^{1}H, ^{19}F, ^{11}B, ^{31}P, and ^{13}C-NMR) data

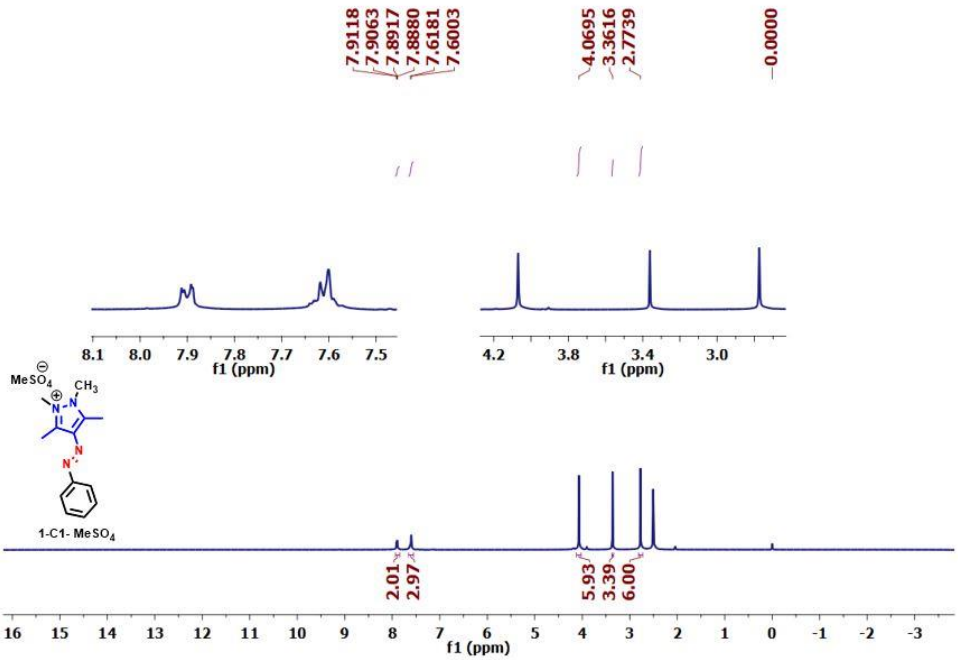

^{1}H NMR spectrum of (*E*)-1,2,3,5-tetramethyl-4-(phenyldiazenyl)-1*H*-pyrazol-2-ium methanesulfonate, **1-C1-MeSO$_4$** (400 MHz, DMSO-d$_6$).

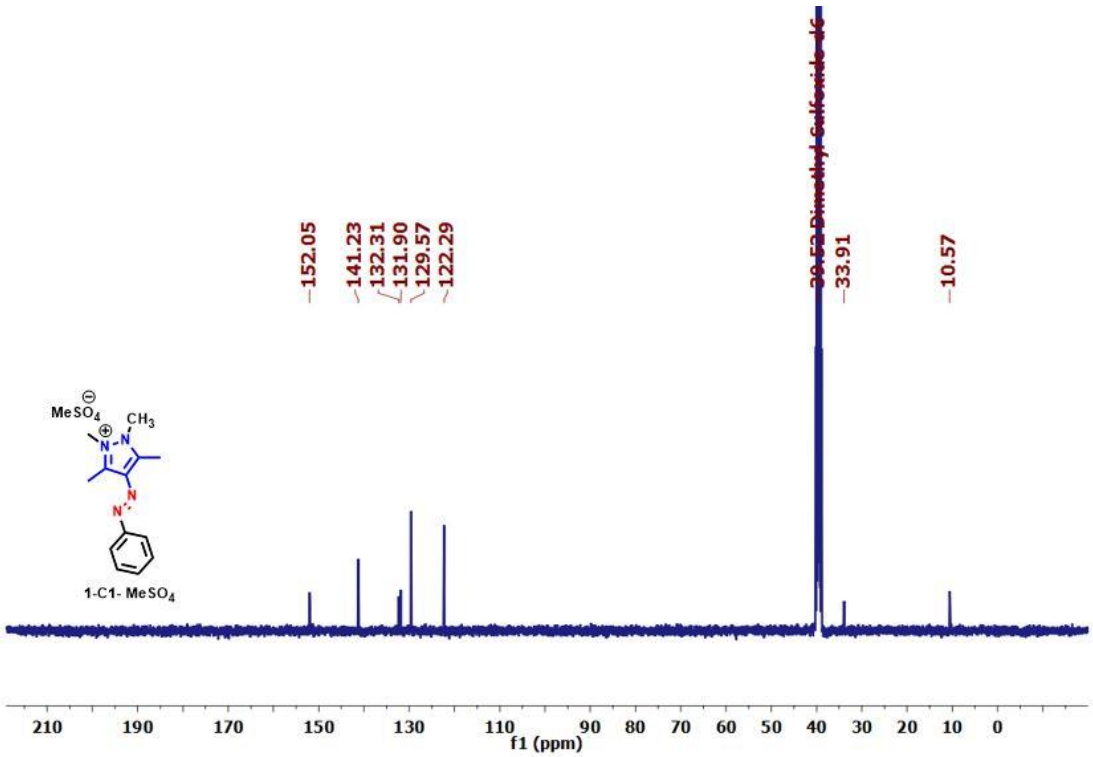

^{13}C NMR spectrum of (*E*)-1,2,3,5-tetramethyl-4-(phenyldiazenyl)-1*H*-pyrazol-2-ium methanesulfonate, **1-C1-MeSO$_4$** (100 MHz, DMSO-d$_6$).

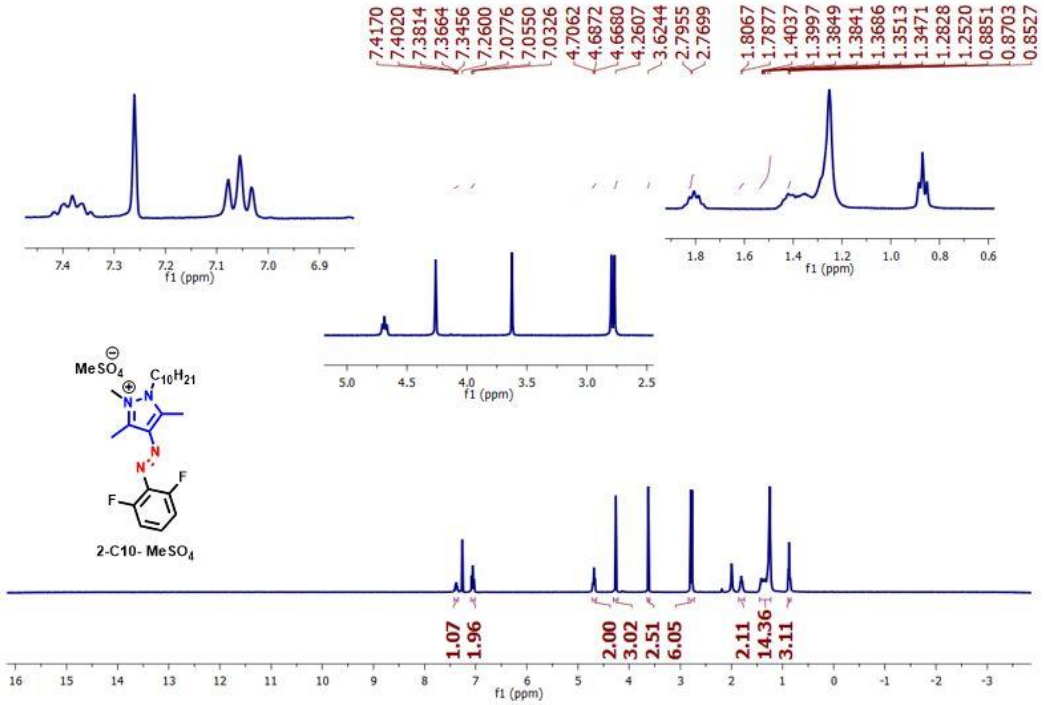

^{1}H NMR spectrum of (*E*)-1-decyl-4-((2,6-difluorophenyl)diazenyl)-2,3,5-trimethyl-1*H*-pyrazol-2-ium methanesulfonate, **2-C10- MeSO$_4$** (400 MHz, $CDCl_3$).

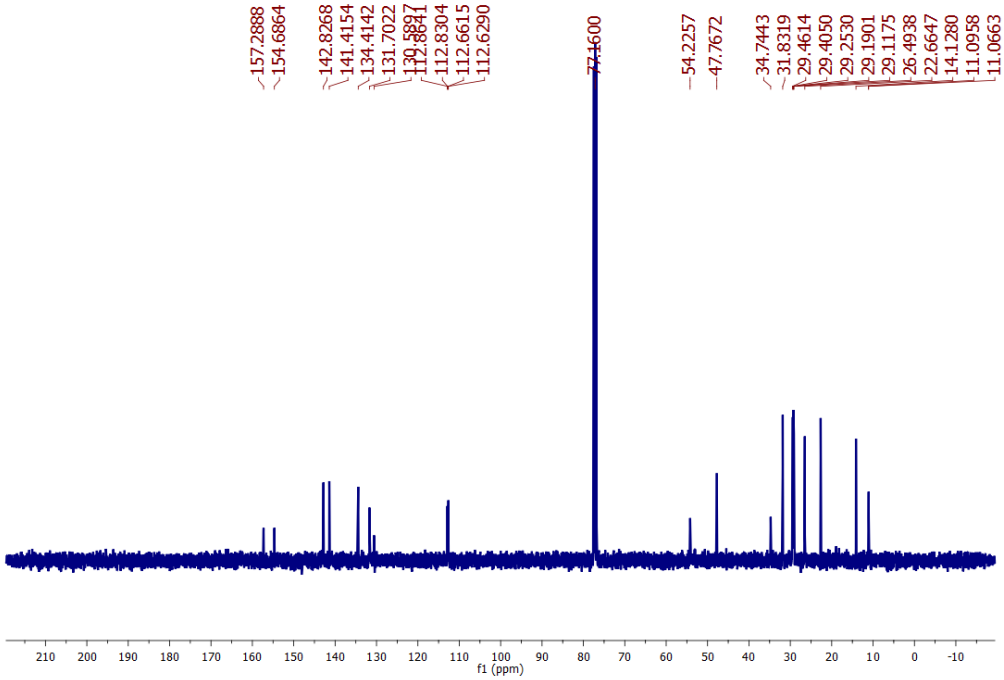

^{13}C NMR spectrum of (*E*)-1-decyl-4-((2,6-difluorophenyl)diazenyl)-2,3,5-trimethyl-1*H*-pyrazol-2-ium methanesulfonate, **2-C10- MeSO$_4$** (100 MHz, $CDCl_3$).

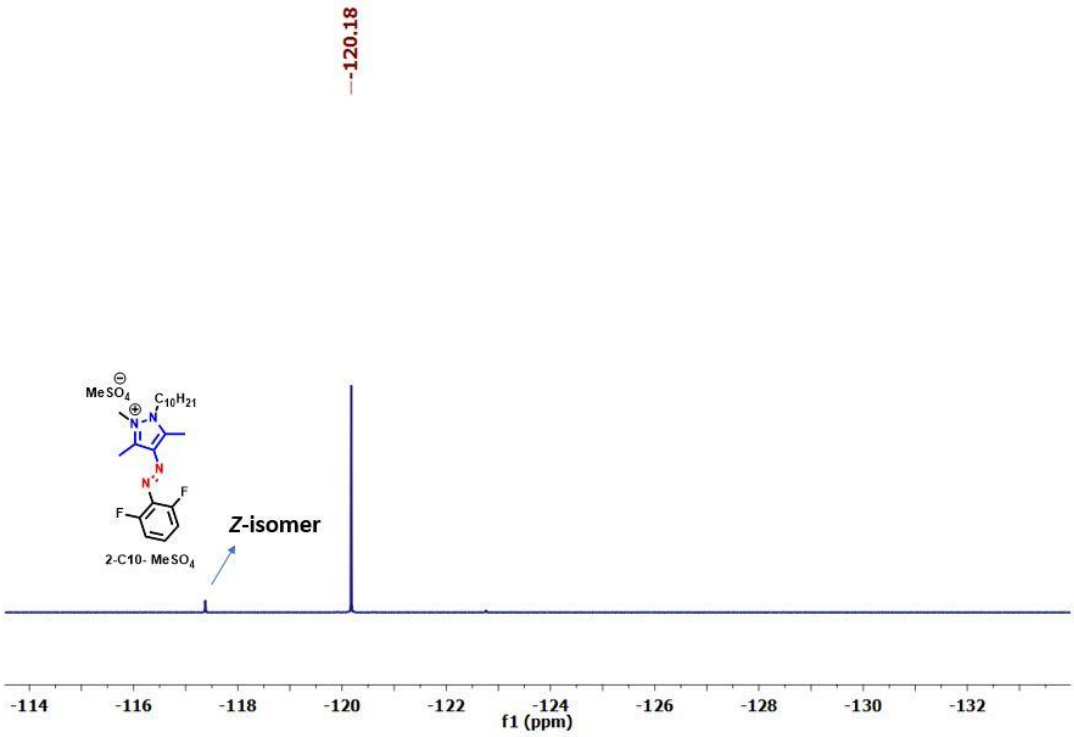

^{19}F NMR spectrum of (*E*)-1-decyl-4-((2,6-difluorophenyl)diazenyl)-2,3,5-trimethyl-1*H*-pyrazol-2-ium methanesulfonate, **2-C10- MeSO$_4$** (376.5 MHz, $CDCl_3$).

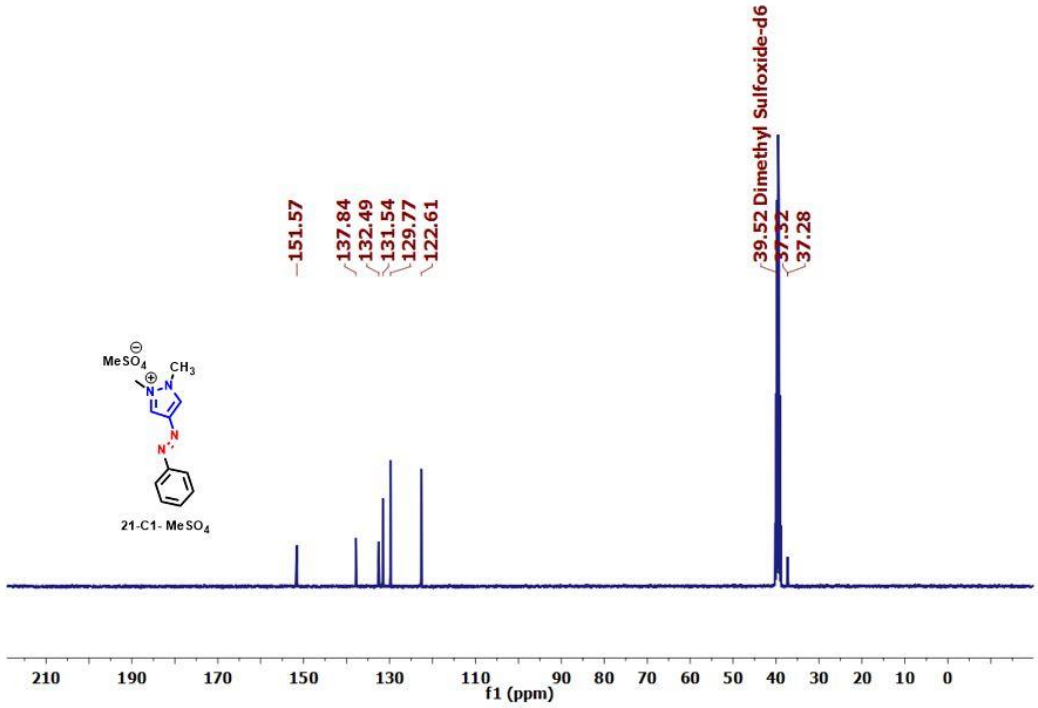

^{13}C NMR spectrum of (*E*)-4-((2-fluorophenyl)diazenyl)-3,5-diphenylisoxazole, **14ac** (100 MHz, $CDCl_3$)

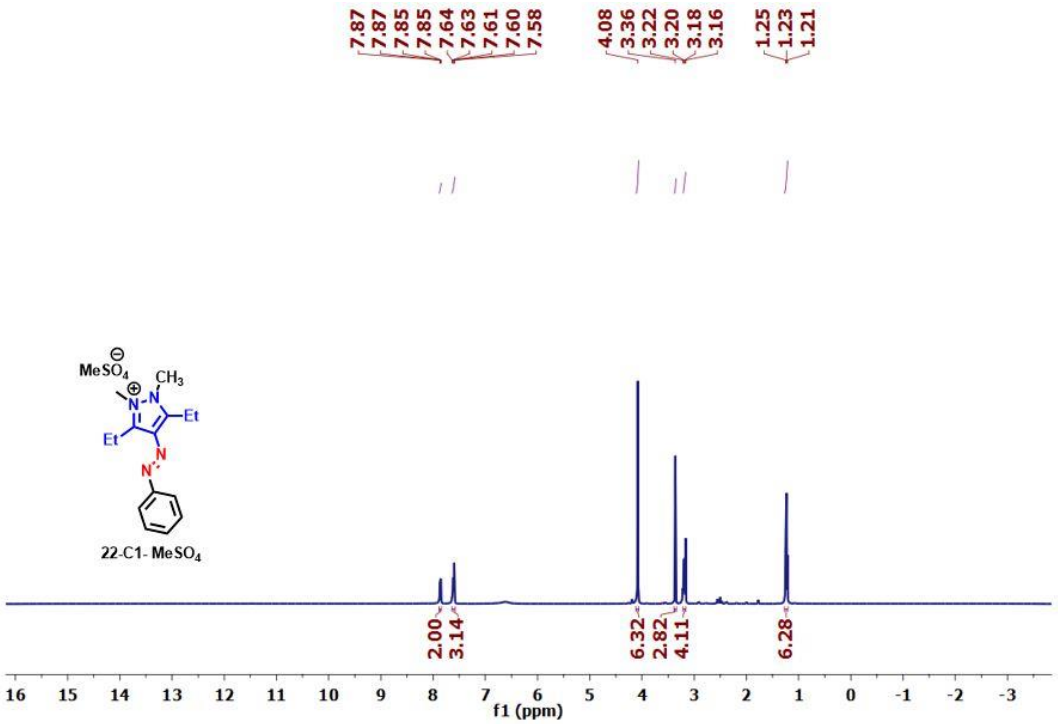

[1]H NMR spectrum of (*E*)-4-((2-fluorophenyl)diazenyl)-3,5-diphenylisoxazole, **15aa** (400 MHz, $CDCl_3$)

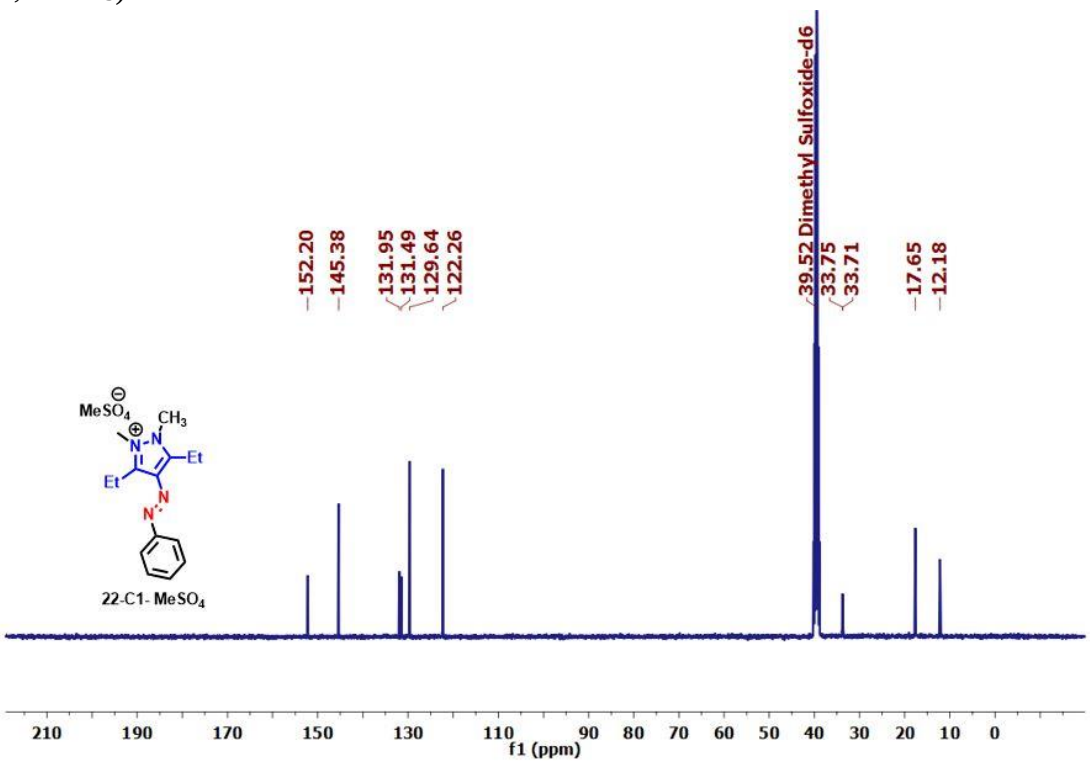

[13]C NMR spectrum of (*E*)-3,5-diethyl-1,2-dimethyl-4-(phenyldiazenyl)-1*H*-pyrazol-2-ium methanesulfonate, **22-C1-MeSO4** (100 MHz, $CDCl_3$).

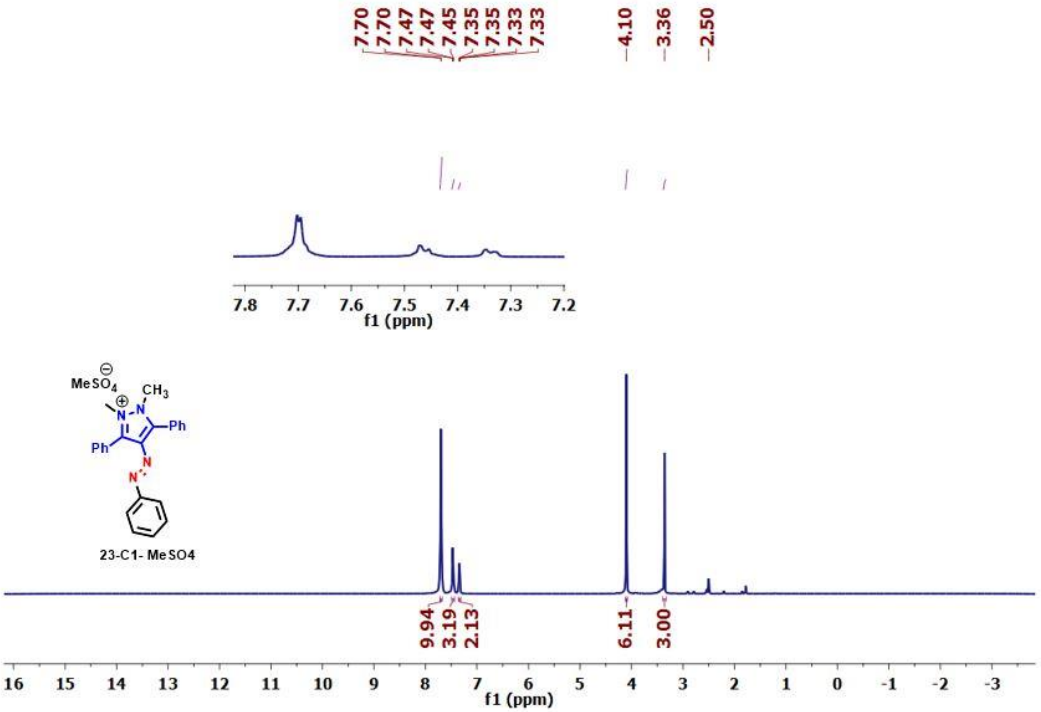

[1]H NMR spectrum of ((*E*)-1,2-dimethyl-3,5-diphenyl-4-(phenyldiazenyl)-1*H*-pyrazol-2-ium methanesulfonate, **23-C1-MeSO4** (400 MHz, $CDCl_3$).

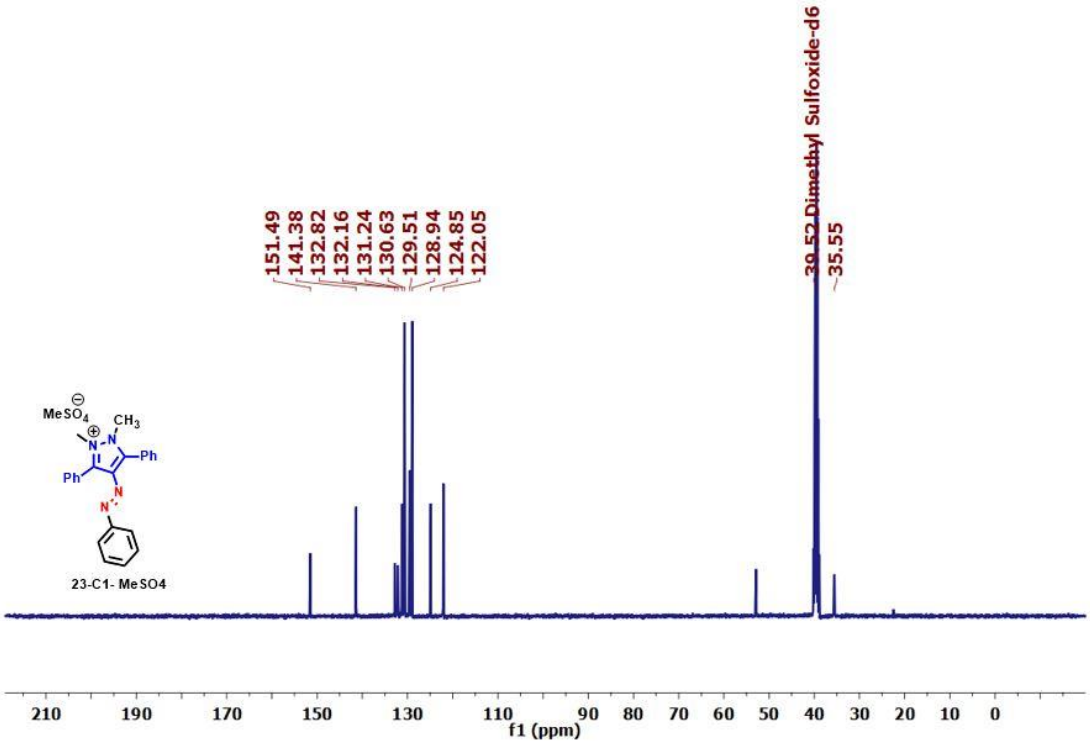

[13]C NMR spectrum of (*E*)-1,2-dimethyl-3,5-diphenyl-4-(phenyldiazenyl)-1*H*-pyrazol-2-ium methanesulfonate, **23-C1-MeSO4** (100 MHz, $CDCl_3$).

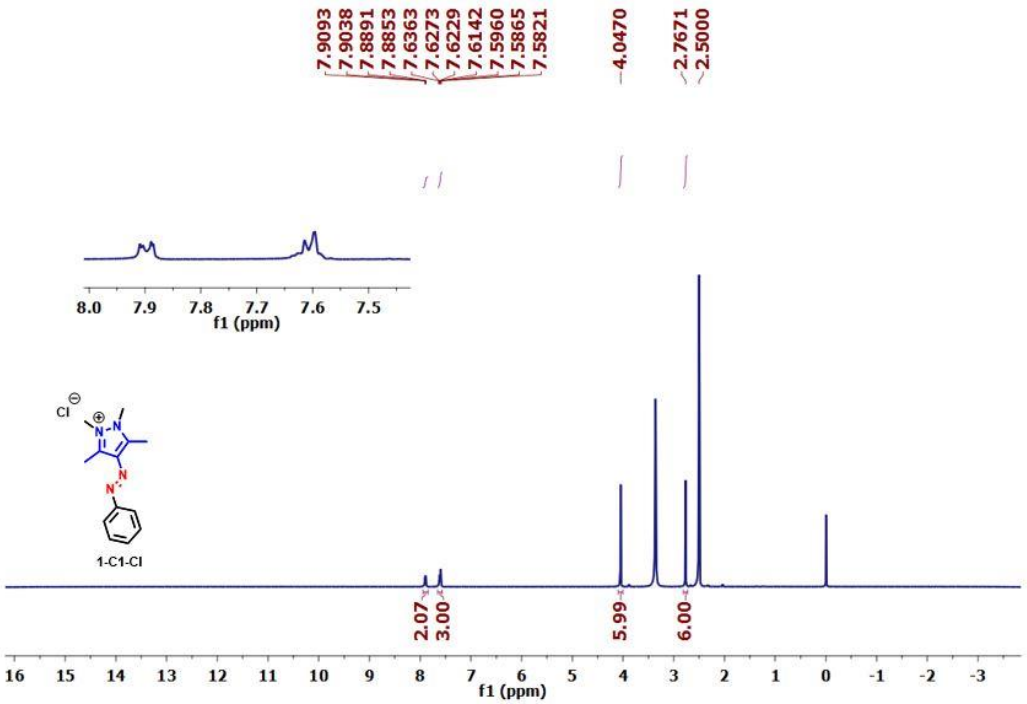

^{1}H NMR spectrum of (*E*)-1,2,3,5-tetramethyl-4-(phenyldiazenyl)-1H-pyrazol-2-ium chloride, **1-C1-Cl** (400 MHz, $CDCl_3$).

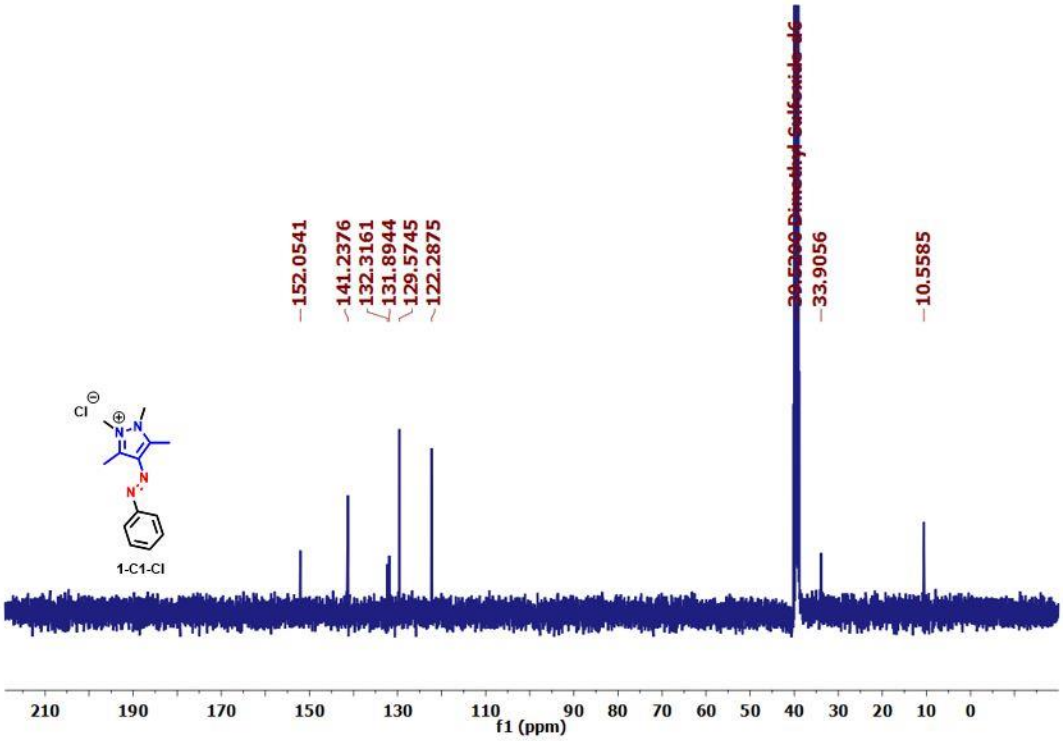

^{13}C NMR spectrum of (*E*)-1,2,3,5-tetramethyl-4-(phenyldiazenyl)-1H-pyrazol-2-ium chloride, **1-C1-Cl** (100 MHz, $CDCl_3$).

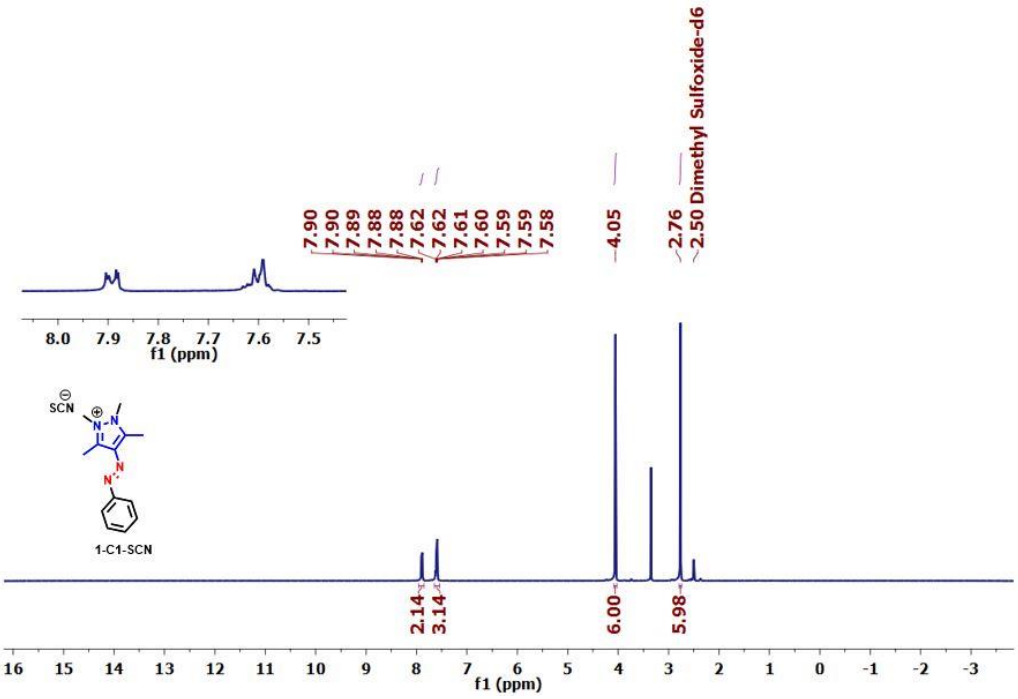

[1]H NMR spectrum of **(***E*)-1,2,3,5-tetramethyl-4-(phenyldiazenyl)-1H-pyrazol-2-ium thiocyanate, **1-C1-SCN** (400 MHz, $CDCl_3$).

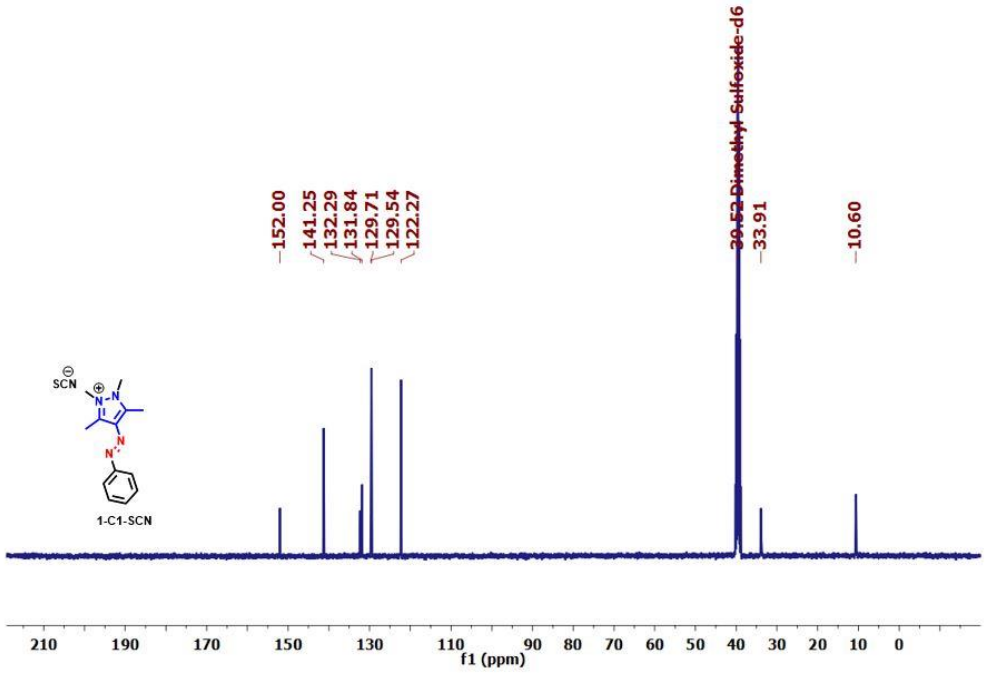

[13]C NMR spectrum of (*E*)-1,2,3,5-tetramethyl-4-(phenyldiazenyl)-1H-pyrazol-2-ium thiocyanate, **1-C1-SCN** (100 MHz, $CDCl_3$).

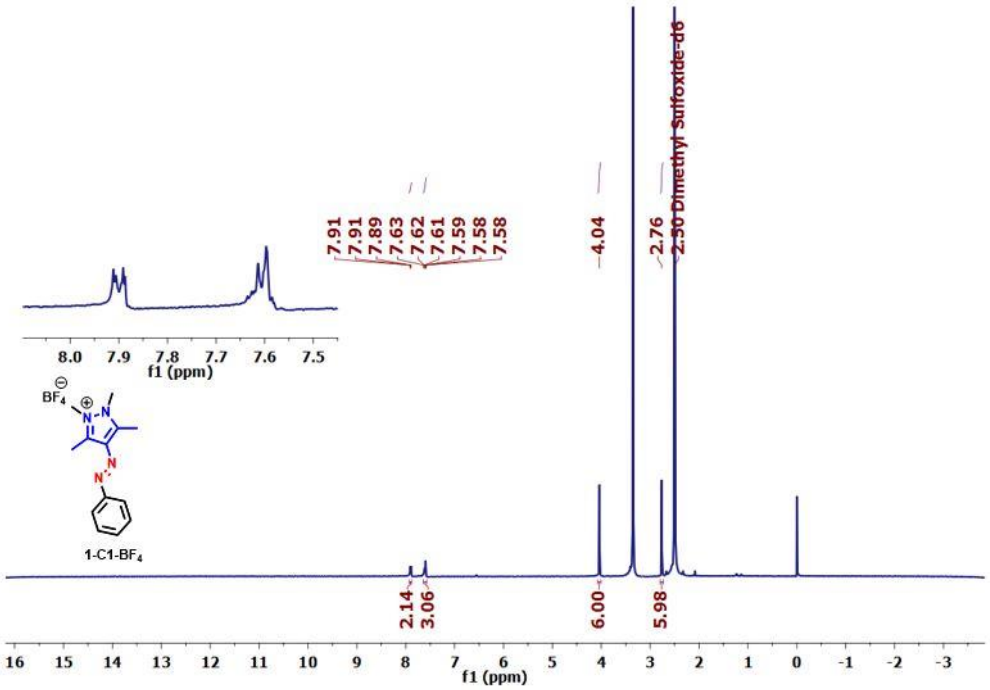

^{1}H NMR spectrum of (*E*)-1,2,3,5-tetramethyl-4-(phenyldiazenyl)-1H-pyrazol-2-ium tetrafluoroborate, **1-C1-BF$_4$** (400 MHz, $CDCl_3$).

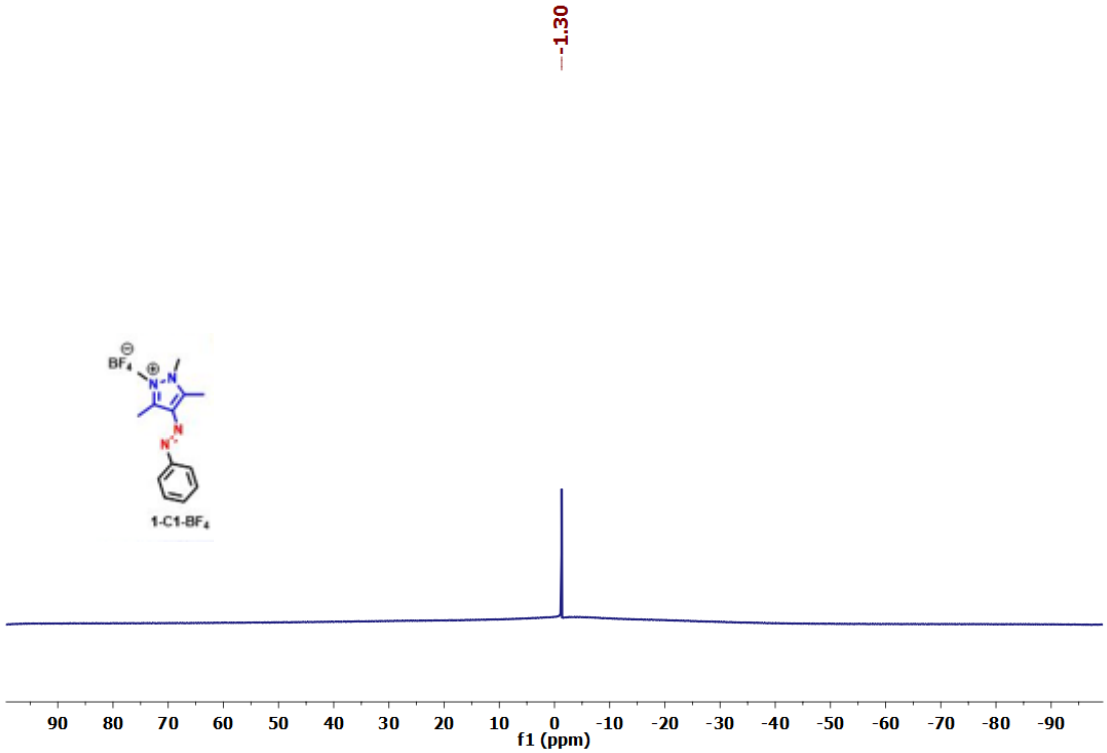

^{11}B NMR spectrum of (*E*)-1,2,3,5-tetramethyl-4-(phenyldiazenyl)-1H-pyrazol-2-ium tetrafluoroborate, **1-C1-BF$_4$** (128.3 MHz, $CDCl_3$).

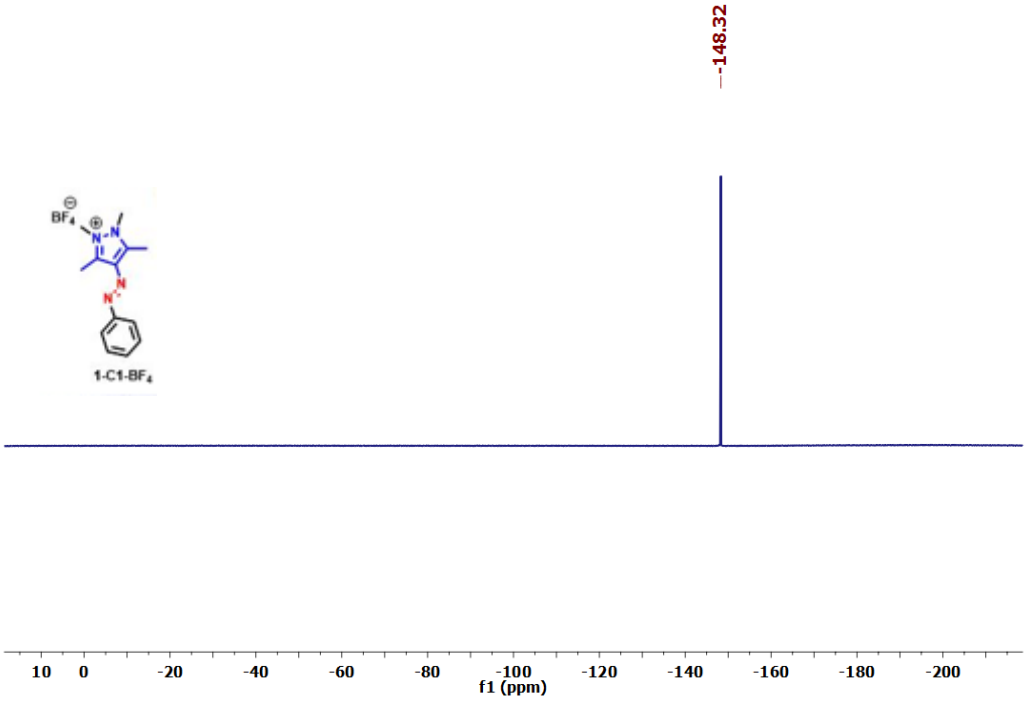

^{19}F NMR spectrum of (*E*)-1,2,3,5-tetramethyl-4-(phenyldiazenyl)-1H-pyrazol-2-ium tetrafluoroborate, **1-C1-BF$_4$** (376.5 MHz, $CDCl_3$).

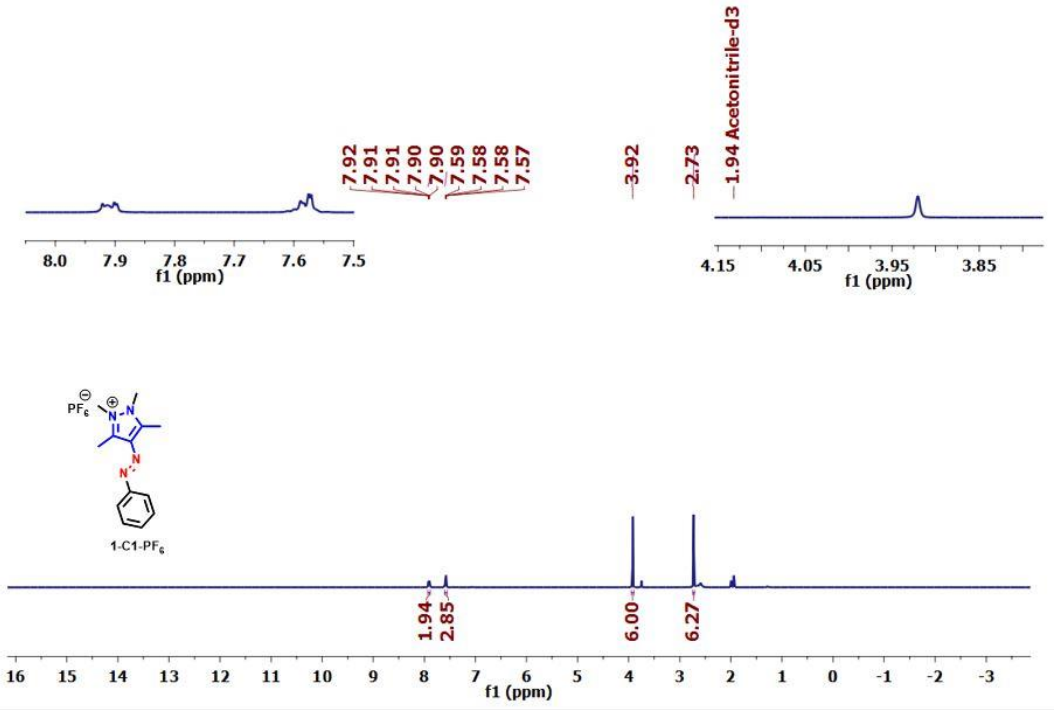

^{1}H NMR spectrum of (*E*)-1,2,3,5-tetramethyl-4-(phenyldiazenyl)-1H-pyrazol-2-ium hexafluorophosphate, **1-C1-PF$_6$** (400 MHz, $CDCl_3$).

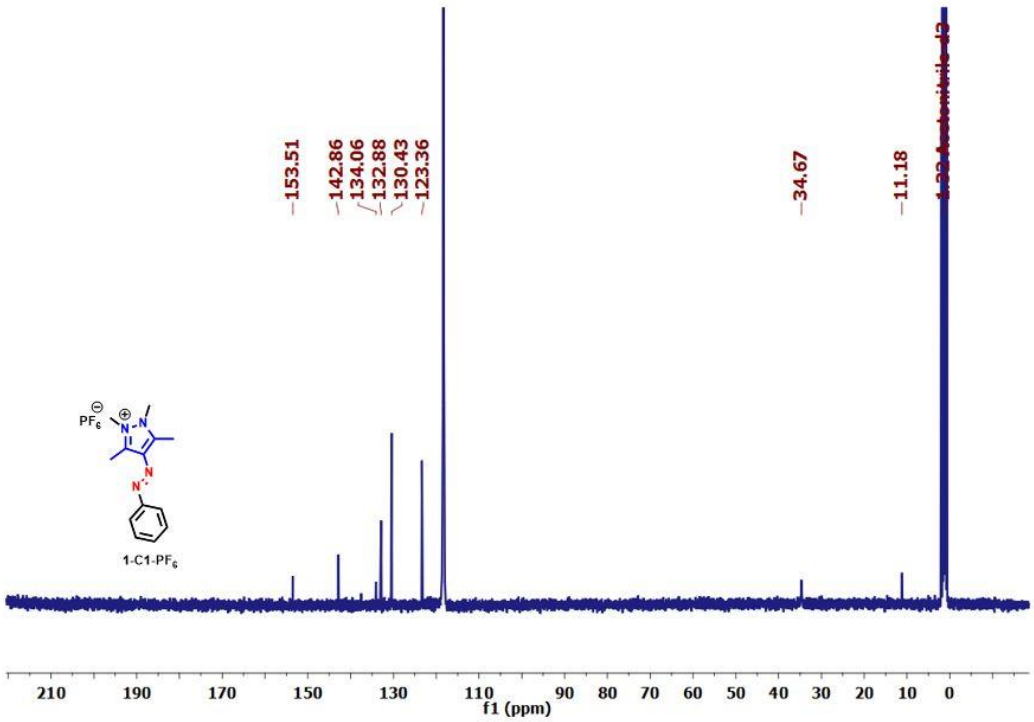

^{13}C NMR spectrum of (*E*)-1,2,3,5-tetramethyl-4-(phenyldiazenyl)-1H-pyrazol-2-ium hexafluorophosphate, **1-C1-PF$_6$** (100 MHz, $CDCl_3$).

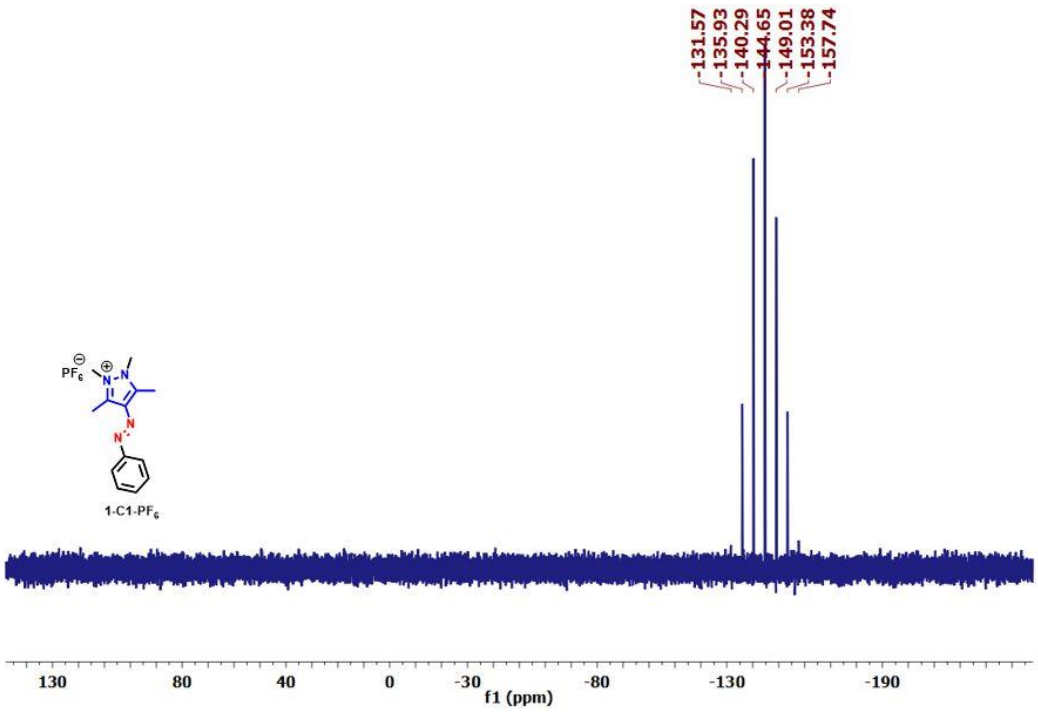

^{31}P NMR spectrum of (*E*)-1,2,3,5-tetramethyl-4-(phenyldiazenyl)-1H-pyrazol-2-ium hexafluorophosphate, **1-C1-PF$_6$** (162.1 MHz, $CDCl_3$).

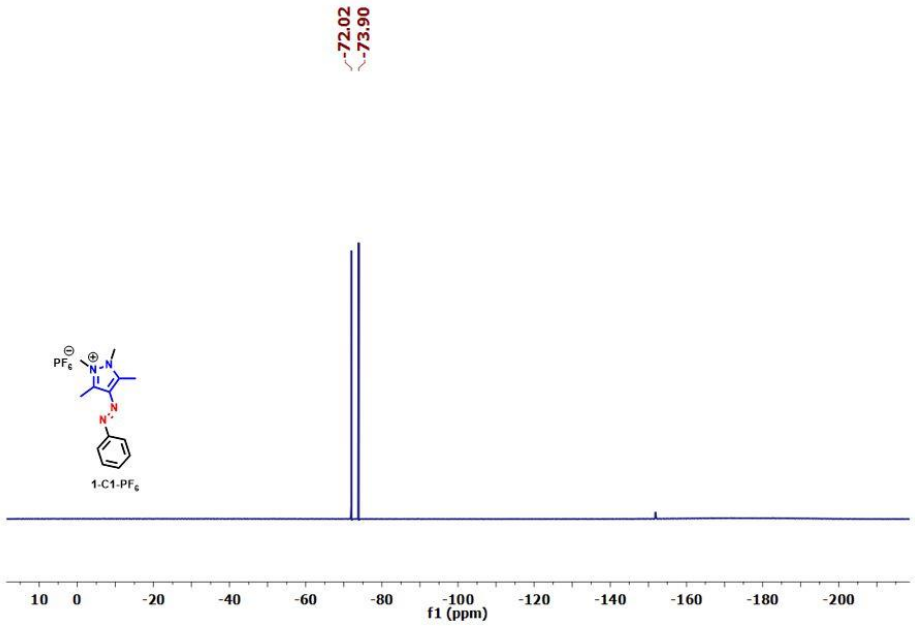

^{19}F NMR spectrum of (*E*)-1,2,3,5-tetramethyl-4-(phenyldiazenyl)-1H-pyrazol-2-ium hexafluorophosphate, **1-C1-PF$_6$** (376.5 MHz, $CDCl_3$).

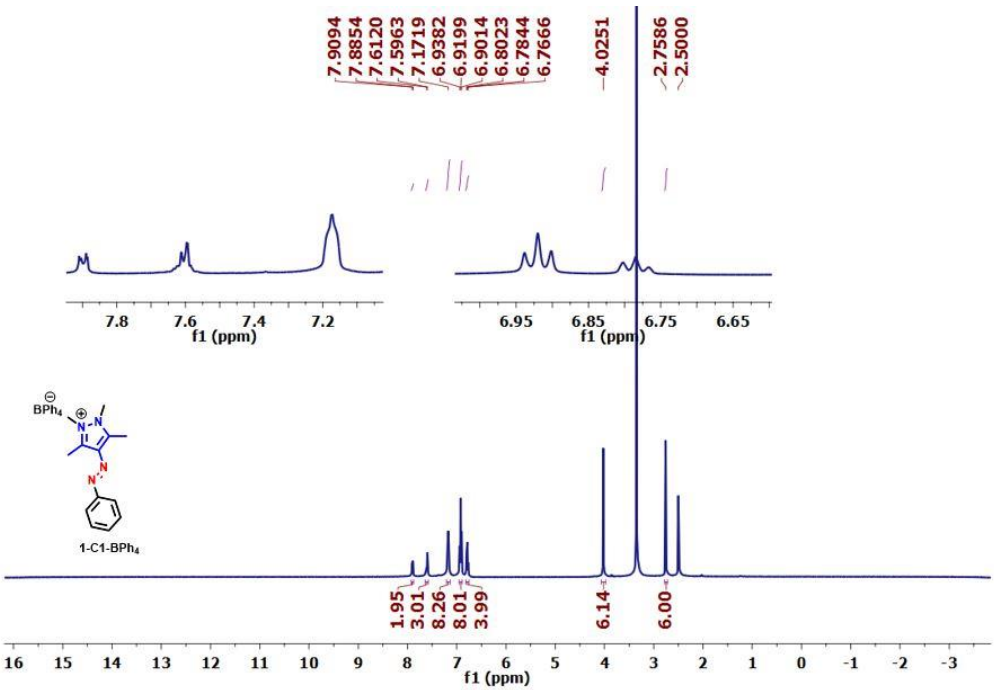

^{1}H NMR spectrum of (*E*)-1,2,3,5-tetramethyl-4-(phenyldiazenyl)-1*H*-pyrazol-2-ium tetraphenyl-l4-borane, **1-C1-BPh$_4$** (400 MHz, $CDCl_3$).

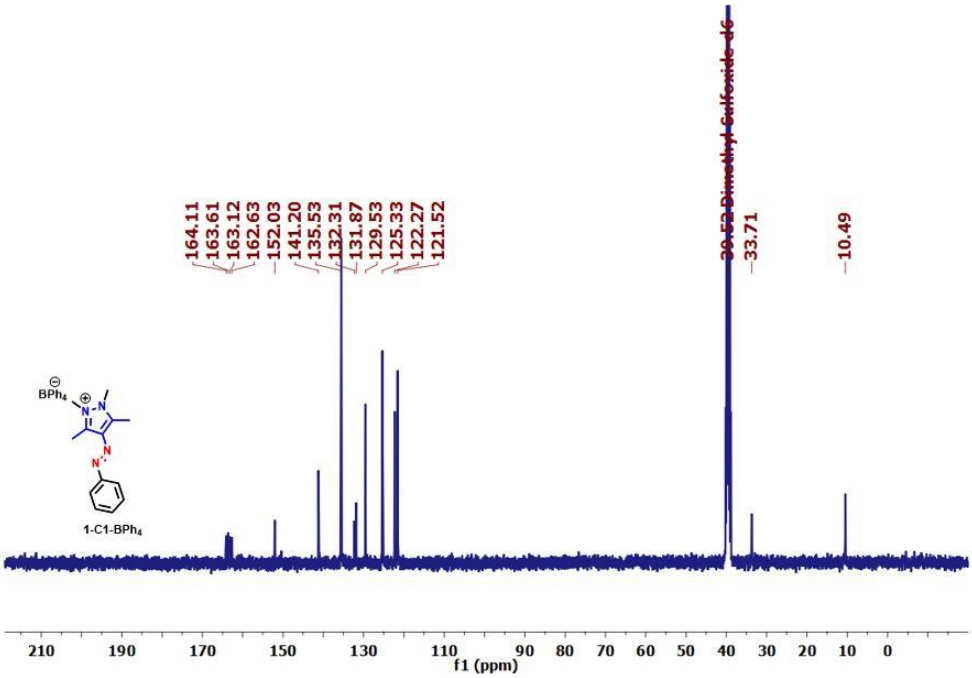

^{13}C NMR spectrum of (*E*)-1,2,3,5-tetramethyl-4-(phenyldiazenyl)-1*H*-pyrazol-2-ium tetraphenyl-l4-borane, **1-C1-BPh4** (100 MHz, $CDCl_3$).

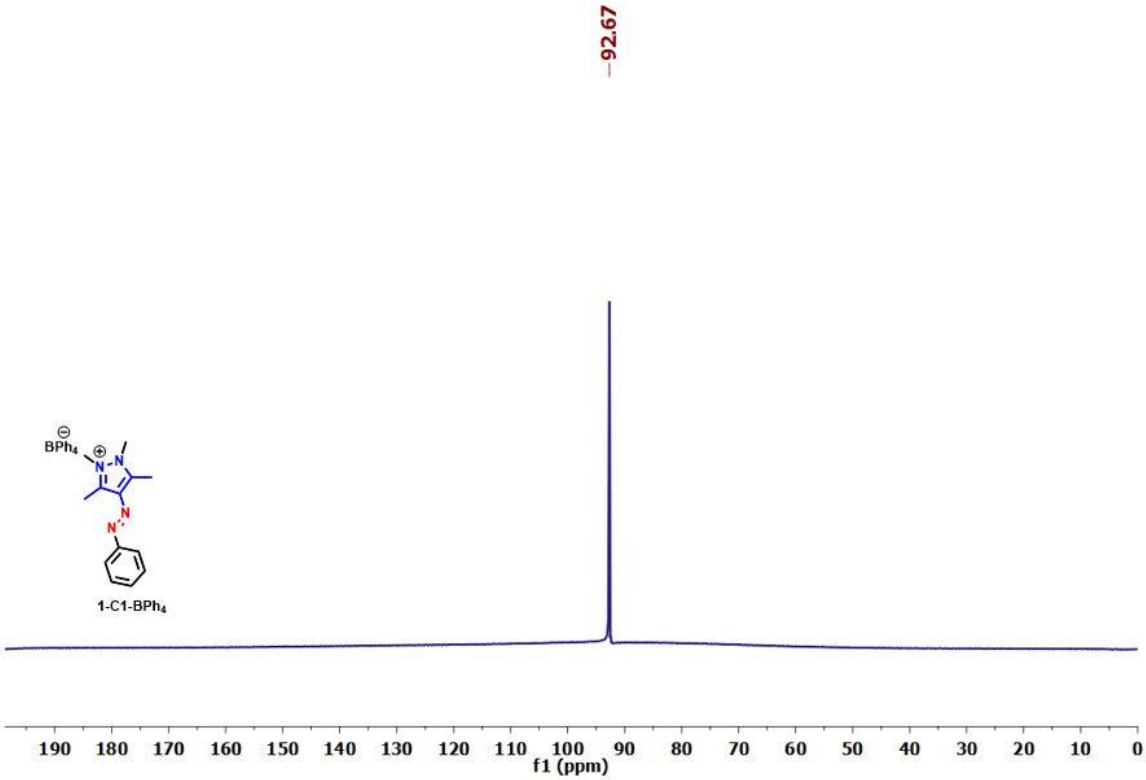

^{11}B NMR spectrum of (*E*)-1,2,3,5-tetramethyl-4-(phenyldiazenyl)-1*H*-pyrazol-2-ium tetraphenyl-l4-borane, **1-C1-BPh4** (128.3 MHz, $CDCl_3$).

Chapter 4. Photochromic multi-azo(hetero)arene connected systems

4.1 Introduction

Molecules exhibiting reversible photochromic properties are useful for devloping smart light triggered devices such as energy storage, actuator, field-effect transistor, and photodetector, etc.[1-3] In this regard, various photoswitches have been developed to satisy the needs.[4] Among all, azobenzenes are widely used for their versatility, ease of synthesis, functionalization prospects, tunable thermal stability, bidirectional photoswitching, and excellent photo rigidity under light.[5] Ineed, all these properties make him suitable candidate for various applications.

In recent decades, photoswitching ability of azoheteroarenes such azoimidazole, azopyrazole, azotriazole, azotetrazole, azothiophene, azoindole, etc. have shown the excellent photoswitching, and tunable *Z*-isomer stability.[6] Particularly the *N*-methylphenylazopyrazoles made way for many diverse applications owing to their long half-life of *Z*-isomer.[7-9] In contrast, the corresponding *Z*-isomer of 1*H*-3,5-dimethylpyrazole derivatives showed three orders of magnitude lower stability.[10] Substituent effects on such systems revealed the presence of substantial steric, electronic effects, and apart from concentration dependent hydrogen bonding interactions, through either intermolecular or solvent-assisted tautomerism destabilize the *Z*-isomer. However, the free NH of the pyrazole moiety allow additional possibilities in N-functionalization of the arylazopyrazole derivatives readily. The resulting new *N*-functionalized arylazopyrazoles can exhibit enhanced *Z*-isomer stability in solution phase.

In the recent decades, the efficiency of solution phase photoswitching of azoarenes has been tremendously improved. However, for practical applications, solid-state photoswtiching is highly desirable. Applications such as rewritable printing and imaging demand solid state bistable compounds.[11] A wide range of structurally diverse classes of molecules are known for their solid-state photochromic properties. In majority of those cases, the light driven switching has been used for printing, however, thermal conditions are required for erasing. Apart from that, the systems need extensive synthesis or polymeric linkages for enabling the reversible writing and erasing processes.[12-15] Another important challenge in this regard is to design molecular systems with large free-volume that requires control in molecular packing and aggregation. Particularly π–π stacking and other supramolecular interactions such as

hydrogen bonding needs to be controlled for better efficiency in the light-driven isomerization processes.[16] In this regard, we planned to develop solid-state switchable systems using arylazo-1*H*-3,5-dimethylpyrazoles owing to their versatility and synthetic prospects.

In the design part, we intended to attach multiple arylazopyrazoles to a core moiety for improving the absorption characteristics. Furthermore, we have also considered the following aspects: (a) symmetry (for avoiding the spectral congestion); (b) π–π stacking (the two methyl groups attached to each of the pyrazole moiety have been considered to inhibit it); (c) hydrogen bonding (introduction of linkages and core groups to minimize it); (d) introducing of flexible units; (e) comparison of C_3 tripodal multiple azobenzenes with azoheteroarenes. Based on these, we designed six C_3 tripodal molecular systems with different connections.

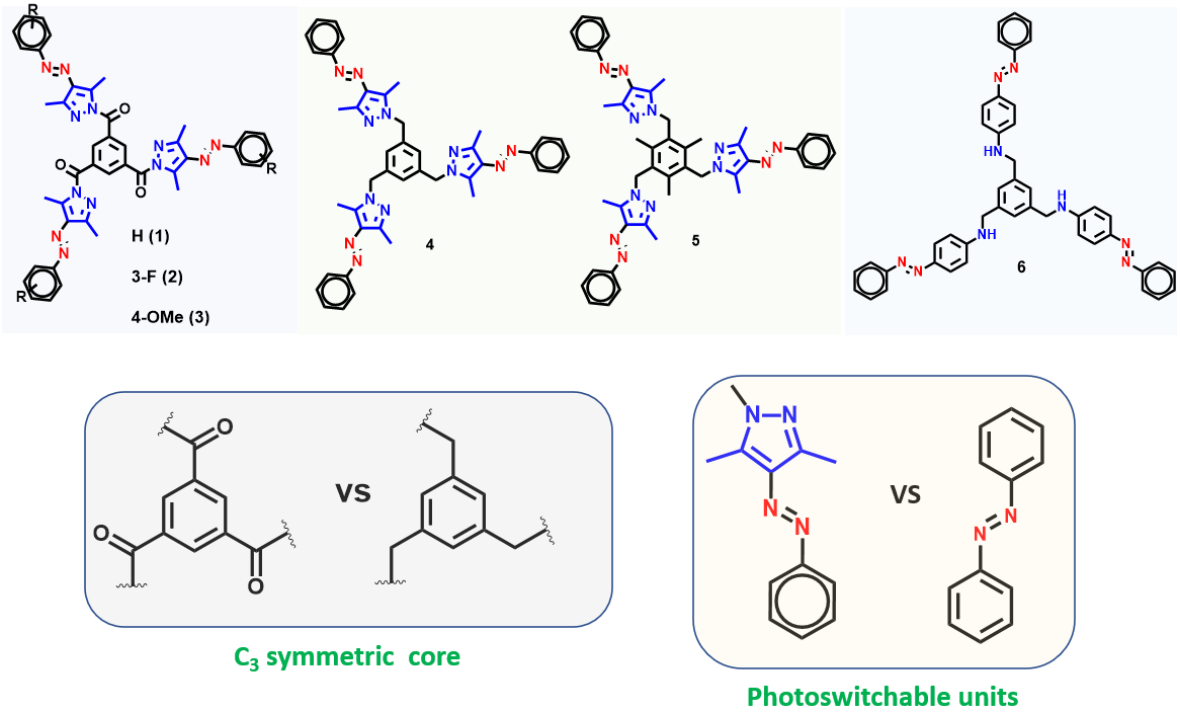

Scheme 4.1. Design scheme of C_3-connected azo(hetero)arene photoswitches.

4.2 Synthesis

We have synthesized all the 6 tripodal targets using the procedures adopted from the literature (**Scheme 4.1**).[17] For accessing derivatives **1-3**, their corresponding azopyrazole derivatives were treated with the in situ generated trimesoyl chloride, derived from trimesic

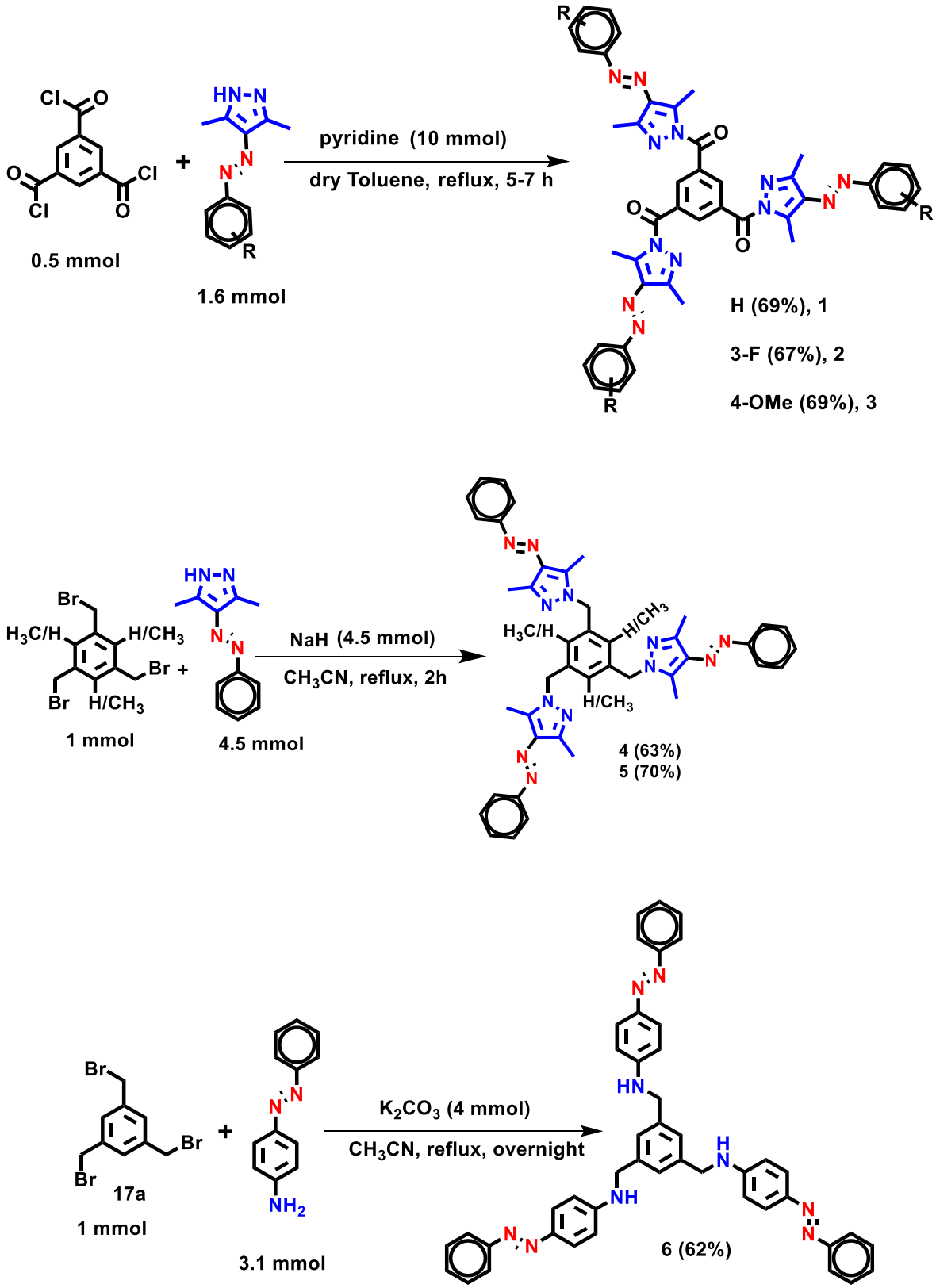

Scheme 4.2. Synthesis scheme of C_3-connected azo(hetero)arene photoswitches.

acid. The targets **4** and **5** were synthesized through a nucleophilic substitution strategy under basic condition using phenylazo-1*H*-3,5-dimethylpyrazole with 1,3,5-

tris(bromomethyl)benzene, and 1,3,5-tris(bromomethyl)mesitylene respectively. Similarly, target **6** was synthesized under similar methods using 4-aminoazobenzene and 1,3,5-tris(bromomethyl)benzene using K_2CO_3 as a base.

4.3 Photoswitching studies

UV-Vis spectroscopic studies

Foremost, we carried out UV-Vis spectroscopic studies for all the tripodal targets **4-6** in DMSO as a solvent. Whereas, $CHCl_3$ was used for derivatives **1-3** due to insolubility in DMSO. Due to the azo chromophores, all the targets in their native state (*EEE*) exhibited strong π–π* absorption bands (**Figure 4.1** and **Appendix**) and weak n–π* features. The derivative **6** showed overlapping π–π* and n–π* bands. For targets with flexible connections, such as **4**, **5**, and **6** the π–π* absorption features were observed at 338, 342, and 413 nm, respectively. Compared to those λ_{max} values, the corresponding simple photoswitches, *N*-methyl phenylazo-3,5-dimethyl-pyrazole, and 4-(*N*-methylamino)azobenzene absorb at 339 and 416 nm, respectively (**Appendix**). This indicates that the flexible connections exhibit no or a weak electronic influence on the azo chromophore of the photoswitches. Despite connected together, the tripodal targets essentially behave like three independent photoswitches. The electronic effect arising due to the donating power of the amine linker in **6** leads to an overlap of π–π* and n–π* bands (aminoazobenzene type).[5a]

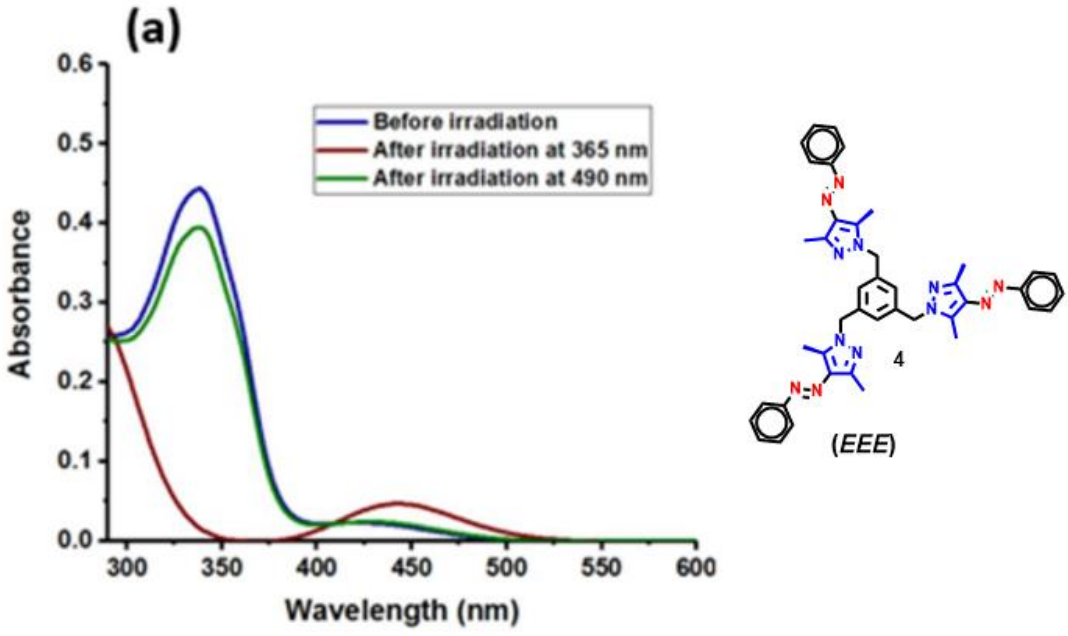

Figure 4.1. Photoswitching studies of derivative **4** in DMSO.

Due to the appearance of only one set of π–π* and n–π* absorption bands, UV-Vis spectroscopy was unable to differentiate among the individual *EEZ*, *EZZ* and *ZZZ*-isomers (**Figure 4.1**). All of the derivatives have been subjected to reverse isomerization using different wavelengths of light.

Pyrazole derivatives **4** and **5** exhibited quantitative forward photoisomerization upon irradiation with 365 nm light whereas the reverse photoisomerization happened with 490 nm light. The derivative **6** showed forward photoisomerization with 405 nm light whereas the reverse photoisomerization was achieved by 535 nm light. Apart from photoisomerization studies, we have also tested the long-term stability of all these derivatives over five cycles. None of the derivatives showed any fatigue.

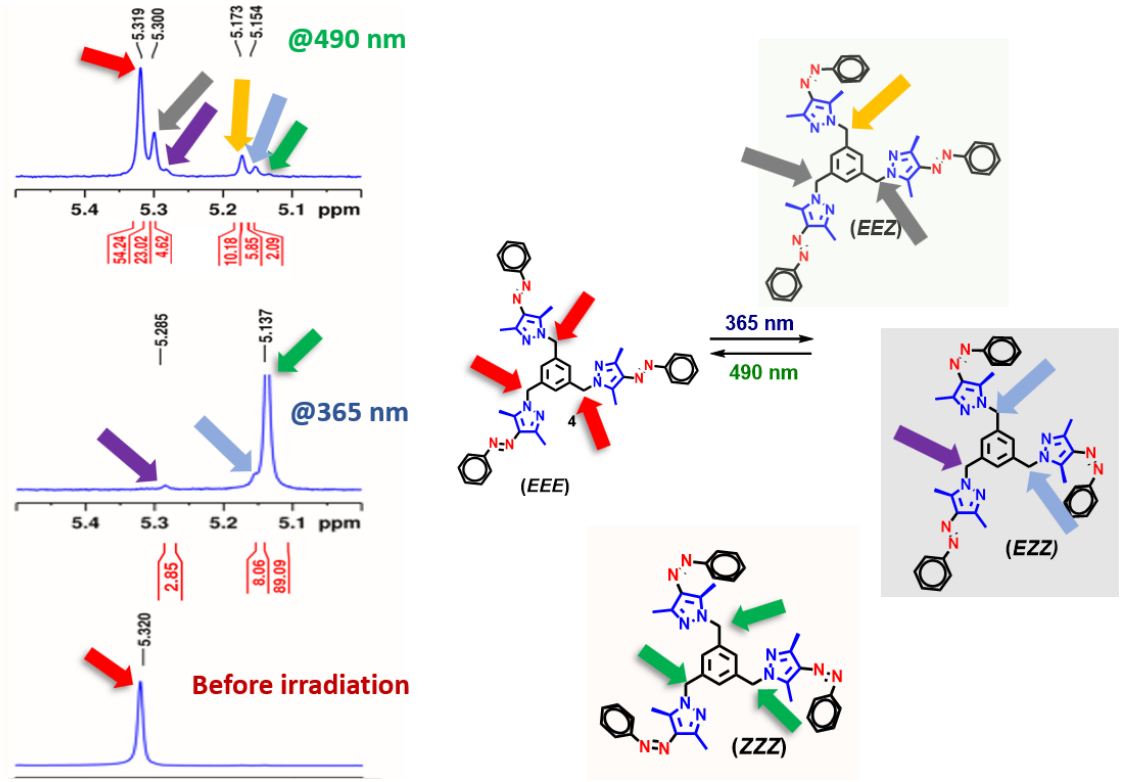

Figure 4.2. PSS composition with different photoisomers representation of **4** (DMSO-d_6, 4.16 mM) (partial ^{1}H NMR of derivative **4**).

For understanding bistability, the estimation of the individual photoisomers (PSS composition) for the forward and reverse isomerization steps is necessary. Towards this, we conducted the photoswitching studies of all targets (**1-3** in $CDCl_3$ **4**, **5** in DMSO-d_6 at mM concentrations). The analysis of the PSS compositions has been carried out using ^{1}H-NMR spectroscopy (**Figure 4.2** and **Appendix**).

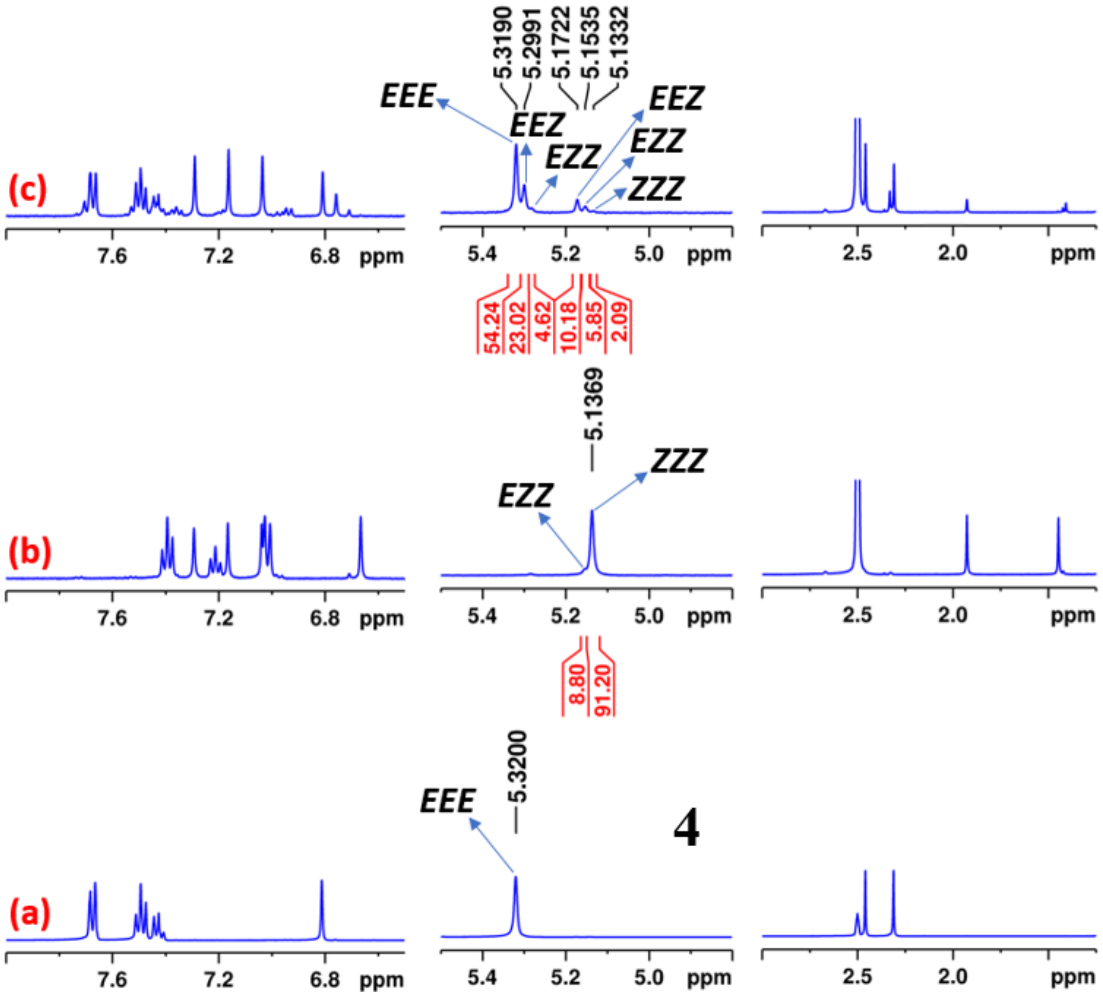

Figure 4.3. PSS composition in **4** (DMSO-d_6, 4.16 mM) (a) Before irradiation; (b) After irradiation at 365 nm; (c) After irradiation at 490 nm (For forward and reverse isomerization steps, PSS composition has been estimated using the normalized integral values of signals due to the linker CH_2 protons).

Due to broadness and overlapping in signals in the derivative **6**, we did not perform such experiments**.** Derivatives **4**, and **5** showed identical conversions of 91% *ZZZ* and 9% *EZZ* upon irradiation with 365 nm light. Conversily, upon irradiation at 490 nm, the derivative **4** led to 55% *EEE*, 33% *EEZ*, 10% *EEZ*, and 2% *ZZZ*; whereas, the derivative **5** formed 24% *EEE*, 33% *EEZ*, 28% *EEZ*, and 15% *ZZZ*.

Thermal reverse isomerization kinetics

Apart from the photoswitching characteristics, the stability of the metastable states under ambient conditions is quite significant in the application point of view. In general, a *Z*-isomer of the azoarene can undergo *Z*-*E* reverse thermal isomerization through inversion or rotational pathways that depend on substitution, type of azoarene, etc.[5a]

Table 4.1. UV-Vis photoswitching studies in solution state

S. No.	Compound	Electronic spectral data				PSS composition in solution phase photoswitching		Conc. (μM)
		Before photoswitching		After photoswitching		Forward *EEE*-*ZZZ* photoisomerization (in terms of % *EEE*)	Reverse *ZZZ*-*EEE* photoisomerization (in terms of %*EEE*)	
		λmax/ π–π* (ε)	λmax/ n–π*	λmax/ π–π*	λmax/ n–π*			
1	**1**	334 (64126 ± 1172)	440	293	442	76	91	10.0
2	**2**	336 (84181 ± 5251)	445	286	439	79	95	9.0
3	**3**	352 (77889 ± 2225)	443	313	446	87	86	9.4
4	**4**	338 (26671 ± 922)	421	282	443	96	88	16.7
5	**5**	342 (81029 ± 796)	407	289	443	94	88	7.3
6	**6**	413 (177832 ± 2097)	-	368	439	72	89	2.0

Thermal barriers and the half-lives associated with the individual metastable states can be tuned by changing the design. Since multiple photoswitchable units containing systems lead to different photoisomers, unraveling the thermal stability of the metastable states involves certain difficulties. This situation is due to the involvement of individual reverse thermal isomerization steps. All our 6 targets contain three photoswitchable groups each, and so the thermal reverse isomerization reactions happen over three consecutive steps, namely, *ZZZ-EZZ*, *EZZ-EEZ*, and *EEZ-EEE* with rate constants k_1, k_2 and k_3, respectively. Indeed, the thermal reverse isomerization kinetics of the derivative **1** in $CDCl_3$ was previously reported by following ^{1}H-NMR spectroscopic data.[17a] For other selected derivatives (**4, 5, 6**) we have done the kinetics study at elevated temperature in DMSO. Derivatives **4**, and **5** showed a half-life of 18, and 17 min, respectively at 90 ^{o}C. While derivative **6** showed a shorter life half (6.9 min) even at a lower temperature (60 ^{o}C) (**Figure 4.3**).

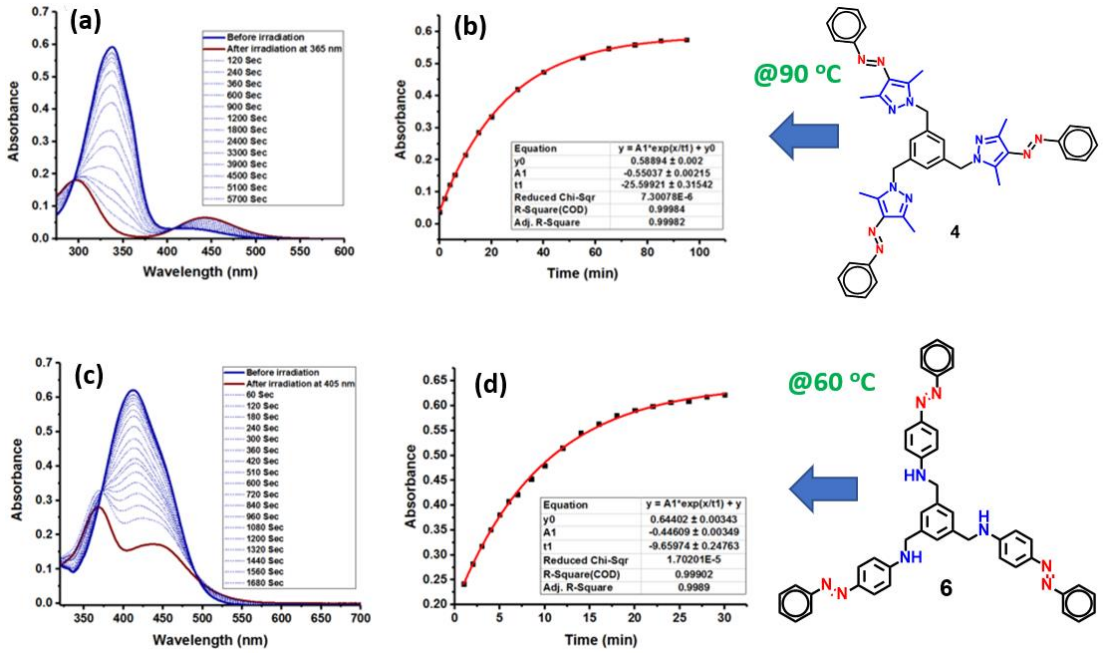

Figure 4.4. (a) & (b) Stepwise thermal reverse isomerization kinetics measurements of derivatives **4** & **6** at 90 & 60 ^{o}C, respectively; (c) & (d) corresponding first order thermal reverse isomerization kinetics plot and exponential fit of derivatives **4** & **6**.

Photoswitching in solid-state

In order to understand the solid-state photoswitching, we have used UV-Vis spectroscopic studies through reflectance mode in KBr medium (**Figure 4.4**). For derivative **1**, we observed prominent changes in the n–π^* band upon irradiation at 365 nm that clearly depicted the solid-state isomerization. The C_3 derivatives of azopyrazole (**1-5**) showed

photochromic behavior in solution as well as in solid-state. Indeed, the derivatives **1-5** exhibited a yellow to red color change upon irradiation with 365 nm light the in forward direction. Derivatives **1-3** showed the photochromic property in the reverse direction with light too; however, more flexible derivatives **4** & **5** showed color changes only upon heating in the reverse direction (**Figure 4.4 e-g**). Taking advantage of photochromic properties in the solid state, one of the derivatives **3** was dip coated on top of a filter paper. By keeping a mask and exposure of 365 nm light induced the color changes in the coated area, which made way to the printing of images.

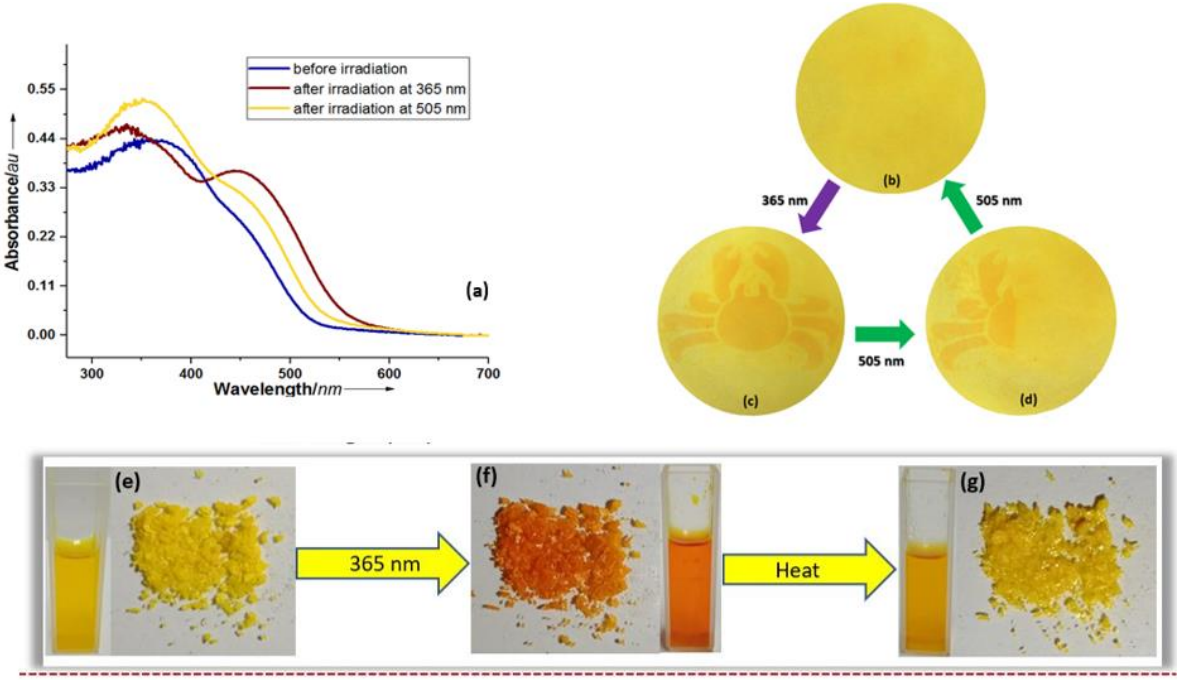

Figure 4.5. (a) Analysis of solid-state photoswitching of **3** in KBr medium using UV/Vis absorption spectroscopy. Printing and erasing of a "Crab" image on top of a filter paper: b) A filter paper dip coated with **3** (using a $CHCl_3$ solution of **3**); c) After irradiation at 365 nm through a Crab shaped stencil; d) Partial exposure to 505 nm light (by blocking half-of-the filter paper to erase half-of the image). By irradiating the entire filter paper, the image can be completely erased; Photo- and thermochromism in **4**: (e) yellow-colored solid-state and solution phase (in CH_3CN) samples of **4** in native state; (f) after exposure to a light of wavelength 365 nm exhibiting solid-state and solution phase photochromism; (g) after heating at 90 ^oC for 30 min (for the solid sample) and 70 ^oC for 1 h (for solution phase sample) to obtain thermochromism in reversing to the native state.

Similarly, the use of green light (505 nm) led to erasing of the images. Through this experiment, a completely light-driven image printing and erasing process was demonstrated in solid-state (**Figure 4.4 c-d**). The salient feature is the stability of the images that were unaffected for more than a week even in the presence of ambient light.

Powder X-ray diffraction (PXRD) studies

For gaining additional insights in the solid-state photochromism, one of the derivatives, **3** having 4-OCH_3 group, was subjected to PXRD studies. The PXRD data for the solid samples before and after irradiation were collected. After 365 nm irradiation, we obtained a red-coloured solid, which showed more amorphous nature compared to the native yellow coloured solid corresponding to *EEE*-isomer. Based on the inspection of data, upon changing the wavelength to 505 nm, the solid sample showed a partially recovery of crystallinity (**Figure 4.5**). The extent of changes from crystallinity to amorphous nature was consistent with the PSS compositions observed upon irradiation.

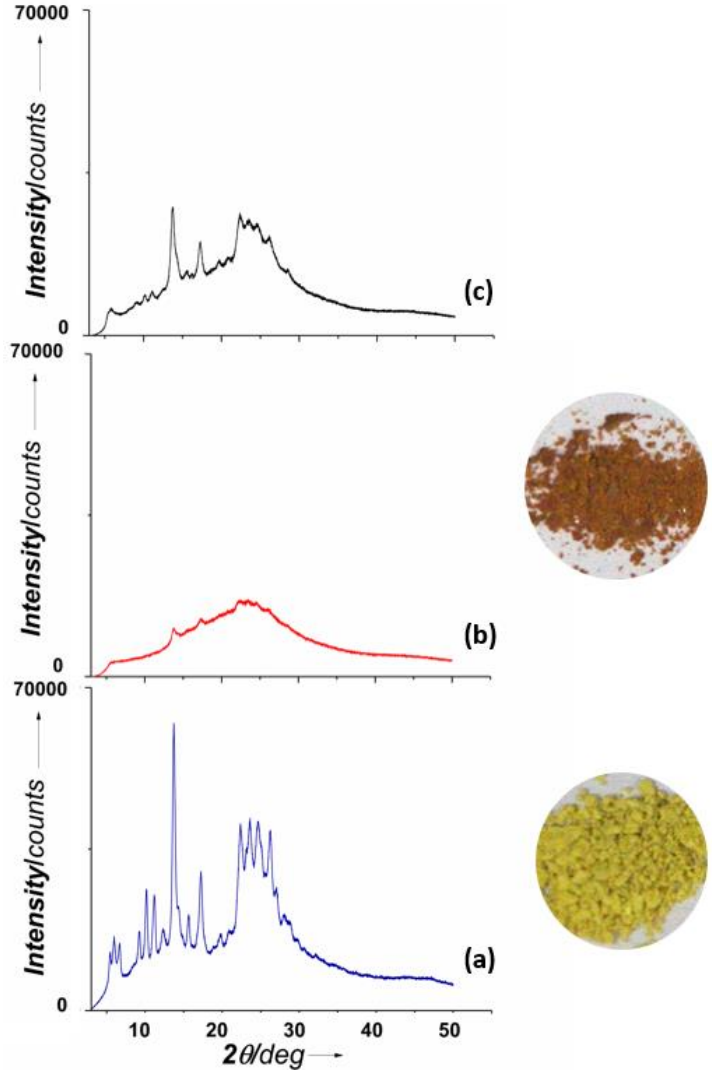

Figure 4.6. PXRD data of **3** corresponding to: a) The yellow-coloured native solid (before irradiation); b) The red-coloured solid (after irradiation of the $CHCl_3$ solution of the native sample at 365 nm, followed by evaporation of the solvent, and drying under high vacuum); c) After irradiation of the red $CHCl_3$ solution at 505 nm for 2 h, followed by evaporation of the solvent, and drying under high vacuum.

4.4 Experimental section

1,3,5-tris((3,5-dimethyl-4-((*E*)-phenyldiazenyl)-1*H*-pyrazol-1-yl)methyl)benzene (4)

Phenylazo-1*H*-3,5-dimethylpyrazole (0.90 g, 4.5 mmol) was dissolved in dry acetonitrile. Sodium hydride (60 % dispersion in mineral oil, 4.5 mmol) was added to it and the mixture was stirred at room temperature for 2 hours under a nitrogen atmosphere. 1,3,5-*tris*(bromomethyl)benzene (0.36 g, 1.0 mmol) was added, and the reaction mixture was refluxed overnight. The reaction was quenched with water and extracted with ethyl acetate. The combined ethyl acetate layers were dried over anhydrous sodium sulfate and the product was purified by column chromatography over silica gel using ethyl acetate and hexane (75:25) as an eluent (Yield = 63%).

1,3,5-tris((3,5-dimethyl-4-((*E*)-phenyldiazenyl)-1*H*-pyrazol-1-yl)methyl)benzene (4):Yellow solid, mp = 200-201 ^{o}C

^{1}H NMR (400 MHz, $CDCl_3$): δ 2.45 (s, 9H), 2.47 (s, 9H), 5.21 (s, 6H), 6.75 (s, 3H), 7.37 (t, *J* = 6.9 Hz, 3H), 7.44 (t, *J* = 7.3 Hz ,6H), 7.74 (d, *J*=7.8 Hz, 6H) ppm; ^{13}C (100 MHz, $CDCl_3$): δ 10.08, 14.08, 52.54, 121.96, 124.23, 129.02, 129.58, 135.55, 139.03, 140.36, 143.23, 153.59 ppm; HRMS-ESI: *m*/*z* $C_{42}H_{42}N_{12}$ $[M+H]^+$ calc. 715.3733, obs. 715.3741; IR (ATR, cm^{-1}): 509, 517,533, 540, 551, 576, 630, 645, 682, 699, 716, 763, 848, 1003, 1068, 1155, 1264, 1303, 1373, 1394, 1417, 1458, 1502, 1557, 2923, 3081.

1,1',1''-((2,4,6-trimethylbenzene-1,3,5-triyl)tris(methylene))tris(3,5-dimethyl-4-((*E*)-phenyldiazenyl)-1*H*-pyrazole) (7)

To obtain **5**, the same procedure as in the synthesis of **4** was adopted using 2,4,6-*tris*(bromomethyl)mesitylene (Yield = 70%).

1,1',1''-((2,4,6-trimethylbenzene-1,3,5-triyl)tris(methylene))tris(3,5-dimethyl-4-((*E*)-phenyldiazenyl)-1*H*-pyrazole) (4): Yellow solid, mp = 255-256 ^{o}C

^{1}H NMR (400 MHz, $CDCl_3$): δ 2.36 (s, 9H), 2.44 (s, 9H) 5.32 (s, 6H), 7.36 (t, *J* = 7.4 Hz, 3H), 7.45 (t, *J* = 7.5 Hz, 6H), 7.76 (d, *J* = 7.8 Hz, 6H) ppm; ^{13}C (100 MHz, $CDCl_3$): δ 10.06, 14.32, 17.07, 48.61, 121.88, 129.02, 129.42, 130.86, 135.32, 138.95, 139.31, 142.34, 153.75 ppm; HRMS-ESI: *m*/*z* $C_{45}H_{48}N_{12}$ $[M+H]^+$ calc. 757.4203, obs. 757.4211; IR (ATR, cm^{-1}): 509, 551, 583, 644, 667, 686, 700, 766, 832, 863, 895, 921, 994, 1019, 1070, 1277, 1302, 1370, 1414, 1455, 1493, 1553, 2923.

***N*,*N*',*N*''-(benzene-1,3,5-triyltris(methylene))tris(4-((*E*)-phenyldiazenyl)aniline) (5)**

A mixture of 1,3,5-Tris(bromomethyl)benzene (0.36 g, 1.0 mmol), (*E*)-4-(phenyldiazenyl)aniline (0.61 g, 3.1 mmol) and anhydrous potassium carbonate (0.52 g, 4.0 mmol) were stirred in dry acetonitrile (10 ml) under nitrogen atmosphere, and the reaction mixture was refluxed overnight. The reaction mixture was then cooled to room temperature and quenched with water, filtered and washed with ethanol to remove the starting material. The crude product was dried and further purified with column chromatography over silica gel using a mixture of ethyl acetate and hexane (50:50) as an eluent (Yield = 62%).

***N*,*N*',*N*''-(benzene-1,3,5-triyltris(methylene))tris(4-((*E*)-phenyldiazenyl)aniline) (6):**Orange yellow solid, mp = 135-136 ^{o}C

^{1}H NMR (400 MHz, $CDCl_3$): δ 3.98-4.69 (br, 9H), 6.32-7.00 (br, 9H), 7.28-7.59 (br, 9H), 7.65-7.87 (br, 9H) ppm (Note: ^{1}H NMR exhibited broad and low intense signals in both [D_6]DMSO and $CDCl_3$ irrespective of the concentration; In $CDCl_3$, the amine protons were absent due to exchange.); ^{13}C (100 MHz, [D_6]DMSO): δ 79.57, 112.41, 112.68, 122.19, 122.30, 125.36, 129.62, 129.91, 143.43, 152.27, 152.81, ppm; HRMS-ESI: *m*/*z* $C_{45}H_{39}N_9$ $[M+H]^+$ calc. 706.3406, obs. 706.3397; IR (ATR, cm^{-1}): 639, 663, 687, 722 , 765, 823, 916, 966, 1019, 1070, 1138, 1232, 1270, 1327, 1408, 1429, 1455, 1511, 1598, 1698, 2926, 3032, 3064, 3409.

4.5 Conclusions

All pyrazole substituted C_3 symmetric derivative showed an excellent photoswitching and photochromic behavior in solution as well as bulk state. We have demonstrated rewritable printing and erasing. In the tripodal aroylazole derivative, the reversible printing and erasing phenomena were induced fully by light, whereas the flexible tripodal derivatives showed by light (photochromism) in the forward step, whereas heat was necessary for the reverse step (thermochromism). Such changes have also been supported by PXRD and IR spectroscopic studies. But the introduction of *p*-amino azobenzene instead of azopyrazoles did not offer solid-state photoswitching.

4.6 References

1 (a) Bouas-Laurent, H.; Dürr, H.; *Pure Appl. Chem.* **2001**, *73*, 639-665; (b) Dürr, H.; Bouas-Laurent, H. *Photochromism: Molecules and Systems*, Elsevier, Amsterdam, **2003**; (c) Irie, M.; Fukaminato, T.; Matsuda, K.; Kobatake, S. *Chem. Rev.* **2014**, *114*, 12174-12277; (d) Irie, M. *Pure Appl. Chem.* **2015**, *87*, 617-626; (e) Zhang, J.; Zou, Q.; Tian, H. *Adv. Mater*. **2013**, *25*, 378– 399; (f) Mukhopadhyay, A.; Moorthy, J. N. *J. Photochem. Photobiol. C* **2016**, *29*, 73- 106.

2 (a) Irie, M. *Photoreactive Materials for Ultrahigh-density Optical Memory*, Elsevier, Amsterdam, **1994**; (b) Ikeda, T.; Tsutsumi, O. *Science* **1995**, *268*, 1873-1875; (c) Irie, M. *Chem. Rev.* **2000**, *100*, 1685-1716.

3 (a) Klajn, R. Chem. Soc. Rev. **2014**, *43*, 148-184; (b) Xie, X.; Mistlberger, G.; Bakker, E. *J. Am. Chem. Soc.* **2012**, *134*, 16929-16932.

4 Gonzalez, A.; Kengmana, E. S.; Fonseca, M. V.; Han, G. G. D. *Mater. Today Adv.* **2020**, *6*, 100058.

5 (a) Bandara, H. M. D.; Burdette, S. C. *Chem. Soc. Rev.* **2012**, *41*, 1809-1825; (b) Garcia-Amorós, J.; Velasco, D. *Beilstein J. Org. Chem.* **2012**, *8*, 1003- 1017; (c) Bléger, D.; Schwarz, J.; Brouwer, A. M.; Hecht, S. *J. Am. Chem. Soc.* **2012**, *134*, 20597-20600; (d) Beharry, A. A.; Sadovski, O.; Woolley, G. A. *J. Am. Chem. Soc.* **2011**, *133*, 19684-19687.

6 (a) Wendler, T.; Schütt, C.; Näther, C.; Herges, R. *J. Org. Chem.* **2012**, *77*, 3284-3287; (b) Weston, C. E.; Richardson, R. D.; Haycock, P. R.; White, A. J. P.; Fuchter, M. J. *J. Am. Chem. Soc.* **2014**, *136*, 11878-11881; (c) Calbo, J.; Weston, C. E.; White, A. J. P.; Rzepa, H. S.; Contreras-García, J.; Fuchter, M. J. *J. Am. Chem. Soc.* **2017**, *139*, 1261-1274; (d) Simeth, N. A.; Crespi, S.; Fagnoni, M.; König, B. *J. Am. Chem. Soc.* **2018**, *140*, 2940-2946; (e) Heindl, A. H.; Wegner, H. A. *Chem. Eur. J.* **2020**, *26*, 13730-13737.

7 Weston, C. E.; Kramer, A.; Colin, F.; Yildiz, Ö.; Baud, M. G. J.; Meyer-Almes, F. J.; Fuchter, M. *J. ACS Infect. Dis.* **2017**, *3*, 152-161.

8 Stricker, L.; Fritz, E. C.; Peterlechner, M.; Doltsinis, N. L.; Ravoo, B. J. *J. Am. Chem. Soc.* **2016**, *138*, 4547-4554.

9 Ghebreyessus, K.; Cooper Jr., S. M. *Organometallics* **2017**, *36*, 3360-3370.

10 Devi, S.; Saraswat, M.; Grewal, S.; Venkataramani, S. *J. Org. Chem.* **2018**, *83*, 4307-4322.

11 (a) Harada, J.; Kawazoe, Y.; Ogawa, K. *Chem. Commun.* **2010**, *46*, 2593-2595; (b) Hadjoudis, E.; Mavridis, I. M. *Chem. Soc. Rev.* **2004**, *33*, 579-588; (c) Guo, J.; Jia, D.; Liu, L.; Yuan, H.; Li, F. *J. Mater. Chem.* **2011**, *21*, 3210-3215; (d) Robert, F.; Naik, A. D.; Tinant, B.; Robiette, R.; Garcia, Y. *Chem. Eur. J.* **2009**, *15*, 4327-4342.

12 Qi, Q.; Li, C.; Liu, X.; Jiang, S.; Xu, Z.; Lee, R.; Zhu, M.; Xu, B.; Tian, W. *J. Am. Chem. Soc.* **2017**, *139*, 16036-16039.

13 Zhou, H.; Xue, C.; Weis, P.; Suzuki, Y.; Huang, S.; Koynov, K.; Auernhammer, G. K.; Berger, R.; Butt, H. J.; Wu, S. *Nat. Chem.* **2017**, *9*, 145-151.

14 Kobatake, S.; Yamashita, I. *Tetrahedron* **2008**, *64*, 7611-7618.

15 Frolova, L. A.; Rezvanova, A. A.; Lukyanov B. S.; Sanina, N. A.; Troshin, P. A.; Aldoshin, S. M. *J. Mater. Chem. C* **2015**, *3*, 11675-11680.

16 (a) Kind, J.; Kaltschnee, L.; Leyendecker, M.; Thiele, C. M. *Chem. Commun.* **2016**, *52*, 12506-12509; (b) Burganov, T. I.; Katsyuba, S. A.; Vakhonina, T. A.; Sharipova, A. V.; Fominykh, O. D.; Balakina, M. Y. *J. Phys. Chem. C* **2018**, *122*, 1779-1785.

17 (a) Devi, S. Tuning, Controlling and Applications of *Cis*-isomer Stability in Azoheteroarenes and Multiple Azoarenes Connected Systems. **2018** (Thesis); (b) Yu, H-C; Li, L.; Gao, J.; Tong, J.; Zheng, W.; Cametti, M.; Famulari, A.; Meille, S. V.; Guo, F.; Rujas, J. M. *Dalton Trans.* **2015**, *44*, 15960–15965.

Appendix 4A.

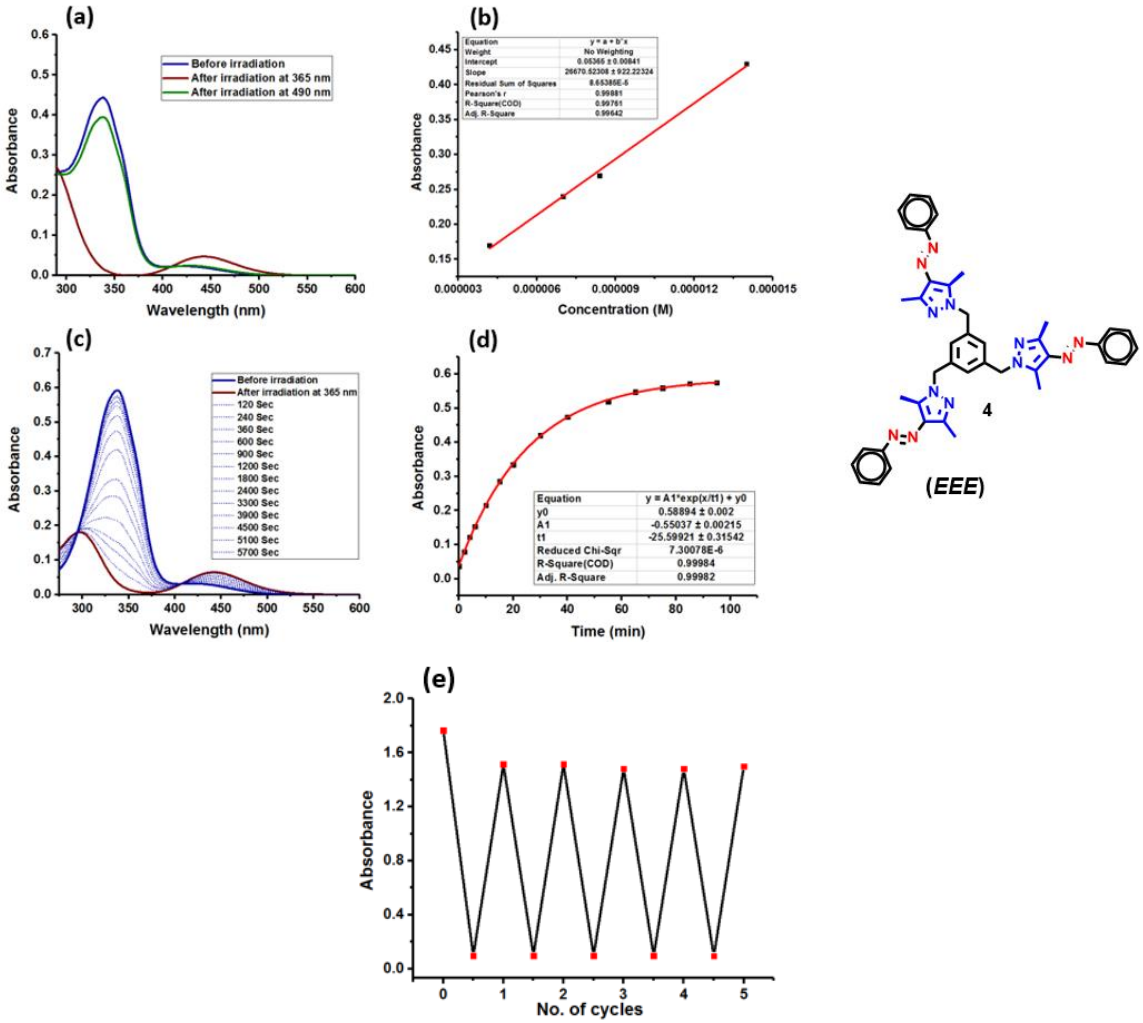

Figure 4A.1. Photoswitching and thermal stability aspects **4** (a) Forward and reverse isomerization (DMSO, 16.7 μM); (b) Estimation of molar extinction coefficient (in DMSO) for the π−π* absorption; (c) Stepwise thermal reverse isomerization kinetics measurements of **5** (UV-Vis spectroscopic monitoring of the 22.0 μM solution at 90 °C); (d) First order thermal reverse isomerization kinetics plot and exponential fit of **6** (22.0 μM solution at 90 °C), (e) Photoswitching stability test upto five cycles of **5** in DMSO (forward isomerization step: 365 nm; reverse isomerization step: 490 nm).

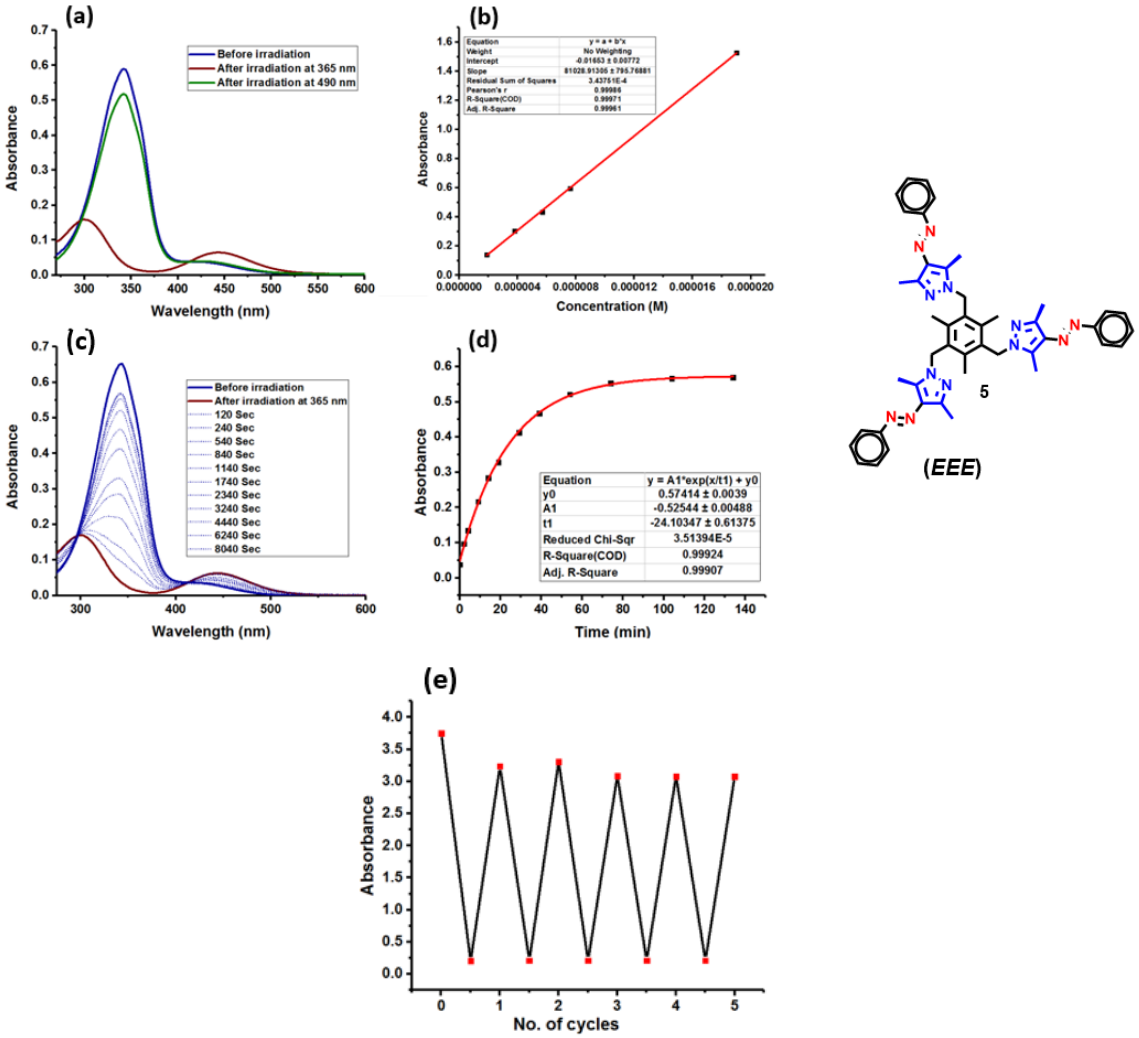

Figure 4A.2. Photoswitching and thermal stability aspects **5** (a) Forward and reverse isomerization (DMSO, 7.3 μM); (b) Estimation of molar extinction coefficient (in DMSO) for the π−π* absorption; (c) Stepwise thermal reverse isomerization kinetics measurements of **7** (UV-Vis spectroscopic monitoring of the 8.1 μM solution at 90 °C); (d) First order thermal reverse isomerization kinetics plot and exponential fit of **5** (8.1 μM solution at 90 °C), (e) Photoswitching stability test upto five cycles of **5** in DMSO (forward isomerization step: 365 nm; reverse isomerization step: 490 nm).

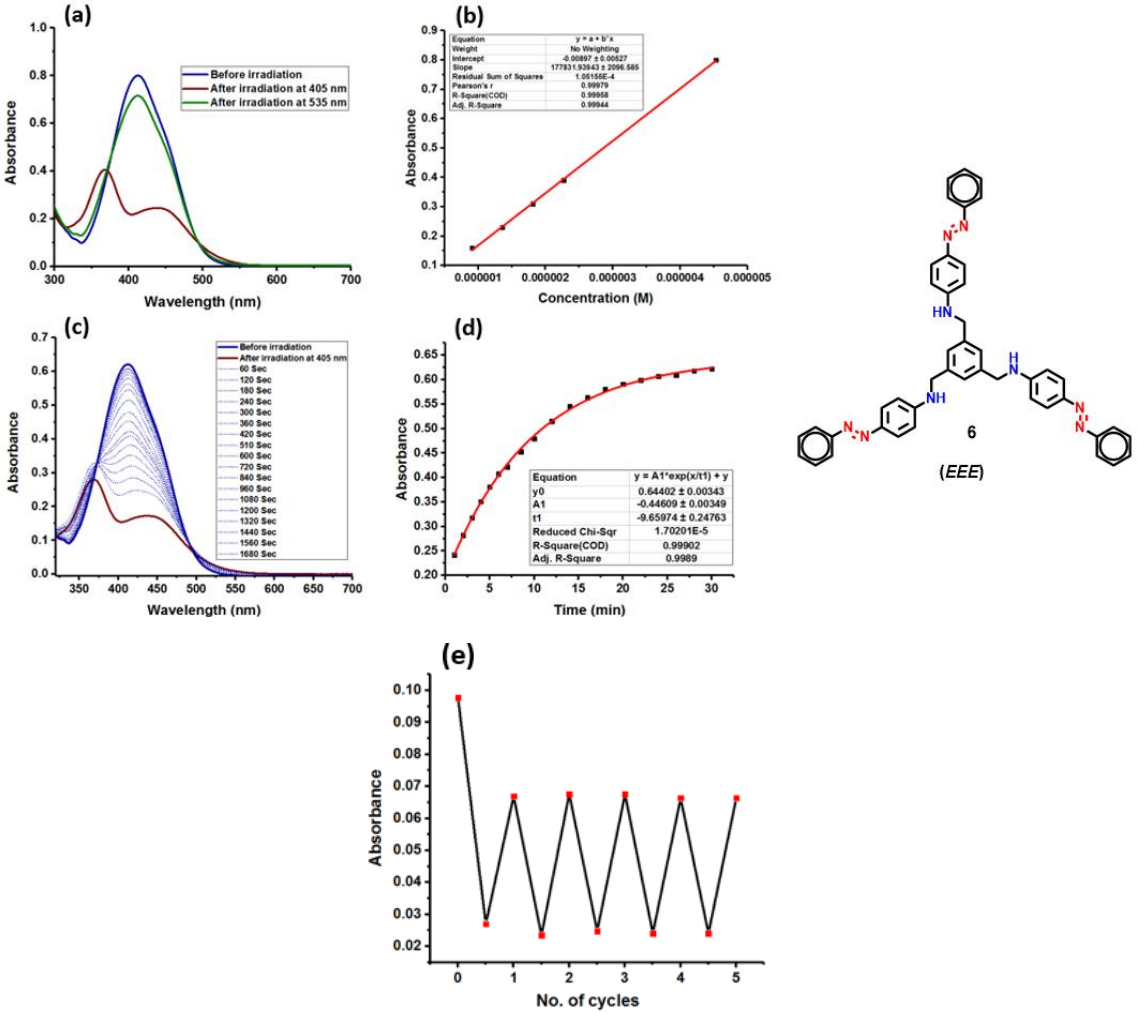

Figure 4.3. Photoswitching and thermal stability aspects **6** (a) Forward and reverse isomerization (DMSO, 2.0 μM); (b) Estimation of molar extinction coefficient (in DMSO) for the π−π* absorption; (c) Stepwise thermal reverse isomerization kinetics measurements of **8** (UV-Vis spectroscopic monitoring of the 3.5 μM solution at 60 °C); (d) First order thermal reverse isomerization kinetics plot and exponential fit of **6** (3.5 μM solution at 60 °C), (e) Photoswitching stability test upto five cycles of **6** in DMSO (forward isomerization step: 405 nm; reverse isomerization step: 535 nm).

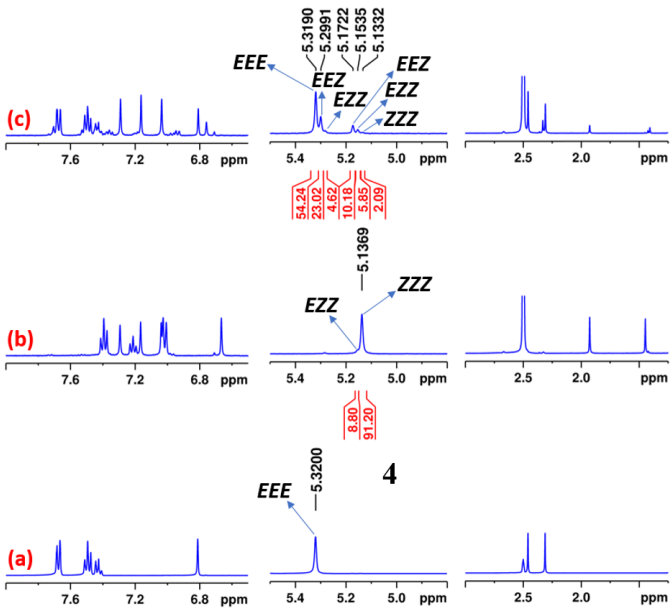

Figure 4.4. PSS composition in **4** (DMSO-d_6, 4.16 mM) (a) Before irradiation; (b) After irradiation at 365 nm; (c) After irradiation at 490 nm (For forward and reverse isomerization steps, PSS composition has been estimated using the normalized integral values of signals due to the linker CH_2 protons)

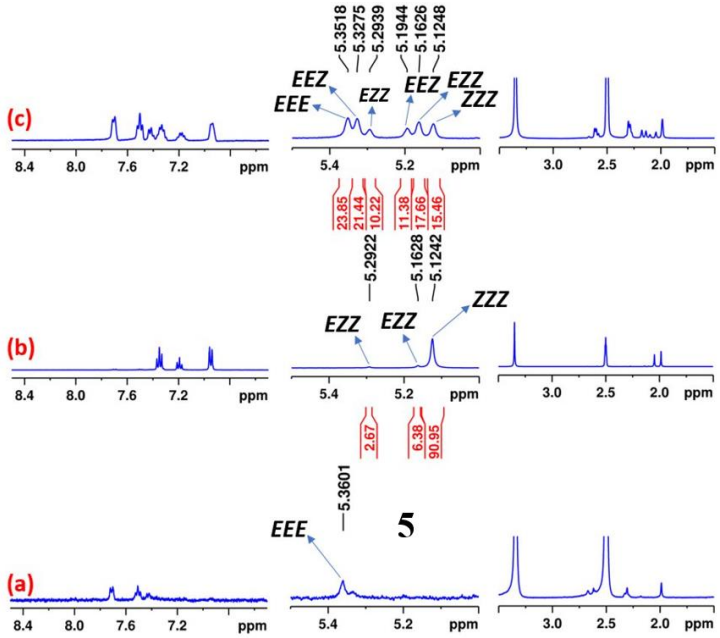

Figure 4.5. PSS composition in **5** (DMSO-d_6, 4.16 mM) (a) Before irradiation; (b) After irradiation at 365 nm; (c) After irradiation at 490 nm (For forward and reverse isomerization steps, PSS composition has been estimated using the normalized integral values of signals due to the linker CH_2 protons). (Note: The ^{1}H-NMR spectrum of the native state in "a" showed poor signal to noise ratio due to solubility issues. Attempts have also been made to improve the signal to noise ratio by increasing the number of scans. However, due to poor solubility at room temperature, the solution led to precipitation during the course of the measurements. However, it has improved after forward photoisomerization step).

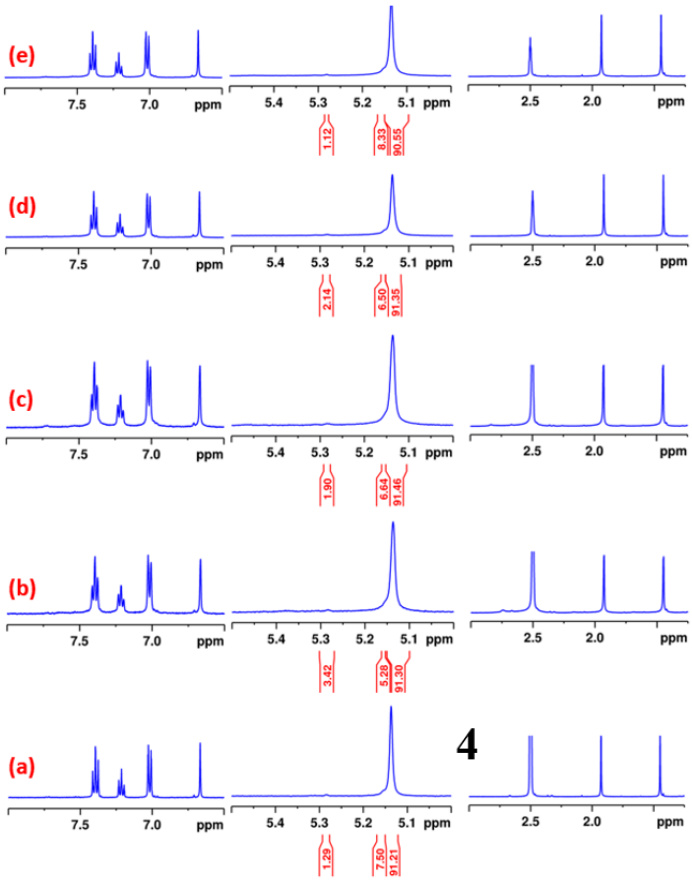

Figure 4.6. Stacking plots depicting the studies on the concentration dependency of **4** in the forward isomerization step (at different concentrations in DMSO-d_6 the samples have been irradiated at 365 nm to attain PSS).

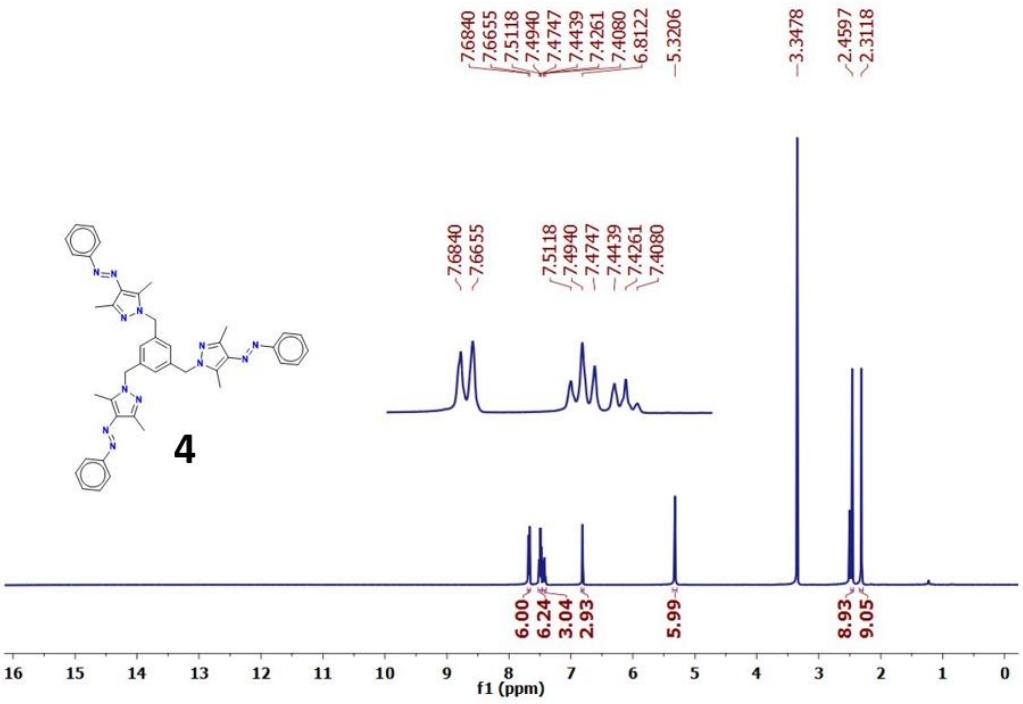

^{1}H NMR spectrum of **4** in $CDCl_3$

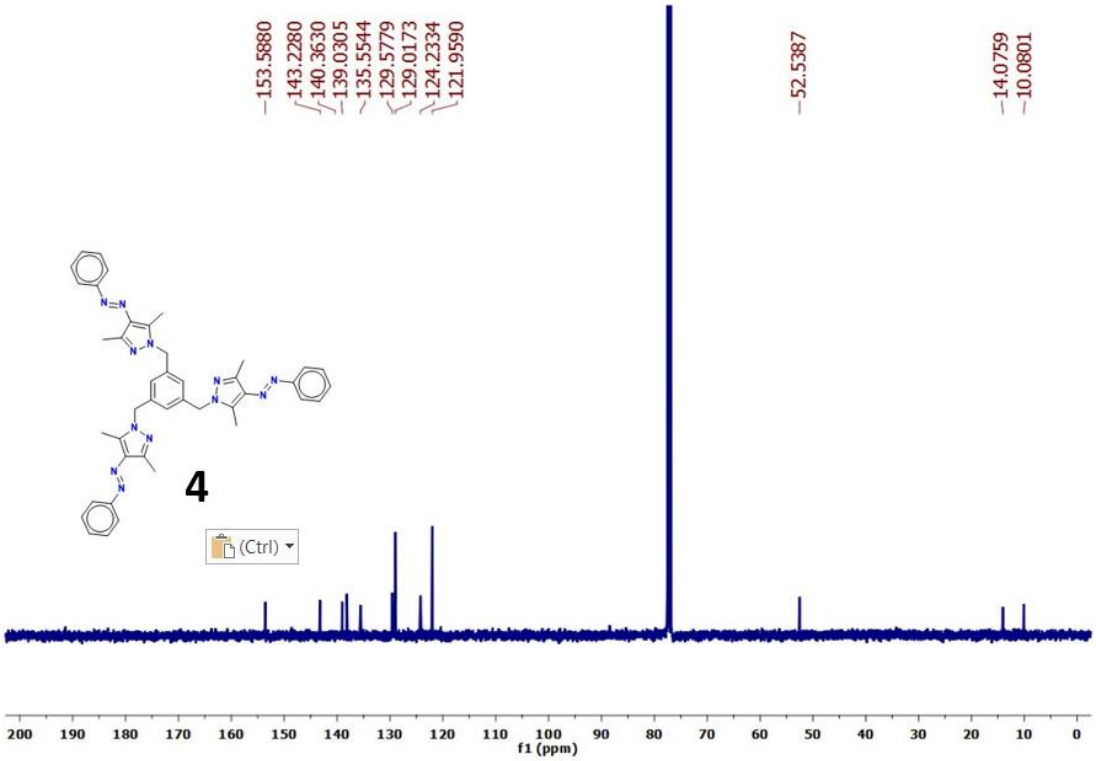

^{13}C NMR spectrum of **4** in $CDCl_3$

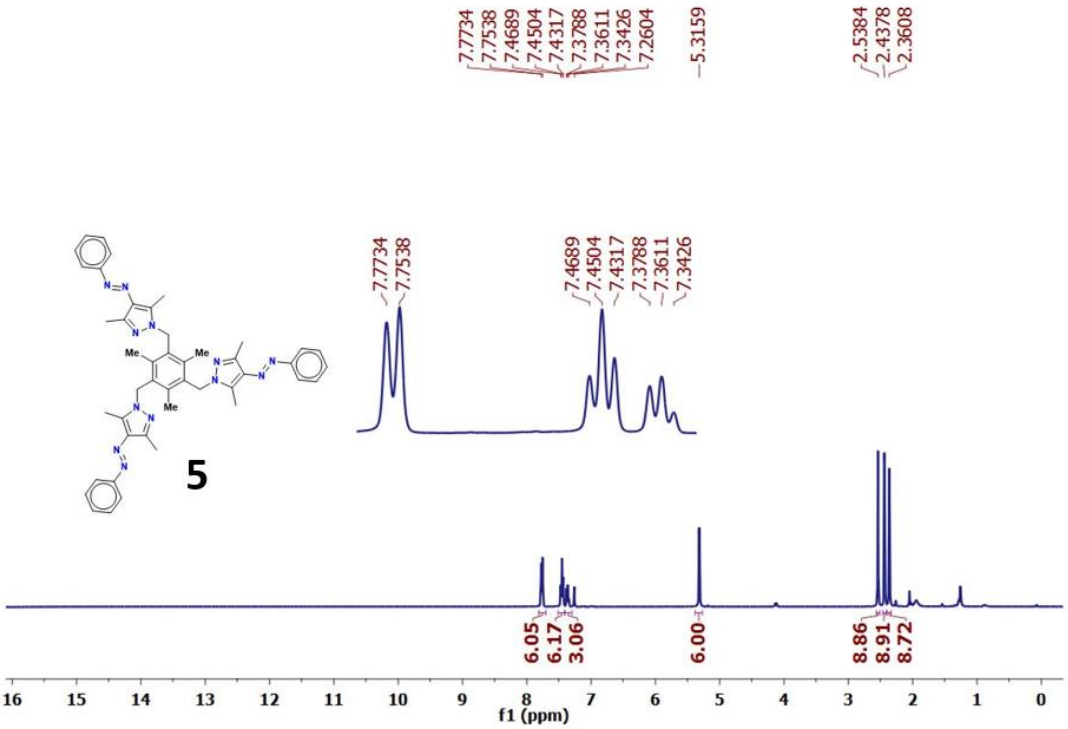

^{1}H NMR spectrum of **5** in $CDCl_3$

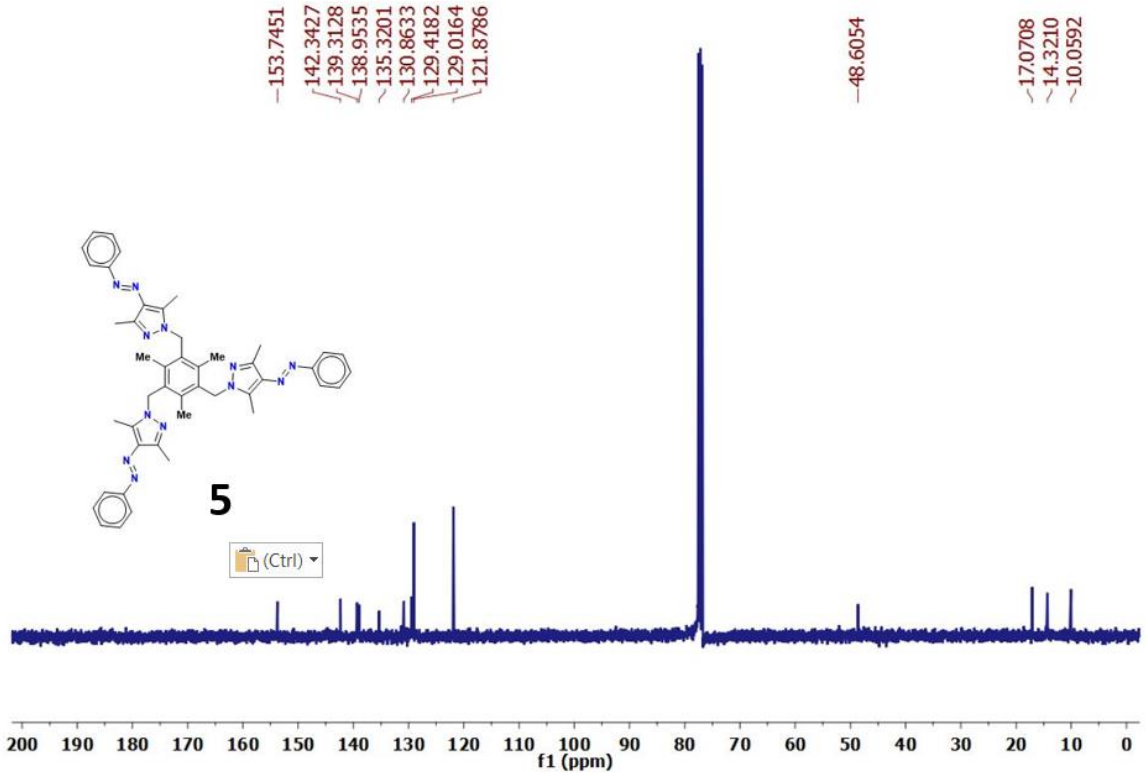

^{13}C NMR spectrum of **5** in $CDCl_3$

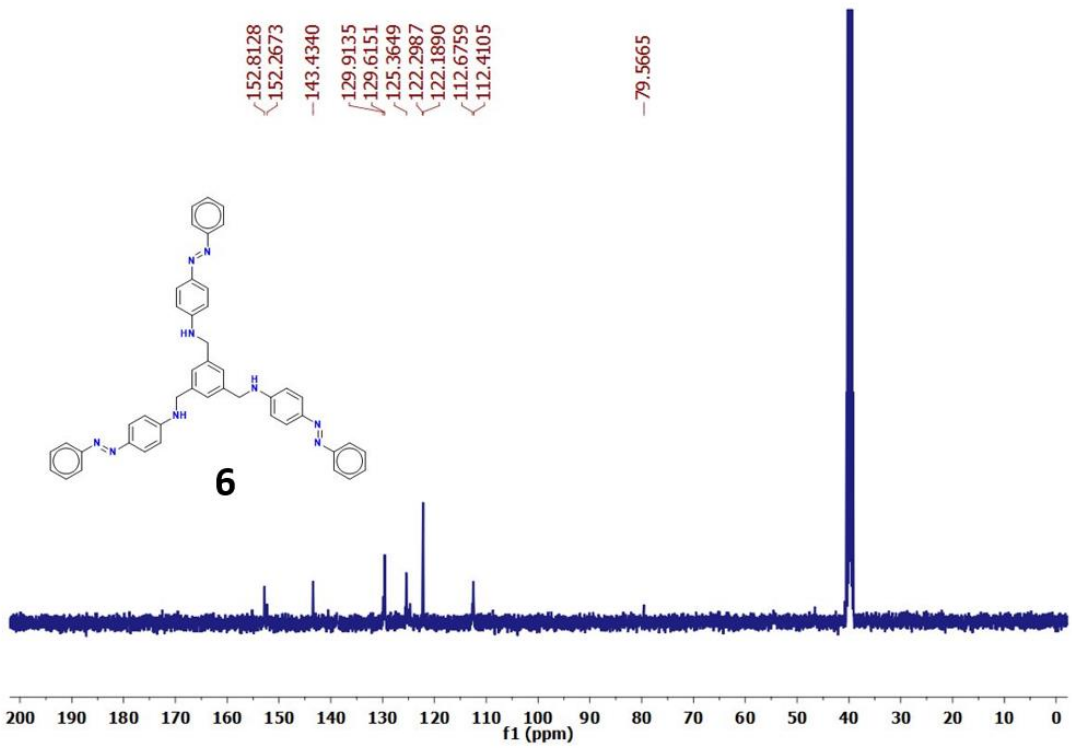

^{13}C NMR spectrum of **6** in DMSO-d_6

Chapter 5. Conclusions and Perspectives

Azoheteroarene photoswitches: Structure-property relationship towards photoswitching using visible light, in the water medium, and solid state

Visible light azoheteroarenes photswitches

In this chapter, we have synthesized 22 derivatives of azoheteroarenes (azoisoxazole, azopyrazoles, and azopyrroles) with different substitution pattern in the heterocycle and aryl ring in good to excellent yields. The connection of cyclic amines (*ortho* or para position) in the aryl group enables them to undergo photoswitching under visibe light. photoswitches. In addition, the *ortho* fluorination allowed the photoswitched (*Z*-isomeric) state to exhibit higher half-life. Furthermore, the half-lives can be tuned by means of the heterocycles, their substitutions and also the ring size of the cyclic amine and fluoro substitution.

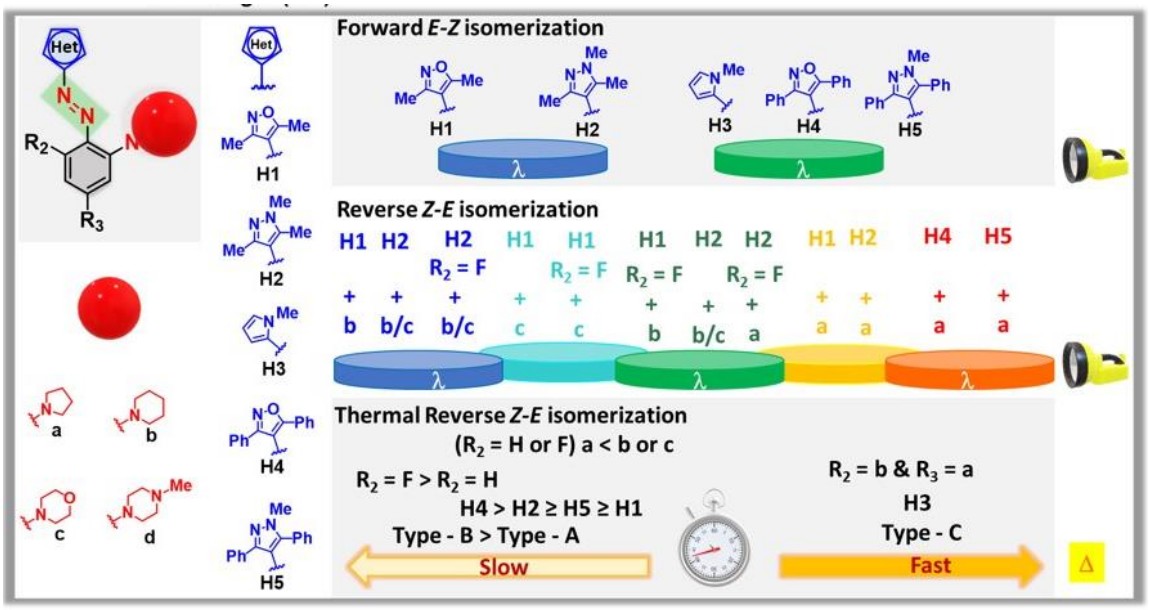

Figure 5.1. Summary depicting the structure-property relationship of azoheteroarene photoswitches.

Most of the photoswitches show good to moderate bidirectional photoswitching under the irradiation of visible light. We also unraveled a new class of 3,5-diphenylheteroazoarenes capable of bidirectional visible light photoswitching and possessing longer half-lives of the *Z*-isomer. To the best of our knowledge, there are no reports on azoheteroarene that can switch in both directions under longer wavelengths compared to blue light irradiation conditions and concurrently unveil extended thermal stability of the photoswitched state.

Water soluble azoheteroarene photoswitches

Water is an essential component of living beings. Developing water-soluble molecular photoswitches, particularly for biological-related applications is one of the current challenges. Among various approaches, converting ionic compounds with high bistability has never been attempted. In this regard, we considered this approach with two diverse azoheteroarene systems. Chapter 3 is subdivided into two parts.

Part A. Heteroaryl azopyrdinium ionic photoswitches (HAPIPs)

In this chapter, we designed 8 heteroazoarene pyridinium ionic photoswitches (HAPIPs) with different five-membered heterocycle units (pyrazole and isoxazole), changes in the counter ions, and the position of the azo relative to the pyridinium center, and substitution at the heterocycle (3,5-dimethyl vs 3,5-diphenyl). Photoswitching properties have been explored in water and other organic solvents through UV-Vis spectroscopy and NMR. HAPIPs exhibited a good to moderate forward *E*-*Z* and reverse *Z*-*E* photoisomerization conversion and thermal stability of *Z*-isomer from seconds to days on varying, solvent, heteroarene or counter ion and 3,5-substitution at heteroarene rings.

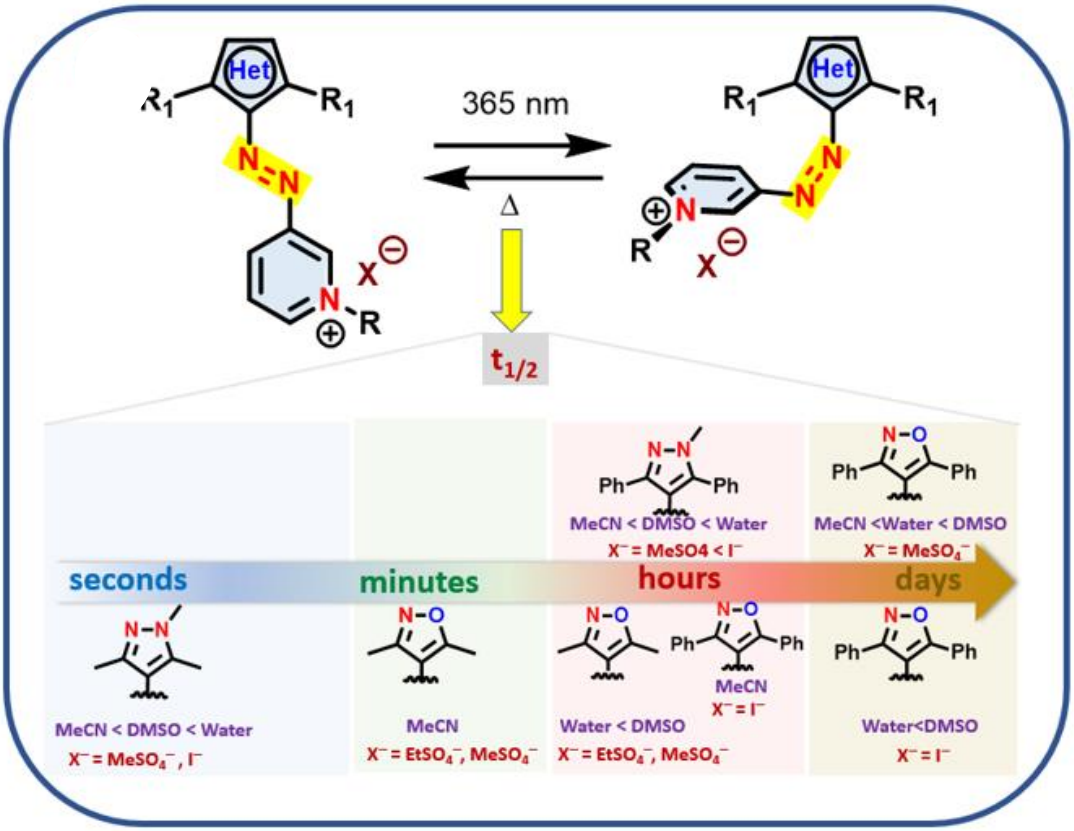

Figure 5.2. Summary of heteroaryl azopyridinium-based ionic photoswitches (HAPIPs).

Derivative **ph-iso-*m*-C1-MeSO$_4$** showed 75% forward photoisomerization and 83% reverse photoisomerization and a half-life of 6.4 d in water. While in previous reports other pyridinium derivatives were known for their fast reverse photoisomerization, our HAPIPs showed tuneable thermal stability and moderate photoisomerization, and high photo reversibility in water.

Part B. Arylazopyrazolium ionic photoswitches (AAPIPs)

As an alternative approach, we synthesized 37 novel water-soluble arylazopyrazolium ionic photoswitches (AAPIPs) by quaternization of azopyrazole derivatives with dimethyl sulfate as an alkylating agent. Almost all AIPIPs showed near quantitative (>90%) forward photoisomerization (*E*-*Z*) while reverse photoisomerization was good to excellent (49-89%). Apart from excellent bidirectional photoswitching, these molecules exhibited very high *Z*-isomer thermal stability in water. The derivative **1-C1-MeSO$_4$** showed a half-life of 55 days in DMSO and 157 days in water. Besides such exceptional thermal stability in water, we observed high photostability and good tolerance in a wide range of pH.

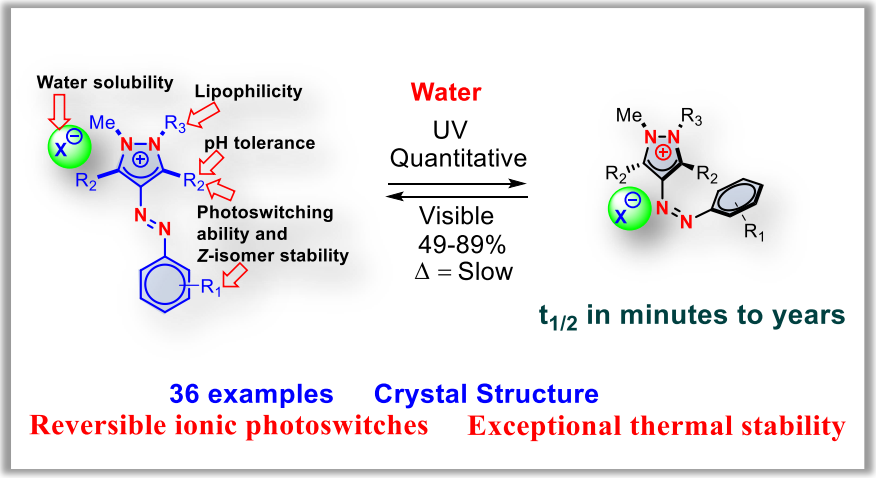

Figure 5.3. Summary of arylazopyrazolium ionic photoswitches (AAPIPs).

Chapter 4. Photochromic multi-azo(hetero)arene connected systems

To enable solid-state photoswitching, the molecules should have enough room, limited intermolecular interactions, and disabled electronic coupling between multiple photoswitches.[ref: chem record] In this regard, we synthesized C_3-symmetric tripodal azopyrazoles or *p*-amino azobenzene-connected derivatives. Tripodal-connected azoarylpyrazole derivatives exhibited excellent photochromic properties in solution and solid state. By using the excellent photochromic properties of such derivatives, we have demonstrated rewritable

printing and erasing. In the tripodal aroylazole derivative, the reversible printing and erasing phenomena were induced fully by light, whereas the flexible tripodal derivatives showed by light (photochromism) in the forward step, whereas heat was necessary for the reverse step (thermochromism). Such changes have also been supported by PXRD and IR spectroscopic studies. But the introduction of *p*-amino azobenzene instead of azopyrazoles did not offer solid-state photoswitching.

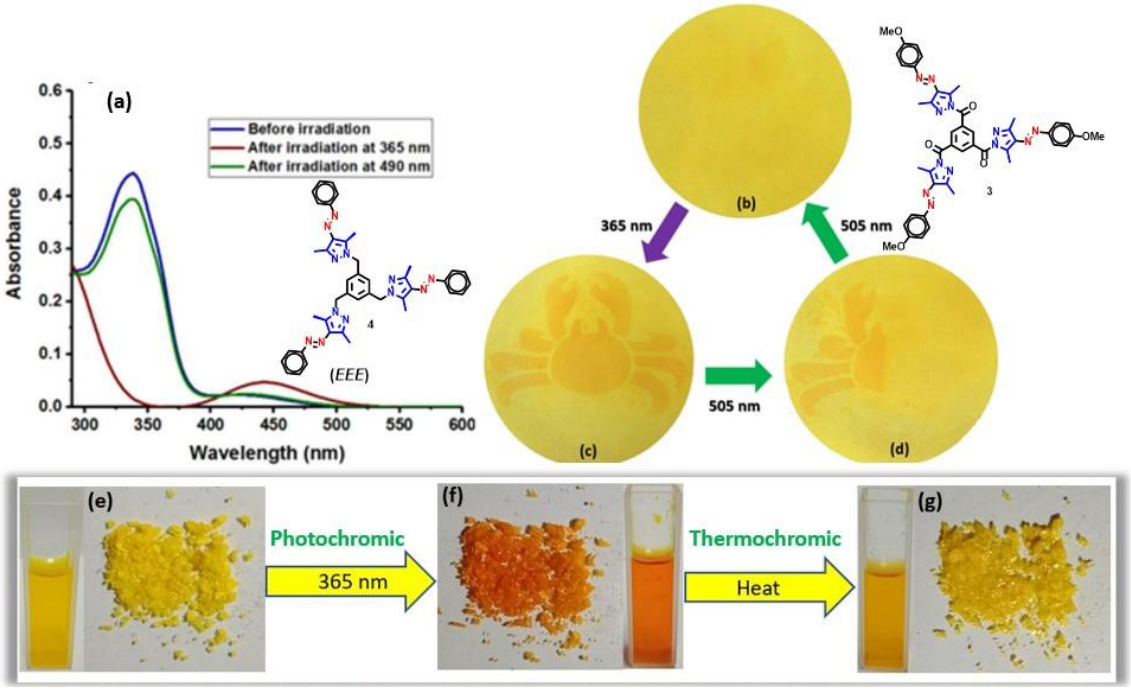

Figure 5.4. (a) Analysis of photoswitching of **4** in DMSO using UV-Vis spectroscopy; Printing and erasing of a "Crab" image on top of a filter paper: (b) A filter paper dip coated with **3** (using $CHCl_3$ solution of 4q); (c) After irradiation at 365 nm through a Crab shaped stencil; (d) Partial exposure to 505 nm light; (e) Yellow coloured solid-state and solution phase (in CH_3CN) samples of **4** in native state; (f) After exposure to a light of wavelength 365 nm exhibiting solid-state and solution phase photochromism; (g) After heating at 90 ^oC for 30 min (for the solid sample) and 70 ^oC for 1 h (for solution phase sample) to obtain thermochromism in reversing to the native state.

Perspectives

Considering the increasing importance and application potential of the azoheteroarenes, many diverging prospects are possible. Particularly, imparting visible light sensitivity for isomerization in water-soluble photoswitches can be one of the future directions that can exhibit usefulness in photopharmocology and MOST materials. Also, systems containing dual stimuli-responsive molecules in a water medium are not explored. In this

direction, a redox-active ferrocene moiety can be coupled with water-soluble photoswitchable ionic derivatives. Based on the recent trends in applications of azobenzenes in energy storage material, the visible light photoswitchable systems can be explored as they convert visible light absorption to store heat energy. Many ionic molecules have solubility in water as well as organic solvents; these systems are potentially applicable for various applications such as photoswitchable surfactants and phase transfer catalysts. Also, these photoswitches can be explored in photoswitchable liquid crystal, adhesive material, bioinspired photoswitchable materials, simple harmonic oscillator (SHO).

Chapter 6. Materials and methods

6.1 Synthesis

Solvent and reagents were purchased from commercially available sources such as Sigma Aldrich, TCI, Avra, Rankem, Promochem, CIL, BLD Pharma etc., which were used without further purification. For anhydrous condition reactions dry solvents such as 1,2-dichloroethane (DCE), toluene, acetonitrile, THF, etc., were obtained from MBRAUN solvent purification system (MB-SPS) and further stored on molecular sieves. N_2 or Ar gases were used for anhydrous condition reactions. Hexane is distilled for column chromatography. UV-vis spectroscopic studies were performed using solvents of spectroscopic or HPLC grade. Reaction progress was monitored by thin-layer chromatography (TLC) purchased from Merck Silica gel 60 F_{254} TLC plates and visualized in a UV chamber (λ = 254 nm). Compounds were purified on a silica gel (mesh size 100-200 Å or 60-120 Å) or neutral/basic alumina using n-hexane/ethyl acetate as an eluent.

6.2 Photoswitching and Characterisation

Nuclear Magnetic Resonance (NMR) spectroscopy: ^{1}H and ^{13}C NMR spectra of all the compounds were carried out on a Bruker Avance-III 400 MHz spectrometer at 400 MHz and 100 MHz, respectively, or a Bruker Avance Neo 500 MHz spectrometer (or 125 MHz for ^{13}C), which are indicated appropriately. The chemical shift (δ) values are reported in parts per million (ppm) and coupling constant (*J*) in hertz (Hz), respectively. The signal multiplicities were abbreviated as follows: s-singlet, d-doublet, t-triplet, q-quartet, p-pentet, sep-septet, dd-doublet of doublets, dt (doublet of triplets), br-broad, m-multiplet, etc. For calibration residual solvent signals were used as internal standard (^{1}H NMR: $CDCl_3$ = 7.26 ppm, DMSO-d_6 = 2.50 ppm; ^{13}C NMR: $CDCl_3$ = 77.16 ppm, DMSO-d_6 = 39.52 ppm).

High-resolution mass spectrometry (HRMS): HRMS was recorded on a Waters Synapt G2-Si Q-TOF mass spectrometer under the electrospray ionization (ESI) method in positive and negative modes.

FT-IR spectroscopy: Infrared spectra (IR) were recorded on a Bruker Alpha spectrometer in transmittance mode using a ZnSe Attenuated Total Reflectance (ATR) assembly or on a Perkin Elmer Spectrum FT-IR spectrometer as a KBr pellet and reported in cm^{-1}.

Melting points (MPs): MPs were recorded on a Stuart SMP20 melting point apparatus which are uncorrected.

UV-vis spectroscopy, photoswitching, kinetics studies, and light sources used

Analysis of photoswitching and kinetics studies of all the azo-compounds were carried out using a UV-vis spectrophotometer either a Cary 5000 UV-Vis-NIR or a Cary 60 spectrophotometer of Agilent technology equipped with a Peltier cell assembly as a temperature controller. In most of the cases, for *trans* (*E*) to *cis* (*Z*) photoisomerization light of 365 nm wavelength, whereas for reverse *cis* (*Z*) to *trans* (*E*) photoisomerization, light of CFL bulb of 35 W, 470 nm, 490 nm, and 505 nm wavelengths have been used. The torch of 365 nm (Convoy S2+) was purchased from commercial sources, whereas visible range wavelengths such as 470 nm, 490nm, 505 nm, etc were used from the LED light source (Applied Photophysics, SX/LED with a bandwidth of 20 nm). For photoswitching studies irradiation was performed either in a quartz cuvette of 1 cm path length or quartz NMR tubes from Sigma Aldrich until photostationary states (PSSs) was reached.

Kinetics studies: ^{1}H NMR spectroscopic studies

Similarly, the thermal reverse isomerization kinetics was performed using ^{1}H NMR spectroscopy. The sample was irradiated in a quartz NMR sample tube using 365 nm UV light, and the sample was introduced immediately into the NMR instrument, and the spectra were recorded. PSS was confirmed by repeating the irradiation sequences until no further changes in spectral data. The kinetics mode of recording was done by keeping the sample tube in a thermostat for different intervals of time. The normalized integral values corresponding to the *cis* and *trans* isomers were used for the kinetics plot.

Estimation of PSS composition and error analysis

(a) UV-vis spectroscopic studies

The estimation of the percentage of PSS composition of *cis* and *trans* isomers in the solution state was performed using UV-vis spectroscopy. The following equation was used in this regard.[(1)]

$$\%cis = \frac{A_{trans} - A_{cis}}{A_{trans}} \times 100 \quad \ldots\ldots (1)$$

or $$\%cis = \left(1 - \frac{A_{cis}}{A_{trans}}\right) \times 100$$

Where A_{trans} is the absorbance corresponding to the *trans*-isomer at λ_{max}, A_{cis} is the absorbance corresponding to the *cis*-isomer at the same wavelength of absorption estimated at PSS.

For the estimation of PSS composition in the solid state, the following expression was used. Using the same expression PSS composition of reverse photoisomerization was also estimated.

$$\%\text{conversion of } \textit{EEE}\text{-isomer} = \left(1 - \frac{A_{n-\pi^*} \text{ absorption before irradiation}}{A_{n-\pi^*} \text{absorption after irradiation}}\right) \times 100$$

Where $A_{n\text{-}\pi^*}$ is the absorption of *trans* and *cis*-isomer at λ_{max} (n to π^*) of *trans*-isomer. The error in PSS estimation using UV-vis spectroscopy was found up to 5%.[1b]

(b) ^{1}H-NMR spectroscopic studies

A milli molar concentration solution was prepared in a quartz NMR tube and was subjected to the recording of the ^{1}H NMR spectrum before irradiation. Then the NMR sample tube was irradiated at 365 nm and a spectrum was recorded immediately. Irradiation and spectral recording steps were repeated until a PSS was attained. Then the direct integration of the peaks of *trans* and *cis*-isomers was followed by the normalization of selected non-overlapping signals corresponding to those isomers that give the PSS composition of both isomers. Similar studies were done for reverse photoisomerization and kinetics studies as well.

In our analysis of NMR experimental data using integral values, we did not account for error. However, to minimize the error, we considered the following:

1. We have chosen one type of signal during the forward and reverse isomerization steps.
2. We have also attempted to use those signals whose overlap is minimal so that a clear integration can be made and normalized to obtain the %conversions.
3. The samples were continuously irradiated such that a photostationary state (PSS) is reached, which was followed by ^{1}H-NMR. This way, we ensured that no further isomerization is possible. Also, the experiments were repeated for reproducibility.
4. For a few cases, the signal-to-noise ratio cannot be improved any further owing to the poor solubility. Particularly, during the reverse photoisomerization step, the conversion into *EEE*-isomer is accompanied by precipitation. In the solution containing the native state (*EEE*-isomer), this situation can be overcome by heating to dissolve the sample; whereas it is not possible under photoirradiation (reverse photoisomerization) conditions.
5. Along the line, the normalized integration values have been estimated using the basic version of the software (TopSpin). Moreover, we did not perform the line-shape simulations or deconvolution procedures, which are critical for minimizing the error during quantification for close-lying signals.

6. Based on repeated measurements in certain cases (or during the attainment of PSS), we observed a marginal error of 2-3% in the normalized integral values.[1b]

Thermal reverse isomerization kinetics

Thermal reverse isomerization kinetics of *cis* to *trans* isomerization was followed by either using UV-vis or NMR spectroscopy. Since *cis*-isomer is thermodynamically less stable it spontaneously converts into the thermodynamically more stable *trans*-isomer at room temperature. Kinetics of *cis* to *trans* thermal reverse isomerization follow first-order exponential decay. Thermal stability of *cis*-isomer can be understood by the comparison of rate constant or half-life. For higher temperature kinetics studies DMSO as a solvent was chosen due to its aprotic nature and high boiling point. The following equations have been used for the first-order exponential decay of *cis*-isomer or growth of *trans*-isomer.

The rate constant has been calculated using the following first-order rate equation:

$$[A] = [A]_o e^{-kt} \quad \text{..... (1)}$$

Half-life was estimated from the rate constant using the following equation

$$t_{1/2} = \frac{0.693}{k} \quad \text{..... (2)}$$

The activation parameters for the *cis* to *trans* thermal reverse isomerization step were obtained using variable temperature kinetics plots. Rate constants obtained from these plots were utilized to plot Eyring and Arrhenius plots.

Eyring equation

$$k = \frac{k_B T}{h} e^{\left(\frac{-\Delta G^{\ddagger}}{RT}\right)} \quad \text{..... (3)}$$

$$k = \frac{k_B T}{h} e^{\left(\frac{\Delta S^{\ddagger}}{R}\right)} e^{\frac{-\Delta H^{\ddagger}}{RT}} \quad \text{..... (4)}$$

The linear form of the Eyring equation (**equation 5**) was used for the estimation of activation parameters, enthalpy of activation ($\Delta H^{\ddagger}$), and entropy of activation ($\Delta S^{\ddagger}$). The slope $-(\Delta H^{\ddagger}/R)$ of ln(k/T) vs 1/T plot gives the value of ($\Delta H^{\ddagger}$) whereas the intercept ($\ln(k_B/h) + \Delta S^{\ddagger}/R$) gives the value of ($\Delta S^{\ddagger}$).

The linear form of the equation

$$\ln\left(\frac{k}{T}\right) = -\left(\frac{\Delta H^{\ddagger}}{R}\right)\left(\frac{1}{T}\right) + \left(ln\left(\frac{k_B}{h}\right) + \frac{\Delta S^{\ddagger}}{R}\right) \text{.....(5)}$$

The linear form of the Arrhenius equation (**equation 8**) was used for the estimation of activation energy (Ea). The slope (–Ea/R) of ln (k) vs (1/T) plot gives the value of activation energy (Ea).

Arrhenius equation

$$k = A\, e^{\left(\frac{-E_a}{RT}\right)} \text{ ..... (6)}$$

$$lnk = lnA - \frac{E_a}{RT} \text{ ..... (7)}$$

$$lnk = -\frac{E_a}{R}\left(\frac{1}{T}\right) + lnA \text{ .... (8)}$$

The first-order exponential fitting of plots was used for estimation of error in rate constant and half-life using Origin software. The error estimation in activation parameters was performed according to the literature reports.[1b, 2)]

Quantum yield

Quantum yield was calculated using previously reported method[,1b].

The rate of a unidirectional photochemical reaction initiated with monochromatic light is given by:

$$r_{A\rightarrow B} = \frac{q_{in}\Phi_{A\rightarrow B}}{V}(1 - 10^{-\varepsilon_A[A]l}) \qquad (1)$$

When the absorbance is much less than 0.43, Taylor expansion of the exponential and truncation at the linear term gives an approximate first-order rate equation (2) from which an expression relating the quantum yield to an observed first-order rate constant, photon flux and measurable properties of the sample can be derived (3):

$$r_{A\rightarrow B} = \frac{q_{in}\Phi_{A\rightarrow B}\varepsilon_A l}{V}[A] \qquad (2)$$

$$\Phi_{A\rightarrow B} = \frac{kV}{q_{in}\varepsilon_A l\, ln\, 10} \qquad (3)$$

Where Φ = quantum yield; k= rate constant (obtained from the exponential fit of a graph of A vs. time); V = sample volume; ε_A= molar extinction coefficient; l = pathlength; and q = molar photon flux.

Molar photon flux was calculated using equation

$$q_{in} = \frac{P\lambda}{hcN_A} \qquad (4)$$

where P = power (of the laser); λ = pump wavelength; h = Planck's constant; c = speed of light; and N_A = Avogadro's number.

6.3 References

1. Ghebreyessus, K.; Cooper, S. M. *Organometallics* **2017**, *36*, 3360–3370; b) Weston, C. E.; Richardson, R. D.; Haycock, P. R.; White, A. J. P.; Fuchter, M. J. *J. Am. Chem. Soc*. **2014**, *136*, 11878−11881; c) Devi, S.; Gaur, A. K.; Gupta, D.; Saraswat, M.; Venkataramani, S. *ChemPhotoChem* **2018**, *2*, 806–810.
2. Lente, G.; Fábián, I.; Poë, A. J. *New J. Chem*. **2005**, *29*, 759-760.

Copyright permissions for published work(s):

3/19/23, 12:25 PM Rightslink® by Copyright Clearance Center

CCC RightsLink

Home | Help | Live Chat | Ankit Gaur

Structure–Property Relationship for Visible Light Bidirectional Photoswitchable Azoheteroarenes and Thermal Stability of Z-Isomers

ACS Publications Most Trusted. Most Cited. Most Read.

Author: Ankit Kumar Gaur, Himanshu Kumar, Debapriya Gupta, et al
Publication: The Journal of Organic Chemistry
Publisher: American Chemical Society
Date: May 1, 2022

Copyright © 2022, American Chemical Society

PERMISSION/LICENSE IS GRANTED FOR YOUR ORDER AT NO CHARGE

This type of permission/license, instead of the standard Terms and Conditions, is sent to you because no fee is being charged for your order. Please note the following:

- Permission is granted for your request in both print and electronic formats, and translations.
- If figures and/or tables were requested, they may be adapted or used in part.
- Please print this page for your records and send a copy of it to your publisher/graduate school.
- Appropriate credit for the requested material should be given as follows: "Reprinted (adapted) with permission from {COMPLETE REFERENCE CITATION}. Copyright {YEAR} American Chemical Society." Insert appropriate information in place of the capitalized words.
- One-time permission is granted only for the use specified in your RightsLink request. No additional uses are granted (such as derivative works or other editions). For any uses, please submit a new request.

If credit is given to another source for the material you requested from RightsLink, permission must be obtained from that source.

BACK CLOSE WINDOW

JOHN WILEY AND SONS LICENSE
TERMS AND CONDITIONS

Mar 19, 2023

This Agreement between IISER Mohali -- Ankit Gaur ("You") and John Wiley and Sons ("John Wiley and Sons") consists of your license details and the terms and conditions provided by John Wiley and Sons and Copyright Clearance Center.

License Number	5512351200811
License date	Mar 19, 2023
Licensed Content Publisher	John Wiley and Sons
Licensed Content Publication	The Chemical Record
Licensed Content Title	Multiple Azoarenes Based Systems -- Photoswitching, Supramolecular Chemistry and Application Prospects
Licensed Content Author	Sugumar Venkataramani, Ankit Kumar Gaur, Anjali Srivastava, et al
Licensed Content Date	Jul 21, 2022
Licensed Content Volume	22
Licensed Content Issue	11
Licensed Content Pages	42
Type of use	Dissertation/Thesis
Requestor type	Author of this Wiley article

Format	Print and electronic
Portion	Full article
Will you be translating?	No
Title	Azoheteroarene photoswitches: Structure-property relationship towards photoswitching using visible light, in the water medium, and solid state
Institution name	IISER Mohali
Expected presentation date	Mar 2023
Order reference number	26
Requestor Location	IISER Mohali SAS Nagar, IISER Mohali (Punjab) Mohali, 140306 India Attn: IISER Mohali
Publisher Tax ID	EU826007151
Total	0.00 USD

Terms and Conditions

JOHN WILEY AND SONS LICENSE
TERMS AND CONDITIONS

Mar 19, 2023

This Agreement between IISER Mohali -- Ankit Gaur ("You") and John Wiley and Sons ("John Wiley and Sons") consists of your license details and the terms and conditions provided by John Wiley and Sons and Copyright Clearance Center.

License Number	5512350801612
License date	Mar 19, 2023
Licensed Content Publisher	John Wiley and Sons
Licensed Content Publication	ChemPhotoChem
Licensed Content Title	Tripodal N-Functionalized Aryluro-3,5-dimethylpyrazole Derivatives of Trimesic Acid: Photochromic Materials for Rewritable Imaging Applications
Licensed Content Author	Sugumar Venkataramani, Mayank Saraswat, Debapriya Gupta, et al
Licensed Content Date	Aug 1, 2018
Licensed Content Volume	2
Licensed Content Issue	9
Licensed Content Pages	5
Type of use	Dissertation/Thesis

Requestor type	Author of this Wiley article
Format	Print and electronic
Portion	Full article
Will you be translating?	No
Title	Azoheteroarene photoswitches: Structure-property relationship towards photoswitching using visible light, in the water medium, and solid state
Institution name	IISER Mohali
Expected presentation date	Mar 2023
Order reference number	25
Requestor Location	IISER Mohali SAS Nagar, IISER Mohali (Punjab) Mohali, 140306 India Attn: IISER Mohali
Publisher Tax ID	EU826007151
Total	0.00 USD
Terms and Conditions	

JOHN WILEY AND SONS LICENSE
TERMS AND CONDITIONS

Mar 19, 2023

This Agreement between IISER Mohali -- Ankit Gaur ("You") and John Wiley and Sons ("John Wiley and Sons") consists of your license details and the terms and conditions provided by John Wiley and Sons and Copyright Clearance Center.

License Number	5512341093667
License date	Mar 19, 2023
Licensed Content Publisher	John Wiley and Sons
Licensed Content Publication	Chemistry - A European Journal
Licensed Content Title	Tuning of Bistability, Thermal Stability of the Metastable States, and Application Prospects in the C3-Symmetric Designs of Multiple Azo(hetero)arenes Systems
Licensed Content Author	Sugumar Venkataramani, Saonli Roy, Sadhu Devi, et al
Licensed Content Date	Jan 15, 2021
Licensed Content Volume	27
Licensed Content Issue	10
Licensed Content Pages	10
Type of use	Dissertation/Thesis

Requestor type	Author of this Wiley article
Format	Print and electronic
Portion	Full article
Will you be translating?	No
Title	Azoheteroarene photoswitches: Structure-property relationship towards photoswitching using visible light, in the water medium, and solid state
Institution name	IISER Mohali
Expected presentation date	Mar 2023
Order reference number	24
Requestor Location	IISER Mohali SAS Nagar, IISER Mohali (Punjab) Mohali, 140306 India Attn: IISER Mohali
Publisher Tax ID	EU826007151
Total	0.00 USD

Terms and Conditions

Ankit Kumar Gaur
Indian Institute of Science Education and Research (IISER) Mohali, India
ankitkumargaur1008@gmail.com ph16012@iisermohali.ac.in +91-8288996574

PhD Chemistry

08/2018–07/2021 **Senior Research Fellow**
Indian Institute of Science Education and Research (IISER) Mohali, India

08/2016–07/2018 **Junior Research Fellow**
Indian Institute of Science Education 014and Research (IISER) Mohali, India

Education

07/2014–06/2016 Master of Science (Chemistry), National Institute of Technology, Rourkela (Odisha), India

07/2011–06/2014 Bachelor of Science, Gurukula Kangri University, Haridwar (Uttarakhand), India

Academic Achievements

- Received **the Best Poster Award** from the organizers of the " International Symposium on Recent Advances in Self-assembled Materials a Supramolecular Chemistry" held at Guru Nanak Dev University (GNDU) Amritsar held on 19th March 2022.
- Awarded **INSPIRE Fellowship** from the Department of Science and Technology (DST), Government of India, from 2011 to 2016.
- Qualified **NET** (**National Eligibility Test**) Conducted by CSIR–UGC December 2015.
- Qualified **GATE** (**Graduate Aptitude Test in Engineering**) Chemistry–2016. All India Rank **– 457**.

Teaching contributions

Indian Institute of Science Education and Research (IISER) Mohali (Teaching Assistant) (2017-18) for undergraduate Chemistry courses

- Assisted in the CHM211 & CHM112 laboratory courses for the BS-MS students. Roles and responsibilities: To demonstrate the experiments to a small group and assist them to execute the experiments; troubleshoot the experiments and address questions; evaluation of lab records and assist the instructors in grading.
- Co-guided master thesis students (Irin P. Tom (2018-19), Anees Rahman (2019-2020), Dhanyaj N. Nampoothiry (2020-2021), and Roshan Nasare 2021-22)
- Mentored undergraduate students during summer internships and mentored junior colleagues.

List of publications

Part of the thesis:

1) **Gaur, A. K**.;‡ Kumar, H.;‡ Gupta, D.;‡ Tom, I. P.;‡ Nampoothry, D. N.; Thakur, S. K.; Mahadevan, A.; Singh' S.; Venkataramani, S. *J. Org. Chem.* **2022**, *87*, 6541−6551. (‡ = equally contributed)
2) **Gaur, A. K.**;† Gupta, D.;† Nampoothiry, D. N.;† Kaur, N.; Kaur, R.; Venkataramani, S. Modulation of Thermal Half-Life of *Z*-Isomers of Heteroaryl Azopyridinium Ionic Photoswitches (HAPIPs) in Aqueous Media (**Manuscript under preparation**). († = equally contributed)
3) **Gaur, A. K**.;‡ Gupta, D.;‡ Mahadevan, A.; Kumar, P.; Kumar, H.; Nampoothry, D. N.; Kaur, N.; Thakur, S. K.; Singh' S.; Slanina, T.; Venkataramani, S. *J. Am. Chem. Soc.* **2023**, *145*, 19, 10584–10594. († = equally contributed)
4) Devi, S.;# **Gaur, A. K**.;# Gupta, D.;# Saraswat, M.;# Venkataramani, S. *ChemPhotoChem,* **2018**, *2*, 9, 806-810. (#Equally contributed)
5) Gupta, D.;‡ **Gaur, A. K**.;‡ Kumar, P.;‡ Kumar, H.;‡ Mahadevan, A.;‡ Devi, S.; Roy, S., Venkataramani S. *Chem*. *Eur*. *J*. **2021**, *27*, 3463–3472. (‡ = equally contributed)
6) Kumar, P.;‡ Gupta, D.;‡ Grewal, S.;‡ Srivastava, A.;‡ **Gaur, A. K**.,‡ Venkataramani, S. *Chem. Rec.* 2022, *22*, 11, e202200074. (‡ = equally contributed)
7) Grewal, S.;# Gupta, D.;# **Gaur, A. K**.;# Saraswat, M.;# Venkataramani, S. *Photoisomerization: Causes, Behavior and Effects*, Nova Publishers: New York, 2019. (#Equally contributed)

Other contributions:

1) Gupta, D.;‡ **Gaur, A. K**.;‡ Chauhan, D.;‡ Thakur, S. K.;‡ Jeyapalan, V.; Singh, S.; Rajaraman, G.; Venkataramani, S. *Inorg. Chem. Front.* **2022**, *9*, 2315–2327. (‡ = equally contributed)
2) Gupta, D.;‡ **Gaur, A. K**.;‡ Thakur, S. K.;‡ Jeyapalan, V.; Singh, S.; Venkataramani, S. Photoswitchable Cu(II) and Cu(I) Complexes of Phenylazo-3,5-dimethylpyrazole Incorporated Ligands (https://doi.org/10.1002/cptc.202200338). (‡ = equally contributed)
3) "Light-switchable" metal complexes- Introducing phototunability through azoheterarenes (**Manuscript under revision**).
4) **Gaur, A. K**.;+ Nasare, R.;+ Kumar, H.;+ Kumar, P.;+ Gupta, D.;+ Parthiban, G.; Sugumar Venkataramani, Extended π-Conjugated Azopyrazole and Azoisoxazole Derivatives (**Manuscript under preparation**).